

Parameterization of Stillinger-Weber Potential for Two-Dimensional Atomic Crystals

Jin-Wu Jiang* and Yu-Ping Zhou

*Shanghai Institute of Applied Mathematics and Mechanics,
Shanghai Key Laboratory of Mechanics in Energy Engineering,
Shanghai University, Shanghai 200072, People's Republic of China*

(Dated: April 28, 2017)

Abstract

We parametrize the Stillinger-Weber potential for 156 two-dimensional atomic crystals. Parameters for the Stillinger-Weber potential are obtained from the valence force field model following the analytic approach (Nanotechnology **26**, 315706 (2015)), in which the valence force constants are determined by the phonon spectrum. The Stillinger-Weber potential is an efficient nonlinear interaction, and is applicable for numerical simulations of nonlinear physical or mechanical processes. The supplemental resources for all simulations in the present work are available online in Ref. 1, including a fortran code to generate crystals' structures, files for molecular dynamics simulations using LAMMPS, files for phonon calculations with the Stillinger-Weber potential using GULP, and files for phonon calculations with the valence force field model using GULP.

PACS numbers: 78.20.Bh, 63.22.-m, 62.25.-g

Keywords: Layered Crystal, Stillinger-Weber Potential, Molecular Dynamics Simulation, Empirical Potential

I. INTRODUCTION

The atomic interaction is of essential importance in the numerical investigation of most physical or mechanical processes. The present work provides parameters for the Stillinger-Weber (SW) empirical potential for 156 two-dimensional atomic crystal (TDACs). In practical applications, these layered materials are usually played as lego on atomic scale to construct the van der Waals heterostructures with comprehensive properties.² The computational cost of *ab initio* for the heterostructure will be substantially increased as compared with one individual atomic layer, because the unit cell for the heterostructure is typically very large resulting from the mismatch of the lattice constants of different layered components. The empirical potential will be a competitive alternative to help out this difficult situation, considering their high efficiency.

In the early stage before 1980s, the computation ability of the scientific community was quite limited. At that time, the valence force field (VFF) model was one popular empirical potential for the description of the atomic interaction, since the VFF model is linear and can be applied in the analytic derivation of most elastic quantities.³ In this model, each VFF term corresponds to a particular motion style in the crystal. Hence, each parameter in the VFF model usually has clear physical essence, which is beneficial for the parameterization of this model. For instance, the bond stretching term in the VFF model is directly related to the frequency of the longitudinal optical phonon modes, so the force constant of the bond stretching term can be determined from the frequencies of the longitudinal optical phonon modes. The VFF model can thus serve as the starting point for developing atomic empirical potentials for different crystals.

While the VFF model is beneficial for the fastest numerical simulation, its strong limitation is the absence of nonlinear effect. Due to this limitation, the VFF model is not applicable to nonlinear phenomena, for which other potential models with nonlinear components are required. Some representative potential models are (in the order of their simulation costs) SW potential,⁴ Tersoff potential,⁵ Brenner potential,⁶ *ab initio* approaches, and etc. The SW potential is one of the simplest potential forms with nonlinear effects included. An advanced feature for the SW potential is that it includes the nonlinear effect, and keeps the numerical simulation at a very fast level.

Considering its distinct advantages, the present article aims at providing the SW potential

for 156 TDACs. We will determine parameters for the SW potential from the VFF model, following the analytic approach proposed by one of the present author (J.W.J).⁷ The VFF constants are fitted to the phonon spectrum or the elastic properties in the TDACs.

In this paper, we parametrize the SW potential for 156 TDACs. All structures discussed in the present work are listed in Tables I, II, III, IV, V, VI, VII, VIII, and IX. The supplemental materials are freely available online in Ref. 1, including a fortran code to generate crystals' structures, files for molecular dynamics simulations using LAMMPS, files for phonon calculations with the SW potential using GULP, and files for phonon calculations with the valence force field model using GULP.

TABLE I: 1H-MX₂, with M as the transition metal and X as oxygen or dichalcogenide. The structure is shown in Fig. 1.

1H-ScO ₂	1H-ScS ₂	1H-ScSe ₂	1H-ScTe ₂	1H-TiTe ₂	1H-VO ₂	1H-VS ₂	1H-VSe ₂	1H-VTe ₂
1H-CrO ₂	1H-CrS ₂	1H-CrSe ₂	1H-CrTe ₂	1H-MnO ₂	1H-FeO ₂	1H-FeS ₂	1H-FeSe ₂	1H-FeTe ₂
1H-CoTe ₂	1H-NiS ₂	1H-NiSe ₂	1H-NiTe ₂	1H-NbS ₂	1H-NbSe ₂	1H-MoO ₂	1H-MoS ₂	1H-MoSe ₂
1H-MoTe ₂	1H-TaS ₂	1H-TaSe ₂	1H-WO ₂	1H-WS ₂	1H-WSe ₂	1H-WTe ₂		

TABLE II: 1T-MX₂, with M as the transition metal and X as oxygen or dichalcogenide. The structure is shown in Fig. 71.

1T-ScO ₂	1T-ScS ₂	1T-ScSe ₂	1T-ScTe ₂	1T-TiS ₂	1T-TiSe ₂	1T-TiTe ₂	1T-VS ₂	1T-VSe ₂
1T-VTe ₂	1T-MnO ₂	1T-MnS ₂	1T-MnSe ₂	1T-MnTe ₂	1T-CoTe ₂	1T-NiO ₂	1T-NiS ₂	1T-NiSe ₂
1T-NiTe ₂	1T-ZrS ₂	1T-ZrSe ₂	1T-ZrTe ₂	1T-NbS ₂	1T-NbSe ₂	1T-NbTe ₂	1T-MoS ₂	1T-MoSe ₂
1T-MoTe ₂	1T-TcS ₂	1T-TcSe ₂	1T-TcTe ₂	1T-RhTe ₂	1T-PdS ₂	1T-PdSe ₂	1T-PdTe ₂	1T-SnS ₂
1T-SnSe ₂	1T-HfS ₂	1T-HfSe ₂	1T-HfTe ₂	1T-TaS ₂	1T-TaSe ₂	1T-TaTe ₂	1T-WS ₂	1T-WSe ₂
1T-WTe ₂	1T-ReS ₂	1T-ReSe ₂	1T-ReTe ₂	1T-IrTe ₂	1T-PtS ₂	1T-PtSe ₂	1T-PtTe ₂	

TABLE III: Puckered (p-) M, with M from group V. The structure is shown in Fig. 178 or Fig. 183.

black phosphorus	p-arsenene	p-antimonene	p-bismuthene
------------------	------------	--------------	--------------

TABLE IV: Puckered MX, with M from group IV and X from group VI. The structure is shown in Fig. 189, and particularly Fig. 191 for p-MX with X=O.

	p-SiO	p-GeO	p-SnO
p-CS	p-SiS	p-GeS	p-SnS
p-CSe	p-SiSe	p-GeSe	p-SnSe
p-CTe	p-SiTe	p-GeTe	p-SnTe

TABLE V: Buckled (b-) M, with M from group IV or V. The structure is shown in Fig. 222.

silicene	germanene	stanene	indiene
blue phosphorus	b-arsenene	b-antimonene	b-bismuthene

TABLE VI: Buckled MX, with M from group IV and X from group VI. The structure is shown in Fig. 239.

b-CO	b-SiO	b-GeO	b-SnO
b-CS	b-SiS	b-GeS	b-SnS
b-CSe	b-SiSe	b-GeSe	b-SnSe
b-CTe	b-SiTe	b-GeTe	b-SnTe

TABLE VII: Buckled MX, with both M and X from group IV, or M from group III and X from group V. The structure is shown in Fig. 239.

b-SnGe	b-SiGe	b-SnSi	b-InP	b-InAs	b-InSb	b-GaAs	b-GaP	b-AlSb
--------	--------	--------	-------	--------	--------	--------	-------	--------

TABLE VIII: Bi-buckled MX, with M from group III and X from group VI. The structure is shown in Fig. 290.

BO	AlO	GaO	InO
BS	AlS	GaS	InS
BSe	AlSe	GaSe	InSe
BTe	AlTe	GaTe	InTe

TABLE IX: Others.

borophene

II. VFF MODEL AND SW POTENTIAL

A. VFF model

The VFF model is one of the most widely used linear model for the description of atomic interactions.³ The bond stretching and the angle bending are two typical motion styles for most covalent bonding materials. The bond stretching describes the energy variation for a bond due to a bond variation $\Delta r = r - r_0$, with r_0 as the initial bond length. The angle bending gives the energy increment for an angle resulting from an angle variation $\Delta\theta = \theta - \theta_0$, with θ_0 as the initial angle. In the VFF model, the energy variations for the bond stretching and the angle bending are described by the following quadratic forms,

$$V_r = \frac{1}{2}K_r (\Delta r)^2, \quad (1)$$

$$V_\theta = \frac{1}{2}K_\theta (\Delta\theta)^2, \quad (2)$$

where K_r and K_θ are two force constant parameters. These two potential expressions in Eqs. (1) and (2) are directly related to the optical phonon modes in the crystal. Hence, their force constant parameters K_r and K_θ are usually determined by fitting to the phonon dispersion.

B. SW potential

In the SW potential, energy increments for the bond stretching and angle bending are described by the following two-body and three-body forms,

$$V_2(r_{ij}) = A(B/r_{ij} - 1)e^{\rho/(r_{ij}-r_{max})}, \quad (3)$$

$$V_3(\theta_{ijk}) = Ke^{[\rho_1/(r_{ij}-r_{max12})+\rho_2/(r_{ik}-r_{max13})]}(\cos\theta_{ijk} - \cos\theta_0)^2 \quad (4)$$

where V_2 corresponds to the bond stretching and V_3 associates with the angle bending. The cut-offs r_{max} , r_{max12} and r_{max13} are geometrically determined by the material's structure. There are five unknown geometrical parameters, i.e., ρ and B in the two-body V_2 term and ρ_1 , ρ_2 , and θ_0 in the three-body V_3 term, and two energy parameters A and K . There is a

constraint among these parameters due to the equilibrium condition,⁷

$$\rho = \frac{-4B(d - r_{max})^2}{(Bd - d^5)}, \quad (5)$$

where d is the equilibrium bond length from experiments. Eq. (5) ensures that the bond has an equilibrium length of d and the V_2 interaction for this bond is at the energy minimum state at the equilibrium configuration.

The energy parameters A and K in the SW potential can be analytically derived from the VFF model as follows,

$$A = \frac{K_r}{\alpha e^{[\rho/(d-r_{max})]}}, \quad (6)$$

$$K = \frac{K_\theta}{2 \sin^2 \theta_0 e^{[\rho_1/(d_1-r_{max12})+\rho_2/(d_2-r_{max13})]}}, \quad (7)$$

where the coefficient α in Eq. (6) is,

$$\begin{aligned} \alpha = & \left[\frac{\rho}{(d - r_{max})^2} \right]^2 (B/d^4 - 1) \\ & + \left[\frac{2\rho}{(d - r_{max})^3} \right] (B/d^4 - 1) \\ & + \left[\frac{\rho}{(d - r_{max})^2} \right] \left(\frac{8B}{d^5} \right) + \left(\frac{20B}{d^6} \right). \end{aligned} \quad (8)$$

In some situations, the SW potential is also written into the following form,

$$V_2(r_{ij}) = \epsilon A_L (B_L \sigma^p r_{ij}^{-p} - \sigma^q r_{ij}^{-q}) e^{[\sigma/(r_{ij}-a\sigma)]}, \quad (9)$$

$$\begin{aligned} V_3(\theta_{ijk}) = & \epsilon \lambda e^{[\gamma\sigma/(r_{ij}-a\sigma)+\gamma\sigma/(r_{jk}-a\sigma)]} \\ & (\cos \theta_{ijk} - \cos \theta_0)^2. \end{aligned} \quad (10)$$

The parameters here can be determined by comparing the SW potential forms in Eqs. (9) and (10) with Eqs. (3) and (4). It is obvious that $p = 4$ and $q = 0$. Eqs. (9) and (10) have two more parameters than Eqs. (3) and (4), so we can set $\epsilon = 1.0$ eV and $\gamma = 1.0$. The other parameters in Eqs. (9) and (10) are related to these parameters in Eqs. (3) and (4) by the following equations

$$A_L = A, \quad (11)$$

$$\sigma = \rho, \quad (12)$$

$$B_L = B/\rho^4, \quad (13)$$

$$a = r_{max}/\rho, \quad (14)$$

$$\lambda = K. \quad (15)$$

TABLE X: The VFF model for single-layer 1H-ScO₂. The second line gives an explicit expression for each VFF term. The third line is the force constant parameters. Parameters are in the unit of $\frac{\text{eV}}{\text{\AA}^2}$ for the bond stretching interactions, and in the unit of eV for the angle bending interaction. The fourth line gives the initial bond length (in unit of \AA) for the bond stretching interaction and the initial angle (in unit of degrees) for the angle bending interaction. The angle θ_{ijk} has atom i as the apex.

VFF type	bond stretching		angle bending	
expression	$\frac{1}{2}K_{\text{Sc-O}}(\Delta r)^2$	$\frac{1}{2}K_{\text{Sc-O-O}}(\Delta\theta)^2$	$\frac{1}{2}K_{\text{Sc-O-O}'}(\Delta\theta)^2$	$\frac{1}{2}K_{\text{O-Sc-Sc}}(\Delta\theta)^2$
parameter	9.417	4.825	4.825	4.825
r_0 or θ_0	2.090	98.222	58.398	98.222

TABLE XI: Two-body SW potential parameters for single-layer 1H-ScO₂ used by GULP⁸ as expressed in Eq. (3).

	A (eV)	ρ (\AA)	B (\AA^4)	r_{min} (\AA)	r_{max} (\AA)
Sc-O	7.506	1.380	9.540	0.0	2.939

The SW potential is implemented in GULP using Eqs. (3) and (4). The SW potential is implemented in LAMMPS using Eqs. (9) and (10).

In the rest of this article, we will develop the VFF model and the SW potential for layered crystals. The VFF model will be developed by fitting to the phonon dispersion from experiments or first-principles calculations. The SW potential will be developed following the above analytic parameterization approach. In this work, GULP⁸ is used for the calculation of phonon dispersion and the fitting process, while LAMMPS⁹ is used for molecular dynamics simulations. The OVITO¹⁰ and XCRYSDEN¹¹ packages are used for visualization. All simulation scripts for GULP and LAMMPS are available online in Ref. 1.

III. 1H-SCO₂

Most existing theoretical studies on the single-layer 1H-ScO₂ are based on the first-principles calculations. In this section, we will develop the SW potential for the single-layer 1H-ScO₂.

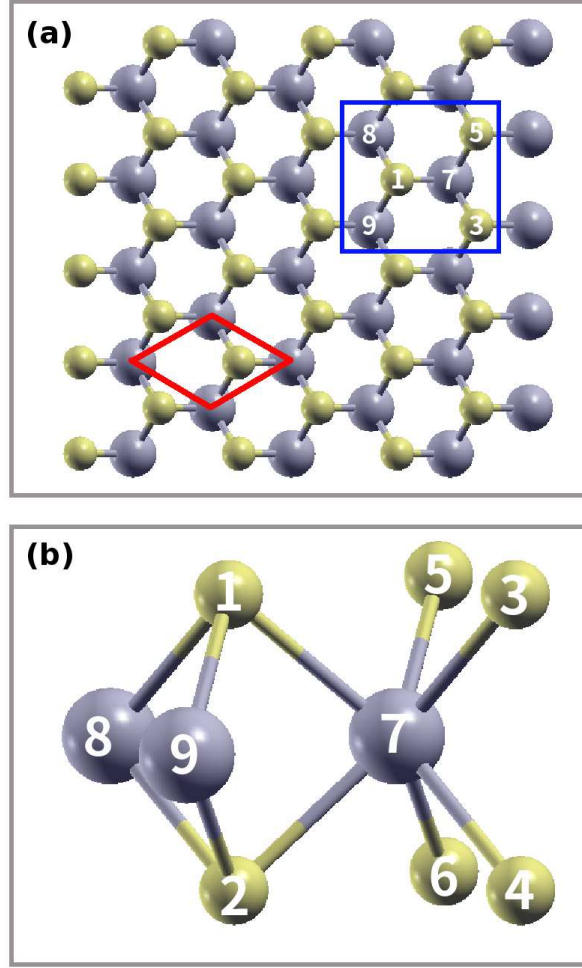


FIG. 1: (Color online) Configuration of the 1H-MX₂ in the 1H phase. (a) Top view. The unit cell is highlighted by a red parallelogram. (b) Enlarged view of atoms in the blue box in (a). Each M atom is surrounded by six X atoms, which are categorized into the top and bottom groups. Atoms X 1, 3, and 5 are from the top group, while atoms X 2, 4, and 6 are from the bottom group. M atoms are represented by larger gray balls. X atoms are represented by smaller yellow balls.

The structure for the single-layer 1H-ScO₂ is shown in Fig. 1 (with M=Sc and X=O). Each Sc atom is surrounded by six O atoms. These O atoms are categorized into the top group (eg. atoms 1, 3, and 5) and bottom group (eg. atoms 2, 4, and 6). Each O atom is connected to three Sc atoms. The structural parameters are from the first-principles calculations,¹² including the lattice constant $a = 3.16 \text{ \AA}$, and the bond length $d_{\text{Sc-O}} = 2.09 \text{ \AA}$. The resultant angles are $\theta_{\text{ScOO}} = \theta_{\text{OScSc}} = 98.222^\circ$ and $\theta_{\text{ScOO}'} = 58.398^\circ$, in which atoms O and O' are from different (top or bottom) group.

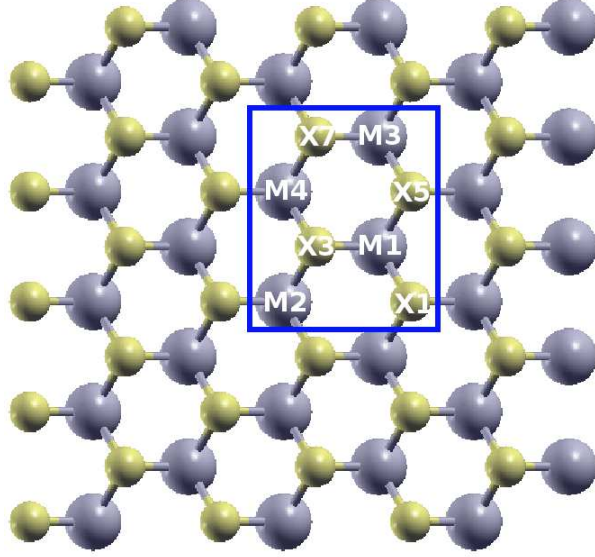


FIG. 2: (Color online) Twelve atom types are introduced to distinguish angles around each M atom for the single-layer 1H-MX₂. Atoms X₁, X₃, X₅, and X₇ are from the top layer. The other four atoms X₂, X₄, X₆, and X₈ are from the bottom layer, which are not displayed in the figure.

TABLE XII: Three-body SW potential parameters for single-layer 1H-ScO₂ used by GULP⁸ as expressed in Eq. (4). The angle θ_{ijk} in the first line indicates the bending energy for the angle with atom i as the apex.

	K (eV)	θ_0 (degree)	ρ_1 (Å)	ρ_2 (Å)	$r_{\min 12}$ (Å)	$r_{\max 12}$ (Å)	$r_{\min 13}$ (Å)	$r_{\max 13}$ (Å)	$r_{\min 23}$ (Å)	$r_{\max 23}$ (Å)
$\theta_{\text{Sc-O-O}}$	63.576	98.222	1.380	1.380	0.0	2.939	0.0	2.939	0.0	3.460
$\theta_{\text{Sc-O-O}'}$	85.850	58.398	1.380	1.380	0.0	2.939	0.0	2.939	0.0	3.460
$\theta_{\text{O-Sc-Sc}}$	63.576	98.222	1.380	1.380	0.0	2.939	0.0	2.939	0.0	3.460

Table X shows four VFF terms for the single-layer 1H-ScO₂, one of which is the bond stretching interaction shown by Eq. (1) while the other three terms are the angle bending interaction shown by Eq. (2). These force constant parameters are determined by fitting to the acoustic branches in the phonon dispersion along ΓM as shown in Fig. 3 (a). The *ab initio* calculations for the phonon dispersion are from Ref. 12. Fig. 3 (b) shows that the VFF model and the SW potential give exactly the same phonon dispersion, as the SW potential is derived from the VFF model.

The parameters for the two-body SW potential used by GULP are shown in Tab. XI. The

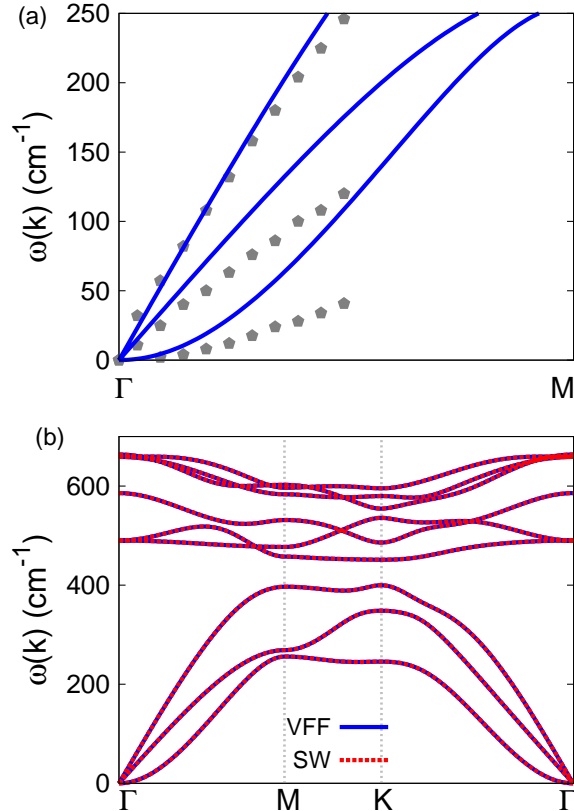


FIG. 3: (Color online) Phonon spectrum for single-layer 1H-ScO₂. (a) Phonon dispersion along the Γ M direction in the Brillouin zone. The results from the VFF model (lines) are comparable with the *ab initio* results (pentagons) from Ref. 12. (b) The phonon dispersion from the SW potential is exactly the same as that from the VFF model.

parameters for the three-body SW potential used by GULP are shown in Tab. XII. Some representative parameters for the SW potential used by LAMMPS are listed in Tab. XIII. We note that twelve atom types have been introduced for the simulation of the single-layer 1H-ScO₂ using LAMMPS, because the angles around atom Sc in Fig. 1 (with M=Sc and X=O) are not distinguishable in LAMMPS. We have suggested two options to differentiate these angles by implementing some additional constraints in LAMMPS, which can be accomplished by modifying the source file of LAMMPS.^{13,14} According to our experience, it is not so convenient for some users to implement these constraints and recompile the LAMMPS package. Hence, in the present work, we differentiate the angles by introducing more atom types, so it is not necessary to modify the LAMMPS package. Fig. 2 (with M=Sc and X=O)

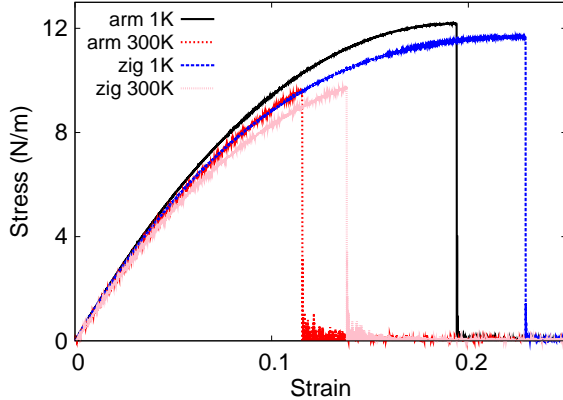


FIG. 4: (Color online) Stress-strain for single-layer 1H-ScO₂ of dimension $100 \times 100 \text{ \AA}$ along the armchair and zigzag directions.

TABLE XIII: SW potential parameters for single-layer 1H-ScO₂ used by LAMMPS⁹ as expressed in Eqs. (9) and (10).

	ϵ (eV)	σ (\AA)	a	λ	γ	$\cos \theta_0$	A_L	B_L	p	q	tol
Sc ₁ -O ₁ -O ₁	1.000	1.380	2.129	0.000	1.000	0.000	7.506	2.627	4	0	0.0
Sc ₁ -O ₁ -O ₃	1.000	0.000	0.000	63.576	1.000	-0.143	0.000	0.000	4	0	0.0
Sc ₁ -O ₁ -O ₂	1.000	0.000	0.000	85.850	1.000	0.524	0.000	0.000	4	0	0.0
O ₁ -Sc ₁ -Sc ₃	1.000	0.000	0.000	63.576	1.000	-0.143	0.000	0.000	4	0	0.0

shows that, for 1H-ScO₂, we can differentiate these angles around the Sc atom by assigning these six neighboring O atoms with different atom types. It can be found that twelve atom types are necessary for the purpose of differentiating all six neighbors around one Sc atom.

We use LAMMPS to perform MD simulations for the mechanical behavior of the single-layer 1H-ScO₂ under uniaxial tension at 1.0 K and 300.0 K. Fig. 4 shows the stress-strain curve for the tension of a single-layer 1H-ScO₂ of dimension $100 \times 100 \text{ \AA}$. Periodic boundary conditions are applied in both armchair and zigzag directions. The single-layer 1H-ScO₂ is stretched uniaxially along the armchair or zigzag direction. The stress is calculated without involving the actual thickness of the quasi-two-dimensional structure of the single-layer 1H-ScO₂. The Young's modulus can be obtained by a linear fitting of the stress-strain relation in the small strain range of $[0, 0.01]$. The Young's modulus are 126.3 N/m and 125.4 N/m along the armchair and zigzag directions, respectively. The Young's modulus is essentially

TABLE XIV: The VFF model for single-layer 1H-ScS₂. The second line gives an explicit expression for each VFF term. The third line is the force constant parameters. Parameters are in the unit of $\frac{\text{eV}}{\text{\AA}^2}$ for the bond stretching interactions, and in the unit of eV for the angle bending interaction. The fourth line gives the initial bond length (in unit of \AA) for the bond stretching interaction and the initial angle (in unit of degrees) for the angle bending interaction. The angle θ_{ijk} has atom i as the apex.

VFF type	bond stretching		angle bending	
expression	$\frac{1}{2}K_{\text{Sc-S}}(\Delta r)^2$	$\frac{1}{2}K_{\text{Sc-S-S}}(\Delta\theta)^2$	$\frac{1}{2}K_{\text{Sc-S-S}'}(\Delta\theta)^2$	$\frac{1}{2}K_{\text{S-Sc-Sc}}(\Delta\theta)^2$
parameter	5.192	2.027	2.027	2.027
r_0 or θ_0	2.520	94.467	64.076	94.467

TABLE XV: Two-body SW potential parameters for single-layer 1H-ScS₂ used by GULP⁸ as expressed in Eq. (3).

	A (eV)	ρ (\AA)	B (\AA^4)	r_{min} (\AA)	r_{max} (\AA)
Sc-S	5.505	1.519	20.164	0.0	3.498

isotropic in the armchair and zigzag directions. The Poisson's ratio from the VFF model and the SW potential is $\nu_{xy} = \nu_{yx} = 0.16$.

There is no available value for nonlinear quantities in the single-layer 1H-ScO₂. We have thus used the nonlinear parameter $B = 0.5d^4$ in Eq. (5), which is close to the value of B in most materials. The value of the third order nonlinear elasticity D can be extracted by fitting the stress-strain relation to the function $\sigma = E\epsilon + \frac{1}{2}D\epsilon^2$ with E as the Young's modulus. The values of D from the present SW potential are -652.8 N/m and -683.3 N/m along the armchair and zigzag directions, respectively. The ultimate stress is about 12.2 Nm^{-1} at the ultimate strain of 0.19 in the armchair direction at the low temperature of 1 K. The ultimate stress is about 11.7 Nm^{-1} at the ultimate strain of 0.23 in the zigzag direction at the low temperature of 1 K.

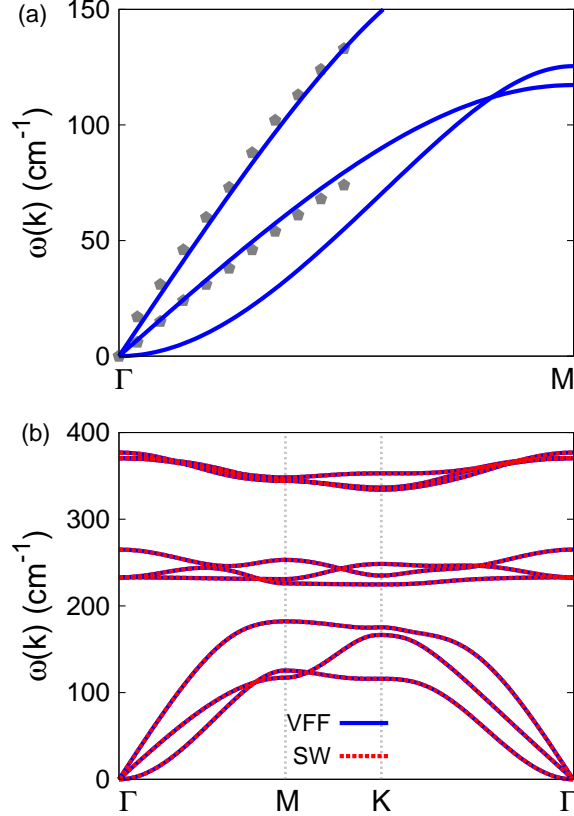


FIG. 5: (Color online) Phonon spectrum for single-layer 1H-ScS₂. (a) Phonon dispersion along the Γ M direction in the Brillouin zone. The results from the VFF model (lines) are comparable with the *ab initio* results (pentagons) from Ref. 12. (b) The phonon dispersion from the SW potential is exactly the same as that from the VFF model.

IV. 1H-SCS₂

Most existing theoretical studies on the single-layer 1H-ScS₂ are based on the first-principles calculations. In this section, we will develop the SW potential for the single-layer 1H-ScS₂.

The structure for the single-layer 1H-ScS₂ is shown in Fig. 1 (with M=Sc and X=S). Each Sc atom is surrounded by six S atoms. These S atoms are categorized into the top group (eg. atoms 1, 3, and 5) and bottom group (eg. atoms 2, 4, and 6). Each S atom is connected to three Sc atoms. The structural parameters are from the first-principles calculations,¹² including the lattice constant $a = 3.70 \text{ \AA}$, and the bond length $d_{\text{Sc-S}} = 2.52 \text{ \AA}$. The resultant

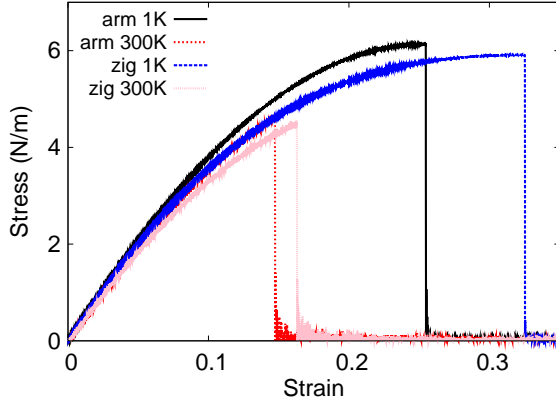


FIG. 6: (Color online) Stress-strain for single-layer 1H-ScS₂ of dimension $100 \times 100 \text{ \AA}$ along the armchair and zigzag directions.

TABLE XVI: Three-body SW potential parameters for single-layer 1H-ScS₂ used by GULP⁸ as expressed in Eq. (4). The angle θ_{ijk} in the first line indicates the bending energy for the angle with atom i as the apex.

	K (eV)	θ_0 (degree)	ρ_1 (Å)	ρ_2 (Å)	$r_{\min 12}$ (Å)	$r_{\max 12}$ (Å)	$r_{\min 13}$ (Å)	$r_{\max 13}$ (Å)	$r_{\min 23}$ (Å)	$r_{\max 23}$ (Å)
$\theta_{\text{Sc-S-S}}$	22.768	94.467	1.519	1.519	0.0	3.498	0.0	3.498	0.0	4.132
$\theta_{\text{Sc-S-S}'}$	27.977	64.076	1.519	1.519	0.0	3.498	0.0	3.498	0.0	4.132
$\theta_{\text{S-Sc-Sc}}$	22.768	94.467	1.519	1.519	0.0	3.498	0.0	3.498	0.0	4.132

angles are $\theta_{\text{ScSS}} = \theta_{\text{SScSc}} = 94.467^\circ$ and $\theta_{\text{ScSS}'} = 64.076^\circ$, in which atoms S and S' are from different (top or bottom) group.

Table XIV shows four VFF terms for the single-layer 1H-ScS₂, one of which is the bond stretching interaction shown by Eq. (1) while the other three terms are the angle bending interaction shown by Eq. (2). These force constant parameters are determined by fitting to the acoustic branches in the phonon dispersion along the ΓM as shown in Fig. 5 (a). The *ab initio* calculations for the phonon dispersion are from Ref. 12. Fig. 5 (b) shows that the VFF model and the SW potential give exactly the same phonon dispersion, as the SW potential is derived from the VFF model.

The parameters for the two-body SW potential used by GULP are shown in Tab. XV. The parameters for the three-body SW potential used by GULP are shown in Tab. XVI. Some representative parameters for the SW potential used by LAMMPS are listed in Tab. XVII.

TABLE XVII: SW potential parameters for single-layer 1H-ScS₂ used by LAMMPS⁹ as expressed in Eqs. (9) and (10).

	ϵ (eV)	σ (Å)	a	λ	γ	$\cos \theta_0$	A_L	B_L	p	q	tol
Sc ₁ -S ₁ -S ₁	1.000	1.519	2.303	0.000	1.000	0.000	5.505	3.784	4	0	0.0
Sc ₁ -S ₁ -S ₃	1.000	0.000	0.000	22.768	1.000	-0.078	0.000	0.000	4	0	0.0
Sc ₁ -S ₁ -S ₂	1.000	0.000	0.000	27.977	1.000	0.437	0.000	0.000	4	0	0.0
S ₁ -Sc ₁ -Sc ₃	1.000	0.000	0.000	22.768	1.000	-0.078	0.000	0.000	4	0	0.0

We note that twelve atom types have been introduced for the simulation of the single-layer 1H-ScS₂ using LAMMPS, because the angles around atom Sc in Fig. 1 (with M=Sc and X=S) are not distinguishable in LAMMPS. We have suggested two options to differentiate these angles by implementing some additional constraints in LAMMPS, which can be accomplished by modifying the source file of LAMMPS.^{13,14} According to our experience, it is not so convenient for some users to implement these constraints and recompile the LAMMPS package. Hence, in the present work, we differentiate the angles by introducing more atom types, so it is not necessary to modify the LAMMPS package. Fig. 2 (with M=Sc and X=S) shows that, for 1H-ScS₂, we can differentiate these angles around the Sc atom by assigning these six neighboring S atoms with different atom types. It can be found that twelve atom types are necessary for the purpose of differentiating all six neighbors around one Sc atom.

We use LAMMPS to perform MD simulations for the mechanical behavior of the single-layer 1H-ScS₂ under uniaxial tension at 1.0 K and 300.0 K. Fig. 6 shows the stress-strain curve for the tension of a single-layer 1H-ScS₂ of dimension 100×100 Å. Periodic boundary conditions are applied in both armchair and zigzag directions. The single-layer 1H-ScS₂ is stretched uniaxially along the armchair or zigzag direction. The stress is calculated without involving the actual thickness of the quasi-two-dimensional structure of the single-layer 1H-ScS₂. The Young's modulus can be obtained by a linear fitting of the stress-strain relation in the small strain range of [0, 0.01]. The Young's modulus are 43.8 N/m and 43.2 N/m along the armchair and zigzag directions, respectively. The Young's modulus is essentially isotropic in the armchair and zigzag directions. The Poisson's ratio from the VFF model and the SW potential is $\nu_{xy} = \nu_{yx} = 0.30$.

There is no available value for nonlinear quantities in the single-layer 1H-ScS₂. We have

TABLE XVIII: The VFF model for single-layer 1H-ScSe₂. The second line gives an explicit expression for each VFF term. The third line is the force constant parameters. Parameters are in the unit of $\frac{\text{eV}}{\text{Å}^2}$ for the bond stretching interactions, and in the unit of eV for the angle bending interaction. The fourth line gives the initial bond length (in unit of Å) for the bond stretching interaction and the initial angle (in unit of degrees) for the angle bending interaction. The angle θ_{ijk} has atom i as the apex.

VFF type	bond stretching		angle bending	
expression	$\frac{1}{2}K_{\text{Sc-Se}}(\Delta r)^2$	$\frac{1}{2}K_{\text{Sc-Se-Se}}(\Delta\theta)^2$	$\frac{1}{2}K_{\text{Sc-Se-Se'}}(\Delta\theta)^2$	$\frac{1}{2}K_{\text{Se-Sc-Sc}}(\Delta\theta)^2$
parameter	5.192	2.027	2.027	2.027
r_0 or θ_0	2.650	92.859	66.432	92.859

TABLE XIX: Two-body SW potential parameters for single-layer 1H-ScSe₂ used by GULP⁸ as expressed in Eq. (3).

	A (eV)	ρ (Å)	B (Å ⁴)	r_{min} (Å)	r_{max} (Å)
Sc-Se	5.853	1.533	24.658	0.0	3.658

thus used the nonlinear parameter $B = 0.5d^4$ in Eq. (5), which is close to the value of B in most materials. The value of the third order nonlinear elasticity D can be extracted by fitting the stress-strain relation to the function $\sigma = E\epsilon + \frac{1}{2}D\epsilon^2$ with E as the Young's modulus. The values of D from the present SW potential are -146.9 N/m and -159.1 N/m along the armchair and zigzag directions, respectively. The ultimate stress is about 6.1 Nm⁻¹ at the ultimate strain of 0.25 in the armchair direction at the low temperature of 1 K. The ultimate stress is about 5.9 Nm⁻¹ at the ultimate strain of 0.32 in the zigzag direction at the low temperature of 1 K.

V. 1H-SCSE₂

Most existing theoretical studies on the single-layer 1H-ScSe₂ are based on the first-principles calculations. In this section, we will develop the SW potential for the single-layer 1H-ScSe₂.

The structure for the single-layer 1H-ScSe₂ is shown in Fig. 1 (with M=Sc and X=Se).

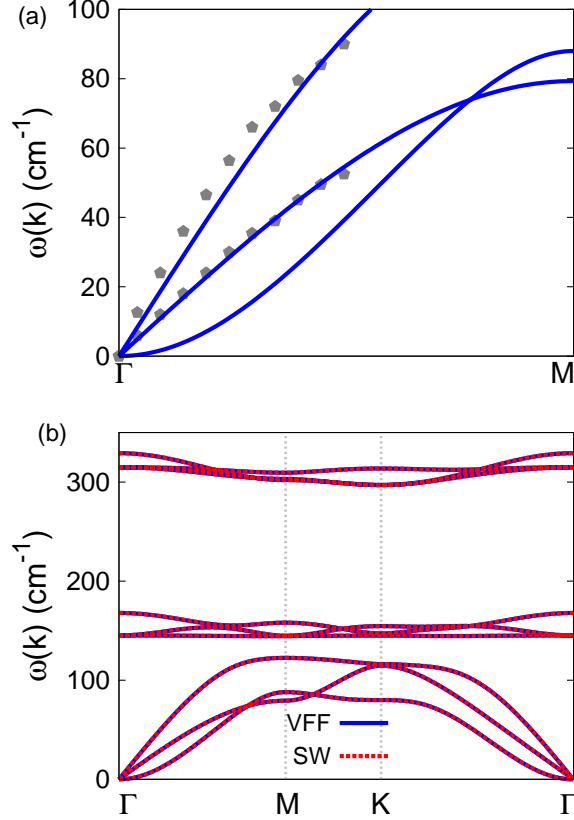


FIG. 7: (Color online) Phonon spectrum for single-layer 1H-ScSe₂. (a) Phonon dispersion along the Γ M direction in the Brillouin zone. The results from the VFF model (lines) are comparable with the *ab initio* results (pentagons) from Ref. 12. (b) The phonon dispersion from the SW potential is exactly the same as that from the VFF model.

Each Sc atom is surrounded by six Se atoms. These Se atoms are categorized into the top group (eg. atoms 1, 3, and 5) and bottom group (eg. atoms 2, 4, and 6). Each Se atom is connected to three Sc atoms. The structural parameters are from the first-principles calculations,¹² including the lattice constant $a = 3.84 \text{ \AA}$, and the bond length $d_{\text{Sc-Se}} = 2.65 \text{ \AA}$. The resultant angles are $\theta_{\text{ScSeSe}} = \theta_{\text{SeScSc}} = 92.859^\circ$ and $\theta_{\text{ScSeSe}'} = 66.432^\circ$, in which atoms Se and Se' are from different (top or bottom) group.

Table XVIII shows four VFF terms for the single-layer 1H-ScSe₂, one of which is the bond stretching interaction shown by Eq. (1) while the other three terms are the angle bending interaction shown by Eq. (2). These force constant parameters are determined by fitting to the acoustic branches in the phonon dispersion along the Γ M as shown in Fig. 7 (a). The *ab*

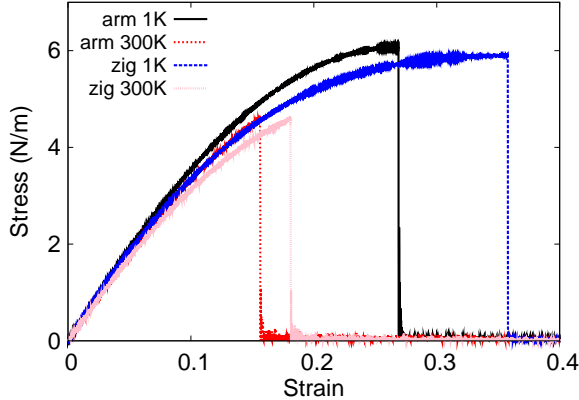


FIG. 8: (Color online) Stress-strain for single-layer 1H-ScSe₂ of dimension $100 \times 100 \text{ \AA}$ along the armchair and zigzag directions.

TABLE XX: Three-body SW potential parameters for single-layer 1H-ScSe₂ used by GULP⁸ as expressed in Eq. (4). The angle θ_{ijk} in the first line indicates the bending energy for the angle with atom i as the apex.

	K (eV)	θ_0 (degree)	ρ_1 (Å)	ρ_2 (Å)	$r_{\min 12}$ (Å)	$r_{\max 12}$ (Å)	$r_{\min 13}$ (Å)	$r_{\max 13}$ (Å)	$r_{\min 23}$ (Å)	$r_{\max 23}$ (Å)
$\theta_{\text{Sc-Se-Se}}$	21.292	92.859	1.533	1.533	0.0	3.658	0.0	3.658	0.0	4.327
$\theta_{\text{Sc-Se-Se}'}$	25.280	66.432	1.533	1.533	0.0	3.658	0.0	3.658	0.0	4.327
$\theta_{\text{Se-Sc-Sc}}$	21.292	92.859	1.533	1.533	0.0	3.658	0.0	3.658	0.0	4.327

initio calculations for the phonon dispersion are from Ref. 12. Fig. 7 (b) shows that the VFF model and the SW potential give exactly the same phonon dispersion, as the SW potential is derived from the VFF model.

The parameters for the two-body SW potential used by GULP are shown in Tab. XIX. The parameters for the three-body SW potential used by GULP are shown in Tab. XX. Some representative parameters for the SW potential used by LAMMPS are listed in Tab. XXI. We note that twelve atom types have been introduced for the simulation of the single-layer 1H-ScSe₂ using LAMMPS, because the angles around atom Sc in Fig. 1 (with M=Sc and X=Se) are not distinguishable in LAMMPS. We have suggested two options to differentiate these angles by implementing some additional constraints in LAMMPS, which can be accomplished by modifying the source file of LAMMPS.^{13,14} According to our experience, it is not so convenient for some users to implement these constraints and recompile the

TABLE XXI: SW potential parameters for single-layer 1H-ScSe₂ used by LAMMPS⁹ as expressed in Eqs. (9) and (10).

	ϵ (eV)	σ (Å)	a	λ	γ	$\cos \theta_0$	A_L	B_L	p	q	tol
Sc ₁ -Se ₁ -Se ₁	1.000	1.533	2.386	0.000	1.000	0.000	5.853	4.464	4	0	0.0
Sc ₁ -Se ₁ -Se ₃	1.000	0.000	0.000	21.292	1.000	-0.050	0.000	0.000	4	0	0.0
Sc ₁ -Se ₁ -Se ₂	1.000	0.000	0.000	25.280	1.000	0.400	0.000	0.000	4	0	0.0
Se ₁ -Sc ₁ -Sc ₃	1.000	0.000	0.000	21.292	1.000	-0.050	0.000	0.000	4	0	0.0

LAMMPS package. Hence, in the present work, we differentiate the angles by introducing more atom types, so it is not necessary to modify the LAMMPS package. Fig. 2 (with M=Sc and X=Se) shows that, for 1H-ScSe₂, we can differentiate these angles around the Sc atom by assigning these six neighboring Se atoms with different atom types. It can be found that twelve atom types are necessary for the purpose of differentiating all six neighbors around one Sc atom.

We use LAMMPS to perform MD simulations for the mechanical behavior of the single-layer 1H-ScSe₂ under uniaxial tension at 1.0 K and 300.0 K. Fig. 8 shows the stress-strain curve for the tension of a single-layer 1H-ScSe₂ of dimension 100 × 100 Å. Periodic boundary conditions are applied in both armchair and zigzag directions. The single-layer 1H-ScSe₂ is stretched uniaxially along the armchair or zigzag direction. The stress is calculated without involving the actual thickness of the quasi-two-dimensional structure of the single-layer 1H-ScSe₂. The Young's modulus can be obtained by a linear fitting of the stress-strain relation in the small strain range of [0, 0.01]. The Young's modulus are 39.4 N/m and 39.9 N/m along the armchair and zigzag directions, respectively. The Young's modulus is essentially isotropic in the armchair and zigzag directions. The Poisson's ratio from the VFF model and the SW potential is $\nu_{xy} = \nu_{yx} = 0.32$.

There is no available value for nonlinear quantities in the single-layer 1H-ScSe₂. We have thus used the nonlinear parameter $B = 0.5d^4$ in Eq. (5), which is close to the value of B in most materials. The value of the third order nonlinear elasticity D can be extracted by fitting the stress-strain relation to the function $\sigma = E\epsilon + \frac{1}{2}D\epsilon^2$ with E as the Young's modulus. The values of D from the present SW potential are -115.7 N/m and -135.7 N/m along the armchair and zigzag directions, respectively. The ultimate stress is about 6.1 Nm⁻¹

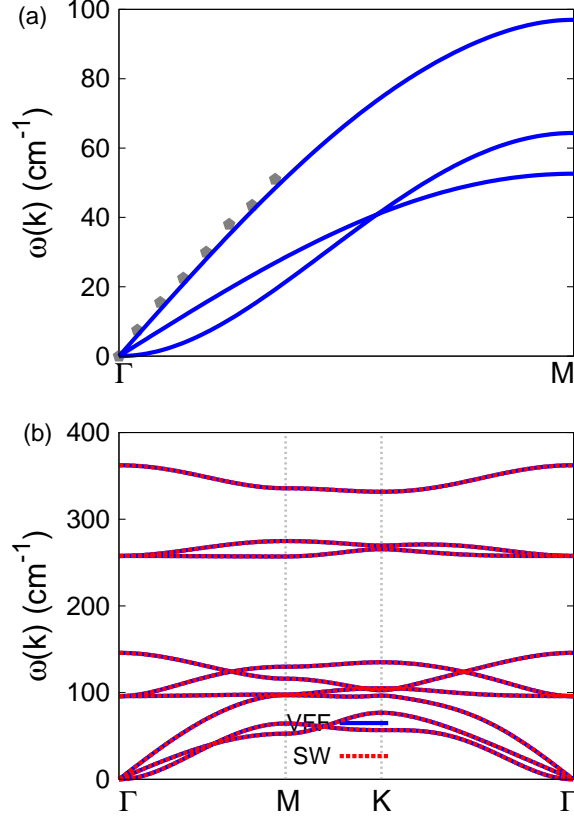


FIG. 9: (Color online) Phonon spectrum for single-layer 1H-ScTe₂. (a) Phonon dispersion along the Γ M direction in the Brillouin zone. The results from the VFF model (lines) are comparable with the *ab initio* results (pentagons) from Ref. 12. (b) The phonon dispersion from the SW potential is exactly the same as that from the VFF model.

at the ultimate strain of 0.27 in the armchair direction at the low temperature of 1 K. The ultimate stress is about 5.9 Nm^{-1} at the ultimate strain of 0.35 in the zigzag direction at the low temperature of 1 K.

VI. 1H-SCTE₂

Most existing theoretical studies on the single-layer 1H-ScTe₂ are based on the first-principles calculations. In this section, we will develop the SW potential for the single-layer 1H-ScTe₂.

The structure for the single-layer 1H-ScTe₂ is shown in Fig. 1 (with M=Sc and X=Te).

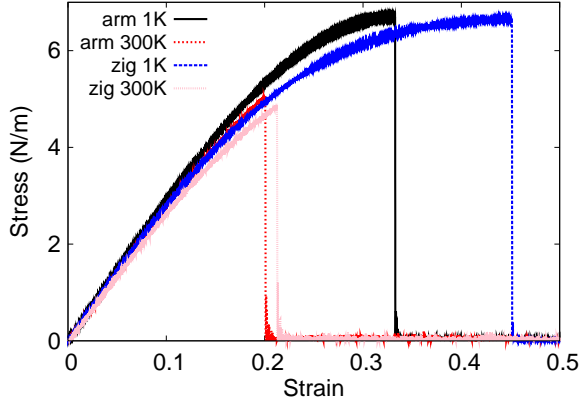


FIG. 10: (Color online) Stress-strain for single-layer 1H-ScTe₂ of dimension $100 \times 100 \text{ \AA}$ along the armchair and zigzag directions.

TABLE XXII: The VFF model for single-layer 1H-ScTe₂. The second line gives an explicit expression for each VFF term. The third line is the force constant parameters. Parameters are in the unit of $\frac{eV}{\text{\AA}^2}$ for the bond stretching interactions, and in the unit of eV for the angle bending interaction. The fourth line gives the initial bond length (in unit of \AA) for the bond stretching interaction and the initial angle (in unit of degrees) for the angle bending interaction. The angle θ_{ijk} has atom i as the apex.

VFF type	bond stretching	angle bending		
expression	$\frac{1}{2}K_{\text{Sc-Te}}(\Delta r)^2$	$\frac{1}{2}K_{\text{Sc-Te-Te}}(\Delta\theta)^2$	$\frac{1}{2}K_{\text{Sc-Te-Te}'}(\Delta\theta)^2$	$\frac{1}{2}K_{\text{Te-Sc-Sc}}(\Delta\theta)^2$
parameter	5.192	2.027	2.027	2.027
r_0 or θ_0	2.890	77.555	87.364	87.364

Each Sc atom is surrounded by six Te atoms. These Te atoms are categorized into the top group (eg. atoms 1, 3, and 5) and bottom group (eg. atoms 2, 4, and 6). Each Te atom is connected to three Sc atoms. The structural parameters are from the first-principles calculations,¹² including the lattice constant $a = 3.62 \text{ \AA}$, and the bond length $d_{\text{Sc-Te}} = 2.89 \text{ \AA}$. The resultant angles are $\theta_{\text{ScTeTe}} = \theta_{\text{TeScSc}} = 77.555^\circ$ and $\theta_{\text{ScTeTe}'} = 87.364^\circ$, in which atoms Te and Te' are from different (top or bottom) group.

Table XXII shows four VFF terms for the single-layer 1H-ScTe₂, one of which is the bond stretching interaction shown by Eq. (1) while the other three terms are the angle bending

TABLE XXIII: Two-body SW potential parameters for single-layer 1H-ScTe₂ used by GULP⁸ as expressed in Eq. (3).

	A (eV)	ρ (Å)	B (Å ⁴)	r_{\min} (Å)	r_{\max} (Å)
Sc-Te	4.630	1.050	34.879	0.0	3.761

TABLE XXIV: Three-body SW potential parameters for single-layer 1H-ScTe₂ used by GULP⁸ as expressed in Eq. (4). The angle θ_{ijk} in the first line indicates the bending energy for the angle with atom i as the apex.

	K (eV)	θ_0 (degree)	ρ_1 (Å)	ρ_2 (Å)	$r_{\min12}$ (Å)	$r_{\max12}$ (Å)	$r_{\min13}$ (Å)	$r_{\max13}$ (Å)	$r_{\min23}$ (Å)	$r_{\max23}$ (Å)
$\theta_{\text{Sc-Te-Te}}$	11.848	77.555	1.050	1.050	0.0	3.761	0.0	3.761	0.0	4.504
$\theta_{\text{Sc-Te-Te}'}$	11.322	87.364	1.050	1.050	0.0	3.761	0.0	3.761	0.0	4.504
$\theta_{\text{Te-Sc-Sc}}$	11.848	77.555	1.050	1.050	0.0	3.761	0.0	3.761	0.0	4.504

interaction shown by Eq. (2). These force constant parameters are determined by fitting to the acoustic branches in the phonon dispersion along the ΓM as shown in Fig. 9 (a). The *ab initio* calculations for the phonon dispersion are from Ref. 12. There is only one (longitudinal) acoustic branch available. We find that the VFF parameters can be chosen to be the same as that of the 1H-ScSe₂, from which the longitudinal acoustic branch agrees with the *ab initio* results as shown in Fig. 9 (a). It has also been shown that the VFF parameters can be the same for TaSe₂ and NbSe₂ of similar structure.¹⁵ Fig. 9 (b) shows that the VFF model and the SW potential give exactly the same phonon dispersion, as the SW potential is derived from the VFF model.

TABLE XXV: SW potential parameters for single-layer 1H-ScTe₂ used by LAMMPS⁹ as expressed in Eqs. (9) and (10).

	ϵ (eV)	σ (Å)	a	λ	γ	$\cos\theta_0$	A_L	B_L	p	q	tol
Sc ₁ -Te ₁ -Te ₁	1.000	1.050	3.581	0.000	1.000	0.000	4.630	28.679	4	0	0.0
Sc ₁ -Te ₁ -Te ₃	1.000	0.000	0.000	11.848	1.000	0.216	0.000	0.000	4	0	0.0
Sc ₁ -Te ₁ -Te ₂	1.000	0.000	0.000	11.322	1.000	0.046	0.000	0.000	4	0	0.0
Te ₁ -Sc ₁ -Sc ₃	1.000	0.000	0.000	11.848	1.000	0.216	0.000	0.000	4	0	0.0

The parameters for the two-body SW potential used by GULP are shown in Tab. XXIII. The parameters for the three-body SW potential used by GULP are shown in Tab. XXIV. Some representative parameters for the SW potential used by LAMMPS are listed in Tab. XXV. We note that twelve atom types have been introduced for the simulation of the single-layer 1H-ScTe₂ using LAMMPS, because the angles around atom Sc in Fig. 1 (with M=Sc and X=Te) are not distinguishable in LAMMPS. We have suggested two options to differentiate these angles by implementing some additional constraints in LAMMPS, which can be accomplished by modifying the source file of LAMMPS.^{13,14} According to our experience, it is not so convenient for some users to implement these constraints and re-compile the LAMMPS package. Hence, in the present work, we differentiate the angles by introducing more atom types, so it is not necessary to modify the LAMMPS package. Fig. 2 (with M=Sc and X=Te) shows that, for 1H-ScTe₂, we can differentiate these angles around the Sc atom by assigning these six neighboring Te atoms with different atom types. It can be found that twelve atom types are necessary for the purpose of differentiating all six neighbors around one Sc atom.

We use LAMMPS to perform MD simulations for the mechanical behavior of the single-layer 1H-ScTe₂ under uniaxial tension at 1.0 K and 300.0 K. Fig. 10 shows the stress-strain curve for the tension of a single-layer 1H-ScTe₂ of dimension 100 × 100 Å. Periodic boundary conditions are applied in both armchair and zigzag directions. The single-layer 1H-ScTe₂ is stretched uniaxially along the armchair or zigzag direction. The stress is calculated without involving the actual thickness of the quasi-two-dimensional structure of the single-layer 1H-ScTe₂. The Young's modulus can be obtained by a linear fitting of the stress-strain relation in the small strain range of [0, 0.01]. The Young's modulus are 29.3 N/m and 28.8 N/m along the armchair and zigzag directions, respectively. The Young's modulus is essentially isotropic in the armchair and zigzag directions. The Poisson's ratio from the VFF model and the SW potential is $\nu_{xy} = \nu_{yx} = 0.38$.

There is no available value for nonlinear quantities in the single-layer 1H-ScTe₂. We have thus used the nonlinear parameter $B = 0.5d^4$ in Eq. (5), which is close to the value of B in most materials. The value of the third order nonlinear elasticity D can be extracted by fitting the stress-strain relation to the function $\sigma = E\epsilon + \frac{1}{2}D\epsilon^2$ with E as the Young's modulus. The values of D from the present SW potential are -43.2 N/m and -59.3 N/m along the armchair and zigzag directions, respectively. The ultimate stress is about 6.7 Nm⁻¹ at

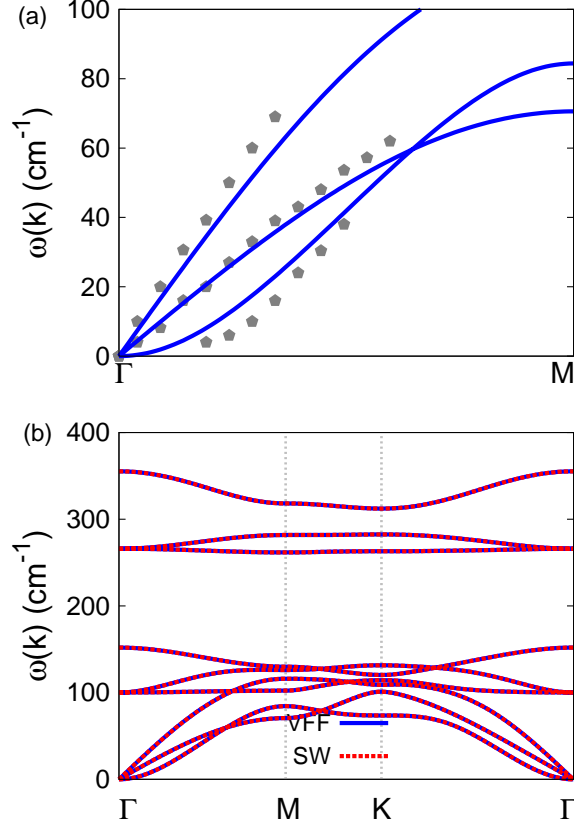


FIG. 11: (Color online) Phonon dispersion for single-layer 1H-TiTe₂. (a) The VFF model is fitted to the three acoustic branches in the long wave limit along the Γ M direction. The *ab initio* results (gray pentagons) are from Ref. 12. (b) The VFF model (blue lines) and the SW potential (red lines) give the same phonon dispersion for single-layer 1H-TiTe₂ along Γ MK Γ .

the ultimate strain of 0.33 in the armchair direction at the low temperature of 1 K. The ultimate stress is about 6.7 Nm^{-1} at the ultimate strain of 0.45 in the zigzag direction at the low temperature of 1 K.

VII. 1H-TITE₂

Most existing theoretical studies on the single-layer 1H-TiTe₂ are based on the first-principles calculations. In this section, we will develop both VFF model and the SW potential for the single-layer 1H-TiTe₂.

The structure for the single-layer 1H-TiTe₂ is shown in Fig. 1 (with M=Ti and X=Se).

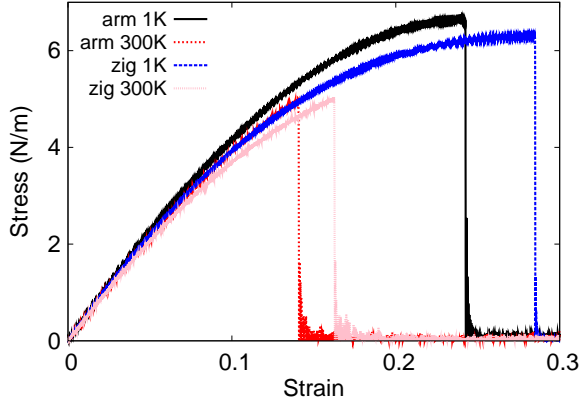


FIG. 12: (Color online) Stress-strain for single-layer 1H-TiTe₂ of dimension $100 \times 100 \text{ \AA}$ along the armchair and zigzag directions.

TABLE XXVI: The VFF model for single-layer 1H-TiTe₂. The second line gives an explicit expression for each VFF term. The third line is the force constant parameters. Parameters are in the unit of $\frac{eV}{\text{Å}^2}$ for the bond stretching interactions, and in the unit of eV for the angle bending interaction. The fourth line gives the initial bond length (in unit of Å) for the bond stretching interaction and the initial angle (in unit of degrees) for the angle bending interaction. The angle θ_{ijk} has atom *i* as the apex.

VFF type	bond stretching	angle bending		
expression	$\frac{1}{2}K_{\text{Ti-Te}}(\Delta r)^2$	$\frac{1}{2}K_{\text{Ti-Te-Te}}(\Delta\theta)^2$	$\frac{1}{2}K_{\text{Ti-Te-Te}'}(\Delta\theta)^2$	$\frac{1}{2}K_{\text{Te-Ti-Ti}}(\Delta\theta)^2$
parameter	4.782	3.216	3.216	3.216
r_0 or θ_0	2.750	82.323	81.071	82.323

Each Ti atom is surrounded by six Te atoms. These Te atoms are categorized into the top group (eg. atoms 1, 3, and 5) and bottom group (eg. atoms 2, 4, and 6). Each Te atom is connected to three Ti atoms. The structural parameters are from Ref. 12, including the lattice constant $a = 3.62 \text{ \AA}$, and the bond length $d_{\text{Ti-Te}} = 2.75 \text{ \AA}$. The resultant angles are $\theta_{\text{TiTeTe}} = \theta_{\text{TeTiTi}} = 82.323^\circ$ and $\theta_{\text{TiTeTe}'} = 81.071^\circ$, in which atoms Te and Te' are from different (top or bottom) group.

Table XXVI shows the VFF terms for the 1H-TiTe₂, one of which is the bond stretching interaction shown by Eq. (1) while the other terms are the angle bending interaction shown

TABLE XXVII: Two-body SW potential parameters for single-layer 1H-TiTe₂ used by GULP⁸ as expressed in Eq. (3).

	A (eV)	ρ (Å)	B (Å ⁴)	r_{\min} (Å)	r_{\max} (Å)
Ti-Te	4.414	1.173	28.596	0.0	3.648

TABLE XXVIII: Three-body SW potential parameters for single-layer 1H-TiTe₂ used by GULP⁸ as expressed in Eq. (4). The angle θ_{ijk} in the first line indicates the bending energy for the angle with atom i as the apex.

	K (eV)	θ_0 (degree)	ρ_1 (Å)	ρ_2 (Å)	$r_{\min12}$ (Å)	$r_{\max12}$ (Å)	$r_{\min13}$ (Å)	$r_{\max13}$ (Å)	$r_{\min23}$ (Å)	$r_{\max23}$ (Å)
$\theta_{\text{Ti-Te-Te}}$	22.321	82.323	1.173	1.173	0.0	3.648	0.0	3.648	0.0	4.354
$\theta_{\text{Ti-Te-Te}'}$	22.463	81.071	1.173	1.173	0.0	3.648	0.0	3.648	0.0	4.354
$\theta_{\text{Te-Ti-Ti}}$	11.321	82.323	1.173	1.173	0.0	3.648	0.0	3.648	0.0	4.354

by Eq. (2). These force constant parameters are determined by fitting to the three acoustic branches in the phonon dispersion along the ΓM as shown in Fig. 11 (a). The *ab initio* calculations for the phonon dispersion are from Ref. 12. Fig. 11 (b) shows that the VFF model and the SW potential give exactly the same phonon dispersion, as the SW potential is derived from the VFF model.

The parameters for the two-body SW potential used by GULP are shown in Tab. XXVII. The parameters for the three-body SW potential used by GULP are shown in Tab. XXVIII. Parameters for the SW potential used by LAMMPS are listed in Tab. XXIX. We note that twelve atom types have been introduced for the simulation of the single-layer 1H-TiTe₂ using

TABLE XXIX: SW potential parameters for single-layer 1H-TiTe₂ used by LAMMPS⁹ as expressed in Eqs. (9) and (10). Atom types in the first column are displayed in Fig. 2 (with M=Ti and X=Te).

	ϵ (eV)	σ (Å)	a	λ	γ	$\cos\theta_0$	A_L	B_L	p	q	tol
Ti ₁ -Te ₁ -Te ₁	1.000	1.173	3.110	0.000	1.000	0.000	4.414	15.100	4	0	0.0
Ti ₁ -Te ₁ -Te ₃	1.000	0.000	0.000	22.321	1.000	0.134	0.000	0.000	4	0	0.0
Ti ₁ -Te ₁ -Te ₂	1.000	0.000	0.000	22.463	1.000	0.155	0.000	0.000	4	0	0.0
Te ₁ -Ti ₁ -Ti ₃	1.000	0.000	0.000	22.321	1.000	0.134	0.000	0.000	4	0	0.0

LAMMPS, because the angles around atom Ti in Fig. 1 (with M=Ti and X=Te) are not distinguishable in LAMMPS. We have suggested two options to differentiate these angles by implementing some additional constraints in LAMMPS, which can be accomplished by modifying the source file of LAMMPS.^{13,14} According to our experience, it is not so convenient for some users to implement these constraints and recompile the LAMMPS package. Hence, in the present work, we differentiate the angles by introducing more atom types, so it is not necessary to modify the LAMMPS package. Fig. 2 (with M=Ti and X=Te) shows that, for 1H-TiTe₂, we can differentiate these angles around the Ti atom by assigning these six neighboring Te atoms with different atom types. It can be found that twelve atom types are necessary for the purpose of differentiating all six neighbors around one Ti atom.

We use LAMMPS to perform MD simulations for the mechanical behavior of the single-layer 1H-TiTe₂ under uniaxial tension at 1.0 K and 300.0 K. Fig. 12 shows the stress-strain curve for the tension of a single-layer 1H-TiTe₂ of dimension 100 × 100 Å. Periodic boundary conditions are applied in both armchair and zigzag directions. The single-layer 1H-TiTe₂ is stretched uniaxially along the armchair or zigzag direction. The stress is calculated without involving the actual thickness of the quasi-two-dimensional structure of the single-layer 1H-TiTe₂. The Young's modulus can be obtained by a linear fitting of the stress-strain relation in the small strain range of [0, 0.01]. The Young's modulus are 47.9 N/m and 47.1 N/m along the armchair and zigzag directions, respectively. The Young's modulus is essentially isotropic in the armchair and zigzag directions. The Poisson's ratio from the VFF model and the SW potential is $\nu_{xy} = \nu_{yx} = 0.29$.

There is no available value for the nonlinear quantities in the single-layer 1H-TiTe₂. We have thus used the nonlinear parameter $B = 0.5d^4$ in Eq. (5), which is close to the value of B in most materials. The value of the third order nonlinear elasticity D can be extracted by fitting the stress-strain relation to the function $\sigma = E\epsilon + \frac{1}{2}D\epsilon^2$ with E as the Young's modulus. The values of D from the present SW potential are -158.6 N/m and -176.3 N/m along the armchair and zigzag directions, respectively. The ultimate stress is about 6.6 Nm⁻¹ at the ultimate strain of 0.24 in the armchair direction at the low temperature of 1 K. The ultimate stress is about 6.3 Nm⁻¹ at the ultimate strain of 0.28 in the zigzag direction at the low temperature of 1 K.

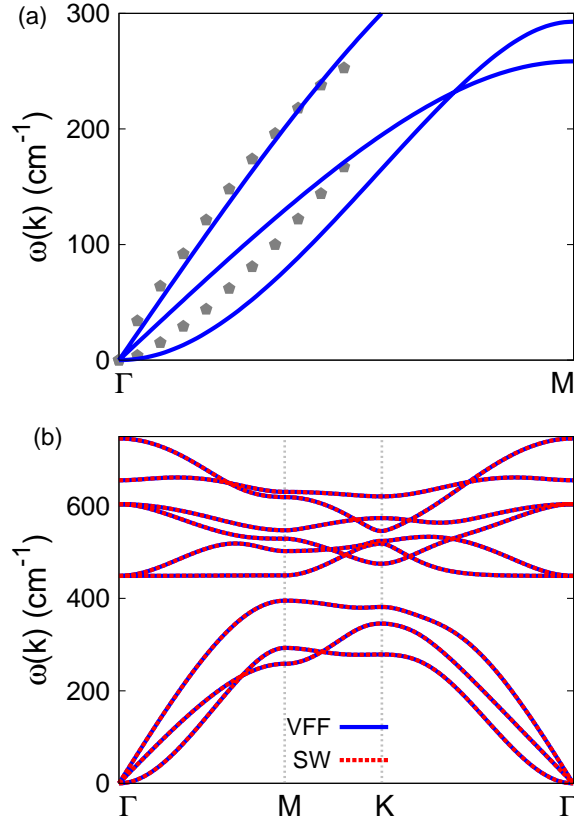


FIG. 13: (Color online) Phonon spectrum for single-layer 1H-VO₂. (a) Phonon dispersion along the Γ M direction in the Brillouin zone. The results from the VFF model (lines) are comparable with the *ab initio* results (pentagons) from Ref. 12. (b) The phonon dispersion from the SW potential is exactly the same as that from the VFF model.

VIII. 1H-VO₂

Most existing theoretical studies on the single-layer 1H-VO₂ are based on the first-principles calculations. In this section, we will develop the SW potential for the single-layer 1H-VO₂.

The structure for the single-layer 1H-VO₂ is shown in Fig. 1 (with M=V and X=O). Each V atom is surrounded by six O atoms. These O atoms are categorized into the top group (eg. atoms 1, 3, and 5) and bottom group (eg. atoms 2, 4, and 6). Each O atom is connected to three V atoms. The structural parameters are from the first-principles calculations,¹² including the lattice constant $a = 2.70$ Å, and the bond length $d_{V-O} = 1.92$ Å. The resultant

TABLE XXX: The VFF model for single-layer 1H-VO₂. The second line gives an explicit expression for each VFF term. The third line is the force constant parameters. Parameters are in the unit of $\frac{\text{eV}}{\text{\AA}^2}$ for the bond stretching interactions, and in the unit of eV for the angle bending interaction. The fourth line gives the initial bond length (in unit of \AA) for the bond stretching interaction and the initial angle (in unit of degrees) for the angle bending interaction. The angle θ_{ijk} has atom i as the apex.

VFF type	bond stretching	angle bending		
expression	$\frac{1}{2}K_{\text{V-O}}(\Delta r)^2$	$\frac{1}{2}K_{\text{V-O-O}}(\Delta\theta)^2$	$\frac{1}{2}K_{\text{V-O-O'}}(\Delta\theta)^2$	$\frac{1}{2}K_{\text{O-V-V}}(\Delta\theta)^2$
parameter	9.417	4.825	4.825	4.825
r_0 or θ_0	1.920	89.356	71.436	89.356

TABLE XXXI: Two-body SW potential parameters for single-layer 1H-VO₂ used by GULP⁸ as expressed in Eq. (3).

	A (eV)	ρ (\AA)	B (\AA ⁴)	r_{min} (\AA)	r_{max} (\AA)
V-O	5.105	1.011	6.795	0.0	2.617

TABLE XXXII: Three-body SW potential parameters for single-layer 1H-VO₂ used by GULP⁸ as expressed in Eq. (4). The angle θ_{ijk} in the first line indicates the bending energy for the angle with atom i as the apex.

	K (eV)	θ_0 (degree)	ρ_1 (\AA)	ρ_2 (\AA)	$r_{\text{min}12}$ (\AA)	$r_{\text{max}12}$ (\AA)	$r_{\text{min}13}$ (\AA)	$r_{\text{max}13}$ (\AA)	$r_{\text{min}23}$ (\AA)	$r_{\text{max}23}$ (\AA)
$\theta_{\text{V-O-O}}$	43.951	89.356	1.011	1.011	0.0	2.617	0.0	2.617	0.0	3.105
$\theta_{\text{V-O-O}'}$	48.902	71.436	1.011	1.011	0.0	2.617	0.0	2.617	0.0	3.105
$\theta_{\text{O-V-V}}$	43.951	89.356	1.011	1.011	0.0	2.617	0.0	2.617	0.0	3.105

TABLE XXXIII: SW potential parameters for single-layer 1H-VO₂ used by LAMMPS⁹ as expressed in Eqs. (9) and (10).

	ϵ (eV)	σ (\AA)	a	λ	γ	$\cos\theta_0$	A_L	B_L	p	q	tol
V ₁ -O ₁ -O ₁	1.000	1.011	2.589	0.000	1.000	0.000	5.105	6.509	4	0	0.0
V ₁ -O ₁ -O ₃	1.000	0.000	0.000	43.951	1.000	0.011	0.000	0.000	4	0	0.0
V ₁ -O ₁ -O ₂	1.000	0.000	0.000	48.902	1.000	0.318	0.000	0.000	4	0	0.0
O ₁ -V ₁ -V ₃	1.000	0.000	0.000	43.951	1.000	0.011	0.000	0.000	4	0	0.0

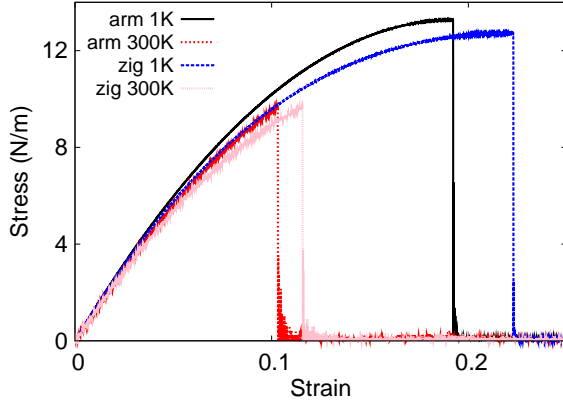


FIG. 14: (Color online) Stress-strain for single-layer 1H-VO₂ of dimension 100 × 100 Å along the armchair and zigzag directions.

angles are $\theta_{VOO} = \theta_{OVV} = 89.356^\circ$ and $\theta_{VOO'} = 71.436^\circ$, in which atoms O and O' are from different (top or bottom) group.

Table XXX shows four VFF terms for the single-layer 1H-VO₂, one of which is the bond stretching interaction shown by Eq. (1) while the other three terms are the angle bending interaction shown by Eq. (2). These force constant parameters are determined by fitting to the acoustic branches in the phonon dispersion along the ΓM as shown in Fig. 13 (a). The *ab initio* calculations for the phonon dispersion are from Ref. 12. Fig. 13 (b) shows that the VFF model and the SW potential give exactly the same phonon dispersion, as the SW potential is derived from the VFF model.

The parameters for the two-body SW potential used by GULP are shown in Tab. XXXI. The parameters for the three-body SW potential used by GULP are shown in Tab. XXXII. Some representative parameters for the SW potential used by LAMMPS are listed in Tab. XXXIII. We note that twelve atom types have been introduced for the simulation of the single-layer 1H-VO₂ using LAMMPS, because the angles around atom V in Fig. 1 (with M=V and X=O) are not distinguishable in LAMMPS. We have suggested two options to differentiate these angles by implementing some additional constraints in LAMMPS, which can be accomplished by modifying the source file of LAMMPS.^{13,14} According to our experience, it is not so convenient for some users to implement these constraints and recompile the LAMMPS package. Hence, in the present work, we differentiate the angles by introducing more atom types, so it is not necessary to modify the LAMMPS package. Fig. 2 (with M=V

and X=O) shows that, for 1H-VO₂, we can differentiate these angles around the V atom by assigning these six neighboring O atoms with different atom types. It can be found that twelve atom types are necessary for the purpose of differentiating all six neighbors around one V atom.

We use LAMMPS to perform MD simulations for the mechanical behavior of the single-layer 1H-VO₂ under uniaxial tension at 1.0 K and 300.0 K. Fig. 14 shows the stress-strain curve for the tension of a single-layer 1H-VO₂ of dimension 100 × 100 Å. Periodic boundary conditions are applied in both armchair and zigzag directions. The single-layer 1H-VO₂ is stretched uniaxially along the armchair or zigzag direction. The stress is calculated without involving the actual thickness of the quasi-two-dimensional structure of the single-layer 1H-VO₂. The Young's modulus can be obtained by a linear fitting of the stress-strain relation in the small strain range of [0, 0.01]. The Young's modulus are 133.0 N/m and 132.9 N/m along the armchair and zigzag directions, respectively. The Young's modulus is essentially isotropic in the armchair and zigzag directions. The Poisson's ratio from the VFF model and the SW potential is $\nu_{xy} = \nu_{yx} = 0.17$.

There is no available value for nonlinear quantities in the single-layer 1H-VO₂. We have thus used the nonlinear parameter $B = 0.5d^4$ in Eq. (5), which is close to the value of B in most materials. The value of the third order nonlinear elasticity D can be extracted by fitting the stress-strain relation to the function $\sigma = E\epsilon + \frac{1}{2}D\epsilon^2$ with E as the Young's modulus. The values of D from the present SW potential are -652.3 N/m and -705.8 N/m along the armchair and zigzag directions, respectively. The ultimate stress is about 13.3 Nm⁻¹ at the ultimate strain of 0.19 in the armchair direction at the low temperature of 1 K. The ultimate stress is about 12.7 Nm⁻¹ at the ultimate strain of 0.22 in the zigzag direction at the low temperature of 1 K.

IX. 1H-VS₂

Most existing theoretical studies on the single-layer 1H-VS₂ are based on the first-principles calculations. In this section, we will develop both VFF model and the SW potential for the single-layer 1H-VS₂.

The structure for the single-layer 1H-VS₂ is shown in Fig. 1 (with M=V and X=S). Each V atom is surrounded by six S atoms. These S atoms are categorized into the top

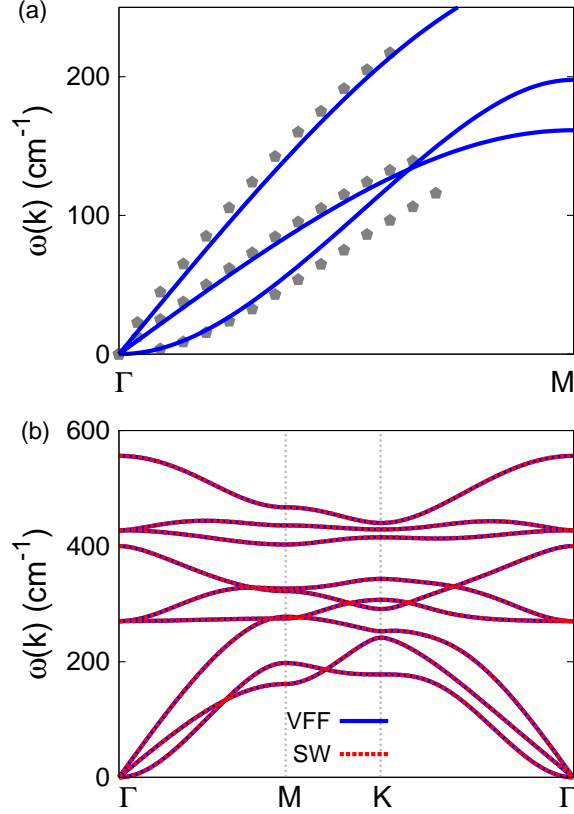


FIG. 15: (Color online) Phonon dispersion for single-layer 1H-VS₂. (a) The VFF model is fitted to the three acoustic branches in the long wave limit along the ΓM direction. The *ab initio* results (gray pentagons) are from Ref. 16. (b) The VFF model (blue lines) and the SW potential (red lines) give the same phonon dispersion for single-layer 1H-VS₂ along $\Gamma\text{MK}\Gamma$.

group (eg. atoms 1, 3, and 5) and bottom group (eg. atoms 2, 4, and 6). Each S atom is connected to three V atoms. The structural parameters are from Ref. 12, including the lattice constant $a = 3.09 \text{ \AA}$, and the bond length $d_{\text{V-S}} = 2.31 \text{ \AA}$. The resultant angles are $\theta_{\text{VSS}} = \theta_{\text{SVV}} = 83.954^\circ$ and $\theta_{\text{VSS}'} = 78.878^\circ$, in which atoms S and S' are from different (top or bottom) group.

Table XXXIV shows the VFF terms for the 1H-VS₂, one of which is the bond stretching interaction shown by Eq. (1) while the other terms are the angle bending interaction shown by Eq. (2). These force constant parameters are determined by fitting to the three acoustic branches in the phonon dispersion along the ΓM as shown in Fig. 15 (a). The *ab initio* calculations for the phonon dispersion are from Ref. 16. The phonon dispersion can also be

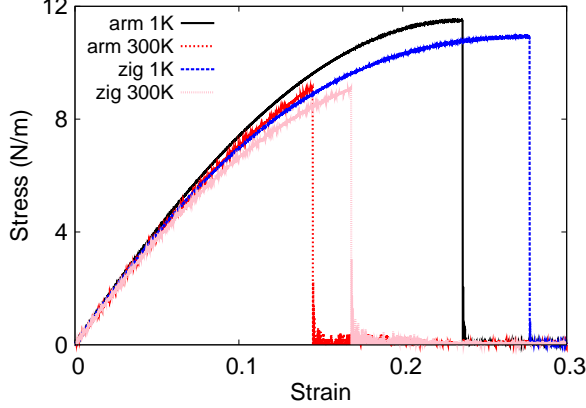


FIG. 16: (Color online) Stress-strain for single-layer 1H-VS₂ of dimension 100 × 100 Å along the armchair and zigzag directions.

TABLE XXXIV: The VFF model for single-layer 1H-VS₂. The second line gives an explicit expression for each VFF term. The third line is the force constant parameters. Parameters are in the unit of $\frac{eV}{\text{Å}^2}$ for the bond stretching interactions, and in the unit of eV for the angle bending interaction. The fourth line gives the initial bond length (in unit of Å) for the bond stretching interaction and the initial angle (in unit of degrees) for the angle bending interaction. The angle θ_{ijk} has atom *i* as the apex.

VFF type	bond stretching	angle bending		
expression	$\frac{1}{2}K_{V-S}(\Delta r)^2$	$\frac{1}{2}K_{V-S-S}(\Delta\theta)^2$	$\frac{1}{2}K_{V-S-S'}(\Delta\theta)^2$	$\frac{1}{2}K_{S-V-V}(\Delta\theta)^2$
parameter	8.392	4.074	4.074	4.074
r_0 or θ_0	2.310	83.954	78.878	83.954

found in other *ab initio* calculations.¹² Fig. 15 (b) shows that the VFF model and the SW potential give exactly the same phonon dispersion, as the SW potential is derived from the VFF model.

The parameters for the two-body SW potential used by GULP are shown in Tab. XXXV. The parameters for the three-body SW potential used by GULP are shown in Tab. XXXVI. Parameters for the SW potential used by LAMMPS are listed in Tab. XXXVII. We note that twelve atom types have been introduced for the simulation of the single-layer 1H-VS₂ using LAMMPS, because the angles around atom V in Fig. 1 (with M=V and X=S) are not

TABLE XXXV: Two-body SW potential parameters for single-layer 1H-VS₂ used by GULP⁸ as expressed in Eq. (3).

	A (eV)	ρ (Å)	B (Å ⁴)	r_{\min} (Å)	r_{\max} (Å)
V-S	5.714	1.037	14.237	0.0	3.084

TABLE XXXVI: Three-body SW potential parameters for single-layer 1H-VS₂ used by GULP⁸ as expressed in Eq. (4). The angle θ_{ijk} in the first line indicates the bending energy for the angle with atom i as the apex.

	K (eV)	θ_0 (degree)	ρ_1 (Å)	ρ_2 (Å)	$r_{\min12}$ (Å)	$r_{\max12}$ (Å)	$r_{\min13}$ (Å)	$r_{\max13}$ (Å)	$r_{\min23}$ (Å)	$r_{\max23}$ (Å)
θ_{V-S-S}	30.059	83.954	1.037	1.037	0.0	3.084	0.0	3.084	0.0	3.676
$\theta_{V-S-S'}$	30.874	78.878	1.037	1.037	0.0	3.084	0.0	3.084	0.0	3.676
θ_{S-V-V}	30.059	83.954	1.037	1.037	0.0	3.084	0.0	3.084	0.0	3.676

distinguishable in LAMMPS. We have suggested two options to differentiate these angles by implementing some additional constraints in LAMMPS, which can be accomplished by modifying the source file of LAMMPS.^{13,14} According to our experience, it is not so convenient for some users to implement these constraints and recompile the LAMMPS package. Hence, in the present work, we differentiate the angles by introducing more atom types, so it is not necessary to modify the LAMMPS package. Fig. 2 (with M=V and X=S) shows that, for 1H-VS₂, we can differentiate these angles around the V atom by assigning these six neighboring S atoms with different atom types. It can be found that twelve atom types are necessary for the purpose of differentiating all six neighbors around one V atom.

TABLE XXXVII: SW potential parameters for single-layer 1H-VS₂ used by LAMMPS⁹ as expressed in Eqs. (9) and (10). Atom types in the first column are displayed in Fig. 2 (with M=V and X=S).

	ϵ (eV)	σ (Å)	a	λ	γ	$\cos\theta_0$	A_L	B_L	p	q	tol
V ₁ -S ₁ -S ₁	1.000	1.037	2.973	0.000	1.000	0.000	5.714	12.294	4	0	0.0
V ₁ -S ₁ -S ₃	1.000	0.000	0.000	30.059	1.000	0.105	0.000	0.000	4	0	0.0
V ₁ -S ₁ -S ₂	1.000	0.000	0.000	30.874	1.000	0.193	0.000	0.000	4	0	0.0
S ₁ -V ₁ -V ₃	1.000	0.000	0.000	30.059	1.000	0.105	0.000	0.000	4	0	0.0

We use LAMMPS to perform MD simulations for the mechanical behavior of the single-layer 1H-VS₂ under uniaxial tension at 1.0 K and 300.0 K. Fig. 16 shows the stress-strain curve for the tension of a single-layer 1H-VS₂ of dimension 100 × 100 Å. Periodic boundary conditions are applied in both armchair and zigzag directions. The single-layer 1H-VS₂ is stretched uniaxially along the armchair or zigzag direction. The stress is calculated without involving the actual thickness of the quasi-two-dimensional structure of the single-layer 1H-VS₂. The Young's modulus can be obtained by a linear fitting of the stress-strain relation in the small strain range of [0, 0.01]. The Young's modulus are 86.5 N/m and 85.3 N/m along the armchair and zigzag directions, respectively. The Young's modulus is essentially isotropic in the armchair and zigzag directions. The Poisson's ratio from the VFF model and the SW potential is $\nu_{xy} = \nu_{yx} = 0.28$.

There is no available value for the nonlinear quantities in the single-layer 1H-VS₂. We have thus used the nonlinear parameter $B = 0.5d^4$ in Eq. (5), which is close to the value of B in most materials. The value of the third order nonlinear elasticity D can be extracted by fitting the stress-strain relation to the function $\sigma = E\epsilon + \frac{1}{2}D\epsilon^2$ with E as the Young's modulus. The values of D from the present SW potential are -302.0 N/m and -334.7 N/m along the armchair and zigzag directions, respectively. The ultimate stress is about 11.5 Nm⁻¹ at the ultimate strain of 0.23 in the armchair direction at the low temperature of 1 K. The ultimate stress is about 10.9 Nm⁻¹ at the ultimate strain of 0.27 in the zigzag direction at the low temperature of 1 K.

X. 1H-VSe₂

Most existing theoretical studies on the single-layer 1H-VSe₂ are based on the first-principles calculations. In this section, we will develop both VFF model and the SW potential for the single-layer 1H-VSe₂.

The structure for the single-layer 1H-VSe₂ is shown in Fig. 1 (with M=V and X=Se). Each V atom is surrounded by six Se atoms. These Se atoms are categorized into the top group (eg. atoms 1, 3, and 5) and bottom group (eg. atoms 2, 4, and 6). Each Se atom is connected to three V atoms. The structural parameters are from Ref. 12, including the lattice constant $a = 3.24$ Å, and the bond length $d_{V-Se} = 2.45$ Å. The resultant angles are $\theta_{VSeSe} = \theta_{SeV} = 82.787^\circ$ and $\theta_{VSeSe'} = 80.450^\circ$, in which atoms Se and Se' are from different

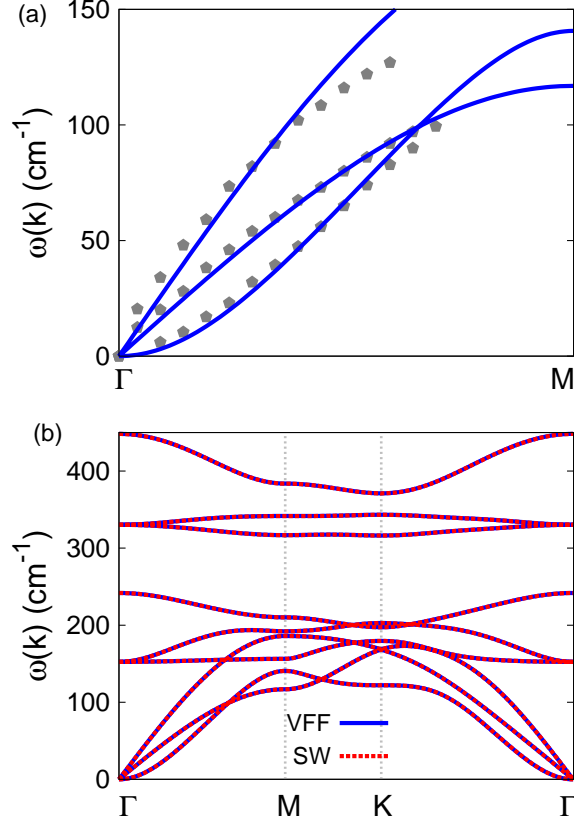


FIG. 17: (Color online) Phonon dispersion for single-layer 1H-VSe₂. (a) The VFF model is fitted to the three acoustic branches in the long wave limit along the Γ M direction. The *ab initio* results (gray pentagons) are from Ref. 12. (b) The VFF model (blue lines) and the SW potential (red lines) give the same phonon dispersion for single-layer 1H-VSe₂ along Γ MKT Γ .

(top or bottom) group.

Table XXXVIII shows the VFF terms for the 1H-VSe₂, one of which is the bond stretching interaction shown by Eq. (1) while the other terms are the angle bending interaction shown by Eq. (2). These force constant parameters are determined by fitting to the three acoustic branches in the phonon dispersion along the Γ M as shown in Fig. 17 (a). The *ab initio* calculations for the phonon dispersion are from Ref. 12. Fig. 17 (b) shows that the VFF model and the SW potential give exactly the same phonon dispersion, as the SW potential is derived from the VFF model.

The parameters for the two-body SW potential used by GULP are shown in Tab. XXXIX. The parameters for the three-body SW potential used by GULP are shown in Tab. XL. Pa-

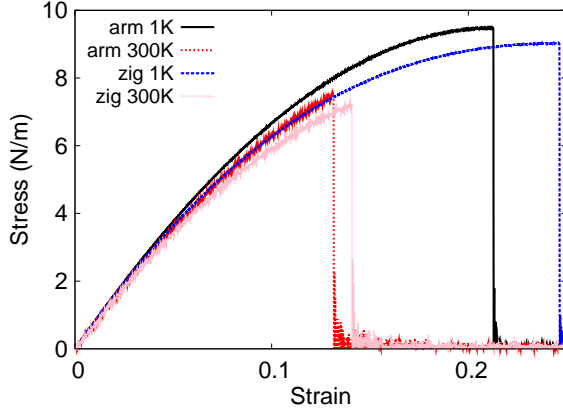


FIG. 18: (Color online) Stress-strain for single-layer 1H-VSe₂ of dimension 100 × 100 Å along the armchair and zigzag directions.

TABLE XXXVIII: The VFF model for single-layer 1H-VSe₂. The second line gives an explicit expression for each VFF term. The third line is the force constant parameters. Parameters are in the unit of $\frac{eV}{\text{Å}^2}$ for the bond stretching interactions, and in the unit of eV for the angle bending interaction. The fourth line gives the initial bond length (in unit of Å) for the bond stretching interaction and the initial angle (in unit of degrees) for the angle bending interaction. The angle θ_{ijk} has atom *i* as the apex.

VFF type	bond stretching	angle bending		
expression	$\frac{1}{2}K_{V-Se}(\Delta r)^2$	$\frac{1}{2}K_{V-Se-Se}(\Delta\theta)^2$	$\frac{1}{2}K_{V-Se-Se'}(\Delta\theta)^2$	$\frac{1}{2}K_{Se-V-V}(\Delta\theta)^2$
parameter	6.492	4.716	4.716	4.716
r_0 or θ_0	2.450	82.787	80.450	82.787

parameters for the SW potential used by LAMMPS are listed in Tab. XLI. We note that twelve atom types have been introduced for the simulation of the single-layer 1H-VSe₂ using LAMMPS, because the angles around atom V in Fig. 1 (with M=V and X=Se) are not distinguishable in LAMMPS. We have suggested two options to differentiate these angles by implementing some additional constraints in LAMMPS, which can be accomplished by modifying the source file of LAMMPS.^{13,14} According to our experience, it is not so convenient for some users to implement these constraints and recompile the LAMMPS package. Hence, in the present work, we differentiate the angles by introducing more atom types, so

TABLE XXXIX: Two-body SW potential parameters for single-layer 1H-VSe₂ used by GULP⁸ as expressed in Eq. (3).

	A (eV)	ρ (Å)	B (Å ⁴)	r_{\min} (Å)	r_{\max} (Å)
V-Se	4.817	1.061	18.015	0.0	3.256

TABLE XL: Three-body SW potential parameters for single-layer 1H-VSe₂ used by GULP⁸ as expressed in Eq. (4). The angle θ_{ijk} in the first line indicates the bending energy for the angle with atom i as the apex.

	K (eV)	θ_0 (degree)	ρ_1 (Å)	ρ_2 (Å)	$r_{\min12}$ (Å)	$r_{\max12}$ (Å)	$r_{\min13}$ (Å)	$r_{\max13}$ (Å)	$r_{\min23}$ (Å)	$r_{\max23}$ (Å)
$\theta_{V-Se-Se}$	33.299	82.787	1.061	1.061	0.0	3.256	0.0	3.256	0.0	3.884
$\theta_{V-Se-Se'}$	33.702	80.450	1.061	1.061	0.0	3.256	0.0	3.256	0.0	3.884
θ_{Se-V-V}	33.299	82.787	1.061	1.061	0.0	3.256	0.0	3.256	0.0	3.884

it is not necessary to modify the LAMMPS package. Fig. 2 (with M=V and X=Se) shows that, for 1H-VSe₂, we can differentiate these angles around the V atom by assigning these six neighboring Se atoms with different atom types. It can be found that twelve atom types are necessary for the purpose of differentiating all six neighbors around one V atom.

We use LAMMPS to perform MD simulations for the mechanical behavior of the single-layer 1H-VSe₂ under uniaxial tension at 1.0 K and 300.0 K. Fig. 18 shows the stress-strain curve for the tension of a single-layer 1H-VSe₂ of dimension 100×100 Å. Periodic boundary conditions are applied in both armchair and zigzag directions. The single-layer 1H-VSe₂ is stretched uniaxially along the armchair or zigzag direction. The stress is calculated without

TABLE XLI: SW potential parameters for single-layer 1H-VSe₂ used by LAMMPS⁹ as expressed in Eqs. (9) and (10). Atom types in the first column are displayed in Fig. 2 (with M=V and X=Se).

	ϵ (eV)	σ (Å)	a	λ	γ	$\cos \theta_0$	A_L	B_L	p	q	tol
V ₁ -Se ₁ -Se ₁	1.000	1.061	3.070	0.000	1.000	0.000	4.817	14.236	4	0	0.0
V ₁ -Se ₁ -Se ₃	1.000	0.000	0.000	33.299	1.000	0.126	0.000	0.000	4	0	0.0
V ₁ -Se ₁ -Se ₂	1.000	0.000	0.000	33.702	1.000	0.166	0.000	0.000	4	0	0.0
Se ₁ -V ₁ -V ₃	1.000	0.000	0.000	33.299	1.000	0.126	0.000	0.000	4	0	0.0

TABLE XLII: The VFF model for single-layer 1H-VTe₂. The second line gives an explicit expression for each VFF term. The third line is the force constant parameters. Parameters are in the unit of $\frac{\text{eV}}{\text{\AA}^2}$ for the bond stretching interactions, and in the unit of eV for the angle bending interaction. The fourth line gives the initial bond length (in unit of \AA) for the bond stretching interaction and the initial angle (in unit of degrees) for the angle bending interaction. The angle θ_{ijk} has atom i as the apex.

VFF type	bond stretching	angle bending		
expression	$\frac{1}{2}K_{\text{V-Te}}(\Delta r)^2$	$\frac{1}{2}K_{\text{V-Te-Te}}(\Delta\theta)^2$	$\frac{1}{2}K_{\text{V-Te-Te}'}(\Delta\theta)^2$	$\frac{1}{2}K_{\text{Te-V-V}}(\Delta\theta)^2$
parameter	6.371	4.384	4.384	4.384
r_0 or θ_0	2.660	81.708	81.891	81.708

involving the actual thickness of the quasi-two-dimensional structure of the single-layer 1H-VSe₂. The Young's modulus can be obtained by a linear fitting of the stress-strain relation in the small strain range of $[0, 0.01]$. The Young's modulus are 81.7 N/m and 80.6 N/m along the armchair and zigzag directions, respectively. The Young's modulus is essentially isotropic in the armchair and zigzag directions. The Poisson's ratio from the VFF model and the SW potential is $\nu_{xy} = \nu_{yx} = 0.23$.

There is no available value for the nonlinear quantities in the single-layer 1H-VSe₂. We have thus used the nonlinear parameter $B = 0.5d^4$ in Eq. (5), which is close to the value of B in most materials. The value of the third order nonlinear elasticity D can be extracted by fitting the stress-strain relation to the function $\sigma = E\epsilon + \frac{1}{2}D\epsilon^2$ with E as the Young's modulus. The values of D from the present SW potential are -335.2 N/m and -363.3 N/m along the armchair and zigzag directions, respectively. The ultimate stress is about 9.5 Nm⁻¹ at the ultimate strain of 0.21 in the armchair direction at the low temperature of 1 K. The ultimate stress is about 9.0 Nm⁻¹ at the ultimate strain of 0.24 in the zigzag direction at the low temperature of 1 K.

XI. 1H-VTE₂

Most existing theoretical studies on the single-layer 1H-VTe₂ are based on the first-principles calculations. In this section, we will develop both VFF model and the SW poten-

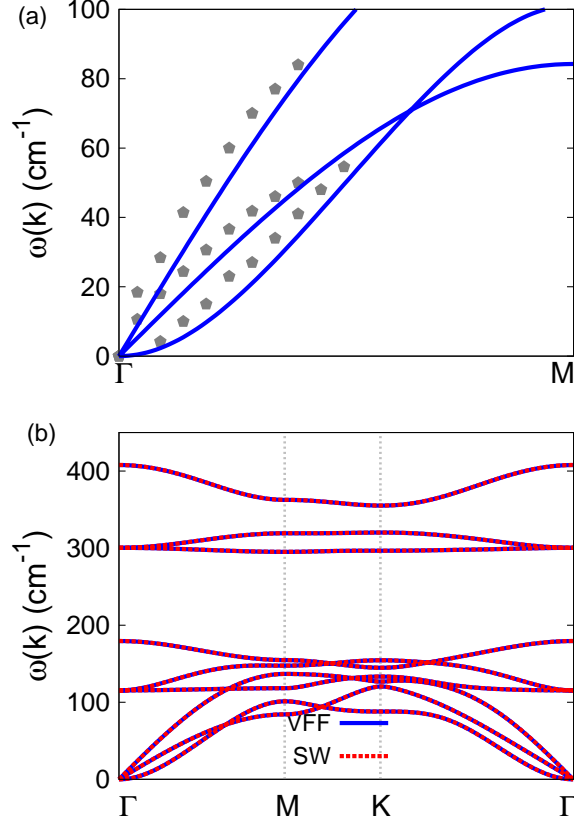


FIG. 19: (Color online) Phonon dispersion for single-layer 1H-VTe₂. (a) The VFF model is fitted to the three acoustic branches in the long wave limit along the Γ M direction. The *ab initio* results (gray pentagons) are from Ref. 12. (b) The VFF model (blue lines) and the SW potential (red lines) give the same phonon dispersion for single-layer 1H-VTe₂ along Γ MK Γ .

TABLE XLIII: Two-body SW potential parameters for single-layer 1H-VTe₂ used by GULP⁸ as expressed in Eq. (3).

	A (eV)	ρ (\AA)	B (\AA^4)	r_{\min} (\AA)	r_{\max} (\AA)
V-Te	5.410	1.112	25.032	0.0	3.520

tial for the single-layer 1H-VTe₂.

The structure for the single-layer 1H-VTe₂ is shown in Fig. 1 (with M=V and X=Te). Each V atom is surrounded by six Te atoms. These Te atoms are categorized into the top group (eg. atoms 1, 3, and 5) and bottom group (eg. atoms 2, 4, and 6). Each Te atom is connected to three V atoms. The structural parameters are from Ref. 12, including the

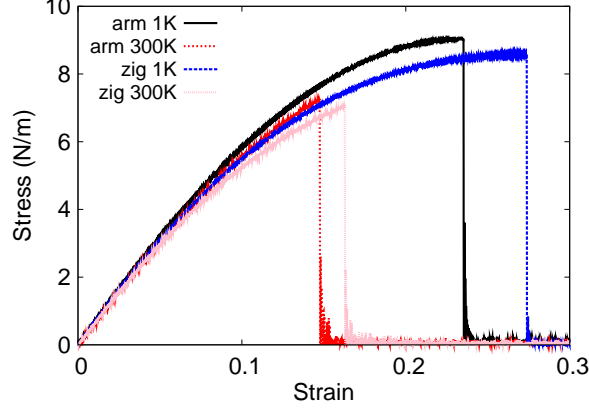


FIG. 20: (Color online) Stress-strain for single-layer 1H-VTe₂ of dimension $100 \times 100 \text{ \AA}$ along the armchair and zigzag directions.

TABLE XLIV: Three-body SW potential parameters for single-layer 1H-VTe₂ used by GULP⁸ as expressed in Eq. (4). The angle θ_{ijk} in the first line indicates the bending energy for the angle with atom i as the apex.

	K (eV)	θ_0 (degree)	ρ_1 (Å)	ρ_2 (Å)	$r_{\min 12}$ (Å)	$r_{\max 12}$ (Å)	$r_{\min 13}$ (Å)	$r_{\max 13}$ (Å)	$r_{\min 23}$ (Å)	$r_{\max 23}$ (Å)
$\theta_{V-\text{Te}-\text{Te}}$	29.743	81.708	1.112	1.112	0.0	3.520	0.0	3.520	0.0	4.203
$\theta_{V-\text{Te}-\text{Te}'}$	29.716	81.891	1.112	1.112	0.0	3.520	0.0	3.520	0.0	4.203
$\theta_{\text{Te}-V-V}$	29.743	81.708	1.112	1.112	0.0	3.520	0.0	3.520	0.0	4.203

lattice constant $a = 3.48 \text{ \AA}$, and the bond length $d_{V-\text{Te}} = 2.66 \text{ \AA}$. The resultant angles are $\theta_{V\text{TeTe}} = \theta_{\text{Te}V\text{V}} = 81.708^\circ$ and $\theta_{V\text{TeTe}'} = 81.891^\circ$, in which atoms Te and Te' are from different (top or bottom) group.

Table XLII shows the VFF terms for the 1H-VTe₂, one of which is the bond stretching interaction shown by Eq. (1) while the other terms are the angle bending interaction shown by Eq. (2). These force constant parameters are determined by fitting to the three acoustic branches in the phonon dispersion along the ΓM as shown in Fig. 19 (a). The *ab initio* calculations for the phonon dispersion are from Ref. 12. Fig. 19 (b) shows that the VFF model and the SW potential give exactly the same phonon dispersion, as the SW potential is derived from the VFF model.

The parameters for the two-body SW potential used by GULP are shown in Tab. XLIII. The parameters for the three-body SW potential used by GULP are shown in Tab. XLIV.

TABLE XLV: SW potential parameters for single-layer 1H-VTe₂ used by LAMMPS⁹ as expressed in Eqs. (9) and (10). Atom types in the first column are displayed in Fig. 2 (with M=V and X=Te).

	ϵ (eV)	σ (Å)	a	λ	γ	$\cos \theta_0$	A_L	B_L	p	q	tol
V ₁ -Te ₁ -Te ₁	1.000	1.112	3.164	0.000	1.000	0.000	5.410	16.345	4	0	0.0
V ₁ -Te ₁ -Te ₃	1.000	0.000	0.000	29.743	1.000	0.144	0.000	0.000	4	0	0.0
V ₁ -Te ₁ -Te ₂	1.000	0.000	0.000	29.716	1.000	0.141	0.000	0.000	4	0	0.0
Te ₁ -V ₁ -V ₃	1.000	0.000	0.000	29.743	1.000	0.144	0.000	0.000	4	0	0.0

Parameters for the SW potential used by LAMMPS are listed in Tab. XLV. We note that twelve atom types have been introduced for the simulation of the single-layer 1H-VTe₂ using LAMMPS, because the angles around atom V in Fig. 1 (with M=V and X=Te) are not distinguishable in LAMMPS. We have suggested two options to differentiate these angles by implementing some additional constraints in LAMMPS, which can be accomplished by modifying the source file of LAMMPS.^{13,14} According to our experience, it is not so convenient for some users to implement these constraints and recompile the LAMMPS package. Hence, in the present work, we differentiate the angles by introducing more atom types, so it is not necessary to modify the LAMMPS package. Fig. 2 (with M=V and X=Te) shows that, for 1H-VTe₂, we can differentiate these angles around the V atom by assigning these six neighboring Te atoms with different atom types. It can be found that twelve atom types are necessary for the purpose of differentiating all six neighbors around one V atom.

We use LAMMPS to perform MD simulations for the mechanical behavior of the single-layer 1H-VTe₂ under uniaxial tension at 1.0 K and 300.0 K. Fig. 20 shows the stress-strain curve for the tension of a single-layer 1H-VTe₂ of dimension 100×100 Å. Periodic boundary conditions are applied in both armchair and zigzag directions. The single-layer 1H-VTe₂ is stretched uniaxially along the armchair or zigzag direction. The stress is calculated without involving the actual thickness of the quasi-two-dimensional structure of the single-layer 1H-VTe₂. The Young's modulus can be obtained by a linear fitting of the stress-strain relation in the small strain range of $[0, 0.01]$. The Young's modulus are 68.1 N/m and 66.8 N/m along the armchair and zigzag directions, respectively. The Young's modulus is essentially isotropic in the armchair and zigzag directions. The Poisson's ratio from the VFF model and the SW potential is $\nu_{xy} = \nu_{yx} = 0.28$.

TABLE XLVI: The VFF model for single-layer 1H-CrO₂. The second line gives an explicit expression for each VFF term. The third line is the force constant parameters. Parameters are in the unit of $\frac{\text{eV}}{\text{Å}^2}$ for the bond stretching interactions, and in the unit of eV for the angle bending interaction. The fourth line gives the initial bond length (in unit of Å) for the bond stretching interaction and the initial angle (in unit of degrees) for the angle bending interaction. The angle θ_{ijk} has atom *i* as the apex.

VFF type	bond stretching		angle bending	
expression	$\frac{1}{2}K_{\text{Cr-O}}(\Delta r)^2$	$\frac{1}{2}K_{\text{Cr-O-O}}(\Delta\theta)^2$	$\frac{1}{2}K_{\text{Cr-O-O}'}(\Delta\theta)^2$	$\frac{1}{2}K_{\text{O-Cr-Cr}}(\Delta\theta)^2$
parameter	12.881	8.039	8.039	8.039
r_0 or θ_0	1.880	86.655	75.194	86.655

TABLE XLVII: Two-body SW potential parameters for single-layer 1H-CrO₂ used by GULP⁸ as expressed in Eq. (3).

	A (eV)	ρ (Å)	B (Å ⁴)	r_{min} (Å)	r_{max} (Å)
Cr-O	6.343	0.916	6.246	0.0	2.536

There is no available value for the nonlinear quantities in the single-layer 1H-VTe₂. We have thus used the nonlinear parameter $B = 0.5d^4$ in Eq. (5), which is close to the value of B in most materials. The value of the third order nonlinear elasticity D can be extracted by fitting the stress-strain relation to the function $\sigma = E\epsilon + \frac{1}{2}D\epsilon^2$ with E as the Young's modulus. The values of D from the present SW potential are -237.4 N/m and -260.4 N/m along the armchair and zigzag directions, respectively. The ultimate stress is about 9.0 Nm⁻¹ at the ultimate strain of 0.23 in the armchair direction at the low temperature of 1 K. The ultimate stress is about 8.6 Nm⁻¹ at the ultimate strain of 0.27 in the zigzag direction at the low temperature of 1 K.

XII. 1H-CRO₂

Most existing theoretical studies on the single-layer 1H-CrO₂ are based on the first-principles calculations. In this section, we will develop the SW potential for the single-layer 1H-CrO₂.

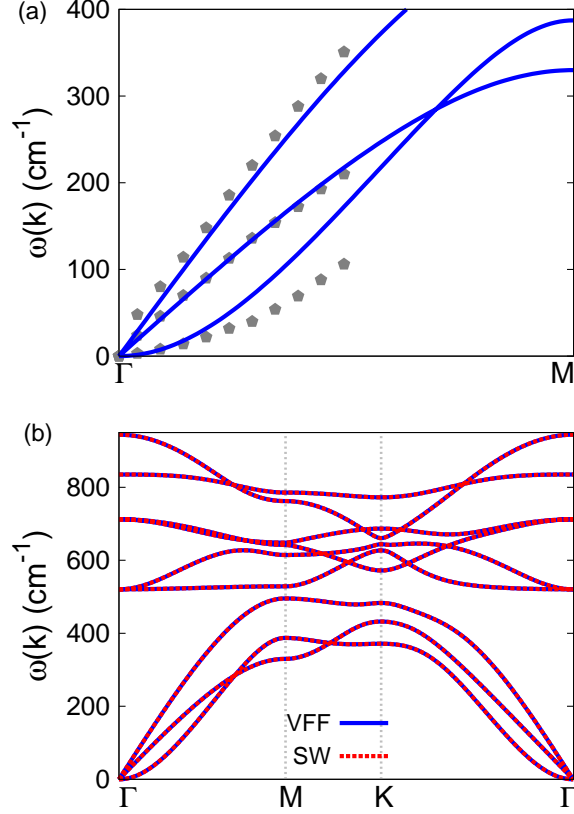


FIG. 21: (Color online) Phonon spectrum for single-layer 1H-CrO₂. (a) Phonon dispersion along the Γ M direction in the Brillouin zone. The results from the VFF model (lines) are comparable with the *ab initio* results (pentagons) from Ref. 12. (b) The phonon dispersion from the SW potential is exactly the same as that from the VFF model.

The structure for the single-layer 1H-CrO₂ is shown in Fig. 1 (with M=Cr and X=O). Each Cr atom is surrounded by six O atoms. These O atoms are categorized into the top group (eg. atoms 1, 3, and 5) and bottom group (eg. atoms 2, 4, and 6). Each O atom is connected to three Cr atoms. The structural parameters are from the first-principles calculations,¹² including the lattice constant $a = 2.58 \text{ \AA}$, and the bond length $d_{\text{Cr-O}} = 1.88 \text{ \AA}$. The resultant angles are $\theta_{\text{CrOO}} = \theta_{\text{OCrCr}} = 86.655^\circ$ and $\theta_{\text{CrOO}'} = 75.194^\circ$, in which atoms O and O' are from different (top or bottom) group.

Table XLVI shows four VFF terms for the single-layer 1H-CrO₂, one of which is the bond stretching interaction shown by Eq. (1) while the other three terms are the angle bending interaction shown by Eq. (2). These force constant parameters are determined by fitting to

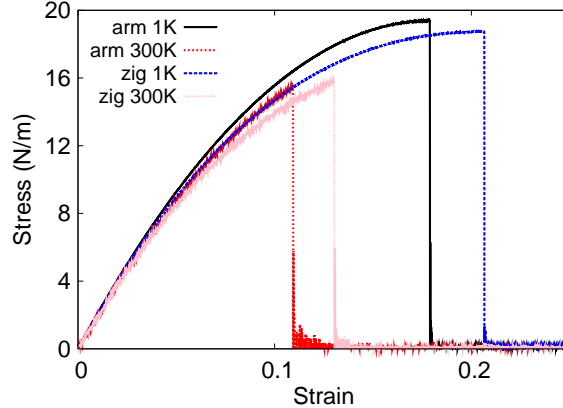


FIG. 22: (Color online) Stress-strain for single-layer 1H-CrO₂ of dimension 100 × 100 Å along the armchair and zigzag directions.

TABLE XLVIII: Three-body SW potential parameters for single-layer 1H-CrO₂ used by GULP⁸ as expressed in Eq. (4). The angle θ_{ijk} in the first line indicates the bending energy for the angle with atom i as the apex.

	K (eV)	θ_0 (degree)	ρ_1 (Å)	ρ_2 (Å)	$r_{\min 12}$ (Å)	$r_{\max 12}$ (Å)	$r_{\min 13}$ (Å)	$r_{\max 13}$ (Å)	$r_{\min 23}$ (Å)	$r_{\max 23}$ (Å)
$\theta_{\text{Cr-O-O}}$	65.805	86.655	0.916	0.916	0.0	2.536	0.0	2.536	0.0	3.016
$\theta_{\text{Cr-O-O}'}$	70.163	75.194	0.916	0.916	0.0	2.536	0.0	2.536	0.0	3.016
$\theta_{\text{O-Cr-Cr}}$	65.805	86.655	0.916	0.916	0.0	2.536	0.0	2.536	0.0	3.016

the acoustic branches in the phonon dispersion along the ΓM as shown in Fig. 21 (a). The *ab initio* calculations for the phonon dispersion are from Ref. 12. Fig. 21 (b) shows that the VFF model and the SW potential give exactly the same phonon dispersion, as the SW potential is derived from the VFF model.

The parameters for the two-body SW potential used by GULP are shown in Tab. XLVII. The parameters for the three-body SW potential used by GULP are shown in Tab. XLVIII. Some representative parameters for the SW potential used by LAMMPS are listed in Tab. XLIX. We note that twelve atom types have been introduced for the simulation of the single-layer 1H-CrO₂ using LAMMPS, because the angles around atom Cr in Fig. 1 (with M=Cr and X=O) are not distinguishable in LAMMPS. We have suggested two options to differentiate these angles by implementing some additional constraints in LAMMPS, which can be accomplished by modifying the source file of LAMMPS.^{13,14} According to our

TABLE XLIX: SW potential parameters for single-layer 1H-CrO₂ used by LAMMPS⁹ as expressed in Eqs. (9) and (10).

	ϵ (eV)	σ (Å)	a	λ	γ	$\cos \theta_0$	A_L	B_L	p	q	tol
Cr ₁ -O ₁ -O ₁	1.000	0.916	2.769	0.000	1.000	0.000	6.242	8.871	4	0	0.0
Cr ₁ -O ₁ -O ₃	1.000	0.000	0.000	65.805	1.000	0.058	0.000	0.000	4	0	0.0
Cr ₁ -O ₁ -O ₂	1.000	0.000	0.000	70.163	1.000	0.256	0.000	0.000	4	0	0.0
O ₁ -Cr ₁ -Cr ₃	1.000	0.000	0.000	65.805	1.000	0.058	0.000	0.000	4	0	0.0

experience, it is not so convenient for some users to implement these constraints and re-compile the LAMMPS package. Hence, in the present work, we differentiate the angles by introducing more atom types, so it is not necessary to modify the LAMMPS package. Fig. 2 (with M=Cr and X=O) shows that, for 1H-CrO₂, we can differentiate these angles around the Cr atom by assigning these six neighboring O atoms with different atom types. It can be found that twelve atom types are necessary for the purpose of differentiating all six neighbors around one Cr atom.

We use LAMMPS to perform MD simulations for the mechanical behavior of the single-layer 1H-CrO₂ under uniaxial tension at 1.0 K and 300.0 K. Fig. 22 shows the stress-strain curve for the tension of a single-layer 1H-CrO₂ of dimension 100×100 Å. Periodic boundary conditions are applied in both armchair and zigzag directions. The single-layer 1H-CrO₂ is stretched uniaxially along the armchair or zigzag direction. The stress is calculated without involving the actual thickness of the quasi-two-dimensional structure of the single-layer 1H-CrO₂. The Young's modulus can be obtained by a linear fitting of the stress-strain relation in the small strain range of $[0, 0.01]$. The Young's modulus are 210.6 N/m and 209.0 N/m along the armchair and zigzag directions, respectively. The Young's modulus is essentially isotropic in the armchair and zigzag directions. The Poisson's ratio from the VFF model and the SW potential is $\nu_{xy} = \nu_{yx} = 0.13$.

There is no available value for nonlinear quantities in the single-layer 1H-CrO₂. We have thus used the nonlinear parameter $B = 0.5d^4$ in Eq. (5), which is close to the value of B in most materials. The value of the third order nonlinear elasticity D can be extracted by fitting the stress-strain relation to the function $\sigma = E\epsilon + \frac{1}{2}D\epsilon^2$ with E as the Young's modulus. The values of D from the present SW potential are -1127.7 N/m and -1185.8 N/m along

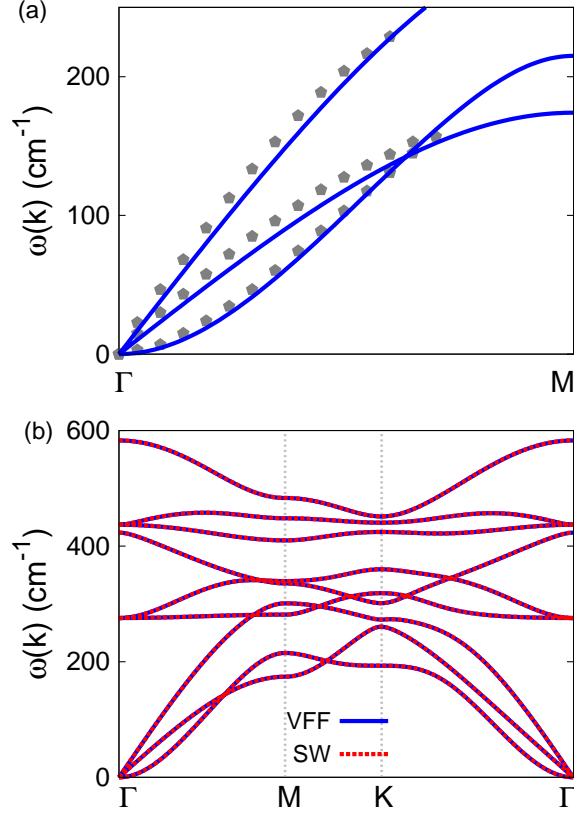


FIG. 23: (Color online) Phonon dispersion for single-layer 1H-CrS₂. (a) The VFF model is fitted to the three acoustic branches in the long wave limit along the Γ M direction. The *ab initio* results (gray pentagons) are from Ref. 17. (b) The VFF model (blue lines) and the SW potential (red lines) give the same phonon dispersion for single-layer 1H-CrS₂ along Γ MKT Γ .

the armchair and zigzag directions, respectively. The ultimate stress is about 19.4 Nm^{-1} at the ultimate strain of 0.18 in the armchair direction at the low temperature of 1 K. The ultimate stress is about 18.7 Nm^{-1} at the ultimate strain of 0.20 in the zigzag direction at the low temperature of 1 K.

XIII. 1H-CRS₂

Most existing theoretical studies on the single-layer 1H-CrS₂ are based on the first-principles calculations. In this section, we will develop both VFF model and the SW potential for the single-layer 1H-CrS₂.

TABLE L: The VFF model for single-layer 1H-CrS₂. The second line gives an explicit expression for each VFF term. The third line is the force constant parameters. Parameters are in the unit of $\frac{eV}{\text{\AA}^2}$ for the bond stretching interactions, and in the unit of eV for the angle bending interaction. The fourth line gives the initial bond length (in unit of \AA) for the bond stretching interaction and the initial angle (in unit of degrees) for the angle bending interaction. The angle θ_{ijk} has atom i as the apex.

VFF type	bond stretching	angle bending		
expression	$\frac{1}{2}K_{Cr-S}(\Delta r)^2$	$\frac{1}{2}K_{Cr-S-S}(\Delta\theta)^2$	$\frac{1}{2}K_{Cr-S-S'}(\Delta\theta)^2$	$\frac{1}{2}K_{S-Cr-Cr}(\Delta\theta)^2$
parameter	8.752	4.614	4.614	4.614
r_0 or θ_0	2.254	83.099	80.031	83.099

TABLE LI: Two-body SW potential parameters for single-layer 1HCrS₂ used by GULP⁸ as expressed in Eq. (3).

	A (eV)	ρ (\AA)	B (\AA^4)	r_{\min} (\AA)	r_{\max} (\AA)
Cr-S	5.544	0.985	12.906	0.0	2.999

TABLE LII: Three-body SW potential parameters for single-layer 1H-CrS₂ used by GULP⁸ as expressed in Eq. (4). The angle θ_{ijk} in the first line indicates the bending energy for the angle with atom i as the apex.

	K (eV)	θ_0 (degree)	ρ_1 (\AA)	ρ_2 (\AA)	$r_{\min12}$ (\AA)	$r_{\max12}$ (\AA)	$r_{\min13}$ (\AA)	$r_{\max13}$ (\AA)	$r_{\min23}$ (\AA)	$r_{\max23}$ (\AA)
θ_{Cr-S-S}	32.963	83.099	0.985	0.985	0.0	2.999	0.0	2.999	0.0	3.577
$\theta_{Cr-S-S'}$	33.491	80.031	0.985	0.985	0.0	2.999	0.0	2.999	0.0	3.577
$\theta_{S-Cr-Cr}$	32.963	83.099	0.985	0.985	0.0	2.999	0.0	2.999	0.0	3.577

TABLE LIII: SW potential parameters for single-layer 1H-CrS₂ used by LAMMPS⁹ as expressed in Eqs. (9) and (10). Atom types in the first column are displayed in Fig. 2 (with M=Cr and X=S).

	ϵ (eV)	σ (\AA)	a	λ	γ	$\cos\theta_0$	A_L	B_L	p	q	tol
Cr ₁ -S ₁ -S ₁	1.000	0.985	3.043	0.000	1.000	0.000	5.544	13.683	4	0	0.0
Cr ₁ -S ₁ -S ₃	1.000	0.000	0.000	32.963	1.000	0.120	0.000	0.000	4	0	0.0
Cr ₁ -S ₁ -S ₂	1.000	0.000	0.000	33.491	1.000	0.173	0.000	0.000	4	0	0.0
S ₁ -Cr ₁ -Cr ₃	1.000	0.000	0.000	32.963	1.000	0.120	0.000	0.000	4	0	0.0

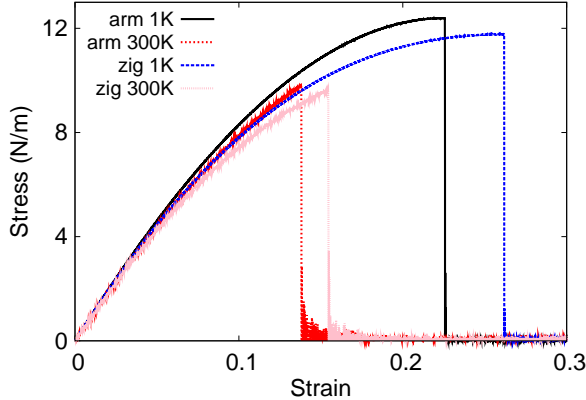


FIG. 24: (Color online) Stress-strain for single-layer 1H-CrS₂ of dimension 100 × 100 Å along the armchair and zigzag directions.

The structure for the single-layer 1H-CrS₂ is shown in Fig. 1 (with M=Cr and X=S). Each Cr atom is surrounded by six S atoms. These S atoms are categorized into the top group (eg. atoms 1, 3, and 5) and bottom group (eg. atoms 2, 4, and 6). Each S atom is connected to three Cr atoms. The structural parameters are from Ref. 17, including the lattice constant $a = 2.99$ Å, and the bond length $d_{\text{Cr-S}} = 2.254$ Å. The resultant angles are $\theta_{\text{CrSS}} = \theta_{\text{SCrCr}} = 83.099^\circ$ and $\theta_{\text{CrSS}'} = 80.031^\circ$, in which atoms S and S' are from different (top or bottom) group.

Table L shows four VFF terms for the 1H-CrS₂, one of which is the bond stretching interaction shown by Eq. (1) while the other three terms are the angle bending interaction shown by Eq. (2). These force constant parameters are determined by fitting to the three acoustic branches in the phonon dispersion along the ΓM as shown in Fig. 23 (a). The *ab initio* calculations for the phonon dispersion are from Ref. 17. Similar phonon dispersion can also be found in other *ab initio* calculations.¹² Fig. 23 (b) shows that the VFF model and the SW potential give exactly the same phonon dispersion, as the SW potential is derived from the VFF model.

The parameters for the two-body SW potential used by GULP are shown in Tab. LI. The parameters for the three-body SW potential used by GULP are shown in Tab. LII. Parameters for the SW potential used by LAMMPS are listed in Tab. LIII. We note that twelve atom types have been introduced for the simulation of the single-layer 1H-CrS₂ using LAMMPS, because the angles around atom Cr in Fig. 1 (with M=Cr and X=S) are not

distinguishable in LAMMPS. We have suggested two options to differentiate these angles by implementing some additional constraints in LAMMPS, which can be accomplished by modifying the source file of LAMMPS.^{13,14} According to our experience, it is not so convenient for some users to implement these constraints and recompile the LAMMPS package. Hence, in the present work, we differentiate the angles by introducing more atom types, so it is not necessary to modify the LAMMPS package. Fig. 2 (with M=Cr and X=S) shows that, for 1H-CrS₂, we can differentiate these angles around the Cr atom by assigning these six neighboring S atoms with different atom types. It can be found that twelve atom types are necessary for the purpose of differentiating all six neighbors around one Cr atom.

We use LAMMPS to perform MD simulations for the mechanical behavior of the single-layer 1H-CrS₂ under uniaxial tension at 1.0 K and 300.0 K. Fig. 24 shows the stress-strain curve for the tension of a single-layer 1H-CrS₂ of dimension 100 × 100 Å. Periodic boundary conditions are applied in both armchair and zigzag directions. The single-layer 1H-CrS₂ is stretched uniaxially along the armchair or zigzag direction. The stress is calculated without involving the actual thickness of the quasi-two-dimensional structure of the single-layer 1H-CrS₂. The Young's modulus can be obtained by a linear fitting of the stress-strain relation in the small strain range of [0, 0.01]. The Young's modulus are 98.4 N/m and 97.8 N/m along the armchair and zigzag directions, respectively. The Young's modulus is essentially isotropic in the armchair and zigzag directions. These values are in reasonably agreement with the *ab initio* results, eg. 112.0 N/m from Refs 18, or 111.9 N/m from Ref. 19. The Poisson's ratio from the VFF model and the SW potential is $\nu_{xy} = \nu_{yx} = 0.26$, which agrees with the *ab initio* value of 0.27.^{18,19}

There is no available value for the nonlinear quantities in the single-layer 1H-CrS₂. We have thus used the nonlinear parameter $B = 0.5d^4$ in Eq. (5), which is close to the value of B in most materials. The value of the third order nonlinear elasticity D can be extracted by fitting the stress-strain relation to the function $\sigma = E\epsilon + \frac{1}{2}D\epsilon^2$ with E as the Young's modulus. The values of D from the present SW potential are -364.8 N/m and -409.3 N/m along the armchair and zigzag directions, respectively. The ultimate stress is about 12.4 Nm⁻¹ at the ultimate strain of 0.22 in the armchair direction at the low temperature of 1 K. The ultimate stress is about 11.8 Nm⁻¹ at the ultimate strain of 0.26 in the zigzag direction at the low temperature of 1 K.

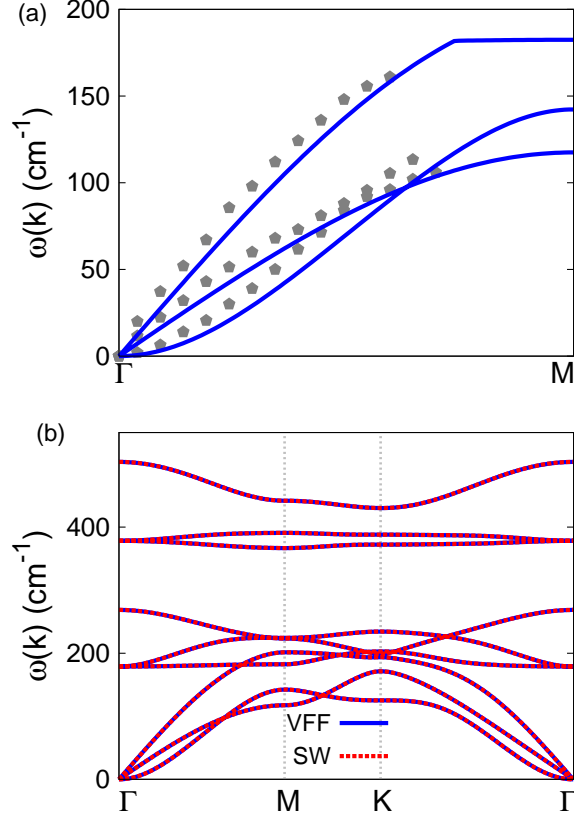


FIG. 25: (Color online) Phonon dispersion for single-layer 1H-CrSe₂. (a) The VFF model is fitted to the three acoustic branches in the long wave limit along the Γ M direction. The *ab initio* results (gray pentagons) are from Ref. 12. (b) The VFF model (blue lines) and the SW potential (red lines) give the same phonon dispersion for single-layer 1H-CrSe₂ along Γ MKT Γ .

XIV. 1H-CRSE₂

Most existing theoretical studies on the single-layer 1H-CrSe₂ are based on the first-principles calculations. In this section, we will develop both VFF model and the SW potential for the single-layer 1H-CrSe₂.

The structure for the single-layer 1H-CrSe₂ is shown in Fig. 1 (with M=Cr and X=Se). Each Cr atom is surrounded by six Se atoms. These Se atoms are categorized into the top group (eg. atoms 1, 3, and 5) and bottom group (eg. atoms 2, 4, and 6). Each Se atom is connected to three Cr atoms. The structural parameters are from Ref. 12, including the lattice constant $a = 3.13$ Å, and the bond length $d_{\text{Cr-Se}} = 2.38$ Å. The resultant angles

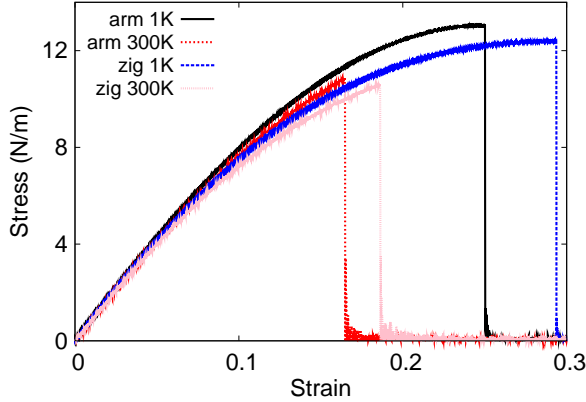


FIG. 26: (Color online) Stress-strain for single-layer 1H-CrSe₂ of dimension $100 \times 100 \text{ \AA}$ along the armchair and zigzag directions.

TABLE LIV: The VFF model for single-layer 1H-CrSe₂. The second line gives an explicit expression for each VFF term. The third line is the force constant parameters. Parameters are in the unit of $\frac{eV}{\text{Å}^2}$ for the bond stretching interactions, and in the unit of eV for the angle bending interaction. The fourth line gives the initial bond length (in unit of Å) for the bond stretching interaction and the initial angle (in unit of degrees) for the angle bending interaction. The angle θ_{ijk} has atom i as the apex.

VFF type	bond stretching	angle bending		
expression	$\frac{1}{2}K_{Cr-Se}(\Delta r)^2$	$\frac{1}{2}K_{Cr-Se-Se}(\Delta\theta)^2$	$\frac{1}{2}K_{Cr-Se-Se'}(\Delta\theta)^2$	$\frac{1}{2}K_{Se-Cr-Cr}(\Delta\theta)^2$
parameter	9.542	4.465	4.465	4.465
r_0 or θ_0	2.380	82.229	81.197	82.229

are $\theta_{CrSeSe} = \theta_{SeCrCr} = 82.229^\circ$ and $\theta_{CrSeSe'} = 81.197^\circ$, in which atoms Se and Se' are from different (top or bottom) group.

Table LIV shows four VFF terms for the 1H-CrSe₂, one of which is the bond stretching interaction shown by Eq. (1) while the other three terms are the angle bending interaction shown by Eq. (2). These force constant parameters are determined by fitting to the three acoustic branches in the phonon dispersion along the ΓM as shown in Fig. 25 (a). The *ab initio* calculations for the phonon dispersion are from Ref. 12. Fig. 25 (b) shows that the VFF model and the SW potential give exactly the same phonon dispersion, as the SW potential is derived from the VFF model.

TABLE LV: Two-body SW potential parameters for single-layer 1H-CrSe₂ used by GULP⁸ as expressed in Eq. (3).

	A (eV)	ρ (Å)	B (Å ⁴)	r_{\min} (Å)	r_{\max} (Å)
Cr-Se	6.581	1.012	16.043	0.0	3.156

TABLE LVI: Three-body SW potential parameters for single-layer 1H-CrSe₂ used by GULP⁸ as expressed in Eq. (4). The angle θ_{ijk} in the first line indicates the bending energy for the angle with atom i as the apex.

	K (eV)	θ_0 (degree)	ρ_1 (Å)	ρ_2 (Å)	$r_{\min12}$ (Å)	$r_{\max12}$ (Å)	$r_{\min13}$ (Å)	$r_{\max13}$ (Å)	$r_{\min23}$ (Å)	$r_{\max23}$ (Å)
$\theta_{\text{Cr-Se-Se}}$	30.881	82.229	1.012	1.012	0.0	3.156	0.0	3.156	0.0	3.767
$\theta_{\text{Cr-Se-Se}'}$	31.044	81.197	1.012	1.012	0.0	3.156	0.0	3.156	0.0	3.767
$\theta_{\text{Se-Cr-Cr}}$	30.881	82.229	1.012	1.012	0.0	3.156	0.0	3.156	0.0	3.767

The parameters for the two-body SW potential used by GULP are shown in Tab. LV. The parameters for the three-body SW potential used by GULP are shown in Tab. LVI. Parameters for the SW potential used by LAMMPS are listed in Tab. LVII. We note that twelve atom types have been introduced for the simulation of the single-layer 1H-CrSe₂ using LAMMPS, because the angles around atom Cr in Fig. 1 (with M=Cr and X=Se) are not distinguishable in LAMMPS. We have suggested two options to differentiate these angles by implementing some additional constraints in LAMMPS, which can be accomplished by modifying the source file of LAMMPS.^{13,14} According to our experience, it is not so conve-

TABLE LVII: SW potential parameters for single-layer 1H-CrSe₂ used by LAMMPS⁹ as expressed in Eqs. (9) and (10). Atom types in the first column are displayed in Fig. 2 (with M=Cr and X=Se).

	ϵ (eV)	σ (Å)	a	λ	γ	$\cos\theta_0$	A_L	B_L	p	q	tol
Cr ₁ -Se ₁ -Se ₁	1.000	1.012	3.118	0.000	1.000	0.000	6.581	15.284	4	0	0.0
Cr ₁ -Se ₁ -Se ₃	1.000	0.000	0.000	30.881	1.000	0.135	0.000	0.000	4	0	0.0
Cr ₁ -Se ₁ -Se ₂	1.000	0.000	0.000	31.044	1.000	0.153	0.000	0.000	4	0	0.0
Se ₁ -Cr ₁ -Cr ₃	1.000	0.000	0.000	30.881	1.000	0.135	0.000	0.000	4	0	0.0

nient for some users to implement these constraints and recompile the LAMMPS package. Hence, in the present work, we differentiate the angles by introducing more atom types, so it is not necessary to modify the LAMMPS package. Fig. 2 (with M=Cr and X=Se) shows that, for 1H-CrSe₂, we can differentiate these angles around the Cr atom by assigning these six neighboring Se atoms with different atom types. It can be found that twelve atom types are necessary for the purpose of differentiating all six neighbors around one Cr atom.

We use LAMMPS to perform MD simulations for the mechanical behavior of the single-layer 1H-CrSe₂ under uniaxial tension at 1.0 K and 300.0 K. Fig. 26 shows the stress-strain curve for the tension of a single-layer 1H-CrSe₂ of dimension 100 × 100 Å. Periodic boundary conditions are applied in both armchair and zigzag directions. The single-layer 1H-CrSe₂ is stretched uniaxially along the armchair or zigzag direction. The stress is calculated without involving the actual thickness of the quasi-two-dimensional structure of the single-layer 1H-CrSe₂. The Young's modulus can be obtained by a linear fitting of the stress-strain relation in the small strain range of [0, 0.01]. The Young's modulus are 90.0 N/m and 89.0 N/m along the armchair and zigzag directions, respectively. The Young's modulus is essentially isotropic in the armchair and zigzag directions. These values are in reasonably agreement with the *ab initio* results, eg. 88.0 N/m from Refs 18, or 87.9 N/m from Ref. 19. The Poisson's ratio from the VFF model and the SW potential is $\nu_{xy} = \nu_{yx} = 0.30$, which agrees with the *ab initio* value of 0.30.^{18,19}

There is no available value for the nonlinear quantities in the single-layer 1H-CrSe₂. We have thus used the nonlinear parameter $B = 0.5d^4$ in Eq. (5), which is close to the value of B in most two-dimensional atomic layered materials. The value of the third order nonlinear elasticity D can be extracted by fitting the stress-strain relation to the function $\sigma = E\epsilon + \frac{1}{2}D\epsilon^2$ with E as the Young's modulus. The values of D from the present SW potential are -279.6 N/m and -318.8 N/m along the armchair and zigzag directions, respectively. The ultimate stress is about 13.0 Nm⁻¹ at the ultimate strain of 0.25 in the armchair direction at the low temperature of 1 K. The ultimate stress is about 12.4 Nm⁻¹ at the ultimate strain of 0.29 in the zigzag direction at the low temperature of 1 K.

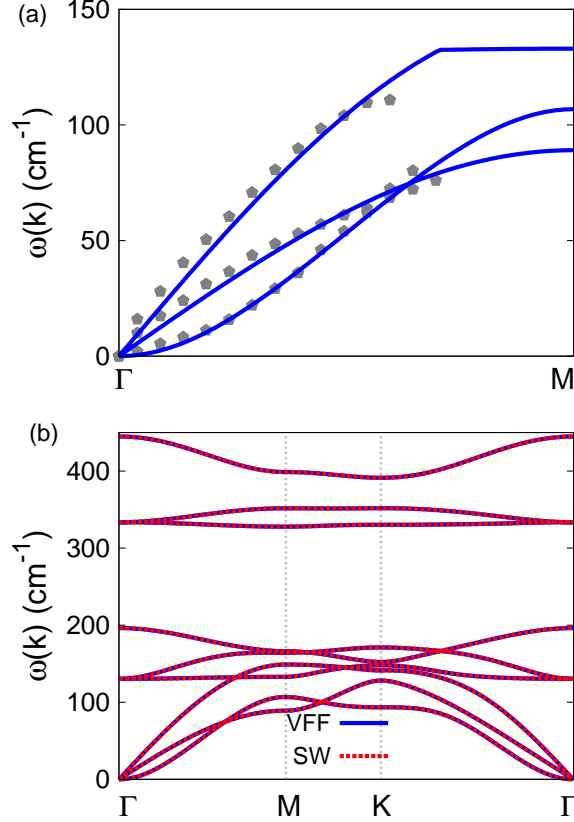


FIG. 27: (Color online) Phonon dispersion for single-layer 1H-CrTe₂. (a) The VFF model is fitted to the three acoustic branches in the long wave limit along the Γ M direction. The *ab initio* results (gray pentagons) are from Ref. 12. (b) The VFF model (blue lines) and the SW potential (red lines) give the same phonon dispersion for single-layer 1H-CrTe₂ along Γ MK Γ .

XV. 1H-CRTE₂

Most existing theoretical studies on the single-layer 1H-CrTe₂ are based on the first-principles calculations. In this section, we will develop both VFF model and the SW potential for the single-layer 1H-CrTe₂.

The structure for the single-layer 1H-CrTe₂ is shown in Fig. 1 (with M=Cr and X=Te). Each Cr atom is surrounded by six Te atoms. These Te atoms are categorized into the top group (eg. atoms 1, 3, and 5) and bottom group (eg. atoms 2, 4, and 6). Each Te atom is connected to three Cr atoms. The structural parameters are from Ref. 12, including the lattice constant $a = 3.39$ Å, and the bond length $d_{\text{Cr-Te}} = 2.58$ Å. The resultant angles

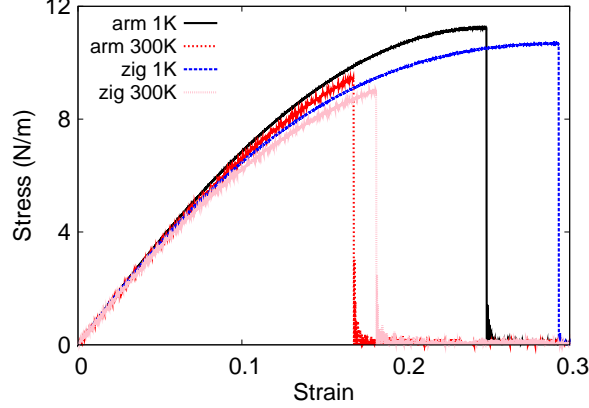


FIG. 28: (Color online) Stress-strain for single-layer 1H-CrTe₂ of dimension $100 \times 100 \text{ \AA}$ along the armchair and zigzag directions.

TABLE LVIII: The VFF model for single-layer 1H-CrTe₂. The second line gives an explicit expression for each VFF term. The third line is the force constant parameters. Parameters are in the unit of $\frac{eV}{\text{Å}^2}$ for the bond stretching interactions, and in the unit of eV for the angle bending interaction. The fourth line gives the initial bond length (in unit of Å) for the bond stretching interaction and the initial angle (in unit of degrees) for the angle bending interaction. The angle θ_{ijk} has atom *i* as the apex.

VFF type	bond stretching	angle bending		
expression	$\frac{1}{2}K_{Cr-Te}(\Delta r)^2$	$\frac{1}{2}K_{Cr-Te-Te}(\Delta\theta)^2$	$\frac{1}{2}K_{Cr-Te-Te'}(\Delta\theta)^2$	$\frac{1}{2}K_{Te-Cr-Cr}(\Delta\theta)^2$
parameter	8.197	4.543	4.543	4.543
r_0 or θ_0	2.580	82.139	81.316	82.139

are $\theta_{CrTeTe} = \theta_{TeCrCr} = 82.139^\circ$ and $\theta_{CrTeTe'} = 81.316^\circ$, in which atoms Te and Te' are from different (top or bottom) group.

Table LVIII shows three VFF terms for the 1H-CrTe₂, one of which is the bond stretching interaction shown by Eq. (1) while the other two terms are the angle bending interaction shown by Eq. (2). These force constant parameters are determined by fitting to the three acoustic branches in the phonon dispersion along the ΓM as shown in Fig. 27 (a). The *ab initio* calculations for the phonon dispersion are from Ref. 12. Fig. 27 (b) shows that the VFF model and the SW potential give exactly the same phonon dispersion, as the SW

TABLE LIX: Two-body SW potential parameters for single-layer 1H-CrTe₂ used by GULP⁸ as expressed in Eq. (3).

	A (eV)	ρ (Å)	B (Å ⁴)	r_{\min} (Å)	r_{\max} (Å)
Cr-Te	6.627	1.094	22.154	0.0	3.420

TABLE LX: Three-body SW potential parameters for single-layer 1H-CrTe₂ used by GULP⁸ as expressed in Eq. (4). The angle θ_{ijk} in the first line indicates the bending energy for the angle with atom i as the apex.

	K (eV)	θ_0 (degree)	ρ_1 (Å)	ρ_2 (Å)	$r_{\min12}$ (Å)	$r_{\max12}$ (Å)	$r_{\min13}$ (Å)	$r_{\max13}$ (Å)	$r_{\min23}$ (Å)	$r_{\max23}$ (Å)
$\theta_{\text{Cr-Te-Te}}$	31.316	82.139	1.094	1.094	0.0	3.420	0.0	3.420	0.0	4.082
$\theta_{\text{Cr-Te-Te}'}$	31.447	81.316	1.094	1.094	0.0	3.420	0.0	3.420	0.0	4.082
$\theta_{\text{Te-Cr-Cr}}$	31.316	82.139	1.094	1.094	0.0	3.420	0.0	3.420	0.0	4.082

potential is derived from the VFF model.

The parameters for the two-body SW potential used by GULP are shown in Tab. LIX. The parameters for the three-body SW potential used by GULP are shown in Tab. LX. Parameters for the SW potential used by LAMMPS are listed in Tab. LXI. We note that twelve atom types have been introduced for the simulation of the single-layer 1H-CrTe₂ using LAMMPS, because the angles around atom Cr in Fig. 1 (with M=Cr and X=Te) are not distinguishable in LAMMPS. We have suggested two options to differentiate these angles by implementing some additional constraints in LAMMPS, which can be accomplished by

TABLE LXI: SW potential parameters for single-layer 1H-CrTe₂ used by LAMMPS⁹ as expressed in Eqs. (9) and (10). Atom types in the first column are displayed in Fig. 2 (with M=Cr and X=Te).

	ϵ (eV)	σ (Å)	a	λ	γ	$\cos\theta_0$	A_L	B_L	p	q	tol
Cr ₁ -Te ₁ -Te ₁	1.000	1.094	3.126	0.000	1.000	0.000	6.627	15.461	4	0	0.0
Cr ₁ -Te ₁ -Te ₃	1.000	0.000	0.000	31.316	1.000	0.137	0.000	0.000	4	0	0.0
Cr ₁ -Te ₁ -Te ₂	1.000	0.000	0.000	31.447	1.000	0.151	0.000	0.000	4	0	0.0
Te ₁ -Cr ₁ -Cr ₃	1.000	0.000	0.000	31.316	1.000	0.137	0.000	0.000	4	0	0.0

modifying the source file of LAMMPS.^{13,14} According to our experience, it is not so convenient for some users to implement these constraints and recompile the LAMMPS package. Hence, in the present work, we differentiate the angles by introducing more atom types, so it is not necessary to modify the LAMMPS package. Fig. 2 (with M=Cr and X=Te) shows that, for 1H-CrTe₂, we can differentiate these angles around the Cr atom by assigning these six neighboring Te atoms with different atom types. It can be found that twelve atom types are necessary for the purpose of differentiating all six neighbors around one Cr atom.

We use LAMMPS to perform MD simulations for the mechanical behavior of the single-layer 1H-CrTe₂ under uniaxial tension at 1.0 K and 300.0 K. Fig. 28 shows the stress-strain curve for the tension of a single-layer 1H-CrTe₂ of dimension $100 \times 100 \text{ \AA}$. Periodic boundary conditions are applied in both armchair and zigzag directions. The single-layer 1H-CrTe₂ is stretched uniaxially along the armchair or zigzag direction. The stress is calculated without involving the actual thickness of the quasi-two-dimensional structure of the single-layer 1H-CrTe₂. The Young's modulus can be obtained by a linear fitting of the stress-strain relation in the small strain range of $[0, 0.01]$. The Young's modulus are 77.2 N/m and 76.4 N/m along the armchair and zigzag directions, respectively. The Young's modulus is essentially isotropic in the armchair and zigzag directions. These values are in reasonably agreement with the *ab initio* results, eg. 63.9 N/m from Refs 18 and 19. The Poisson's ratio from the VFF model and the SW potential is $\nu_{xy} = \nu_{yx} = 0.30$, which agrees with the *ab initio* value of 0.30.^{18,19}

There is no available value for the nonlinear quantities in the single-layer 1H-CrTe₂. We have thus used the nonlinear parameter $B = 0.5d^4$ in Eq. (5), which is close to the value of B in most two-dimensional atomic layered materials. The value of the third order nonlinear elasticity D can be extracted by fitting the stress-strain relation to the function $\sigma = E\epsilon + \frac{1}{2}D\epsilon^2$ with E as the Young's modulus. The values of D from the present SW potential are -237.1 N/m and -280.8 N/m along the armchair and zigzag directions, respectively. The ultimate stress is about 11.2 Nm^{-1} at the ultimate strain of 0.25 in the armchair direction at the low temperature of 1 K. The ultimate stress is about 10.7 Nm^{-1} at the ultimate strain of 0.29 in the zigzag direction at the low temperature of 1 K.

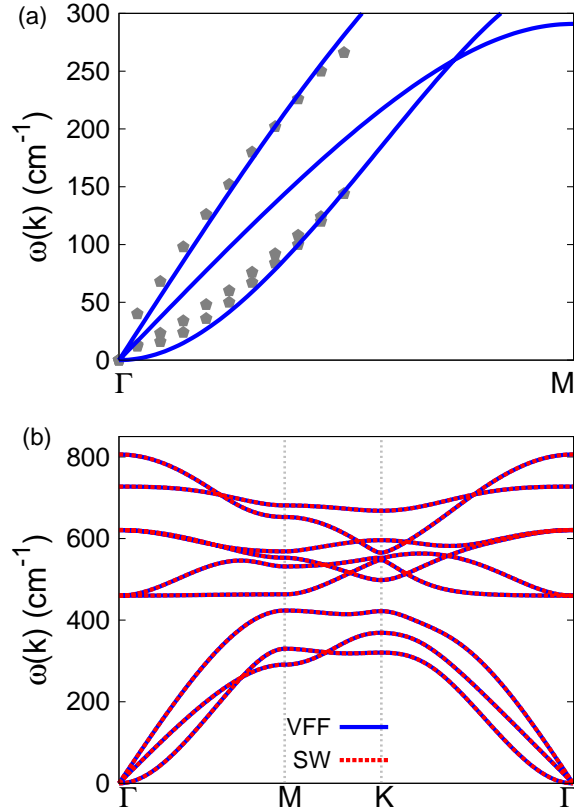


FIG. 29: (Color online) Phonon spectrum for single-layer 1H-MnO₂. (a) Phonon dispersion along the Γ M direction in the Brillouin zone. The results from the VFF model (lines) are comparable with the *ab initio* results (pentagons) from Ref. 12. (b) The phonon dispersion from the SW potential is exactly the same as that from the VFF model.

XVI. 1H-MNO₂

Most existing theoretical studies on the single-layer 1H-MnO₂ are based on the first-principles calculations. In this section, we will develop the SW potential for the single-layer 1H-MnO₂.

The structure for the single-layer 1H-MnO₂ is shown in Fig. 1 (with M=Mn and X=O). Each Mn atom is surrounded by six O atoms. These O atoms are categorized into the top group (eg. atoms 1, 3, and 5) and bottom group (eg. atoms 2, 4, and 6). Each O atom is connected to three Mn atoms. The structural parameters are from the first-principles calculations,¹² including the lattice constant $a = 2.61 \text{ \AA}$, and the bond length

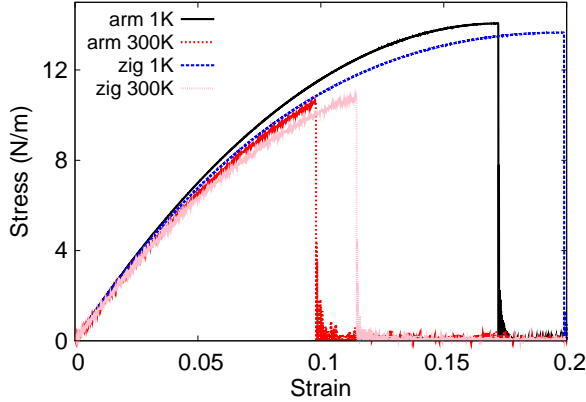


FIG. 30: (Color online) Stress-strain for single-layer 1H-MnO₂ of dimension $100 \times 100 \text{ \AA}$ along the armchair and zigzag directions.

TABLE LXII: The VFF model for single-layer 1H-MnO₂. The second line gives an explicit expression for each VFF term. The third line is the force constant parameters. Parameters are in the unit of $\frac{eV}{\text{\AA}^2}$ for the bond stretching interactions, and in the unit of eV for the angle bending interaction. The fourth line gives the initial bond length (in unit of \AA) for the bond stretching interaction and the initial angle (in unit of degrees) for the angle bending interaction. The angle θ_{ijk} has atom i as the apex.

VFF type	bond stretching	angle bending		
expression	$\frac{1}{2}K_{\text{Mn-O}}(\Delta r)^2$	$\frac{1}{2}K_{\text{Mn-O-O}}(\Delta\theta)^2$	$\frac{1}{2}K_{\text{Mn-O-O'}}(\Delta\theta)^2$	$\frac{1}{2}K_{\text{O-Mn-Mn}}(\Delta\theta)^2$
parameter	9.382	6.253	6.253	6.253
r_0 or θ_0	1.870	88.511	72.621	88.511

$d_{\text{Mn-O}} = 1.87 \text{ \AA}$. The resultant angles are $\theta_{\text{MnOO}} = \theta_{\text{OMnMn}} = 88.511^\circ$ and $\theta_{\text{MnOO'}} = 72.621^\circ$, in which atoms O and O' are from different (top or bottom) group.

Table LXII shows four VFF terms for the single-layer 1H-MnO₂, one of which is the bond stretching interaction shown by Eq. (1) while the other three terms are the angle bending interaction shown by Eq. (2). These force constant parameters are determined by fitting to the acoustic branches in the phonon dispersion along the ΓM as shown in Fig. 29 (a). The *ab initio* calculations for the phonon dispersion are from Ref. 12. Typically, the transverse acoustic branch has a linear dispersion, so is higher than the flexural branch. However, it can

TABLE LXIII: Two-body SW potential parameters for single-layer 1H-MnO₂ used by GULP⁸ as expressed in Eq. (3).

	A (eV)	ρ (Å)	B (Å ⁴)	r_{\min} (Å)	r_{\max} (Å)
Mn-O	4.721	0.961	6.114	0.0	2.540

TABLE LXIV: Three-body SW potential parameters for single-layer 1H-MnO₂ used by GULP⁸ as expressed in Eq. (4). The angle θ_{ijk} in the first line indicates the bending energy for the angle with atom i as the apex.

	K (eV)	θ_0 (degree)	ρ_1 (Å)	ρ_2 (Å)	$r_{\min12}$ (Å)	$r_{\max12}$ (Å)	$r_{\min13}$ (Å)	$r_{\max13}$ (Å)	$r_{\min23}$ (Å)	$r_{\max23}$ (Å)
$\theta_{\text{Mn-O-O}}$	55.070	88.511	0.961	0.961	0.0	2.540	0.0	2.540	0.0	3.016
$\theta_{\text{Mn-O-O}'}$	60.424	72.621	0.961	0.961	0.0	2.540	0.0	2.540	0.0	3.016
$\theta_{\text{O-Mn-Mn}}$	55.070	88.511	0.961	0.961	0.0	2.540	0.0	2.540	0.0	3.016

be seen that the transverse acoustic branch is close to the flexural branch, which should be due to the underestimation from the *ab initio* calculations. Fig. 29 (b) shows that the VFF model and the SW potential give exactly the same phonon dispersion, as the SW potential is derived from the VFF model.

The parameters for the two-body SW potential used by GULP are shown in Tab. LXIII. The parameters for the three-body SW potential used by GULP are shown in Tab. LXIV. Some representative parameters for the SW potential used by LAMMPS are listed in Tab. LXV. We note that twelve atom types have been introduced for the simulation of the single-layer 1H-MnO₂ using LAMMPS, because the angles around atom Mn in Fig. 1

TABLE LXV: SW potential parameters for single-layer 1H-MnO₂ used by LAMMPS⁹ as expressed in Eqs. (9) and (10).

	ϵ (eV)	σ (Å)	a	λ	γ	$\cos \theta_0$	A_L	B_L	p	q	tol
Mn ₁ -O ₁ -O ₁	1.000	0.961	2.643	0.000	1.000	0.000	4.721	7.158	4	0	0.0
Mn ₁ -O ₁ -O ₃	1.000	0.000	0.000	55.070	1.000	0.026	0.000	0.000	4	0	0.0
Mn ₁ -O ₁ -O ₂	1.000	0.000	0.000	60.424	1.000	0.299	0.000	0.000	4	0	0.0
O ₁ -Mn ₁ -Mn ₃	1.000	0.000	0.000	55.070	1.000	0.026	0.000	0.000	4	0	0.0

(with $M=\text{Mn}$ and $X=\text{O}$) are not distinguishable in LAMMPS. We have suggested two options to differentiate these angles by implementing some additional constraints in LAMMPS, which can be accomplished by modifying the source file of LAMMPS.^{13,14} According to our experience, it is not so convenient for some users to implement these constraints and re-compile the LAMMPS package. Hence, in the present work, we differentiate the angles by introducing more atom types, so it is not necessary to modify the LAMMPS package. Fig. 2 (with $M=\text{Mn}$ and $X=\text{O}$) shows that, for 1H-MnO₂, we can differentiate these angles around the Mn atom by assigning these six neighboring O atoms with different atom types. It can be found that twelve atom types are necessary for the purpose of differentiating all six neighbors around one Mn atom.

We use LAMMPS to perform MD simulations for the mechanical behavior of the single-layer 1H-MnO₂ under uniaxial tension at 1.0 K and 300.0 K. Fig. 30 shows the stress-strain curve for the tension of a single-layer 1H-MnO₂ of dimension $100 \times 100 \text{ \AA}$. Periodic boundary conditions are applied in both armchair and zigzag directions. The single-layer 1H-MnO₂ is stretched uniaxially along the armchair or zigzag direction. The stress is calculated without involving the actual thickness of the quasi-two-dimensional structure of the single-layer 1H-MnO₂. The Young's modulus can be obtained by a linear fitting of the stress-strain relation in the small strain range of $[0, 0.01]$. The Young's modulus are 161.1 N/m and 160.2 N/m along the armchair and zigzag directions, respectively. The Young's modulus is essentially isotropic in the armchair and zigzag directions. The Poisson's ratio from the VFF model and the SW potential is $\nu_{xy} = \nu_{yx} = 0.10$.

There is no available value for nonlinear quantities in the single-layer 1H-MnO₂. We have thus used the nonlinear parameter $B = 0.5d^4$ in Eq. (5), which is close to the value of B in most materials. The value of the third order nonlinear elasticity D can be extracted by fitting the stress-strain relation to the function $\sigma = E\epsilon + \frac{1}{2}D\epsilon^2$ with E as the Young's modulus. The values of D from the present SW potential are -915.9 N/m and -957.1 N/m along the armchair and zigzag directions, respectively. The ultimate stress is about 14.1 Nm^{-1} at the ultimate strain of 0.17 in the armchair direction at the low temperature of 1 K. The ultimate stress is about 13.7 Nm^{-1} at the ultimate strain of 0.20 in the zigzag direction at the low temperature of 1 K.

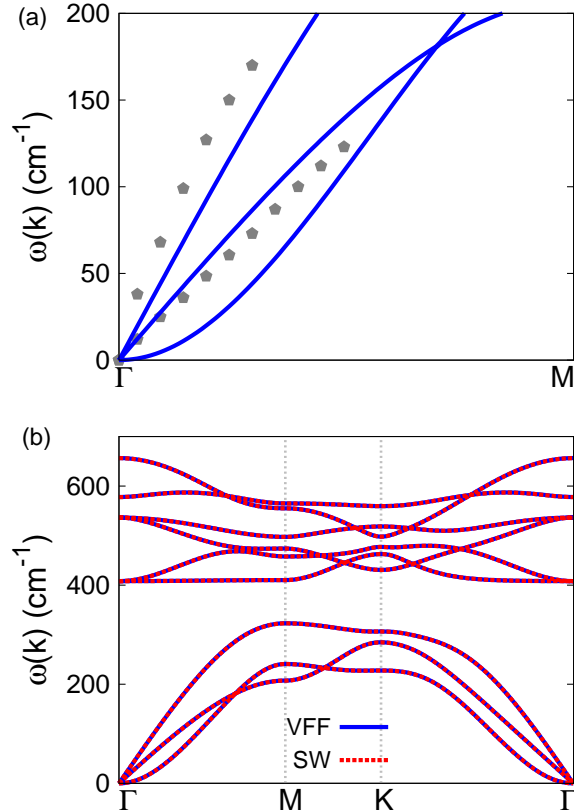


FIG. 31: (Color online) Phonon spectrum for single-layer 1H-FeO₂. (a) Phonon dispersion along the Γ M direction in the Brillouin zone. The results from the VFF model (lines) are comparable with the *ab initio* results (pentagons) from Ref. 12. (b) The phonon dispersion from the SW potential is exactly the same as that from the VFF model.

XVII. 1H-FEO₂

Most existing theoretical studies on the single-layer 1H-FeO₂ are based on the first-principles calculations. In this section, we will develop the SW potential for the single-layer 1H-FeO₂.

The structure for the single-layer 1H-FeO₂ is shown in Fig. 1 (with M=Fe and X=O). Each Fe atom is surrounded by six O atoms. These O atoms are categorized into the top group (eg. atoms 1, 3, and 5) and bottom group (eg. atoms 2, 4, and 6). Each O atom is connected to three Fe atoms. The structural parameters are from the first-principles calculations,¹² including the lattice constant $a = 2.62 \text{ \AA}$, and the bond length $d_{\text{Fe-O}} = 1.88 \text{ \AA}$. The resultant

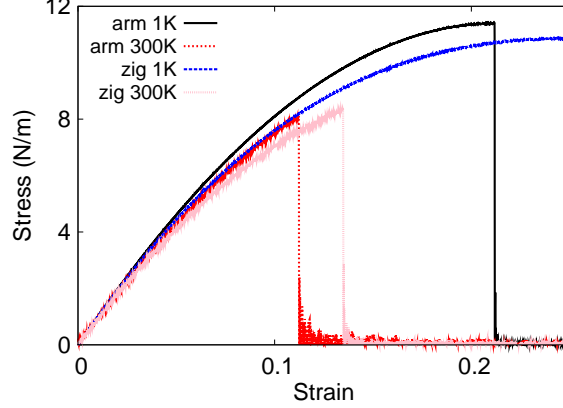


FIG. 32: (Color online) Stress-strain for single-layer 1H-FeO₂ of dimension 100 × 100 Å along the armchair and zigzag directions.

TABLE LXVI: The VFF model for single-layer 1H-FeO₂. The second line gives an explicit expression for each VFF term. The third line is the force constant parameters. Parameters are in the unit of $\frac{eV}{\text{Å}^2}$ for the bond stretching interactions, and in the unit of eV for the angle bending interaction. The fourth line gives the initial bond length (in unit of Å) for the bond stretching interaction and the initial angle (in unit of degrees) for the angle bending interaction. The angle θ_{ijk} has atom *i* as the apex.

VFF type	bond stretching	angle bending		
expression	$\frac{1}{2}K_{\text{Fe-O}}(\Delta r)^2$	$\frac{1}{2}K_{\text{Fe-O-O}}(\Delta\theta)^2$	$\frac{1}{2}K_{\text{Fe-O-O}'}(\Delta\theta)^2$	$\frac{1}{2}K_{\text{O-Fe-Fe}}(\Delta\theta)^2$
parameter	8.377	3.213	3.213	3.213
r_0 or θ_0	1.880	88.343	72.856	88.343

angles are $\theta_{\text{FeOO}} = \theta_{\text{OFeFe}} = 88.343^\circ$ and $\theta_{\text{FeOO}'} = 72.856^\circ$, in which atoms O and O' are from different (top or bottom) group.

Table LXVI shows four VFF terms for the single-layer 1H-FeO₂, one of which is the bond stretching interaction shown by Eq. (1) while the other three terms are the angle bending interaction shown by Eq. (2). These force constant parameters are determined by fitting to the three acoustic branches in the phonon dispersion along the ΓM as shown in Fig. 31 (a). The *ab initio* calculations for the phonon dispersion are from Ref. 12. Fig. 31 (b) shows that the VFF model and the SW potential give exactly the same phonon dispersion, as the SW

TABLE LXVII: Two-body SW potential parameters for single-layer 1H-FeO₂ used by GULP⁸ as expressed in Eq. (3).

	A (eV)	ρ (Å)	B (Å ⁴)	r_{\min} (Å)	r_{\max} (Å)
Fe-O	4.242	0.962	6.246	0.0	2.552

TABLE LXVIII: Three-body SW potential parameters for single-layer 1H-FeO₂ used by GULP⁸ as expressed in Eq. (4). The angle θ_{ijk} in the first line indicates the bending energy for the angle with atom i as the apex.

	K (eV)	θ_0 (degree)	ρ_1 (Å)	ρ_2 (Å)	$r_{\min12}$ (Å)	$r_{\max12}$ (Å)	$r_{\min13}$ (Å)	$r_{\max13}$ (Å)	$r_{\min23}$ (Å)	$r_{\max23}$ (Å)
$\theta_{\text{Fe-O-O}}$	28.105	88.343	0.962	0.962	0.0	2.552	0.0	2.552	0.0	3.031
$\theta_{\text{Fe-O-O}'}$	30.754	72.856	0.962	0.962	0.0	2.552	0.0	2.552	0.0	3.031
$\theta_{\text{O-Fe-Fe}}$	28.105	88.343	0.962	0.962	0.0	2.552	0.0	2.552	0.0	3.031

potential is derived from the VFF model.

The parameters for the two-body SW potential used by GULP are shown in Tab. LXVII. The parameters for the three-body SW potential used by GULP are shown in Tab. LXVIII. Some representative parameters for the SW potential used by LAMMPS are listed in Tab. LXIX. We note that twelve atom types have been introduced for the simulation of the single-layer 1H-FeO₂ using LAMMPS, because the angles around atom Fe in Fig. 1 (with M=Fe and X=O) are not distinguishable in LAMMPS. We have suggested two options to differentiate these angles by implementing some additional constraints in LAMMPS, which can be accomplished by modifying the source file of LAMMPS.^{13,14} According to our experi-

TABLE LXIX: SW potential parameters for single-layer 1H-FeO₂ used by LAMMPS⁹ as expressed in Eqs. (9) and (10).

	ϵ (eV)	σ (Å)	a	λ	γ	$\cos \theta_0$	A_L	B_L	p	q	tol
Fe ₁ -O ₁ -O ₁	1.000	0.962	2.654	0.000	1.000	0.000	4.242	7.298	4	0	0.0
Fe ₁ -O ₁ -O ₃	1.000	0.000	0.000	28.105	1.000	0.029	0.000	0.000	4	0	0.0
Fe ₁ -O ₁ -O ₂	1.000	0.000	0.000	30.754	1.000	0.295	0.000	0.000	4	0	0.0
O ₁ -Fe ₁ -Fe ₃	1.000	0.000	0.000	28.105	1.000	0.029	0.000	0.000	4	0	0.0

ence, it is not so convenient for some users to implement these constraints and recompile the LAMMPS package. Hence, in the present work, we differentiate the angles by introducing more atom types, so it is not necessary to modify the LAMMPS package. Fig. 2 (with M=Fe and X=O) shows that, for 1H-FeO₂, we can differentiate these angles around the Fe atom by assigning these six neighboring O atoms with different atom types. It can be found that twelve atom types are necessary for the purpose of differentiating all six neighbors around one Fe atom.

We use LAMMPS to perform MD simulations for the mechanical behavior of the single-layer 1H-FeO₂ under uniaxial tension at 1.0 K and 300.0 K. Fig. 32 shows the stress-strain curve for the tension of a single-layer 1H-FeO₂ of dimension 100 × 100 Å. Periodic boundary conditions are applied in both armchair and zigzag directions. The single-layer 1H-FeO₂ is stretched uniaxially along the armchair or zigzag direction. The stress is calculated without involving the actual thickness of the quasi-two-dimensional structure of the single-layer 1H-FeO₂. The Young's modulus can be obtained by a linear fitting of the stress-strain relation in the small strain range of [0, 0.01]. The Young's modulus are 100.2 N/m and 99.3 N/m along the armchair and zigzag directions, respectively. The Young's modulus is essentially isotropic in the armchair and zigzag directions. The Poisson's ratio from the VFF model and the SW potential is $\nu_{xy} = \nu_{yx} = 0.23$.

There is no available value for nonlinear quantities in the single-layer 1H-FeO₂. We have thus used the nonlinear parameter $B = 0.5d^4$ in Eq. (5), which is close to the value of B in most materials. The value of the third order nonlinear elasticity D can be extracted by fitting the stress-strain relation to the function $\sigma = E\epsilon + \frac{1}{2}D\epsilon^2$ with E as the Young's modulus. The values of D from the present SW potential are -423.4 N/m and -460.2 N/m along the armchair and zigzag directions, respectively. The ultimate stress is about 11.4 Nm⁻¹ at the ultimate strain of 0.21 in the armchair direction at the low temperature of 1 K. The ultimate stress is about 10.9 Nm⁻¹ at the ultimate strain of 0.25 in the zigzag direction at the low temperature of 1 K.

XVIII. 1H-FES₂

Most existing theoretical studies on the single-layer 1H-FeS₂ are based on the first-principles calculations. In this section, we will develop the SW potential for the single-layer

TABLE LXX: The VFF model for single-layer 1H-FeS₂. The second line gives an explicit expression for each VFF term. The third line is the force constant parameters. Parameters are in the unit of $\frac{\text{eV}}{\text{\AA}^2}$ for the bond stretching interactions, and in the unit of eV for the angle bending interaction. The fourth line gives the initial bond length (in unit of \AA) for the bond stretching interaction and the initial angle (in unit of degrees) for the angle bending interaction. The angle θ_{ijk} has atom i as the apex.

VFF type	bond stretching		angle bending	
expression	$\frac{1}{2}K_{\text{Fe-S}}(\Delta r)^2$	$\frac{1}{2}K_{\text{Fe-S-S}}(\Delta\theta)^2$	$\frac{1}{2}K_{\text{Fe-S-S'}}(\Delta\theta)^2$	$\frac{1}{2}K_{\text{S-Fe-Fe}}(\Delta\theta)^2$
parameter	6.338	3.964	3.964	3.964
r_0 or θ_0	2.220	87.132	74.537	87.132

TABLE LXXI: Two-body SW potential parameters for single-layer 1H-FeS₂ used by GULP⁸ as expressed in Eq. (3).

	A (eV)	ρ (\AA)	B (\AA^4)	r_{\min} (\AA)	r_{\max} (\AA)
Fe-S	4.337	1.097	12.145	0.0	3.000

TABLE LXXII: Three-body SW potential parameters for single-layer 1H-FeS₂ used by GULP⁸ as expressed in Eq. (4). The angle θ_{ijk} in the first line indicates the bending energy for the angle with atom i as the apex.

	K (eV)	θ_0 (degree)	ρ_1 (\AA)	ρ_2 (\AA)	$r_{\min12}$ (\AA)	$r_{\max12}$ (\AA)	$r_{\min13}$ (\AA)	$r_{\max13}$ (\AA)	$r_{\min23}$ (\AA)	$r_{\max23}$ (\AA)
$\theta_{\text{Fe-S-S}}$	33.060	87.132	1.097	1.097	0.0	3.000	0.0	3.000	0.0	3.567
$\theta_{\text{Fe-S-S'}}$	35.501	74.537	1.097	1.097	0.0	3.000	0.0	3.000	0.0	3.567
$\theta_{\text{S-Fe-Fe}}$	33.060	87.132	1.097	1.097	0.0	3.000	0.0	3.000	0.0	3.567

TABLE LXXIII: SW potential parameters for single-layer 1H-FeS₂ used by LAMMPS⁹ as expressed in Eqs. (9) and (10).

	ϵ (eV)	σ (\AA)	a	λ	γ	$\cos\theta_0$	A_L	B_L	p	q	tol
Fe ₁ -S ₁ -S ₁	1.000	1.097	2.735	0.000	1.000	0.000	4.337	8.338	4	0	0.0
Fe ₁ -S ₁ -S ₃	1.000	0.000	0.000	33.060	1.000	0.050	0.000	0.000	4	0	0.0
Fe ₁ -S ₁ -S ₂	1.000	0.000	0.000	35.501	1.000	0.267	0.000	0.000	4	0	0.0
S ₁ -Fe ₁ -Fe ₃	1.000	0.000	0.000	33.060	1.000	0.050	0.000	0.000	4	0	0.0

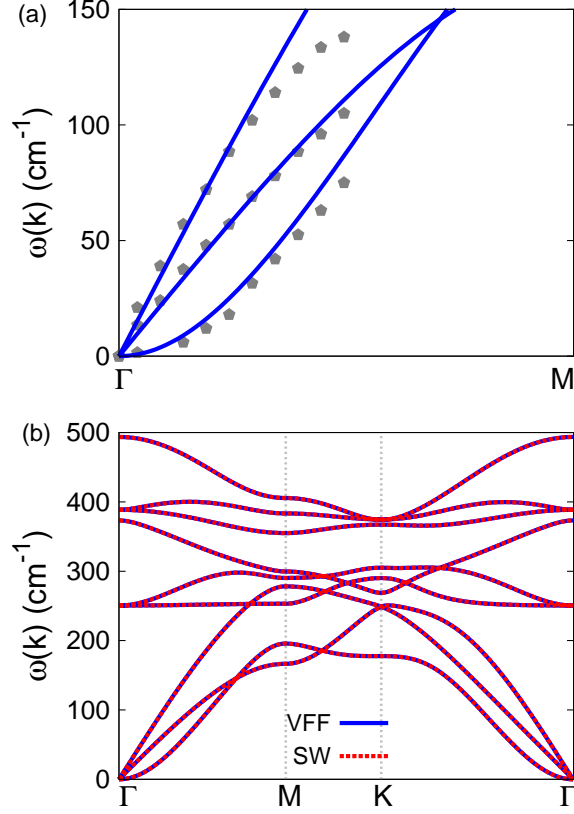


FIG. 33: (Color online) Phonon spectrum for single-layer 1H-FeS₂. (a) Phonon dispersion along the Γ M direction in the Brillouin zone. The results from the VFF model (lines) are comparable with the *ab initio* results (pentagons) from Ref. 12. (b) The phonon dispersion from the SW potential is exactly the same as that from the VFF model.

1H-FeS₂.

The structure for the single-layer 1H-FeS₂ is shown in Fig. 1 (with M=Fe and X=S). Each Fe atom is surrounded by six S atoms. These S atoms are categorized into the top group (eg. atoms 1, 3, and 5) and bottom group (eg. atoms 2, 4, and 6). Each S atom is connected to three Fe atoms. The structural parameters are from the first-principles calculations,¹² including the lattice constant $a = 3.06 \text{ \AA}$, and the bond length $d_{\text{Fe-S}} = 2.22 \text{ \AA}$. The resultant angles are $\theta_{\text{FeSS}} = \theta_{\text{SFeFe}} = 87.132^\circ$ and $\theta_{\text{FeSS}'} = 74.537^\circ$, in which atoms S and S' are from different (top or bottom) group.

Table LXX shows four VFF terms for the single-layer 1H-FeS₂, one of which is the bond stretching interaction shown by Eq. (1) while the other three terms are the angle bending

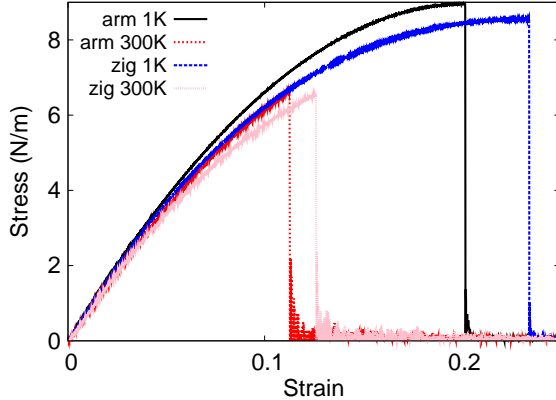


FIG. 34: (Color online) Stress-strain for single-layer 1H-FeS₂ of dimension $100 \times 100 \text{ \AA}$ along the armchair and zigzag directions.

interaction shown by Eq. (2). These force constant parameters are determined by fitting to the three acoustic branches in the phonon dispersion along the ΓM as shown in Fig. 33 (a). The *ab initio* calculations for the phonon dispersion are from Ref. 12. Fig. 33 (b) shows that the VFF model and the SW potential give exactly the same phonon dispersion, as the SW potential is derived from the VFF model.

The parameters for the two-body SW potential used by GULP are shown in Tab. LXXI. The parameters for the three-body SW potential used by GULP are shown in Tab. LXXII. Some representative parameters for the SW potential used by LAMMPS are listed in Tab. LXXIII. We note that twelve atom types have been introduced for the simulation of the single-layer 1H-FeS₂ using LAMMPS, because the angles around atom Fe in Fig. 1 (with M=Fe and X=S) are not distinguishable in LAMMPS. We have suggested two options to differentiate these angles by implementing some additional constraints in LAMMPS, which can be accomplished by modifying the source file of LAMMPS.^{13,14} According to our experience, it is not so convenient for some users to implement these constraints and recompile the LAMMPS package. Hence, in the present work, we differentiate the angles by introducing more atom types, so it is not necessary to modify the LAMMPS package. Fig. 2 (with M=Fe and X=S) shows that, for 1H-FeS₂, we can differentiate these angles around the Fe atom by assigning these six neighboring S atoms with different atom types. It can be found that twelve atom types are necessary for the purpose of differentiating all six neighbors around one Fe atom.

We use LAMMPS to perform MD simulations for the mechanical behavior of the single-layer 1H-FeS₂ under uniaxial tension at 1.0 K and 300.0 K. Fig. 34 shows the stress-strain curve for the tension of a single-layer 1H-FeS₂ of dimension 100 × 100 Å. Periodic boundary conditions are applied in both armchair and zigzag directions. The single-layer 1H-FeS₂ is stretched uniaxially along the armchair or zigzag direction. The stress is calculated without involving the actual thickness of the quasi-two-dimensional structure of the single-layer 1H-FeS₂. The Young's modulus can be obtained by a linear fitting of the stress-strain relation in the small strain range of [0, 0.01]. The Young's modulus are 83.6 N/m and 83.4 N/m along the armchair and zigzag directions, respectively. The Young's modulus is essentially isotropic in the armchair and zigzag directions. The Poisson's ratio from the VFF model and the SW potential is $\nu_{xy} = \nu_{yx} = 0.20$.

There is no available value for nonlinear quantities in the single-layer 1H-FeS₂. We have thus used the nonlinear parameter $B = 0.5d^4$ in Eq. (5), which is close to the value of B in most materials. The value of the third order nonlinear elasticity D can be extracted by fitting the stress-strain relation to the function $\sigma = E\epsilon + \frac{1}{2}D\epsilon^2$ with E as the Young's modulus. The values of D from the present SW potential are -377.5 N/m and -412.7 N/m along the armchair and zigzag directions, respectively. The ultimate stress is about 9.0 Nm⁻¹ at the ultimate strain of 0.20 in the armchair direction at the low temperature of 1 K. The ultimate stress is about 8.6 Nm⁻¹ at the ultimate strain of 0.23 in the zigzag direction at the low temperature of 1 K.

XIX. 1H-FESE₂

Most existing theoretical studies on the single-layer 1H-FeSe₂ are based on the first-principles calculations. In this section, we will develop the SW potential for the single-layer 1H-FeSe₂.

The structure for the single-layer 1H-FeSe₂ is shown in Fig. 1 (with M=Fe and X=Se). Each Fe atom is surrounded by six Se atoms. These Se atoms are categorized into the top group (eg. atoms 1, 3, and 5) and bottom group (eg. atoms 2, 4, and 6). Each Se atom is connected to three Fe atoms. The structural parameters are from the first-principles calculations,¹² including the lattice constant $a = 3.22$ Å, and the bond length $d_{\text{Fe-Se}} = 2.35$ Å. The resultant angles are $\theta_{\text{FeSeSe}} = \theta_{\text{SeFeFe}} = 86.488^\circ$ and $\theta_{\text{FeSeSe}'} = 75.424^\circ$,

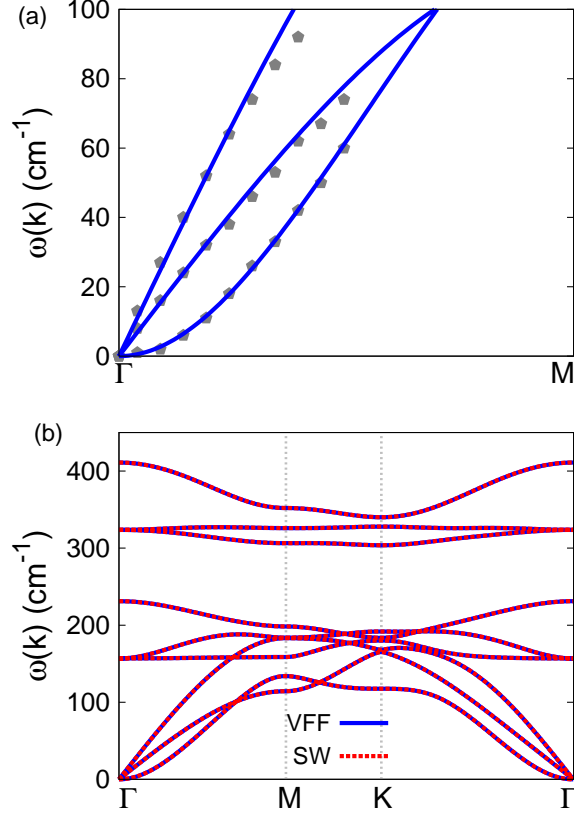


FIG. 35: (Color online) Phonon spectrum for single-layer 1H-FeSe₂. (a) Phonon dispersion along the Γ M direction in the Brillouin zone. The results from the VFF model (lines) are comparable with the *ab initio* results (pentagons) from Ref. 12. (b) The phonon dispersion from the SW potential is exactly the same as that from the VFF model.

in which atoms Se and Se' are from different (top or bottom) group.

Table LXXIV shows four VFF terms for the single-layer 1H-FeSe₂, one of which is the bond stretching interaction shown by Eq. (1) while the other three terms are the angle bending interaction shown by Eq. (2). These force constant parameters are determined by fitting to the three acoustic branches in the phonon dispersion along the Γ M as shown in Fig. 35 (a). The *ab initio* calculations for the phonon dispersion are from Ref. 12. Fig. 35 (b) shows that the VFF model and the SW potential give exactly the same phonon dispersion, as the SW potential is derived from the VFF model.

The parameters for the two-body SW potential used by GULP are shown in Tab. LXXV. The parameters for the three-body SW potential used by GULP are shown in Tab. LXXVI.

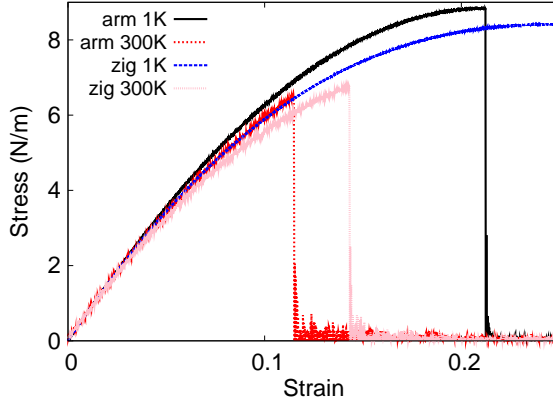


FIG. 36: (Color online) Stress-strain for single-layer 1H-FeSe₂ of dimension $100 \times 100 \text{ \AA}$ along the armchair and zigzag directions.

TABLE LXXIV: The VFF model for single-layer 1H-FeSe₂. The second line gives an explicit expression for each VFF term. The third line is the force constant parameters. Parameters are in the unit of $\frac{eV}{\text{Å}^2}$ for the bond stretching interactions, and in the unit of eV for the angle bending interaction. The fourth line gives the initial bond length (in unit of Å) for the bond stretching interaction and the initial angle (in unit of degrees) for the angle bending interaction. The angle θ_{ijk} has atom *i* as the apex.

VFF type	bond stretching	angle bending		
expression	$\frac{1}{2}K_{\text{Fe-Se}}(\Delta r)^2$	$\frac{1}{2}K_{\text{Fe-Se-Se}}(\Delta\theta)^2$	$\frac{1}{2}K_{\text{Fe-Se-Se'}}(\Delta\theta)^2$	$\frac{1}{2}K_{\text{Se-Fe-Fe}}(\Delta\theta)^2$
parameter	6.338	3.964	3.964	3.964
r_0 or θ_0	2.350	86.488	75.424	86.488

Some representative parameters for the SW potential used by LAMMPS are listed in Tab. LXXVII. We note that twelve atom types have been introduced for the simulation of the single-layer 1H-FeSe₂ using LAMMPS, because the angles around atom Fe in Fig. 1 (with M=Fe and X=Se) are not distinguishable in LAMMPS. We have suggested two options to differentiate these angles by implementing some additional constraints in LAMMPS, which can be accomplished by modifying the source file of LAMMPS.^{13,14} According to our experience, it is not so convenient for some users to implement these constraints and recompile the LAMMPS package. Hence, in the present work, we differentiate the angles

TABLE LXXV: Two-body SW potential parameters for single-layer 1H-FeSe₂ used by GULP⁸ as expressed in Eq. (3).

	A (eV)	ρ (Å)	B (Å ⁴)	r_{\min} (Å)	r_{\max} (Å)
Fe-Se	4.778	1.139	15.249	0.0	3.168

TABLE LXXVI: Three-body SW potential parameters for single-layer 1H-FeSe₂ used by GULP⁸ as expressed in Eq. (4). The angle θ_{ijk} in the first line indicates the bending energy for the angle with atom i as the apex.

	K (eV)	θ_0 (degree)	ρ_1 (Å)	ρ_2 (Å)	$r_{\min12}$ (Å)	$r_{\max12}$ (Å)	$r_{\min13}$ (Å)	$r_{\max13}$ (Å)	$r_{\min23}$ (Å)	$r_{\max23}$ (Å)
$\theta_{\text{Fe-Se-Se}}$	32.235	86.488	1.139	1.139	0.0	3.168	0.0	3.168	0.0	3.768
$\theta_{\text{Fe-Se-Se}'}$	34.286	75.424	1.139	1.139	0.0	3.168	0.0	3.168	0.0	3.768
$\theta_{\text{Se-Fe-Fe}}$	32.235	86.488	1.139	1.139	0.0	3.168	0.0	3.168	0.0	3.768

by introducing more atom types, so it is not necessary to modify the LAMMPS package. Fig. 2 (with M=Fe and X=Se) shows that, for 1H-FeSe₂, we can differentiate these angles around the Fe atom by assigning these six neighboring Se atoms with different atom types. It can be found that twelve atom types are necessary for the purpose of differentiating all six neighbors around one Fe atom.

We use LAMMPS to perform MD simulations for the mechanical behavior of the single-layer 1H-FeSe₂ under uniaxial tension at 1.0 K and 300.0 K. Fig. 36 shows the stress-strain curve for the tension of a single-layer 1H-FeSe₂ of dimension 100 × 100 Å. Periodic boundary conditions are applied in both armchair and zigzag directions. The single-layer 1H-FeSe₂ is

TABLE LXXVII: SW potential parameters for single-layer 1H-FeSe₂ used by LAMMPS⁹ as expressed in Eqs. (9) and (10).

	ϵ (eV)	σ (Å)	a	λ	γ	$\cos \theta_0$	A_L	B_L	p	q	tol
Fe ₁ -Se ₁ -Se ₁	1.000	1.139	2.781	0.000	1.000	0.000	4.778	9.049	4	0	0.0
Fe ₁ -Se ₁ -Se ₃	1.000	0.000	0.000	32.235	1.000	0.061	0.000	0.000	4	0	0.0
Fe ₁ -Se ₁ -Se ₂	1.000	0.000	0.000	34.286	1.000	0.252	0.000	0.000	4	0	0.0
Se ₁ -Fe ₁ -Fe ₃	1.000	0.000	0.000	32.235	1.000	0.061	0.000	0.000	4	0	0.0

TABLE LXXVIII: The VFF model for single-layer 1H-FeTe₂. The second line gives an explicit expression for each VFF term. The third line is the force constant parameters. Parameters are in the unit of $\frac{\text{eV}}{\text{\AA}^2}$ for the bond stretching interactions, and in the unit of eV for the angle bending interaction. The fourth line gives the initial bond length (in unit of \AA) for the bond stretching interaction and the initial angle (in unit of degrees) for the angle bending interaction. The angle θ_{ijk} has atom i as the apex.

VFF type	bond stretching		angle bending	
expression	$\frac{1}{2}K_{\text{Fe-Te}}(\Delta r)^2$	$\frac{1}{2}K_{\text{Fe-Te-Te}}(\Delta\theta)^2$	$\frac{1}{2}K_{\text{Fe-Te-Te}'}(\Delta\theta)^2$	$\frac{1}{2}K_{\text{Te-Fe-Fe}}(\Delta\theta)^2$
parameter	6.338	3.964	3.964	3.964
r_0 or θ_0	2.530	86.904	74.851	86.904

stretched uniaxially along the armchair or zigzag direction. The stress is calculated without involving the actual thickness of the quasi-two-dimensional structure of the single-layer 1H-FeSe₂. The Young's modulus can be obtained by a linear fitting of the stress-strain relation in the small strain range of [0, 0.01]. The Young's modulus are 77.3 N/m and 77.4 N/m along the armchair and zigzag directions, respectively. The Young's modulus is essentially isotropic in the armchair and zigzag directions. The Poisson's ratio from the VFF model and the SW potential is $\nu_{xy} = \nu_{yx} = 0.23$.

There is no available value for nonlinear quantities in the single-layer 1H-FeSe₂. We have thus used the nonlinear parameter $B = 0.5d^4$ in Eq. (5), which is close to the value of B in most materials. The value of the third order nonlinear elasticity D can be extracted by fitting the stress-strain relation to the function $\sigma = E\epsilon + \frac{1}{2}D\epsilon^2$ with E as the Young's modulus. The values of D from the present SW potential are -323.8 N/m and -360.8 N/m along the armchair and zigzag directions, respectively. The ultimate stress is about 8.8 Nm⁻¹ at the ultimate strain of 0.21 in the armchair direction at the low temperature of 1 K. The ultimate stress is about 8.4 Nm⁻¹ at the ultimate strain of 0.25 in the zigzag direction at the low temperature of 1 K.

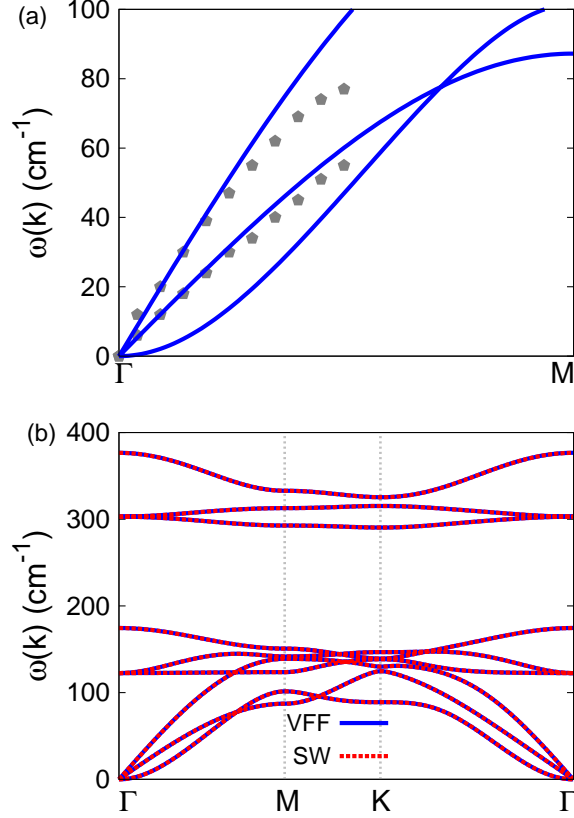


FIG. 37: (Color online) Phonon spectrum for single-layer 1H-FeTe₂. (a) Phonon dispersion along the Γ M direction in the Brillouin zone. The results from the VFF model (lines) are comparable with the *ab initio* results (pentagons) from Ref. 12. (b) The phonon dispersion from the SW potential is exactly the same as that from the VFF model.

TABLE LXXIX: Two-body SW potential parameters for single-layer 1H-FeTe₂ used by GULP⁸ as expressed in Eq. (3).

	A (eV)	ρ (\AA)	B (\AA^4)	r_{\min} (\AA)	r_{\max} (\AA)
Fe-Te	5.599	1.242	20.486	0.0	3.416

XX. 1H-FETE₂

Most existing theoretical studies on the single-layer 1H-FeTe₂ are based on the first-principles calculations. In this section, we will develop the SW potential for the single-layer 1H-FeTe₂.

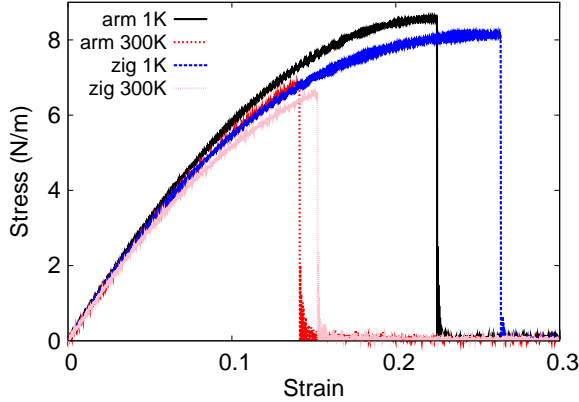


FIG. 38: (Color online) Stress-strain for single-layer 1H-FeTe₂ of dimension $100 \times 100 \text{ \AA}$ along the armchair and zigzag directions.

TABLE LXXX: Three-body SW potential parameters for single-layer 1H-FeTe₂ used by GULP⁸ as expressed in Eq. (4). The angle θ_{ijk} in the first line indicates the bending energy for the angle with atom i as the apex.

	K (eV)	θ_0 (degree)	ρ_1 (Å)	ρ_2 (Å)	$r_{\min 12}$ (Å)	$r_{\max 12}$ (Å)	$r_{\min 13}$ (Å)	$r_{\max 13}$ (Å)	$r_{\min 23}$ (Å)	$r_{\max 23}$ (Å)
$\theta_{\text{Fe}-\text{Te}-\text{Te}}$	32.766	86.904	1.242	1.242	0.0	3.416	0.0	3.416	0.0	4.062
$\theta_{\text{Fe}-\text{Te}-\text{Te}'}$	35.065	74.851	1.242	1.242	0.0	3.416	0.0	3.416	0.0	4.062
$\theta_{\text{Te}-\text{Fe}-\text{Fe}}$	32.766	86.904	1.242	1.242	0.0	3.416	0.0	3.416	0.0	4.062

The structure for the single-layer 1H-FeTe₂ is shown in Fig. 1 (with M=Fe and X=Te). Each Fe atom is surrounded by six Te atoms. These Te atoms are categorized into the top group (eg. atoms 1, 3, and 5) and bottom group (eg. atoms 2, 4, and 6). Each Te atom is connected to three Fe atoms. The structural parameters are from the first-principles calculations,¹² including the lattice constant $a = 3.48 \text{ \AA}$, and the bond length $d_{\text{Fe}-\text{Te}} = 2.53 \text{ \AA}$. The resultant angles are $\theta_{\text{FeTeTe}} = \theta_{\text{TeFeFe}} = 86.904^\circ$ and $\theta_{\text{FeTeTe}'}$ = 74.851° , in which atoms Te and Te' are from different (top or bottom) group.

Table LXXVIII shows four VFF terms for the single-layer 1H-FeTe₂, one of which is the bond stretching interaction shown by Eq. (1) while the other three terms are the angle bending interaction shown by Eq. (2). These force constant parameters are determined by fitting to the two in-plane acoustic branches in the phonon dispersion along the ΓM as shown in Fig. 37 (a). The *ab initio* calculations for the phonon dispersion are from Ref. 12.

TABLE LXXXI: SW potential parameters for single-layer 1H-FeTe₂ used by LAMMPS⁹ as expressed in Eqs. (9) and (10).

	ϵ (eV)	σ (Å)	a	λ	γ	$\cos \theta_0$	A_L	B_L	p	q	tol
Fe ₁ -Te ₁ -Te ₁	1.000	1.242	2.751	0.000	1.000	0.000	5.599	8.615	4	0	0.0
Fe ₁ -Te ₁ -Te ₃	1.000	0.000	0.000	32.766	1.000	0.054	0.000	0.000	4	0	0.0
Fe ₁ -Te ₁ -Te ₂	1.000	0.000	0.000	35.065	1.000	0.261	0.000	0.000	4	0	0.0
Te ₁ -Fe ₁ -Fe ₃	1.000	0.000	0.000	32.766	1.000	0.054	0.000	0.000	4	0	0.0

Fig. 37 (b) shows that the VFF model and the SW potential give exactly the same phonon dispersion, as the SW potential is derived from the VFF model.

The parameters for the two-body SW potential used by GULP are shown in Tab. LXXIX. The parameters for the three-body SW potential used by GULP are shown in Tab. LXXX. Some representative parameters for the SW potential used by LAMMPS are listed in Tab. LXXXI. We note that twelve atom types have been introduced for the simulation of the single-layer 1H-FeTe₂ using LAMMPS, because the angles around atom Fe in Fig. 1 (with M=Fe and X=Te) are not distinguishable in LAMMPS. We have suggested two options to differentiate these angles by implementing some additional constraints in LAMMPS, which can be accomplished by modifying the source file of LAMMPS.^{13,14} According to our experience, it is not so convenient for some users to implement these constraints and re-compile the LAMMPS package. Hence, in the present work, we differentiate the angles by introducing more atom types, so it is not necessary to modify the LAMMPS package. Fig. 2 (with M=Fe and X=Te) shows that, for 1H-FeTe₂, we can differentiate these angles around the Fe atom by assigning these six neighboring Te atoms with different atom types. It can be found that twelve atom types are necessary for the purpose of differentiating all six neighbors around one Fe atom.

We use LAMMPS to perform MD simulations for the mechanical behavior of the single-layer 1H-FeTe₂ under uniaxial tension at 1.0 K and 300.0 K. Fig. 38 shows the stress-strain curve for the tension of a single-layer 1H-FeTe₂ of dimension 100 × 100 Å. Periodic boundary conditions are applied in both armchair and zigzag directions. The single-layer 1H-FeTe₂ is stretched uniaxially along the armchair or zigzag direction. The stress is calculated without involving the actual thickness of the quasi-two-dimensional structure of the single-layer 1H-

TABLE LXXXII: The VFF model for single-layer 1H-CoTe₂. The second line gives an explicit expression for each VFF term. The third line is the force constant parameters. Parameters are in the unit of $\frac{\text{eV}}{\text{Å}^2}$ for the bond stretching interactions, and in the unit of eV for the angle bending interaction. The fourth line gives the initial bond length (in unit of Å) for the bond stretching interaction and the initial angle (in unit of degrees) for the angle bending interaction. The angle θ_{ijk} has atom i as the apex.

VFF type	bond stretching	angle bending		
expression	$\frac{1}{2}K_{\text{Co-Te}}(\Delta r)^2$	$\frac{1}{2}K_{\text{Co-Te-Te}}(\Delta\theta)^2$	$\frac{1}{2}K_{\text{Co-Te-Te}'}(\Delta\theta)^2$	$\frac{1}{2}K_{\text{Te-Co-Co}}(\Delta\theta)^2$
parameter	6.712	2.656	2.656	2.656
r_0 or θ_0	2.510	89.046	71.873	89.046

FeTe₂. The Young's modulus can be obtained by a linear fitting of the stress-strain relation in the small strain range of [0, 0.01]. The Young's modulus are 69.6 N/m and 69.8 N/m along the armchair and zigzag directions, respectively. The Young's modulus is essentially isotropic in the armchair and zigzag directions. The Poisson's ratio from the VFF model and the SW potential is $\nu_{xy} = \nu_{yx} = 0.25$.

There is no available value for nonlinear quantities in the single-layer 1H-FeTe₂. We have thus used the nonlinear parameter $B = 0.5d^4$ in Eq. (5), which is close to the value of B in most materials. The value of the third order nonlinear elasticity D can be extracted by fitting the stress-strain relation to the function $\sigma = E\epsilon + \frac{1}{2}D\epsilon^2$ with E as the Young's modulus. The values of D from the present SW potential are -267.5 N/m and -302.8 N/m along the armchair and zigzag directions, respectively. The ultimate stress is about 8.6 Nm⁻¹ at the ultimate strain of 0.22 in the armchair direction at the low temperature of 1 K. The ultimate stress is about 8.1 Nm⁻¹ at the ultimate strain of 0.26 in the zigzag direction at the low temperature of 1 K.

XXI. 1H-COTE₂

Most existing theoretical studies on the single-layer 1H-CoTe₂ are based on the first-principles calculations. In this section, we will develop the SW potential for the single-layer 1H-CoTe₂.

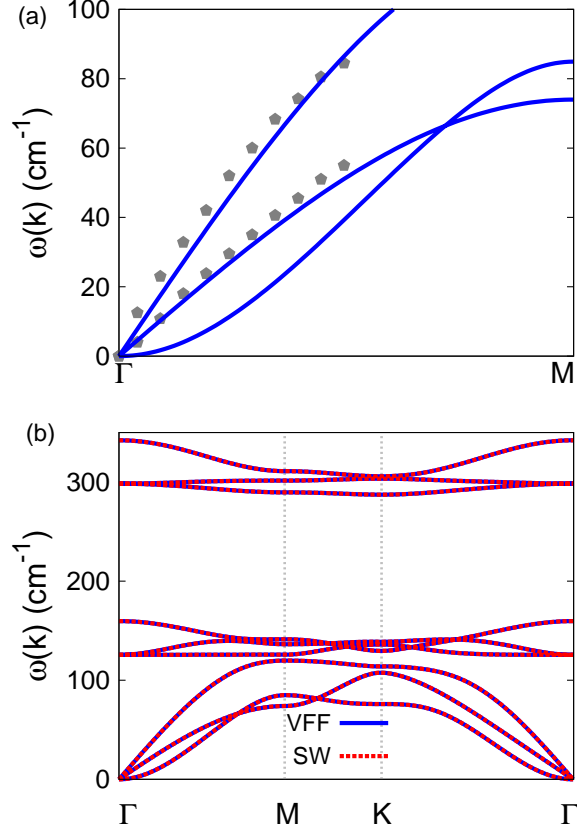


FIG. 39: (Color online) Phonon spectrum for single-layer 1H-CoTe₂. (a) Phonon dispersion along the Γ M direction in the Brillouin zone. The results from the VFF model (lines) are comparable with the *ab initio* results (pentagons) from Ref. 12. (b) The phonon dispersion from the SW potential is exactly the same as that from the VFF model.

TABLE LXXXIII: Two-body SW potential parameters for single-layer 1H-CoTe₂ used by GULP⁸ as expressed in Eq. (3).

	A (eV)	ρ (\AA)	B (\AA^4)	r_{\min} (\AA)	r_{\max} (\AA)
Co-Te	6.169	1.310	19.846	0.0	3.417

The structure for the single-layer 1H-CoTe₂ is shown in Fig. 1 (with M=Co and X=Te). Each Co atom is surrounded by six Te atoms. These Te atoms are categorized into the top group (eg. atoms 1, 3, and 5) and bottom group (eg. atoms 2, 4, and 6). Each Te atom is connected to three Co atoms. The structural parameters are from the first-principles calculations,¹² including the lattice constant $a = 3.52 \text{ \AA}$, and the bond length

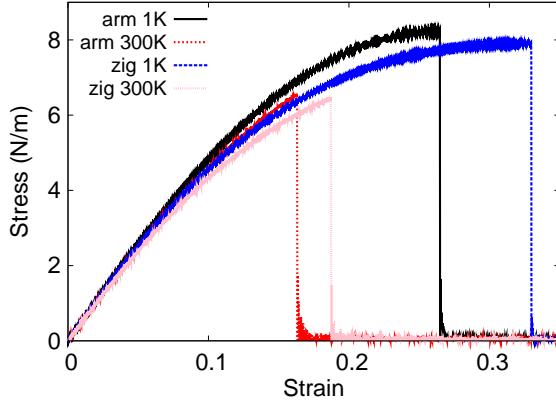


FIG. 40: (Color online) Stress-strain for single-layer 1H-CoTe₂ of dimension $100 \times 100 \text{ \AA}$ along the armchair and zigzag directions.

TABLE LXXXIV: Three-body SW potential parameters for single-layer 1H-CoTe₂ used by GULP⁸ as expressed in Eq. (4). The angle θ_{ijk} in the first line indicates the bending energy for the angle with atom i as the apex.

	K (eV)	θ_0 (degree)	ρ_1 (Å)	ρ_2 (Å)	$r_{\min 12}$ (Å)	$r_{\max 12}$ (Å)	$r_{\min 13}$ (Å)	$r_{\max 13}$ (Å)	$r_{\min 23}$ (Å)	$r_{\max 23}$ (Å)
$\theta_{\text{Co-Te-Te}}$	23.895	89.046	1.310	1.310	0.0	3.417	0.0	3.417	0.0	4.055
$\theta_{\text{Co-Te-Te}'}$	26.449	71.873	1.310	1.310	0.0	3.417	0.0	3.417	0.0	4.055
$\theta_{\text{Te-Co-Co}}$	23.895	89.046	1.310	1.310	0.0	3.417	0.0	3.417	0.0	4.055

$d_{\text{Co-Te}} = 2.51 \text{ \AA}$. The resultant angles are $\theta_{\text{CoTeTe}} = \theta_{\text{TeCoCo}} = 89.046^\circ$ and $\theta_{\text{CoTeTe}'} = 71.873^\circ$, in which atoms Te and Te' are from different (top or bottom) group.

Table LXXXII shows four VFF terms for the single-layer 1H-CoTe₂, one of which is the bond stretching interaction shown by Eq. (1) while the other three terms are the angle bending interaction shown by Eq. (2). These force constant parameters are determined by fitting to the acoustic branches in the phonon dispersion along the ΓM as shown in Fig. 39 (a). The *ab initio* calculations for the phonon dispersion are from Ref. 12. Fig. 39 (b) shows that the VFF model and the SW potential give exactly the same phonon dispersion, as the SW potential is derived from the VFF model.

The parameters for the two-body SW potential used by GULP are shown in Tab. LXXXIII. The parameters for the three-body SW potential used by GULP are shown in Tab. LXXXIV. Some representative parameters for the SW potential used by LAMMPS

TABLE LXXXV: SW potential parameters for single-layer 1H-CoTe₂ used by LAMMPS⁹ as expressed in Eqs. (9) and (10).

	ϵ (eV)	σ (Å)	a	λ	γ	$\cos \theta_0$	A_L	B_L	p	q	tol
Co ₁ -Te ₁ -Te ₁	1.000	1.310	2.608	0.000	1.000	0.000	6.169	6.739	4	0	0.0
Co ₁ -Te ₁ -Te ₃	1.000	0.000	0.000	23.895	1.000	0.017	0.000	0.000	4	0	0.0
Co ₁ -Te ₁ -Te ₂	1.000	0.000	0.000	26.449	1.000	0.311	0.000	0.000	4	0	0.0
Te ₁ -Co ₁ -Co ₃	1.000	0.000	0.000	23.895	1.000	0.017	0.000	0.000	4	0	0.0

are listed in Tab. LXXXV. We note that twelve atom types have been introduced for the simulation of the single-layer 1H-CoTe₂ using LAMMPS, because the angles around atom Co in Fig. 1 (with M=Co and X=Te) are not distinguishable in LAMMPS. We have suggested two options to differentiate these angles by implementing some additional constraints in LAMMPS, which can be accomplished by modifying the source file of LAMMPS.^{13,14} According to our experience, it is not so convenient for some users to implement these constraints and recompile the LAMMPS package. Hence, in the present work, we differentiate the angles by introducing more atom types, so it is not necessary to modify the LAMMPS package. Fig. 2 (with M=Co and X=Te) shows that, for 1H-CoTe₂, we can differentiate these angles around the Co atom by assigning these six neighboring Te atoms with different atom types. It can be found that twelve atom types are necessary for the purpose of differentiating all six neighbors around one Co atom.

We use LAMMPS to perform MD simulations for the mechanical behavior of the single-layer 1H-CoTe₂ under uniaxial tension at 1.0 K and 300.0 K. Fig. 40 shows the stress-strain curve for the tension of a single-layer 1H-CoTe₂ of dimension 100×100 Å. Periodic boundary conditions are applied in both armchair and zigzag directions. The single-layer 1H-CoTe₂ is stretched uniaxially along the armchair or zigzag direction. The stress is calculated without involving the actual thickness of the quasi-two-dimensional structure of the single-layer 1H-CoTe₂. The Young's modulus can be obtained by a linear fitting of the stress-strain relation in the small strain range of $[0, 0.01]$. The Young's modulus are 53.7 N/m and 54.3 N/m along the armchair and zigzag directions, respectively. The Young's modulus is essentially isotropic in the armchair and zigzag directions. The Poisson's ratio from the VFF model and the SW potential is $\nu_{xy} = \nu_{yx} = 0.32$.

TABLE LXXXVI: The VFF model for single-layer 1H-NiS₂. The second line gives an explicit expression for each VFF term. The third line is the force constant parameters. Parameters are in the unit of $\frac{\text{eV}}{\text{Å}^2}$ for the bond stretching interactions, and in the unit of eV for the angle bending interaction. The fourth line gives the initial bond length (in unit of Å) for the bond stretching interaction and the initial angle (in unit of degrees) for the angle bending interaction. The angle θ_{ijk} has atom i as the apex.

VFF type	bond stretching		angle bending	
expression	$\frac{1}{2}K_{\text{Ni-S}}(\Delta r)^2$	$\frac{1}{2}K_{\text{Ni-S-S}}(\Delta\theta)^2$	$\frac{1}{2}K_{\text{Ni-S-S}'}(\Delta\theta)^2$	$\frac{1}{2}K_{\text{S-Ni-Ni}}(\Delta\theta)^2$
parameter	6.933	3.418	3.418	3.418
r_0 or θ_0	2.240	98.740	57.593	98.740

TABLE LXXXVII: Two-body SW potential parameters for single-layer 1H-NiS₂ used by GULP⁸ as expressed in Eq. (3).

	A (eV)	ρ (Å)	B (Å ⁴)	r_{min} (Å)	r_{max} (Å)
Ni-S	6.425	1.498	12.588	0.0	3.156

There is no available value for nonlinear quantities in the single-layer 1H-CoTe₂. We have thus used the nonlinear parameter $B = 0.5d^4$ in Eq. (5), which is close to the value of B in most materials. The value of the third order nonlinear elasticity D can be extracted by fitting the stress-strain relation to the function $\sigma = E\epsilon + \frac{1}{2}D\epsilon^2$ with E as the Young's modulus. The values of D from the present SW potential are -157.2 N/m and -187.9 N/m along the armchair and zigzag directions, respectively. The ultimate stress is about 8.2 Nm⁻¹ at the ultimate strain of 0.26 in the armchair direction at the low temperature of 1 K. The ultimate stress is about 7.9 Nm⁻¹ at the ultimate strain of 0.33 in the zigzag direction at the low temperature of 1 K.

XXII. 1H-NIS₂

Most existing theoretical studies on the single-layer 1H-NiS₂ are based on the first-principles calculations. In this section, we will develop the SW potential for the single-layer 1H-NiS₂.

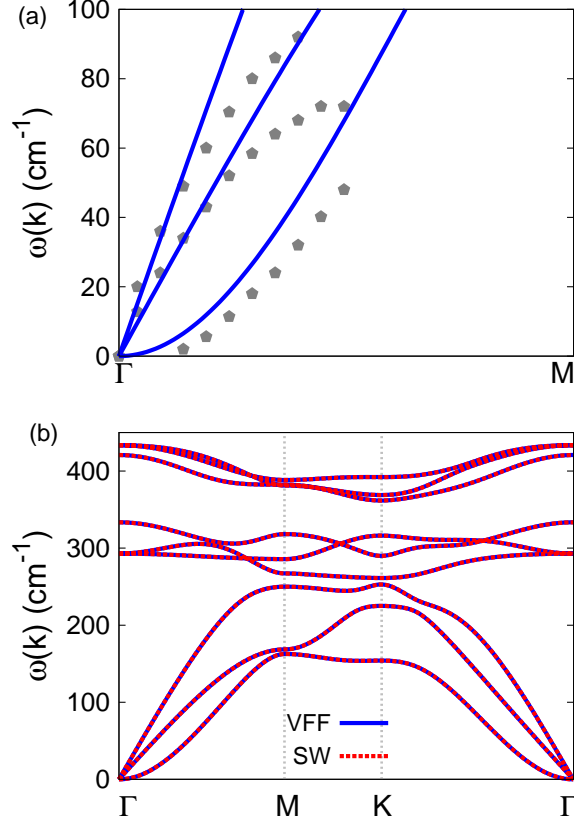


FIG. 41: (Color online) Phonon spectrum for single-layer 1H-NiS₂. (a) Phonon dispersion along the Γ M direction in the Brillouin zone. The results from the VFF model (lines) are comparable with the *ab initio* results (pentagons) from Ref. 12. (b) The phonon dispersion from the SW potential is exactly the same as that from the VFF model.

The structure for the single-layer 1H-NiS₂ is shown in Fig. 1 (with M=Ni and X=S). Each Ni atom is surrounded by six S atoms. These S atoms are categorized into the top group (eg. atoms 1, 3, and 5) and bottom group (eg. atoms 2, 4, and 6). Each S atom is connected to three Ni atoms. The structural parameters are from the first-principles calculations,¹² including the lattice constant $a = 3.40 \text{ \AA}$, and the bond length $d_{\text{Ni-S}} = 2.24 \text{ \AA}$. The resultant angles are $\theta_{\text{NiSS}} = \theta_{\text{S Ni Ni}} = 98.740^\circ$ and $\theta_{\text{NiSS}'} = 57.593^\circ$, in which atoms S and S' are from different (top or bottom) group.

Table LXXXVI shows four VFF terms for the single-layer 1H-NiS₂, one of which is the bond stretching interaction shown by Eq. (1) while the other three terms are the angle bending interaction shown by Eq. (2). These force constant parameters are determined by

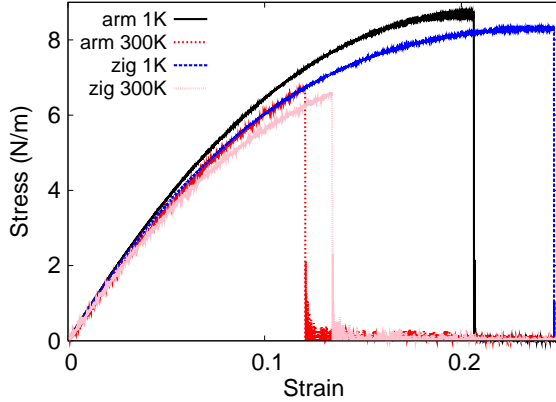


FIG. 42: (Color online) Stress-strain for single-layer 1H-NiS₂ of dimension 100 × 100 Å along the armchair and zigzag directions.

TABLE LXXXVIII: Three-body SW potential parameters for single-layer 1H-NiS₂ used by GULP⁸ as expressed in Eq. (4). The angle θ_{ijk} in the first line indicates the bending energy for the angle with atom i as the apex.

	K (eV)	θ_0 (degree)	ρ_1 (Å)	ρ_2 (Å)	$r_{\min 12}$ (Å)	$r_{\max 12}$ (Å)	$r_{\min 13}$ (Å)	$r_{\max 13}$ (Å)	$r_{\min 23}$ (Å)	$r_{\max 23}$ (Å)
$\theta_{\text{Ni-S-S}}$	46.062	98.740	1.498	1.498	0.0	3.156	0.0	3.156	0.0	3.713
$\theta_{\text{Ni-S-S}'}$	63.130	57.593	1.498	1.498	0.0	3.156	0.0	3.156	0.0	3.713
$\theta_{\text{S-Ni-Ni}}$	46.062	98.740	1.498	1.498	0.0	3.156	0.0	3.156	0.0	3.713

fitting to the acoustic branches in the phonon dispersion along the ΓM as shown in Fig. 41 (a). The *ab initio* calculations for the phonon dispersion are from Ref. 12. Fig. 41 (b) shows that the VFF model and the SW potential give exactly the same phonon dispersion, as the SW potential is derived from the VFF model.

The parameters for the two-body SW potential used by GULP are shown in Tab. LXXXVII. The parameters for the three-body SW potential used by GULP are shown in Tab. LXXXVIII. Some representative parameters for the SW potential used by LAMMPS are listed in Tab. LXXXIX. We note that twelve atom types have been introduced for the simulation of the single-layer 1H-NiS₂ using LAMMPS, because the angles around atom Ni in Fig. 1 (with M=Ni and X=S) are not distinguishable in LAMMPS. We have suggested two options to differentiate these angles by implementing some additional constraints in LAMMPS, which can be accomplished by modifying the source file of LAMMPS.^{13,14}

TABLE LXXXIX: SW potential parameters for single-layer 1H-NiS₂ used by LAMMPS⁹ as expressed in Eqs. (9) and (10).

	ϵ (eV)	σ (Å)	a	λ	γ	$\cos\theta_0$	A_L	B_L	p	q	tol
Ni ₁ -S ₁ -S ₁	1.000	1.498	2.107	0.000	1.000	0.000	6.425	2.502	4	0	0.0
Ni ₁ -S ₁ -S ₃	1.000	0.000	0.000	46.062	1.000	-0.152	0.000	0.000	4	0	0.0
Ni ₁ -S ₁ -S ₂	1.000	0.000	0.000	63.130	1.000	0.536	0.000	0.000	4	0	0.0
S ₁ -Ni ₁ -Ni ₃	1.000	0.000	0.000	46.062	1.000	-0.152	0.000	0.000	4	0	0.0

According to our experience, it is not so convenient for some users to implement these constraints and recompile the LAMMPS package. Hence, in the present work, we differentiate the angles by introducing more atom types, so it is not necessary to modify the LAMMPS package. Fig. 2 (with M=Ni and X=S) shows that, for 1H-NiS₂, we can differentiate these angles around the Ni atom by assigning these six neighboring S atoms with different atom types. It can be found that twelve atom types are necessary for the purpose of differentiating all six neighbors around one Ni atom.

We use LAMMPS to perform MD simulations for the mechanical behavior of the single-layer 1H-NiS₂ under uniaxial tension at 1.0 K and 300.0 K. Fig. 42 shows the stress-strain curve for the tension of a single-layer 1H-NiS₂ of dimension 100×100 Å. Periodic boundary conditions are applied in both armchair and zigzag directions. The single-layer 1H-NiS₂ is stretched uniaxially along the armchair or zigzag direction. The stress is calculated without involving the actual thickness of the quasi-two-dimensional structure of the single-layer 1H-NiS₂. The Young's modulus can be obtained by a linear fitting of the stress-strain relation in the small strain range of [0, 0.01]. The Young's modulus are 84.0 N/m and 82.5 N/m along the armchair and zigzag directions, respectively. The Young's modulus is essentially isotropic in the armchair and zigzag directions. The Poisson's ratio from the VFF model and the SW potential is $\nu_{xy} = \nu_{yx} = 0.19$.

There is no available value for nonlinear quantities in the single-layer 1H-NiS₂. We have thus used the nonlinear parameter $B = 0.5d^4$ in Eq. (5), which is close to the value of B in most materials. The value of the third order nonlinear elasticity D can be extracted by fitting the stress-strain relation to the function $\sigma = E\epsilon + \frac{1}{2}D\epsilon^2$ with E as the Young's modulus. The values of D from the present SW potential are -403.2 N/m and -414.8 N/m

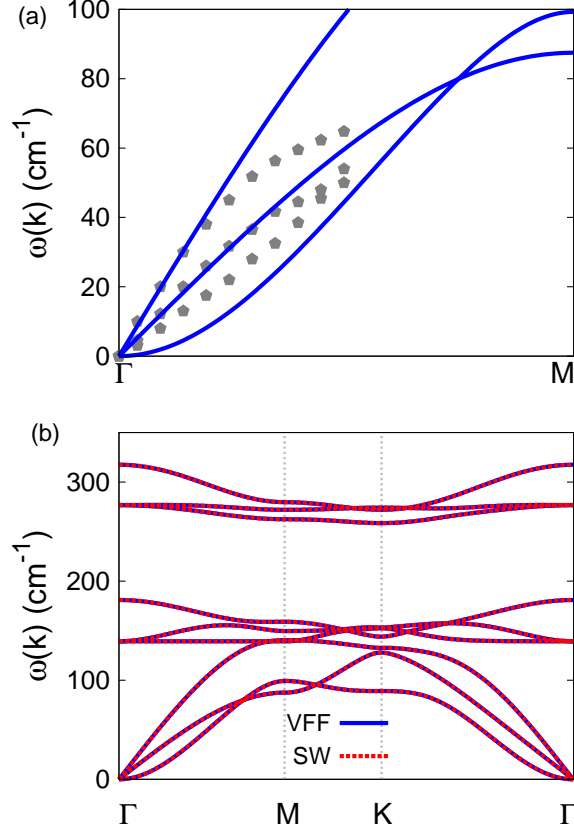


FIG. 43: (Color online) Phonon spectrum for single-layer 1H-NiSe₂. (a) Phonon dispersion along the Γ M direction in the Brillouin zone. The results from the VFF model (lines) are comparable with the *ab initio* results (pentagons) from Ref. 12. (b) The phonon dispersion from the SW potential is exactly the same as that from the VFF model.

along the armchair and zigzag directions, respectively. The ultimate stress is about 8.7 Nm^{-1} at the ultimate strain of 0.20 in the armchair direction at the low temperature of 1 K. The ultimate stress is about 8.3 Nm^{-1} at the ultimate strain of 0.24 in the zigzag direction at the low temperature of 1 K.

XXIII. 1H-NiSe₂

Most existing theoretical studies on the single-layer 1H-NiSe₂ are based on the first-principles calculations. In this section, we will develop the SW potential for the single-layer 1H-NiSe₂.

TABLE XC: The VFF model for single-layer 1H-NiSe₂. The second line gives an explicit expression for each VFF term. The third line is the force constant parameters. Parameters are in the unit of $\frac{eV}{\text{\AA}^2}$ for the bond stretching interactions, and in the unit of eV for the angle bending interaction. The fourth line gives the initial bond length (in unit of \AA) for the bond stretching interaction and the initial angle (in unit of degrees) for the angle bending interaction. The angle θ_{ijk} has atom i as the apex.

VFF type	bond stretching	angle bending		
expression	$\frac{1}{2}K_{\text{Ni-Se}}(\Delta r)^2$	$\frac{1}{2}K_{\text{Ni-Se-Se}}(\Delta\theta)^2$	$\frac{1}{2}K_{\text{Ni-Se-Se'}}(\Delta\theta)^2$	$\frac{1}{2}K_{\text{Se-Ni-Ni}}(\Delta\theta)^2$
parameter	4.823	2.171	2.171	2.171
r_0 or θ_0	2.350	90.228	70.206	90.228

TABLE XCI: Two-body SW potential parameters for single-layer 1H-NiSe₂ used by GULP⁸ as expressed in Eq. (3).

	A (eV)	ρ (\AA)	B (\AA^4)	r_{\min} (\AA)	r_{\max} (\AA)
Ni-Se	4.004	1.267	15.249	0.0	3.213

TABLE XCII: Three-body SW potential parameters for single-layer 1H-NiSe₂ used by GULP⁸ as expressed in Eq. (4). The angle θ_{ijk} in the first line indicates the bending energy for the angle with atom i as the apex.

	K (eV)	θ_0 (degree)	ρ_1 (\AA)	ρ_2 (\AA)	$r_{\min12}$ (\AA)	$r_{\max12}$ (\AA)	$r_{\min13}$ (\AA)	$r_{\max13}$ (\AA)	$r_{\min23}$ (\AA)	$r_{\max23}$ (\AA)
$\theta_{\text{Ni-Se-Se}}$	20.479	90.228	1.267	1.267	0.0	3.213	0.0	3.213	0.0	3.809
$\theta_{\text{Ni-Se-Se'}}$	23.132	70.206	1.267	1.267	0.0	3.213	0.0	3.213	0.0	3.809
$\theta_{\text{Se-Ni-Ni}}$	20.479	90.228	1.267	1.267	0.0	3.213	0.0	3.213	0.0	3.809

TABLE XCIII: SW potential parameters for single-layer 1H-NiSe₂ used by LAMMPS⁹ as expressed in Eqs. (9) and (10).

	ϵ (eV)	σ (\AA)	a	λ	γ	$\cos\theta_0$	A_L	B_L	p	q	tol
Ni ₁ -Se ₁ -Se ₁	1.000	1.267	2.535	0.000	1.000	0.000	4.004	5.913	4	0	0.0
Ni ₁ -Se ₁ -Se ₃	1.000	0.000	0.000	20.479	1.000	-0.004	0.000	0.000	4	0	0.0
Ni ₁ -Se ₁ -Se ₂	1.000	0.000	0.000	23.132	1.000	0.339	0.000	0.000	4	0	0.0
Se ₁ -Ni ₁ -Ni ₃	1.000	0.000	0.000	20.479	1.000	-0.004	0.000	0.000	4	0	0.0

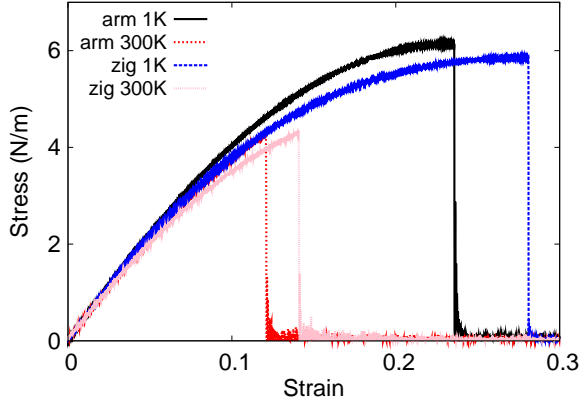


FIG. 44: (Color online) Stress-strain for single-layer 1H-NiSe₂ of dimension $100 \times 100 \text{ \AA}$ along the armchair and zigzag directions.

The structure for the single-layer 1H-NiSe₂ is shown in Fig. 1 (with M=Ni and X=Se). Each Ni atom is surrounded by six Se atoms. These Se atoms are categorized into the top group (eg. atoms 1, 3, and 5) and bottom group (eg. atoms 2, 4, and 6). Each Se atom is connected to three Ni atoms. The structural parameters are from the first-principles calculations,¹² including the lattice constant $a = 3.33 \text{ \AA}$, and the bond length $d_{\text{Ni-Se}} = 2.35 \text{ \AA}$. The resultant angles are $\theta_{\text{NiSeSe}} = \theta_{\text{SeNiNi}} = 90.228^\circ$ and $\theta_{\text{NiSeSe}'} = 70.206^\circ$, in which atoms Se and Se' are from different (top or bottom) group.

Table XC shows four VFF terms for the single-layer 1H-NiSe₂, one of which is the bond stretching interaction shown by Eq. (1) while the other three terms are the angle bending interaction shown by Eq. (2). These force constant parameters are determined by fitting to the acoustic branches in the phonon dispersion along the ΓM as shown in Fig. 43 (a). The *ab initio* calculations for the phonon dispersion are from Ref. 12. The lowest acoustic branch (flexural mode) is almost linear in the *ab initio* calculations, which may due to the violation of the rigid rotational invariance.²⁰ Fig. 43 (b) shows that the VFF model and the SW potential give exactly the same phonon dispersion, as the SW potential is derived from the VFF model.

The parameters for the two-body SW potential used by GULP are shown in Tab. XCI. The parameters for the three-body SW potential used by GULP are shown in Tab. XCII. Some representative parameters for the SW potential used by LAMMPS are listed in Tab. XCIII. We note that twelve atom types have been introduced for the simulation of the single-layer

1H-NiSe₂ using LAMMPS, because the angles around atom Ni in Fig. 1 (with M=Ni and X=Se) are not distinguishable in LAMMPS. We have suggested two options to differentiate these angles by implementing some additional constraints in LAMMPS, which can be accomplished by modifying the source file of LAMMPS.^{13,14} According to our experience, it is not so convenient for some users to implement these constraints and recompile the LAMMPS package. Hence, in the present work, we differentiate the angles by introducing more atom types, so it is not necessary to modify the LAMMPS package. Fig. 2 (with M=Ni and X=Se) shows that, for 1H-NiSe₂, we can differentiate these angles around the Ni atom by assigning these six neighboring Se atoms with different atom types. It can be found that twelve atom types are necessary for the purpose of differentiating all six neighbors around one Ni atom.

We use LAMMPS to perform MD simulations for the mechanical behavior of the single-layer 1H-NiSe₂ under uniaxial tension at 1.0 K and 300.0 K. Fig. 44 shows the stress-strain curve for the tension of a single-layer 1H-NiSe₂ of dimension $100 \times 100 \text{ \AA}$. Periodic boundary conditions are applied in both armchair and zigzag directions. The single-layer 1H-NiSe₂ is stretched uniaxially along the armchair or zigzag direction. The stress is calculated without involving the actual thickness of the quasi-two-dimensional structure of the single-layer 1H-NiSe₂. The Young's modulus can be obtained by a linear fitting of the stress-strain relation in the small strain range of $[0, 0.01]$. The Young's modulus are 47.6 N/m and 47.8 N/m along the armchair and zigzag directions, respectively. The Young's modulus is essentially isotropic in the armchair and zigzag directions. The Poisson's ratio from the VFF model and the SW potential is $\nu_{xy} = \nu_{yx} = 0.27$.

There is no available value for nonlinear quantities in the single-layer 1H-NiSe₂. We have thus used the nonlinear parameter $B = 0.5d^4$ in Eq. (5), which is close to the value of B in most materials. The value of the third order nonlinear elasticity D can be extracted by fitting the stress-strain relation to the function $\sigma = E\epsilon + \frac{1}{2}D\epsilon^2$ with E as the Young's modulus. The values of D from the present SW potential are -173.9 N/m and -197.6 N/m along the armchair and zigzag directions, respectively. The ultimate stress is about 6.1 Nm^{-1} at the ultimate strain of 0.23 in the armchair direction at the low temperature of 1 K. The ultimate stress is about 5.9 Nm^{-1} at the ultimate strain of 0.28 in the zigzag direction at the low temperature of 1 K.

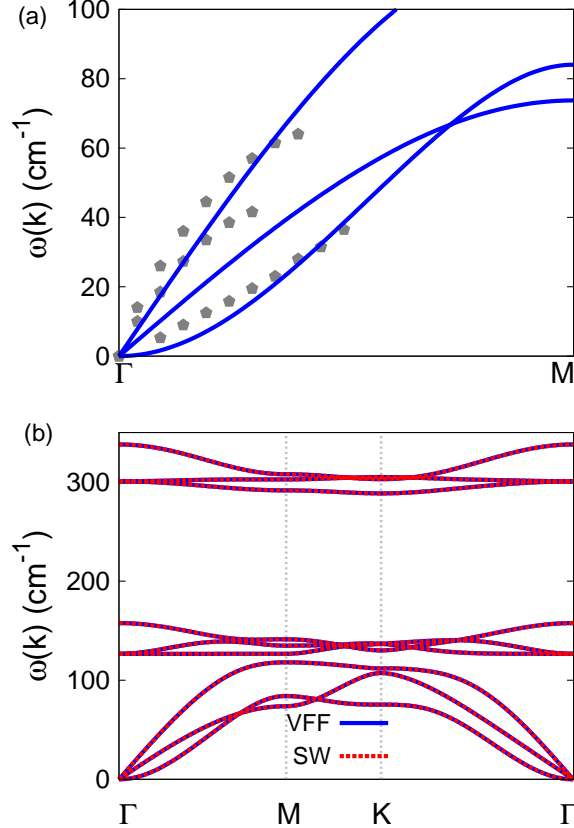


FIG. 45: (Color online) Phonon spectrum for single-layer 1H-NiTe₂. (a) Phonon dispersion along the Γ M direction in the Brillouin zone. The results from the VFF model (lines) are comparable with the *ab initio* results (pentagons) from Ref. 12. (b) The phonon dispersion from the SW potential is exactly the same as that from the VFF model.

XXIV. 1H-NITE₂

Most existing theoretical studies on the single-layer 1H-NiTe₂ are based on the first-principles calculations. In this section, we will develop the SW potential for the single-layer 1H-NiTe₂.

The structure for the single-layer 1H-NiTe₂ is shown in Fig. 1 (with M=Ni and X=Te). Each Ni atom is surrounded by six Te atoms. These Te atoms are categorized into the top group (eg. atoms 1, 3, and 5) and bottom group (eg. atoms 2, 4, and 6). Each Te atom is connected to three Ni atoms. The structural parameters are from the first-principles calculations,¹² including the lattice constant $a = 3.59 \text{ \AA}$, and the bond length

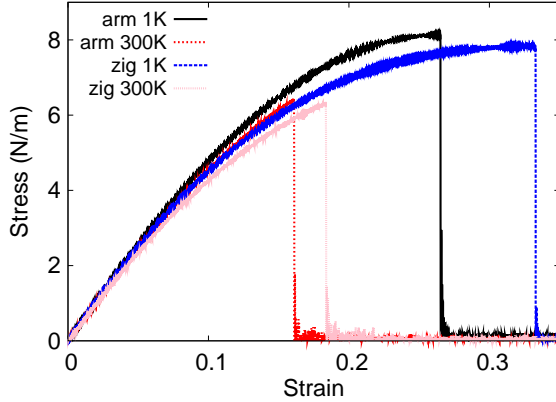


FIG. 46: (Color online) Stress-strain for single-layer 1H-NiTe₂ of dimension $100 \times 100 \text{ \AA}$ along the armchair and zigzag directions.

TABLE XCIV: The VFF model for single-layer 1H-NiTe₂. The second line gives an explicit expression for each VFF term. The third line is the force constant parameters. Parameters are in the unit of $\frac{eV}{\text{Å}^2}$ for the bond stretching interactions, and in the unit of eV for the angle bending interaction. The fourth line gives the initial bond length (in unit of Å) for the bond stretching interaction and the initial angle (in unit of degrees) for the angle bending interaction. The angle θ_{ijk} has atom *i* as the apex.

VFF type	bond stretching	angle bending		
expression	$\frac{1}{2}K_{\text{Ni-Te}}(\Delta r)^2$	$\frac{1}{2}K_{\text{Ni-Te-Te}}(\Delta\theta)^2$	$\frac{1}{2}K_{\text{Ni-Te-Te'}}(\Delta\theta)^2$	$\frac{1}{2}K_{\text{Te-Ni-Ni}}(\Delta\theta)^2$
parameter	6.712	2.656	2.656	2.656
r_0 or θ_0	2.540	89.933	70.624	89.933

$d_{\text{Ni-Te}} = 2.54 \text{ \AA}$. The resultant angles are $\theta_{\text{NiTeTe}} = \theta_{\text{TeNiNi}} = 89.933^\circ$ and $\theta_{\text{NiTeTe'}} = 70.624^\circ$, in which atoms Te and Te' are from different (top or bottom) group.

Table XCIV shows four VFF terms for the single-layer 1H-NiTe₂, one of which is the bond stretching interaction shown by Eq. (1) while the other three terms are the angle bending interaction shown by Eq. (2). These force constant parameters are determined by fitting to the acoustic branches in the phonon dispersion along the ΓM as shown in Fig. 45 (a). The *ab initio* calculations for the phonon dispersion are from Ref. 12. The lowest acoustic branch (flexural mode) is almost linear in the *ab initio* calculations, which may due to the

TABLE XCV: Two-body SW potential parameters for single-layer 1H-NiTe₂ used by GULP⁸ as expressed in Eq. (3).

	A (eV)	ρ (Å)	B (Å ⁴)	r_{\min} (Å)	r_{\max} (Å)
Ni-Te	6.461	1.359	20.812	0.0	3.469

TABLE XCVI: Three-body SW potential parameters for single-layer 1H-NiTe₂ used by GULP⁸ as expressed in Eq. (4). The angle θ_{ijk} in the first line indicates the bending energy for the angle with atom i as the apex.

	K (eV)	θ_0 (degree)	ρ_1 (Å)	ρ_2 (Å)	$r_{\min12}$ (Å)	$r_{\max12}$ (Å)	$r_{\min13}$ (Å)	$r_{\max13}$ (Å)	$r_{\min23}$ (Å)	$r_{\max23}$ (Å)
$\theta_{\text{Ni-Te-Te}}$	24.759	89.933	1.359	1.359	0.0	3.469	0.0	3.469	0.0	4.114
$\theta_{\text{Ni-Te-Te}'}$	27.821	70.624	1.359	1.359	0.0	3.469	0.0	3.469	0.0	4.114
$\theta_{\text{Te-Ni-Ni}}$	24.759	89.933	1.359	1.359	0.0	3.469	0.0	3.469	0.0	4.114

violation of the rigid rotational invariance.²⁰ The transverse acoustic branch is very close to the longitudinal acoustic branch in the *ab initio* calculations. Fig. 45 (b) shows that the VFF model and the SW potential give exactly the same phonon dispersion, as the SW potential is derived from the VFF model.

The parameters for the two-body SW potential used by GULP are shown in Tab. XCV. The parameters for the three-body SW potential used by GULP are shown in Tab. XCVI. Some representative parameters for the SW potential used by LAMMPS are listed in Tab. XCVII. We note that twelve atom types have been introduced for the simulation of the single-layer 1H-NiTe₂ using LAMMPS, because the angles around atom Ni in Fig. 1 (with

TABLE XCVII: SW potential parameters for single-layer 1H-NiTe₂ used by LAMMPS⁹ as expressed in Eqs. (9) and (10).

	ϵ (eV)	σ (Å)	a	λ	γ	$\cos \theta_0$	A_L	B_L	p	q	tol
Ni ₁ -Te ₁ -Te ₁	1.000	1.359	2.553	0.000	1.000	0.000	6.461	6.107	4	0	0.0
Ni ₁ -Te ₁ -Te ₃	1.000	0.000	0.000	24.759	1.000	0.001	0.000	0.000	4	0	0.0
Ni ₁ -Te ₁ -Te ₂	1.000	0.000	0.000	27.821	1.000	0.332	0.000	0.000	4	0	0.0
Te ₁ -Ni ₁ -Ni ₃	1.000	0.000	0.000	24.759	1.000	0.001	0.000	0.000	4	0	0.0

M=Ni and X=Te) are not distinguishable in LAMMPS. We have suggested two options to differentiate these angles by implementing some additional constraints in LAMMPS, which can be accomplished by modifying the source file of LAMMPS.^{13,14} According to our experience, it is not so convenient for some users to implement these constraints and recompile the LAMMPS package. Hence, in the present work, we differentiate the angles by introducing more atom types, so it is not necessary to modify the LAMMPS package. Fig. 2 (with M=Ni and X=Te) shows that, for 1H-NiTe₂, we can differentiate these angles around the Ni atom by assigning these six neighboring Te atoms with different atom types. It can be found that twelve atom types are necessary for the purpose of differentiating all six neighbors around one Ni atom.

We use LAMMPS to perform MD simulations for the mechanical behavior of the single-layer 1H-NiTe₂ under uniaxial tension at 1.0 K and 300.0 K. Fig. 46 shows the stress-strain curve for the tension of a single-layer 1H-NiTe₂ of dimension 100 × 100 Å. Periodic boundary conditions are applied in both armchair and zigzag directions. The single-layer 1H-NiTe₂ is stretched uniaxially along the armchair or zigzag direction. The stress is calculated without involving the actual thickness of the quasi-two-dimensional structure of the single-layer 1H-NiTe₂. The Young's modulus can be obtained by a linear fitting of the stress-strain relation in the small strain range of [0, 0.01]. The Young's modulus are 53.2 N/m and 53.6 N/m along the armchair and zigzag directions, respectively. The Young's modulus is essentially isotropic in the armchair and zigzag directions. The Poisson's ratio from the VFF model and the SW potential is $\nu_{xy} = \nu_{yx} = 0.32$.

There is no available value for nonlinear quantities in the single-layer 1H-NiTe₂. We have thus used the nonlinear parameter $B = 0.5d^4$ in Eq. (5), which is close to the value of B in most materials. The value of the third order nonlinear elasticity D can be extracted by fitting the stress-strain relation to the function $\sigma = E\epsilon + \frac{1}{2}D\epsilon^2$ with E as the Young's modulus. The values of D from the present SW potential are -156.6 N/m and -184.8 N/m along the armchair and zigzag directions, respectively. The ultimate stress is about 8.1 Nm⁻¹ at the ultimate strain of 0.26 in the armchair direction at the low temperature of 1 K. The ultimate stress is about 7.8 Nm⁻¹ at the ultimate strain of 0.33 in the zigzag direction at the low temperature of 1 K.

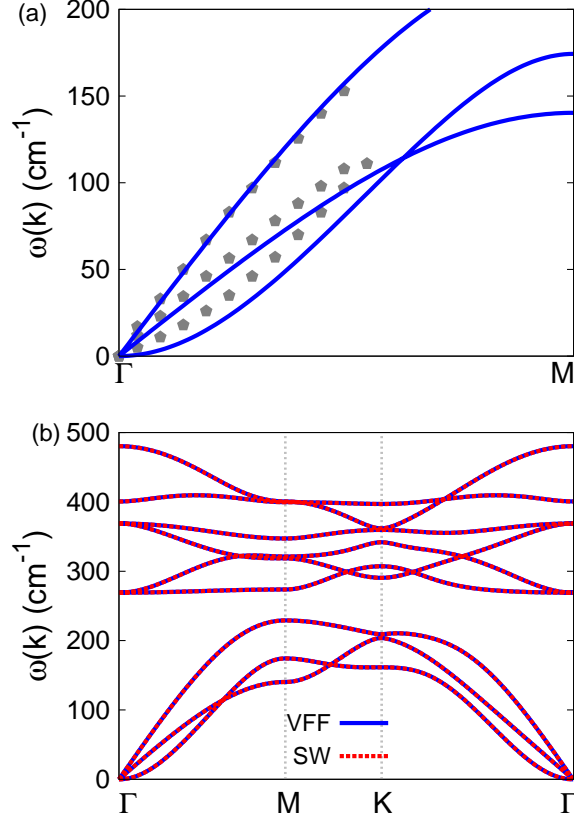


FIG. 47: (Color online) Phonon dispersion for single-layer 1H-NbS₂. (a) The VFF model is fitted to the three acoustic branches in the long wave limit along the Γ M direction. The theoretical results (gray pentagons) are from Ref. 21. The blue lines are from the present VFF model. (b) The VFF model (blue lines) and the SW potential (red lines) give the same phonon dispersion for single-layer 1H-NbS₂ along Γ MK Γ .

XXV. 1H-NbS₂

In 1983, the VFF model was developed to investigate the lattice dynamical properties in the bulk 2H-NbS₂.²¹ In this section, we will develop the SW potential for the single-layer 1H-NbS₂.

The structure for the single-layer 1H-NbS₂ is shown in Fig. 1 (with M=Nb and X=S). Each Nb atom is surrounded by six S atoms. These S atoms are categorized into the top group (eg. atoms 1, 3, and 5) and bottom group (eg. atoms 2, 4, and 6). Each S atom is connected to three Nb atoms. The structural parameters are from Ref. 21, including the

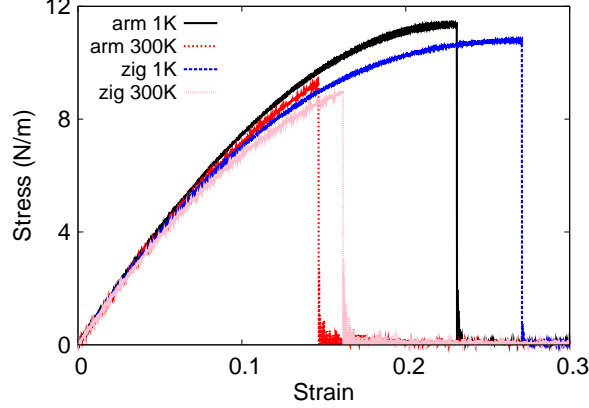


FIG. 48: (Color online) Stress-strain for single-layer 1H-NbS₂ of dimension 100 × 100 Å along the armchair and zigzag directions.

TABLE XCVIII: The VFF model for single-layer 1H-NbS₂. The second line gives an explicit expression for each VFF term. The third line is the force constant parameters. Parameters are in the unit of $\frac{eV}{\text{Å}^2}$ for the bond stretching interactions, and in the unit of eV for the angle bending interaction. The fourth line gives the initial bond length (in unit of Å) for the bond stretching interaction and the initial angle (in unit of degrees) for the angle bending interaction. The angle θ_{ijk} has atom *i* as the apex.

VFF type	bond stretching	angle bending		
expression	$\frac{1}{2}K_{Nb-S}(\Delta r)^2$	$\frac{1}{2}K_{Nb-S-S}(\Delta\theta)^2$	$\frac{1}{2}K_{Nb-S-S'}(\Delta\theta)^2$	$\frac{1}{2}K_{S-Nb-Nb}(\Delta\theta)^2$
parameter	8.230	4.811	4.811	4.811
r_0 or θ_0	2.470	84.140	78.626	84.140

lattice constant $a = 3.31$ Å, and the bond length $d_{Nb-S} = 2.47$ Å. The resultant angles are $\theta_{NbSS} = \theta_{SNbNb} = 84.140^\circ$ and $\theta_{NbSS'} = 78.626^\circ$, in which atoms S and S' are from different (top or bottom) group.

Table XCVIII shows four VFF terms for the 1H-NbS₂, one of which is the bond stretching interaction shown by Eq. (1) while the other three terms are the angle bending interaction shown by Eq. (2). These force constant parameters are determined by fitting to the three acoustic branches in the phonon dispersion along the ΓM as shown in Fig. 47 (a). The theoretical phonon frequencies (gray pentagons) are from Ref. 21, which are the phonon

TABLE XCIX: Two-body SW potential parameters for single-layer 1H-NbS₂ used by GULP⁸ as expressed in Eq. (3).

	A (eV)	ρ (Å)	B (Å ⁴)	r_{\min} (Å)	r_{\max} (Å)
Nb-S	6.439	1.116	18.610	0.0	3.300

TABLE C: Three-body SW potential parameters for single-layer 1H-NbS₂ used by GULP⁸ as expressed in Eq. (4). The angle θ_{ijk} in the first line indicates the bending energy for the angle with atom i as the apex.

	K (eV)	θ_0 (degree)	ρ_1 (Å)	ρ_2 (Å)	$r_{\min12}$ (Å)	$r_{\max12}$ (Å)	$r_{\min13}$ (Å)	$r_{\max13}$ (Å)	$r_{\min23}$ (Å)	$r_{\max23}$ (Å)
$\theta_{\text{Nb-S-S}}$	35.748	84.140	1.116	1.116	0.0	3.300	0.0	3.300	0.0	3.933
$\theta_{\text{Nb-S-S}'}$	36.807	78.626	1.116	1.116	0.0	3.300	0.0	3.300	0.0	3.933
$\theta_{\text{S-Nb-Nb}}$	35.748	84.140	1.116	1.116	0.0	3.300	0.0	3.300	0.0	3.933

dispersion of bulk 2H-NbS₂. We have used these phonon frequencies as the phonon dispersion of the single-layer 1H-NbS₂, as the inter-layer interaction in the bulk 2H-NbS₂ only induces weak effects on the two inplane acoustic branches. The inter-layer coupling will strengthen the out-of-plane acoustic branch (flexural branch), so the flexural branch from the present VFF model (blue line) is lower than the theoretical results for bulk 2H-NbS₂ (gray pentagons). Fig. 47 (b) shows that the VFF model and the SW potential give exactly the same phonon dispersion, as the SW potential is derived from the VFF model.

The parameters for the two-body SW potential used by GULP are shown in Tab. XCIX. The parameters for the three-body SW potential used by GULP are shown in Tab. C.

TABLE CI: SW potential parameters for single-layer 1H-NbS₂ used by LAMMPS⁹ as expressed in Eqs. (9) and (10). Atom types in the first column are displayed in Fig. 2 (with M=Nb and X=S).

	ϵ (eV)	σ (Å)	a	λ	γ	$\cos\theta_0$	A_L	B_L	p	q	tol
Nb ₁ -S ₁ -S ₁	1.000	1.116	2.958	0.000	1.000	0.000	6.439	12.014	4	0	0.0
Nb ₁ -S ₁ -S ₃	1.000	0.000	0.000	35.748	1.000	0.102	0.000	0.000	4	0	0.0
Nb ₁ -S ₁ -S ₂	1.000	0.000	0.000	36.807	1.000	0.197	0.000	0.000	4	0	0.0
S ₁ -Nb ₁ -Nb ₃	1.000	0.000	0.000	35.748	1.000	0.102	0.000	0.000	4	0	0.0

Parameters for the SW potential used by LAMMPS are listed in Tab. CI. We note that twelve atom types have been introduced for the simulation of the single-layer 1H-NbS₂ using LAMMPS, because the angles around atom Nb in Fig. 1 (with M=Nb and X=S) are not distinguishable in LAMMPS. We have suggested two options to differentiate these angles by implementing some additional constraints in LAMMPS, which can be accomplished by modifying the source file of LAMMPS.^{13,14} According to our experience, it is not so convenient for some users to implement these constraints and recompile the LAMMPS package. Hence, in the present work, we differentiate the angles by introducing more atom types, so it is not necessary to modify the LAMMPS package. Fig. 2 (with M=Nb and X=S) shows that, for 1H-NbS₂, we can differentiate these angles around the Nb atom by assigning these six neighboring S atoms with different atom types. It can be found that twelve atom types are necessary for the purpose of differentiating all six neighbors around one Nb atom.

We use LAMMPS to perform MD simulations for the mechanical behavior of the single-layer 1H-NbS₂ under uniaxial tension at 1.0 K and 300.0 K. Fig. 48 shows the stress-strain curve for the tension of a single-layer 1H-NbS₂ of dimension 100 × 100 Å. Periodic boundary conditions are applied in both armchair and zigzag directions. The single-layer 1H-NbS₂ is stretched uniaxially along the armchair or zigzag direction. The stress is calculated without involving the actual thickness of the quasi-two-dimensional structure of the single-layer 1H-NbS₂. The Young's modulus can be obtained by a linear fitting of the stress-strain relation in the small strain range of [0, 0.01]. The Young's modulus are 87.7 N/m and 87.2 N/m along the armchair and zigzag directions, respectively. The Young's modulus is essentially isotropic in the armchair and zigzag directions. The Poisson's ratio from the VFF model and the SW potential is $\nu_{xy} = \nu_{yx} = 0.27$.

There is no available value for the nonlinear quantities in the single-layer 1H-NbS₂. We have thus used the nonlinear parameter $B = 0.5d^4$ in Eq. (5), which is close to the value of B in most materials. The value of the third order nonlinear elasticity D can be extracted by fitting the stress-strain relation to the function $\sigma = E\epsilon + \frac{1}{2}D\epsilon^2$ with E as the Young's modulus. The values of D from the present SW potential are -315.3 N/m and -355.1 N/m along the armchair and zigzag directions, respectively. The ultimate stress is about 11.4 Nm⁻¹ at the ultimate strain of 0.23 in the armchair direction at the low temperature of 1 K. The ultimate stress is about 10.8 Nm⁻¹ at the ultimate strain of 0.27 in the zigzag direction at the low temperature of 1 K.

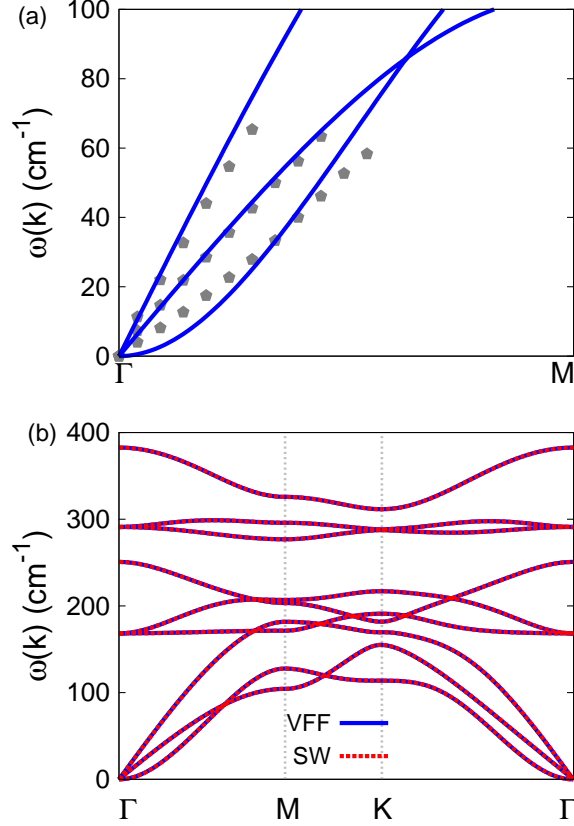


FIG. 49: (Color online) Phonon dispersion for single-layer 1H-NbSe₂. (a) The VFF model is fitted to the three acoustic branches in the long wave limit along the Γ M direction. The theoretical results (gray pentagons) are from Ref. 15. The blue lines are from the present VFF model. (b) The VFF model (blue lines) and the SW potential (red lines) give the same phonon dispersion for single-layer 1H-NbSe₂ along Γ MK Γ .

XXVI. 1H-NBSE₂

In 1983, the VFF model was developed to investigate the lattice dynamical properties in the bulk 2H-NbSe₂.^{15,21} In this section, we will develop the SW potential for the single-layer 1H-NbSe₂.

The structure for the single-layer 1H-NbSe₂ is shown in Fig. 1 (with M=Nb and X=Se). Each Nb atom is surrounded by six Se atoms. These Se atoms are categorized into the top group (eg. atoms 1, 3, and 5) and bottom group (eg. atoms 2, 4, and 6). Each Se atom is connected to three Nb atoms. The structural parameters are from Ref. 21, including the

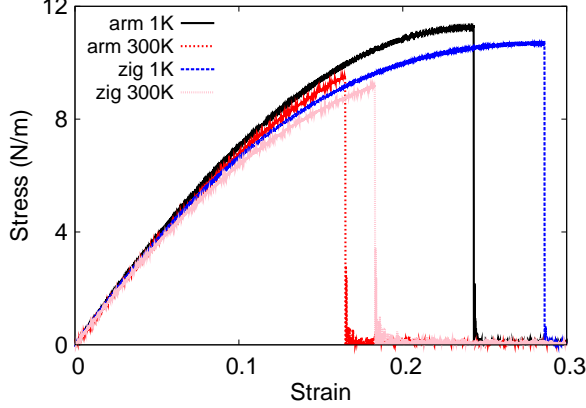


FIG. 50: (Color online) Stress-strain for single-layer 1H-NbSe₂ of dimension $100 \times 100 \text{ \AA}$ along the armchair and zigzag directions.

TABLE CII: The VFF model for single-layer 1H-NbSe₂. The second line gives an explicit expression for each VFF term. The third line is the force constant parameters. Parameters are in the unit of $\frac{eV}{\text{Å}^2}$ for the bond stretching interactions, and in the unit of eV for the angle bending interaction. The fourth line gives the initial bond length (in unit of Å) for the bond stretching interaction and the initial angle (in unit of degrees) for the angle bending interaction. The angle θ_{ijk} has atom i as the apex.

VFF type	bond stretching	angle bending		
expression	$\frac{1}{2}K_{\text{Nb-Se}}(\Delta r)^2$	$\frac{1}{2}K_{\text{Nb-Se-Se}}(\Delta\theta)^2$	$\frac{1}{2}K_{\text{Nb-Se-Se}'}(\Delta\theta)^2$	$\frac{1}{2}K_{\text{Se-Nb-Nb}}(\Delta\theta)^2$
parameter	8.230	4.811	4.811	4.811
r_0 or θ_0	2.600	83.129	79.990	83.129

lattice constant $a = 3.45 \text{ \AA}$, and the bond length $d_{\text{Nb-Se}} = 2.60 \text{ \AA}$. The resultant angles are $\theta_{\text{NbSeSe}} = \theta_{\text{SNbNb}} = 83.129^\circ$ and $\theta_{\text{NbSeSe}'} = 79.990^\circ$, in which atoms Se and Se' are from different (top or bottom) group.

Table CII shows four VFF terms for the 1H-NbSe₂, one of which is the bond stretching interaction shown by Eq. (1) while the other three terms are the angle bending interaction shown by Eq. (2). These force constant parameters are determined by fitting to the three acoustic branches in the phonon dispersion along the ΓM as shown in Fig. 49 (a). The theoretical phonon frequencies (gray pentagons) are from Ref. 21, which are the phonon dispersion of bulk 2H-NbSe₂. We have used these phonon frequencies as the phonon disper-

TABLE CIII: Two-body SW potential parameters for single-layer 1H-NbSe₂ used by GULP⁸ as expressed in Eq. (3).

	A (eV)	ρ (Å)	B (Å ⁴)	r_{\min} (Å)	r_{\max} (Å)
Nb-Se	6.942	1.138	22.849	0.0	3.460

TABLE CIV: Three-body SW potential parameters for single-layer 1H-NbSe₂ used by GULP⁸ as expressed in Eq. (4). The angle θ_{ijk} in the first line indicates the bending energy for the angle with atom i as the apex.

	K (eV)	θ_0 (degree)	ρ_1 (Å)	ρ_2 (Å)	$r_{\min12}$ (Å)	$r_{\max12}$ (Å)	$r_{\min13}$ (Å)	$r_{\max13}$ (Å)	$r_{\min23}$ (Å)	$r_{\max23}$ (Å)
$\theta_{\text{Nb-Se-Se}}$	34.409	83.129	1.138	1.138	0.0	3.460	0.0	3.460	0.0	4.127
$\theta_{\text{Nb-Se-Se}'}$	34.973	79.990	1.138	1.138	0.0	3.460	0.0	3.460	0.0	4.127
$\theta_{\text{Se-Nb-Nb}}$	34.409	83.129	1.138	1.138	0.0	3.460	0.0	3.460	0.0	4.127

sion of the single-layer 1H-NbSe₂, as the inter-layer interaction in the bulk 2H-NbSe₂ only induces weak effects on the two inplane acoustic branches. The inter-layer coupling will strengthen the out-of-plane acoustic branch (flexural branch), so the flexural branch from the present VFF model (blue line) is lower than the theoretical results for bulk 2H-NbSe₂ (gray pentagons). It turns out that the VFF parameters for the single-layer 1H-NbSe₂ are the same as the single-layer NbS₂. The phonon dispersion for single-layer 1H-NbSe₂ was also shown in Ref. 12. Fig. 49 (b) shows that the VFF model and the SW potential give exactly the same phonon dispersion, as the SW potential is derived from the VFF model.

TABLE CV: SW potential parameters for single-layer 1H-NbSe₂ used by LAMMPS⁹ as expressed in Eqs. (9) and (10). Atom types in the first column are displayed in Fig. 2 (with M=Nb and X=Se).

	ϵ (eV)	σ (Å)	a	λ	γ	$\cos \theta_0$	A_L	B_L	p	q	tol
Nb ₁ -Se ₁ -Se ₁	1.000	1.138	3.041	0.000	1.000	0.000	6.942	13.631	4	0	0.0
Nb ₁ -Se ₁ -Se ₃	1.000	0.000	0.000	34.409	1.000	0.120	0.000	0.000	4	0	0.0
Nb ₁ -Se ₁ -Se ₂	1.000	0.000	0.000	34.973	1.000	0.174	0.000	0.000	4	0	0.0
Se ₁ -Nb ₁ -Nb ₃	1.000	0.000	0.000	34.409	1.000	0.120	0.000	0.000	4	0	0.0

The parameters for the two-body SW potential used by GULP are shown in Tab. CIII. The parameters for the three-body SW potential used by GULP are shown in Tab. CIV. Parameters for the SW potential used by LAMMPS are listed in Tab. CV. We note that twelve atom types have been introduced for the simulation of the single-layer 1H-NbSe₂ using LAMMPS, because the angles around atom Nb in Fig. 1 (with M=Nb and X=Se) are not distinguishable in LAMMPS. We have suggested two options to differentiate these angles by implementing some additional constraints in LAMMPS, which can be accomplished by modifying the source file of LAMMPS.^{13,14} According to our experience, it is not so convenient for some users to implement these constraints and recompile the LAMMPS package. Hence, in the present work, we differentiate the angles by introducing more atom types, so it is not necessary to modify the LAMMPS package. Fig. 2 (with M=Nb and X=Se) shows that, for 1H-NbSe₂, we can differentiate these angles around the Nb atom by assigning these six neighboring Se atoms with different atom types. It can be found that twelve atom types are necessary for the purpose of differentiating all six neighbors around one Nb atom.

We use LAMMPS to perform MD simulations for the mechanical behavior of the single-layer 1H-NbSe₂ under uniaxial tension at 1.0 K and 300.0 K. Fig. 50 shows the stress-strain curve for the tension of a single-layer 1H-NbSe₂ of dimension 100 × 100 Å. Periodic boundary conditions are applied in both armchair and zigzag directions. The single-layer 1H-NbSe₂ is stretched uniaxially along the armchair or zigzag direction. The stress is calculated without involving the actual thickness of the quasi-two-dimensional structure of the single-layer 1H-NbSe₂. The Young's modulus can be obtained by a linear fitting of the stress-strain relation in the small strain range of [0, 0.01]. The Young's modulus are 80.2 N/m and 80.7 N/m along the armchair and zigzag directions, respectively. The Young's modulus is essentially isotropic in the armchair and zigzag directions. The Poisson's ratio from the VFF model and the SW potential is $\nu_{xy} = \nu_{yx} = 0.29$.

There is no available value for the nonlinear quantities in the single-layer 1H-NbSe₂. We have thus used the nonlinear parameter $B = 0.5d^4$ in Eq. (5), which is close to the value of B in most materials. The value of the third order nonlinear elasticity D can be extracted by fitting the stress-strain relation to the function $\sigma = E\epsilon + \frac{1}{2}D\epsilon^2$ with E as the Young's modulus. The values of D from the present SW potential are -258.8 N/m and -306.1 N/m along the armchair and zigzag directions, respectively. The ultimate stress is about 11.2 Nm⁻¹ at the ultimate strain of 0.24 in the armchair direction at the low

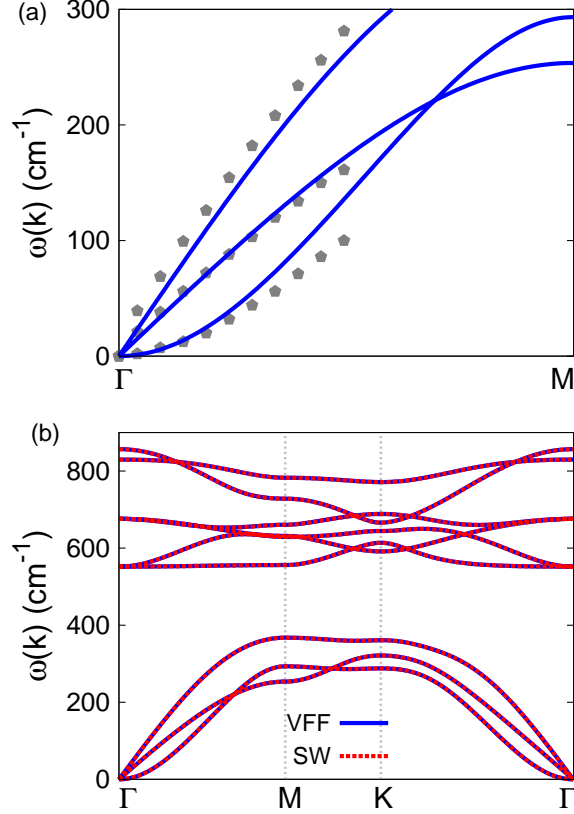


FIG. 51: (Color online) Phonon spectrum for single-layer 1H-MoO₂. (a) Phonon dispersion along the Γ M direction in the Brillouin zone. The results from the VFF model (lines) are comparable with the *ab initio* results (pentagons) from Ref. 12. (b) The phonon dispersion from the SW potential is exactly the same as that from the VFF model.

temperature of 1 K. The ultimate stress is about 10.7 Nm^{-1} at the ultimate strain of 0.28 in the zigzag direction at the low temperature of 1 K.

XXVII. 1H-MOO₂

Most existing theoretical studies on the single-layer 1H-MoO₂ are based on the first-principles calculations. In this section, we will develop the SW potential for the single-layer 1H-MoO₂.

The structure for the single-layer 1H-MoO₂ is shown in Fig. 1 (with M=Mo and X=O). Each Mo atom is surrounded by six O atoms. These O atoms are categorized into the

TABLE CVI: The VFF model for single-layer 1H-MoO₂. The second line gives an explicit expression for each VFF term. The third line is the force constant parameters. Parameters are in the unit of $\frac{eV}{\text{Å}^2}$ for the bond stretching interactions, and in the unit of eV for the angle bending interaction. The fourth line gives the initial bond length (in unit of Å) for the bond stretching interaction and the initial angle (in unit of degrees) for the angle bending interaction. The angle θ_{ijk} has atom *i* as the apex.

VFF type	bond stretching	angle bending		
expression	$\frac{1}{2}K_{\text{Mo-O}}(\Delta r)^2$	$\frac{1}{2}K_{\text{Mo-O-O}}(\Delta\theta)^2$	$\frac{1}{2}K_{\text{Mo-O-O}'}(\Delta\theta)^2$	$\frac{1}{2}K_{\text{O-Mo-Mo}}(\Delta\theta)^2$
parameter	14.622	8.410	8.410	8.410
r_0 or θ_0	2.000	88.054	73.258	88.054

TABLE CVII: Two-body SW potential parameters for single-layer 1H-MoO₂ used by GULP⁸ as expressed in Eq. (3).

	A (eV)	ρ (Å)	B (Å ⁴)	r_{\min} (Å)	r_{\max} (Å)
Mo-O	8.317	1.015	8.000	0.0	2.712

TABLE CVIII: Three-body SW potential parameters for single-layer 1H-MoO₂ used by GULP⁸ as expressed in Eq. (4). The angle θ_{ijk} in the first line indicates the bending energy for the angle with atom *i* as the apex.

	K (eV)	θ_0 (degree)	ρ_1 (Å)	ρ_2 (Å)	$r_{\min12}$ (Å)	$r_{\max12}$ (Å)	$r_{\min13}$ (Å)	$r_{\max13}$ (Å)	$r_{\min23}$ (Å)	$r_{\max23}$ (Å)
$\theta_{\text{Mo-O-O}}$	72.735	88.054	1.015	1.015	0.0	2.712	0.0	2.712	0.0	3.222
$\theta_{\text{Mo-O-O}'}$	79.226	73.258	1.015	1.015	0.0	2.712	0.0	2.712	0.0	3.222
$\theta_{\text{O-Mo-Mo}}$	72.735	88.054	1.015	1.015	0.0	2.712	0.0	2.712	0.0	3.222

TABLE CIX: SW potential parameters for single-layer 1H-MoO₂ used by LAMMPS⁹ as expressed in Eqs. (9) and (10).

	ϵ (eV)	σ (Å)	a	λ	γ	$\cos\theta_0$	A_L	B_L	p	q	tol
Mo ₁ -O ₁ -O ₁	1.000	1.015	2.673	0.000	1.000	0.000	8.317	7.541	4	0	0.0
Mo ₁ -O ₁ -O ₃	1.000	0.000	0.000	72.735	1.000	0.034	0.000	0.000	4	0	0.0
Mo ₁ -O ₁ -O ₂	1.000	0.000	0.000	79.226	1.000	0.288	0.000	0.000	4	0	0.0
O ₁ -Mo ₁ -Mo ₃	1.000	0.000	0.000	72.735	1.000	0.034	0.000	0.000	4	0	0.0

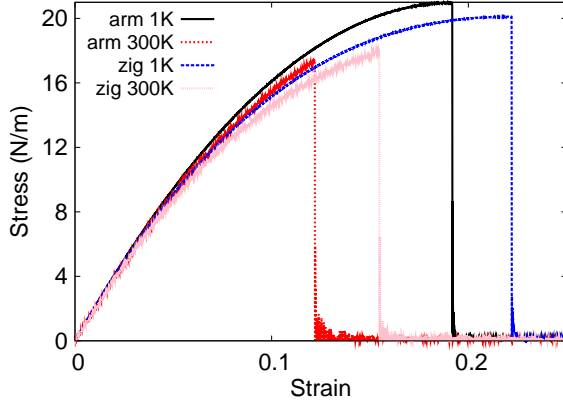


FIG. 52: (Color online) Stress-strain for single-layer 1H-MoO₂ of dimension $100 \times 100 \text{ \AA}$ along the armchair and zigzag directions.

top group (eg. atoms 1, 3, and 5) and bottom group (eg. atoms 2, 4, and 6). Each O atom is connected to three Mo atoms. The structural parameters are from the first-principles calculations,¹² including the lattice constant $a = 2.78 \text{ \AA}$, and the bond length $d_{\text{Mo-O}} = 2.00 \text{ \AA}$. The resultant angles are $\theta_{\text{MoOO}} = \theta_{\text{OMoMo}} = 88.054^\circ$ and $\theta_{\text{MoOO}'} = 73.258^\circ$, in which atoms O and O' are from different (top or bottom) group.

Table CVI shows four VFF terms for the single-layer 1H-MoO₂, one of which is the bond stretching interaction shown by Eq. (1) while the other three terms are the angle bending interaction shown by Eq. (2). These force constant parameters are determined by fitting to the acoustic branches in the phonon dispersion along the ΓM as shown in Fig. 51 (a). The *ab initio* calculations for the phonon dispersion are from Ref. 12. Fig. 51 (b) shows that the VFF model and the SW potential give exactly the same phonon dispersion, as the SW potential is derived from the VFF model.

The parameters for the two-body SW potential used by GULP are shown in Tab. CVII. The parameters for the three-body SW potential used by GULP are shown in Tab. CVIII. Some representative parameters for the SW potential used by LAMMPS are listed in Tab. CIX. We note that twelve atom types have been introduced for the simulation of the single-layer 1H-MoO₂ using LAMMPS, because the angles around atom Mo in Fig. 1 (with M=Mo and X=O) are not distinguishable in LAMMPS. We have suggested two options to differentiate these angles by implementing some additional constraints in LAMMPS, which can be accomplished by modifying the source file of LAMMPS.^{13,14} According to our

experience, it is not so convenient for some users to implement these constraints and re-compile the LAMMPS package. Hence, in the present work, we differentiate the angles by introducing more atom types, so it is not necessary to modify the LAMMPS package. Fig. 2 (with $M=Mo$ and $X=O$) shows that, for 1H-MoO₂, we can differentiate these angles around the Mo atom by assigning these six neighboring O atoms with different atom types. It can be found that twelve atom types are necessary for the purpose of differentiating all six neighbors around one Mo atom.

We use LAMMPS to perform MD simulations for the mechanical behavior of the single-layer 1H-MoO₂ under uniaxial tension at 1.0 K and 300.0 K. Fig. 52 shows the stress-strain curve for the tension of a single-layer 1H-MoO₂ of dimension $100 \times 100 \text{ \AA}$. Periodic boundary conditions are applied in both armchair and zigzag directions. The single-layer 1H-MoO₂ is stretched uniaxially along the armchair or zigzag direction. The stress is calculated without involving the actual thickness of the quasi-two-dimensional structure of the single-layer 1H-MoO₂. The Young's modulus can be obtained by a linear fitting of the stress-strain relation in the small strain range of $[0, 0.01]$. The Young's modulus are 210.0 N/m and 209.3 N/m along the armchair and zigzag directions, respectively. The Young's modulus is essentially isotropic in the armchair and zigzag directions. The Poisson's ratio from the VFF model and the SW potential is $\nu_{xy} = \nu_{yx} = 0.17$.

There is no available value for nonlinear quantities in the single-layer 1H-MoO₂. We have thus used the nonlinear parameter $B = 0.5d^4$ in Eq. (5), which is close to the value of B in most materials. The value of the third order nonlinear elasticity D can be extracted by fitting the stress-strain relation to the function $\sigma = E\epsilon + \frac{1}{2}D\epsilon^2$ with E as the Young's modulus. The values of D from the present SW potential are -1027.8 N/m and -1106.8 N/m along the armchair and zigzag directions, respectively. The ultimate stress is about 21.0 Nm^{-1} at the ultimate strain of 0.19 in the armchair direction at the low temperature of 1 K. The ultimate stress is about 20.1 Nm^{-1} at the ultimate strain of 0.22 in the zigzag direction at the low temperature of 1 K.

XXVIII. 1H-MOS₂

Several potentials have been proposed to describe the interaction for the single-layer 1H-MoS₂. In 1975, Wakabayashi et al. developed a VFF model to calculate the phonon

TABLE CX: The VFF model parameters for single-layer 1H-MoS₂ from Ref. 22. The second line gives the expression for each VFF term. Parameters are in the unit of $\frac{eV}{\text{Å}^2}$ for the bond stretching interactions, and in the unit of eV for the angle bending interaction. The fourth line gives the initial bond length (in unit of Å) for the bond stretching interaction and the initial angle (in unit of degrees) for the angle bending interaction. The angle θ_{ijk} has atom i as the apex.

VFF type	bond stretching	angle bending	
expression	$\frac{1}{2}K_{Mo-S}(\Delta r_{Mo-S})^2$	$\frac{1}{2}K_{MoSS}(\Delta\theta_{MoSS})^2$	$\frac{1}{2}K_{SMoMo}(\Delta\theta_{SMoMo})^2$
parameter	8.640	5.316	4.891
r_0 or θ_0	2.382	80.581	80.581

TABLE CXI: Two-body SW potential parameters for single-layer 1H-MoS₂ used by GULP⁸ as expressed in Eq. (3).

	A (eV)	ρ (Å)	B (Å ⁴)	r_{\min} (Å)	r_{\max} (Å)
r_{Mo-S}	6.918	1.252	17.771	0.0	3.16

TABLE CXII: Three-body SW potential parameters for single-layer 1H-MoS₂ used by GULP⁸ as expressed in Eq. (4). The angle θ_{ijk} in the first line indicates the bending energy for the angle with atom i as the apex.

	K (eV)	θ_0 (degree)	ρ_1 (Å)	ρ_2 (Å)	$r_{\min12}$ (Å)	$r_{\max12}$ (Å)	$r_{\min13}$ (Å)	$r_{\max13}$ (Å)	$r_{\min23}$ (Å)	$r_{\max23}$ (Å)
θ_{MoSS}	67.883	81.788	1.252	1.252	0.0	3.16	0.0	3.16	0.0	3.78
θ_{SMoMo}	62.449	81.788	1.252	1.252	0.0	3.16	0.0	3.16	0.0	4.27

TABLE CXIII: SW potential parameters for single-layer 1H-MoS₂ used by LAMMPS⁹ as expressed in Eqs. (9) and (10). Atom types in the first column are displayed in Fig. 2 (with M=Mo and X=S).

	ϵ (eV)	σ (Å)	a	λ	γ	$\cos\theta_0$	A_L	B_L	p	q	tol
Mo ₁ -S ₁ -S ₁	1.000	1.252	2.523	0.000	1.000	0.000	6.918	7.223	4	0	0.0
Mo ₁ -S ₁ -S ₃	1.000	0.000	0.000	67.883	1.000	0.143	0.000	0.000	4	0	0.0
S ₁ -Mo ₁ -Mo ₃	1.000	0.000	0.000	62.449	1.000	0.143	0.000	0.000	4	0	0.0

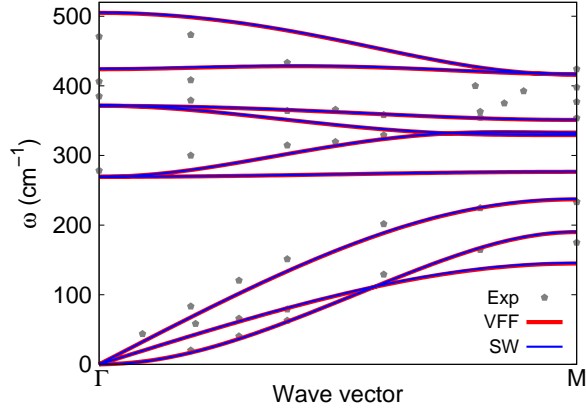


FIG. 53: (Color online) Phonon spectrum for single-layer 1H-MoS₂. Phonon dispersion along the Γ M direction in the Brillouin zone. The results from the VFF model (lines) are comparable with the experiment data (pentagons) from Ref. 22. The phonon dispersion from the SW potential is exactly the same as that from the VFF model.

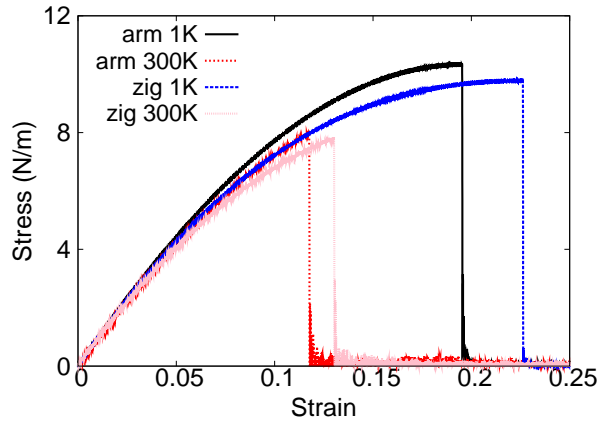


FIG. 54: (Color online) Stress-strain for single-layer 1H-MoS₂ of dimension $100 \times 100 \text{ \AA}$ along the armchair and zigzag directions.

spectrum of the bulk 2H-MoS₂.²² In 2009, Liang et al. parameterized a bond-order potential for 1H-MoS₂,²³ which is based on the bond order concept underlying the Brenner potential.⁶ A separate force field model was parameterized in 2010 for MD simulations of bulk 2H-MoS₂.²⁴ The present author (J.W.J.) and his collaborators parameterized the SW potential for 1H-MoS₂ in 2013,¹³ which was improved by one of the present author (J.W.J.) in 2015.⁷ Recently, another set of parameters for the SW potential were proposed for the single-layer

1H-MoS₂.²⁵

We show the VFF model and the SW potential for single-layer 1H-MoS₂ in this section. These potentials have been developed in previous works. The VFF model presented here is from Ref. 22, while the SW potential presented in this section is from Ref. 7.

The structural parameters for the single-layer 1H-MoS₂ are from the first-principles calculations as shown in Fig. 1 (with M=Mo and X=S).²⁶ The Mo atom layer in the single-layer 1H-MoS₂ is sandwiched by two S atom layers. Accordingly, each Mo atom is surrounded by six S atoms, while each S atom is connected to three Mo atoms. The bond length between neighboring Mo and S atoms is $d = 2.382 \text{ \AA}$, and the angles are $\theta_{\text{MoSS}} = 80.581^\circ$ and $\theta_{\text{SMoMo}} = 80.581^\circ$.

The VFF model for single-layer 1H-MoS₂ is from Ref. 22, which is able to describe the phonon spectrum and the sound velocity accurately. We have listed the first three leading force constants for single-layer 1H-MoS₂ in Tab. CX, neglecting other weak interaction terms. The SW potential parameters for single-layer 1H-MoS₂ used by GULP are listed in Tabs. CXI and CXII. The SW potential parameters for single-layer 1H-MoS₂ used by LAMMPS⁹ are listed in Tab. CXIII. We note that twelve atom types have been introduced for the simulation of the single-layer 1H-MoS₂ using LAMMPS, because the angles around atom Mo in Fig. 1 (with M=Mo and X=S) are not distinguishable in LAMMPS. We have suggested two options to differentiate these angles by implementing some additional constraints in LAMMPS, which can be accomplished by modifying the source file of LAMMPS.^{13,14} According to our experience, it is not so convenient for some users to implement these constraints and recompile the LAMMPS package. Hence, in the present work, we differentiate the angles by introducing more atom types, so it is not necessary to modify the LAMMPS package. Fig. 2 (with M=Mo and X=S) shows that, for 1H-MoS₂, we can differentiate these angles around the Mo atom by assigning these six neighboring S atoms with different atom types. It can be found that twelve atom types are necessary for the purpose of differentiating all six neighbors around one Mo atom.

We use GULP to compute the phonon dispersion for the single-layer 1H-MoS₂ as shown in Fig. 53. The results from the VFF model are quite comparable with the experiment data. The phonon dispersion from the SW potential is the same as that from the VFF model, which indicates that the SW potential has fully inherited the linear portion of the interaction from the VFF model.

TABLE CXIV: The VFF model for single-layer 1H-MoSe₂. The second line gives an explicit expression for each VFF term. The third line is the force constant parameters. Parameters are in the unit of $\frac{\text{eV}}{\text{Å}^2}$ for the bond stretching interactions, and in the unit of eV for the angle bending interaction. The fourth line gives the initial bond length (in unit of Å) for the bond stretching interaction and the initial angle (in unit of degrees) for the angle bending interaction. The angle θ_{ijk} has atom i as the apex.

VFF type	bond stretching	angle bending		
expression	$\frac{1}{2}K_{Mo-Se}(\Delta r)^2$	$\frac{1}{2}K_{Mo-Se-Se}(\Delta\theta)^2$	$\frac{1}{2}K_{Mo-Se-Se'}(\Delta\theta)^2$	$\frac{1}{2}K_{Se-Mo-Mo}(\Delta\theta)^2$
parameter	7.928	6.945	6.945	5.782
r_0 or θ_0	2.528	82.119	81.343	82.119

We use LAMMPS to perform MD simulations for the mechanical behavior of the single-layer 1H-MoS₂ under uniaxial tension at 1.0 K and 300.0 K. Fig. 54 shows the stress-strain curve during the tension of a single-layer 1H-MoS₂ of dimension 100×100 Å. Periodic boundary conditions are applied in both armchair and zigzag directions. The single-layer 1H-MoS₂ is stretched uniaxially along the armchair or zigzag direction. The stress is calculated without involving the actual thickness of the quasi-two-dimensional structure of the single-layer 1H-MoS₂. The Young's modulus can be obtained by a linear fitting of the stress-strain relation in the small strain range of $[0, 0.01]$. The Young's modulus are 97 N/m and 96 N/m along the armchair and zigzag directions, respectively. The Young's modulus is isotropic in the armchair and zigzag directions. These values are in considerable agreement with the experimental results, eg. 120 ± 30 N/m from Refs 27,28, or 180 ± 60 N/m from Ref. 29. The third-order nonlinear elastic constant D can be obtained by fitting the stress-strain relation to $\sigma = E\epsilon + \frac{1}{2}D\epsilon^2$ with E as the Young's modulus. The values of D are -418 N/m and -461 N/m along the armchair and zigzag directions, respectively. The Poisson's ratio from the VFF model and the SW potential is $\nu_{xy} = \nu_{yx} = 0.27$.

XXIX. 1H-MOSE₂

There is a recent parameter set for the SW potential in the single-layer 1H-MoSe₂.²⁵ In this section, we will develop both VFF model and the SW potential for the single-layer

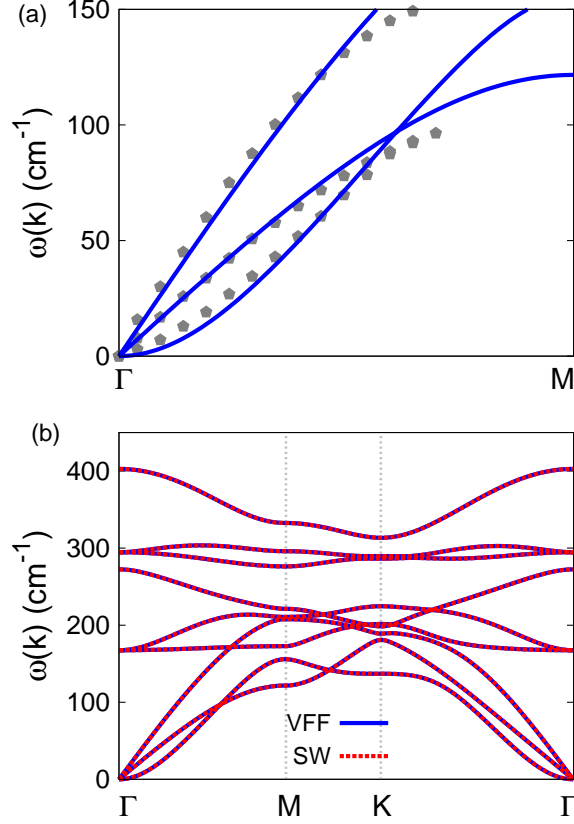


FIG. 55: (Color online) Phonon dispersion for single-layer 1H-MoSe₂. (a) The VFF model is fitted to the three acoustic branches in the long wave limit along the ΓM direction. The *ab initio* results (gray pentagons) are from Ref. 30. (b) The VFF model (blue lines) and the SW potential (red lines) give the same phonon dispersion for single-layer 1H-MoSe₂ along $\Gamma\text{MK}\Gamma$.

TABLE CXV: Two-body SW potential parameters for single-layer 1H-MoSe₂ used by GULP⁸ as expressed in Eq. (3).

	A (eV)	ρ (\AA)	B (\AA^4)	r_{\min} (\AA)	r_{\max} (\AA)
Mo-Se	5.737	0.913	18.787	0.0	3.351

1H-MoSe₂.

The structure for the single-layer 1H-MoSe₂ is shown in Fig. 1 (with M=Mo and X=Se). Each Mo atom is surrounded by six Se atoms. These Se atoms are categorized into the top group (eg. atoms 1, 3, and 5) and bottom group (eg. atoms 2, 4, and 6). Each Se atom is connected to three Mo atoms. The structural parameters are from Ref. 30, including the

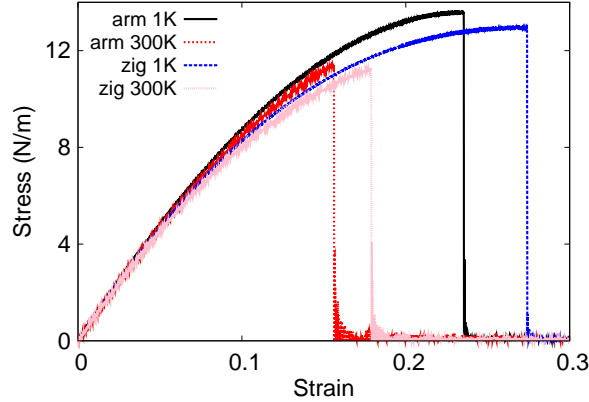


FIG. 56: (Color online) Stress-strain for single-layer 1H-MoSe₂ of dimension $100 \times 100 \text{ \AA}$ along the armchair and zigzag directions.

TABLE CXVI: Three-body SW potential parameters for single-layer 1H-MoSe₂ used by GULP⁸ as expressed in Eq. (4). The angle θ_{ijk} in the first line indicates the bending energy for the angle with atom i as the apex.

	K (eV)	θ_0 (degree)	ρ_1 (\AA)	ρ_2 (\AA)	$r_{\min 12}$ (\AA)	$r_{\max 12}$ (\AA)	$r_{\min 13}$ (\AA)	$r_{\max 13}$ (\AA)	$r_{\min 23}$ (\AA)	$r_{\max 23}$ (\AA)
$\theta_{\text{Mo-Se-Se}}$	32.526	82.119	0.913	0.913	0.0	3.351	0.0	3.351	0.0	4.000
$\theta_{\text{Mo-Se-Se}'}$	32.654	81.343	0.913	0.913	0.0	3.351	0.0	3.351	0.0	4.000
$\theta_{\text{Se-Mo-Mo}}$	27.079	82.119	0.913	0.913	0.0	3.351	0.0	3.351	0.0	4.000

lattice constant $a = 3.321 \text{ \AA}$, and the bond length $d_{\text{Mo-Se}} = 2.528 \text{ \AA}$. The resultant angles are $\theta_{\text{MoSeSe}} = \theta_{\text{SeMoMo}} = 82.119^\circ$ and $\theta_{\text{MoSeSe}'}$ = 81.343° , in which atoms Se and Se' are from different (top or bottom) group.

Table CXIV shows four VFF terms for the 1H-MoSe₂, one of which is the bond stretching interaction shown by Eq. (1) while the other three terms are the angle bending interaction shown by Eq. (2). These force constant parameters are determined by fitting to the three acoustic branches in the phonon dispersion along the ΓM as shown in Fig. 55 (a). The *ab initio* calculations for the phonon dispersion are from Ref. 30. Similar phonon dispersion can also be found in other *ab initio* calculations.^{12,31-34} Fig. 55 (b) shows that the VFF model and the SW potential give exactly the same phonon dispersion, as the SW potential is derived from the VFF model.

The parameters for the two-body SW potential used by GULP are shown in Tab. CXV.

TABLE CXVII: SW potential parameters for single-layer 1H-MoSe₂ used by LAMMPS⁹ as expressed in Eqs. (9) and (10). Atom types in the first column are displayed in Fig. 2 (with M=Mo and X=Se).

	ϵ (eV)	σ (Å)	a	λ	γ	$\cos \theta_0$	A_L	B_L	p	q	tol
Mo ₁ -Se ₁ -Se ₁	1.000	0.913	3.672	0.000	1.000	0.000	5.737	27.084	4	0	0.0
Mo ₁ -Se ₁ -Se ₃	1.000	0.000	0.000	32.526	1.000	0.137	0.000	0.000	4	0	0.0
Mo ₁ -Se ₁ -Se ₂	1.000	0.000	0.000	32.654	1.000	0.151	0.000	0.000	4	0	0.0
Se ₁ -Mo ₁ -Mo ₃	1.000	0.000	0.000	27.079	1.000	0.137	0.000	0.000	4	0	0.0

The parameters for the three-body SW potential used by GULP are shown in Tab. CXVI. Parameters for the SW potential used by LAMMPS are listed in Tab. CXVII. We note that twelve atom types have been introduced for the simulation of the single-layer 1H-MoSe₂ using LAMMPS, because the angles around atom Mo in Fig. 1 (with M=Mo and X=Se) are not distinguishable in LAMMPS. We have suggested two options to differentiate these angles by implementing some additional constraints in LAMMPS, which can be accomplished by modifying the source file of LAMMPS.^{13,14} According to our experience, it is not so convenient for some users to implement these constraints and recompile the LAMMPS package. Hence, in the present work, we differentiate the angles by introducing more atom types, so it is not necessary to modify the LAMMPS package. Fig. 2 (with M=Mo and X=Se) shows that, for 1H-MoSe₂, we can differentiate these angles around the Mo atom by assigning these six neighboring Se atoms with different atom types. It can be found that twelve atom types are necessary for the purpose of differentiating all six neighbors around one Mo atom.

We use LAMMPS to perform MD simulations for the mechanical behavior of the single-layer 1H-MoSe₂ under uniaxial tension at 1.0 K and 300.0 K. Fig. 56 shows the stress-strain curve during the tension of a single-layer 1H-MoSe₂ of dimension 100×100 Å. Periodic boundary conditions are applied in both armchair and zigzag directions. The single-layer 1H-MoSe₂ is stretched uniaxially along the armchair or zigzag direction. The stress is calculated without involving the actual thickness of the quasi-two-dimensional structure of the single-layer 1H-MoSe₂. The Young's modulus can be obtained by a linear fitting of the stress-strain relation in the small strain range of $[0, 0.01]$. The Young's modulus are 103.0 N/m and 101.8 N/m along the armchair and zigzag directions, respectively. The

TABLE CXVIII: The VFF model for single-layer 1H-MoTe₂. The second line gives an explicit expression for each VFF term. The third line is the force constant parameters. Parameters are in the unit of $\frac{\text{eV}}{\text{Å}^2}$ for the bond stretching interactions, and in the unit of eV for the angle bending interaction. The fourth line gives the initial bond length (in unit of Å) for the bond stretching interaction and the initial angle (in unit of degrees) for the angle bending interaction. The angle θ_{ijk} has atom *i* as the apex.

VFF type	bond stretching	angle bending		
expression	$\frac{1}{2}K_{\text{Mo-Te}}(\Delta r)^2$	$\frac{1}{2}K_{\text{Mo-Te-Te}}(\Delta\theta)^2$	$\frac{1}{2}K_{\text{Mo-Te-Te'}}(\Delta\theta)^2$	$\frac{1}{2}K_{\text{Te-Mo-Mo}}(\Delta\theta)^2$
parameter	6.317	6.184	6.184	5.225
r_0 or θ_0	2.730	81.111	82.686	81.111

Young's modulus is essentially isotropic in the armchair and zigzag directions. These values are in considerable agreement with the experimental results, eg. 103.9 N/m from Refs 18, or 113.9 N/m from Ref. 35. The Poisson's ratio from the VFF model and the SW potential is $\nu_{xy} = \nu_{yx} = 0.24$, which agrees quite well with the *ab initio* value of 0.23.¹⁸

We have determined the nonlinear parameter to be $B = 0.46d^4$ in Eq. (5) by fitting to the third-order nonlinear elastic constant D from the *ab initio* calculations.³⁵ We have extracted the value of $D = -383.7$ N/m by fitting the stress-strain relation along the armchair direction in the *ab initio* calculations to the function $\sigma = E\epsilon + \frac{1}{2}D\epsilon^2$ with E as the Young's modulus. The values of D from the present SW potential are -365.4 N/m and -402.4 N/m along the armchair and zigzag directions, respectively. The ultimate stress is about 13.6 Nm⁻¹ at the ultimate strain of 0.23 in the armchair direction at the low temperature of 1 K. The ultimate stress is about 13.0 Nm⁻¹ at the ultimate strain of 0.27 in the zigzag direction at the low temperature of 1 K.

XXX. 1H-MOTE₂

Most existing theoretical studies on the single-layer 1H-MoTe₂ are based on the first-principles calculations. In this section, we will develop both VFF model and the SW potential for the single-layer 1H-MoTe₂.

The structure for the single-layer 1H-MoTe₂ is shown in Fig. 1 (with M=Mo and X=Te).

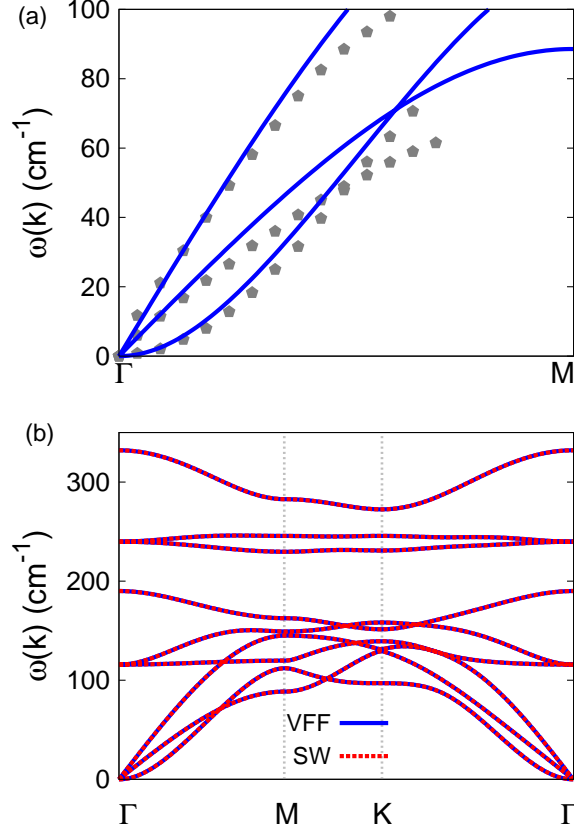


FIG. 57: (Color online) Phonon dispersion for single-layer 1H-MoTe₂. (a) The VFF model is fitted to the three acoustic branches in the long wave limit along the ΓM direction. The *ab initio* results (gray pentagons) are from Ref. 36. (b) The VFF model (blue lines) and the SW potential (red lines) give the same phonon dispersion for single-layer 1H-MoTe₂ along $\Gamma\text{MK}\Gamma$.

TABLE CXIX: Two-body SW potential parameters for single-layer 1H-MoTe₂ used by GULP⁸ as expressed in Eq. (3).

	A (eV)	ρ (\AA)	B (\AA^4)	r_{\min} (\AA)	r_{\max} (\AA)
Mo-Te	5.086	0.880	24.440	0.0	3.604

Each Mo atom is surrounded by six Te atoms. These Te atoms are categorized into the top group (eg. atoms 1, 3, and 5) and bottom group (eg. atoms 2, 4, and 6). Each Te atom is connected to three Mo atoms. The structural parameters are from Ref. 36, including the lattice constant $a = 3.55 \text{ \AA}$, and the bond length $d_{\text{Mo-Te}} = 2.73 \text{ \AA}$. The resultant angles are $\theta_{\text{MoTeTe}} = \theta_{\text{TeMoMo}} = 81.111^\circ$ and $\theta_{\text{MoTeTe}'} = 82.686^\circ$, in which atoms Te and Te' are from

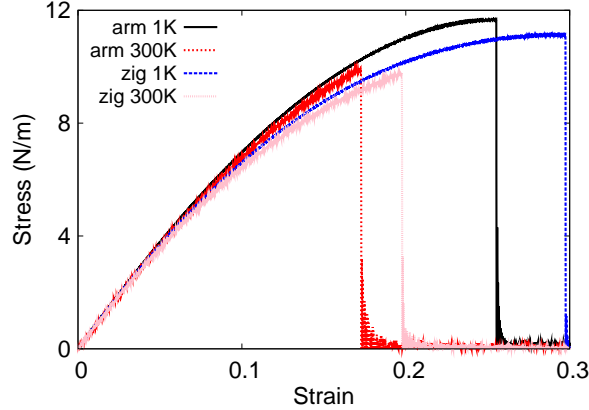


FIG. 58: (Color online) Stress-strain for single-layer 1H-MoTe₂ of dimension $100 \times 100 \text{ \AA}$ along the armchair and zigzag directions.

TABLE CXX: Three-body SW potential parameters for single-layer 1H-MoTe₂ used by GULP⁸ as expressed in Eq. (4). The angle θ_{ijk} in the first line indicates the bending energy for the angle with atom i as the apex.

	K (eV)	θ_0 (degree)	ρ_1 (Å)	ρ_2 (Å)	$r_{\min 12}$ (Å)	$r_{\max 12}$ (Å)	$r_{\min 13}$ (Å)	$r_{\max 13}$ (Å)	$r_{\min 23}$ (Å)	$r_{\max 23}$ (Å)
$\theta_{\text{Mo-Te-Te}}$	23.705	81.111	0.880	0.880	0.0	3.604	0.0	3.604	0.0	4.305
$\theta_{\text{Mo-Te-Te}'}$	23.520	82.686	0.880	0.880	0.0	3.604	0.0	3.604	0.0	4.305
$\theta_{\text{Te-Mo-Mo}}$	20.029	81.111	0.880	0.880	0.0	3.604	0.0	3.604	0.0	4.305

different (top or bottom) group.

Table CXVIII shows four VFF terms for the 1H-MoTe₂, one of which is the bond stretching interaction shown by Eq. (1) while the other three terms are the angle bending interaction shown by Eq. (2). These force constant parameters are determined by fitting to the three acoustic branches in the phonon dispersion along the ΓM as shown in Fig. 57 (a). The *ab initio* calculations for the phonon dispersion are from Ref. 36. Similar phonon dispersion can also be found in other *ab initio* calculations.^{12,34,37} Fig. 57 (b) shows that the VFF model and the SW potential give exactly the same phonon dispersion, as the SW potential is derived from the VFF model.

The parameters for the two-body SW potential used by GULP are shown in Tab. CXIX. The parameters for the three-body SW potential used by GULP are shown in Tab. CXX. Parameters for the SW potential used by LAMMPS are listed in Tab. CXXI. We note that

TABLE CXXI: SW potential parameters for single-layer 1H-MoTe₂ used by LAMMPS⁹ as expressed in Eqs. (9) and (10). Atom types in the first column are displayed in Fig. 2 (with M=Mo and X=Te).

	ϵ (eV)	σ (Å)	a	λ	γ	$\cos \theta_0$	A_L	B_L	p	q	tol
Mo ₁ -Te ₁ -Te ₁	1.000	0.900	4.016	0.000	1.000	0.000	5.169	37.250	4	0	0.0
Mo ₁ -Te ₁ -Te ₃	1.000	0.000	0.000	24.163	1.000	0.143	0.000	0.000	4	0	0.0
Te ₁ -Mo ₁ -Mo ₃	1.000	0.000	0.000	20.416	1.000	0.143	0.000	0.000	4	0	0.0

twelve atom types have been introduced for the simulation of the single-layer 1H-MoTe₂ using LAMMPS, because the angles around atom Mo in Fig. 1 (with M=Mo and X=Te) are not distinguishable in LAMMPS. We have suggested two options to differentiate these angles by implementing some additional constraints in LAMMPS, which can be accomplished by modifying the source file of LAMMPS.^{13,14} According to our experience, it is not so convenient for some users to implement these constraints and recompile the LAMMPS package. Hence, in the present work, we differentiate the angles by introducing more atom types, so it is not necessary to modify the LAMMPS package. Fig. 2 (with M=Mo and X=Te) shows that, for 1H-MoTe₂, we can differentiate these angles around the Mo atom by assigning these six neighboring Te atoms with different atom types. It can be found that twelve atom types are necessary for the purpose of differentiating all six neighbors around one Mo atom.

We use LAMMPS to perform MD simulations for the mechanical behavior of the single-layer 1H-MoTe₂ under uniaxial tension at 1.0 K and 300.0 K. Fig. 58 shows the stress-strain curve for the tension of a single-layer 1H-MoTe₂ of dimension 100 × 100 Å. Periodic boundary conditions are applied in both armchair and zigzag directions. The single-layer 1H-MoTe₂ is stretched uniaxially along the armchair or zigzag direction. The stress is calculated without involving the actual thickness of the quasi-two-dimensional structure of the single-layer 1H-MoTe₂. The Young's modulus can be obtained by a linear fitting of the stress-strain relation in the small strain range of [0, 0.01]. The Young's modulus are 79.8 N/m and 78.5 N/m along the armchair and zigzag directions, respectively. The Young's modulus is essentially isotropic in the armchair and zigzag directions. These values are in considerable agreement with the experimental results, eg. 79.4 N/m from Refs 18, or 87.0 N/m from Ref. 35. The Poisson's ratio from the VFF model and the SW potential is $\nu_{xy} = \nu_{yx} = 0.25$, which agrees

TABLE CXXII: The VFF model for single-layer 1H-TaS₂. The second line gives an explicit expression for each VFF term. The third line is the force constant parameters. Parameters are in the unit of $\frac{\text{eV}}{\text{Å}^2}$ for the bond stretching interactions, and in the unit of eV for the angle bending interaction. The fourth line gives the initial bond length (in unit of Å) for the bond stretching interaction and the initial angle (in unit of degrees) for the angle bending interaction. The angle θ_{ijk} has atom i as the apex.

VFF type	bond stretching		angle bending	
expression	$\frac{1}{2}K_{\text{Ta-S}}(\Delta r)^2$	$\frac{1}{2}K_{\text{Ta-S-S}}(\Delta\theta)^2$	$\frac{1}{2}K_{\text{Ta-S-S'}}(\Delta\theta)^2$	$\frac{1}{2}K_{\text{S-Ta-Ta}}(\Delta\theta)^2$
parameter	8.230	4.811	4.811	4.811
r_0 or θ_0	2.480	83.879	78.979	83.879

TABLE CXXIII: Two-body SW potential parameters for single-layer 1H-TaS₂ used by GULP⁸ as expressed in Eq. (3).

	A (eV)	ρ (Å)	B (Å ⁴)	r_{min} (Å)	r_{max} (Å)
Ta-S	6.446	1.111	18.914	0.0	3.310

with the *ab initio* value of 0.24.¹⁸

We have determined the nonlinear parameter to be $B = 0.44d^4$ in Eq. (5) by fitting to the third-order nonlinear elastic constant D from the *ab initio* calculations.³⁵ We have extracted the value of $D = -278.2$ N/m by fitting the stress-strain relation along the armchair direction in the *ab initio* calculations to the function $\sigma = E\epsilon + \frac{1}{2}D\epsilon^2$ with E as the Young's modulus. The values of D from the present SW potential are -250.5 N/m and -276.6 N/m along the armchair and zigzag directions, respectively. The ultimate stress is about 11.7 Nm⁻¹ at the ultimate strain of 0.25 in the armchair direction at the low temperature of 1 K. The ultimate stress is about 11.1 Nm⁻¹ at the ultimate strain of 0.29 in the zigzag direction at the low temperature of 1 K.

XXXI. 1H-TAS₂

In 1983, the VFF model was developed to investigate the lattice dynamical properties in the bulk 2H-TaS₂.²¹ In this section, we will develop the SW potential for the single-layer

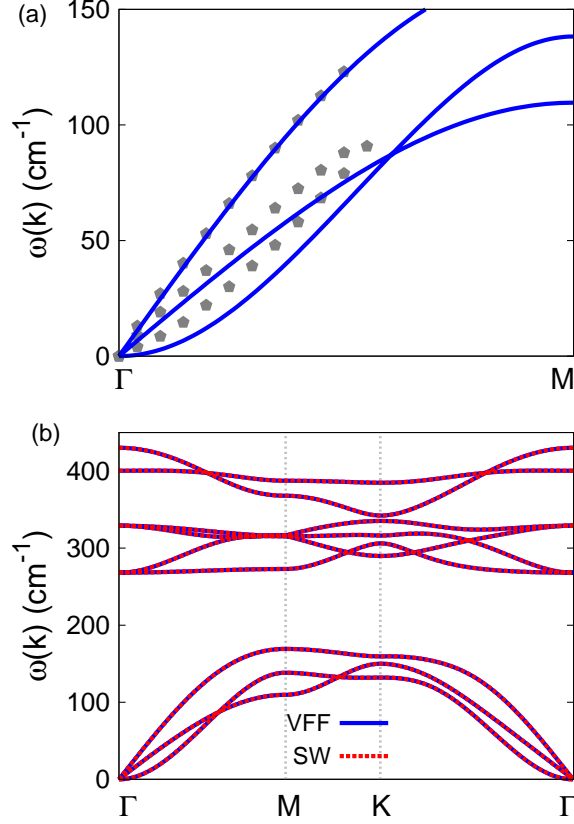


FIG. 59: (Color online) Phonon dispersion for single-layer 1H-TaS₂. (a) The VFF model is fitted to the three acoustic branches in the long wave limit along the Γ M direction. The theoretical results (gray pentagons) are from Ref. 21. The blue lines are from the present VFF model. (b) The VFF model (blue lines) and the SW potential (red lines) give the same phonon dispersion for single-layer 1H-TaS₂ along Γ MK Γ .

1H-TaS₂.

The structure for the single-layer 1H-TaS₂ is shown in Fig. 1 (with M=Ta and X=S). Each Ta atom is surrounded by six S atoms. These S atoms are categorized into the top group (eg. atoms 1, 3, and 5) and bottom group (eg. atoms 2, 4, and 6). Each S atom is connected to three Ta atoms. The structural parameters are from Ref. 21, including the lattice constant $a = 3.315 \text{ \AA}$, and the bond length $d_{\text{Ta-S}} = 2.48 \text{ \AA}$. The resultant angles are $\theta_{\text{TaSS}} = \theta_{\text{STaTa}} = 83.879^\circ$ and $\theta_{\text{TaSS}'} = 78.979^\circ$, in which atoms S and S' are from different (top or bottom) group.

Table CXXII shows the VFF terms for the 1H-TaS₂, one of which is the bond stretching

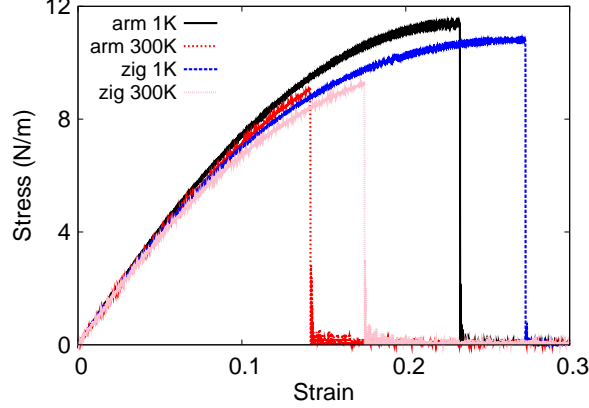


FIG. 60: (Color online) Stress-strain for single-layer 1H-TaS₂ of dimension 100 × 100 Å along the armchair and zigzag directions.

TABLE CXXIV: Three-body SW potential parameters for single-layer 1H-TaS₂ used by GULP⁸ as expressed in Eq. (4). The angle θ_{ijk} in the first line indicates the bending energy for the angle with atom i as the apex.

	K (eV)	θ_0 (degree)	ρ_1 (Å)	ρ_2 (Å)	$r_{\min 12}$ (Å)	$r_{\max 12}$ (Å)	$r_{\min 13}$ (Å)	$r_{\max 13}$ (Å)	$r_{\min 23}$ (Å)	$r_{\max 23}$ (Å)
$\theta_{\text{Ta-S-S}}$	35.396	83.879	1.111	1.111	0.0	3.310	0.0	3.310	0.0	3.945
$\theta_{\text{Ta-S-S}'}$	36.321	78.979	1.111	1.111	0.0	3.310	0.0	3.310	0.0	3.945
$\theta_{\text{S-Ta-Ta}}$	35.396	83.879	1.111	1.111	0.0	3.310	0.0	3.310	0.0	3.945

interaction shown by Eq. (1) while the others are the angle bending interaction shown by Eq. (2). These force constant parameters are determined by fitting to the three acoustic branches in the phonon dispersion along the ΓM as shown in Fig. 59 (a). The theoretical phonon frequencies (gray pentagons) are from Ref. 21, which are the phonon dispersion of bulk 2H-TaS₂. We have used these phonon frequencies as the phonon dispersion of the single-layer 1H-TaS₂, as the inter-layer interaction in the bulk 2H-TaS₂ only induces weak effects on the two inplane acoustic branches. The inter-layer coupling will strengthen the out-of-plane acoustic (flexural) branch, so the flexural branch from the present VFF model (blue line) is lower than the theoretical results for bulk 2H-TaS₂ (gray pentagons). Fig. 59 (b) shows that the VFF model and the SW potential give exactly the same phonon dispersion, as the SW potential is derived from the VFF model.

The parameters for the two-body SW potential used by GULP are shown in Tab. CXXIII.

TABLE CXXV: SW potential parameters for single-layer 1H-TaS₂ used by LAMMPS⁹ as expressed in Eqs. (9) and (10). Atom types in the first column are displayed in Fig. 2 (with M=Ta and X=S).

	ϵ (eV)	σ (Å)	a	λ	γ	$\cos \theta_0$	A_L	B_L	p	q	tol
Ta ₁ -S ₁ -S ₁	1.000	1.111	2.979	0.000	1.000	0.000	6.446	12.408	4	0	0.0
Ta ₁ -S ₁ -S ₃	1.000	0.000	0.000	35.396	1.000	0.107	0.000	0.000	4	0	0.0
Ta ₁ -S ₁ -S ₂	1.000	0.000	0.000	36.321	1.000	0.191	0.000	0.000	4	0	0.0
S ₁ -Ta ₁ -Ta ₃	1.000	0.000	0.000	35.396	1.000	0.107	0.000	0.000	4	0	0.0

The parameters for the three-body SW potential used by GULP are shown in Tab. CXXIV. Parameters for the SW potential used by LAMMPS are listed in Tab. CXXV. We note that twelve atom types have been introduced for the simulation of the single-layer 1H-TaS₂ using LAMMPS, because the angles around atom Ta in Fig. 1 (with M=Ta and X=S) are not distinguishable in LAMMPS. We have suggested two options to differentiate these angles by implementing some additional constraints in LAMMPS, which can be accomplished by modifying the source file of LAMMPS.^{13,14} According to our experience, it is not so convenient for some users to implement these constraints and recompile the LAMMPS package. Hence, in the present work, we differentiate the angles by introducing more atom types, so it is not necessary to modify the LAMMPS package. Fig. 2 (with M=Ta and X=S) shows that, for 1H-TaS₂, we can differentiate these angles around the Ta atom by assigning these six neighboring S atoms with different atom types. It can be found that twelve atom types are necessary for the purpose of differentiating all six neighbors around one Ta atom.

We use LAMMPS to perform MD simulations for the mechanical behavior of the single-layer 1H-TaS₂ under uniaxial tension at 1.0 K and 300.0 K. Fig. 60 shows the stress-strain curve for the tension of a single-layer 1H-TaS₂ of dimension 100 × 100 Å. Periodic boundary conditions are applied in both armchair and zigzag directions. The single-layer 1H-TaS₂ is stretched uniaxially along the armchair or zigzag direction. The stress is calculated without involving the actual thickness of the quasi-two-dimensional structure of the single-layer 1H-TaS₂. The Young's modulus can be obtained by a linear fitting of the stress-strain relation in the small strain range of [0, 0.01]. The Young's modulus is 87.4 N/m and 86.6 N/m along the armchair and zigzag directions, respectively. The Poisson's ratio from the VFF model and the SW potential is $\nu_{xy} = \nu_{yx} = 0.27$.

TABLE CXXVI: The VFF model for single-layer 1H-TaSe₂. The second line gives an explicit expression for each VFF term. The third line is the force constant parameters. Parameters are in the unit of $\frac{\text{eV}}{\text{Å}^2}$ for the bond stretching interactions, and in the unit of eV for the angle bending interaction. The fourth line gives the initial bond length (in unit of Å) for the bond stretching interaction and the initial angle (in unit of degrees) for the angle bending interaction. The angle θ_{ijk} has atom i as the apex.

VFF type	bond stretching	angle bending		
expression	$\frac{1}{2}K_{\text{Ta-Se}}(\Delta r)^2$	$\frac{1}{2}K_{\text{Ta-Se-Se}}(\Delta\theta)^2$	$\frac{1}{2}K_{\text{Ta-Se-Se'}}(\Delta\theta)^2$	$\frac{1}{2}K_{\text{Se-Ta-Ta}}(\Delta\theta)^2$
parameter	8.230	4.811	4.811	4.811
r_0 or θ_0	2.590	83.107	80.019	83.107

TABLE CXXVII: Two-body SW potential parameters for single-layer 1H-TaSe₂ used by GULP⁸ as expressed in Eq. (3).

	A (eV)	ρ (Å)	B (Å ⁴)	r_{min} (Å)	r_{max} (Å)
Ta-Se	6.885	1.133	22.499	0.0	3.446

There is no available value for the nonlinear quantities in the single-layer 1H-TaS₂. We have thus used the nonlinear parameter $B = 0.5d^4$ in Eq. (5), which is close to the value of B in most materials. The value of the third order nonlinear elasticity D can be extracted by fitting the stress-strain relation to the function $\sigma = E\epsilon + \frac{1}{2}D\epsilon^2$ with E as the Young's modulus. The values of D from the present SW potential are -313.0 N/m and -349.3 N/m along the armchair and zigzag directions, respectively. The ultimate stress is about 11.4 Nm⁻¹ at the ultimate strain of 0.23 in the armchair direction at the low temperature of 1 K. The ultimate stress is about 10.8 Nm⁻¹ at the ultimate strain of 0.27 in the zigzag direction at the low temperature of 1 K.

XXXII. 1H-TASE₂

The VFF model was developed to investigate the lattice dynamical properties in the bulk 2H-TaSe₂.^{15,21} In this section, we will develop the SW potential for the single-layer 1H-TaSe₂.

The structure for the single-layer 1H-TaSe₂ is shown in Fig. 1 (with M=Ta and X=Se).

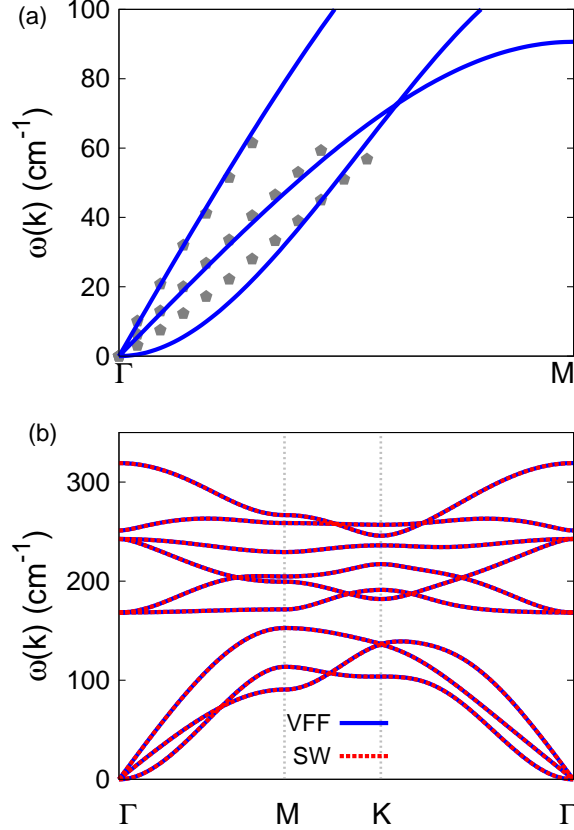


FIG. 61: (Color online) Phonon dispersion for single-layer 1H-TaSe₂. (a) The VFF model is fitted to the three acoustic branches in the long wave limit along the Γ M direction. The theoretical results (gray pentagons) are from Ref. 15. The blue lines are from the present VFF model. (b) The VFF model (blue lines) and the SW potential (red lines) give the same phonon dispersion for single-layer 1H-TaSe₂ along Γ MK Γ .

Each Ta atom is surrounded by six Se atoms. These Se atoms are categorized into the top group (eg. atoms 1, 3, and 5) and bottom group (eg. atoms 2, 4, and 6). Each Se atom is connected to three Ta atoms. The structural parameters are from Ref. 21, including the lattice constant $a = 3.436 \text{ \AA}$, and the bond length $d_{\text{Ta-Se}} = 2.59 \text{ \AA}$. The resultant angles are $\theta_{\text{TaSeSe}} = \theta_{\text{SeTaTa}} = 83.107^\circ$ and $\theta_{\text{TaSeSe}'} = 80.019^\circ$, in which atoms Se and Se' are from different (top or bottom) group.

Table CXXXVI shows the VFF terms for the 1H-TaSe₂, one of which is the bond stretching interaction shown by Eq. (1) while the others are the angle bending interaction shown by Eq. (2). These force constant parameters are determined by fitting to the three acoustic

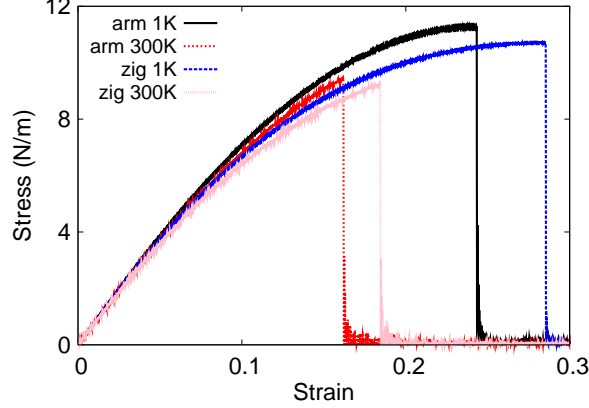


FIG. 62: (Color online) Stress-strain for single-layer 1H-TaSe₂ of dimension $100 \times 100 \text{ \AA}$ along the armchair and zigzag directions.

TABLE CXXVIII: Three-body SW potential parameters for single-layer 1H-TaSe₂ used by GULP⁸ as expressed in Eq. (4). The angle θ_{ijk} in the first line indicates the bending energy for the angle with atom i as the apex.

	K (eV)	θ_0 (degree)	ρ_1 (Å)	ρ_2 (Å)	$r_{\min 12}$ (Å)	$r_{\max 12}$ (Å)	$r_{\min 13}$ (Å)	$r_{\max 13}$ (Å)	$r_{\min 23}$ (Å)	$r_{\max 23}$ (Å)
$\theta_{\text{Ta-Se-Se}}$	34.381	83.107	1.133	1.133	0.0	3.446	0.0	3.446	0.0	4.111
$\theta_{\text{Ta-Se-Se}'}$	34.936	80.019	1.133	1.133	0.0	3.446	0.0	3.446	0.0	4.111
$\theta_{\text{Se-Ta-Ta}}$	34.381	83.107	1.133	1.133	0.0	3.446	0.0	3.446	0.0	4.111

branches in the phonon dispersion along the ΓM as shown in Fig. 61 (a). The theoretical phonon frequencies (gray pentagons) are from Ref. 21, which are the phonon dispersion of bulk 2H-TaSe₂. We have used these phonon frequencies as the phonon dispersion of the single-layer 1H-TaSe₂, as the inter-layer interaction in the bulk 2H-TaSe₂ only induces weak effects on the two in-plane acoustic branches. The inter-layer coupling will strengthen the out-of-plane acoustic branch (flexural branch), so the flexural branch from the present VFF model (blue line) is lower than the theoretical results for bulk 2H-TaSe₂ (gray pentagons). Fig. 61 (b) shows that the VFF model and the SW potential give exactly the same phonon dispersion, as the SW potential is derived from the VFF model.

The parameters for the two-body SW potential used by GULP are shown in Tab. CXXVII. The parameters for the three-body SW potential used by GULP are shown in Tab. CXXVIII. Parameters for the SW potential used by LAMMPS are listed in Tab. CXXIX. We note that

TABLE CXXIX: SW potential parameters for single-layer 1H-TaSe₂ used by LAMMPS⁹ as expressed in Eqs. (9) and (10). Atom types in the first column are displayed in Fig. 2 (with M=Ta and X=Se).

	ϵ (eV)	σ (Å)	a	λ	γ	$\cos \theta_0$	A_L	B_L	p	q	tol
Ta ₁ -Se ₁ -Se ₁	1.000	1.133	3.043	0.000	1.000	0.000	6.885	13.668	4	0	0.0
Ta ₁ -Se ₁ -Se ₃	1.000	0.000	0.000	34.381	1.000	0.120	0.000	0.000	4	0	0.0
Ta ₁ -Se ₁ -Se ₂	1.000	0.000	0.000	34.936	1.000	0.173	0.000	0.000	4	0	0.0
Se ₁ -Ta ₁ -Ta ₃	1.000	0.000	0.000	34.381	1.000	0.120	0.000	0.000	4	0	0.0

twelve atom types have been introduced for the simulation of the single-layer 1H-TaSe₂ using LAMMPS, because the angles around atom Ta in Fig. 1 (with M=Ta and X=Se) are not distinguishable in LAMMPS. We have suggested two options to differentiate these angles by implementing some additional constraints in LAMMPS, which can be accomplished by modifying the source file of LAMMPS.^{13,14} According to our experience, it is not so convenient for some users to implement these constraints and recompile the LAMMPS package. Hence, in the present work, we differentiate the angles by introducing more atom types, so it is not necessary to modify the LAMMPS package. Fig. 2 (with M=Ta and X=Se) shows that, for 1H-TaSe₂, we can differentiate these angles around the Ta atom by assigning these six neighboring Se atoms with different atom types. It can be found that twelve atom types are necessary for the purpose of differentiating all six neighbors around one Ta atom.

We use LAMMPS to perform MD simulations for the mechanical behavior of the single-layer 1H-TaSe₂ under uniaxial tension at 1.0 K and 300.0 K. Fig. 62 shows the stress-strain curve for the tension of a single-layer 1H-TaSe₂ of dimension 100 × 100 Å. Periodic boundary conditions are applied in both armchair and zigzag directions. The single-layer 1H-TaSe₂ is stretched uniaxially along the armchair or zigzag direction. The stress is calculated without involving the actual thickness of the quasi-two-dimensional structure of the single-layer 1H-TaSe₂. The Young's modulus can be obtained by a linear fitting of the stress-strain relation in the small strain range of [0, 0.01]. The Young's modulus are 80.8 N/m and 81.1 N/m along the armchair and zigzag directions, respectively. The Young's modulus is essentially isotropic in the armchair and zigzag directions. The Poisson's ratio from the VFF model and the SW potential is $\nu_{xy} = \nu_{yx} = 0.29$.

TABLE CXXX: The VFF model for single-layer 1H-WO₂. The second line gives an explicit expression for each VFF term. The third line is the force constant parameters. Parameters are in the unit of $\frac{\text{eV}}{\text{\AA}^2}$ for the bond stretching interactions, and in the unit of eV for the angle bending interaction. The fourth line gives the initial bond length (in unit of \AA) for the bond stretching interaction and the initial angle (in unit of degrees) for the angle bending interaction. The angle θ_{ijk} has atom *i* as the apex.

VFF type	bond stretching	angle bending		
expression	$\frac{1}{2}K_{\text{W-O}}(\Delta r)^2$	$\frac{1}{2}K_{\text{W-O-O}}(\Delta\theta)^2$	$\frac{1}{2}K_{\text{W-O-O}'}(\Delta\theta)^2$	$\frac{1}{2}K_{\text{O-W-W}}(\Delta\theta)^2$
parameter	15.318	10.276	10.276	10.276
r_0 or θ_0	2.030	87.206	74.435	87.206

TABLE CXXXI: Two-body SW potential parameters for single-layer 1H-WO₂ used by GULP⁸ as expressed in Eq. (3).

	A (eV)	ρ (\AA)	B (\AA^4)	r_{min} (\AA)	r_{max} (\AA)
W-O	8.781	1.005	8.491	0.0	2.744

There is no available value for the nonlinear quantities in the single-layer 1H-TaSe₂. We have thus used the nonlinear parameter $B = 0.5d^4$ in Eq. (5), which is close to the value of B in most materials. The value of the third order nonlinear elasticity D can be extracted by fitting the stress-strain relation to the function $\sigma = E\epsilon + \frac{1}{2}D\epsilon^2$ with E as the Young's modulus. The values of D from the present SW potential are -263.3 N/m and -308.6 N/m along the armchair and zigzag directions, respectively. The ultimate stress is about 11.3 Nm⁻¹ at the ultimate strain of 0.24 in the armchair direction at the low temperature of 1 K. The ultimate stress is about 10.7 Nm⁻¹ at the ultimate strain of 0.28 in the zigzag direction at the low temperature of 1 K.

XXXIII. 1H-WO₂

Most existing theoretical studies on the single-layer 1H-WO₂ are based on the first-principles calculations. In this section, we will develop the SW potential for the single-layer 1H-WO₂.

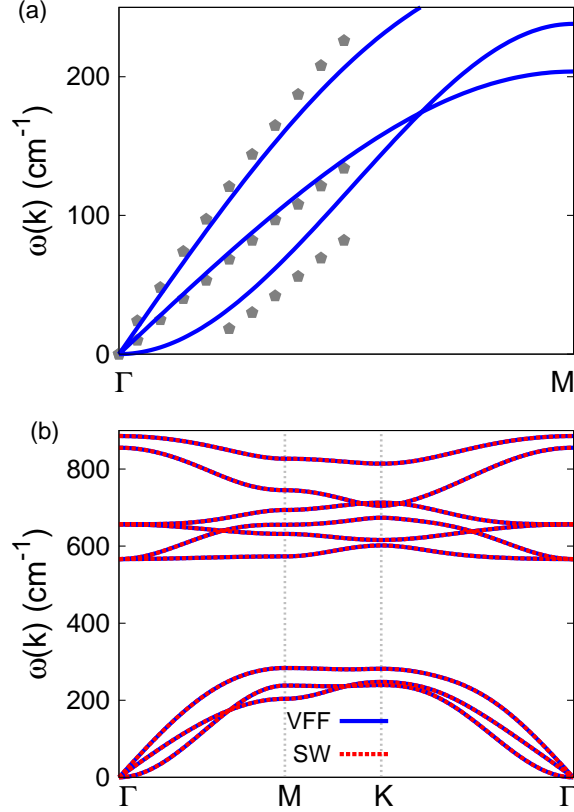


FIG. 63: (Color online) Phonon spectrum for single-layer 1H-WO₂. (a) Phonon dispersion along the Γ M direction in the Brillouin zone. The results from the VFF model (lines) are comparable with the *ab initio* results (pentagons) from Ref. 12. (b) The phonon dispersion from the SW potential is exactly the same as that from the VFF model.

The structure for the single-layer 1H-WO₂ is shown in Fig. 1 (with M=W and X=O). Each W atom is surrounded by six O atoms. These O atoms are categorized into the top group (eg. atoms 1, 3, and 5) and bottom group (eg. atoms 2, 4, and 6). Each O atom is connected to three W atoms. The structural parameters are from the first-principles calculations,¹² including the lattice constant $a = 2.80 \text{ \AA}$, and the bond length $d_{\text{W-O}} = 2.03 \text{ \AA}$. The resultant angles are $\theta_{\text{WOO}} = \theta_{\text{OWW}} = 87.206^\circ$ and $\theta_{\text{WOO}'} = 74.435^\circ$, in which atoms O and O' are from different (top or bottom) group.

Table CXXX shows four VFF terms for the single-layer 1H-WO₂, one of which is the bond stretching interaction shown by Eq. (1) while the other three terms are the angle bending interaction shown by Eq. (2). These force constant parameters are determined by fitting to

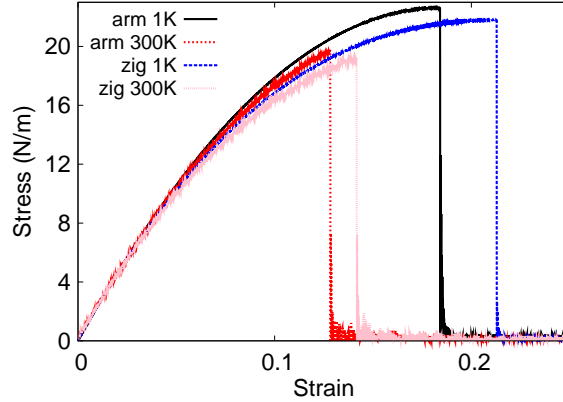


FIG. 64: (Color online) Stress-strain for single-layer 1H-WO₂ of dimension 100 × 100 Å along the armchair and zigzag directions.

TABLE CXXXII: Three-body SW potential parameters for single-layer 1H-WO₂ used by GULP⁸ as expressed in Eq. (4). The angle θ_{ijk} in the first line indicates the bending energy for the angle with atom i as the apex.

	K (eV)	θ_0 (degree)	ρ_1 (Å)	ρ_2 (Å)	$r_{\min 12}$ (Å)	$r_{\max 12}$ (Å)	$r_{\min 13}$ (Å)	$r_{\max 13}$ (Å)	$r_{\min 23}$ (Å)	$r_{\max 23}$ (Å)
θ_{W-O-O}	85.955	87.206	1.005	1.005	0.0	2.744	0.0	2.744	0.0	3.262
$\theta_{W-O-O'}$	92.404	74.435	1.005	1.005	0.0	2.744	0.0	2.744	0.0	3.262
θ_{O-W-W}	85.955	87.206	1.005	1.005	0.0	2.744	0.0	2.744	0.0	3.262

the acoustic branches in the phonon dispersion along the ΓM as shown in Fig. 63 (a). The *ab initio* calculations for the phonon dispersion are from Ref. 12. Fig. 63 (b) shows that the VFF model and the SW potential give exactly the same phonon dispersion, as the SW potential is derived from the VFF model.

The parameters for the two-body SW potential used by GULP are shown in Tab. CXXXI. The parameters for the three-body SW potential used by GULP are shown in Tab. CXXXII. Some representative parameters for the SW potential used by LAMMPS are listed in Tab. CXXXIII. We note that twelve atom types have been introduced for the simulation of the single-layer 1H-WO₂ using LAMMPS, because the angles around atom W in Fig. 1 (with M=W and X=O) are not distinguishable in LAMMPS. We have suggested two options to differentiate these angles by implementing some additional constraints in LAMMPS, which can be accomplished by modifying the source file of LAMMPS.^{13,14} According to our experi-

TABLE CXXXIII: SW potential parameters for single-layer 1H-WO₂ used by LAMMPS⁹ as expressed in Eqs. (9) and (10).

	ϵ (eV)	σ (Å)	a	λ	γ	$\cos \theta_0$	A_L	B_L	p	q	tol
W ₁ -O ₁ -O ₁	1.000	1.005	2.730	0.000	1.000	0.000	8.781	8.316	4	0	0.0
W ₁ -O ₁ -O ₃	1.000	0.000	0.000	85.955	1.000	0.049	0.000	0.000	4	0	0.0
W ₁ -O ₁ -O ₂	1.000	0.000	0.000	92.404	1.000	0.268	0.000	0.000	4	0	0.0
O ₁ -W ₁ -W ₃	1.000	0.000	0.000	85.955	1.000	0.049	0.000	0.000	4	0	0.0

ence, it is not so convenient for some users to implement these constraints and recompile the LAMMPS package. Hence, in the present work, we differentiate the angles by introducing more atom types, so it is not necessary to modify the LAMMPS package. Fig. 2 (with M=W and X=O) shows that, for 1H-WO₂, we can differentiate these angles around the W atom by assigning these six neighboring O atoms with different atom types. It can be found that twelve atom types are necessary for the purpose of differentiating all six neighbors around one W atom.

We use LAMMPS to perform MD simulations for the mechanical behavior of the single-layer 1H-WO₂ under uniaxial tension at 1.0 K and 300.0 K. Fig. 64 shows the stress-strain curve for the tension of a single-layer 1H-WO₂ of dimension 100×100 Å. Periodic boundary conditions are applied in both armchair and zigzag directions. The single-layer 1H-WO₂ is stretched uniaxially along the armchair or zigzag direction. The stress is calculated without involving the actual thickness of the quasi-two-dimensional structure of the single-layer 1H-WO₂. The Young's modulus can be obtained by a linear fitting of the stress-strain relation in the small strain range of $[0, 0.01]$. The Young's modulus are 237.1 N/m and 237.2 N/m along the armchair and zigzag directions, respectively. The Young's modulus is essentially isotropic in the armchair and zigzag directions. The Poisson's ratio from the VFF model and the SW potential is $\nu_{xy} = \nu_{yx} = 0.15$.

There is no available value for nonlinear quantities in the single-layer 1H-WO₂. We have thus used the nonlinear parameter $B = 0.5d^4$ in Eq. (5), which is close to the value of B in most materials. The value of the third order nonlinear elasticity D can be extracted by fitting the stress-strain relation to the function $\sigma = E\epsilon + \frac{1}{2}D\epsilon^2$ with E as the Young's modulus. The values of D from the present SW potential are -1218.0 N/m and -1312.9 N/m along

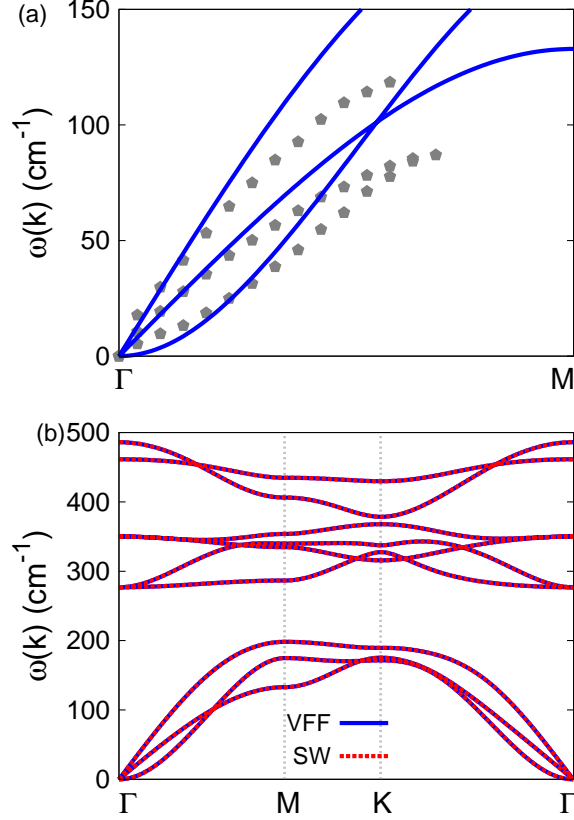


FIG. 65: (Color online) Phonon dispersion for single-layer 1H-WS₂. (a) The VFF model is fitted to the three acoustic branches in the long wave limit along the Γ M direction. The *ab initio* results (gray pentagons) are from Ref. 31. (b) The VFF model (blue lines) and the SW potential (red lines) give the same phonon dispersion for single-layer 1H-WS₂ along Γ MK Γ .

the armchair and zigzag directions, respectively. The ultimate stress is about 22.6 Nm⁻¹ at the ultimate strain of 0.18 in the armchair direction at the low temperature of 1 K. The ultimate stress is about 21.8 Nm⁻¹ at the ultimate strain of 0.21 in the zigzag direction at the low temperature of 1 K.

XXXIV. 1H-WS₂

Most existing theoretical studies on the single-layer 1H-WS₂ are based on the first-principles calculations. In this section, we will develop both VFF model and the SW potential for the single-layer 1H-WS₂.

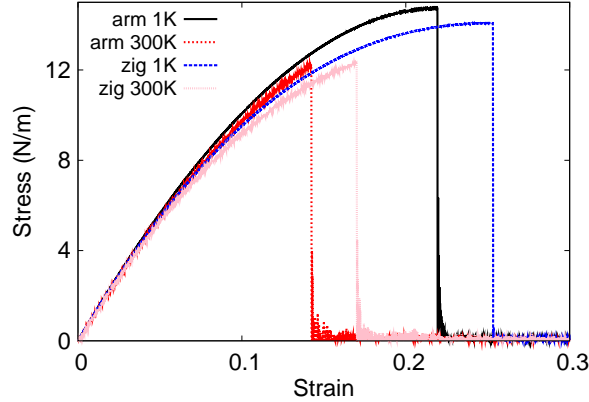


FIG. 66: (Color online) Stress-strain for single-layer 1H-WS₂ of dimension 100 × 100 Å along the armchair and zigzag directions.

TABLE CXXXIV: The VFF model for single-layer 1H-WS₂. The second line gives an explicit expression for each VFF term. The third line is the force constant parameters. Parameters are in the unit of $\frac{eV}{\text{Å}^2}$ for the bond stretching interactions, and in the unit of eV for the angle bending interaction. The fourth line gives the initial bond length (in unit of Å) for the bond stretching interaction and the initial angle (in unit of degrees) for the angle bending interaction. The angle θ_{ijk} has atom i as the apex.

VFF type	bond stretching	angle bending		
expression	$\frac{1}{2}K_{W-S}(\Delta r)^2$	$\frac{1}{2}K_{W-S-S}(\Delta\theta)^2$	$\frac{1}{2}K_{W-S-S'}(\Delta\theta)^2$	$\frac{1}{2}K_{S-W-W}(\Delta\theta)^2$
parameter	8.701	7.421	7.421	6.607
r_0 or θ_0	2.390	81.811	81.755	81.811

The structure for the single-layer 1H-WS₂ is shown in Fig. 1 (with M=W and X=S). Each W atom is surrounded by six S atoms. These S atoms are categorized into the top group (eg. atoms 1, 3, and 5) and bottom group (eg. atoms 2, 4, and 6). Each S atom is connected to three W atoms. The structural parameters are from Ref. 12, including the lattice constant $a = 3.13$ Å, and the bond length $d_{W-S} = 2.39$ Å. The resultant angles are $\theta_{WSS} = \theta_{SWW} = 81.811^\circ$ and $\theta_{WSS'} = 81.755^\circ$, in which atoms S and S' are from different (top or bottom) group.

Table CXXXIV shows the VFF terms for the 1H-WS₂, one of which is the bond stretching

TABLE CXXXV: Two-body SW potential parameters for single-layer 1H-WS₂ used by GULP⁸ as expressed in Eq. (3).

	A (eV)	ρ (Å)	B (Å ⁴)	r_{\min} (Å)	r_{\max} (Å)
W-S	5.664	0.889	15.335	0.0	3.164

TABLE CXXXVI: Three-body SW potential parameters for single-layer 1H-WS₂ used by GULP⁸ as expressed in Eq. (4). The angle θ_{ijk} in the first line indicates the bending energy for the angle with atom i as the apex.

	K (eV)	θ_0 (degree)	ρ_1 (Å)	ρ_2 (Å)	$r_{\min12}$ (Å)	$r_{\max12}$ (Å)	$r_{\min13}$ (Å)	$r_{\max13}$ (Å)	$r_{\min23}$ (Å)	$r_{\max23}$ (Å)
θ_{W-S-S}	37.687	81.811	0.889	0.889	0.0	3.164	0.0	3.164	0.0	3.778
$\theta_{W-S-S'}$	37.697	81.755	0.889	0.889	0.0	3.164	0.0	3.164	0.0	3.778
θ_{S-W-W}	33.553	81.811	0.889	0.889	0.0	3.164	0.0	3.164	0.0	3.778

interaction shown by Eq. (1) while the other terms are the angle bending interaction shown by Eq. (2). These force constant parameters are determined by fitting to the three acoustic branches in the phonon dispersion along the ΓM as shown in Fig. 65 (a). The *ab initio* calculations for the phonon dispersion are from Ref. 31. Similar phonon dispersion can also be found in other *ab initio* calculations.^{12,26,34,38,39} Fig. 65 (b) shows that the VFF model and the SW potential give exactly the same phonon dispersion, as the SW potential is derived from the VFF model.

The parameters for the two-body SW potential used by GULP are shown in Tab. CXXXV.

TABLE CXXXVII: SW potential parameters for single-layer 1H-WS₂ used by LAMMPS⁹ as expressed in Eqs. (9) and (10). Atom types in the first column are displayed in Fig. 2 (with M=W and X=S).

	ϵ (eV)	σ (Å)	a	λ	γ	$\cos \theta_0$	A_L	B_L	p	q	tol
W ₁ -S ₁ -S ₁	1.000	0.889	3.558	0.000	1.000	0.000	5.664	24.525	4	0	0.0
W ₁ -S ₁ -S ₃	1.000	0.000	0.000	37.687	1.000	0.142	0.000	0.000	4	0	0.0
W ₁ -S ₁ -S ₂	1.000	0.000	0.000	37.697	1.000	0.143	0.000	0.000	4	0	0.0
S ₁ -W ₁ -W ₃	1.000	0.000	0.000	33.553	1.000	0.142	0.000	0.000	4	0	0.0

The parameters for the three-body SW potential used by GULP are shown in Tab. CXXXVI. Parameters for the SW potential used by LAMMPS are listed in Tab. CXXXVII. We note that twelve atom types have been introduced for the simulation of the single-layer 1H-WS₂ using LAMMPS, because the angles around atom W in Fig. 1 (with M=W and X=S) are not distinguishable in LAMMPS. We have suggested two options to differentiate these angles by implementing some additional constraints in LAMMPS, which can be accomplished by modifying the source file of LAMMPS.^{13,14} According to our experience, it is not so convenient for some users to implement these constraints and recompile the LAMMPS package. Hence, in the present work, we differentiate the angles by introducing more atom types, so it is not necessary to modify the LAMMPS package. Fig. 2 (with M=W and X=S) shows that, for 1H-WS₂, we can differentiate these angles around the W atom by assigning these six neighboring S atoms with different atom types. It can be found that twelve atom types are necessary for the purpose of differentiating all six neighbors around one W atom.

We use LAMMPS to perform MD simulations for the mechanical behavior of the single-layer 1H-WS₂ under uniaxial tension at 1.0 K and 300.0 K. Fig. 66 shows the stress-strain curve for the tension of a single-layer 1H-WS₂ of dimension 100 × 100 Å. Periodic boundary conditions are applied in both armchair and zigzag directions. The single-layer 1H-WS₂ is stretched uniaxially along the armchair or zigzag direction. The stress is calculated without involving the actual thickness of the quasi-two-dimensional structure of the single-layer 1H-WS₂. The Young's modulus can be obtained by a linear fitting of the stress-strain relation in the small strain range of [0, 0.01]. The Young's modulus are 121.5 N/m along both armchair and zigzag directions. These values are in reasonably agreement with the *ab initio* results, eg. 139.6 N/m from Ref. 18, or 148.5 N/m from Ref. 35. The Poisson's ratio from the VFF model and the SW potential is $\nu_{xy} = \nu_{yx} = 0.21$, which agrees with the *ab initio* value of 0.22.¹⁸

We have determined the nonlinear parameter to be $B = 0.47d^4$ in Eq. (5) by fitting to the third-order nonlinear elastic constant D from the *ab initio* calculations.³⁵ We have extracted the value of $D = -502.9$ N/m by fitting the stress-strain relation along the armchair direction in the *ab initio* calculations to the function $\sigma = E\epsilon + \frac{1}{2}D\epsilon^2$ with E as the Young's modulus. The values of D from the present SW potential are -472.8 N/m and -529.6 N/m along the armchair and zigzag directions, respectively. The ultimate stress is about 14.7 Nm⁻¹ at the ultimate strain of 0.22 in the armchair direction at the low temperature of 1 K. The ultimate

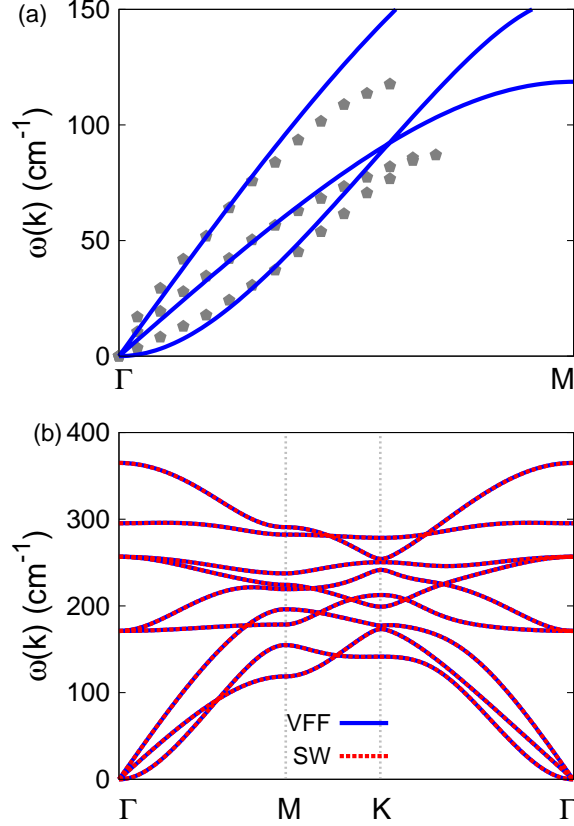


FIG. 67: (Color online) Phonon dispersion for single-layer 1H-WSe₂. (a) The VFF model is fitted to the three acoustic branches in the long wave limit along the Γ M direction. The *ab initio* results (gray pentagons) are from Ref. 31. (b) The VFF model (blue lines) and the SW potential (red lines) give the same phonon dispersion for single-layer 1H-WSe₂ along Γ MK Γ .

stress is about 14.1 Nm^{-1} at the ultimate strain of 0.25 in the zigzag direction at the low temperature of 1 K.

XXXV. 1H-WSE₂

Most existing theoretical studies on the single-layer 1H-WSe₂ are based on the first-principles calculations. Norouzzadeh and Singh provided one set of parameters for the SW potential for the single-layer 1H-WSe₂.⁴⁰ In this section, we will develop both VFF model and the SW potential for the single-layer 1H-WSe₂.

The structure for the single-layer 1H-WSe₂ is shown in Fig. 1 (with M=W and X=Se).

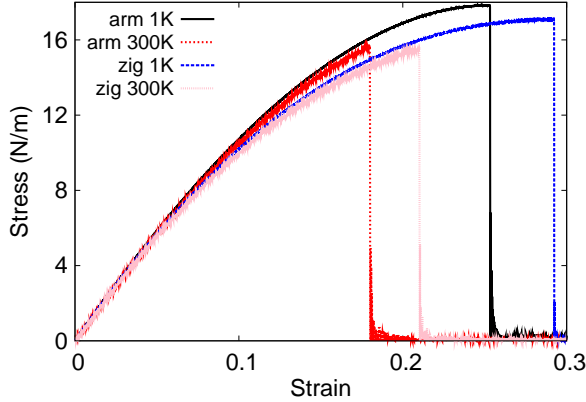


FIG. 68: (Color online) Stress-strain for single-layer 1H-WSe₂ of dimension $100 \times 100 \text{ \AA}$ along the armchair and zigzag directions.

TABLE CXXXVIII: The VFF model for single-layer 1H-WSe₂. The second line gives an explicit expression for each VFF term. The third line is the force constant parameters. Parameters are in the unit of $\frac{eV}{\text{Å}^2}$ for the bond stretching interactions, and in the unit of eV for the angle bending interaction. The fourth line gives the initial bond length (in unit of Å) for the bond stretching interaction and the initial angle (in unit of degrees) for the angle bending interaction. The angle θ_{ijk} has atom *i* as the apex.

VFF type	bond stretching	angle bending		
expression	$\frac{1}{2}K_{W-Se}(\Delta r)^2$	$\frac{1}{2}K_{W-Se-Se}(\Delta\theta)^2$	$\frac{1}{2}K_{W-Se-Se'}(\Delta\theta)^2$	$\frac{1}{2}K_{Se-W-W}(\Delta\theta)^2$
parameter	8.286	8.513	8.513	7.719
r_0 or θ_0	2.510	80.693	83.140	80.693

Each W atom is surrounded by six Se atoms. These Se atoms are categorized into the top group (eg. atoms 1, 3, and 5) and bottom group (eg. atoms 2, 4, and 6). Each Se atom is connected to three W atoms. The structural parameters are from Ref. 12, including the lattice constant $a = 3.25 \text{ \AA}$, and the bond length $d_{W-Se} = 2.51 \text{ \AA}$. The resultant angles are $\theta_{WSeSe} = \theta_{SeWW} = 80.693^\circ$ and $\theta_{WSeSe'} = 83.240^\circ$, in which atoms Se and Se' are from different (top or bottom) group.

Table CXXXVIII shows three VFF terms for the 1H-WSe₂, one of which is the bond stretching interaction shown by Eq. (1) while the other two terms are the angle bending

TABLE CXXXIX: Two-body SW potential parameters for single-layer 1H-WSe₂ used by GULP⁸ as expressed in Eq. (3).

	A (eV)	ρ (Å)	B (Å ⁴)	r_{\min} (Å)	r_{\max} (Å)
W-Se	5.476	0.706	16.273	0.0	3.308

TABLE CXL: Three-body SW potential parameters for single-layer 1H-WSe₂ used by GULP⁸ as expressed in Eq. (4). The angle θ_{ijk} in the first line indicates the bending energy for the angle with atom i as the apex.

	K (eV)	θ_0 (degree)	ρ_1 (Å)	ρ_2 (Å)	$r_{\min12}$ (Å)	$r_{\max12}$ (Å)	$r_{\min13}$ (Å)	$r_{\max13}$ (Å)	$r_{\min23}$ (Å)	$r_{\max23}$ (Å)
$\theta_{\text{W-Se-Se}}$	25.607	80.693	0.706	0.706	0.0	3.308	0.0	3.308	0.0	3.953
$\theta_{\text{W-Se-Se}'}$	25.287	83.240	0.706	0.706	0.0	3.308	0.0	3.308	0.0	3.953
$\theta_{\text{Se-W-W}}$	23.218	80.693	0.706	0.706	0.0	3.308	0.0	3.308	0.0	3.953

interaction shown by Eq. (2). These force constant parameters are determined by fitting to the three acoustic branches in the phonon dispersion along the ΓM as shown in Fig. 67 (a). The *ab initio* calculations for the phonon dispersion are from Ref. 31. Similar phonon dispersion can also be found in other *ab initio* calculations.^{12,33,34,39,41} Fig. 67 (b) shows that the VFF model and the SW potential give exactly the same phonon dispersion, as the SW potential is derived from the VFF model.

The parameters for the two-body SW potential used by GULP are shown in Tab. CXXXIX. The parameters for the three-body SW potential used by GULP are shown in Tab. CXL. Parameters for the SW potential used by LAMMPS are listed in Tab. CXLI.

TABLE CXLI: SW potential parameters for single-layer 1H-WSe₂ used by LAMMPS⁹ as expressed in Eqs. (9) and (10). Atom types in the first column are displayed in Fig. 2 (with M=W and X=Se).

	ϵ (eV)	σ (Å)	a	λ	γ	$\cos \theta_0$	A_L	B_L	p	q	tol
W ₁ -Se ₁ -Se ₁	1.000	0.706	4.689	0.000	1.000	0.000	5.476	65.662	4	0	0.0
W ₁ -Se ₁ -Se ₃	1.000	0.000	0.000	25.607	1.000	0.162	0.000	0.000	4	0	0.0
W ₁ -Se ₁ -Se ₂	1.000	0.000	0.000	25.287	1.000	0.118	0.000	0.000	4	0	0.0
Se ₁ -W ₁ -W ₃	1.000	0.000	0.000	23.218	1.000	0.162	0.000	0.000	4	0	0.0

We note that twelve atom types have been introduced for the simulation of the single-layer 1H-WSe₂ using LAMMPS, because the angles around atom W in Fig. 1 (with M=W and X=Se) are not distinguishable in LAMMPS. We have suggested two options to differentiate these angles by implementing some additional constraints in LAMMPS, which can be accomplished by modifying the source file of LAMMPS.^{13,14} According to our experience, it is not so convenient for some users to implement these constraints and recompile the LAMMPS package. Hence, in the present work, we differentiate the angles by introducing more atom types, so it is not necessary to modify the LAMMPS package. Fig. 2 (with M=W and X=Se) shows that, for 1H-WSe₂, we can differentiate these angles around the W atom by assigning these six neighboring Se atoms with different atom types. It can be found that twelve atom types are necessary for the purpose of differentiating all six neighbors around one W atom.

We use LAMMPS to perform MD simulations for the mechanical behavior of the single-layer 1H-WSe₂ under uniaxial tension at 1.0 K and 300.0 K. Fig. 68 shows the stress-strain curve for the tension of a single-layer 1H-WSe₂ of dimension 100 × 100 Å. Periodic boundary conditions are applied in both armchair and zigzag directions. The single-layer 1H-WSe₂ is stretched uniaxially along the armchair or zigzag direction. The stress is calculated without involving the actual thickness of the quasi-two-dimensional structure of the single-layer 1H-WSe₂. The Young's modulus can be obtained by a linear fitting of the stress-strain relation in the small strain range of [0, 0.01]. The Young's modulus are 124.1 N/m and 123.0 N/m along the armchair and zigzag directions, respectively. The Young's modulus is essentially isotropic in the armchair and zigzag directions. These values are in reasonably agreement with the *ab initio* results, eg. 116.0 N/m from Ref. 18, or 126.2 N/m from Ref. 35. The Poisson's ratio from the VFF model and the SW potential is $\nu_{xy} = \nu_{yx} = 0.20$, which agrees with the *ab initio* value of 0.19.¹⁸

We have determined the nonlinear parameter to be $B = 0.41d^4$ in Eq. (5) by fitting to the third-order nonlinear elastic constant D from the *ab initio* calculations.³⁵ We have extracted the value of $D = -413.1$ N/m by fitting the stress-strain relation along the armchair direction in the *ab initio* calculations to the function $\sigma = E\epsilon + \frac{1}{2}D\epsilon^2$ with E as the Young's modulus. The values of D from the present SW potential are -400.4 N/m and -444.3 N/m along the armchair and zigzag directions, respectively. The ultimate stress is about 17.8 Nm⁻¹ at the ultimate strain of 0.25 in the armchair direction at the low temperature of 1 K. The ultimate

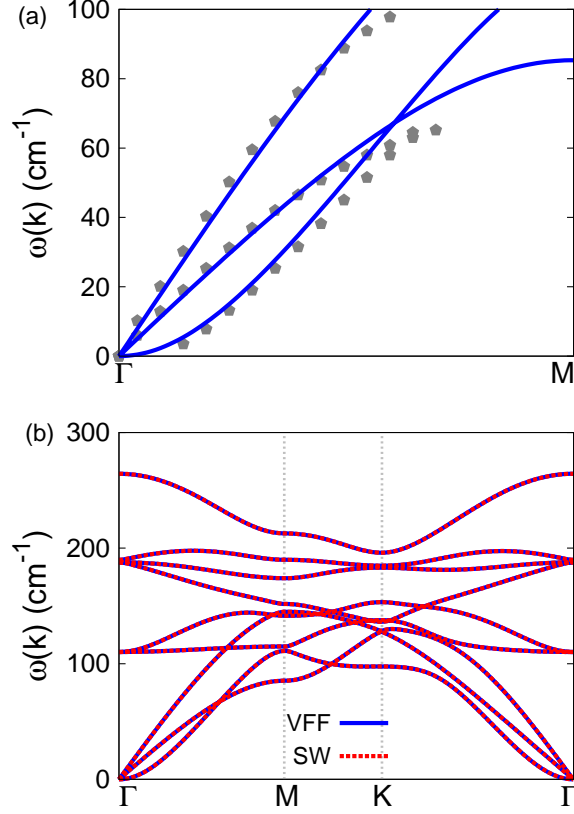


FIG. 69: (Color online) Phonon dispersion for single-layer 1H-WTe₂. (a) The VFF model is fitted to the three acoustic branches in the long wave limit along the Γ M direction. The *ab initio* results (gray pentagons) are from Ref. 42. (b) The VFF model (blue lines) and the SW potential (red lines) give the same phonon dispersion for single-layer 1H-WTe₂ along Γ MK Γ .

stress is about 17.1 Nm^{-1} at the ultimate strain of 0.29 in the zigzag direction at the low temperature of 1 K.

XXXVI. 1H-WTE₂

Most existing theoretical studies on the single-layer 1H-WTe₂ are based on the first-principles calculations. In this section, we will develop both VFF model and the SW potential for the single-layer 1H-WTe₂.

The bulk WTe₂ has the trigonally coordinated H phase structure.⁴³ However, it has been predicted that the structure of the single-layer WTe₂ can be either the trigonally coordinated

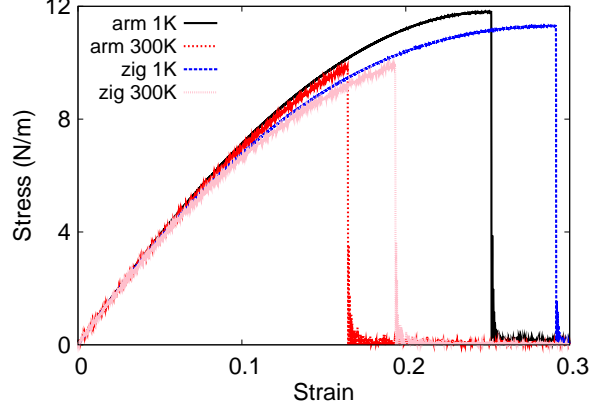


FIG. 70: (Color online) Stress-strain for single-layer 1H-WTe₂ of dimension $100 \times 100 \text{ \AA}$ along the armchair and zigzag directions.

TABLE CXLII: The VFF model for single-layer 1H-WTe₂. The second line gives an explicit expression for each VFF term. The third line is the force constant parameters. Parameters are in the unit of $\frac{eV}{\text{Å}^2}$ for the bond stretching interactions, and in the unit of eV for the angle bending interaction. The fourth line gives the initial bond length (in unit of Å) for the bond stretching interaction and the initial angle (in unit of degrees) for the angle bending interaction. The angle θ_{ijk} has atom *i* as the apex.

VFF type	bond stretching	angle bending		
expression	$\frac{1}{2}K_{W-Te}(\Delta r)^2$	$\frac{1}{2}K_{W-Te-Te}(\Delta\theta)^2$	$\frac{1}{2}K_{W-Te-Te'}(\Delta\theta)^2$	$\frac{1}{2}K_{Te-W-W}(\Delta\theta)^2$
parameter	5.483	7.016	7.016	5.718
r_0 or θ_0	2.730	81.111	82.686	81.111

H phase¹² or the octahedrally coordinated T_d phase,⁴⁴⁻⁴⁷ with T_d phase as the more stable structure.⁴² We will thus consider both phases in the present paper. This section is devoted to the H phase for the WTe₂ (1H-WTe₂), while the SW potential for the T_d -WTe₂ (1T-WTe₂) is presented in another section.

The structure for the single-layer 1H-WTe₂ is shown in Fig. 1 (with M=W and X=Te). Each W atom is surrounded by six Te atoms. These Te atoms are categorized into the top group (eg. atoms 1, 3, and 5) and bottom group (eg. atoms 2, 4, and 6). Each Te atom is connected to three W atoms. The structural parameters are from Ref. 42, including the

TABLE CXLIII: Two-body SW potential parameters for single-layer 1H-WTe₂ used by GULP⁸ as expressed in Eq. (3).

	A (eV)	ρ (Å)	B (Å ⁴)	r_{\min} (Å)	r_{\max} (Å)
W-Te	4.326	0.778	22.774	0.0	3.604

TABLE CXLIV: Three-body SW potential parameters for single-layer 1H-WTe₂ used by GULP⁸ as expressed in Eq. (4). The angle θ_{ijk} in the first line indicates the bending energy for the angle with atom i as the apex.

	K (eV)	θ_0 (degree)	ρ_1 (Å)	ρ_2 (Å)	$r_{\min12}$ (Å)	$r_{\max12}$ (Å)	$r_{\min13}$ (Å)	$r_{\max13}$ (Å)	$r_{\min23}$ (Å)	$r_{\max23}$ (Å)
$\theta_{\text{W-Te-Te}}$	21.313	81.111	0.778	0.778	0.0	3.604	0.0	3.604	0.0	4.305
$\theta_{\text{W-Te-Te}'}$	21.147	82.686	0.778	0.778	0.0	3.604	0.0	3.604	0.0	4.305
$\theta_{\text{Te-W-W}}$	17.370	81.111	0.778	0.778	0.0	3.604	0.0	3.604	0.0	4.305

lattice constant $a = 3.55$ Å, and the bond length $d_{\text{W-Te}} = 2.73$ Å. The resultant angles are $\theta_{\text{WTeTe}} = \theta_{\text{TeWW}} = 81.111^\circ$ and $\theta_{\text{WTeTe}'} = 82.686^\circ$, in which atoms Te and Te' are from different (top or bottom) group.

Table CXLII shows the VFF terms for the 1H-WTe₂, one of which is the bond stretching interaction shown by Eq. (1) while the other terms are the angle bending interaction shown by Eq. (2). These force constant parameters are determined by fitting to the three acoustic branches in the phonon dispersion along the ΓM as shown in Fig. 69 (a). The *ab initio* calculations for the phonon dispersion are from Ref. 42. Similar phonon dispersion can also be found in other *ab initio* calculations.¹² Fig. 69 (b) shows that the VFF model and the

TABLE CXLV: SW potential parameters for single-layer 1H-WTe₂ used by LAMMPS⁹ as expressed in Eqs. (9) and (10). Atom types in the first column are displayed in Fig. 2 (with M=W and X=Te).

	ϵ (eV)	σ (Å)	a	λ	γ	$\cos\theta_0$	A_L	B_L	p	q	tol
W ₁ -Te ₁ -Te ₁	1.000	0.778	4.632	0.000	1.000	0.000	4.326	62.148	4	0	0.0
W ₁ -Te ₁ -Te ₃	1.000	0.000	0.000	21.313	1.000	0.155	0.000	0.000	4	0	0.0
W ₁ -Te ₁ -Te ₂	1.000	0.000	0.000	21.147	1.000	0.127	0.000	0.000	4	0	0.0
Te ₁ -W ₁ -W ₃	1.000	0.000	0.000	17.370	1.000	0.155	0.000	0.000	4	0	0.0

SW potential give exactly the same phonon dispersion, as the SW potential is derived from the VFF model.

The parameters for the two-body SW potential used by GULP are shown in Tab. CXLIII. The parameters for the three-body SW potential used by GULP are shown in Tab. CXLIV. Parameters for the SW potential used by LAMMPS are listed in Tab. CXLV. We note that twelve atom types have been introduced for the simulation of the single-layer 1H-WTe₂ using LAMMPS, because the angles around atom W in Fig. 1 (with M=W and X=Te) are not distinguishable in LAMMPS. We have suggested two options to differentiate these angles by implementing some additional constraints in LAMMPS, which can be accomplished by modifying the source file of LAMMPS.^{13,14} According to our experience, it is not so convenient for some users to implement these constraints and recompile the LAMMPS package. Hence, in the present work, we differentiate the angles by introducing more atom types, so it is not necessary to modify the LAMMPS package. Fig. 2 (with M=W and X=Te) shows that, for 1H-WTe₂, we can differentiate these angles around the W atom by assigning these six neighboring Te atoms with different atom types. It can be found that twelve atom types are necessary for the purpose of differentiating all six neighbors around one W atom.

We use LAMMPS to perform MD simulations for the mechanical behavior of the single-layer 1H-WTe₂ under uniaxial tension at 1.0 K and 300.0 K. Fig. 70 shows the stress-strain curve for the tension of a single-layer 1H-WTe₂ of dimension 100 × 100 Å. Periodic boundary conditions are applied in both armchair and zigzag directions. The single-layer 1H-WTe₂ is stretched uniaxially along the armchair or zigzag direction. The stress is calculated without involving the actual thickness of the quasi-two-dimensional structure of the single-layer 1H-WTe₂. The Young's modulus can be obtained by a linear fitting of the stress-strain relation in the small strain range of [0, 0.01]. The Young's modulus are 82.7 N/m and 81.9 N/m along the armchair and zigzag directions, respectively. The Young's modulus is essentially isotropic in the armchair and zigzag directions. These values are in reasonably agreement with the *ab initio* results, eg. 86.4 N/m from Ref. 18, or 93.9 N/m from Ref. 35. The Poisson's ratio from the VFF model and the SW potential is $\nu_{xy} = \nu_{yx} = 0.20$, which agrees with the *ab initio* value of 0.18.¹⁸

We have determined the nonlinear parameter to be $B = 0.41d^4$ in Eq. (5) by fitting to the third-order nonlinear elastic constant D from the *ab initio* calculations.³⁵ We have extracted the value of $D = -280.3$ N/m by fitting the stress-strain relation along the armchair direction

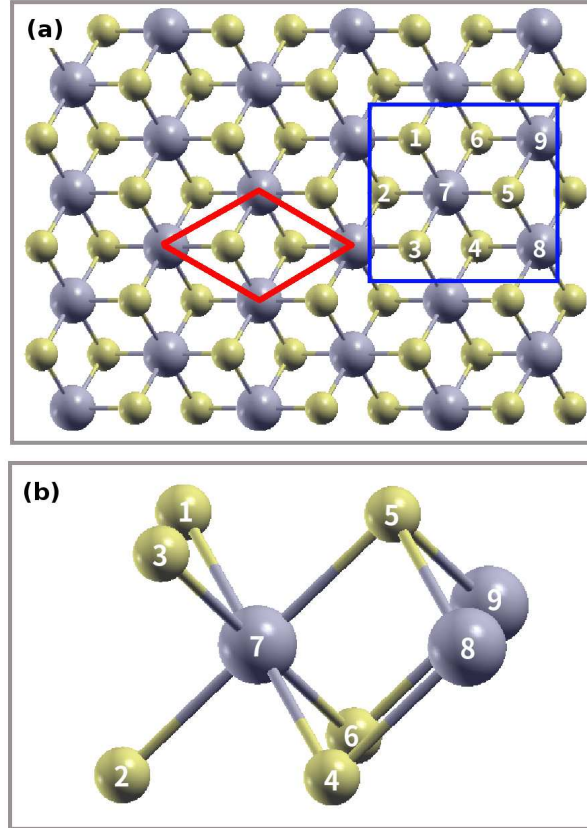


FIG. 71: (Color online) Configuration of the 1T-MX₂ in the 1T phase. (a) Top view. The unit cell is highlighted by a red parallelogram. The armchair direction is defined to be along the horizontal direction. The zigzag direction is along the vertical direction. (b) Enlarged view of atoms in the blue box in (a). Each M atom is surrounded by six X atoms, which are categorized into the top and bottom groups. Atoms X 1, 3, and 5 are from the top group, while atoms X 2, 4, and 6 are from the bottom group. M atoms are represented by larger gray balls. X atoms are represented by smaller yellow balls.

in the *ab initio* calculations to the function $\sigma = E\epsilon + \frac{1}{2}D\epsilon^2$ with E as the Young's modulus. The values of D from the present SW potential are -269.4 N/m and -297.9 N/m along the armchair and zigzag directions, respectively. The ultimate stress is about 11.8 Nm⁻¹ at the ultimate strain of 0.25 in the armchair direction at the low temperature of 1 K. The ultimate stress is about 11.3 Nm⁻¹ at the ultimate strain of 0.29 in the zigzag direction at the low temperature of 1 K.

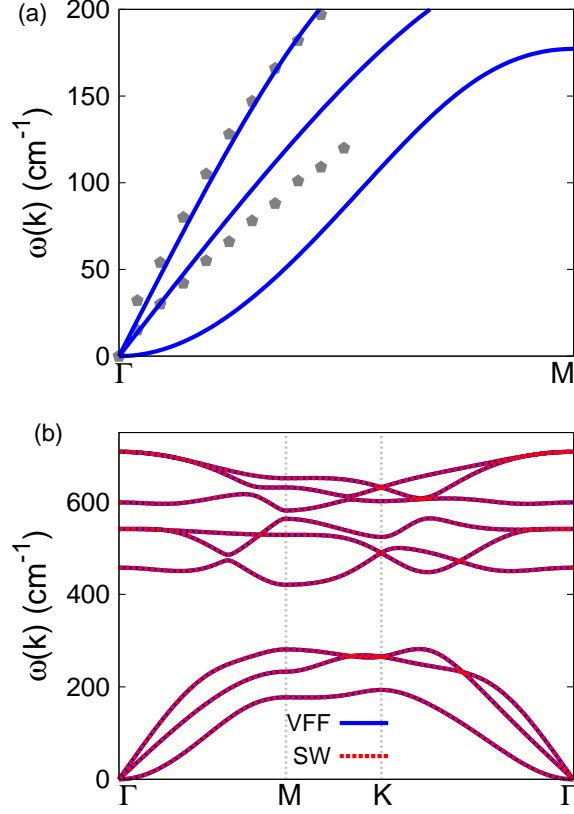


FIG. 72: (Color online) Phonon spectrum for single-layer 1T-ScO₂. (a) Phonon dispersion along the Γ M direction in the Brillouin zone. The results from the VFF model (lines) are comparable with the *ab initio* results (pentagons) from Ref. 12. (b) The phonon dispersion from the SW potential is exactly the same as that from the VFF model.

XXXVII. 1T-SCO₂

Most existing theoretical studies on the single-layer 1T-ScO₂ are based on the first-principles calculations. In this section, we will develop the SW potential for the single-layer 1T-ScO₂.

The structure for the single-layer 1T-ScO₂ is shown in Fig. 71 (with M=Sc and X=O). Each Ni atom is surrounded by six O atoms. These O atoms are categorized into the top group (eg. atoms 1, 3, and 5) and bottom group (eg. atoms 2, 4, and 6). Each O atom is connected to three Sc atoms. The structural parameters are from the first-principles calculations,¹² including the lattice constant $a = 3.22 \text{ \AA}$ and the bond length $d_{\text{Sc-O}} = 2.07 \text{ \AA}$.

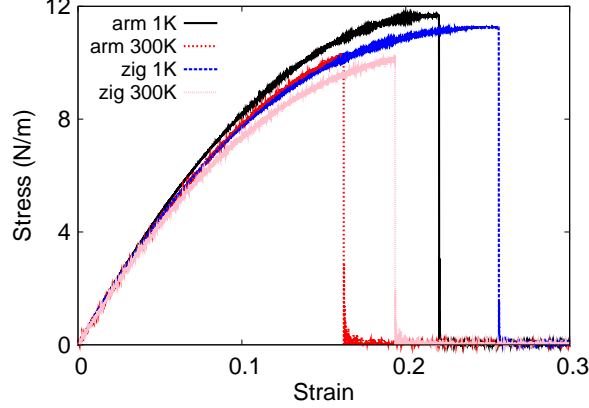


FIG. 73: (Color online) Stress-strain for single-layer 1T-ScO₂ of dimension 100 × 100 Å along the armchair and zigzag directions.

TABLE CXLVI: The VFF model for single-layer 1T-ScO₂. The second line gives an explicit expression for each VFF term. The third line is the force constant parameters. Parameters are in the unit of $\frac{eV}{\text{Å}^2}$ for the bond stretching interactions, and in the unit of eV for the angle bending interaction. The fourth line gives the initial bond length (in unit of Å) for the bond stretching interaction and the initial angle (in unit of degrees) for the angle bending interaction. The angle θ_{ijk} has atom *i* as the apex.

VFF type	bond stretching	angle bending	
expression	$\frac{1}{2}K_{\text{Sc-O}}(\Delta r)^2$	$\frac{1}{2}K_{\text{Sc-O-O}}(\Delta\theta)^2$	$\frac{1}{2}K_{\text{O-Sc-Sc}}(\Delta\theta)^2$
parameter	11.926	3.258	3.258
r_0 or θ_0	2.07	102.115	102.115

The resultant angles are $\theta_{\text{ScOO}} = 102.115^\circ$ with O atoms from the same (top or bottom) group, and $\theta_{\text{OScSc}} = 102.115^\circ$.

Table CXLVI shows three VFF terms for the single-layer 1T-ScO₂, one of which is the bond stretching interaction shown by Eq. (1) while the other two terms are the angle bending interaction shown by Eq. (2). We note that the angle bending term $K_{\text{Sc-O-O}}$ is for the angle $\theta_{\text{Sc-O-O}}$ with both O atoms from the same (top or bottom) group. These force constant parameters are determined by fitting to the two in-plane acoustic branches in the phonon dispersion along the ΓM as shown in Fig. 72 (a). The *ab initio* calculations for the phonon

TABLE CXLVII: Two-body SW potential parameters for single-layer 1T-ScO₂ used by GULP⁸ as expressed in Eq. (3).

	A (eV)	ρ (Å)	B (Å ⁴)	r_{\min} (Å)	r_{\max} (Å)
Sc-O	10.187	1.493	9.180	0.0	2.949

TABLE CXLVIII: Three-body SW potential parameters for single-layer 1T-ScO₂ used by GULP⁸ as expressed in Eq. (4). The angle θ_{ijk} in the first line indicates the bending energy for the angle with atom i as the apex.

	K (eV)	θ_0 (degree)	ρ_1 (Å)	ρ_2 (Å)	$r_{\min12}$ (Å)	$r_{\max12}$ (Å)	$r_{\min13}$ (Å)	$r_{\max13}$ (Å)	$r_{\min23}$ (Å)	$r_{\max23}$ (Å)
$\theta_{\text{Sc-O-O}}$	50.913	102.115	1.493	1.493	0.0	2.949	0.0	2.949	0.0	4.399
$\theta_{\text{O-Sc-Sc}}$	50.913	102.115	1.493	1.493	0.0	2.949	0.0	2.949	0.0	4.399

dispersion are from Ref. 12. Fig. 72 (b) shows that the VFF model and the SW potential give exactly the same phonon dispersion, as the SW potential is derived from the VFF model.

The parameters for the two-body SW potential used by GULP are shown in Tab. CXLVII. The parameters for the three-body SW potential used by GULP are shown in Tab. CXLVIII. Some representative parameters for the SW potential used by LAMMPS are listed in Tab. CXLIX.

We use LAMMPS to perform MD simulations for the mechanical behavior of the single-layer 1T-ScO₂ under uniaxial tension at 1.0 K and 300.0 K. Fig. 73 shows the stress-strain curve for the tension of a single-layer 1T-ScO₂ of dimension 100×100 Å. Periodic boundary conditions are applied in both armchair and zigzag directions. The single-layer 1T-ScO₂ is stretched uniaxially along the armchair or zigzag direction. The stress is calculated without involving the actual thickness of the quasi-two-dimensional structure of the single-layer 1T-ScO₂. The Young's modulus can be obtained by a linear fitting of the stress-strain relation in the small strain range of $[0, 0.01]$. The Young's modulus are 100.9 N/m and 100.4 N/m

TABLE CXLIX: SW potential parameters for single-layer 1T-ScO₂ used by LAMMPS⁹ as expressed in Eqs. (9) and (10).

	ϵ (eV)	σ (Å)	a	λ	γ	$\cos \theta_0$	A_L	B_L	p	q	tol
Sc-O ₁ -O ₁	1.000	1.493	1.975	50.913	1.000	-0.210	10.187	1.847	4	0	0.0

TABLE CL: The VFF model for single-layer 1T-ScS₂. The second line gives an explicit expression for each VFF term. The third line is the force constant parameters. Parameters are in the unit of $\frac{\text{eV}}{\text{\AA}^2}$ for the bond stretching interactions, and in the unit of eV for the angle bending interaction. The fourth line gives the initial bond length (in unit of \AA) for the bond stretching interaction and the initial angle (in unit of degrees) for the angle bending interaction. The angle θ_{ijk} has atom i as the apex.

VFF type	bond stretching	angle bending	
expression	$\frac{1}{2}K_{\text{Sc-S}}(\Delta r)^2$	$\frac{1}{2}K_{\text{Sc-S-S}}(\Delta\theta)^2$	$\frac{1}{2}K_{\text{S-Sc-S}}(\Delta\theta)^2$
parameter	3.512	1.593	1.593
r_0 or θ_0	2.50	92.771	92.771

TABLE CLI: Two-body SW potential parameters for single-layer 1T-ScS₂ used by GULP⁸ as expressed in Eq. (3).

	A (eV)	ρ (\AA)	B (\AA^4)	r_{min} (\AA)	r_{max} (\AA)
Sc-S	3.516	1.443	19.531	0.0	3.450

along the armchair and zigzag directions, respectively. The Young's modulus is essentially isotropic in the armchair and zigzag directions. The Poisson's ratio from the VFF model and the SW potential is $\nu_{xy} = \nu_{yx} = 0.15$.

There is no available value for nonlinear quantities in the single-layer 1T-ScO₂. We have thus used the nonlinear parameter $B = 0.5d^4$ in Eq. (5), which is close to the value of B in most materials. The value of the third order nonlinear elasticity D can be extracted by fitting the stress-strain relation to the function $\sigma = E\epsilon + \frac{1}{2}D\epsilon^2$ with E as the Young's modulus. The values of D from the present SW potential are -422.4 N/m and -453.7 N/m along the armchair and zigzag directions, respectively. The ultimate stress is about 11.7 Nm⁻¹ at the ultimate strain of 0.22 in the armchair direction at the low temperature of 1 K. The ultimate stress is about 11.3 Nm⁻¹ at the ultimate strain of 0.25 in the zigzag direction at the low temperature of 1 K.

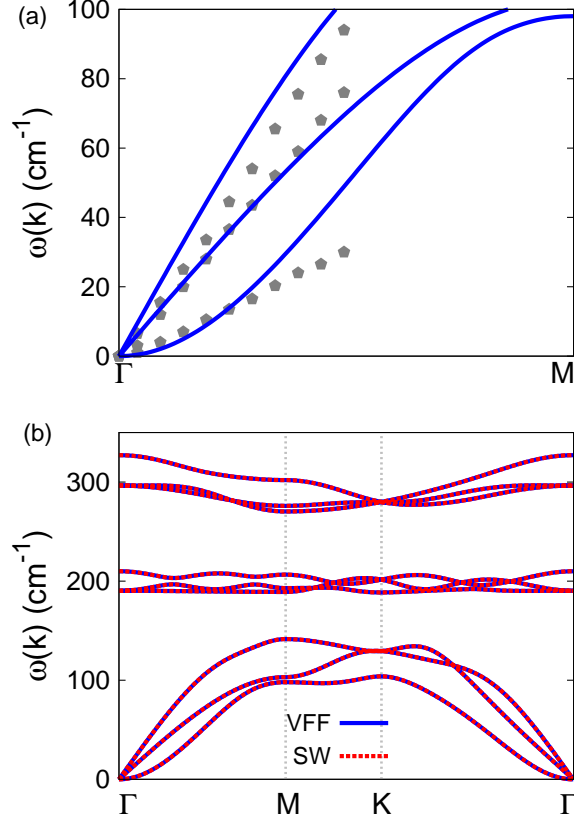


FIG. 74: (Color online) Phonon spectrum for single-layer 1T-ScS₂. (a) Phonon dispersion along the Γ M direction in the Brillouin zone. The results from the VFF model (lines) are comparable with the *ab initio* results (pentagons) from Ref. 12. (b) The phonon dispersion from the SW potential is exactly the same as that from the VFF model.

XXXVIII. 1T-SCS₂

Most existing theoretical studies on the single-layer 1T-ScS₂ are based on the first-principles calculations. In this section, we will develop the SW potential for the single-layer 1T-ScS₂.

The structure for the single-layer 1T-ScS₂ is shown in Fig. 71 (with M=Sc and X=S). Each Sc atom is surrounded by six S atoms. These S atoms are categorized into the top group (eg. atoms 1, 3, and 5) and bottom group (eg. atoms 2, 4, and 6). Each S atom is connected to three Sc atoms. The structural parameters are from the first-principles calculations,¹² including the lattice constant $a = 3.62 \text{ \AA}$, and the bond length $d_{\text{Sc-S}} = 2.50 \text{ \AA}$. The resultant

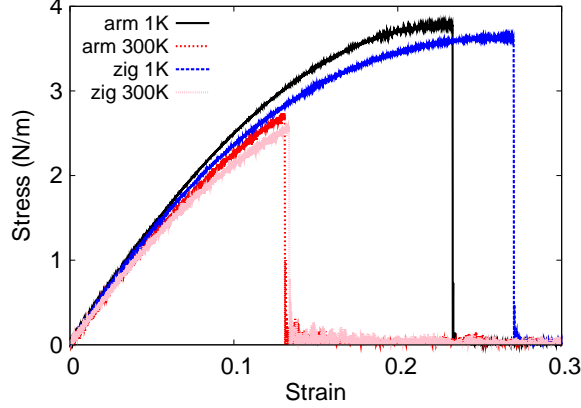


FIG. 75: (Color online) Stress-strain for single-layer 1T-ScS₂ of dimension 100 × 100 Å along the armchair and zigzag directions.

TABLE CLII: Three-body SW potential parameters for single-layer 1T-ScS₂ used by GULP⁸ as expressed in Eq. (4). The angle θ_{ijk} in the first line indicates the bending energy for the angle with atom i as the apex.

	K (eV)	θ_0 (degree)	ρ_1 (Å)	ρ_2 (Å)	$r_{\min 12}$ (Å)	$r_{\max 12}$ (Å)	$r_{\min 13}$ (Å)	$r_{\max 13}$ (Å)	$r_{\min 23}$ (Å)	$r_{\max 23}$ (Å)
$\theta_{\text{Sc-S-S}}$	16.674	92.771	1.443	1.443	0.0	3.450	0.0	3.450	0.0	4.945
$\theta_{\text{S-Sc-Sc}}$	16.674	92.771	1.443	1.443	0.0	3.450	0.0	3.450	0.0	4.945

angle is $\theta_{\text{SScSc}} = 92.771^\circ$ and $\theta_{\text{ScSS}} = 92.771^\circ$ with S atoms from the same (top or bottom) group.

Table CL shows three VFF terms for the single-layer 1T-ScS₂, one of which is the bond stretching interaction shown by Eq. (1) while the other two terms are the angle bending interaction shown by Eq. (2). We note that the angle bending term $K_{\text{Sc-S-S}}$ is for the angle $\theta_{\text{Sc-S-S}}$ with both S atoms from the same (top or bottom) group. These force constant parameters are determined by fitting to the three acoustic branches in the phonon dispersion

TABLE CLIII: SW potential parameters for single-layer 1T-ScS₂ used by LAMMPS⁹ as expressed in Eqs. (9) and (10).

	ϵ (eV)	σ (Å)	a	λ	γ	$\cos \theta_0$	A_L	B_L	p	q	tol
Sc-S ₁ -S ₁	1.000	1.443	2.390	16.674	1.000	-0.048	3.516	4.504	4	0	0.0

along the ΓM as shown in Fig. 74 (a). The *ab initio* calculations for the phonon dispersion are from Ref. 12. Fig. 74 (b) shows that the VFF model and the SW potential give exactly the same phonon dispersion, as the SW potential is derived from the VFF model.

The parameters for the two-body SW potential used by GULP are shown in Tab. CLI. The parameters for the three-body SW potential used by GULP are shown in Tab. CLII. Some representative parameters for the SW potential used by LAMMPS are listed in Tab. CLIII.

We use LAMMPS to perform MD simulations for the mechanical behavior of the single-layer 1T-ScS₂ under uniaxial tension at 1.0 K and 300.0 K. Fig. 75 shows the stress-strain curve for the tension of a single-layer 1T-ScS₂ of dimension 100×100 Å. Periodic boundary conditions are applied in both armchair and zigzag directions. The single-layer 1T-ScS₂ is stretched uniaxially along the armchair or zigzag direction. The stress is calculated without involving the actual thickness of the quasi-two-dimensional structure of the single-layer 1T-ScS₂. The Young's modulus can be obtained by a linear fitting of the stress-strain relation in the small strain range of $[0, 0.01]$. The Young's modulus are 30.0 N/m and 29.9 N/m along the armchair and zigzag directions, respectively. The Young's modulus is essentially isotropic in the armchair and zigzag directions. The Poisson's ratio from the VFF model and the SW potential is $\nu_{xy} = \nu_{yx} = 0.17$.

There is no available value for nonlinear quantities in the single-layer 1T-ScS₂. We have thus used the nonlinear parameter $B = 0.5d^4$ in Eq. (5), which is close to the value of B in most materials. The value of the third order nonlinear elasticity D can be extracted by fitting the stress-strain relation to the function $\sigma = E\epsilon + \frac{1}{2}D\epsilon^2$ with E as the Young's modulus. The values of D from the present SW potential are -113.7 N/m and -124.6 N/m along the armchair and zigzag directions, respectively. The ultimate stress is about 3.8 Nm^{-1} at the ultimate strain of 0.23 in the armchair direction at the low temperature of 1 K. The ultimate stress is about 3.6 Nm^{-1} at the ultimate strain of 0.27 in the zigzag direction at the low temperature of 1 K.

XXXIX. 1T-SCSE₂

Most existing theoretical studies on the single-layer 1T-ScSe₂ are based on the first-principles calculations. In this section, we will develop the SW potential for the single-layer 1T-ScSe₂.

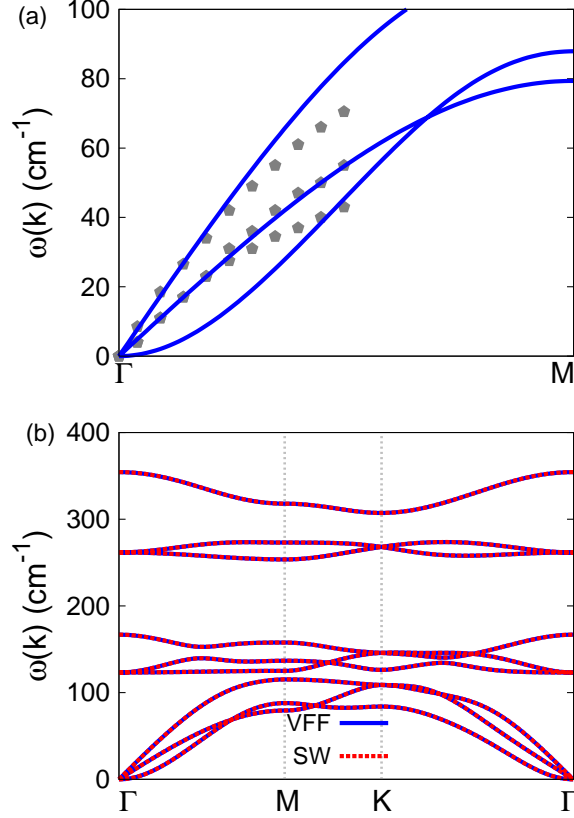


FIG. 76: (Color online) Phonon spectrum for single-layer 1T-ScSe₂. (a) Phonon dispersion along the Γ M direction in the Brillouin zone. The results from the VFF model (lines) are comparable with the *ab initio* results (pentagons) from Ref. 12. (b) The phonon dispersion from the SW potential is exactly the same as that from the VFF model.

The structure for the single-layer 1T-ScSe₂ is shown in Fig. 71 (with M=Sc and X=Se). Each Sc atom is surrounded by six Se atoms. These Se atoms are categorized into the top group (eg. atoms 1, 3, and 5) and bottom group (eg. atoms 2, 4, and 6). Each Se atom is connected to three Sc atoms. The structural parameters are from the first-principles calculations,¹² including the lattice constant $a = 3.52 \text{ \AA}$, and the bond length $d_{\text{Sc-Se}} = 2.64 \text{ \AA}$. The resultant angle is $\theta_{\text{SeScSc}} = 83.621^\circ$ and $\theta_{\text{ScSeSe}} = 83.621^\circ$ with Se atoms from the same (top or bottom) group.

Table CLIV shows three VFF terms for the single-layer 1T-ScSe₂, one of which is the bond stretching interaction shown by Eq. (1) while the other two terms are the angle bending interaction shown by Eq. (2). We note that the angle bending term $K_{\text{Sc-Se-Se}}$ is for the angle

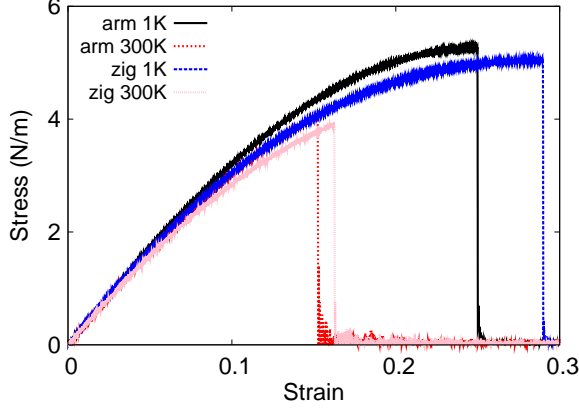


FIG. 77: (Color online) Stress-strain for single-layer 1T-ScSe₂ of dimension $100 \times 100 \text{ \AA}$ along the armchair and zigzag directions.

TABLE CLIV: The VFF model for single-layer 1T-ScSe₂. The second line gives an explicit expression for each VFF term. The third line is the force constant parameters. Parameters are in the unit of $\frac{eV}{\text{\AA}^2}$ for the bond stretching interactions, and in the unit of eV for the angle bending interaction. The fourth line gives the initial bond length (in unit of \AA) for the bond stretching interaction and the initial angle (in unit of degrees) for the angle bending interaction. The angle θ_{ijk} has atom i as the apex.

VFF type	bond stretching	angle bending	
expression	$\frac{1}{2}K_{\text{Sc-Se}}(\Delta r)^2$	$\frac{1}{2}K_{\text{Sc-Se-Se}}(\Delta\theta)^2$	$\frac{1}{2}K_{\text{Se-Sc-Se}}(\Delta\theta)^2$
parameter	4.407	2.399	2.399
r_0 or θ_0	2.64	83.621	83.621

$\theta_{\text{Sc-Se-Se}}$ with both Se atoms from the same (top or bottom) group. These force constant parameters are determined by fitting to the three acoustic branches in the phonon dispersion along the ΓM as shown in Fig. 76 (a). The *ab initio* calculations for the phonon dispersion are from Ref. 12. We note that the lowest-frequency branch around the Γ point from the VFF model is lower than the *ab initio* results. This branch is the flexural branch, which should be a quadratic dispersion. However, the *ab initio* calculations give a linear dispersion for the flexural branch due to the violation of the rigid rotational invariance in the first-principles package,²⁰ so *ab initio* calculations typically overestimate the frequency of this

TABLE CLV: Two-body SW potential parameters for single-layer 1T-ScSe₂ used by GULP⁸ as expressed in Eq. (3).

	A (eV)	ρ (Å)	B (Å ⁴)	r_{\min} (Å)	r_{\max} (Å)
Sc-Se	3.884	1.173	24.288	0.0	3.520

TABLE CLVI: Three-body SW potential parameters for single-layer 1T-ScSe₂ used by GULP⁸ as expressed in Eq. (4). The angle θ_{ijk} in the first line indicates the bending energy for the angle with atom i as the apex.

	K (eV)	θ_0 (degree)	ρ_1 (Å)	ρ_2 (Å)	$r_{\min 12}$ (Å)	$r_{\max 12}$ (Å)	$r_{\min 13}$ (Å)	$r_{\max 13}$ (Å)	$r_{\min 23}$ (Å)	$r_{\max 23}$ (Å)
$\theta_{\text{Sc-Se-Se}}$	17.479	83.621	1.173	1.173	0.0	3.520	0.0	3.520	0.0	4.808
$\theta_{\text{Se-Sc-Sc}}$	17.479	83.621	1.173	1.173	0.0	3.520	0.0	3.520	0.0	4.808

branch. Fig. 76 (b) shows that the VFF model and the SW potential give exactly the same phonon dispersion, as the SW potential is derived from the VFF model.

The parameters for the two-body SW potential used by GULP are shown in Tab. CLV. The parameters for the three-body SW potential used by GULP are shown in Tab. CLVI. Some representative parameters for the SW potential used by LAMMPS are listed in Tab. CLVII.

We use LAMMPS to perform MD simulations for the mechanical behavior of the single-layer 1T-ScSe₂ under uniaxial tension at 1.0 K and 300.0 K. Fig. 77 shows the stress-strain curve for the tension of a single-layer 1T-ScSe₂ of dimension 100×100 Å. Periodic boundary conditions are applied in both armchair and zigzag directions. The single-layer 1T-ScSe₂ is stretched uniaxially along the armchair or zigzag direction. The stress is calculated without involving the actual thickness of the quasi-two-dimensional structure of the single-layer 1T-ScSe₂. The Young's modulus can be obtained by a linear fitting of the stress-strain relation in the small strain range of $[0, 0.01]$. The Young's modulus are 36.4 N/m and 36.3 N/m

TABLE CLVII: SW potential parameters for single-layer 1T-ScSe₂ used by LAMMPS⁹ as expressed in Eqs. (9) and (10).

	ϵ (eV)	σ (Å)	a	λ	γ	$\cos \theta_0$	A_L	B_L	p	q	tol
Sc-Se ₁ -Se ₁	1.000	1.173	3.000	17.479	1.000	0.111	3.884	12.814	4	0	0.0

TABLE CLVIII: The VFF model for single-layer 1T-ScTe₂. The second line gives an explicit expression for each VFF term. The third line is the force constant parameters. Parameters are in the unit of $\frac{\text{eV}}{\text{\AA}^2}$ for the bond stretching interactions, and in the unit of eV for the angle bending interaction. The fourth line gives the initial bond length (in unit of \AA) for the bond stretching interaction and the initial angle (in unit of degrees) for the angle bending interaction. The angle θ_{ijk} has atom *i* as the apex.

VFF type	bond stretching	angle bending	
expression	$\frac{1}{2}K_{\text{Sc-Te}}(\Delta r)^2$	$\frac{1}{2}K_{\text{Sc-Te-Te}}(\Delta\theta)^2$	$\frac{1}{2}K_{\text{Te-Sc-Sc}}(\Delta\theta)^2$
parameter	4.407	2.399	2.399
r_0 or θ_0	2.85	81.481	81.481

TABLE CLIX: Two-body SW potential parameters for single-layer 1T-ScTe₂ used by GULP⁸ as expressed in Eq. (3).

	A (eV)	ρ (\AA)	B (\AA^4)	r_{min} (\AA)	r_{max} (\AA)
Sc-Te	4.269	1.183	32.988	0.0	3.768

along the armchair and zigzag directions, respectively. The Young's modulus is essentially isotropic in the armchair and zigzag directions. The Poisson's ratio from the VFF model and the SW potential is $\nu_{xy} = \nu_{yx} = 0.20$.

There is no available value for nonlinear quantities in the single-layer 1T-ScSe₂. We have thus used the nonlinear parameter $B = 0.5d^4$ in Eq. (5), which is close to the value of B in most materials. The value of the third order nonlinear elasticity D can be extracted by fitting the stress-strain relation to the function $\sigma = E\epsilon + \frac{1}{2}D\epsilon^2$ with E as the Young's modulus. The values of D from the present SW potential are -113.7 N/m and -130.3 N/m along the armchair and zigzag directions, respectively. The ultimate stress is about 5.3 Nm^{-1} at the ultimate strain of 0.25 in the armchair direction at the low temperature of 1 K. The ultimate stress is about 5.0 Nm^{-1} at the ultimate strain of 0.29 in the zigzag direction at the low temperature of 1 K.

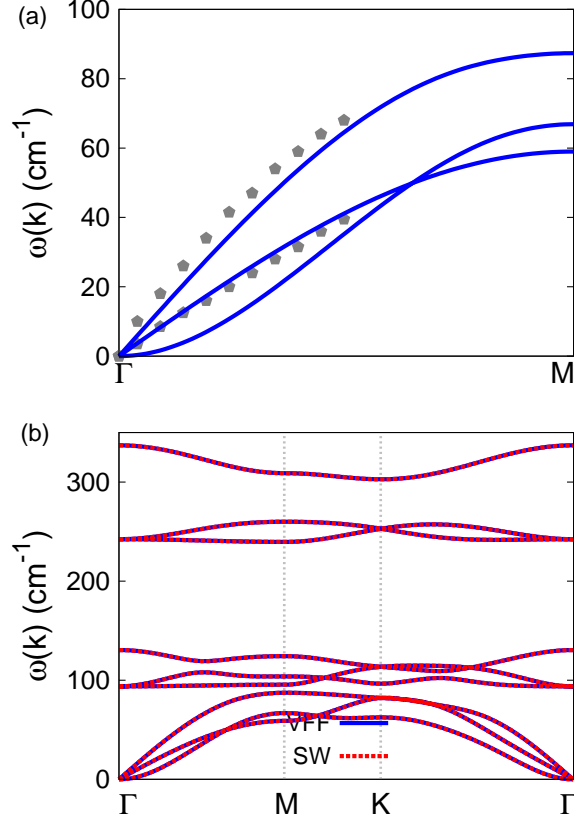


FIG. 78: (Color online) Phonon spectrum for single-layer 1T-ScTe₂. (a) Phonon dispersion along the Γ M direction in the Brillouin zone. The results from the VFF model (lines) are comparable with the *ab initio* results (pentagons) from Ref. 12. (b) The phonon dispersion from the SW potential is exactly the same as that from the VFF model.

XL. 1T-SCTE₂

Most existing theoretical studies on the single-layer 1T-ScTe₂ are based on the first-principles calculations. In this section, we will develop the SW potential for the single-layer 1T-ScTe₂.

The structure for the single-layer 1T-ScTe₂ is shown in Fig. 71 (with M=Sc and X=Te). Each Sc atom is surrounded by six Te atoms. These Te atoms are categorized into the top group (eg. atoms 1, 3, and 5) and bottom group (eg. atoms 2, 4, and 6). Each Te atom is connected to three Sc atoms. The structural parameters are from the first-principles calculations,¹² including the lattice constant $a = 3.72 \text{ \AA}$, and the bond length

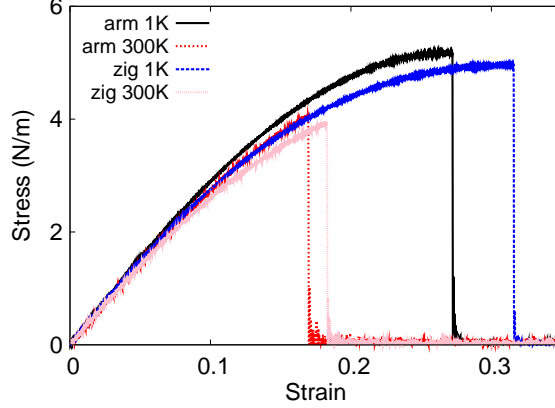


FIG. 79: (Color online) Stress-strain for single-layer 1T-ScTe₂ of dimension 100 × 100 Å along the armchair and zigzag directions.

TABLE CLX: Three-body SW potential parameters for single-layer 1T-ScTe₂ used by GULP⁸ as expressed in Eq. (4). The angle θ_{ijk} in the first line indicates the bending energy for the angle with atom i as the apex.

	K (eV)	θ_0 (degree)	ρ_1 (Å)	ρ_2 (Å)	$r_{\min 12}$ (Å)	$r_{\max 12}$ (Å)	$r_{\min 13}$ (Å)	$r_{\max 13}$ (Å)	$r_{\min 23}$ (Å)	$r_{\max 23}$ (Å)
$\theta_{\text{Sc-Te-Te}}$	16.139	81.481	1.183	1.183	0.0	3.768	0.0	3.768	0.0	5.082
$\theta_{\text{Te-Sc-Sc}}$	16.139	81.481	1.183	1.183	0.0	3.768	0.0	3.768	0.0	5.082

$d_{\text{Sc-Te}} = 2.85$ Å. The resultant angle is $\theta_{\text{TeScSc}} = 81.481^\circ$ and $\theta_{\text{ScTeTe}} = 81.481^\circ$ with Se atoms from the same (top or bottom) group.

Table CLVIII shows three VFF terms for the single-layer 1T-ScTe₂, one of which is the bond stretching interaction shown by Eq. (1) while the other two terms are the angle bending interaction shown by Eq. (2). We note that the angle bending term $K_{\text{Sc-Te-Te}}$ is for the angle $\theta_{\text{Sc-Te-Te}}$ with both Te atoms from the same (top or bottom) group. These force constant parameters are determined by fitting to the two in-plane acoustic branches in the

TABLE CLXI: SW potential parameters for single-layer 1T-ScTe₂ used by LAMMPS⁹ as expressed in Eqs. (9) and (10).

	ϵ (eV)	σ (Å)	a	λ	γ	$\cos \theta_0$	A_L	B_L	p	q	tol
Sc-Te ₁ -Te ₁	1.000	1.183	3.185	16.139	1.000	0.148	4.269	16.841	4	0	0.0

phonon dispersion along the Γ M as shown in Fig. 78 (a). The *ab initio* calculations for the phonon dispersion are from Ref. 12. Fig. 78 (b) shows that the VFF model and the SW potential give exactly the same phonon dispersion, as the SW potential is derived from the VFF model.

The parameters for the two-body SW potential used by GULP are shown in Tab. CLIX. The parameters for the three-body SW potential used by GULP are shown in Tab. CLX. Some representative parameters for the SW potential used by LAMMPS are listed in Tab. CLXI.

We use LAMMPS to perform MD simulations for the mechanical behavior of the single-layer 1T-ScTe₂ under uniaxial tension at 1.0 K and 300.0 K. Fig. 79 shows the stress-strain curve for the tension of a single-layer 1T-ScTe₂ of dimension 100×100 Å. Periodic boundary conditions are applied in both armchair and zigzag directions. The single-layer 1T-ScTe₂ is stretched uniaxially along the armchair or zigzag direction. The stress is calculated without involving the actual thickness of the quasi-two-dimensional structure of the single-layer 1T-ScTe₂. The Young's modulus can be obtained by a linear fitting of the stress-strain relation in the small strain range of $[0, 0.01]$. The Young's modulus are 31.4 N/m and 31.3 N/m along the armchair and zigzag directions, respectively. The Young's modulus is essentially isotropic in the armchair and zigzag directions. The Poisson's ratio from the VFF model and the SW potential is $\nu_{xy} = \nu_{yx} = 0.22$.

There is no available value for nonlinear quantities in the single-layer 1T-ScTe₂. We have thus used the nonlinear parameter $B = 0.5d^4$ in Eq. (5), which is close to the value of B in most materials. The value of the third order nonlinear elasticity D can be extracted by fitting the stress-strain relation to the function $\sigma = E\epsilon + \frac{1}{2}D\epsilon^2$ with E as the Young's modulus. The values of D from the present SW potential are -81.2 N/m and -96.7 N/m along the armchair and zigzag directions, respectively. The ultimate stress is about 5.2 Nm^{-1} at the ultimate strain of 0.27 in the armchair direction at the low temperature of 1 K. The ultimate stress is about 5.0 Nm^{-1} at the ultimate strain of 0.31 in the zigzag direction at the low temperature of 1 K.

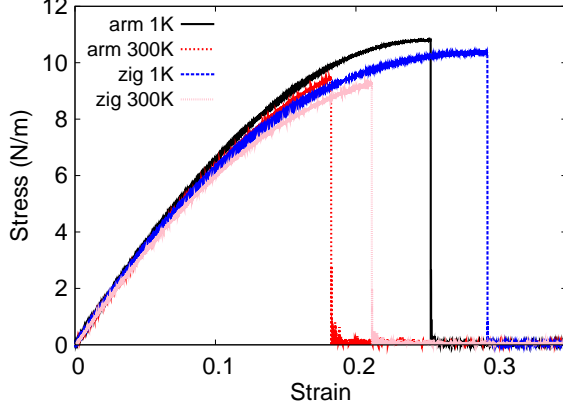


FIG. 80: (Color online) Stress-strain for single-layer 1T-TiS₂ of dimension $100 \times 100 \text{ \AA}$ along the armchair and zigzag directions.

TABLE CLXII: The VFF model for single-layer 1T-TiS₂. The second line gives an explicit expression for each VFF term. The third line is the force constant parameters. Parameters are in the unit of $\frac{\text{eV}}{\text{\AA}^2}$ for the bond stretching interactions, and in the unit of eV for the angle bending interaction. The fourth line gives the initial bond length (in unit of \AA) for the bond stretching interaction and the initial angle (in unit of degrees) for the angle bending interaction. The angle θ_{ijk} has atom i as the apex.

VFF type	bond stretching	angle bending	
expression	$\frac{1}{2}K_{\text{Ti-S}}(\Delta r)^2$	$\frac{1}{2}K_{\text{Ti-S-S}}(\Delta\theta)^2$	$\frac{1}{2}K_{\text{S-Ti-Ti}}(\Delta\theta)^2$
parameter	9.815	3.754	3.754
r_0 or θ_0	2.390	87.984	87.984

XLI. 1T-TIS₂

Most existing theoretical studies on the single-layer 1T-TiS₂ are based on the first-principles calculations. In this section, we will develop the SW potential for the single-layer 1T-TiS₂.

The structure for the single-layer 1T-TiS₂ is shown in Fig. 71 (with M=Ti and X=S). Each Ti atom is surrounded by six S atoms. These S atoms are categorized into the top group (eg. atoms 1, 3, and 5) and bottom group (eg. atoms 2, 4, and 6). Each S atom is connected to three Ti atoms. The structural parameters are from the first-principles

TABLE CLXIII: Two-body SW potential parameters for single-layer 1T-TiS₂ used by GULP⁸ as expressed in Eq. (3).

	A (eV)	ρ (Å)	B (Å ⁴)	r_{\min} (Å)	r_{\max} (Å)
Ti-S	7.958	1.210	16.314	0.0	3.240

TABLE CLXIV: Three-body SW potential parameters for single-layer 1T-TiS₂ used by GULP⁸ as expressed in Eq. (4). The angle θ_{ijk} in the first line indicates the bending energy for the angle with atom i as the apex.

	K (eV)	θ_0 (degree)	ρ_1 (Å)	ρ_2 (Å)	$r_{\min12}$ (Å)	$r_{\max12}$ (Å)	$r_{\min13}$ (Å)	$r_{\max13}$ (Å)	$r_{\min23}$ (Å)	$r_{\max23}$ (Å)
$\theta_{\text{Ti-S-S}}$	32.377	87.984	1.210	1.210	0.0	3.240	0.0	3.240	0.0	4.535
$\theta_{\text{S-Ti-Ti}}$	32.377	87.984	1.210	1.210	0.0	3.240	0.0	3.240	0.0	4.535

calculations,¹² including the lattice constant $a = 3.32$ Å and the bond length $d_{\text{Ti-S}} = 2.39$ Å. The resultant angles are $\theta_{\text{TiSS}} = 87.984^\circ$ with S atoms from the same (top or bottom) group, and $\theta_{\text{STiTi}} = 87.984^\circ$.

Table CLXII shows three VFF terms for the single-layer 1T-TiS₂, one of which is the bond stretching interaction shown by Eq. (1) while the other two terms are the angle bending interaction shown by Eq. (2). We note that the angle bending term $K_{\text{Ti-S-S}}$ is for the angle $\theta_{\text{Ti-S-S}}$ with both S atoms from the same (top or bottom) group. We find that there are actually only two parameters in the VFF model, so we can determine their value by fitting to the Young's modulus and the Poisson's ratio of the system. The *ab initio* calculations have predicted the Young's modulus to be 85 N/m and the Poisson's ratio as 0.20.⁴⁸

The parameters for the two-body SW potential used by GULP are shown in Tab. CLXIII. The parameters for the three-body SW potential used by GULP are shown in Tab. CLXIV. Some representative parameters for the SW potential used by LAMMPS are listed in Tab. CLXV.

TABLE CLXV: SW potential parameters for single-layer 1T-TiS₂ used by LAMMPS⁹ as expressed in Eqs. (9) and (10).

	ϵ (eV)	σ (Å)	a	λ	γ	$\cos \theta_0$	A_L	B_L	p	q	tol
Ti-S-S	1.000	1.210	2.677	32.377	1.000	0.035	7.958	7.602	4	0	0.0

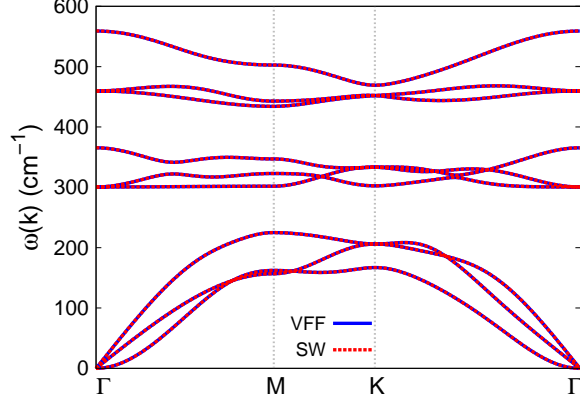


FIG. 81: (Color online) Phonon spectrum for single-layer 1T-TiS₂ along the Γ MK Γ direction in the Brillouin zone. The phonon dispersion from the SW potential is exactly the same as that from the VFF model.

We use LAMMPS to perform MD simulations for the mechanical behavior of the single-layer 1T-TiS₂ under uniaxial tension at 1.0 K and 300.0 K. Fig. 80 shows the stress-strain curve for the tension of a single-layer 1T-TiS₂ of dimension 100×100 Å. Periodic boundary conditions are applied in both armchair and zigzag directions. The single-layer 1T-TiS₂ is stretched uniaxially along the armchair or zigzag direction. The stress is calculated without involving the actual thickness of the quasi-two-dimensional structure of the single-layer 1T-TiS₂. The Young's modulus can be obtained by a linear fitting of the stress-strain relation in the small strain range of $[0, 0.01]$. The Young's modulus are 75.0 N/m and 74.6 N/m along the armchair and zigzag directions, respectively. The Young's modulus is essentially isotropic in the armchair and zigzag directions. The Poisson's ratio from the VFF model and the SW potential is $\nu_{xy} = \nu_{yx} = 0.20$. The fitted Young's modulus value is about 10% smaller than the *ab initio* result of 85 N/m,⁴⁸ as only short-range interactions are considered in the present work. The long-range interactions are ignored, which typically leads to about 10% underestimation for the value of the Young's modulus.

There is no available value for nonlinear quantities in the single-layer 1T-TiS₂. We have thus used the nonlinear parameter $B = 0.5d^4$ in Eq. (5), which is close to the value of B in most materials. The value of the third order nonlinear elasticity D can be extracted by fitting the stress-strain relation to the function $\sigma = E\epsilon + \frac{1}{2}D\epsilon^2$ with E as the Young's modulus. The values of D from the present SW potential are -220.8 N/m and -264.4 N/m along the

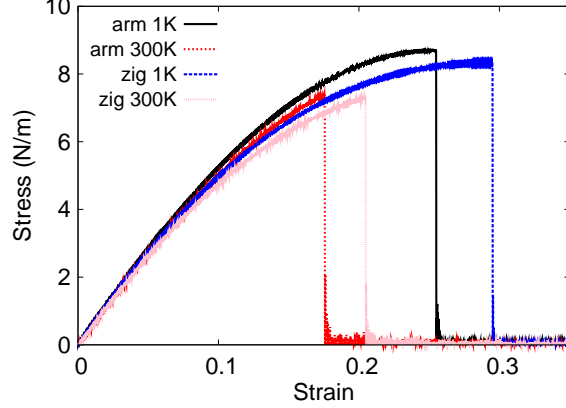


FIG. 82: (Color online) Stress-strain for single-layer 1T-TiSe₂ of dimension $100 \times 100 \text{ \AA}$ along the armchair and zigzag directions.

TABLE CLXVI: The VFF model for single-layer 1T-TiSe₂. The second line gives an explicit expression for each VFF term. The third line is the force constant parameters. Parameters are in the unit of $\frac{\text{eV}}{\text{\AA}^2}$ for the bond stretching interactions, and in the unit of eV for the angle bending interaction. The fourth line gives the initial bond length (in unit of \AA) for the bond stretching interaction and the initial angle (in unit of degrees) for the angle bending interaction. The angle θ_{ijk} has atom *i* as the apex.

VFF type	bond stretching	angle bending	
expression	$\frac{1}{2}K_{\text{Ti-Se}}(\Delta r)^2$	$\frac{1}{2}K_{\text{Ti-Se-Se}}(\Delta\theta)^2$	$\frac{1}{2}K_{\text{Se-Ti-Ti}}(\Delta\theta)^2$
parameter	7.712	3.363	3.363
r_0 or θ_0	2.510	86.199	86.199

armchair and zigzag directions, respectively. The ultimate stress is about 10.8 Nm^{-1} at the ultimate strain of 0.25 in the armchair direction at the low temperature of 1 K. The ultimate stress is about 10.4 Nm^{-1} at the ultimate strain of 0.29 in the zigzag direction at the low temperature of 1 K.

Fig. 81 shows that the VFF model and the SW potential give exactly the same phonon dispersion, as the SW potential is derived from the VFF model.

TABLE CLXVII: Two-body SW potential parameters for single-layer 1T-TiSe₂ used by GULP⁸ as expressed in Eq. (3).

	A (eV)	ρ (Å)	B (Å ⁴)	r_{\min} (Å)	r_{\max} (Å)
Ti-Se	6.582	1.207	19.846	0.0	3.380

TABLE CLXVIII: Three-body SW potential parameters for single-layer 1T-TiSe₂ used by GULP⁸ as expressed in Eq. (4). The angle θ_{ijk} in the first line indicates the bending energy for the angle with atom i as the apex.

	K (eV)	θ_0 (degree)	ρ_1 (Å)	ρ_2 (Å)	$r_{\min12}$ (Å)	$r_{\max12}$ (Å)	$r_{\min13}$ (Å)	$r_{\max13}$ (Å)	$r_{\min23}$ (Å)	$r_{\max23}$ (Å)
$\theta_{\text{Ti-Se-Se}}$	27.044	86.199	1.207	1.207	0.0	3.380	0.0	3.380	0.0	4.685
$\theta_{\text{Se-Ti-Ti}}$	27.044	86.199	1.207	1.207	0.0	3.380	0.0	3.380	0.0	4.685

XLII. 1T-TiSe₂

Most existing theoretical studies on the single-layer 1T-TiSe₂ are based on the first-principles calculations. In this section, we will develop the SW potential for the single-layer 1T-TiSe₂.

The structure for the single-layer 1T-TiSe₂ is shown in Fig. 71 (with M=Ti and X=Se). Each Ti atom is surrounded by six Se atoms. These Se atoms are categorized into the top group (eg. atoms 1, 3, and 5) and bottom group (eg. atoms 2, 4, and 6). Each Se atom is connected to three Ti atoms. The structural parameters are from the first-principles calculations,¹² including the lattice constant $a = 3.43$ Å and the bond length $d_{\text{Ti-Se}} = 2.51$ Å. The resultant angles are $\theta_{\text{TiSeSe}} = 86.199^\circ$ with Se atoms from the same (top or bottom) group, and $\theta_{\text{SeTiTi}} = 86.199^\circ$.

Table CLXVI shows three VFF terms for the single-layer 1T-TiSe₂, one of which is the bond stretching interaction shown by Eq. (1) while the other two terms are the angle bending

TABLE CLXIX: SW potential parameters for single-layer 1T-TiSe₂ used by LAMMPS⁹ as expressed in Eqs. (9) and (10).

	ϵ (eV)	σ (Å)	a	λ	γ	$\cos \theta_0$	A_L	B_L	p	q	tol
Ti-Se-Se	1.000	1.207	2.801	27.044	1.000	0.066	6.582	9.362	4	0	0.0

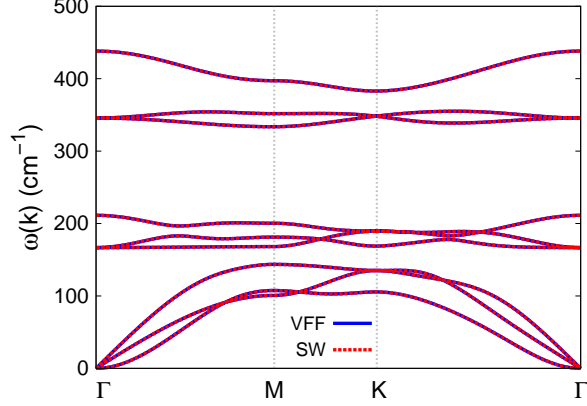


FIG. 83: (Color online) Phonon spectrum for single-layer 1T-TiSe₂ along the Γ MK Γ direction in the Brillouin zone. The phonon dispersion from the SW potential is exactly the same as that from the VFF model.

interaction shown by Eq. (2). We note that the angle bending term $K_{\text{Ti-Se-Se}}$ is for the angle $\theta_{\text{Ti-Se-Se}}$ with both Se atoms from the same (top or bottom) group. We find that there are actually only two parameters in the VFF model, so we can determine their value by fitting to the Young's modulus and the Poisson's ratio of the system. The *ab initio* calculations have predicted the Young's modulus to be 70 N/m and the Poisson's ratio as 0.20.⁴⁸

The parameters for the two-body SW potential used by GULP are shown in Tab. CLXVII. The parameters for the three-body SW potential used by GULP are shown in Tab. CLXVIII. Some representative parameters for the SW potential used by LAMMPS are listed in Tab. CLXIX.

We use LAMMPS to perform MD simulations for the mechanical behavior of the single-layer 1T-TiSe₂ under uniaxial tension at 1.0 K and 300.0 K. Fig. 82 shows the stress-strain curve for the tension of a single-layer 1T-TiSe₂ of dimension $100 \times 100 \text{ \AA}$. Periodic boundary conditions are applied in both armchair and zigzag directions. The single-layer 1T-TiSe₂ is stretched uniaxially along the armchair or zigzag direction. The stress is calculated without involving the actual thickness of the quasi-two-dimensional structure of the single-layer 1T-TiSe₂. The Young's modulus can be obtained by a linear fitting of the stress-strain relation in the small strain range of $[0, 0.01]$. The Young's modulus are 59.2 N/m and 58.9 N/m along the armchair and zigzag directions, respectively. The Young's modulus is essentially isotropic in the armchair and zigzag directions. The Poisson's ratio from the VFF model

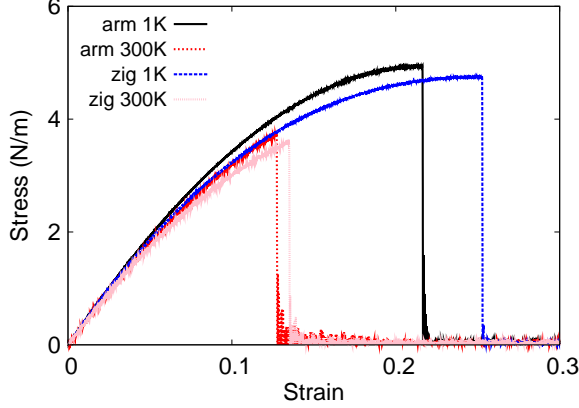


FIG. 84: (Color online) Stress-strain for single-layer 1T-TiTe₂ of dimension $100 \times 100 \text{ \AA}$ along the armchair and zigzag directions.

and the SW potential is $\nu_{xy} = \nu_{yx} = 0.20$. The fitted Young's modulus value is about 10% smaller than the *ab initio* result of 70 N/m ,⁴⁸ as only short-range interactions are considered in the present work. The long-range interactions are ignored, which typically leads to about 10% underestimation for the value of the Young's modulus.

There is no available value for nonlinear quantities in the single-layer 1T-TiSe₂. We have thus used the nonlinear parameter $B = 0.5d^4$ in Eq. (5), which is close to the value of B in most materials. The value of the third order nonlinear elasticity D can be extracted by fitting the stress-strain relation to the function $\sigma = E\epsilon + \frac{1}{2}D\epsilon^2$ with E as the Young's modulus. The values of D from the present SW potential are -166.5 N/m and -201.6 N/m along the armchair and zigzag directions, respectively. The ultimate stress is about 8.7 Nm^{-1} at the ultimate strain of 0.25 in the armchair direction at the low temperature of 1 K. The ultimate stress is about 8.3 Nm^{-1} at the ultimate strain of 0.29 in the zigzag direction at the low temperature of 1 K.

Fig. 83 shows that the VFF model and the SW potential give exactly the same phonon dispersion, as the SW potential is derived from the VFF model.

XLIII. 1T-TITE₂

Most existing theoretical studies on the single-layer 1T-TiTe₂ are based on the first-principles calculations. In this section, we will develop the SW potential for the single-layer

TABLE CLXX: The VFF model for single-layer 1T-TiTe₂. The second line gives an explicit expression for each VFF term. The third line is the force constant parameters. Parameters are in the unit of $\frac{\text{eV}}{\text{Å}^2}$ for the bond stretching interactions, and in the unit of eV for the angle bending interaction. The fourth line gives the initial bond length (in unit of Å) for the bond stretching interaction and the initial angle (in unit of degrees) for the angle bending interaction. The angle θ_{ijk} has atom i as the apex.

VFF type	bond stretching	angle bending	
expression	$\frac{1}{2}K_{\text{Ti-Te}}(\Delta r)^2$	$\frac{1}{2}K_{\text{Ti-Te-Te}}(\Delta\theta)^2$	$\frac{1}{2}K_{\text{Te-Ti-Ti}}(\Delta\theta)^2$
parameter	3.758	3.217	3.217
r_0 or θ_0	2.730	83.621	83.621

TABLE CLXXI: Two-body SW potential parameters for single-layer 1T-TiTe₂ used by GULP⁸ as expressed in Eq. (3).

	A (eV)	ρ (Å)	B (Å ⁴)	r_{\min} (Å)	r_{\max} (Å)
Ti-Te	3.542	1.213	27.773	0.0	3.640

1T-TiTe₂.

The structure for the single-layer 1T-TiTe₂ is shown in Fig. 71 (with M=Ti and X=Te). Each Ti atom is surrounded by six Te atoms. These Te atoms are categorized into the top group (eg. atoms 1, 3, and 5) and bottom group (eg. atoms 2, 4, and 6). Each Te atom is connected to three Ti atoms. The structural parameters are from the first-principles calculations,¹² including the lattice constant $a = 3.64$ Å and the bond length $d_{\text{Ti-Te}} = 2.73$ Å. The resultant angles are $\theta_{\text{TiTeTe}} = 83.621^\circ$ with Te atoms from the same (top or bottom)

TABLE CLXXII: Three-body SW potential parameters for single-layer 1T-TiTe₂ used by GULP⁸ as expressed in Eq. (4). The angle θ_{ijk} in the first line indicates the bending energy for the angle with atom i as the apex.

	K (eV)	θ_0 (degree)	ρ_1 (Å)	ρ_2 (Å)	$r_{\min12}$ (Å)	$r_{\max12}$ (Å)	$r_{\min13}$ (Å)	$r_{\max13}$ (Å)	$r_{\min23}$ (Å)	$r_{\max23}$ (Å)
$\theta_{\text{Ti-Te-Te}}$	23.439	83.621	1.213	1.213	0.0	3.640	0.0	3.640	0.0	4.972
$\theta_{\text{Te-Ti-Ti}}$	23.439	83.621	1.213	1.213	0.0	3.640	0.0	3.640	0.0	4.972

TABLE CLXXIII: SW potential parameters for single-layer 1T-TiTe₂ used by LAMMPS⁹ as expressed in Eqs. (9) and (10).

	ϵ (eV)	σ (Å)	a	λ	γ	$\cos \theta_0$	A_L	B_L	p	q	tol
Ti-Te-Te	1.000	1.213	3.000	23.439	1.000	0.111	3.542	12.814	4	0	0.0

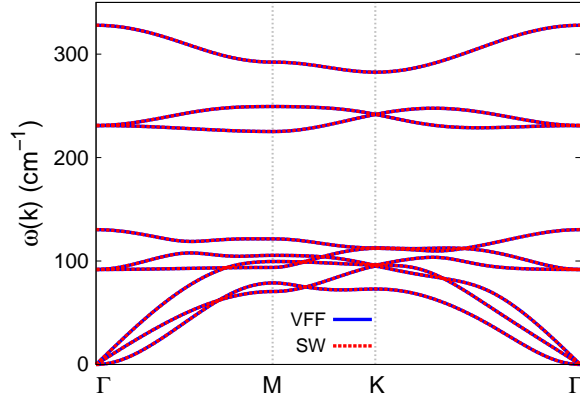


FIG. 85: (Color online) Phonon spectrum for single-layer 1T-TiTe₂ along the Γ MK Γ direction in the Brillouin zone. The phonon dispersion from the SW potential is exactly the same as that from the VFF model.

group, and $\theta_{\text{TeTiTi}} = 83.621^\circ$.

Table CLXX shows three VFF terms for the single-layer 1T-TiTe₂, one of which is the bond stretching interaction shown by Eq. (1) while the other two terms are the angle bending interaction shown by Eq. (2). We note that the angle bending term $K_{\text{Ti-Te-Te}}$ is for the angle $\theta_{\text{Ti-Te-Te}}$ with both Te atoms from the same (top or bottom) group. We find that there are actually only two parameters in the VFF model, so we can determine their value by fitting to the Young's modulus and the Poisson's ratio of the system. The *ab initio* calculations have predicted the Young's modulus to be 46 N/m and the Poisson's ratio as 0.15.⁴⁸

The parameters for the two-body SW potential used by GULP are shown in Tab. CLXXI. The parameters for the three-body SW potential used by GULP are shown in Tab. CLXXII. Some representative parameters for the SW potential used by LAMMPS are listed in Tab. CLXXIII.

We use LAMMPS to perform MD simulations for the mechanical behavior of the single-layer 1T-TiTe₂ under uniaxial tension at 1.0 K and 300.0 K. Fig. 84 shows the stress-strain

curve for the tension of a single-layer 1T-TiTe₂ of dimension 100×100 Å. Periodic boundary conditions are applied in both armchair and zigzag directions. The single-layer 1T-TiTe₂ is stretched uniaxially along the armchair or zigzag direction. The stress is calculated without involving the actual thickness of the quasi-two-dimensional structure of the single-layer 1T-TiTe₂. The Young's modulus can be obtained by a linear fitting of the stress-strain relation in the small strain range of $[0, 0.01]$. The Young's modulus are 41.4 N/m and 41.2 N/m along the armchair and zigzag directions, respectively. The Young's modulus is essentially isotropic in the armchair and zigzag directions. The Poisson's ratio from the VFF model and the SW potential is $\nu_{xy} = \nu_{yx} = 0.15$. The fitted Young's modulus value is about 10% smaller than the *ab initio* result of 46 N/m,⁴⁸ as only short-range interactions are considered in the present work. The long-range interactions are ignored, which typically leads to about 10% underestimation for the value of the Young's modulus.

There is no available value for nonlinear quantities in the single-layer 1T-TiTe₂. We have thus used the nonlinear parameter $B = 0.5d^4$ in Eq. (5), which is close to the value of B in most materials. The value of the third order nonlinear elasticity D can be extracted by fitting the stress-strain relation to the function $\sigma = E\epsilon + \frac{1}{2}D\epsilon^2$ with E as the Young's modulus. The values of D from the present SW potential are -161.3 N/m and -181.4 N/m along the armchair and zigzag directions, respectively. The ultimate stress is about 4.9 Nm^{-1} at the ultimate strain of 0.22 in the armchair direction at the low temperature of 1 K. The ultimate stress is about 4.7 Nm^{-1} at the ultimate strain of 0.25 in the zigzag direction at the low temperature of 1 K.

Fig. 85 shows that the VFF model and the SW potential give exactly the same phonon dispersion, as the SW potential is derived from the VFF model.

XLIV. 1T-VS₂

Most existing theoretical studies on the single-layer 1T-VS₂ are based on the first-principles calculations. In this section, we will develop the SW potential for the single-layer 1T-VS₂.

The structure for the single-layer 1T-VS₂ is shown in Fig. 71 (with M=V and X=S). Each V atom is surrounded by six S atoms. These S atoms are categorized into the top group (eg. atoms 1, 3, and 5) and bottom group (eg. atoms 2, 4, and 6). Each S atom

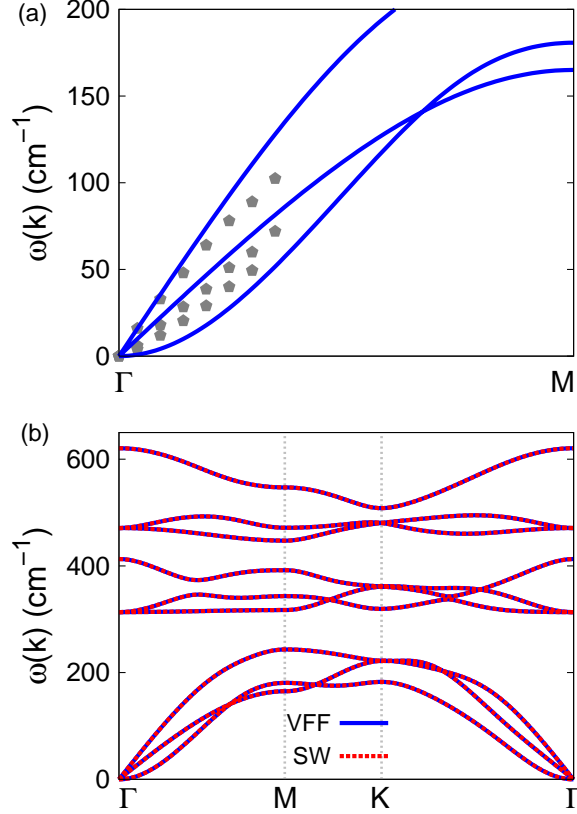


FIG. 86: (Color online) Phonon spectrum for single-layer 1T-VS₂. (a) Phonon dispersion along the Γ M direction in the Brillouin zone. The results from the VFF model (lines) are comparable with the *ab initio* results (pentagons) from Ref. 12. (b) The phonon dispersion from the SW potential is exactly the same as that from the VFF model.

is connected to three V atoms. The structural parameters are from the first-principles calculations,¹² including the lattice constant $a = 3.10 \text{ \AA}$ and the bond length $d_{V-S} = 2.31 \text{ \AA}$. The resultant angles are $\theta_{VSS} = 84.288^\circ$ with S atoms from the same (top or bottom) group, and $\theta_{SVV} = 84.288^\circ$.

Table CLXXIV shows three VFF terms for the single-layer 1T-VS₂, one of which is the bond stretching interaction shown by Eq. (1) while the other two terms are the angle bending interaction shown by Eq. (2). We note that the angle bending term K_{V-S-S} is for the angle θ_{V-S-S} with both S atoms from the same (top or bottom) group. These force constant parameters are determined by fitting to the three acoustic branches in the phonon dispersion along the Γ M as shown in Fig. 86 (a). The *ab initio* calculations for the phonon

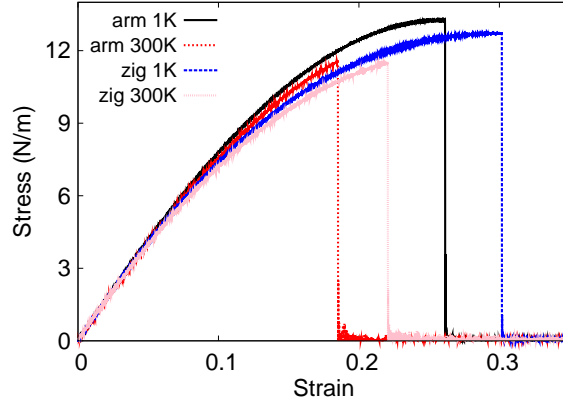


FIG. 87: (Color online) Stress-strain for single-layer 1T-VS₂ of dimension $100 \times 100 \text{ \AA}$ along the armchair and zigzag directions.

TABLE CLXXIV: The VFF model for single-layer 1T-VS₂. The second line gives an explicit expression for each VFF term. The third line is the force constant parameters. Parameters are in the unit of $\frac{\text{eV}}{\text{\AA}^2}$ for the bond stretching interactions, and in the unit of eV for the angle bending interaction. The fourth line gives the initial bond length (in unit of \AA) for the bond stretching interaction and the initial angle (in unit of degrees) for the angle bending interaction. The angle θ_{ijk} has atom i as the apex.

VFF type	bond stretching	angle bending	
expression	$\frac{1}{2}K_{V-S}(\Delta r)^2$	$\frac{1}{2}K_{V-S-S}(\Delta\theta)^2$	$\frac{1}{2}K_{S-V-V}(\Delta\theta)^2$
parameter	11.562	4.237	4.237
r_0 or θ_0	2.310	84.288	84.288

dispersion are from Ref. 12. The lowest acoustic branch (flexural mode) is linear and very close to the inplane transverse acoustic branch in the *ab initio* calculations, which may due to the violation of the rigid rotational invariance.²⁰ Fig. 86 (b) shows that the VFF model and the SW potential give exactly the same phonon dispersion, as the SW potential is derived from the VFF model.

The parameters for the two-body SW potential used by GULP are shown in Tab. CLXXV. The parameters for the three-body SW potential used by GULP are shown in Tab. CLXXVI. Some representative parameters for the SW potential used by LAMMPS are listed in

TABLE CLXXV: Two-body SW potential parameters for single-layer 1T-VS₂ used by GULP⁸ as expressed in Eq. (3).

	A (eV)	ρ (Å)	B (Å ⁴)	r_{\min} (Å)	r_{\max} (Å)
V-S	7.943	1.048	14.237	0.0	3.088

TABLE CLXXVI: Three-body SW potential parameters for single-layer 1T-VS₂ used by GULP⁸ as expressed in Eq. (4). The angle θ_{ijk} in the first line indicates the bending energy for the angle with atom i as the apex.

	K (eV)	θ_0 (degree)	ρ_1 (Å)	ρ_2 (Å)	$r_{\min12}$ (Å)	$r_{\max12}$ (Å)	$r_{\min13}$ (Å)	$r_{\max13}$ (Å)	$r_{\min23}$ (Å)	$r_{\max23}$ (Å)
θ_{V-S-S}	31.659	84.288	1.048	1.048	0.0	3.088	0.0	3.088	0.0	4.235
θ_{S-V-V}	31.659	84.288	1.048	1.048	0.0	3.088	0.0	3.088	0.0	4.235

Tab. CLXXVII.

We use LAMMPS to perform MD simulations for the mechanical behavior of the single-layer 1T-VS₂ under uniaxial tension at 1.0 K and 300.0 K. Fig. 87 shows the stress-strain curve for the tension of a single-layer 1T-VS₂ of dimension 100×100 Å. Periodic boundary conditions are applied in both armchair and zigzag directions. The single-layer 1T-VS₂ is stretched uniaxially along the armchair or zigzag direction. The stress is calculated without involving the actual thickness of the quasi-two-dimensional structure of the single-layer 1T-VS₂. The Young's modulus can be obtained by a linear fitting of the stress-strain relation in the small strain range of $[0, 0.01]$. The Young's modulus are 87.1 N/m and 86.8 N/m along the armchair and zigzag directions, respectively. The Young's modulus is essentially isotropic in the armchair and zigzag directions. The Poisson's ratio from the VFF model and the SW potential is $\nu_{xy} = \nu_{yx} = 0.21$.

There is no available value for nonlinear quantities in the single-layer 1T-VS₂. We have thus used the nonlinear parameter $B = 0.5d^4$ in Eq. (5), which is close to the value of B in

TABLE CLXXVII: SW potential parameters for single-layer 1T-VS₂ used by LAMMPS⁹ as expressed in Eqs. (9) and (10).

	ϵ (eV)	σ (Å)	a	λ	γ	$\cos \theta_0$	A_L	B_L	p	q	tol
V-S ₁ -S ₁	1.000	1.048	2.946	31.659	1.000	0.100	7.943	11.797	4	0	0.0

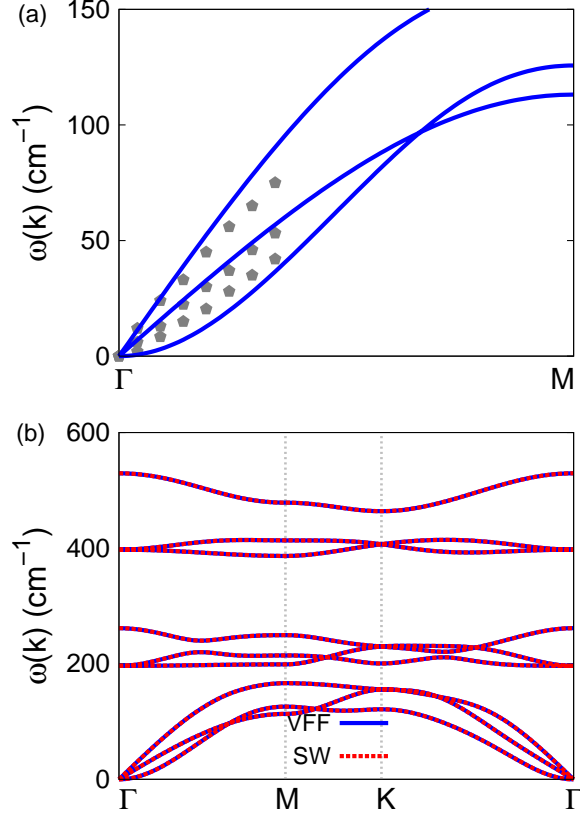


FIG. 88: (Color online) Phonon spectrum for single-layer 1T-VSe₂. (a) Phonon dispersion along the Γ M direction in the Brillouin zone. The results from the VFF model (lines) are comparable with the experiment data (pentagons) from Ref. 12. (b) The phonon dispersion from the SW potential is exactly the same as that from the VFF model.

most materials. The value of the third order nonlinear elasticity D can be extracted by fitting the stress-strain relation to the function $\sigma = E\epsilon + \frac{1}{2}D\epsilon^2$ with E as the Young's modulus. The values of D from the present SW potential are -230.5 N/m and -283.6 N/m along the armchair and zigzag directions, respectively. The ultimate stress is about 13.3 Nm^{-1} at the ultimate strain of 0.26 in the armchair direction at the low temperature of 1 K. The ultimate stress is about 12.7 Nm^{-1} at the ultimate strain of 0.30 in the zigzag direction at the low temperature of 1 K.

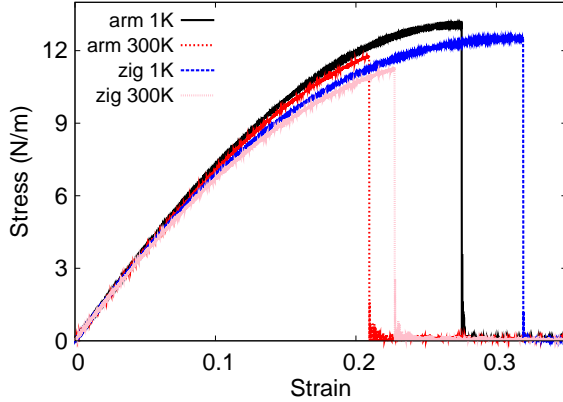


FIG. 89: (Color online) Stress-strain for single-layer 1T-VSe₂ of dimension $100 \times 100 \text{ \AA}$ along the armchair and zigzag directions.

TABLE CLXXVIII: The VFF model for single-layer 1T-VSe₂. The second line gives an explicit expression for each VFF term. The third line is the force constant parameters. Parameters are in the unit of $\frac{eV}{\text{\AA}^2}$ for the bond stretching interactions, and in the unit of eV for the angle bending interaction. The fourth line gives the initial bond length (in unit of \AA) for the bond stretching interaction and the initial angle (in unit of degrees) for the angle bending interaction. The angle θ_{ijk} has atom i as the apex.

VFF type	bond stretching	angle bending	
expression	$\frac{1}{2}K_{V-Se}(\Delta r)^2$	$\frac{1}{2}K_{V-Se-Se}(\Delta\theta)^2$	$\frac{1}{2}K_{Se-V-V}(\Delta\theta)^2$
parameter	11.562	4.237	4.237
r_0 or θ_0	2.440	83.201	83.201

XLV. 1T-VSE₂

Most existing theoretical studies on the single-layer 1T-VSe₂ are based on the first-principles calculations. In this section, we will develop the SW potential for the single-layer 1T-VSe₂.

The structure for the single-layer 1T-VSe₂ is shown in Fig. 71 (with M=V and X=Se). Each V atom is surrounded by six Se atoms. These Se atoms are categorized into the top group (eg. atoms 1, 3, and 5) and bottom group (eg. atoms 2, 4, and 6). Each Se atom is connected to three V atoms. The structural parameters are from the first-principles

TABLE CLXXIX: Two-body SW potential parameters for single-layer 1T-VSe₂ used by GULP⁸ as expressed in Eq. (3).

	A (eV)	ρ (Å)	B (Å ⁴)	r_{\min} (Å)	r_{\max} (Å)
V-Se	8.606	1.070	17.723	0.0	3.248

TABLE CLXXX: Three-body SW potential parameters for single-layer 1T-VSe₂ used by GULP⁸ as expressed in Eq. (4). The angle θ_{ijk} in the first line indicates the bending energy for the angle with atom i as the apex.

	K (eV)	θ_0 (degree)	ρ_1 (Å)	ρ_2 (Å)	$r_{\min12}$ (Å)	$r_{\max12}$ (Å)	$r_{\min13}$ (Å)	$r_{\max13}$ (Å)	$r_{\min23}$ (Å)	$r_{\max23}$ (Å)
$\theta_{V-Se-Se}$	30.387	83.201	1.070	1.070	0.0	3.248	0.0	3.248	0.0	4.426
θ_{Se-V-V}	30.387	83.201	1.070	1.070	0.0	3.248	0.0	3.248	0.0	4.426

calculations,¹² including the lattice constant $a = 3.24$ Å and the bond length $d_{V-Se} = 2.44$ Å. The resultant angles are $\theta_{VSeSe} = 83.201^\circ$ with Se atoms from the same (top or bottom) group, and $\theta_{SeVV} = 83.201^\circ$.

Table CLXXVIII shows three VFF terms for the single-layer 1T-VSe₂, one of which is the bond stretching interaction shown by Eq. (1) while the other two terms are the angle bending interaction shown by Eq. (2). We note that the angle bending term $K_{V-Se-Se}$ is for the angle $\theta_{V-Se-Se}$ with both Se atoms from the same (top or bottom) group. These force constant parameters are determined by fitting to the three acoustic branches in the phonon dispersion along the ΓM as shown in Fig. 88 (a). The *ab initio* calculations for the phonon dispersion are from Ref. 12. The lowest acoustic branch (flexural mode) is almost linear in the *ab initio* calculations, which may due to the violation of the rigid rotational invariance.²⁰ Fig. 88 (b) shows that the VFF model and the SW potential give exactly the same phonon dispersion, as the SW potential is derived from the VFF model.

The parameters for the two-body SW potential used by GULP are shown in

TABLE CLXXXI: SW potential parameters for single-layer 1T-VSe₂ used by LAMMPS⁹ as expressed in Eqs. (9) and (10).

	ϵ (eV)	σ (Å)	a	λ	γ	$\cos \theta_0$	A_L	B_L	p	q	tol
V-Se ₁ -Se ₁	1.000	1.070	3.035	30.387	1.000	0.118	8.606	13.507	4	0	0.0

Tab. CLXXIX. The parameters for the three-body SW potential used by GULP are shown in Tab. CLXXX. Some representative parameters for the SW potential used by LAMMPS are listed in Tab. CLXXXI.

We use LAMMPS to perform MD simulations for the mechanical behavior of the single-layer 1T-VSe₂ under uniaxial tension at 1.0 K and 300.0 K. Fig. 89 shows the stress-strain curve for the tension of a single-layer 1T-VSe₂ of dimension 100 × 100 Å. Periodic boundary conditions are applied in both armchair and zigzag directions. The single-layer 1T-VSe₂ is stretched uniaxially along the armchair or zigzag direction. The stress is calculated without involving the actual thickness of the quasi-two-dimensional structure of the single-layer 1T-VSe₂. The Young's modulus can be obtained by a linear fitting of the stress-strain relation in the small strain range of [0, 0.01]. The Young's modulus are 78.4 N/m and 78.1 N/m along the armchair and zigzag directions, respectively. The Young's modulus is essentially isotropic in the armchair and zigzag directions. The Poisson's ratio from the VFF model and the SW potential is $\nu_{xy} = \nu_{yx} = 0.22$.

There is no available value for nonlinear quantities in the single-layer 1T-VSe₂. We have thus used the nonlinear parameter $B = 0.5d^4$ in Eq. (5), which is close to the value of B in most materials. The value of the third order nonlinear elasticity D can be extracted by fitting the stress-strain relation to the function $\sigma = E\epsilon + \frac{1}{2}D\epsilon^2$ with E as the Young's modulus. The values of D from the present SW potential are -168.5 N/m and -218.6 N/m along the armchair and zigzag directions, respectively. The ultimate stress is about 13.1 Nm⁻¹ at the ultimate strain of 0.27 in the armchair direction at the low temperature of 1 K. The ultimate stress is about 12.5 Nm⁻¹ at the ultimate strain of 0.32 in the zigzag direction at the low temperature of 1 K.

XLVI. 1T-VTe₂

Most existing theoretical studies on the single-layer 1T-VTe₂ are based on the first-principles calculations. In this section, we will develop the SW potential for the single-layer 1T-VTe₂.

The structure for the single-layer 1T-VTe₂ is shown in Fig. 71 (with M=V and X=Te). Each V atom is surrounded by six Te atoms. These Te atoms are categorized into the top group (eg. atoms 1, 3, and 5) and bottom group (eg. atoms 2, 4, and 6). Each Te

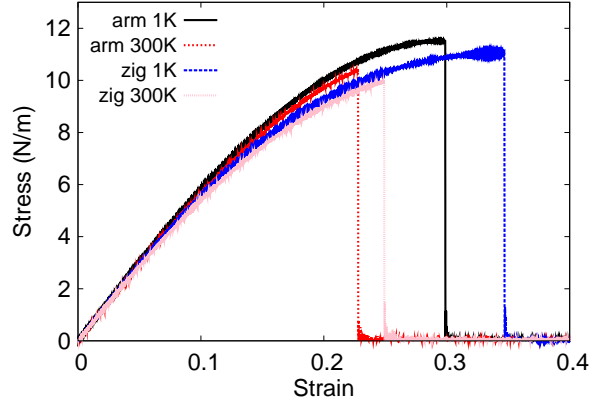


FIG. 90: (Color online) Stress-strain for single-layer 1T-VTe₂ of dimension $100 \times 100 \text{ \AA}$ along the armchair and zigzag directions.

TABLE CLXXXII: The VFF model for single-layer 1T-VTe₂. The second line gives an explicit expression for each VFF term. The third line is the force constant parameters. Parameters are in the unit of $\frac{\text{eV}}{\text{\AA}^2}$ for the bond stretching interactions, and in the unit of eV for the angle bending interaction. The fourth line gives the initial bond length (in unit of \AA) for the bond stretching interaction and the initial angle (in unit of degrees) for the angle bending interaction. The angle θ_{ijk} has atom i as the apex.

VFF type	bond stretching	angle bending	
expression	$\frac{1}{2}K_{\text{V-Te}}(\Delta r)^2$	$\frac{1}{2}K_{\text{V-Te-Te}}(\Delta\theta)^2$	$\frac{1}{2}K_{\text{Te-V-V}}(\Delta\theta)^2$
parameter	10.476	3.814	3.814
r_0 or θ_0	2.640	81.885	81.885

atom is connected to three V atoms. The structural parameters are from the first-principles calculations,¹² including the lattice constant $a = 3.46 \text{ \AA}$ and the bond length $d_{\text{V-Te}} = 2.64 \text{ \AA}$. The resultant angles are $\theta_{\text{VTeTe}} = 81.885^\circ$ with Te atoms from the same (top or bottom) group, and $\theta_{\text{TeVV}} = 81.885^\circ$.

Table CLXXXII shows three VFF terms for the single-layer 1T-VTe₂, one of which is the bond stretching interaction shown by Eq. (1) while the other two terms are the angle bending interaction shown by Eq. (2). We note that the angle bending term $K_{\text{V-Te-Te}}$ is for the angle $\theta_{\text{V-Te-Te}}$ with both Te atoms from the same (top or bottom) group. We find

TABLE CLXXXIII: Two-body SW potential parameters for single-layer 1T-VTe₂ used by GULP⁸ as expressed in Eq. (3).

	A (eV)	ρ (Å)	B (Å ⁴)	r_{\min} (Å)	r_{\max} (Å)
V-Te	8.805	1.110	24.288	0.0	3.496

TABLE CLXXXIV: Three-body SW potential parameters for single-layer 1T-VTe₂ used by GULP⁸ as expressed in Eq. (4). The angle θ_{ijk} in the first line indicates the bending energy for the angle with atom i as the apex.

	K (eV)	θ_0 (degree)	ρ_1 (Å)	ρ_2 (Å)	$r_{\min12}$ (Å)	$r_{\max12}$ (Å)	$r_{\min13}$ (Å)	$r_{\max13}$ (Å)	$r_{\min23}$ (Å)	$r_{\max23}$ (Å)
$\theta_{V-Te-Te}$	26.043	81.885	1.110	1.110	0.0	3.496	0.0	3.496	0.0	4.726
θ_{Te-V-V}	26.043	81.885	1.110	1.110	0.0	3.496	0.0	3.496	0.0	4.726

that there are actually only two parameters in the VFF model, so we can determine their value by fitting to the Young's modulus and the Poisson's ratio of the system. The *ab initio* calculations have predicted the Young's modulus to be 67 N/m and the Poisson's ratio as 0.24.⁴⁸

The parameters for the two-body SW potential used by GULP are shown in Tab. CLXXXIII. The parameters for the three-body SW potential used by GULP are shown in Tab. CLXXXIV. Some representative parameters for the SW potential used by LAMMPS are listed in Tab. CLXXXV.

We use LAMMPS to perform MD simulations for the mechanical behavior of the single-layer 1T-VTe₂ under uniaxial tension at 1.0 K and 300.0 K. Fig. 90 shows the stress-strain curve for the tension of a single-layer 1T-VTe₂ of dimension 100×100 Å. Periodic boundary conditions are applied in both armchair and zigzag directions. The single-layer 1T-VTe₂ is stretched uniaxially along the armchair or zigzag direction. The stress is calculated without involving the actual thickness of the quasi-two-dimensional structure of the single-layer 1T-

TABLE CLXXXV: SW potential parameters for single-layer 1T-VTe₂ used by LAMMPS⁹ as expressed in Eqs. (9) and (10).

	ϵ (eV)	σ (Å)	a	λ	γ	$\cos \theta_0$	A_L	B_L	p	q	tol
V-Te ₁ -Te ₁	1.000	1.110	3.149	26.043	1.000	0.141	8.805	15.980	4	0	0.0

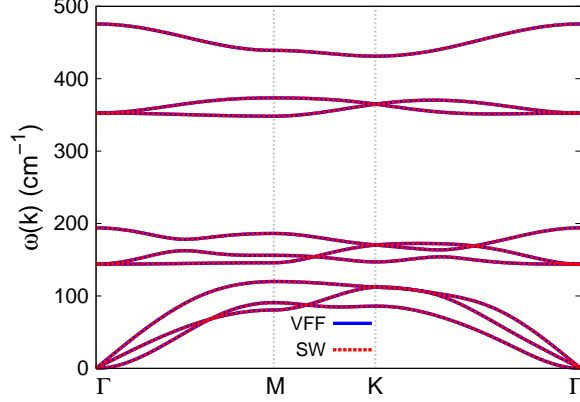


FIG. 91: (Color online) Phonon spectrum for single-layer 1T-VTe₂ along the Γ MK Γ direction in the Brillouin zone. The phonon dispersion from the SW potential is exactly the same as that from the VFF model.

VTe₂. The Young's modulus can be obtained by a linear fitting of the stress-strain relation in the small strain range of $[0, 0.01]$. The Young's modulus are 61.2 N/m and 61.0 N/m along the armchair and zigzag directions, respectively. The Young's modulus is essentially isotropic in the armchair and zigzag directions. The Poisson's ratio from the VFF model and the SW potential is $\nu_{xy} = \nu_{yx} = 0.24$. The fitted Young's modulus value is about 10% smaller than the *ab initio* result of 67 N/m,⁴⁸ as only short-range interactions are considered in the present work. The long-range interactions are ignored, which typically leads to about 10% underestimation for the value of the Young's modulus.

There is no available value for nonlinear quantities in the single-layer 1T-VTe₂. We have thus used the nonlinear parameter $B = 0.5d^4$ in Eq. (5), which is close to the value of B in most materials. The value of the third order nonlinear elasticity D can be extracted by fitting the stress-strain relation to the function $\sigma = E\epsilon + \frac{1}{2}D\epsilon^2$ with E as the Young's modulus. The values of D from the present SW potential are -95.8 N/m and -135.6 N/m along the armchair and zigzag directions, respectively. The ultimate stress is about 11.5 Nm⁻¹ at the ultimate strain of 0.30 in the armchair direction at the low temperature of 1 K. The ultimate stress is about 11.0 Nm⁻¹ at the ultimate strain of 0.34 in the zigzag direction at the low temperature of 1 K.

Fig. 91 shows that the VFF model and the SW potential give exactly the same phonon dispersion, as the SW potential is derived from the VFF model.

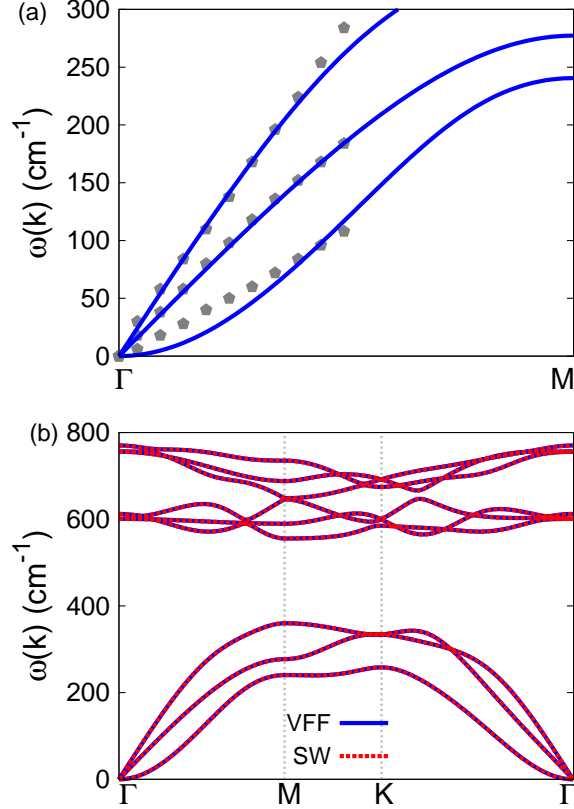


FIG. 92: (Color online) Phonon spectrum for single-layer 1T-MnO₂. (a) Phonon dispersion along the Γ M direction in the Brillouin zone. The results from the VFF model (lines) are comparable with the *ab initio* results (pentagons) from Ref. 12. (b) The phonon dispersion from the SW potential is exactly the same as that from the VFF model.

XLVII. 1T-MNO₂

Most existing theoretical studies on the single-layer 1T-MnO₂ are based on the first-principles calculations. In this section, we will develop the SW potential for the single-layer 1T-MnO₂.

The structure for the single-layer 1T-MnO₂ is shown in Fig. 71 (with M=Mn and X=O). Each Mn atom is surrounded by six O atoms. These O atoms are categorized into the top group (eg. atoms 1, 3, and 5) and bottom group (eg. atoms 2, 4, and 6). Each O atom is connected to three Mn atoms. The structural parameters are from the first-principles calculations,¹² including the lattice constant $a = 2.82 \text{ \AA}$ and the bond length

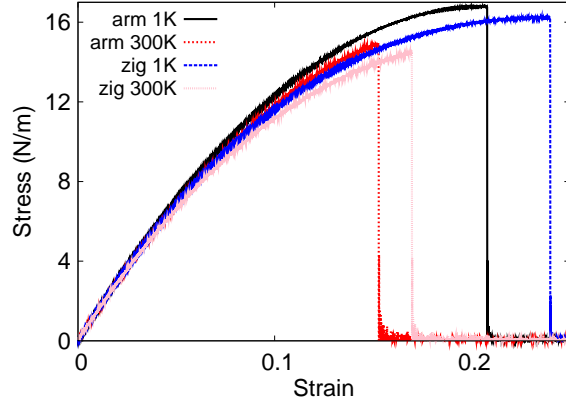


FIG. 93: (Color online) Stress-strain for single-layer 1T-MnO₂ of dimension $100 \times 100 \text{ \AA}$ along the armchair and zigzag directions.

TABLE CLXXXVI: The VFF model for single-layer 1T-MnO₂. The second line gives an explicit expression for each VFF term. The third line is the force constant parameters. Parameters are in the unit of $\frac{\text{eV}}{\text{\AA}^2}$ for the bond stretching interactions, and in the unit of eV for the angle bending interaction. The fourth line gives the initial bond length (in unit of \AA) for the bond stretching interaction and the initial angle (in unit of degrees) for the angle bending interaction. The angle θ_{ijk} has atom i as the apex.

VFF type	bond stretching	angle bending	
expression	$\frac{1}{2}K_{\text{Mn-O}}(\Delta r)^2$	$\frac{1}{2}K_{\text{Mn-O-O}}(\Delta\theta)^2$	$\frac{1}{2}K_{\text{O-Mn-Mn}}(\Delta\theta)^2$
parameter	15.371	4.822	4.822
r_0 or θ_0	1.88	97.181	97.181

$d_{\text{Mn-O}} = 1.88 \text{ \AA}$. The resultant angles are $\theta_{\text{MnOO}} = 97.181^\circ$ with O atoms from the same (top or bottom) group, and $\theta_{\text{OMnMn}} = 97.181^\circ$.

Table CLXXXVI shows three VFF terms for the single-layer 1T-MnO₂, one of which is the bond stretching interaction shown by Eq. (1) while the other two terms are the angle bending interaction shown by Eq. (2). We note that the angle bending term $K_{\text{Mn-O-O}}$ is for the angle $\theta_{\text{Mn-O-O}}$ with both O atoms from the same (top or bottom) group. These force constant parameters are determined by fitting to the two in-plane acoustic branches in the phonon dispersion along the ΓM as shown in Fig. 92 (a). The *ab initio* calculations for the

TABLE CLXXXVII: Two-body SW potential parameters for single-layer 1T-MnO₂ used by GULP⁸ as expressed in Eq. (3).

	A (eV)	ρ (Å)	B (Å ⁴)	r_{\min} (Å)	r_{\max} (Å)
Mn-O	9.675	1.212	6.246	0.0	2.635

TABLE CLXXXVIII: Three-body SW potential parameters for single-layer 1T-MnO₂ used by GULP⁸ as expressed in Eq. (4). The angle θ_{ijk} in the first line indicates the bending energy for the angle with atom i as the apex.

	K (eV)	θ_0 (degree)	ρ_1 (Å)	ρ_2 (Å)	$r_{\min12}$ (Å)	$r_{\max12}$ (Å)	$r_{\min13}$ (Å)	$r_{\max13}$ (Å)	$r_{\min23}$ (Å)	$r_{\max23}$ (Å)
$\theta_{\text{Mn-O-O}}$	60.755	97.181	1.212	1.212	0.0	2.635	0.0	2.635	0.0	3.852
$\theta_{\text{O-Mn-Mn}}$	60.755	97.181	1.212	1.212	0.0	2.635	0.0	2.635	0.0	3.852

phonon dispersion are from Ref. 12. Fig. 92 (b) shows that the VFF model and the SW potential give exactly the same phonon dispersion, as the SW potential is derived from the VFF model.

The parameters for the two-body SW potential used by GULP are shown in Tab. CLXXXVII. The parameters for the three-body SW potential used by GULP are shown in Tab. CLXXXVIII. Some representative parameters for the SW potential used by LAMMPS are listed in Tab. CLXXXIX.

We use LAMMPS to perform MD simulations for the mechanical behavior of the single-layer 1T-MnO₂ under uniaxial tension at 1.0 K and 300.0 K. Fig. 93 shows the stress-strain curve for the tension of a single-layer 1T-MnO₂ of dimension 100×100 Å. Periodic boundary conditions are applied in both armchair and zigzag directions. The single-layer 1T-MnO₂ is stretched uniaxially along the armchair or zigzag direction. The stress is calculated without involving the actual thickness of the quasi-two-dimensional structure of the single-layer 1T-MnO₂. The Young's modulus can be obtained by a linear fitting of the stress-strain relation

TABLE CLXXXIX: SW potential parameters for single-layer 1T-MnO₂ used by LAMMPS⁹ as expressed in Eqs. (9) and (10).

	ϵ (eV)	σ (Å)	a	λ	γ	$\cos \theta_0$	A_L	B_L	p	q	tol
Mn-O ₁ -O ₁	1.000	1.212	2.175	60.755	1.000	-0.125	9.675	2.899	4	0	0.0

TABLE CXC: The VFF model for single-layer 1T-MnS₂. The second line gives an explicit expression for each VFF term. The third line is the force constant parameters. Parameters are in the unit of $\frac{eV}{\text{Å}^2}$ for the bond stretching interactions, and in the unit of eV for the angle bending interaction. The fourth line gives the initial bond length (in unit of Å) for the bond stretching interaction and the initial angle (in unit of degrees) for the angle bending interaction. The angle θ_{ijk} has atom i as the apex.

VFF type	bond stretching	angle bending	
expression	$\frac{1}{2}K_{\text{Mn-S}}(\Delta r)^2$	$\frac{1}{2}K_{\text{Mn-S-S}}(\Delta\theta)^2$	$\frac{1}{2}K_{\text{S-Mn-Mn}}(\Delta\theta)^2$
parameter	4.407	2.399	2.399
r_0 or θ_0	2.27	86.822	86.822

in the small strain range of $[0, 0.01]$. The Young's modulus are 156.3 N/m and 155.4 N/m along the armchair and zigzag directions, respectively. The Young's modulus is essentially isotropic in the armchair and zigzag directions. The Poisson's ratio from the VFF model and the SW potential is $\nu_{xy} = \nu_{yx} = 0.12$.

There is no available value for nonlinear quantities in the single-layer 1T-MnO₂. We have thus used the nonlinear parameter $B = 0.5d^4$ in Eq. (5), which is close to the value of B in most materials. The value of the third order nonlinear elasticity D can be extracted by fitting the stress-strain relation to the function $\sigma = E\epsilon + \frac{1}{2}D\epsilon^2$ with E as the Young's modulus. The values of D from the present SW potential are -711.7 N/m and -756.1 N/m along the armchair and zigzag directions, respectively. The ultimate stress is about 16.8 Nm⁻¹ at the ultimate strain of 0.21 in the armchair direction at the low temperature of 1 K. The ultimate stress is about 16.2 Nm⁻¹ at the ultimate strain of 0.24 in the zigzag direction at the low temperature of 1 K.

XLVIII. 1T-MNS₂

Most existing theoretical studies on the single-layer 1T-MnS₂ are based on the first-principles calculations. In this section, we will develop the SW potential for the single-layer 1T-MnS₂.

The structure for the single-layer 1T-MnS₂ is shown in Fig. 71 (with M=Mn and X=S).

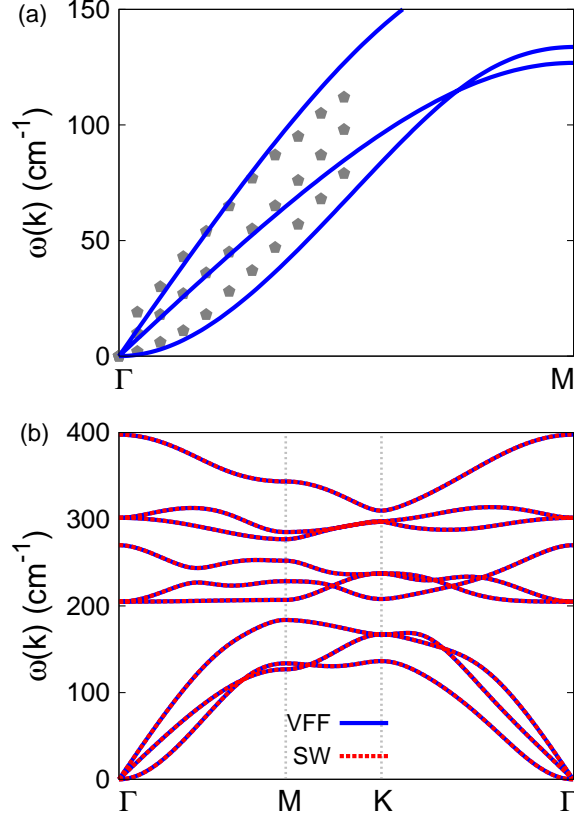


FIG. 94: (Color online) Phonon spectrum for single-layer 1T-MnS₂. (a) Phonon dispersion along the Γ M direction in the Brillouin zone. The results from the VFF model (lines) are comparable with the *ab initio* results (pentagons) from Ref. 12. (b) The phonon dispersion from the SW potential is exactly the same as that from the VFF model.

TABLE CXCI: Two-body SW potential parameters for single-layer 1T-MnS₂ used by GULP⁸ as expressed in Eq. (3).

	A (eV)	ρ (\AA)	B (\AA^4)	r_{\min} (\AA)	r_{\max} (\AA)
Mn-S	3.127	1.111	13.276	0.0	3.064

Each Mn atom is surrounded by six S atoms. These S atoms are categorized into the top group (eg. atoms 1, 3, and 5) and bottom group (eg. atoms 2, 4, and 6). Each S atom is connected to three Mn atoms. The structural parameters are from the first-principles calculations,¹² including the lattice constant $a = 3.12 \text{ \AA}$ and the bond length $d_{\text{Mn-S}} = 2.27 \text{ \AA}$. The resultant angles are $\theta_{\text{MnSS}} = 86.822^\circ$ with S atoms from the same (top or bottom) group,

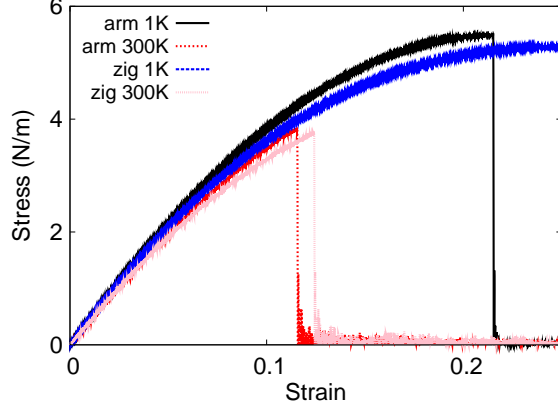


FIG. 95: (Color online) Stress-strain for single-layer 1T-MnS₂ of dimension 100 × 100 Å along the armchair and zigzag directions.

TABLE CXCII: Three-body SW potential parameters for single-layer 1T-MnS₂ used by GULP⁸ as expressed in Eq. (4). The angle θ_{ijk} in the first line indicates the bending energy for the angle with atom i as the apex.

	K (eV)	θ_0 (degree)	ρ_1 (Å)	ρ_2 (Å)	$r_{\min 12}$ (Å)	$r_{\max 12}$ (Å)	$r_{\min 13}$ (Å)	$r_{\max 13}$ (Å)	$r_{\min 23}$ (Å)	$r_{\max 23}$ (Å)
$\theta_{\text{Mn-S-S}}$	19.765	86.822	1.111	1.111	0.0	3.064	0.0	3.064	0.0	4.262
$\theta_{\text{S-Mn-Mn}}$	19.765	86.822	1.111	1.111	0.0	3.064	0.0	3.064	0.0	4.262

and $\theta_{\text{SMnMn}} = 86.822^\circ$.

Table CXC shows three VFF terms for the single-layer 1T-MnS₂, one of which is the bond stretching interaction shown by Eq. (1) while the other two terms are the angle bending interaction shown by Eq. (2). We note that the angle bending term $K_{\text{Mn-S-S}}$ is for the angle $\theta_{\text{Mn-S-S}}$ with both S atoms from the same (top or bottom) group. These force constant parameters are determined by fitting to the acoustic branches in the phonon dispersion along the ΓM as shown in Fig. 94 (a). The *ab initio* calculations for the phonon dispersion

TABLE CXCIII: SW potential parameters for single-layer 1T-MnS₂ used by LAMMPS⁹ as expressed in Eqs. (9) and (10).

	ϵ (eV)	σ (Å)	a	λ	γ	$\cos \theta_0$	A_L	B_L	p	q	tol
Mn-S ₁ -S ₁	1.000	1.111	2.757	19.765	1.000	0.055	3.127	8.700	4	0	0.0

are from Ref. 12. Fig. 94 (b) shows that the VFF model and the SW potential give exactly the same phonon dispersion, as the SW potential is derived from the VFF model.

The parameters for the two-body SW potential used by GULP are shown in Tab. CXCI. The parameters for the three-body SW potential used by GULP are shown in Tab. CXCII. Some representative parameters for the SW potential used by LAMMPS are listed in Tab. CXCIII.

We use LAMMPS to perform MD simulations for the mechanical behavior of the single-layer 1T-MnS₂ under uniaxial tension at 1.0 K and 300.0 K. Fig. 95 shows the stress-strain curve for the tension of a single-layer 1T-MnS₂ of dimension 100 × 100 Å. Periodic boundary conditions are applied in both armchair and zigzag directions. The single-layer 1T-MnS₂ is stretched uniaxially along the armchair or zigzag direction. The stress is calculated without involving the actual thickness of the quasi-two-dimensional structure of the single-layer 1T-MnS₂. The Young's modulus can be obtained by a linear fitting of the stress-strain relation in the small strain range of [0, 0.01]. The Young's modulus are 47.1 N/m and 46.8 N/m along the armchair and zigzag directions, respectively. The Young's modulus is essentially isotropic in the armchair and zigzag directions. The Poisson's ratio from the VFF model and the SW potential is $\nu_{xy} = \nu_{yx} = 0.15$.

There is no available value for nonlinear quantities in the single-layer 1T-MnS₂. We have thus used the nonlinear parameter $B = 0.5d^4$ in Eq. (5), which is close to the value of B in most materials. The value of the third order nonlinear elasticity D can be extracted by fitting the stress-strain relation to the function $\sigma = E\epsilon + \frac{1}{2}D\epsilon^2$ with E as the Young's modulus. The values of D from the present SW potential are -193.8 N/m and -210.1 N/m along the armchair and zigzag directions, respectively. The ultimate stress is about 5.5 Nm⁻¹ at the ultimate strain of 0.21 in the armchair direction at the low temperature of 1 K. The ultimate stress is about 5.3 Nm⁻¹ at the ultimate strain of 0.25 in the zigzag direction at the low temperature of 1 K.

XLIX. 1T-MNSE₂

Most existing theoretical studies on the single-layer 1T-MnSe₂ are based on the first-principles calculations. In this section, we will develop the SW potential for the single-layer 1T-MnSe₂.

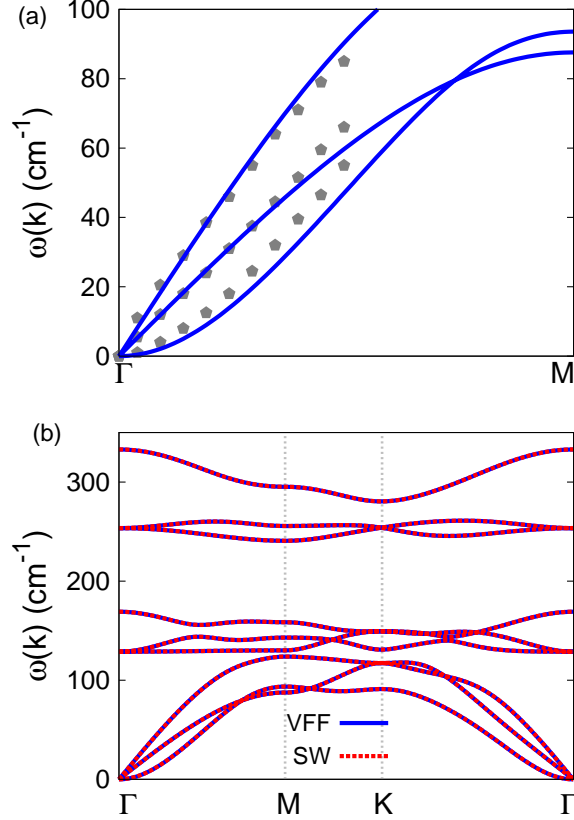


FIG. 96: (Color online) Phonon spectrum for single-layer 1T-MnSe₂. (a) Phonon dispersion along the Γ M direction in the Brillouin zone. The results from the VFF model (lines) are comparable with the *ab initio* results (pentagons) from Ref. 12. (b) The phonon dispersion from the SW potential is exactly the same as that from the VFF model.

The structure for the single-layer 1T-MnSe₂ is shown in Fig. 71 (with M=Mn and X=Se). Each Mn atom is surrounded by six Se atoms. These Se atoms are categorized into the top group (eg. atoms 1, 3, and 5) and bottom group (eg. atoms 2, 4, and 6). Each Se atom is connected to three Mn atoms. The structural parameters are from the first-principles calculations,¹² including the lattice constant $a = 3.27 \text{ \AA}$ and the bond length $d_{\text{Mn-Se}} = 2.39 \text{ \AA}$. The resultant angles are $\theta_{\text{MnSeSe}} = 86.330^\circ$ with Se atoms from the same (top or bottom) group, and $\theta_{\text{SeMnMn}} = 86.330^\circ$.

Table CXCIV shows three VFF terms for the single-layer 1T-MnSe₂, one of which is the bond stretching interaction shown by Eq. (1) while the other two terms are the angle bending interaction shown by Eq. (2). We note that the angle bending term $K_{\text{Mn-Se-Se}}$ is

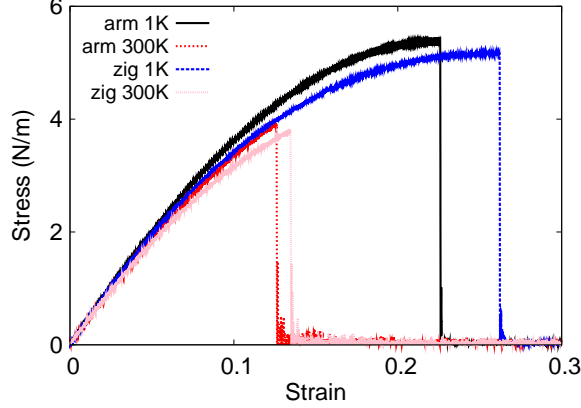


FIG. 97: (Color online) Stress-strain for single-layer 1T-MnSe₂ of dimension $100 \times 100 \text{ \AA}$ along the armchair and zigzag directions.

TABLE CXCIV: The VFF model for single-layer 1T-MnSe₂. The second line gives an explicit expression for each VFF term. The third line is the force constant parameters. Parameters are in the unit of $\frac{\text{eV}}{\text{A}^2}$ for the bond stretching interactions, and in the unit of eV for the angle bending interaction. The fourth line gives the initial bond length (in unit of A) for the bond stretching interaction and the initial angle (in unit of degrees) for the angle bending interaction. The angle θ_{ijk} has atom i as the apex.

VFF type	bond stretching	angle bending	
expression	$\frac{1}{2}K_{\text{Mn-Se}}(\Delta r)^2$	$\frac{1}{2}K_{\text{Mn-Se-Se}}(\Delta\theta)^2$	$\frac{1}{2}K_{\text{Se-Mn-Mn}}(\Delta\theta)^2$
parameter	4.407	2.399	2.399
r_0 or θ_0	2.39	86.330	86.330

for the angle $\theta_{\text{Mn-Se-Se}}$ with both Se atoms from the same (top or bottom) group. These force constant parameters are determined by fitting to the acoustic branches in the phonon dispersion along the ΓM as shown in Fig. 96 (a). The *ab initio* calculations for the phonon dispersion are from Ref. 12. Fig. 96 (b) shows that the VFF model and the SW potential give exactly the same phonon dispersion, as the SW potential is derived from the VFF model.

The parameters for the two-body SW potential used by GULP are shown in Tab. CXCIV. The parameters for the three-body SW potential used by GULP are shown in Tab. CXCVI. Some representative parameters for the SW potential used by LAMMPS are listed in

TABLE CXCIV: Two-body SW potential parameters for single-layer 1T-MnSe₂ used by GULP⁸ as expressed in Eq. (3).

	A (eV)	ρ (Å)	B (Å ⁴)	r_{\min} (Å)	r_{\max} (Å)
Mn-Se	3.422	1.153	16.314	0.0	3.220

TABLE CXCV: Three-body SW potential parameters for single-layer 1T-MnSe₂ used by GULP⁸ as expressed in Eq. (4). The angle θ_{ijk} in the first line indicates the bending energy for the angle with atom i as the apex.

	K (eV)	θ_0 (degree)	ρ_1 (Å)	ρ_2 (Å)	$r_{\min12}$ (Å)	$r_{\max12}$ (Å)	$r_{\min13}$ (Å)	$r_{\max13}$ (Å)	$r_{\min23}$ (Å)	$r_{\max23}$ (Å)
$\theta_{\text{Mn-Se-Se}}$	19.390	86.330	1.153	1.153	0.0	3.220	0.0	3.220	0.0	4.467
$\theta_{\text{Se-Mn-Mn}}$	19.390	86.330	1.153	1.153	0.0	3.220	0.0	3.220	0.0	4.467

Tab. CXCVI.

We use LAMMPS to perform MD simulations for the mechanical behavior of the single-layer 1T-MnSe₂ under uniaxial tension at 1.0 K and 300.0 K. Fig. 97 shows the stress-strain curve for the tension of a single-layer 1T-MnSe₂ of dimension 100×100 Å. Periodic boundary conditions are applied in both armchair and zigzag directions. The single-layer 1T-MnSe₂ is stretched uniaxially along the armchair or zigzag direction. The stress is calculated without involving the actual thickness of the quasi-two-dimensional structure of the single-layer 1T-MnSe₂. The Young's modulus can be obtained by a linear fitting of the stress-strain relation in the small strain range of $[0, 0.01]$. The Young's modulus are 43.2 N/m and 42.9 N/m along the armchair and zigzag directions, respectively. The Young's modulus is essentially isotropic in the armchair and zigzag directions. The Poisson's ratio from the VFF model and the SW potential is $\nu_{xy} = \nu_{yx} = 0.17$.

There is no available value for nonlinear quantities in the single-layer 1T-MnSe₂. We have thus used the nonlinear parameter $B = 0.5d^4$ in Eq. (5), which is close to the value of

TABLE CXCVII: SW potential parameters for single-layer 1T-MnSe₂ used by LAMMPS⁹ as expressed in Eqs. (9) and (10).

	ϵ (eV)	σ (Å)	a	λ	γ	$\cos \theta_0$	A_L	B_L	p	q	tol
Mn-Se ₁ -Se ₁	1.000	1.153	2.792	19.390	1.000	0.064	3.422	9.219	4	0	0.0

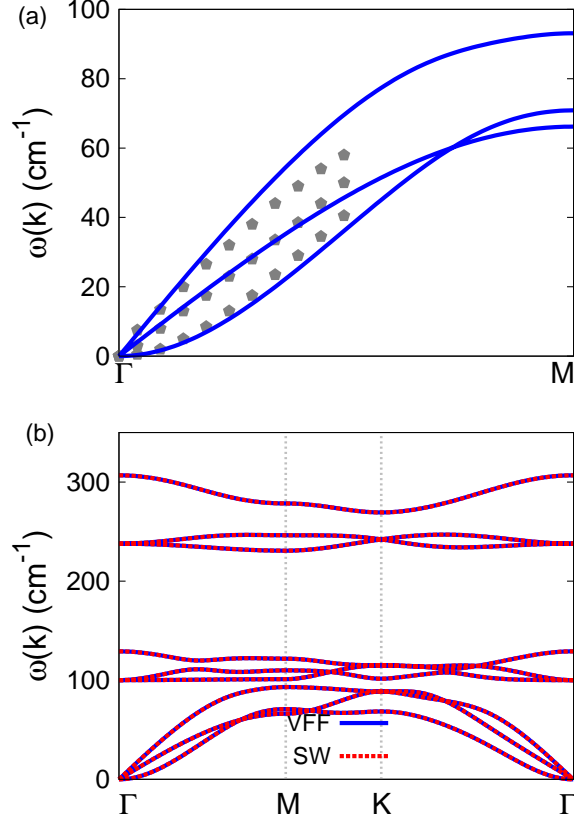


FIG. 98: (Color online) Phonon spectrum for single-layer 1T-MnTe₂. (a) Phonon dispersion along the Γ M direction in the Brillouin zone. The results from the VFF model (lines) are comparable with the *ab initio* results (pentagons) from Ref. 12. (b) The phonon dispersion from the SW potential is exactly the same as that from the VFF model.

B in most materials. The value of the third order nonlinear elasticity D can be extracted by fitting the stress-strain relation to the function $\sigma = E\epsilon + \frac{1}{2}D\epsilon^2$ with E as the Young's modulus. The values of D from the present SW potential are -163.4 N/m and -179.4 N/m along the armchair and zigzag directions, respectively. The ultimate stress is about 5.4 Nm⁻¹ at the ultimate strain of 0.22 in the armchair direction at the low temperature of 1 K. The ultimate stress is about 5.2 Nm⁻¹ at the ultimate strain of 0.26 in the zigzag direction at the low temperature of 1 K.

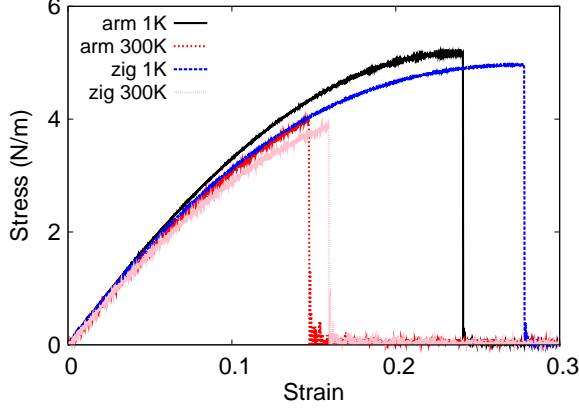


FIG. 99: (Color online) Stress-strain for single-layer 1T-MnTe₂ of dimension $100 \times 100 \text{ \AA}$ along the armchair and zigzag directions.

TABLE CXCVIII: The VFF model for single-layer 1T-MnTe₂. The second line gives an explicit expression for each VFF term. The third line is the force constant parameters. Parameters are in the unit of $\frac{\text{eV}}{\text{Å}^2}$ for the bond stretching interactions, and in the unit of eV for the angle bending interaction. The fourth line gives the initial bond length (in unit of Å) for the bond stretching interaction and the initial angle (in unit of degrees) for the angle bending interaction. The angle θ_{ijk} has atom i as the apex.

VFF type	bond stretching	angle bending	
expression	$\frac{1}{2}K_{\text{Mn-Te}}(\Delta r)^2$	$\frac{1}{2}K_{\text{Mn-Te-Te}}(\Delta\theta)^2$	$\frac{1}{2}K_{\text{Te-Mn-Mn}}(\Delta\theta)^2$
parameter	4.407	2.399	2.399
r_0 or θ_0	2.59	86.219	86.219

L. 1T-MNTE₂

Most existing theoretical studies on the single-layer 1T-MnTe₂ are based on the first-principles calculations. In this section, we will develop the SW potential for the single-layer 1T-MnTe₂.

The structure for the single-layer 1T-MnTe₂ is shown in Fig. 71 (with M=Mn and X=Te). Each Mn atom is surrounded by six Te atoms. These Te atoms are categorized into the top group (eg. atoms 1, 3, and 5) and bottom group (eg. atoms 2, 4, and 6). Each Te atom is connected to three Mn atoms. The structural parameters are from the first-

TABLE CXCIX: Two-body SW potential parameters for single-layer 1T-MnTe₂ used by GULP⁸ as expressed in Eq. (3).

	A (eV)	ρ (Å)	B (Å ⁴)	r_{\min} (Å)	r_{\max} (Å)
Mn-Te	4.007	1.246	22.499	0.0	3.488

TABLE CC: Three-body SW potential parameters for single-layer 1T-MnTe₂ used by GULP⁸ as expressed in Eq. (4). The angle θ_{ijk} in the first line indicates the bending energy for the angle with atom i as the apex.

	K (eV)	θ_0 (degree)	ρ_1 (Å)	ρ_2 (Å)	$r_{\min12}$ (Å)	$r_{\max12}$ (Å)	$r_{\min13}$ (Å)	$r_{\max13}$ (Å)	$r_{\min23}$ (Å)	$r_{\max23}$ (Å)
$\theta_{\text{Mn-Te-Te}}$	19.307	86.219	1.246	1.246	0.0	3.488	0.0	3.488	0.0	4.836
$\theta_{\text{Te-Mn-Mn}}$	19.307	86.219	1.246	1.246	0.0	3.488	0.0	3.488	0.0	4.836

principles calculations,¹² including the lattice constant $a = 3.54$ Å and the bond length $d_{\text{Mn-Te}} = 2.59$ Å. The resultant angles are $\theta_{\text{MnTeTe}} = 86.219^\circ$ with Te atoms from the same (top or bottom) group, and $\theta_{\text{TeMnMn}} = 86.219^\circ$.

Table CXCVIII shows three VFF terms for the single-layer 1T-MnTe₂, one of which is the bond stretching interaction shown by Eq. (1) while the other two terms are the angle bending interaction shown by Eq. (2). We note that the angle bending term $K_{\text{Mn-Te-Te}}$ is for the angle $\theta_{\text{Mn-Te-Te}}$ with both Se atoms from the same (top or bottom) group. These force constant parameters are determined by fitting to the acoustic branches in the phonon dispersion along the ΓM as shown in Fig. 98 (a). The *ab initio* calculations for the phonon dispersion are from Ref. 12. Fig. 98 (b) shows that the VFF model and the SW potential give exactly the same phonon dispersion, as the SW potential is derived from the VFF model.

The parameters for the two-body SW potential used by GULP are shown in Tab. CXCIX. The parameters for the three-body SW potential used by GULP are shown in Tab. CC. Some representative parameters for the SW potential used by LAMMPS are listed in Tab. CCI.

TABLE CCI: SW potential parameters for single-layer 1T-MnTe₂ used by LAMMPS⁹ as expressed in Eqs. (9) and (10).

	ϵ (eV)	σ (Å)	a	λ	γ	$\cos \theta_0$	A_L	B_L	p	q	tol
Mn-Te ₁ -Te ₁	1.000	1.246	2.800	19.307	1.000	0.066	4.007	9.340	4	0	0.0

We use LAMMPS to perform MD simulations for the mechanical behavior of the single-layer 1T-MnTe₂ under uniaxial tension at 1.0 K and 300.0 K. Fig. 99 shows the stress-strain curve for the tension of a single-layer 1T-MnTe₂ of dimension 100×100 Å. Periodic boundary conditions are applied in both armchair and zigzag directions. The single-layer 1T-MnTe₂ is stretched uniaxially along the armchair or zigzag direction. The stress is calculated without involving the actual thickness of the quasi-two-dimensional structure of the single-layer 1T-MnTe₂. The Young’s modulus can be obtained by a linear fitting of the stress-strain relation in the small strain range of [0, 0.01]. The Young’s modulus are 38.5 N/m and 38.4 N/m along the armchair and zigzag directions, respectively. The Young’s modulus is essentially isotropic in the armchair and zigzag directions. The Poisson’s ratio from the VFF model and the SW potential is $\nu_{xy} = \nu_{yx} = 0.19$.

There is no available value for nonlinear quantities in the single-layer 1T-MnTe₂. We have thus used the nonlinear parameter $B = 0.5d^4$ in Eq. (5), which is close to the value of B in most materials. The value of the third order nonlinear elasticity D can be extracted by fitting the stress-strain relation to the function $\sigma = E\epsilon + \frac{1}{2}D\epsilon^2$ with E as the Young’s modulus. The values of D from the present SW potential are -133.5 N/m and -149.5 N/m along the armchair and zigzag directions, respectively. The ultimate stress is about 5.2 Nm⁻¹ at the ultimate strain of 0.24 in the armchair direction at the low temperature of 1 K. The ultimate stress is about 5.0 Nm⁻¹ at the ultimate strain of 0.28 in the zigzag direction at the low temperature of 1 K.

LI. 1T-COTE₂

Most existing theoretical studies on the single-layer 1T-CoTe₂ are based on the first-principles calculations. In this section, we will develop the SW potential for the single-layer 1T-CoTe₂.

The structure for the single-layer 1T-CoTe₂ is shown in Fig. 71 (with M=Co and X=Te). Each Co atom is surrounded by six Te atoms. These Te atoms are categorized into the top group (eg. atoms 1, 3, and 5) and bottom group (eg. atoms 2, 4, and 6). Each Te atom is connected to three Co atoms. The structural parameters are from the first-principles calculations,⁴⁸ including the lattice constant $a = 3.5983$ Å, and the bond length $d_{\text{Co-Te}} = 2.5117$ Å, which is derived from the angle $\theta_{\text{TeCoCo}} = 91.5^\circ$. The other angle is

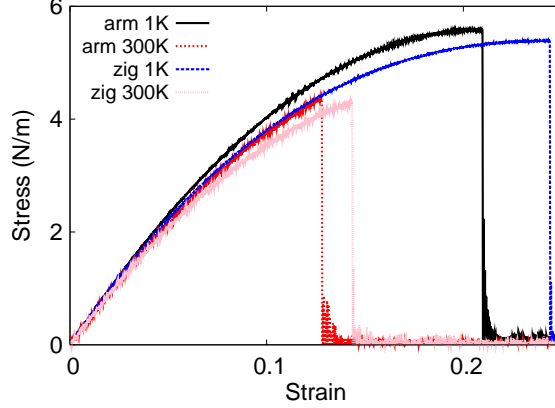


FIG. 100: (Color online) Stress-strain for single-layer 1T-CoTe₂ of dimension $100 \times 100 \text{ \AA}$ along the armchair and zigzag directions.

TABLE CCII: The VFF model for single-layer 1T-CoTe₂. The second line gives an explicit expression for each VFF term. The third line is the force constant parameters. Parameters are in the unit of $\frac{eV}{\text{Å}^2}$ for the bond stretching interactions, and in the unit of eV for the angle bending interaction. The fourth line gives the initial bond length (in unit of Å) for the bond stretching interaction and the initial angle (in unit of degrees) for the angle bending interaction. The angle θ_{ijk} has atom *i* as the apex.

VFF type	bond stretching	angle bending	
expression	$\frac{1}{2}K_{\text{Co-Te}}(\Delta r)^2$	$\frac{1}{2}K_{\text{Co-Te-Te}}(\Delta\theta)^2$	$\frac{1}{2}K_{\text{Te-Co-Co}}(\Delta\theta)^2$
parameter	4.726	3.035	3.035
r_0 or θ_0	2.512	91.501	91.501

$\theta_{\text{CoTeTe}} = 91.5^\circ$ with Te atoms from the same (top or bottom) group.

Table CCII shows three VFF terms for the single-layer 1T-CoTe₂, one of which is the bond stretching interaction shown by Eq. (1) while the other two terms are the angle bending interaction shown by Eq. (2). We note that the angle bending term $K_{\text{Co-Te-Te}}$ is for the angle $\theta_{\text{Co-Te-Te}}$ with both Te atoms from the same (top or bottom) group. We find that there are actually only two parameters in the VFF model, so we can determine their value by fitting to the Young's modulus and the Poisson's ratio of the system. The *ab initio* calculations have predicted the Young's modulus to be 59 N/m and the Poisson's ratio as

TABLE CCIII: Two-body SW potential parameters for single-layer 1T-CoTe₂ used by GULP⁸ as expressed in Eq. (3).

	A (eV)	ρ (Å)	B (Å ⁴)	r_{\min} (Å)	r_{\max} (Å)
Co-Te	4.628	1.402	19.899	0.0	3.450

TABLE CCIV: Three-body SW potential parameters for single-layer 1T-CoTe₂ used by GULP⁸ as expressed in Eq. (4). The angle θ_{ijk} in the first line indicates the bending energy for the angle with atom i as the apex.

	K (eV)	θ_0 (degree)	ρ_1 (Å)	ρ_2 (Å)	$r_{\min12}$ (Å)	$r_{\max12}$ (Å)	$r_{\min13}$ (Å)	$r_{\max13}$ (Å)	$r_{\min23}$ (Å)	$r_{\max23}$ (Å)
$\theta_{\text{Co-Te-Te}}$	30.149	91.501	1.402	1.402	0.0	3.450	0.0	3.450	0.0	4.915
$\theta_{\text{Te-Co-Co}}$	30.149	91.501	1.402	1.402	0.0	3.450	0.0	3.450	0.0	4.915

0.14.⁴⁸

The parameters for the two-body SW potential used by GULP are shown in Tab. CCIII. The parameters for the three-body SW potential used by GULP are shown in Tab. CCIV. Some representative parameters for the SW potential used by LAMMPS are listed in Tab. CCV.

We use LAMMPS to perform MD simulations for the mechanical behavior of the single-layer 1T-CoTe₂ under uniaxial tension at 1.0 K and 300.0 K. Fig. 100 shows the stress-strain curve for the tension of a single-layer 1T-CoTe₂ of dimension 100×100 Å. Periodic boundary conditions are applied in both armchair and zigzag directions. The single-layer 1T-CoTe₂ is stretched uniaxially along the armchair or zigzag direction. The stress is calculated without involving the actual thickness of the quasi-two-dimensional structure of the single-layer 1T-CoTe₂. The Young's modulus can be obtained by a linear fitting of the stress-strain relation in the small strain range of $[0, 0.01]$. The Young's modulus are 50.5 N/m and 50.3 N/m along the armchair and zigzag directions, respectively. The Young's modulus is essentially

TABLE CCV: SW potential parameters for single-layer 1T-CoTe₂ used by LAMMPS⁹ as expressed in Eqs. (9) and (10).

	ϵ (eV)	σ (Å)	a	λ	γ	$\cos \theta_0$	A_L	B_L	p	q	tol
Co-Te ₁ -Te ₁	1.000	1.402	2.461	30.149	1.000	-0.026	4.628	5.151	4	0	0.0

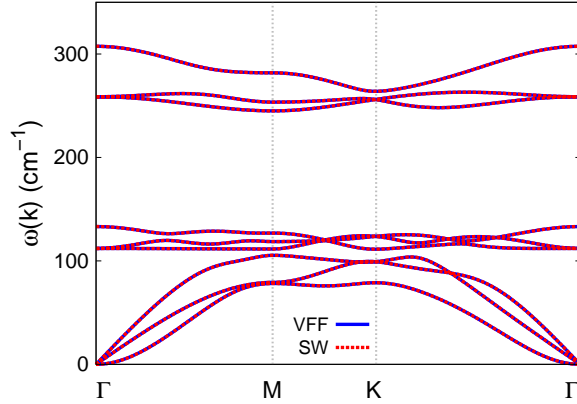


FIG. 101: (Color online) Phonon spectrum for single-layer 1T-CoTe₂ along the Γ MK Γ direction in the Brillouin zone. The phonon dispersion from the SW potential is exactly the same as that from the VFF model.

isotropic in the armchair and zigzag directions. The Poisson's ratio from the VFF model and the SW potential is $\nu_{xy} = \nu_{yx} = 0.13$. The fitted Young's modulus value is about 10% smaller than the *ab initio* result of 59 N/m,⁴⁸ as only short-range interactions are considered in the present work. The long-range interactions are ignored, which typically leads to about 10% underestimation for the value of the Young's modulus.

There is no available value for nonlinear quantities in the single-layer 1T-CoTe₂. We have thus used the nonlinear parameter $B = 0.5d^4$ in Eq. (5), which is close to the value of B in most materials. The value of the third order nonlinear elasticity D can be extracted by fitting the stress-strain relation to the function $\sigma = E\epsilon + \frac{1}{2}D\epsilon^2$ with E as the Young's modulus. The values of D from the present SW potential are -221.5 N/m and -238.3 N/m along the armchair and zigzag directions, respectively. The ultimate stress is about 5.6 Nm⁻¹ at the ultimate strain of 0.21 in the armchair direction at the low temperature of 1 K. The ultimate stress is about 5.4 Nm⁻¹ at the ultimate strain of 0.24 in the zigzag direction at the low temperature of 1 K.

Fig. 101 shows that the VFF model and the SW potential give exactly the same phonon dispersion, as the SW potential is derived from the VFF model.

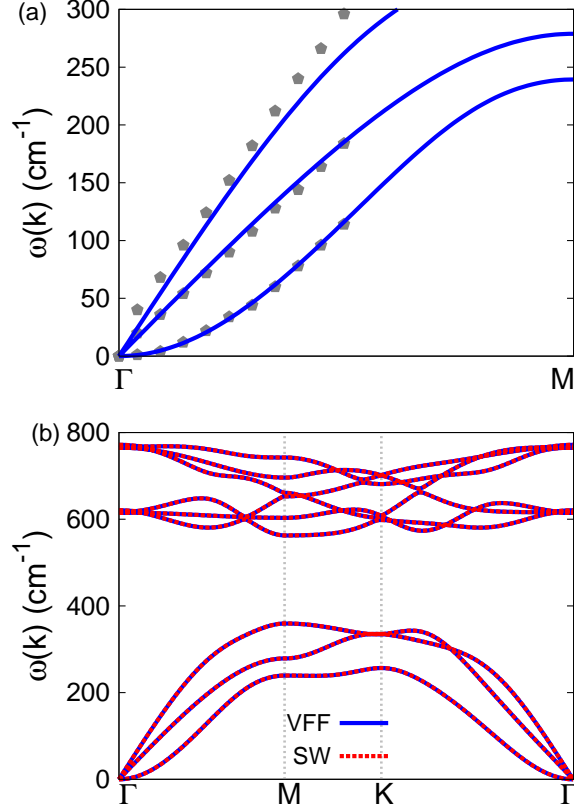


FIG. 102: (Color online) Phonon spectrum for single-layer 1T-NiO₂. (a) Phonon dispersion along the Γ M direction in the Brillouin zone. The results from the VFF model (lines) are comparable with the *ab initio* results (pentagons) from Ref. 12. (b) The phonon dispersion from the SW potential is exactly the same as that from the VFF model.

LII. 1T-NiO₂

Most existing theoretical studies on the single-layer 1T-NiO₂ are based on the first-principles calculations. In this section, we will develop the SW potential for the single-layer 1T-NiO₂.

The structure for the single-layer 1T-NiO₂ is shown in Fig. 71 (with M=Ni and X=O). Each Ni atom is surrounded by six O atoms. These O atoms are categorized into the top group (eg. atoms 1, 3, and 5) and bottom group (eg. atoms 2, 4, and 6). Each O atom is connected to three Ni atoms. The structural parameters are from the first-principles calculations,¹² including the lattice constant $a = 2.77 \text{ \AA}$ and the bond length $d_{\text{Ni-O}} = 1.84 \text{ \AA}$.

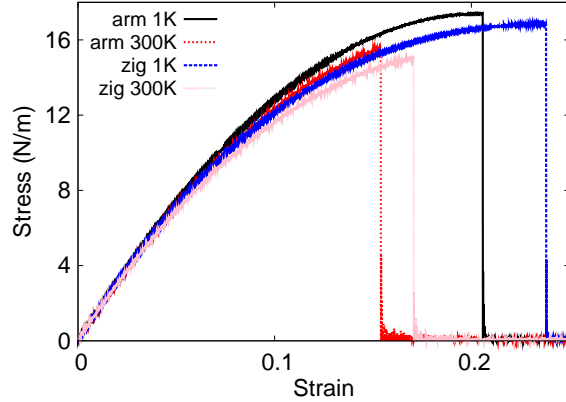


FIG. 103: (Color online) Stress-strain for single-layer 1T-NiO₂ of dimension $100 \times 100 \text{ \AA}$ along the armchair and zigzag directions.

TABLE CCVI: The VFF model for single-layer 1T-NiO₂. The second line gives an explicit expression for each VFF term. The third line is the force constant parameters. Parameters are in the unit of $\frac{eV}{\text{Å}^2}$ for the bond stretching interactions, and in the unit of eV for the angle bending interaction. The fourth line gives the initial bond length (in unit of Å) for the bond stretching interaction and the initial angle (in unit of degrees) for the angle bending interaction. The angle θ_{ijk} has atom i as the apex.

VFF type	bond stretching	angle bending	
expression	$\frac{1}{2}K_{\text{Ni-O}}(\Delta r)^2$	$\frac{1}{2}K_{\text{Ni-O-O}}(\Delta\theta)^2$	$\frac{1}{2}K_{\text{O-Ni-Ni}}(\Delta\theta)^2$
parameter	15.925	4.847	4.847
r_0 or θ_0		97.653	97.653

The resultant angles are $\theta_{\text{NiOO}} = 97.653^\circ$ with O atoms from the same (top or bottom) group, and $\theta_{\text{ONiNi}} = 97.653^\circ$.

Table CCVI shows three VFF terms for the single-layer 1T-NiO₂, one of which is the bond stretching interaction shown by Eq. (1) while the other two terms are the angle bending interaction shown by Eq. (2). We note that the angle bending term $K_{\text{Ni-O-O}}$ is for the angle $\theta_{\text{Ni-O-O}}$ with both O atoms from the same (top or bottom) group. These force constant parameters are determined by fitting to the two in-plane acoustic branches in the phonon dispersion along the ΓM as shown in Fig. 102 (a). The *ab initio* calculations for the phonon

TABLE CCVII: Two-body SW potential parameters for single-layer 1T-NiO₂ used by GULP⁸ as expressed in Eq. (3).

	A (eV)	ρ (Å)	B (Å ⁴)	r_{\min} (Å)	r_{\max} (Å)
Ni-O	9.709	1.199	5.731	0.0	2.583

TABLE CCVIII: Three-body SW potential parameters for single-layer 1T-NiO₂ used by GULP⁸ as expressed in Eq. (4). The angle θ_{ijk} in the first line indicates the bending energy for the angle with atom i as the apex.

	K (eV)	θ_0 (degree)	ρ_1 (Å)	ρ_2 (Å)	$r_{\min12}$ (Å)	$r_{\max12}$ (Å)	$r_{\min13}$ (Å)	$r_{\max13}$ (Å)	$r_{\min23}$ (Å)	$r_{\max23}$ (Å)
$\theta_{\text{Ni-O-O}}$	62.317	97.653	1.199	1.199	0.0	2.583	0.0	2.583	0.0	3.784
$\theta_{\text{O-Ni-Ni}}$	62.317	97.653	1.199	1.199	0.0	2.583	0.0	2.583	0.0	3.784

dispersion are from Ref. 12. Fig. 102 (b) shows that the VFF model and the SW potential give exactly the same phonon dispersion, as the SW potential is derived from the VFF model.

The parameters for the two-body SW potential used by GULP are shown in Tab. CCVII. The parameters for the three-body SW potential used by GULP are shown in Tab. CCVIII. Some representative parameters for the SW potential used by LAMMPS are listed in Tab. CCIX.

We use LAMMPS to perform MD simulations for the mechanical behavior of the single-layer 1T-NiO₂ under uniaxial tension at 1.0 K and 300.0 K. Fig. 103 shows the stress-strain curve for the tension of a single-layer 1T-NiO₂ of dimension 100×100 Å. Periodic boundary conditions are applied in both armchair and zigzag directions. The single-layer 1T-NiO₂ is stretched uniaxially along the armchair or zigzag direction. The stress is calculated without involving the actual thickness of the quasi-two-dimensional structure of the single-layer 1T-NiO₂. The Young's modulus can be obtained by a linear fitting of the stress-strain relation

TABLE CCIX: SW potential parameters for single-layer 1T-NiO₂ used by LAMMPS⁹ as expressed in Eqs. (9) and (10).

	ϵ (eV)	σ (Å)	a	λ	γ	$\cos \theta_0$	A_L	B_L	p	q	tol
Ni-O ₁ -O ₁	1.000	1.199	2.154	62.317	1.000	-0.133	9.709	2.772	4	0	0.0

TABLE CCX: The VFF model for single-layer 1T-NiS₂. The second line gives an explicit expression for each VFF term. The third line is the force constant parameters. Parameters are in the unit of $\frac{\text{eV}}{\text{Å}^2}$ for the bond stretching interactions, and in the unit of eV for the angle bending interaction. The fourth line gives the initial bond length (in unit of Å) for the bond stretching interaction and the initial angle (in unit of degrees) for the angle bending interaction. The angle θ_{ijk} has atom i as the apex.

VFF type	bond stretching	angle bending	
expression	$\frac{1}{2}K_{\text{Ni-S}}(\Delta r)^2$	$\frac{1}{2}K_{\text{Ni-S-S}}(\Delta\theta)^2$	$\frac{1}{2}K_{\text{S-Ni-Ni}}(\Delta\theta)^2$
parameter	9.385	2.952	2.952
r_0 or θ_0	2.232	96.000	96.000

in the small strain range of $[0, 0.01]$. The Young's modulus are 163.3 N/m and 162.4 N/m along the armchair and zigzag directions, respectively. The Young's modulus is essentially isotropic in the armchair and zigzag directions. The Poisson's ratio from the VFF model and the SW potential is $\nu_{xy} = \nu_{yx} = 0.12$.

There is no available value for nonlinear quantities in the single-layer 1T-NiO₂. We have thus used the nonlinear parameter $B = 0.5d^4$ in Eq. (5), which is close to the value of B in most materials. The value of the third order nonlinear elasticity D can be extracted by fitting the stress-strain relation to the function $\sigma = E\epsilon + \frac{1}{2}D\epsilon^2$ with E as the Young's modulus. The values of D from the present SW potential are -748.7 N/m and -796.0 N/m along the armchair and zigzag directions, respectively. The ultimate stress is about 17.4 Nm⁻¹ at the ultimate strain of 0.20 in the armchair direction at the low temperature of 1 K. The ultimate stress is about 16.8 Nm⁻¹ at the ultimate strain of 0.24 in the zigzag direction at the low temperature of 1 K.

LIII. 1T-NIS₂

Most existing theoretical studies on the single-layer 1T-NiS₂ are based on the first-principles calculations. In this section, we will develop the SW potential for the single-layer 1T-NiS₂.

The structure for the single-layer 1T-NiS₂ is shown in Fig. 71 (with M=Ni and X=S).

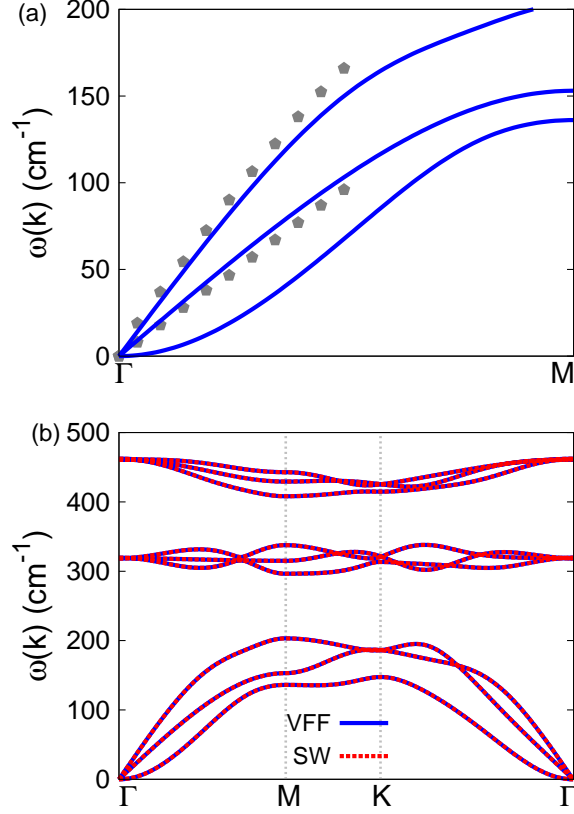


FIG. 104: (Color online) Phonon spectrum for single-layer 1T-NiS₂. (a) Phonon dispersion along the Γ M direction in the Brillouin zone. The results from the VFF model (lines) are comparable with the *ab initio* results (pentagons) from Ref. 12. (b) The phonon dispersion from the SW potential is exactly the same as that from the VFF model.

TABLE CCXI: Two-body SW potential parameters for single-layer 1T-NiS₂ used by GULP⁸ as expressed in Eq. (3).

	A (eV)	ρ (\AA)	B (\AA^4)	r_{\min} (\AA)	r_{\max} (\AA)
Ni-S	8.098	1.398	12.409	0.0	3.115

Each Ni atom is surrounded by six S atoms. These S atoms are categorized into the top group (eg. atoms 1, 3, and 5) and bottom group (eg. atoms 2, 4, and 6). Each S atom is connected to three Ni atoms. The structural parameters are from the first-principles calculations,⁴⁸ including the lattice constant $a = 3.3174 \text{ \AA}$, and the bond length $d_{\text{Ni-S}} = 2.2320 \text{ \AA}$, which is derived from the angle $\theta_{\text{SNiNi}} = 96^\circ$. The other angle is $\theta_{\text{NiSS}} = 96^\circ$ with S atoms from the

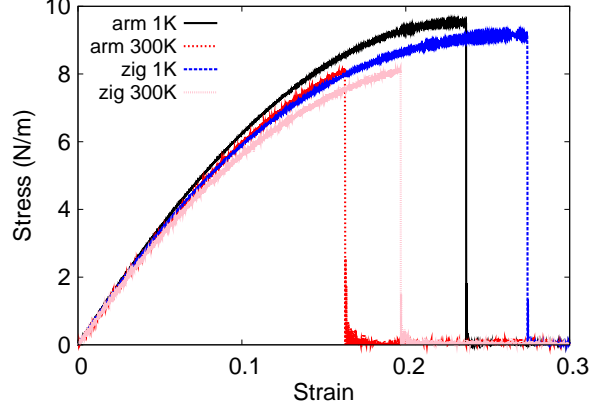


FIG. 105: (Color online) Stress-strain for single-layer 1T-NiS₂ of dimension 100 × 100 Å along the armchair and zigzag directions.

TABLE CCXII: Three-body SW potential parameters for single-layer 1T-NiS₂ used by GULP⁸ as expressed in Eq. (4). The angle θ_{ijk} in the first line indicates the bending energy for the angle with atom i as the apex.

	K (eV)	θ_0 (degree)	ρ_1 (Å)	ρ_2 (Å)	$r_{\min 12}$ (Å)	$r_{\max 12}$ (Å)	$r_{\min 13}$ (Å)	$r_{\max 13}$ (Å)	$r_{\min 23}$ (Å)	$r_{\max 23}$ (Å)
$\theta_{\text{Ni-S-S}}$	35.372	96.000	1.398	1.398	0.0	3.115	0.0	3.115	0.0	4.532
$\theta_{\text{S-Ni-Ni}}$	35.372	96.000	1.398	1.398	0.0	3.115	0.0	3.115	0.0	4.532

same (top or bottom) group.

Table CCX shows three VFF terms for the single-layer 1T-NiS₂, one of which is the bond stretching interaction shown by Eq. (1) while the other two terms are the angle bending interaction shown by Eq. (2). We note that the angle bending term $K_{\text{Ni-S-S}}$ is for the angle $\theta_{\text{Ni-S-S}}$ with both S atoms from the same (top or bottom) group. These force constant parameters are determined by fitting to the two in-plane acoustic branches in the phonon dispersion along the ΓM as shown in Fig. 104 (a). The *ab initio* calculations for the phonon

TABLE CCXIII: SW potential parameters for single-layer 1T-NiS₂ used by LAMMPS⁹ as expressed in Eqs. (9) and (10).

	ϵ (eV)	σ (Å)	a	λ	γ	$\cos \theta_0$	A_L	B_L	p	q	tol
Ni-S ₁ -S ₁	1.000	1.398	2.228	35.372	1.000	-0.105	8.098	3.249	4	0	0.0

dispersion are from Ref. 12. Fig. 104 (b) shows that the VFF model and the SW potential give exactly the same phonon dispersion, as the SW potential is derived from the VFF model.

The parameters for the two-body SW potential used by GULP are shown in Tab. CCXI. The parameters for the three-body SW potential used by GULP are shown in Tab. CCXII. Some representative parameters for the SW potential used by LAMMPS are listed in Tab. CCXIII.

We use LAMMPS to perform MD simulations for the mechanical behavior of the single-layer 1T-NiS₂ under uniaxial tension at 1.0 K and 300.0 K. Fig. 105 shows the stress-strain curve for the tension of a single-layer 1T-NiS₂ of dimension $100 \times 100 \text{ \AA}$. Periodic boundary conditions are applied in both armchair and zigzag directions. The single-layer 1T-NiS₂ is stretched uniaxially along the armchair or zigzag direction. The stress is calculated without involving the actual thickness of the quasi-two-dimensional structure of the single-layer 1T-NiS₂. The Young's modulus can be obtained by a linear fitting of the stress-strain relation in the small strain range of $[0, 0.01]$. The Young's modulus are 74.2 N/m and 73.9 N/m along the armchair and zigzag directions, respectively. The Young's modulus is essentially isotropic in the armchair and zigzag directions. The Poisson's ratio from the VFF model and the SW potential is $\nu_{xy} = \nu_{yx} = 0.17$.

There is no available value for nonlinear quantities in the single-layer 1T-NiS₂. We have thus used the nonlinear parameter $B = 0.5d^4$ in Eq. (5), which is close to the value of B in most materials. The value of the third order nonlinear elasticity D can be extracted by fitting the stress-strain relation to the function $\sigma = E\epsilon + \frac{1}{2}D\epsilon^2$ with E as the Young's modulus. The values of D from the present SW potential are -274.5 N/m and -301.4 N/m along the armchair and zigzag directions, respectively. The ultimate stress is about 9.5 Nm^{-1} at the ultimate strain of 0.23 in the armchair direction at the low temperature of 1 K. The ultimate stress is about 9.2 Nm^{-1} at the ultimate strain of 0.27 in the zigzag direction at the low temperature of 1 K.

LIV. 1T-NiSe₂

Most existing theoretical studies on the single-layer 1T-NiSe₂ are based on the first-principles calculations. In this section, we will develop the SW potential for the single-layer

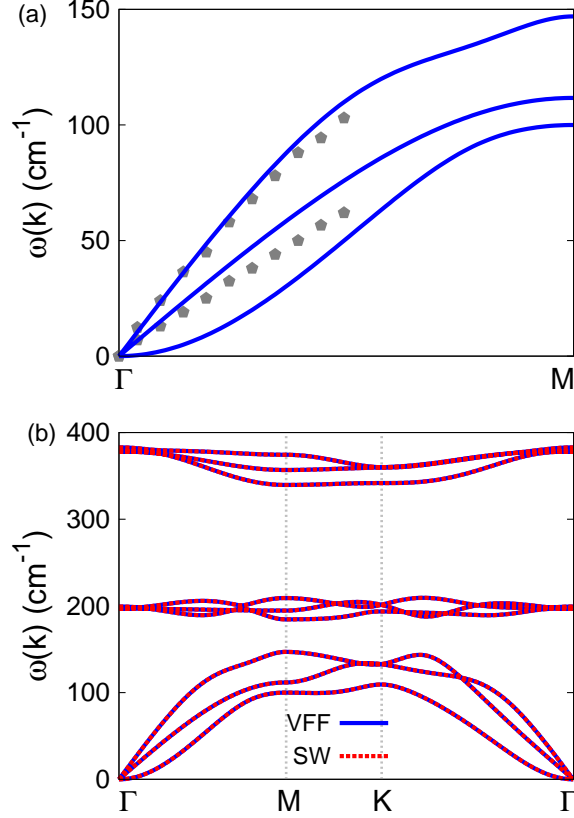


FIG. 106: (Color online) Phonon spectrum for single-layer 1T-NiSe₂. (a) Phonon dispersion along the Γ M direction in the Brillouin zone. The results from the VFF model (lines) are comparable with the *ab initio* results (pentagons) from Ref. 12. (b) The phonon dispersion from the SW potential is exactly the same as that from the VFF model.

1T-NiSe₂.

The structure for the single-layer 1T-NiSe₂ is shown in Fig. 71 (with M=Ni and X=Se). Each Ni atom is surrounded by six Se atoms. These Se atoms are categorized into the top group (eg. atoms 1, 3, and 5) and bottom group (eg. atoms 2, 4, and 6). Each Se atom is connected to three Ni atoms. The structural parameters are from the first-principles calculations,⁴⁸ including the lattice constant $a = 3.4712 \text{ \AA}$, and the bond length $d_{\text{Ni-Se}} = 2.3392 \text{ \AA}$, which is derived from the angle $\theta_{\text{SeNiNi}} = 95.8^\circ$. The other angle is $\theta_{\text{NiSeSe}} = 95.8^\circ$ with Se atoms from the same (top or bottom) group.

Table CCXIV shows three VFF terms for the single-layer 1T-NiSe₂, one of which is the bond stretching interaction shown by Eq. (1) while the other two terms are the angle

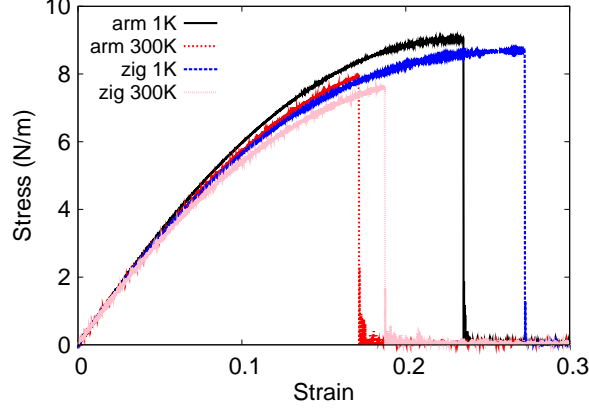


FIG. 107: (Color online) Stress-strain for single-layer 1T-NiSe₂ of dimension $100 \times 100 \text{ \AA}$ along the armchair and zigzag directions.

TABLE CCXIV: The VFF model for single-layer 1T-NiSe₂. The second line gives an explicit expression for each VFF term. The third line is the force constant parameters. Parameters are in the unit of $\frac{\text{eV}}{\text{\AA}^2}$ for the bond stretching interactions, and in the unit of eV for the angle bending interaction. The fourth line gives the initial bond length (in unit of \AA) for the bond stretching interaction and the initial angle (in unit of degrees) for the angle bending interaction. The angle θ_{ijk} has atom i as the apex.

VFF type	bond stretching	angle bending	
expression	$\frac{1}{2}K_{\text{Ni-Se}}(\Delta r)^2$	$\frac{1}{2}K_{\text{Ni-Se-Se}}(\Delta\theta)^2$	$\frac{1}{2}K_{\text{Se-Ni-Ni}}(\Delta\theta)^2$
parameter	8.814	3.149	3.149
r_0 or θ_0	2.339	95.798	95.798

bending interaction shown by Eq. (2). We note that the angle bending term $K_{\text{Ni-Se-Se}}$ is for the angle $\theta_{\text{Ni-Se-Se}}$ with both Se atoms from the same (top or bottom) group. These force constant parameters are determined by fitting to the two in-plane acoustic branches in the phonon dispersion along the ΓM as shown in Fig. 106 (a). The *ab initio* calculations for the phonon dispersion are from Ref. 12. Fig. 106 (b) shows that the VFF model and the SW potential give exactly the same phonon dispersion, as the SW potential is derived from the VFF model.

The parameters for the two-body SW potential used by GULP are shown in Tab. CCXV.

TABLE CCXV: Two-body SW potential parameters for single-layer 1T-NiSe₂ used by GULP⁸ as expressed in Eq. (3).

	A (eV)	ρ (Å)	B (Å ⁴)	r_{\min} (Å)	r_{\max} (Å)
Ni-Se	8.313	1.458	14.971	0.0	3.263

TABLE CCXVI: Three-body SW potential parameters for single-layer 1T-NiSe₂ used by GULP⁸ as expressed in Eq. (4). The angle θ_{ijk} in the first line indicates the bending energy for the angle with atom i as the apex.

	K (eV)	θ_0 (degree)	ρ_1 (Å)	ρ_2 (Å)	$r_{\min12}$ (Å)	$r_{\max12}$ (Å)	$r_{\min13}$ (Å)	$r_{\max13}$ (Å)	$r_{\min23}$ (Å)	$r_{\max23}$ (Å)
$\theta_{\text{Ni-Se-Se}}$	37.407	95.798	1.458	1.458	0.0	3.263	0.0	3.263	0.0	4.742
$\theta_{\text{Se-Ni-Ni}}$	37.407	95.798	1.458	1.458	0.0	3.263	0.0	3.263	0.0	4.742

The parameters for the three-body SW potential used by GULP are shown in Tab. CCXVI. Some representative parameters for the SW potential used by LAMMPS are listed in Tab. CCXVII.

We use LAMMPS to perform MD simulations for the mechanical behavior of the single-layer 1T-NiSe₂ under uniaxial tension at 1.0 K and 300.0 K. Fig. 107 shows the stress-strain curve for the tension of a single-layer 1T-NiSe₂ of dimension 100×100 Å. Periodic boundary conditions are applied in both armchair and zigzag directions. The single-layer 1T-NiSe₂ is stretched uniaxially along the armchair or zigzag direction. The stress is calculated without involving the actual thickness of the quasi-two-dimensional structure of the single-layer 1T-NiSe₂. The Young's modulus can be obtained by a linear fitting of the stress-strain relation in the small strain range of $[0, 0.01]$. The Young's modulus are 70.9 N/m and 70.6 N/m along the armchair and zigzag directions, respectively. The Young's modulus is essentially isotropic in the armchair and zigzag directions. The Poisson's ratio from the VFF model and the SW potential is $\nu_{xy} = \nu_{yx} = 0.17$.

TABLE CCXVII: SW potential parameters for single-layer 1T-NiSe₂ used by LAMMPS⁹ as expressed in Eqs. (9) and (10).

	ϵ (eV)	σ (Å)	a	λ	γ	$\cos \theta_0$	A_L	B_L	p	q	tol
Ni-Se ₁ -Se ₁	1.000	1.458	2.238	37.407	1.000	-0.101	8.313	3.315	4	0	0.0

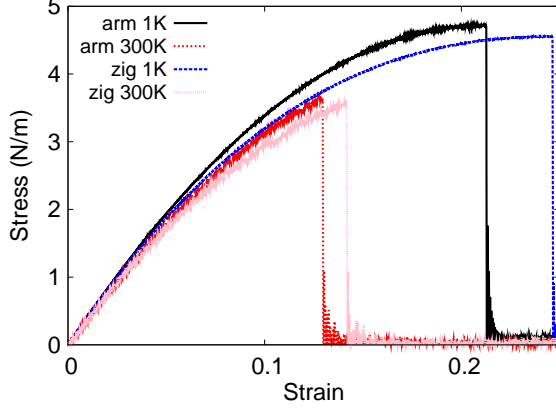


FIG. 108: (Color online) Stress-strain for single-layer 1T-NiTe₂ of dimension $100 \times 100 \text{ \AA}$ along the armchair and zigzag directions.

There is no available value for nonlinear quantities in the single-layer 1T-NiSe₂. We have thus used the nonlinear parameter $B = 0.5d^4$ in Eq. (5), which is close to the value of B in most materials. The value of the third order nonlinear elasticity D can be extracted by fitting the stress-strain relation to the function $\sigma = E\epsilon + \frac{1}{2}D\epsilon^2$ with E as the Young's modulus. The values of D from the present SW potential are -263.7 N/m and -289.5 N/m along the armchair and zigzag directions, respectively. The ultimate stress is about 9.0 Nm^{-1} at the ultimate strain of 0.23 in the armchair direction at the low temperature of 1 K. The ultimate stress is about 8.7 Nm^{-1} at the ultimate strain of 0.27 in the zigzag direction at the low temperature of 1 K.

LV. 1T-NITE₂

Most existing theoretical studies on the single-layer 1T-NiTe₂ are based on the first-principles calculations. In this section, we will develop the SW potential for the single-layer 1T-NiTe₂.

The structure for the single-layer 1T-NiTe₂ is shown in Fig. 71 (with M=Ni and X=Te). Each Ni atom is surrounded by six Te atoms. These Te atoms are categorized into the top group (eg. atoms 1, 3, and 5) and bottom group (eg. atoms 2, 4, and 6). Each Te atom is connected to three Ni atoms. The structural parameters are from the first-principles calculations,⁴⁸ including the lattice constant $a = 3.7248 \text{ \AA}$, and the bond length

TABLE CCXVIII: The VFF model for single-layer 1T-NiTe₂. The second line gives an explicit expression for each VFF term. The third line is the force constant parameters. Parameters are in the unit of $\frac{\text{eV}}{\text{\AA}^2}$ for the bond stretching interactions, and in the unit of eV for the angle bending interaction. The fourth line gives the initial bond length (in unit of \AA) for the bond stretching interaction and the initial angle (in unit of degrees) for the angle bending interaction. The angle θ_{ijk} has atom i as the apex.

VFF type	bond stretching	angle bending	
expression	$\frac{1}{2}K_{\text{Ni-Te}}(\Delta r)^2$	$\frac{1}{2}K_{\text{Ni-Te-Te}}(\Delta\theta)^2$	$\frac{1}{2}K_{\text{Te-Ni-Ni}}(\Delta\theta)^2$
parameter	4.230	2.429	2.429
r_0 or θ_0	2.532	94.702	94.702
or θ_0	2.635	95.999	95.999

TABLE CCXIX: Two-body SW potential parameters for single-layer 1T-NiTe₂ used by GULP⁸ as expressed in Eq. (3).

	A (eV)	ρ (\AA)	B (\AA ⁴)	r_{min} (\AA)	r_{max} (\AA)
Ni-Te	4.554	1.536	20.554	0.0	3.518

TABLE CCXX: Three-body SW potential parameters for single-layer 1T-NiTe₂ used by GULP⁸ as expressed in Eq. (4). The angle θ_{ijk} in the first line indicates the bending energy for the angle with atom i as the apex.

	K (eV)	θ_0 (degree)	ρ_1 (\AA)	ρ_2 (\AA)	$r_{\text{min}12}$ (\AA)	$r_{\text{max}12}$ (\AA)	$r_{\text{min}13}$ (\AA)	$r_{\text{max}13}$ (\AA)	$r_{\text{min}23}$ (\AA)	$r_{\text{max}23}$ (\AA)
$\theta_{\text{Ni-Te-Te}}$	27.553	94.702	1.536	1.536	0.0	3.518	0.0	3.518	0.0	5.088
$\theta_{\text{Te-Ni-Ni}}$	27.553	94.702	1.536	1.536	0.0	3.518	0.0	3.518	0.0	5.088

TABLE CCXXI: SW potential parameters for single-layer 1T-NiTe₂ used by LAMMPS⁹ as expressed in Eqs. (9) and (10).

	ϵ (eV)	σ (\AA)	a	λ	γ	$\cos\theta_0$	A_L	B_L	p	q	tol
Ni-Te ₁ -Te ₁	1.000	1.536	2.291	27.553	1.000	-0.082	4.554	3.696	4	0	0.0

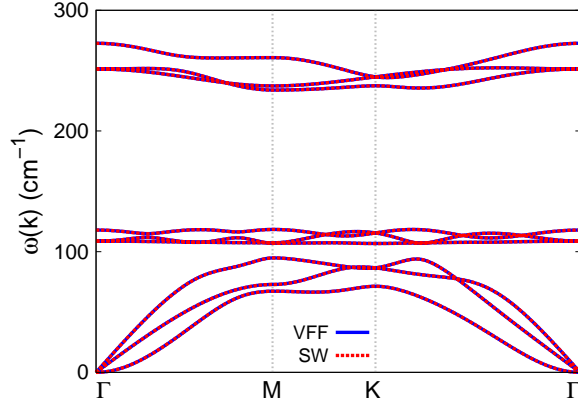


FIG. 109: (Color online) Phonon spectrum for single-layer 1T-NiTe₂ along the Γ MK Γ direction in the Brillouin zone. The phonon dispersion from the SW potential is exactly the same as that from the VFF model.

$d_{\text{Ni-Te}} = 2.5321 \text{ \AA}$, which is derived from the angle $\theta_{\text{TeNiNi}} = 94.7^\circ$. The other angle is $\theta_{\text{NiTeTe}} = 94.7^\circ$ with Te atoms from the same (top or bottom) group.

Table CCXVIII shows three VFF terms for the single-layer 1T-NiTe₂, one of which is the bond stretching interaction shown by Eq. (1) while the other two terms are the angle bending interaction shown by Eq. (2). We note that the angle bending term $K_{\text{Ni-Te-Te}}$ is for the angle $\theta_{\text{Ni-Te-Te}}$ with both Te atoms from the same (top or bottom) group. We find that there are actually only two parameters in the VFF model, so we can determine their value by fitting to the Young's modulus and the Poisson's ratio of the system. The *ab initio* calculations have predicted the Young's modulus to be 44 N/m and the Poisson's ratio as 0.14.⁴⁸

The parameters for the two-body SW potential used by GULP are shown in Tab. CCXIX. The parameters for the three-body SW potential used by GULP are shown in Tab. CCXX. Some representative parameters for the SW potential used by LAMMPS are listed in Tab. CCXXI.

We use LAMMPS to perform MD simulations for the mechanical behavior of the single-layer 1T-NiTe₂ under uniaxial tension at 1.0 K and 300.0 K. Fig. 108 shows the stress-strain curve for the tension of a single-layer 1T-NiTe₂ of dimension $100 \times 100 \text{ \AA}$. Periodic boundary conditions are applied in both armchair and zigzag directions. The single-layer 1T-NiTe₂ is stretched uniaxially along the armchair or zigzag direction. The stress is calculated without

TABLE CCXXII: The VFF model for single-layer 1T-ZrS₂. The second line gives an explicit expression for each VFF term. The third line is the force constant parameters. Parameters are in the unit of $\frac{\text{eV}}{\text{Å}^2}$ for the bond stretching interactions, and in the unit of eV for the angle bending interaction. The fourth line gives the initial bond length (in unit of Å) for the bond stretching interaction and the initial angle (in unit of degrees) for the angle bending interaction. The angle θ_{ijk} has atom i as the apex.

VFF type	bond stretching	angle bending	
expression	$\frac{1}{2}K_{\text{Zr-S}}(\Delta r)^2$	$\frac{1}{2}K_{\text{Zr-S-S}}(\Delta\theta)^2$	$\frac{1}{2}K_{\text{S-Zr-Zr}}(\Delta\theta)^2$
parameter	7.930	4.283	4.283
r_0 or θ_0	2.580	91.305	91.305

involving the actual thickness of the quasi-two-dimensional structure of the single-layer 1T-NiTe₂. The Young's modulus can be obtained by a linear fitting of the stress-strain relation in the small strain range of [0, 0.01]. The Young's modulus are 42.6 N/m and 42.4 N/m along the armchair and zigzag directions, respectively. The Young's modulus is essentially isotropic in the armchair and zigzag directions. The Poisson's ratio from the VFF model and the SW potential is $\nu_{xy} = \nu_{yx} = 0.14$.

There is no available value for nonlinear quantities in the single-layer 1T-NiTe₂. We have thus used the nonlinear parameter $B = 0.5d^4$ in Eq. (5), which is close to the value of B in most materials. The value of the third order nonlinear elasticity D can be extracted by fitting the stress-strain relation to the function $\sigma = E\epsilon + \frac{1}{2}D\epsilon^2$ with E as the Young's modulus. The values of D from the present SW potential are -187.6 N/m and -200.6 N/m along the armchair and zigzag directions, respectively. The ultimate stress is about 4.7 Nm⁻¹ at the ultimate strain of 0.21 in the armchair direction at the low temperature of 1 K. The ultimate stress is about 4.6 Nm⁻¹ at the ultimate strain of 0.24 in the zigzag direction at the low temperature of 1 K.

Fig. 109 shows that the VFF model and the SW potential give exactly the same phonon dispersion, as the SW potential is derived from the VFF model.

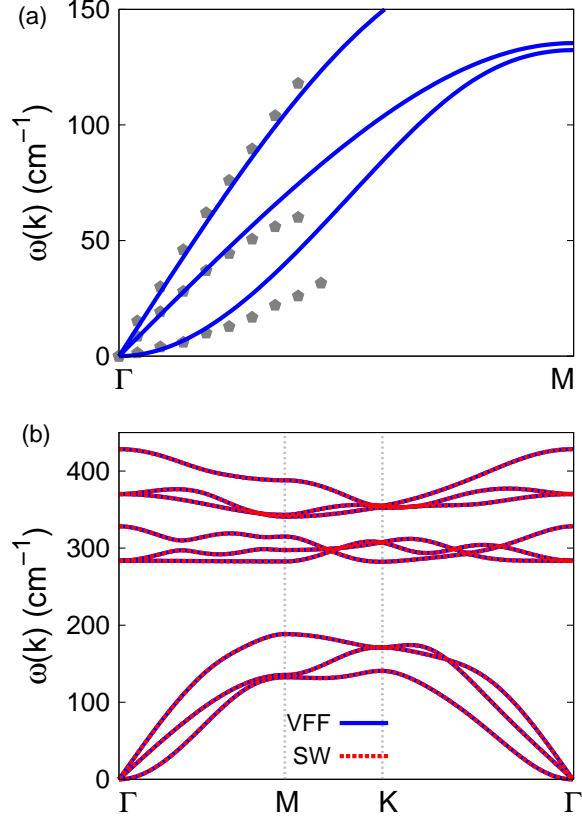


FIG. 110: (Color online) Phonon spectrum for single-layer 1T-ZrS₂. (a) Phonon dispersion along the Γ M direction in the Brillouin zone. The results from the VFF model (lines) are comparable with the experiment data (pentagons) from Ref. 38. (b) The phonon dispersion from the SW potential is exactly the same as that from the VFF model.

TABLE CCXXIII: Two-body SW potential parameters for single-layer 1T-ZrS₂ used by GULP⁸ as expressed in Eq. (3).

	A (eV)	ρ (\AA)	B (\AA^4)	r_{\min} (\AA)	r_{\max} (\AA)
Zr-S	8.149	1.432	22.154	0.0	3.541

LVI. 1T-ZRS₂

Most existing theoretical studies on the single-layer 1T-ZrS₂ are based on the first-principles calculations. In this section, we will develop the SW potential for the single-layer 1T-ZrS₂.

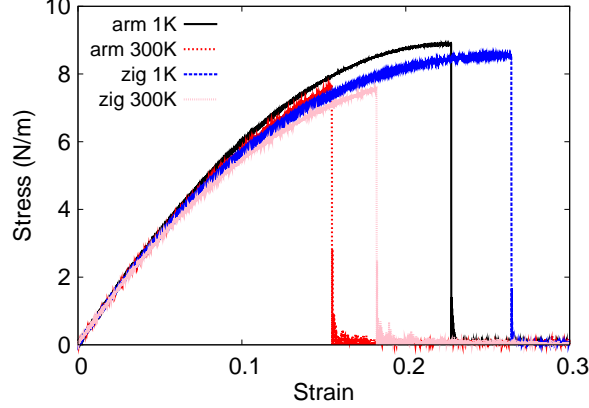


FIG. 111: (Color online) Stress-strain for single-layer 1T-ZrS₂ of dimension 100 × 100 Å along the armchair and zigzag directions.

TABLE CCXXIV: Three-body SW potential parameters for single-layer 1T-ZrS₂ used by GULP⁸ as expressed in Eq. (4). The angle θ_{ijk} in the first line indicates the bending energy for the angle with atom i as the apex.

	K (eV)	θ_0 (degree)	ρ_1 (Å)	ρ_2 (Å)	$r_{\min 12}$ (Å)	$r_{\max 12}$ (Å)	$r_{\min 13}$ (Å)	$r_{\max 13}$ (Å)	$r_{\min 23}$ (Å)	$r_{\max 23}$ (Å)
$\theta_{\text{Zr-S-S}}$	42.170	91.305	1.432	1.432	0.0	3.541	0.0	3.541	0.0	5.041
$\theta_{\text{S-Zr-Zr}}$	42.170	91.305	1.432	1.432	0.0	3.541	0.0	3.541	0.0	5.041

The structure for the single-layer 1T-ZrS₂ is shown in Fig. 71 (with M=Zr and X=S). Each Zr atom is surrounded by six S atoms. These S atoms are categorized into the top group (eg. atoms 1, 3, and 5) and bottom group (eg. atoms 2, 4, and 6). Each S atom is connected to three Zr atoms. The structural parameters are from the first-principles calculations,⁴⁹ including the lattice constant $a = 3.690$ Å and the bond length $d_{\text{Zr-S}} = 2.58$ Å. The resultant angles are $\theta_{\text{ZrSS}} = 91.305^\circ$ with S atoms from the same (top or bottom) group, and

TABLE CCXXV: SW potential parameters for single-layer 1T-ZrS₂ used by LAMMPS⁹ as expressed in Eqs. (9) and (10).

	ϵ (eV)	σ (Å)	a	λ	γ	$\cos \theta_0$	A_L	B_L	p	q	tol
Zr-S1-S1	1.000	1.432	2.473	42.177	1.000	-0.023	8.149	5.268	4	0	0.0
S1-Zr-Zr	1.000	1.432	2.473	42.177	1.000	-0.023	8.149	5.268	4	0	0.0

$$\theta_{\text{SZrZr}} = 91.305^\circ.$$

Table [CCXXII](#) shows three VFF terms for the single-layer 1T-ZrS₂, one of which is the bond stretching interaction shown by Eq. (1) while the other two terms are the angle bending interaction shown by Eq. (2). We note that the angle bending term $K_{\text{Zr-S-S}}$ is for the angle $\theta_{\text{Zr-S-S}}$ with both S atoms from the same (top or bottom) group. These force constant parameters are determined by fitting to the three acoustic branches in the phonon dispersion along the ΓM as shown in Fig. [110](#) (a). The *ab initio* calculations for the phonon dispersion are from Ref. 38. Similar phonon dispersion can also be found in other *ab initio* calculations.³⁴ Fig. [110](#) (b) shows that the VFF model and the SW potential give exactly the same phonon dispersion, as the SW potential is derived from the VFF model.

The parameters for the two-body SW potential used by GULP are shown in Tab. [CCXXIII](#). The parameters for the three-body SW potential used by GULP are shown in Tab. [CCXXIV](#). Some representative parameters for the SW potential used by LAMMPS are listed in Tab. [CCXXV](#).

We use LAMMPS to perform MD simulations for the mechanical behavior of the single-layer 1T-ZrS₂ under uniaxial tension at 1.0 K and 300.0 K. Fig. [111](#) shows the stress-strain curve for the tension of a single-layer 1T-ZrS₂ of dimension 100×100 Å. Periodic boundary conditions are applied in both armchair and zigzag directions. The single-layer 1T-ZrS₂ is stretched uniaxially along the armchair or zigzag direction. The stress is calculated without involving the actual thickness of the quasi-two-dimensional structure of the single-layer 1T-ZrS₂. The Young's modulus can be obtained by a linear fitting of the stress-strain relation in the small strain range of $[0, 0.01]$. The Young's modulus are 71.8 N/m and 71.5 N/m along the armchair and zigzag directions, respectively. The Young's modulus is essentially isotropic in the armchair and zigzag directions. These values are close to the *ab initio* results at 0 K temperature, eg. 75.74 Nm⁻¹ in Ref. 49. The Poisson's ratio from the VFF model and the SW potential is $\nu_{xy} = \nu_{yx} = 0.16$, which are comparable with the *ab initio* result⁴⁹ of 0.22.

There is no available value for nonlinear quantities in the single-layer 1T-ZrS₂. We have thus used the nonlinear parameter $B = 0.5d^4$ in Eq. (5), which is close to the value of B in most materials. The value of the third order nonlinear elasticity D can be extracted by fitting the stress-strain relation to the function $\sigma = E\epsilon + \frac{1}{2}D\epsilon^2$ with E as the Young's modulus. The values of D from the present SW potential are -268.9 N/m and -305.2 N/m

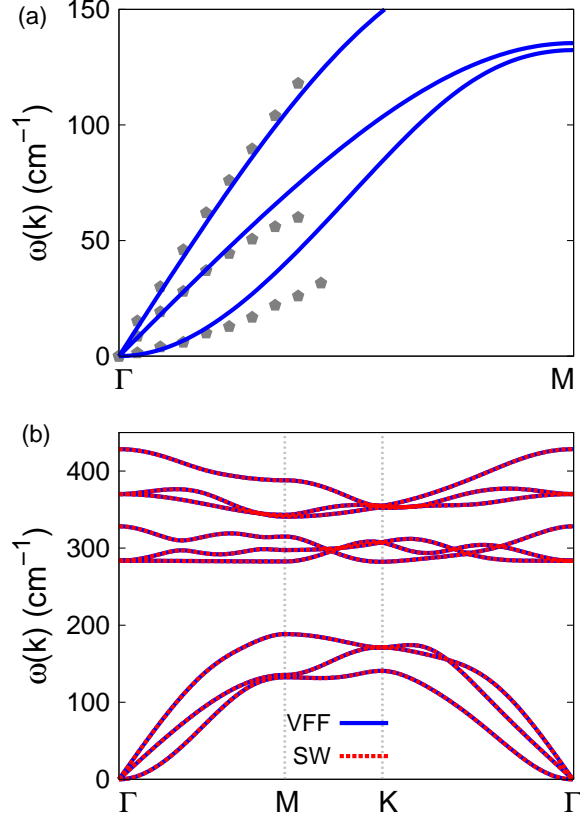


FIG. 112: (Color online) Phonon spectrum for single-layer 1T-ZrSe₂. (a) Phonon dispersion along the Γ M direction in the Brillouin zone. The results from the VFF model (lines) are comparable with the experiment data (pentagons) from Ref. 50. (b) The phonon dispersion from the SW potential is exactly the same as that from the VFF model.

along the armchair and zigzag directions, respectively. The ultimate stress is about 8.9 Nm^{-1} at the ultimate strain of 0.23 in the armchair direction at the low temperature of 1 K. The ultimate stress is about 8.5 Nm^{-1} at the ultimate strain of 0.26 in the zigzag direction at the low temperature of 1 K.

LVII. 1T-ZRSE₂

Most existing theoretical studies on the single-layer 1T-ZrSe₂ are based on the first-principles calculations. In this section, we will develop the SW potential for the single-layer 1T-ZrSe₂.

TABLE CCXXVI: The VFF model for single-layer 1T-ZrSe₂. The second line gives an explicit expression for each VFF term. The third line is the force constant parameters. Parameters are in the unit of $\frac{\text{eV}}{\text{\AA}^2}$ for the bond stretching interactions, and in the unit of eV for the angle bending interaction. The fourth line gives the initial bond length (in unit of \AA) for the bond stretching interaction and the initial angle (in unit of degrees) for the angle bending interaction. The angle θ_{ijk} has atom i as the apex.

VFF type	bond stretching	angle bending	
expression	$\frac{1}{2}K_{\text{Zr-Se}}(\Delta r)^2$	$\frac{1}{2}K_{\text{Zr-Se-Se}}(\Delta\theta)^2$	$\frac{1}{2}K_{\text{Se-Zr-Zr}}(\Delta\theta)^2$
parameter	7.930	4.283	4.283
r_0 or θ_0	2.667	88.058	88.058

TABLE CCXXVII: Two-body SW potential parameters for single-layer 1T-ZrSe₂ used by GULP⁸ as expressed in Eq. (3).

	A (eV)	ρ (\AA)	B (\AA ⁴)	r_{min} (\AA)	r_{max} (\AA)
Zr-Se	8.022	1.354	25.297	0.0	3.617

TABLE CCXXVIII: Three-body SW potential parameters for single-layer 1T-ZrSe₂ used by GULP⁸ as expressed in Eq. (4). The angle θ_{ijk} in the first line indicates the bending energy for the angle with atom i as the apex.

	K (eV)	θ_0 (degree)	ρ_1 (\AA)	ρ_2 (\AA)	$r_{\text{min}12}$ (\AA)	$r_{\text{max}12}$ (\AA)	$r_{\text{min}13}$ (\AA)	$r_{\text{max}13}$ (\AA)	$r_{\text{min}23}$ (\AA)	$r_{\text{max}23}$ (\AA)
$\theta_{\text{Zr-Se-Se}}$	37.051	88.058	1.354	1.354	0.0	3.617	0.0	3.617	0.0	5.064
$\theta_{\text{Se-Zr-Zr}}$	37.051	88.058	1.354	1.354	0.0	3.617	0.0	3.617	0.0	5.064

TABLE CCXXIX: SW potential parameters for single-layer 1T-ZrSe₂ used by LAMMPS⁹ as expressed in Eqs. (9) and (10).

	ϵ (eV)	σ (\AA)	a	λ	γ	$\cos\theta_0$	A_L	B_L	p	q	tol
Zr-Se-Se	1.000	1.354	2.671	37.051	1.000	0.034	8.022	7.527	4	0	0.0
Se-Zr-Zr	1.000	1.354	2.671	37.051	1.000	0.034	8.022	7.527	4	0	0.0

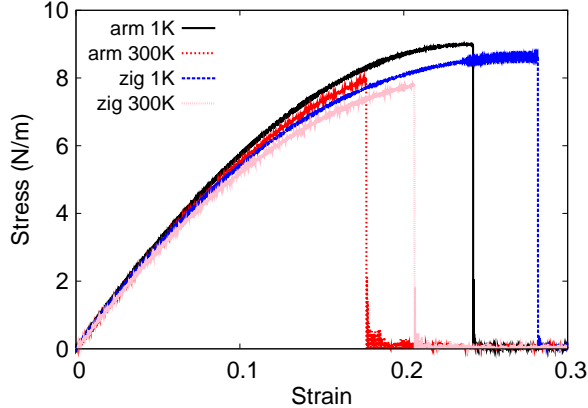


FIG. 113: (Color online) Stress-strain for single-layer 1T-ZrSe₂ of dimension $100 \times 100 \text{ \AA}$ along the armchair and zigzag directions.

The structure for the single-layer 1T-ZrSe₂ is shown in Fig. 71 (with M=Zr and X=Se). Each Zr atom is surrounded by six Se atoms. These Se atoms are categorized into the top group (eg. atoms 1, 3, and 5) and bottom group (eg. atoms 2, 4, and 6). Each Se atom is connected to three Zr atoms. The structural parameters are from the first-principles calculations,⁵¹ including the lattice constant $a = 3.707 \text{ \AA}$, and the position of the Se atom with respect to the Zr atomic plane $h = 1.591 \text{ \AA}$. The resultant angles are $\theta_{\text{ZrSeSe}} = 88.058^\circ$ with Se atoms from the same (top or bottom) group, and $\theta_{\text{SeZrZr}} = 88.058^\circ$.

Table CCXXVI shows three VFF terms for the single-layer 1T-ZrSe₂, one of which is the bond stretching interaction shown by Eq. (1) while the other two terms are the angle bending interaction shown by Eq. (2). We note that the angle bending term $K_{\text{Zr-Se-Se}}$ is for the angle $\theta_{\text{Zr-Se-Se}}$ with both Se atoms from the same (top or bottom) group. These force constant parameters are determined by fitting to the three acoustic branches in the phonon dispersion along the ΓM as shown in Fig. 112 (a). The *ab initio* calculations for the phonon dispersion are from Ref. 50. Similar phonon dispersion can also be found in other *ab initio* calculations.³⁴ Fig. 112 (b) shows that the VFF model and the SW potential give exactly the same phonon dispersion, as the SW potential is derived from the VFF model.

The parameters for the two-body SW potential used by GULP are shown in Tab. CCXXVII. The parameters for the three-body SW potential used by GULP are shown in Tab. CCXXVIII. Some representative parameters for the SW potential used by LAMMPS are listed in Tab. CCXXIX.

We use LAMMPS to perform MD simulations for the mechanical behavior of the single-layer 1T-ZrSe₂ under uniaxial tension at 1.0 K and 300.0 K. Fig. 113 shows the stress-strain curve for the tension of a single-layer 1T-ZrSe₂ of dimension 100 × 100 Å. Periodic boundary conditions are applied in both armchair and zigzag directions. The single-layer 1T-ZrSe₂ is stretched uniaxially along the armchair or zigzag direction. The stress is calculated without involving the actual thickness of the quasi-two-dimensional structure of the single-layer 1T-ZrSe₂. The Young's modulus can be obtained by a linear fitting of the stress-strain relation in the small strain range of [0, 0.01]. The Young's modulus are 66.7 N/m and 66.4 N/m along the armchair and zigzag directions, respectively. The Young's modulus is essentially isotropic in the armchair and zigzag directions. The Poisson's ratio from the VFF model and the SW potential is $\nu_{xy} = \nu_{yx} = 0.19$.

There is no available value for nonlinear quantities in the single-layer 1T-ZrSe₂. We have thus used the nonlinear parameter $B = 0.5d^4$ in Eq. (5), which is close to the value of B in most materials. The value of the third order nonlinear elasticity D can be extracted by fitting the stress-strain relation to the function $\sigma = E\epsilon + \frac{1}{2}D\epsilon^2$ with E as the Young's modulus. The values of D from the present SW potential are -219.6 N/m and -256.6 N/m along the armchair and zigzag directions, respectively. The ultimate stress is about 9.0 Nm⁻¹ at the ultimate strain of 0.24 in the armchair direction at the low temperature of 1 K. The ultimate stress is about 8.6 Nm⁻¹ at the ultimate strain of 0.28 in the zigzag direction at the low temperature of 1 K.

LVIII. 1T-ZRTE₂

Most existing theoretical studies on the single-layer 1T-ZrTe₂ are based on the first-principles calculations. In this section, we will develop the SW potential for the single-layer 1T-ZrTe₂.

The structure for the single-layer 1T-ZrTe₂ is shown in Fig. 71 (with M=Zr and X=Te). Each Zr atom is surrounded by six Te atoms. These Te atoms are categorized into the top group (eg. atoms 1, 3, and 5) and bottom group (eg. atoms 2, 4, and 6). Each Te atom is connected to three Zr atoms. The structural parameters are from the first-principles calculations,⁴⁸ including the lattice constant $a = 4.0064$ Å, and the bond length $d_{\text{Zr-Te}} = 2.9021$ Å, which is derived from the angle $\theta_{\text{TeZrZr}} = 87.3^\circ$. The other angle is

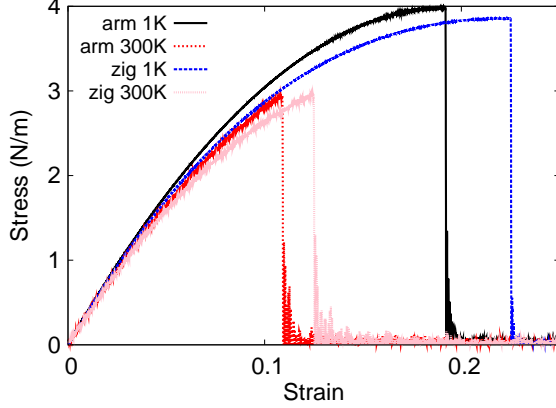


FIG. 114: (Color online) Stress-strain for single-layer 1T-ZrTe₂ of dimension $100 \times 100 \text{ \AA}$ along the armchair and zigzag directions.

TABLE CCXXX: The VFF model for single-layer 1T-ZrTe₂. The second line gives an explicit expression for each VFF term. The third line is the force constant parameters. Parameters are in the unit of $\frac{\text{eV}}{\text{Å}^2}$ for the bond stretching interactions, and in the unit of eV for the angle bending interaction. The fourth line gives the initial bond length (in unit of Å) for the bond stretching interaction and the initial angle (in unit of degrees) for the angle bending interaction. The angle θ_{ijk} has atom *i* as the apex.

VFF type	bond stretching	angle bending	
expression	$\frac{1}{2}K_{\text{Zr-Te}}(\Delta r)^2$	$\frac{1}{2}K_{\text{Zr-Te-Te}}(\Delta\theta)^2$	$\frac{1}{2}K_{\text{Te-Zr-Zr}}(\Delta\theta)^2$
parameter	2.974	3.681	3.681
r_0 or θ_0	2.902	87.301	87.301

$\theta_{\text{ZrTeTe}} = 87.3^\circ$ with Te atoms from the same (top or bottom) group.

Table CCXXX shows three VFF terms for the single-layer 1T-ZrTe₂, one of which is the bond stretching interaction shown by Eq. (1) while the other two terms are the angle bending interaction shown by Eq. (2). We note that the angle bending term $K_{\text{Zr-Te-Te}}$ is for the angle $\theta_{\text{Zr-Te-Te}}$ with both Te atoms from the same (top or bottom) group. We find that there are actually only two parameters in the VFF model, so we can determine their value by fitting to the Young's modulus and the Poisson's ratio of the system. The *ab initio* calculations have predicted the Young's modulus to be 44 N/m and the Poisson's ratio as

TABLE CCXXXI: Two-body SW potential parameters for single-layer 1T-ZrTe₂ used by GULP⁸ as expressed in Eq. (3).

	A (eV)	ρ (Å)	B (Å ⁴)	r_{\min} (Å)	r_{\max} (Å)
Zr-Te	3.493	1.441	35.467	0.0	3.925

TABLE CCXXXII: Three-body SW potential parameters for single-layer 1T-ZrTe₂ used by GULP⁸ as expressed in Eq. (4). The angle θ_{ijk} in the first line indicates the bending energy for the angle with atom i as the apex.

	K (eV)	θ_0 (degree)	ρ_1 (Å)	ρ_2 (Å)	$r_{\min12}$ (Å)	$r_{\max12}$ (Å)	$r_{\min13}$ (Å)	$r_{\max13}$ (Å)	$r_{\min23}$ (Å)	$r_{\max23}$ (Å)
$\theta_{\text{Zr-Te-Te}}$	30.905	87.301	1.441	1.441	0.0	3.925	0.0	3.925	0.0	5.473
$\theta_{\text{Te-Zr-Zr}}$	30.905	87.301	1.441	1.441	0.0	3.925	0.0	3.925	0.0	5.473

0.13.⁴⁸

The parameters for the two-body SW potential used by GULP are shown in Tab. CCXXXI. The parameters for the three-body SW potential used by GULP are shown in Tab. CCXXXII. Some representative parameters for the SW potential used by LAMMPS are listed in Tab. CCXXXIII.

We use LAMMPS to perform MD simulations for the mechanical behavior of the single-layer 1T-ZrTe₂ under uniaxial tension at 1.0 K and 300.0 K. Fig. 114 shows the stress-strain curve for the tension of a single-layer 1T-ZrTe₂ of dimension 100×100 Å. Periodic boundary conditions are applied in both armchair and zigzag directions. The single-layer 1T-ZrTe₂ is stretched uniaxially along the armchair or zigzag direction. The stress is calculated without involving the actual thickness of the quasi-two-dimensional structure of the single-layer 1T-ZrTe₂. The Young's modulus can be obtained by a linear fitting of the stress-strain relation in the small strain range of $[0, 0.01]$. The Young's modulus are 39.2 N/m and 39.1 N/m along the armchair and zigzag directions, respectively. The Young's modulus is essentially

TABLE CCXXXIII: SW potential parameters for single-layer 1T-ZrTe₂ used by LAMMPS⁹ as expressed in Eqs. (9) and (10).

	ϵ (eV)	σ (Å)	a	λ	γ	$\cos \theta_0$	A_L	B_L	p	q	tol
Zr-Te ₁ -Te ₁	1.000	1.441	2.723	30.905	1.000	0.047	3.493	8.225	4	0	0.0

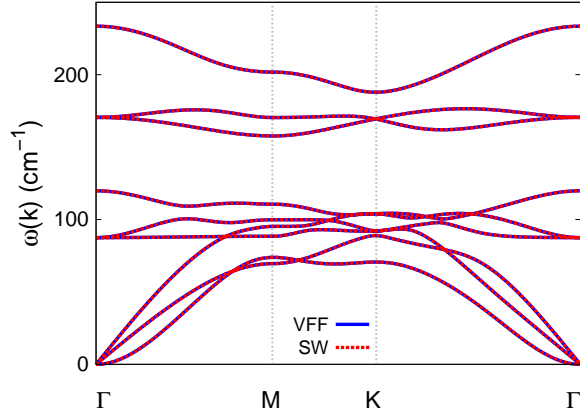


FIG. 115: (Color online) Phonon spectrum for single-layer 1T-ZrTe₂ along the Γ MK Γ direction in the Brillouin zone. The phonon dispersion from the SW potential is exactly the same as that from the VFF model.

isotropic in the armchair and zigzag directions. The Poisson's ratio from the VFF model and the SW potential is $\nu_{xy} = \nu_{yx} = 0.10$. The fitted Young's modulus value is about 10% smaller than the *ab initio* result of 44 N/m,⁴⁸ as only short-range interactions are considered in the present work. The long-range interactions are ignored, which typically leads to about 10% underestimation for the value of the Young's modulus.

There is no available value for nonlinear quantities in the single-layer 1T-ZrTe₂. We have thus used the nonlinear parameter $B = 0.5d^4$ in Eq. (5), which is close to the value of B in most materials. The value of the third order nonlinear elasticity D can be extracted by fitting the stress-strain relation to the function $\sigma = E\epsilon + \frac{1}{2}D\epsilon^2$ with E as the Young's modulus. The values of D from the present SW potential are -187.2 N/m and -201.1 N/m along the armchair and zigzag directions, respectively. The ultimate stress is about 4.0 Nm⁻¹ at the ultimate strain of 0.19 in the armchair direction at the low temperature of 1 K. The ultimate stress is about 3.9 Nm⁻¹ at the ultimate strain of 0.22 in the zigzag direction at the low temperature of 1 K.

Fig. 115 shows that the VFF model and the SW potential give exactly the same phonon dispersion, as the SW potential is derived from the VFF model.

TABLE CCXXXIV: The VFF model for single-layer 1T-NbS₂. The second line gives an explicit expression for each VFF term. The third line is the force constant parameters. Parameters are in the unit of $\frac{\text{eV}}{\text{Å}^2}$ for the bond stretching interactions, and in the unit of eV for the angle bending interaction. The fourth line gives the initial bond length (in unit of Å) for the bond stretching interaction and the initial angle (in unit of degrees) for the angle bending interaction. The angle θ_{ijk} has atom i as the apex.

VFF type	bond stretching		angle bending	
expression	$\frac{1}{2}K_{\text{Nb-S}}(\Delta r)^2$	$\frac{1}{2}K_{\text{Nb-S-S}}(\Delta\theta)^2$	$\frac{1}{2}K_{\text{S-Nb-Nb}}(\Delta\theta)^2$	
parameter	7.930	4.283	4.283	
r_0 or θ_0	2.450	84.671	84.671	

TABLE CCXXXV: Two-body SW potential parameters for single-layer 1T-NbS₂ used by GULP⁸ as expressed in Eq. (3).

	A (eV)	ρ (Å)	B (Å ⁴)	r_{min} (Å)	r_{max} (Å)
Nb-S	6.192	1.125	18.015	0.0	3.280

TABLE CCXXXVI: Three-body SW potential parameters for single-layer 1T-NbS₂ used by GULP⁸ as expressed in Eq. (4). The angle θ_{ijk} in the first line indicates the bending energy for the angle with atom i as the apex.

	K (eV)	θ_0 (degree)	ρ_1 (Å)	ρ_2 (Å)	$r_{\text{min}12}$ (Å)	$r_{\text{max}12}$ (Å)	$r_{\text{min}13}$ (Å)	$r_{\text{max}13}$ (Å)	$r_{\text{min}23}$ (Å)	$r_{\text{max}23}$ (Å)
$\theta_{\text{Nb-S-S}}$	32.472	84.671	1.125	1.125	0.0	3.280	0.0	3.280	0.0	4.508
$\theta_{\text{S-Nb-Nb}}$	32.472	84.671	1.125	1.125	0.0	3.280	0.0	3.280	0.0	4.508

TABLE CCXXXVII: SW potential parameters for single-layer 1T-NbS₂ used by LAMMPS⁹ as expressed in Eqs. (9) and (10).

	ϵ (eV)	σ (Å)	a	λ	γ	$\cos\theta_0$	A_L	B_L	p	q	tol
Nb-S ₁ -S ₁	1.000	1.125	2.916	32.472	1.000	0.093	6.192	11.247	4	0	0.0
S ₁ -Nb-Nb	1.000	1.125	2.916	32.472	1.000	0.093	6.192	11.247	4	0	0.0

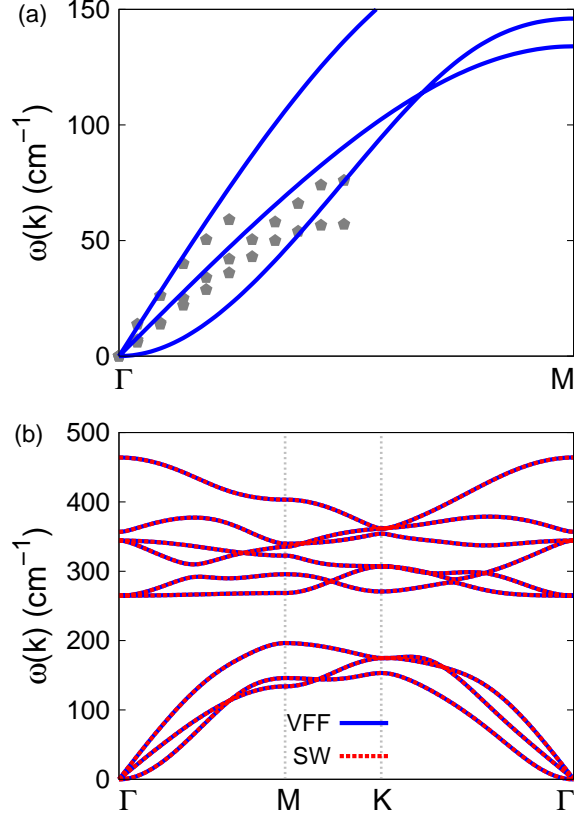


FIG. 116: (Color online) Phonon spectrum for single-layer 1T-NbS₂. (a) Phonon dispersion along the Γ M direction in the Brillouin zone. The results from the VFF model (lines) are comparable with the experiment data (pentagons) from Ref. 12. (b) The phonon dispersion from the SW potential is exactly the same as that from the VFF model.

LIX. 1T-NbS₂

Most existing theoretical studies on the single-layer 1T-NbS₂ are based on the first-principles calculations. In this section, we will develop the SW potential for the single-layer 1T-NbS₂.

The structure for the single-layer 1T-NbS₂ is shown in Fig. 71 (with M=Nb and X=S). Each Nb atom is surrounded by six S atoms. These S atoms are categorized into the top group (eg. atoms 1, 3, and 5) and bottom group (eg. atoms 2, 4, and 6). Each S atom is connected to three Nb atoms. The structural parameters are from the first-principles calculations,¹² including the lattice constant $a = 3.30 \text{ \AA}$ and the bond length $d_{\text{Nb-S}} = 2.45 \text{ \AA}$.

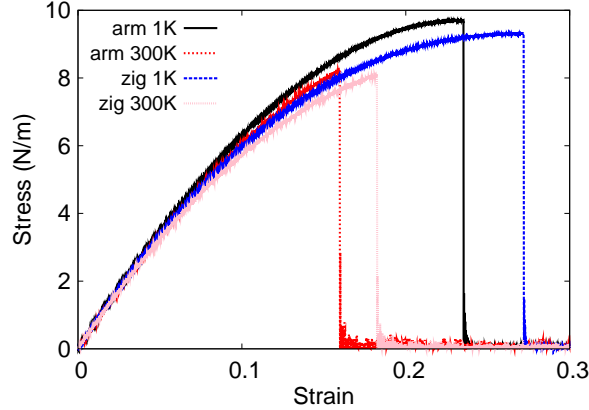


FIG. 117: (Color online) Stress-strain for single-layer 1T-NbS₂ of dimension 100 × 100 Å along the armchair and zigzag directions.

The resultant angles are $\theta_{\text{NbSS}} = 84.671^\circ$ with S atoms from the same (top or bottom) group, and $\theta_{\text{SNbNb}} = 84.671^\circ$.

Table CCXXXIV shows three VFF terms for the single-layer 1T-NbS₂, one of which is the bond stretching interaction shown by Eq. (1) while the other two terms are the angle bending interaction shown by Eq. (2). We note that the angle bending term $K_{\text{Nb-S-S}}$ is for the angle $\theta_{\text{Nb-S-S}}$ with both S atoms from the same (top or bottom) group. These force constant parameters are determined by fitting to the three acoustic branches in the phonon dispersion along the ΓM as shown in Fig. 116 (a). The *ab initio* calculations for the phonon dispersion are from Ref. 12. The lowest acoustic branch (flexural mode) is linear and very close to the inplane transverse acoustic branch in the *ab initio* calculations, which may due to the violation of the rigid rotational invariance.²⁰ Fig. 116 (b) shows that the VFF model and the SW potential give exactly the same phonon dispersion, as the SW potential is derived from the VFF model.

The parameters for the two-body SW potential used by GULP are shown in Tab. CCXXXV. The parameters for the three-body SW potential used by GULP are shown in Tab. CCXXXVI. Some representative parameters for the SW potential used by LAMMPS are listed in Tab. CCXXXVII.

We use LAMMPS to perform MD simulations for the mechanical behavior of the single-layer 1T-NbS₂ under uniaxial tension at 1.0 K and 300.0 K. Fig. 117 shows the stress-strain curve for the tension of a single-layer 1T-NbS₂ of dimension 100 × 100 Å. Periodic boundary

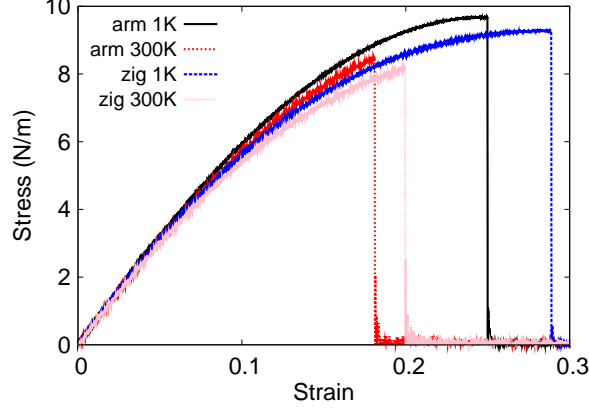


FIG. 118: (Color online) Stress-strain for single-layer 1T-NbSe₂ of dimension $100 \times 100 \text{ \AA}$ along the armchair and zigzag directions.

conditions are applied in both armchair and zigzag directions. The single-layer 1T-NbS₂ is stretched uniaxially along the armchair or zigzag direction. The stress is calculated without involving the actual thickness of the quasi-two-dimensional structure of the single-layer 1T-NbS₂. The Young's modulus can be obtained by a linear fitting of the stress-strain relation in the small strain range of $[0, 0.01]$. The Young's modulus are 73.8 N/m and 73.4 N/m along the armchair and zigzag directions, respectively. The Young's modulus is essentially isotropic in the armchair and zigzag directions. The Poisson's ratio from the VFF model and the SW potential is $\nu_{xy} = \nu_{yx} = 0.18$.

There is no available value for nonlinear quantities in the single-layer 1T-NbS₂. We have thus used the nonlinear parameter $B = 0.5d^4$ in Eq. (5), which is close to the value of B in most materials. The value of the third order nonlinear elasticity D can be extracted by fitting the stress-strain relation to the function $\sigma = E\epsilon + \frac{1}{2}D\epsilon^2$ with E as the Young's modulus. The values of D from the present SW potential are -250.5 N/m and -290.4 N/m along the armchair and zigzag directions, respectively. The ultimate stress is about 9.7 Nm^{-1} at the ultimate strain of 0.23 in the armchair direction at the low temperature of 1 K. The ultimate stress is about 9.4 Nm^{-1} at the ultimate strain of 0.27 in the zigzag direction at the low temperature of 1 K.

TABLE CCXXXVIII: The VFF model for single-layer 1T-NbSe₂. The second line gives an explicit expression for each VFF term. The third line is the force constant parameters. Parameters are in the unit of $\frac{\text{eV}}{\text{\AA}^2}$ for the bond stretching interactions, and in the unit of eV for the angle bending interaction. The fourth line gives the initial bond length (in unit of \AA) for the bond stretching interaction and the initial angle (in unit of degrees) for the angle bending interaction. The angle θ_{ijk} has atom i as the apex.

VFF type	bond stretching	angle bending	
expression	$\frac{1}{2}K_{\text{Nb-Se}}(\Delta r)^2$	$\frac{1}{2}K_{\text{Nb-Se-Se}}(\Delta\theta)^2$	$\frac{1}{2}K_{\text{Se-Nb-Nb}}(\Delta\theta)^2$
parameter	7.930	4.283	4.283
r_0 or θ_0	2.570	82.529	82.529

TABLE CCXXXIX: Two-body SW potential parameters for single-layer 1T-NbSe₂ used by GULP⁸ as expressed in Eq. (3).

	A (eV)	ρ (\AA)	B (\AA^4)	r_{min} (\AA)	r_{max} (\AA)
Nb-Se	6.430	1.104	21.812	0.0	3.412

LX. 1T-NBSE₂

Most existing theoretical studies on the single-layer 1T-NbSe₂ are based on the first-principles calculations. In this section, we will develop the SW potential for the single-layer 1T-NbSe₂.

The structure for the single-layer 1T-NbSe₂ is shown in Fig. 71 (with M=Nb and X=Se). Each Nb atom is surrounded by six Se atoms. These Se atoms are categorized into the top group (eg. atoms 1, 3, and 5) and bottom group (eg. atoms 2, 4, and 6). Each

TABLE CCXL: Three-body SW potential parameters for single-layer 1T-NbSe₂ used by GULP⁸ as expressed in Eq. (4). The angle θ_{ijk} in the first line indicates the bending energy for the angle with atom i as the apex.

	K (eV)	θ_0 (degree)	ρ_1 (\AA)	ρ_2 (\AA)	$r_{\text{min}12}$ (\AA)	$r_{\text{max}12}$ (\AA)	$r_{\text{min}13}$ (\AA)	$r_{\text{max}13}$ (\AA)	$r_{\text{min}23}$ (\AA)	$r_{\text{max}23}$ (\AA)
$\theta_{\text{Nb-Se-Se}}$	29.956	82.528	1.104	1.104	0.0	3.412	0.0	3.412	0.0	4.631
$\theta_{\text{Se-Nb-Nb}}$	29.956	82.528	1.104	1.104	0.0	3.412	0.0	3.412	0.0	4.631

TABLE CCXLI: SW potential parameters for single-layer 1T-NbSe₂ used by LAMMPS⁹ as expressed in Eqs. (9) and (10).

	ϵ (eV)	σ (Å)	a	λ	γ	$\cos \theta_0$	A_L	B_L	p	q	tol
Nb-Se ₁ -Se ₁	1.000	1.104	3.092	29.956	1.000	0.130	6.430	14.706	4	0	0.0

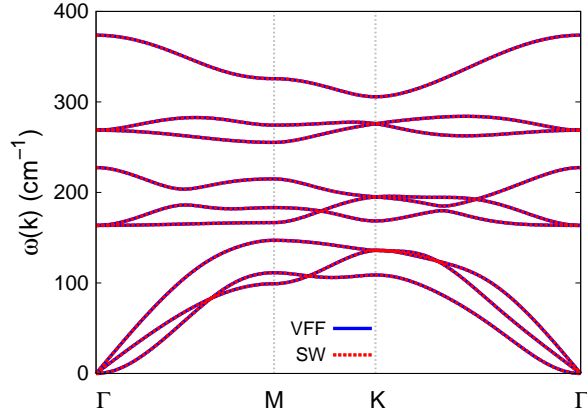


FIG. 119: (Color online) Phonon spectrum for single-layer 1T-NbSe₂ along the Γ MKT direction in the Brillouin zone. The phonon dispersion from the SW potential is exactly the same as that from the VFF model.

Se atom is connected to three Nb atoms. The structural parameters are from the first-principles calculations,¹² including the lattice constant $a = 3.39$ Å and the bond length $d_{\text{Nb-Se}} = 2.57$ Å. The resultant angles are $\theta_{\text{NbSeSe}} = 82.529^\circ$ with Se atoms from the same (top or bottom) group, and $\theta_{\text{SeNbNb}} = 82.529^\circ$.

Table CCXXXVIII shows three VFF terms for the single-layer 1T-NbSe₂, one of which is the bond stretching interaction shown by Eq. (1) while the other two terms are the angle bending interaction shown by Eq. (2). We note that the angle bending term $K_{\text{Nb-Se-Se}}$ is for the angle $\theta_{\text{Nb-Se-Se}}$ with both Se atoms from the same (top or bottom) group. We find that there are actually only two parameters in the VFF model, so we can determine their value by fitting to the Young's modulus and the Poisson's ratio of the system. The *ab initio* calculations have predicted the Young's modulus to be 73 N/m and the Poisson's ratio as 0.20.⁴⁸

The parameters for the two-body SW potential used by GULP are shown in Tab. CCXXXIX. The parameters for the three-body SW potential used by GULP are shown

in Tab. CCXL. Some representative parameters for the SW potential used by LAMMPS are listed in Tab. CCXLI.

We use LAMMPS to perform MD simulations for the mechanical behavior of the single-layer 1T-NbSe₂ under uniaxial tension at 1.0 K and 300.0 K. Fig. 118 shows the stress-strain curve for the tension of a single-layer 1T-NbSe₂ of dimension 100 × 100 Å. Periodic boundary conditions are applied in both armchair and zigzag directions. The single-layer 1T-NbSe₂ is stretched uniaxially along the armchair or zigzag direction. The stress is calculated without involving the actual thickness of the quasi-two-dimensional structure of the single-layer 1T-NbSe₂. The Young's modulus can be obtained by a linear fitting of the stress-strain relation in the small strain range of [0, 0.01]. The Young's modulus are 67.1 N/m and 66.8 N/m along the armchair and zigzag directions, respectively. The Young's modulus is essentially isotropic in the armchair and zigzag directions. The Poisson's ratio from the VFF model and the SW potential is $\nu_{xy} = \nu_{yx} = 0.20$. The fitted Young's modulus value is about 10% smaller than the *ab initio* result of 73 N/m,⁴⁸ as only short-range interactions are considered in the present work. The long-range interactions are ignored, which typically lead to about 10% underestimation for the Young's modulus value.

There is no available value for nonlinear quantities in the single-layer 1T-NbSe₂. We have thus used the nonlinear parameter $B = 0.5d^4$ in Eq. (5), which is close to the value of B in most materials. The value of the third order nonlinear elasticity D can be extracted by fitting the stress-strain relation to the function $\sigma = E\epsilon + \frac{1}{2}D\epsilon^2$ with E as the Young's modulus. The values of D from the present SW potential are -193.5 N/m and -233.4 N/m along the armchair and zigzag directions, respectively. The ultimate stress is about 9.7 Nm⁻¹ at the ultimate strain of 0.25 in the armchair direction at the low temperature of 1 K. The ultimate stress is about 9.3 Nm⁻¹ at the ultimate strain of 0.29 in the zigzag direction at the low temperature of 1 K.

Fig. 119 shows that the VFF model and the SW potential give exactly the same phonon dispersion, as the SW potential is derived from the VFF model.

LXI. 1T-NbTe₂

Most existing theoretical studies on the single-layer 1T-NbTe₂ are based on the first-principles calculations. In this section, we will develop the SW potential for the single-layer

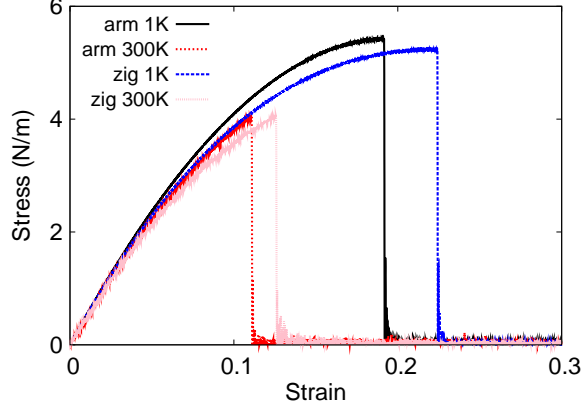


FIG. 120: (Color online) Stress-strain for single-layer 1T-NbTe₂ of dimension $100 \times 100 \text{ \AA}$ along the armchair and zigzag directions.

TABLE CCXLII: The VFF model for single-layer 1T-NbTe₂. The second line gives an explicit expression for each VFF term. The third line is the force constant parameters. Parameters are in the unit of $\frac{eV}{\text{Å}^2}$ for the bond stretching interactions, and in the unit of eV for the angle bending interaction. The fourth line gives the initial bond length (in unit of Å) for the bond stretching interaction and the initial angle (in unit of degrees) for the angle bending interaction. The angle θ_{ijk} has atom i as the apex.

VFF type	bond stretching	angle bending	
expression	$\frac{1}{2}K_{\text{Nb-Te}}(\Delta r)^2$	$\frac{1}{2}K_{\text{Nb-Te-Te}}(\Delta\theta)^2$	$\frac{1}{2}K_{\text{Te-Nb-Nb}}(\Delta\theta)^2$
parameter	3.559	4.863	4.863
r_0 or θ_0	2.770	79.972	79.972

1T-NbTe₂.

The structure for the single-layer 1T-NbTe₂ is shown in Fig. 71 (with M=Nb and X=Te). Each Nb atom is surrounded by six Te atoms. These Te atoms are categorized into the top group (eg. atoms 1, 3, and 5) and bottom group (eg. atoms 2, 4, and 6). Each Te atom is connected to three Nb atoms. The structural parameters are from the first-principles calculations,¹² including the lattice constant $a = 3.56 \text{ \AA}$ and the bond length $d_{\text{Nb-Te}} = 2.77 \text{ \AA}$. The resultant angles are $\theta_{\text{NbTeTe}} = 79.972^\circ$ with Te atoms from the same (top or bottom) group, and $\theta_{\text{TeNbNb}} = 79.972^\circ$.

TABLE CCXLIII: Two-body SW potential parameters for single-layer 1T-NbTe₂ used by GULP⁸ as expressed in Eq. (3).

	A (eV)	ρ (Å)	B (Å ⁴)	r_{\min} (Å)	r_{\max} (Å)
Nb-Te	3.123	1.094	29.437	0.0	3.640

TABLE CCXLIV: Three-body SW potential parameters for single-layer 1T-NbTe₂ used by GULP⁸ as expressed in Eq. (4). The angle θ_{ijk} in the first line indicates the bending energy for the angle with atom i as the apex.

	K (eV)	θ_0 (degree)	ρ_1 (Å)	ρ_2 (Å)	$r_{\min12}$ (Å)	$r_{\max12}$ (Å)	$r_{\min13}$ (Å)	$r_{\max13}$ (Å)	$r_{\min23}$ (Å)	$r_{\max23}$ (Å)
$\theta_{\text{Nb-Te-Te}}$	30.968	79.972	1.094	1.094	0.0	3.640	0.0	3.640	0.0	4.863
$\theta_{\text{Te-Nb-Nb}}$	30.968	79.972	1.094	1.094	0.0	3.640	0.0	3.640	0.0	4.863

Table CCXLII shows three VFF terms for the single-layer 1T-NbTe₂, one of which is the bond stretching interaction shown by Eq. (1) while the other two terms are the angle bending interaction shown by Eq. (2). We note that the angle bending term $K_{\text{Nb-Te-Te}}$ is for the angle $\theta_{\text{Nb-Te-Te}}$ with both Te atoms from the same (top or bottom) group. We find that there are actually only two parameters in the VFF model, so we can determine their value by fitting to the Young's modulus and the Poisson's ratio of the system. The *ab initio* calculations have predicted the Young's modulus to be 56 N/m and the Poisson's ratio as 0.11.⁴⁸

The parameters for the two-body SW potential used by GULP are shown in Tab. CCXLIII. The parameters for the three-body SW potential used by GULP are shown in Tab. CCXLIV. Some representative parameters for the SW potential used by LAMMPS are listed in Tab. CCXLV.

We use LAMMPS to perform MD simulations for the mechanical behavior of the single-layer 1T-NbTe₂ under uniaxial tension at 1.0 K and 300.0 K. Fig. 120 shows the stress-strain

TABLE CCXLV: SW potential parameters for single-layer 1T-NbTe₂ used by LAMMPS⁹ as expressed in Eqs. (9) and (10).

	ϵ (eV)	σ (Å)	a	λ	γ	$\cos \theta_0$	A_L	B_L	p	q	tol
Nb-Te ₁ -Te ₁	1.000	1.094	3.328	30.968	1.000	0.174	3.123	20.560	4	0	0.0

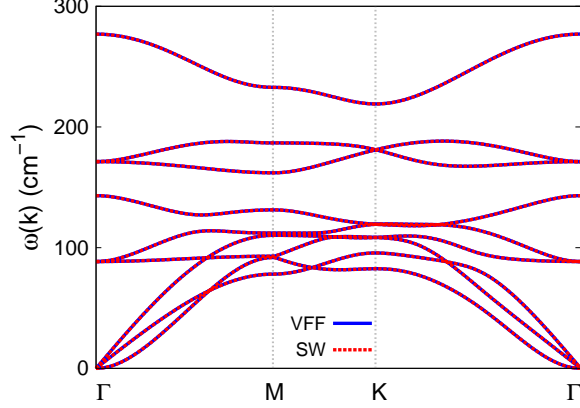


FIG. 121: (Color online) Phonon spectrum for single-layer 1T-NbTe₂ along the Γ MK Γ direction in the Brillouin zone. The phonon dispersion from the SW potential is exactly the same as that from the VFF model.

curve for the tension of a single-layer 1T-NbTe₂ of dimension 100×100 Å. Periodic boundary conditions are applied in both armchair and zigzag directions. The single-layer 1T-NbTe₂ is stretched uniaxially along the armchair or zigzag direction. The stress is calculated without involving the actual thickness of the quasi-two-dimensional structure of the single-layer 1T-NbTe₂. The Young's modulus can be obtained by a linear fitting of the stress-strain relation in the small strain range of $[0, 0.01]$. The Young's modulus are 52.2 N/m and 51.9 N/m along the armchair and zigzag directions, respectively. The Young's modulus is essentially isotropic in the armchair and zigzag directions. The Poisson's ratio from the VFF model and the SW potential is $\nu_{xy} = \nu_{yx} = 0.11$. The fitted Young's modulus value is about 10% smaller than the *ab initio* result of 56 N/m,⁴⁸ as only short-range interactions are considered in the present work. The long-range interactions are ignored, which typically leads to about 10% underestimation for the value of the Young's modulus.

There is no available value for nonlinear quantities in the single-layer 1T-NbTe₂. We have thus used the nonlinear parameter $B = 0.5d^4$ in Eq. (5), which is close to the value of B in most materials. The value of the third order nonlinear elasticity D can be extracted by fitting the stress-strain relation to the function $\sigma = E\epsilon + \frac{1}{2}D\epsilon^2$ with E as the Young's modulus. The values of D from the present SW potential are -237.7 N/m and -265.0 N/m along the armchair and zigzag directions, respectively. The ultimate stress is about 5.4 Nm⁻¹ at the ultimate strain of 0.19 in the armchair direction at the low temperature of 1 K. The

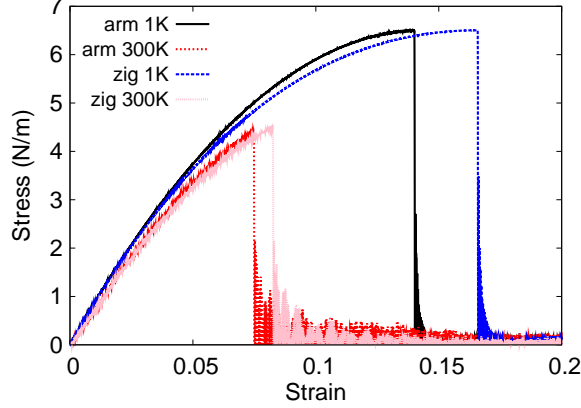


FIG. 122: (Color online) Stress-strain for single-layer 1T-MoS₂ of dimension $100 \times 100 \text{ \AA}$ along the armchair and zigzag directions.

TABLE CCXLVI: The VFF model for single-layer 1T-MoS₂. The second line gives an explicit expression for each VFF term. The third line is the force constant parameters. Parameters are in the unit of $\frac{\text{eV}}{\text{\AA}^2}$ for the bond stretching interactions, and in the unit of eV for the angle bending interaction. The fourth line gives the initial bond length (in unit of \AA) for the bond stretching interaction and the initial angle (in unit of degrees) for the angle bending interaction. The angle θ_{ijk} has atom i as the apex.

VFF type	bond stretching	angle bending	
expression	$\frac{1}{2}K_{\text{Mo-S}}(\Delta r)^2$	$\frac{1}{2}K_{\text{Mo-S-S}}(\Delta\theta)^2$	$\frac{1}{2}K_{\text{S-Mo-Mo}}(\Delta\theta)^2$
parameter	3.523	10.394	10.394
r_0 or θ_0	2.419	82.799	82.799

ultimate stress is about 5.2 Nm^{-1} at the ultimate strain of 0.22 in the zigzag direction at the low temperature of 1 K.

Fig. 121 shows that the VFF model and the SW potential give exactly the same phonon dispersion, as the SW potential is derived from the VFF model.

LXII. 1T-MOS₂

Most existing theoretical studies on the single-layer 1T-MoS₂ are based on the first-principles calculations. In this section, we will develop the SW potential for the single-layer

TABLE CCXLVII: Two-body SW potential parameters for single-layer 1T-MoS₂ used by GULP⁸ as expressed in Eq. (3).

	A (eV)	ρ (Å)	B (Å ⁴)	r_{\min} (Å)	r_{\max} (Å)
Mo-S	2.550	1.048	17.129	0.0	3.215

TABLE CCXLVIII: Three-body SW potential parameters for single-layer 1T-MoS₂ used by GULP⁸ as expressed in Eq. (4). The angle θ_{ijk} in the first line indicates the bending energy for the angle with atom i as the apex.

	K (eV)	θ_0 (degree)	ρ_1 (Å)	ρ_2 (Å)	$r_{\min12}$ (Å)	$r_{\max12}$ (Å)	$r_{\min13}$ (Å)	$r_{\max13}$ (Å)	$r_{\min23}$ (Å)	$r_{\max23}$ (Å)
$\theta_{\text{Mo-S-S}}$	73.436	82.799	1.048	1.048	0.0	3.215	0.0	3.215	0.0	4.371
$\theta_{\text{S-Mo-Mo}}$	73.436	82.799	1.048	1.048	0.0	3.215	0.0	3.215	0.0	4.371

1T-MoS₂.

The structure for the single-layer 1T-MoS₂ is shown in Fig. 71 (with M=Mo and X=S). Each Mo atom is surrounded by six S atoms. These S atoms are categorized into the top group (eg. atoms 1, 3, and 5) and bottom group (eg. atoms 2, 4, and 6). Each S atom is connected to three Mo atoms. The structural parameters are from the first-principles calculations,⁴⁸ including the lattice constant $a = 3.1998$ Å, and the bond length $d_{\text{Mo-S}} = 2.4193$ Å, which is derived from the angle $\theta_{\text{SMoMo}} = 82.8^\circ$. The other angle is $\theta_{\text{MoSS}} = 82.8^\circ$ with S atoms from the same (top or bottom) group.

Table CCXLVI shows three VFF terms for the single-layer 1T-MoS₂, one of which is the bond stretching interaction shown by Eq. (1) while the other two terms are the angle bending interaction shown by Eq. (2). We note that the angle bending term $K_{\text{Mo-S-S}}$ is for the angle $\theta_{\text{Mo-S-S}}$ with both S atoms from the same (top or bottom) group. We find that there are actually only two parameters in the VFF model, so we can determine their value by fitting to the Young's modulus and the Poisson's ratio of the system. The *ab initio*

TABLE CCXLIX: SW potential parameters for single-layer 1T-MoS₂ used by LAMMPS⁹ as expressed in Eqs. (9) and (10).

	ϵ (eV)	σ (Å)	a	λ	γ	$\cos \theta_0$	A_L	B_L	p	q	tol
Mo-S ₁ -S ₁	1.000	1.048	3.069	73.436	1.000	0.125	2.550	14.207	4	0	0.0

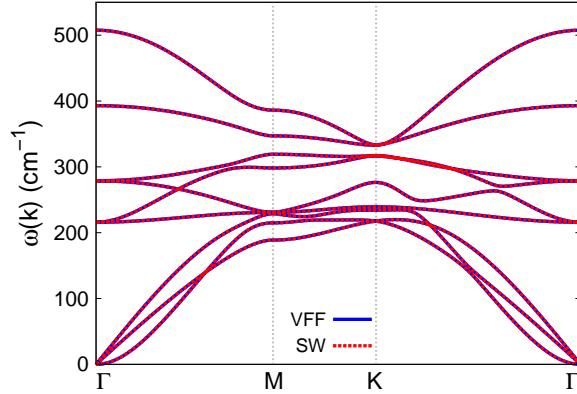


FIG. 123: (Color online) Phonon spectrum for single-layer 1T-MoS₂ along the Γ MK Γ direction in the Brillouin zone. The phonon dispersion from the SW potential is exactly the same as that from the VFF model.

calculations have predicted the Young's modulus to be 103 N/m and the Poisson's ratio as -0.07.⁴⁸ The *ab initio* calculations have predicted a negative Poisson's ratio in the 1T-MoS₂, which was attributed to the orbital coupling in this material. The orbital coupling enhances the angle bending interaction in the VFF model. As a result, the value of the angle bending parameter is much larger than the bond stretching force constant parameter, which is typical in auxetic materials with negative Poisson's ratio.⁵²

The parameters for the two-body SW potential used by GULP are shown in Tab. CCXLVII. The parameters for the three-body SW potential used by GULP are shown in Tab. CCXLVIII. Some representative parameters for the SW potential used by LAMMPS are listed in Tab. CCXLIX.

We use LAMMPS to perform MD simulations for the mechanical behavior of the single-layer 1T-MoS₂ under uniaxial tension at 1.0 K and 300.0 K. Fig. 122 shows the stress-strain curve for the tension of a single-layer 1T-MoS₂ of dimension $100 \times 100 \text{ \AA}$. Periodic boundary conditions are applied in both armchair and zigzag directions. The single-layer 1T-MoS₂ is stretched uniaxially along the armchair or zigzag direction. The stress is calculated without involving the actual thickness of the quasi-two-dimensional structure of the single-layer 1T-MoS₂. The Young's modulus can be obtained by a linear fitting of the stress-strain relation in the small strain range of $[0, 0.01]$. The Young's modulus are 88.7 N/m and 88.3 N/m along the armchair and zigzag directions, respectively. The Young's modulus is essentially

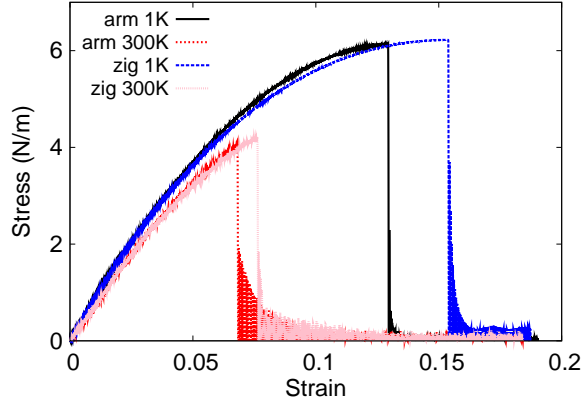


FIG. 124: (Color online) Stress-strain for single-layer 1T-MoSe₂ of dimension $100 \times 100 \text{ \AA}$ along the armchair and zigzag directions.

isotropic in the armchair and zigzag directions. The Poisson's ratio from the VFF model and the SW potential is $\nu_{xy} = \nu_{yx} = -0.07$. The fitted Young's modulus value is about 10% smaller than the *ab initio* result of 103 N/m,⁴⁸ as only short-range interactions are considered in the present work. The long-range interactions are ignored, which typically leads to about 10% underestimation for the value of the Young's modulus.

There is no available value for nonlinear quantities in the single-layer 1T-MoS₂. We have thus used the nonlinear parameter $B = 0.5d^4$ in Eq. (5), which is close to the value of B in most materials. The value of the third order nonlinear elasticity D can be extracted by fitting the stress-strain relation to the function $\sigma = E\epsilon + \frac{1}{2}D\epsilon^2$ with E as the Young's modulus. The values of D from the present SW potential are -595.2 N/m and -624.1 N/m along the armchair and zigzag directions, respectively. The ultimate stress is about 6.5 Nm^{-1} at the ultimate strain of 0.14 in the armchair direction at the low temperature of 1 K. The ultimate stress is about 6.5 Nm^{-1} at the ultimate strain of 0.16 in the zigzag direction at the low temperature of 1 K.

Fig. 123 shows that the VFF model and the SW potential give exactly the same phonon dispersion, as the SW potential is derived from the VFF model.

TABLE CCL: The VFF model for single-layer 1T-MoSe₂. The second line gives an explicit expression for each VFF term. The third line is the force constant parameters. Parameters are in the unit of $\frac{\text{eV}}{\text{\AA}^2}$ for the bond stretching interactions, and in the unit of eV for the angle bending interaction. The fourth line gives the initial bond length (in unit of \AA) for the bond stretching interaction and the initial angle (in unit of degrees) for the angle bending interaction. The angle θ_{ijk} has atom i as the apex.

VFF type	bond stretching	angle bending	
expression	$\frac{1}{2}K_{\text{Mo-Se}}(\Delta r)^2$	$\frac{1}{2}K_{\text{Mo-Se-Se}}(\Delta\theta)^2$	$\frac{1}{2}K_{\text{Se-Mo-Mo}}(\Delta\theta)^2$
parameter	2.964	14.753	14.753
r_0 or θ_0	2.529	80.501	80.501

TABLE CCLI: Two-body SW potential parameters for single-layer 1T-MoSe₂ used by GULP⁸ as expressed in Eq. (3).

	A (eV)	ρ (\AA)	B (\AA^4)	r_{\min} (\AA)	r_{\max} (\AA)
Mo-Se	2.201	1.017	20.463	0.0	3.331

LXIII. 1T-MOSE₂

Most existing theoretical studies on the single-layer 1T-MoSe₂ are based on the first-principles calculations. In this section, we will develop the SW potential for the single-layer 1T-MoSe₂.

The structure for the single-layer 1T-MoSe₂ is shown in Fig. 71 (with M=Mo and X=Se). Each Mo atom is surrounded by six Se atoms. These Se atoms are categorized into the top group (eg. atoms 1, 3, and 5) and bottom group (eg. atoms 2, 4, and 6). Each

TABLE CCLII: Three-body SW potential parameters for single-layer 1T-MoSe₂ used by GULP⁸ as expressed in Eq. (4). The angle θ_{ijk} in the first line indicates the bending energy for the angle with atom i as the apex.

	K (eV)	θ_0 (degree)	ρ_1 (\AA)	ρ_2 (\AA)	$r_{\min12}$ (\AA)	$r_{\max12}$ (\AA)	$r_{\min13}$ (\AA)	$r_{\max13}$ (\AA)	$r_{\min23}$ (\AA)	$r_{\max23}$ (\AA)
$\theta_{\text{Mo-Se-Se}}$	95.770	80.501	1.017	1.017	0.0	3.331	0.0	3.331	0.0	4.465
$\theta_{\text{Se-Mo-Mo}}$	95.770	80.501	1.017	1.017	0.0	3.331	0.0	3.331	0.0	4.465

TABLE CCLIII: SW potential parameters for single-layer 1T-MoSe₂ used by LAMMPS⁹ as expressed in Eqs. (9) and (10).

	ϵ (eV)	σ (Å)	a	λ	γ	$\cos \theta_0$	A_L	B_L	p	q	tol
Mo-Se ₁ -Se ₁	1.000	1.017	3.276	95.770	1.000	0.165	2.201	19.152	4	0	0.0

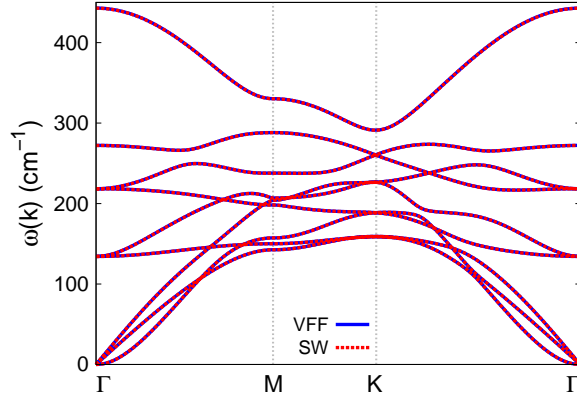


FIG. 125: (Color online) Phonon spectrum for single-layer 1T-MoSe₂ along the Γ MK Γ direction in the Brillouin zone. The phonon dispersion from the SW potential is exactly the same as that from the VFF model.

Se atom is connected to three Mo atoms. The structural parameters are from the first-principles calculations,⁴⁸ including the lattice constant $a = 3.2685$ Å, and the bond length $d_{\text{Mo-Se}} = 2.5293$ Å, which is derived from the angle $\theta_{\text{SeMoMo}} = 80.5^\circ$. The other angle is $\theta_{\text{MoSeSe}} = 80.5^\circ$ with Se atoms from the same (top or bottom) group.

Table CCL shows three VFF terms for the single-layer 1T-MoSe₂, one of which is the bond stretching interaction shown by Eq. (1) while the other two terms are the angle bending interaction shown by Eq. (2). We note that the angle bending term $K_{\text{Mo-Se-Se}}$ is for the angle $\theta_{\text{Mo-Se-Se}}$ with both Se atoms from the same (top or bottom) group. We find that there are actually only two parameters in the VFF model, so we can determine their value by fitting to the Young's modulus and the Poisson's ratio of the system. The *ab initio* calculations have predicted the Young's modulus to be 104 N/m and the Poisson's ratio as -0.13.⁴⁸ The *ab initio* calculations have predicted a negative Poisson's ratio in the 1T-MoSe₂, which was attributed to the orbital coupling in this material. The orbital coupling enhances the angle bending interaction in the VFF model. As a result, the value of the angle bending

parameter is much larger than the bond stretching force constant parameter, which is typical in auxetic materials with negative Poisson’s ratio.⁵²

The parameters for the two-body SW potential used by GULP are shown in Tab. CCLI. The parameters for the three-body SW potential used by GULP are shown in Tab. CCLII. Some representative parameters for the SW potential used by LAMMPS are listed in Tab. CCLIII.

We use LAMMPS to perform MD simulations for the mechanical behavior of the single-layer 1T-MoSe₂ under uniaxial tension at 1.0 K and 300.0 K. Fig. 124 shows the stress-strain curve for the tension of a single-layer 1T-MoSe₂ of dimension 100 × 100 Å. Periodic boundary conditions are applied in both armchair and zigzag directions. The single-layer 1T-MoSe₂ is stretched uniaxially along the armchair or zigzag direction. The stress is calculated without involving the actual thickness of the quasi-two-dimensional structure of the single-layer 1T-MoSe₂. The Young’s modulus can be obtained by a linear fitting of the stress-strain relation in the small strain range of [0, 0.01]. The Young’s modulus are 88.2 N/m and 87.9 N/m along the armchair and zigzag directions, respectively. The Young’s modulus is essentially isotropic in the armchair and zigzag directions. The Poisson’s ratio from the VFF model and the SW potential is $\nu_{xy} = \nu_{yx} = -0.13$. The fitted Young’s modulus value is about 10% smaller than the *ab initio* result of 104 N/m,⁴⁸ as only short-range interactions are considered in the present work. The long-range interactions are ignored, which typically leads to about 10% underestimation for the value of the Young’s modulus.

There is no available value for nonlinear quantities in the single-layer 1T-MoSe₂. We have thus used the nonlinear parameter $B = 0.5d^4$ in Eq. (5), which is close to the value of B in most materials. The value of the third order nonlinear elasticity D can be extracted by fitting the stress-strain relation to the function $\sigma = E\epsilon + \frac{1}{2}D\epsilon^2$ with E as the Young’s modulus. The values of D from the present SW potential are -632.6 N/m and -629.7 N/m along the armchair and zigzag directions, respectively. The ultimate stress is about 6.1 Nm⁻¹ at the ultimate strain of 0.13 in the armchair direction at the low temperature of 1 K. The ultimate stress is about 6.2 Nm⁻¹ at the ultimate strain of 0.15 in the zigzag direction at the low temperature of 1 K.

Fig. 125 shows that the VFF model and the SW potential give exactly the same phonon dispersion, as the SW potential is derived from the VFF model.

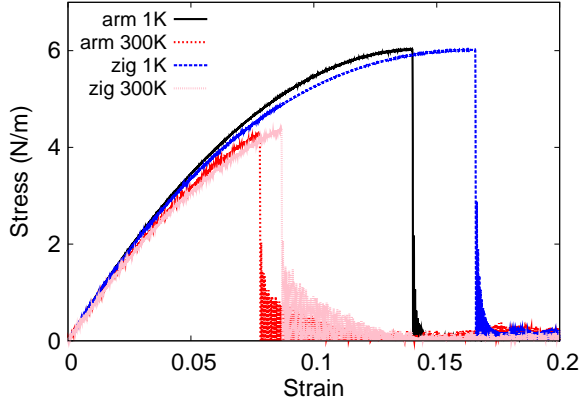


FIG. 126: (Color online) Stress-strain for single-layer 1T-MoTe₂ of dimension $100 \times 100 \text{ \AA}$ along the armchair and zigzag directions.

TABLE CCLIV: The VFF model for single-layer 1T-MoTe₂. The second line gives an explicit expression for each VFF term. The third line is the force constant parameters. Parameters are in the unit of $\frac{\text{eV}}{\text{A}^2}$ for the bond stretching interactions, and in the unit of eV for the angle bending interaction. The fourth line gives the initial bond length (in unit of \AA) for the bond stretching interaction and the initial angle (in unit of degrees) for the angle bending interaction. The angle θ_{ijk} has atom i as the apex.

VFF type	bond stretching	angle bending	
expression	$\frac{1}{2}K_{\text{Mo-Te}}(\Delta r)^2$	$\frac{1}{2}K_{\text{Mo-Te-Te}}(\Delta\theta)^2$	$\frac{1}{2}K_{\text{Te-Mo-Mo}}(\Delta\theta)^2$
parameter	3.074	12.516	12.516
r_0 or θ_0	2.729	79.700	79.700

LXIV. 1T-MOTE₂

Most existing theoretical studies on the single-layer 1T-MoTe₂ are based on the first-principles calculations. In this section, we will develop the SW potential for the single-layer 1T-MoTe₂.

The structure for the single-layer 1T-MoTe₂ is shown in Fig. 71 (with M=Mo and X=Te). Each Mo atom is surrounded by six Te atoms. These Te atoms are categorized into the top group (eg. atoms 1, 3, and 5) and bottom group (eg. atoms 2, 4, and 6). Each Te atom is connected to three Mo atoms. The structural parameters are from the first-

TABLE CCLV: Two-body SW potential parameters for single-layer 1T-MoTe₂ used by GULP⁸ as expressed in Eq. (3).

	A (eV)	ρ (Å)	B (Å ⁴)	r_{\min} (Å)	r_{\max} (Å)
Mo-Te	2.597	1.068	27.720	0.0	3.582

TABLE CCLVI: Three-body SW potential parameters for single-layer 1T-MoTe₂ used by GULP⁸ as expressed in Eq. (4). The angle θ_{ijk} in the first line indicates the bending energy for the angle with atom i as the apex.

	K (eV)	θ_0 (degree)	ρ_1 (Å)	ρ_2 (Å)	$r_{\min12}$ (Å)	$r_{\max12}$ (Å)	$r_{\min13}$ (Å)	$r_{\max13}$ (Å)	$r_{\min23}$ (Å)	$r_{\max23}$ (Å)
$\theta_{\text{Mo-Te-Te}}$	78.925	79.700	1.068	1.068	0.0	3.582	0.0	3.582	0.0	4.777
$\theta_{\text{Te-Mo-Mo}}$	78.925	79.700	1.068	1.068	0.0	3.582	0.0	3.582	0.0	4.777

principles calculations,⁴⁸ including the lattice constant $a = 3.4970$ Å, and the bond length $d_{\text{Mo-Te}} = 2.7287$ Å, which is derived from the angle $\theta_{\text{TeMoMo}} = 79.7^\circ$. The other angle is $\theta_{\text{MoTeTe}} = 79.7^\circ$ with Te atoms from the same (top or bottom) group.

Table CCLIV shows three VFF terms for the single-layer 1T-MoTe₂, one of which is the bond stretching interaction shown by Eq. (1) while the other two terms are the angle bending interaction shown by Eq. (2). We note that the angle bending term $K_{\text{Mo-Te-Te}}$ is for the angle $\theta_{\text{Mo-Te-Te}}$ with both Te atoms from the same (top or bottom) group. We find that there are actually only two parameters in the VFF model, so we can determine their value by fitting to the Young's modulus and the Poisson's ratio of the system. The *ab initio* calculations have predicted the Young's modulus to be 92 N/m and the Poisson's ratio as -0.07.⁴⁸ The *ab initio* calculations have predicted a negative Poisson's ratio in the 1T-MoTe₂, which was attributed to the orbital coupling in this material. The orbital coupling enhances the angle bending interaction in the VFF model. As a result, the value of the angle bending parameter is much larger than the bond stretching force constant parameter, which is typical

TABLE CCLVII: SW potential parameters for single-layer 1T-MoTe₂ used by LAMMPS⁹ as expressed in Eqs. (9) and (10).

	ϵ (eV)	σ (Å)	a	λ	γ	$\cos \theta_0$	A_L	B_L	p	q	tol
Mo-Te ₁ -Te ₁	1.000	1.068	3.355	78.925	1.000	0.179	2.597	21.328	4	0	0.0

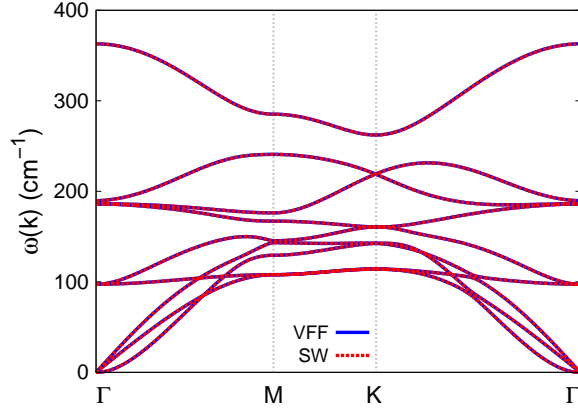


FIG. 127: (Color online) Phonon spectrum for single-layer 1T-MoTe₂ along the Γ MK Γ direction in the Brillouin zone. The phonon dispersion from the SW potential is exactly the same as that from the VFF model.

in auxetic materials with negative Poisson's ratio.⁵²

The parameters for the two-body SW potential used by GULP are shown in Tab. CCLV. The parameters for the three-body SW potential used by GULP are shown in Tab. CCLVI. Some representative parameters for the SW potential used by LAMMPS are listed in Tab. CCLVII.

We use LAMMPS to perform MD simulations for the mechanical behavior of the single-layer 1T-MoTe₂ under uniaxial tension at 1.0 K and 300.0 K. Fig. 126 shows the stress-strain curve for the tension of a single-layer 1T-MoTe₂ of dimension $100 \times 100 \text{ \AA}$. Periodic boundary conditions are applied in both armchair and zigzag directions. The single-layer 1T-MoTe₂ is stretched uniaxially along the armchair or zigzag direction. The stress is calculated without involving the actual thickness of the quasi-two-dimensional structure of the single-layer 1T-MoTe₂. The Young's modulus can be obtained by a linear fitting of the stress-strain relation in the small strain range of $[0, 0.01]$. The Young's modulus are 81.6 N/m and 81.2 N/m along the armchair and zigzag directions, respectively. The Young's modulus is essentially isotropic in the armchair and zigzag directions. The Poisson's ratio from the VFF model and the SW potential is $\nu_{xy} = \nu_{yx} = -0.07$. The fitted Young's modulus value is about 10% smaller than the *ab initio* result of 92 N/m,⁴⁸ as only short-range interactions are considered in the present work. The long-range interactions are ignored, which typically leads to about 10% underestimation for the value of the Young's modulus.

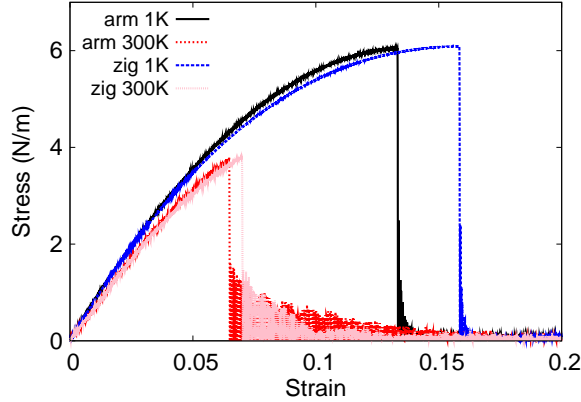


FIG. 128: (Color online) Stress-strain for single-layer 1T-TcS₂ of dimension $100 \times 100 \text{ \AA}$ along the armchair and zigzag directions.

There is no available value for nonlinear quantities in the single-layer 1T-MoTe₂. We have thus used the nonlinear parameter $B = 0.5d^4$ in Eq. (5), which is close to the value of B in most materials. The value of the third order nonlinear elasticity D can be extracted by fitting the stress-strain relation to the function $\sigma = E\epsilon + \frac{1}{2}D\epsilon^2$ with E as the Young's modulus. The values of D from the present SW potential are -543.1 N/m and -558.6 N/m along the armchair and zigzag directions, respectively. The ultimate stress is about 6.0 Nm^{-1} at the ultimate strain of 0.14 in the armchair direction at the low temperature of 1 K. The ultimate stress is about 6.0 Nm^{-1} at the ultimate strain of 0.16 in the zigzag direction at the low temperature of 1 K.

Fig. 127 shows that the VFF model and the SW potential give exactly the same phonon dispersion, as the SW potential is derived from the VFF model.

LXV. 1T-TCS₂

Most existing theoretical studies on the single-layer 1T-TcS₂ are based on the first-principles calculations. In this section, we will develop the SW potential for the single-layer 1T-TcS₂.

The structure for the single-layer 1T-TcS₂ is shown in Fig. 71 (with M=Tc and X=S). Each Tc atom is surrounded by six S atoms. These S atoms are categorized into the top group (eg. atoms 1, 3, and 5) and bottom group (eg. atoms 2, 4, and 6). Each S atom is connected

TABLE CCLVIII: The VFF model for single-layer 1T-TcS₂. The second line gives an explicit expression for each VFF term. The third line is the force constant parameters. Parameters are in the unit of $\frac{\text{eV}}{\text{\AA}^2}$ for the bond stretching interactions, and in the unit of eV for the angle bending interaction. The fourth line gives the initial bond length (in unit of \AA) for the bond stretching interaction and the initial angle (in unit of degrees) for the angle bending interaction. The angle θ_{ijk} has atom i as the apex.

VFF type	bond stretching	angle bending	
expression	$\frac{1}{2}K_{\text{Tc-S}}(\Delta r)^2$	$\frac{1}{2}K_{\text{Tc-S-S}}(\Delta\theta)^2$	$\frac{1}{2}K_{\text{S-Tc-Tc}}(\Delta\theta)^2$
parameter	2.986	11.141	11.141
r_0 or θ_0	2.392	79.800	79.800

TABLE CCLIX: Two-body SW potential parameters for single-layer 1T-TcS₂ used by GULP⁸ as expressed in Eq. (3).

	A (eV)	ρ (\AA)	B (\AA^4)	r_{min} (\AA)	r_{max} (\AA)
Tc-S	1.945	0.939	16.380	0.0	3.142

to three Tc atoms. The structural parameters are from the first-principles calculations,⁴⁸ including the lattice constant $a = 3.0692 \text{ \AA}$, and the bond length $d_{\text{Tc-S}} = 2.3924 \text{ \AA}$, which is derived from the angle $\theta_{\text{STcTc}} = 79.8^\circ$. The other angle is $\theta_{\text{TcSS}} = 79.8^\circ$ with S atoms from the same (top or bottom) group.

Table CCLVIII shows three VFF terms for the single-layer 1T-TcS₂, one of which is the bond stretching interaction shown by Eq. (1) while the other two terms are the angle bending interaction shown by Eq. (2). We note that the angle bending term $K_{\text{Tc-S-S}}$ is for the angle

TABLE CCLX: Three-body SW potential parameters for single-layer 1T-TcS₂ used by GULP⁸ as expressed in Eq. (4). The angle θ_{ijk} in the first line indicates the bending energy for the angle with atom i as the apex.

	K (eV)	θ_0 (degree)	ρ_1 (\AA)	ρ_2 (\AA)	r_{min12} (\AA)	r_{max12} (\AA)	r_{min13} (\AA)	r_{max13} (\AA)	r_{min23} (\AA)	r_{max23} (\AA)
$\theta_{\text{Tc-S-S}}$	70.512	79.800	0.939	0.939	0.0	3.142	0.0	3.142	0.0	4.193
$\theta_{\text{S-Tc-Tc}}$	70.512	79.800	0.939	0.939	0.0	3.142	0.0	3.142	0.0	4.193

TABLE CCLXI: SW potential parameters for single-layer 1T-TcS₂ used by LAMMPS⁹ as expressed in Eqs. (9) and (10).

	ϵ (eV)	σ (Å)	a	λ	γ	$\cos \theta_0$	A_L	B_L	p	q	tol
Tc-S ₁ -S ₁	1.000	0.939	3.345	70.512	1.000	0.177	1.945	21.038	4	0	0.0

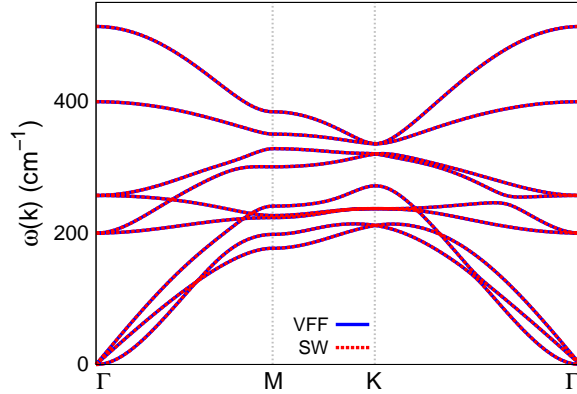


FIG. 129: (Color online) Phonon spectrum for single-layer 1T-TcS₂ along the Γ MK Γ direction in the Brillouin zone. The phonon dispersion from the SW potential is exactly the same as that from the VFF model.

$\theta_{\text{Tc-S-S}}$ with both S atoms from the same (top or bottom) group. We find that there are actually only two parameters in the VFF model, so we can determine their value by fitting to the Young's modulus and the Poisson's ratio of the system. The *ab initio* calculations have predicted the Young's modulus to be 94 N/m and the Poisson's ratio as -0.10.⁴⁸ The *ab initio* calculations have predicted a negative Poisson's ratio in the 1T-TcS₂, which was attributed to the orbital coupling in this material. The orbital coupling enhances the angle bending interaction in the VFF model. As a result, the value of the angle bending parameter is much larger than the bond stretching force constant parameter, which is typical in auxetic materials with negative Poisson's ratio.⁵²

The parameters for the two-body SW potential used by GULP are shown in Tab. CCLIX. The parameters for the three-body SW potential used by GULP are shown in Tab. CCLX. Some representative parameters for the SW potential used by LAMMPS are listed in Tab. CCLXI.

We use LAMMPS to perform MD simulations for the mechanical behavior of the single-

layer 1T-TcS₂ under uniaxial tension at 1.0 K and 300.0 K. Fig. 128 shows the stress-strain curve for the tension of a single-layer 1T-TcS₂ of dimension 100 × 100 Å. Periodic boundary conditions are applied in both armchair and zigzag directions. The single-layer 1T-TcS₂ is stretched uniaxially along the armchair or zigzag direction. The stress is calculated without involving the actual thickness of the quasi-two-dimensional structure of the single-layer 1T-TcS₂. The Young's modulus can be obtained by a linear fitting of the stress-strain relation in the small strain range of [0, 0.01]. The Young's modulus are 84.3 N/m and 84.0 N/m along the armchair and zigzag directions, respectively. The Young's modulus is essentially isotropic in the armchair and zigzag directions. The Poisson's ratio from the VFF model and the SW potential is $\nu_{xy} = \nu_{yx} = -0.10$. The fitted Young's modulus value is about 10% smaller than the *ab initio* result of 94 N/m,⁴⁸ as only short-range interactions are considered in the present work. The long-range interactions are ignored, which typically leads to about 10% underestimation for the value of the Young's modulus.

There is no available value for nonlinear quantities in the single-layer 1T-TcS₂. We have thus used the nonlinear parameter $B = 0.5d^4$ in Eq. (5), which is close to the value of B in most materials. The value of the third order nonlinear elasticity D can be extracted by fitting the stress-strain relation to the function $\sigma = E\epsilon + \frac{1}{2}D\epsilon^2$ with E as the Young's modulus. The values of D from the present SW potential are -572.0 N/m and -588.6 N/m along the armchair and zigzag directions, respectively. The ultimate stress is about 6.0 Nm⁻¹ at the ultimate strain of 0.13 in the armchair direction at the low temperature of 1 K. The ultimate stress is about 6.1 Nm⁻¹ at the ultimate strain of 0.16 in the zigzag direction at the low temperature of 1 K.

Fig. 129 shows that the VFF model and the SW potential give exactly the same phonon dispersion, as the SW potential is derived from the VFF model.

LXVI. 1T-TCSE₂

Most existing theoretical studies on the single-layer 1T-TcSe₂ are based on the first-principles calculations. In this section, we will develop the SW potential for the single-layer 1T-TcSe₂.

The structure for the single-layer 1T-TcSe₂ is shown in Fig. 71 (with M=Tc and X=Se). Each Tc atom is surrounded by six Se atoms. These Se atoms are categorized into the

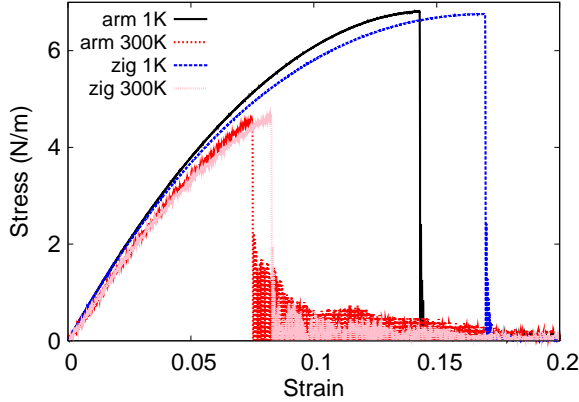


FIG. 130: (Color online) Stress-strain for single-layer 1T-TcSe₂ of dimension $100 \times 100 \text{ \AA}$ along the armchair and zigzag directions.

TABLE CCLXII: The VFF model for single-layer 1T-TcSe₂. The second line gives an explicit expression for each VFF term. The third line is the force constant parameters. Parameters are in the unit of $\frac{eV}{\text{Å}^2}$ for the bond stretching interactions, and in the unit of eV for the angle bending interaction. The fourth line gives the initial bond length (in unit of Å) for the bond stretching interaction and the initial angle (in unit of degrees) for the angle bending interaction. The angle θ_{ijk} has atom *i* as the apex.

VFF type	bond stretching	angle bending	
expression	$\frac{1}{2}K_{\text{Tc-Se}}(\Delta r)^2$	$\frac{1}{2}K_{\text{Tc-Se-Se}}(\Delta\theta)^2$	$\frac{1}{2}K_{\text{Se-Tc-Tc}}(\Delta\theta)^2$
parameter	3.467	10.636	10.636
r_0 or θ_0	2.506	78.001	78.001

top group (eg. atoms 1, 3, and 5) and bottom group (eg. atoms 2, 4, and 6). Each Se atom is connected to three Tc atoms. The structural parameters are from the first-principles calculations,⁴⁸ including the lattice constant $a = 3.1543 \text{ \AA}$, and the bond length $d_{\text{Tc-Se}} = 2.5061 \text{ \AA}$, which is derived from the angle $\theta_{\text{SeTcTc}} = 78^\circ$. The other angle is $\theta_{\text{TcSeSe}} = 78^\circ$ with Se atoms from the same (top or bottom) group.

Table CCLXII shows three VFF terms for the single-layer 1T-TcSe₂, one of which is the bond stretching interaction shown by Eq. (1) while the other two terms are the angle bending interaction shown by Eq. (2). We note that the angle bending term $K_{\text{Tc-Se-Se}}$ is

TABLE CCLXIII: Two-body SW potential parameters for single-layer 1T-TcSe₂ used by GULP⁸ as expressed in Eq. (3).

	A (eV)	ρ (Å)	B (Å ⁴)	r_{\min} (Å)	r_{\max} (Å)
Tc-Se	2.355	0.925	19.723	0.0	3.267

TABLE CCLXIV: Three-body SW potential parameters for single-layer 1T-TcSe₂ used by GULP⁸ as expressed in Eq. (4). The angle θ_{ijk} in the first line indicates the bending energy for the angle with atom i as the apex.

	K (eV)	θ_0 (degree)	ρ_1 (Å)	ρ_2 (Å)	$r_{\min12}$ (Å)	$r_{\max12}$ (Å)	$r_{\min13}$ (Å)	$r_{\max13}$ (Å)	$r_{\min23}$ (Å)	$r_{\max23}$ (Å)
$\theta_{\text{Tc-Se-Se}}$	63.150	78.001	0.925	0.925	0.0	3.267	0.0	3.267	0.0	4.309
$\theta_{\text{Se-Tc-Tc}}$	63.150	78.001	0.925	0.925	0.0	3.267	0.0	3.267	0.0	4.309

for the angle $\theta_{\text{Tc-Se-Se}}$ with both Se atoms from the same (top or bottom) group. We find that there are actually only two parameters in the VFF model, so we can determine their value by fitting to the Young's modulus and the Poisson's ratio of the system. The *ab initio* calculations have predicted the Young's modulus to be 104 N/m and the Poisson's ratio as -0.04.⁴⁸ The *ab initio* calculations have predicted a negative Poisson's ratio in the 1T-TcSe₂, which was attributed to the orbital coupling in this material. The orbital coupling enhances the angle bending interaction in the VFF model. As a result, the value of the angle bending parameter is much larger than the bond stretching force constant parameter, which is typical in auxetic materials with negative Poisson's ratio.⁵²

The parameters for the two-body SW potential used by GULP are shown in Tab. CCLXIII. The parameters for the three-body SW potential used by GULP are shown in Tab. CCLXIV. Some representative parameters for the SW potential used by LAMMPS are listed in Tab. CCLXV.

We use LAMMPS to perform MD simulations for the mechanical behavior of the single-

TABLE CCLXV: SW potential parameters for single-layer 1T-TcSe₂ used by LAMMPS⁹ as expressed in Eqs. (9) and (10).

	ϵ (eV)	σ (Å)	a	λ	γ	$\cos \theta_0$	A_L	B_L	p	q	tol
Tc-Se ₁ -Se ₁	1.000	0.925	3.532	63.150	1.000	0.208	2.355	26.932	4	0	0.0

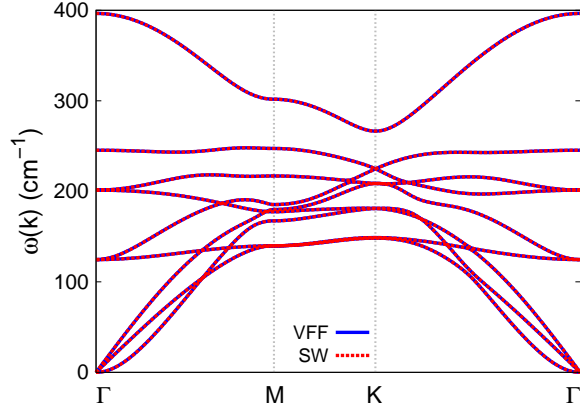


FIG. 131: (Color online) Phonon spectrum for single-layer 1T-TcSe₂ along the Γ MK Γ direction in the Brillouin zone. The phonon dispersion from the SW potential is exactly the same as that from the VFF model.

layer 1T-TcSe₂ under uniaxial tension at 1.0 K and 300.0 K. Fig. 130 shows the stress-strain curve for the tension of a single-layer 1T-TcSe₂ of dimension 100×100 Å. Periodic boundary conditions are applied in both armchair and zigzag directions. The single-layer 1T-TcSe₂ is stretched uniaxially along the armchair or zigzag direction. The stress is calculated without involving the actual thickness of the quasi-two-dimensional structure of the single-layer 1T-TcSe₂. The Young's modulus can be obtained by a linear fitting of the stress-strain relation in the small strain range of $[0, 0.01]$. The Young's modulus are 88.8 N/m and 88.3 N/m along the armchair and zigzag directions, respectively. The Young's modulus is essentially isotropic in the armchair and zigzag directions. The Poisson's ratio from the VFF model and the SW potential is $\nu_{xy} = \nu_{yx} = -0.04$. The fitted Young's modulus value is about 10% smaller than the *ab initio* result of 104 N/m,⁴⁸ as only short-range interactions are considered in the present work. The long-range interactions are ignored, which typically leads to about 10% underestimation for the value of the Young's modulus.

There is no available value for nonlinear quantities in the single-layer 1T-TcSe₂. We have thus used the nonlinear parameter $B = 0.5d^4$ in Eq. (5), which is close to the value of B in most materials. The value of the third order nonlinear elasticity D can be extracted by fitting the stress-strain relation to the function $\sigma = E\epsilon + \frac{1}{2}D\epsilon^2$ with E as the Young's modulus. The values of D from the present SW potential are -565.7 N/m and -587.3 N/m along the armchair and zigzag directions, respectively. The ultimate stress is about 6.8 Nm^{-1}

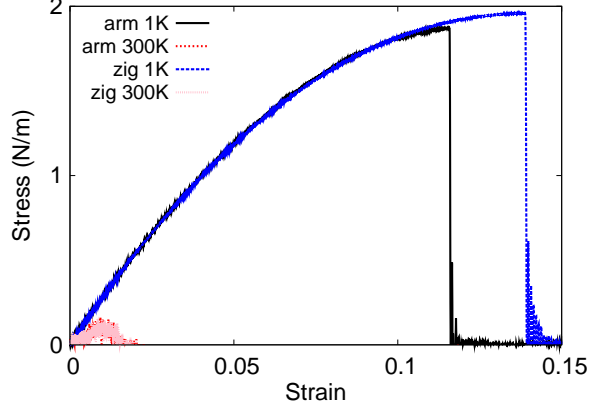


FIG. 132: (Color online) Stress-strain for single-layer 1T-TcTe₂ of dimension $100 \times 100 \text{ \AA}$ along the armchair and zigzag directions.

TABLE CCLXVI: The VFF model for single-layer 1T-TcTe₂. The second line gives an explicit expression for each VFF term. The third line is the force constant parameters. Parameters are in the unit of $\frac{\text{eV}}{\text{\AA}^2}$ for the bond stretching interactions, and in the unit of eV for the angle bending interaction. The fourth line gives the initial bond length (in unit of \AA) for the bond stretching interaction and the initial angle (in unit of degrees) for the angle bending interaction. The angle θ_{ijk} has atom i as the apex.

VFF type	bond stretching	angle bending	
expression	$\frac{1}{2}K_{\text{Tc-Te}}(\Delta r)^2$	$\frac{1}{2}K_{\text{Tc-Te-Te}}(\Delta\theta)^2$	$\frac{1}{2}K_{\text{Te-Te-Tc}}(\Delta\theta)^2$
parameter	0.785	8.894	8.894
r_0 or θ_0	2.690	78.801	78.801

at the ultimate strain of 0.14 in the armchair direction at the low temperature of 1 K. The ultimate stress is about 6.8 Nm^{-1} at the ultimate strain of 0.17 in the zigzag direction at the low temperature of 1 K.

Fig. 131 shows that the VFF model and the SW potential give exactly the same phonon dispersion, as the SW potential is derived from the VFF model.

TABLE CCLXVII: Two-body SW potential parameters for single-layer 1T-TcTe₂ used by GULP⁸ as expressed in Eq. (3).

	A (eV)	ρ (Å)	B (Å ⁴)	r_{\min} (Å)	r_{\max} (Å)
Tc-Te	0.628	1.021	26.181	0.0	3.519

TABLE CCLXVIII: Three-body SW potential parameters for single-layer 1T-TcTe₂ used by GULP⁸ as expressed in Eq. (4). The angle θ_{ijk} in the first line indicates the bending energy for the angle with atom i as the apex.

	K (eV)	θ_0 (degree)	ρ_1 (Å)	ρ_2 (Å)	$r_{\min12}$ (Å)	$r_{\max12}$ (Å)	$r_{\min13}$ (Å)	$r_{\max13}$ (Å)	$r_{\min23}$ (Å)	$r_{\max23}$ (Å)
$\theta_{\text{Tc-Te-Te}}$	54.313	78.801	1.021	1.021	0.0	3.519	0.0	3.519	0.0	4.665
$\theta_{\text{Te-Tc-Tc}}$	54.313	78.801	1.021	1.021	0.0	3.519	0.0	3.519	0.0	4.665

LXVII. 1T-TCTE₂

Most existing theoretical studies on the single-layer 1T-TcTe₂ are based on the first-principles calculations. In this section, we will develop the SW potential for the single-layer 1T-TcTe₂.

The structure for the single-layer 1T-TcTe₂ is shown in Fig. 71 (with M=Tc and X=Te). Each Tc atom is surrounded by six Te atoms. These Te atoms are categorized into the top group (eg. atoms 1, 3, and 5) and bottom group (eg. atoms 2, 4, and 6). Each Te atom is connected to three Tc atoms. The structural parameters are from the first-principles calculations,⁴⁸ including the lattice constant $a = 3.4149$ Å, and the bond length $d_{\text{Tc-Te}} = 2.6900$ Å, which is derived from the angle $\theta_{\text{TeTcTe}} = 78.8^\circ$. The other angle is $\theta_{\text{TcTeTe}} = 78.8^\circ$ with Te atoms from the same (top or bottom) group.

Table CCLXVI shows three VFF terms for the single-layer 1T-TcTe₂, one of which is the bond stretching interaction shown by Eq. (1) while the other two terms are the angle

TABLE CCLXIX: SW potential parameters for single-layer 1T-TcTe₂ used by LAMMPS⁹ as expressed in Eqs. (9) and (10).

	ϵ (eV)	σ (Å)	a	λ	γ	$\cos \theta_0$	A_L	B_L	p	q	tol
Tc-Te ₁ -Te ₁	1.000	1.021	3.447	54.313	1.000	0.194	0.628	24.110	4	0	0.0

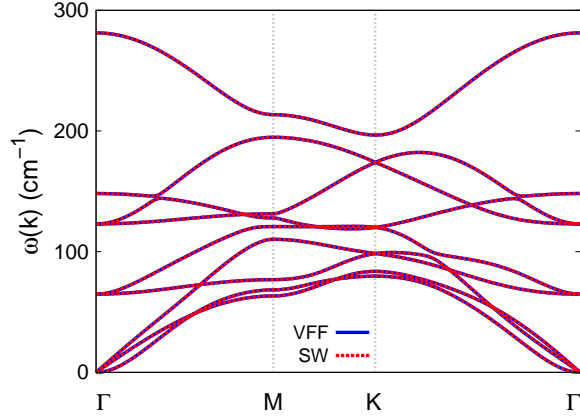


FIG. 133: (Color online) Phonon spectrum for single-layer 1T-TcTe₂ along the Γ MKT direction in the Brillouin zone. The phonon dispersion from the SW potential is exactly the same as that from the VFF model.

bending interaction shown by Eq. (2). We note that the angle bending term $K_{\text{Tc-Te-Te}}$ is for the angle $\theta_{\text{Tc-Te-Te}}$ with both Te atoms from the same (top or bottom) group. We find that there are actually only two parameters in the VFF model, so we can determine their value by fitting to the Young's modulus and the Poisson's ratio of the system. The *ab initio* calculations have predicted the Young's modulus to be 34 N/m and the Poisson's ratio as -0.36.⁴⁸ The *ab initio* calculations have predicted a negative Poisson's ratio in the 1T-TcTe₂, which was attributed to the orbital coupling in this material. The orbital coupling enhances the angle bending interaction in the VFF model. As a result, the value of the angle bending parameter is much larger than the bond stretching force constant parameter, which is typical in auxetic materials with negative Poisson's ratio.⁵²

The parameters for the two-body SW potential used by GULP are shown in Tab. CCLXVII. The parameters for the three-body SW potential used by GULP are shown in Tab. CCLXVIII. Some representative parameters for the SW potential used by LAMMPS are listed in Tab. CCLXIX.

We use LAMMPS to perform MD simulations for the mechanical behavior of the single-layer 1T-TcTe₂ under uniaxial tension at 1.0 K and 300.0 K. Fig. 132 shows the stress-strain curve for the tension of a single-layer 1T-TcTe₂ of dimension $100 \times 100 \text{ \AA}$. Periodic boundary conditions are applied in both armchair and zigzag directions. The single-layer 1T-TcTe₂ is stretched uniaxially along the armchair or zigzag direction. The stress is calculated without

involving the actual thickness of the quasi-two-dimensional structure of the single-layer 1T-TcTe₂. The Young's modulus can be obtained by a linear fitting of the stress-strain relation in the small strain range of [0, 0.01]. The Young's modulus is 28.6 N/m along the armchair and zigzag directions. The Poisson's ratio from the VFF model and the SW potential is $\nu_{xy} = \nu_{yx} = -0.21$. The fitted Young's modulus value is about 10% smaller than the *ab initio* result of 34 N/m,⁴⁸ as only short-range interactions are considered in the present work. The long-range interactions are ignored, which typically leads to about 10% underestimation for the value of the Young's modulus.

There is no available value for nonlinear quantities in the single-layer 1T-TcTe₂. We have thus used the nonlinear parameter $B = 0.5d^4$ in Eq. (5), which is close to the value of B in most materials. The value of the third order nonlinear elasticity D can be extracted by fitting the stress-strain relation to the function $\sigma = E\epsilon + \frac{1}{2}D\epsilon^2$ with E as the Young's modulus. The values of D from the present SW potential are -207.8 N/m and -208.7 N/m along the armchair and zigzag directions, respectively. The ultimate stress is about 1.9 Nm⁻¹ at the ultimate strain of 0.11 in the armchair direction at the low temperature of 1 K. The ultimate stress is about 2.0 Nm⁻¹ at the ultimate strain of 0.14 in the zigzag direction at the low temperature of 1 K. The ultimate strain decreases to be about 0.01 at 300 K, so the single-layer 1T-TcTe₂ is not very stable at higher temperature. It is because this material is very soft and the Poisson's ratio is very small (negative value).

Fig. 133 shows that the VFF model and the SW potential give exactly the same phonon dispersion, as the SW potential is derived from the VFF model.

LXVIII. 1T-RHTE₂

Most existing theoretical studies on the single-layer 1T-RhTe₂ are based on the first-principles calculations. In this section, we will develop the SW potential for the single-layer 1T-RhTe₂.

The structure for the single-layer 1T-RhTe₂ is shown in Fig. 71 (with M=Rh and X=Te). Each Rh atom is surrounded by six Te atoms. These Te atoms are categorized into the top group (eg. atoms 1, 3, and 5) and bottom group (eg. atoms 2, 4, and 6). Each Te atom is connected to three Rh atoms. The structural parameters are from the first-principles calculations,⁴⁸ including the lattice constant $a = 3.7563 \text{ \AA}$, and the bond length

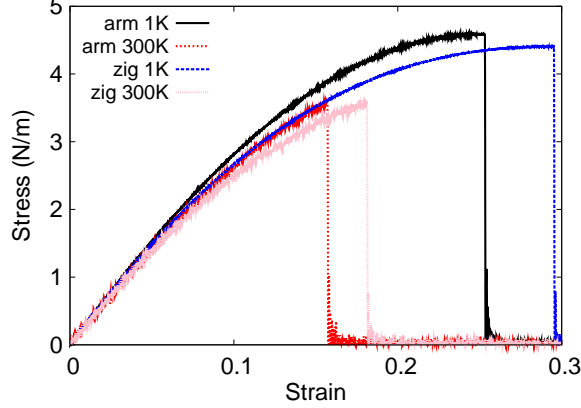


FIG. 134: (Color online) Stress-strain for single-layer 1T-RhTe₂ of dimension $100 \times 100 \text{ \AA}$ along the armchair and zigzag directions.

TABLE CCLXX: The VFF model for single-layer 1T-RhTe₂. The second line gives an explicit expression for each VFF term. The third line is the force constant parameters. Parameters are in the unit of $\frac{eV}{\text{Å}^2}$ for the bond stretching interactions, and in the unit of eV for the angle bending interaction. The fourth line gives the initial bond length (in unit of Å) for the bond stretching interaction and the initial angle (in unit of degrees) for the angle bending interaction. The angle θ_{ijk} has atom i as the apex.

VFF type	bond stretching	angle bending	
expression	$\frac{1}{2}K_{\text{Rh-Te}}(\Delta r)^2$	$\frac{1}{2}K_{\text{Rh-Te-Te}}(\Delta\theta)^2$	$\frac{1}{2}K_{\text{Te-Rh-Rh}}(\Delta\theta)^2$
parameter	4.366	1.869	1.869
r_0 or θ_0	2.633	91.001	91.001

$d_{\text{Rh-Te}} = 2.6332 \text{ \AA}$, which is derived from the angle $\theta_{\text{TeRhRh}} = 91^\circ$. The other angle is $\theta_{\text{RhTeTe}} = 91^\circ$ with Te atoms from the same (top or bottom) group.

Table CCLXX shows three VFF terms for the single-layer 1T-RhTe₂, one of which is the bond stretching interaction shown by Eq. (1) while the other two terms are the angle bending interaction shown by Eq. (2). We note that the angle bending term $K_{\text{Rh-Te-Te}}$ is for the angle $\theta_{\text{Rh-Te-Te}}$ with both Te atoms from the same (top or bottom) group. We find that there are actually only two parameters in the VFF model, so we can determine their value by fitting to the Young's modulus and the Poisson's ratio of the system. The *ab initio*

TABLE CCLXXI: Two-body SW potential parameters for single-layer 1T-RhTe₂ used by GULP⁸ as expressed in Eq. (3).

	A (eV)	ρ (Å)	B (Å ⁴)	r_{\min} (Å)	r_{\max} (Å)
Rh-Te	4.640	1.450	24.038	0.0	3.610

TABLE CCLXXII: Three-body SW potential parameters for single-layer 1T-RhTe₂ used by GULP⁸ as expressed in Eq. (4). The angle θ_{ijk} in the first line indicates the bending energy for the angle with atom i as the apex.

	K (eV)	θ_0 (degree)	ρ_1 (Å)	ρ_2 (Å)	$r_{\min12}$ (Å)	$r_{\max12}$ (Å)	$r_{\min13}$ (Å)	$r_{\max13}$ (Å)	$r_{\min23}$ (Å)	$r_{\max23}$ (Å)
$\theta_{\text{Rh-Te-Te}}$	18.192	91.001	1.450	1.450	0.0	3.610	0.0	3.610	0.0	5.131
$\theta_{\text{Te-Rh-Rh}}$	18.192	91.001	1.450	1.450	0.0	3.610	0.0	3.610	0.0	5.131

calculations have predicted the Young's modulus to be 37 N/m and the Poisson's ratio as 0.20.⁴⁸

The parameters for the two-body SW potential used by GULP are shown in Tab. CCLXXI. The parameters for the three-body SW potential used by GULP are shown in Tab. CCLXXII. Some representative parameters for the SW potential used by LAMMPS are listed in Tab. CCLXXIII.

We use LAMMPS to perform MD simulations for the mechanical behavior of the single-layer 1T-RhTe₂ under uniaxial tension at 1.0 K and 300.0 K. Fig. 134 shows the stress-strain curve for the tension of a single-layer 1T-RhTe₂ of dimension 100×100 Å. Periodic boundary conditions are applied in both armchair and zigzag directions. The single-layer 1T-RhTe₂ is stretched uniaxially along the armchair or zigzag direction. The stress is calculated without involving the actual thickness of the quasi-two-dimensional structure of the single-layer 1T-RhTe₂. The Young's modulus can be obtained by a linear fitting of the stress-strain relation in the small strain range of $[0, 0.01]$. The Young's modulus are 32.1 N/m and 32.0 N/m

TABLE CCLXXIII: SW potential parameters for single-layer 1T-RhTe₂ used by LAMMPS⁹ as expressed in Eqs. (9) and (10).

	ϵ (eV)	σ (Å)	a	λ	γ	$\cos \theta_0$	A_L	B_L	p	q	tol
Rh-Te ₁ -Te ₁	1.000	1.450	2.490	18.192	1.000	-0.017	4.640	5.436	4	0	0.0

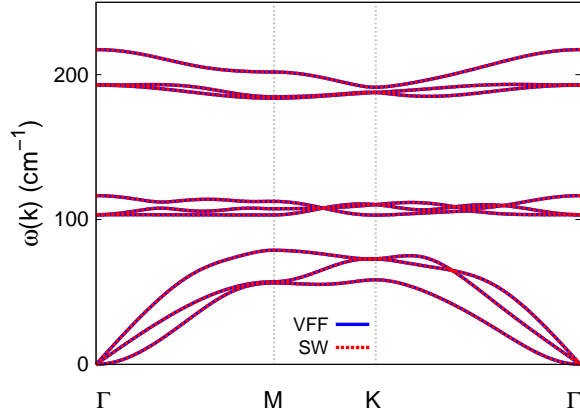


FIG. 135: (Color online) Phonon spectrum for single-layer 1T-RhTe₂ along the Γ MK Γ direction in the Brillouin zone. The phonon dispersion from the SW potential is exactly the same as that from the VFF model.

along the armchair and zigzag directions, respectively. The Young's modulus is essentially isotropic in the armchair and zigzag directions. The Poisson's ratio from the VFF model and the SW potential is $\nu_{xy} = \nu_{yx} = 0.20$. The fitted Young's modulus value is about 10% smaller than the *ab initio* result of 37 N/m,⁴⁸ as only short-range interactions are considered in the present work. The long-range interactions are ignored, which typically leads to about 10% underestimation for the value of the Young's modulus.

There is no available value for nonlinear quantities in the single-layer 1T-RhTe₂. We have thus used the nonlinear parameter $B = 0.5d^4$ in Eq. (5), which is close to the value of B in most materials. The value of the third order nonlinear elasticity D can be extracted by fitting the stress-strain relation to the function $\sigma = E\epsilon + \frac{1}{2}D\epsilon^2$ with E as the Young's modulus. The values of D from the present SW potential are -103.1 N/m and -116.5 N/m along the armchair and zigzag directions, respectively. The ultimate stress is about 4.6 Nm⁻¹ at the ultimate strain of 0.25 in the armchair direction at the low temperature of 1 K. The ultimate stress is about 4.4 Nm⁻¹ at the ultimate strain of 0.29 in the zigzag direction at the low temperature of 1 K.

Fig. 135 shows that the VFF model and the SW potential give exactly the same phonon dispersion, as the SW potential is derived from the VFF model.

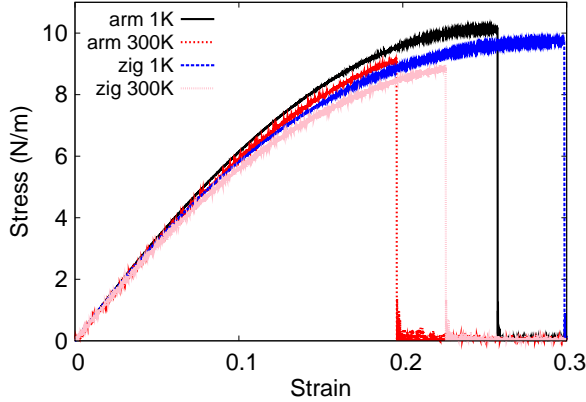


FIG. 136: (Color online) Stress-strain for single-layer 1T-PdS₂ of dimension $100 \times 100 \text{ \AA}$ along the armchair and zigzag directions.

TABLE CCLXXIV: The VFF model for single-layer 1T-PdS₂. The second line gives an explicit expression for each VFF term. The third line is the force constant parameters. Parameters are in the unit of $\frac{\text{eV}}{\text{\AA}^2}$ for the bond stretching interactions, and in the unit of eV for the angle bending interaction. The fourth line gives the initial bond length (in unit of \AA) for the bond stretching interaction and the initial angle (in unit of degrees) for the angle bending interaction. The angle θ_{ijk} has atom i as the apex.

VFF type	bond stretching	angle bending	
expression	$\frac{1}{2}K_{\text{Pd-S}}(\Delta r)^2$	$\frac{1}{2}K_{\text{Pd-S-S}}(\Delta\theta)^2$	$\frac{1}{2}K_{\text{S-Pd-Pd}}(\Delta\theta)^2$
parameter	10.374	3.122	3.122
r_0 or θ_0	2.401	94.998	94.998

LXIX. 1T-PDS₂

Most existing theoretical studies on the single-layer 1T-PdS₂ are based on the first-principles calculations. In this section, we will develop the SW potential for the single-layer 1T-PdS₂.

The structure for the single-layer 1T-PdS₂ is shown in Fig. 71 (with M=Pd and X=S). Each Pd atom is surrounded by six S atoms. These S atoms are categorized into the top group (eg. atoms 1, 3, and 5) and bottom group (eg. atoms 2, 4, and 6). Each S atom is connected to three Pd atoms. The structural parameters are from the first-principles calculations,⁴⁸

TABLE CCLXXV: Two-body SW potential parameters for single-layer 1T-PdS₂ used by GULP⁸ as expressed in Eq. (3).

	A (eV)	ρ (Å)	B (Å ⁴)	r_{\min} (Å)	r_{\max} (Å)
Pd-S	10.116	1.467	16.625	0.0	3.340

TABLE CCLXXVI: Three-body SW potential parameters for single-layer 1T-PdS₂ used by GULP⁸ as expressed in Eq. (4). The angle θ_{ijk} in the first line indicates the bending energy for the angle with atom i as the apex.

	K (eV)	θ_0 (degree)	ρ_1 (Å)	ρ_2 (Å)	$r_{\min12}$ (Å)	$r_{\max12}$ (Å)	$r_{\min13}$ (Å)	$r_{\max13}$ (Å)	$r_{\min23}$ (Å)	$r_{\max23}$ (Å)
$\theta_{\text{Pd-S-S}}$	35.859	94.998	1.467	1.467	0.0	3.340	0.0	3.340	0.0	4.837
$\theta_{\text{S-Pd-Pd}}$	35.859	94.998	1.467	1.467	0.0	3.340	0.0	3.340	0.0	4.837

including the lattice constant $a = 3.5408$ Å, and the bond length $d_{\text{Pd-S}} = 2.4013$ Å, which is derived from the angle $\theta_{\text{SPdPd}} = 95^\circ$. The other angle is $\theta_{\text{PdSS}} = 95^\circ$ with S atoms from the same (top or bottom) group.

Table CCLXXIV shows three VFF terms for the single-layer 1T-PdS₂, one of which is the bond stretching interaction shown by Eq. (1) while the other two terms are the angle bending interaction shown by Eq. (2). We note that the angle bending term $K_{\text{Pd-S-S}}$ is for the angle $\theta_{\text{Pd-S-S}}$ with both S atoms from the same (top or bottom) group. We find that there are actually only two parameters in the VFF model, so we can determine their value by fitting to the Young's modulus and the Poisson's ratio of the system. The *ab initio* calculations have predicted the Young's modulus to be 77 N/m and the Poisson's ratio as 0.53.⁴⁸

The parameters for the two-body SW potential used by GULP are shown in Tab. CCLXXV. The parameters for the three-body SW potential used by GULP are shown in Tab. CCLXXVI. Some representative parameters for the SW potential used by LAMMPS

TABLE CCLXXVII: SW potential parameters for single-layer 1T-PdS₂ used by LAMMPS⁹ as expressed in Eqs. (9) and (10).

	ϵ (eV)	σ (Å)	a	λ	γ	$\cos \theta_0$	A_L	B_L	p	q	tol
Pd-S ₁ -S ₁	1.000	1.467	2.276	35.859	1.000	-0.087	10.116	3.588	4	0	0.0

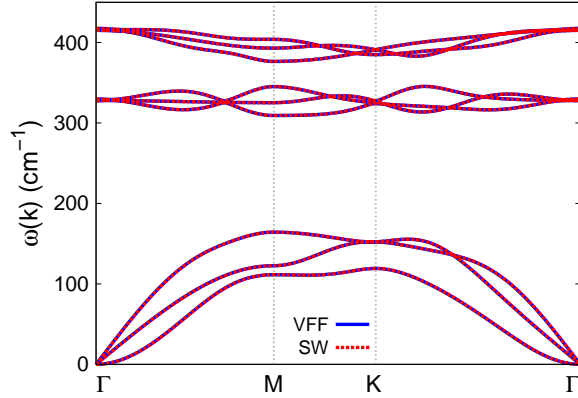


FIG. 137: (Color online) Phonon spectrum for single-layer 1T-PdS₂ along the Γ MK Γ direction in the Brillouin zone. The phonon dispersion from the SW potential is exactly the same as that from the VFF model.

are listed in Tab. [CCLXXVII](#).

We use LAMMPS to perform MD simulations for the mechanical behavior of the single-layer 1T-PdS₂ under uniaxial tension at 1.0 K and 300.0 K. Fig. [136](#) shows the stress-strain curve for the tension of a single-layer 1T-PdS₂ of dimension $100 \times 100 \text{ \AA}$. Periodic boundary conditions are applied in both armchair and zigzag directions. The single-layer 1T-PdS₂ is stretched uniaxially along the armchair or zigzag direction. The stress is calculated without involving the actual thickness of the quasi-two-dimensional structure of the single-layer 1T-PdS₂. The Young's modulus can be obtained by a linear fitting of the stress-strain relation in the small strain range of $[0, 0.01]$. The Young's modulus are 69.9 N/m and 69.5 N/m along the armchair and zigzag directions, respectively. The Young's modulus is essentially isotropic in the armchair and zigzag directions. The Poisson's ratio from the VFF model and the SW potential is $\nu_{xy} = \nu_{yx} = 0.20$. The fitted Young's modulus value is about 10% smaller than the *ab initio* result of 77 N/m,⁴⁸ as only short-range interactions are considered in the present work. The long-range interactions are ignored, which typically leads to about 10% underestimation for the value of the Young's modulus.

There is no available value for nonlinear quantities in the single-layer 1T-PdS₂. We have thus used the nonlinear parameter $B = 0.5d^4$ in Eq. (5), which is close to the value of B in most materials. The value of the third order nonlinear elasticity D can be extracted by fitting the stress-strain relation to the function $\sigma = E\epsilon + \frac{1}{2}D\epsilon^2$ with E as the Young's modulus.

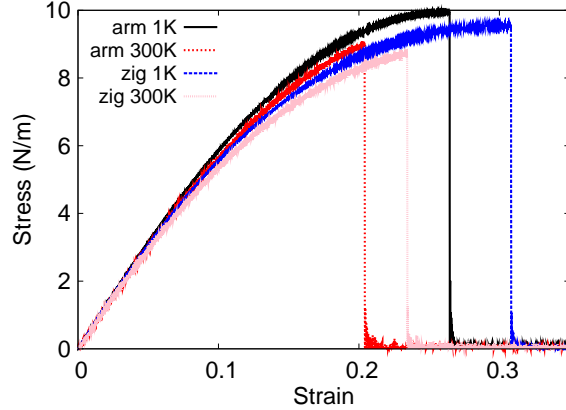


FIG. 138: (Color online) Stress-strain for single-layer 1T-PdSe₂ of dimension $100 \times 100 \text{ \AA}$ along the armchair and zigzag directions.

The values of D from the present SW potential are -222.0 N/m and -248.8 N/m along the armchair and zigzag directions, respectively. The ultimate stress is about 10.1 Nm^{-1} at the ultimate strain of 0.25 in the armchair direction at the low temperature of 1 K . The ultimate stress is about 9.7 Nm^{-1} at the ultimate strain of 0.30 in the zigzag direction at the low temperature of 1 K .

Fig. 137 shows that the VFF model and the SW potential give exactly the same phonon dispersion, as the SW potential is derived from the VFF model.

LXX. 1T-PDSE₂

Most existing theoretical studies on the single-layer 1T-PdSe₂ are based on the first-principles calculations. In this section, we will develop the SW potential for the single-layer 1T-PdSe₂.

The structure for the single-layer 1T-PdSe₂ is shown in Fig. 71 (with $M=\text{Pd}$ and $X=\text{Se}$). Each Pd atom is surrounded by six Se atoms. These Se atoms are categorized into the top group (eg. atoms 1, 3, and 5) and bottom group (eg. atoms 2, 4, and 6). Each Se atom is connected to three Pd atoms. The structural parameters are from the first-principles calculations,⁴⁸ including the lattice constant $a = 3.6759 \text{ \AA}$, and the bond length $d_{\text{Pd-Se}} = 2.4929 \text{ \AA}$, which is derived from the angle $\theta_{\text{SePdPd}} = 95^\circ$. The other angle is $\theta_{\text{PdSeSe}} = 95^\circ$ with Se atoms from the same (top or bottom) group.

TABLE CCLXXVIII: The VFF model for single-layer 1T-PdSe₂. The second line gives an explicit expression for each VFF term. The third line is the force constant parameters. Parameters are in the unit of $\frac{\text{eV}}{\text{Å}^2}$ for the bond stretching interactions, and in the unit of eV for the angle bending interaction. The fourth line gives the initial bond length (in unit of Å) for the bond stretching interaction and the initial angle (in unit of degrees) for the angle bending interaction. The angle θ_{ijk} has atom *i* as the apex.

VFF type	bond stretching	angle bending	
expression	$\frac{1}{2}K_{\text{Pd-Se}}(\Delta r)^2$	$\frac{1}{2}K_{\text{Pd-Se-Se}}(\Delta\theta)^2$	$\frac{1}{2}K_{\text{Se-Pd-Pd}}(\Delta\theta)^2$
parameter	10.374	3.122	3.122
r_0 or θ_0	2.493	94.999	94.999

TABLE CCLXXIX: Two-body SW potential parameters for single-layer 1T-PdSe₂ used by GULP⁸ as expressed in Eq. (3).

	A (eV)	ρ (Å)	B (Å ⁴)	r_{\min} (Å)	r_{\max} (Å)
Pd-Se	10.902	1.523	19.310	0.0	3.467

Table CCLXXVIII shows three VFF terms for the single-layer 1T-PdSe₂, one of which is the bond stretching interaction shown by Eq. (1) while the other two terms are the angle bending interaction shown by Eq. (2). We note that the angle bending term $K_{\text{Pd-Se-Se}}$ is for the angle $\theta_{\text{Pd-Se-Se}}$ with both Se atoms from the same (top or bottom) group. We find that there are actually only two parameters in the VFF model, so we can determine their value by fitting to the Young's modulus and the Poisson's ratio of the system. The *ab initio* calculations have predicted the Young's modulus to be 66 N/m and the Poisson's ratio as 0.45.⁴⁸

TABLE CCLXXX: Three-body SW potential parameters for single-layer 1T-PdSe₂ used by GULP⁸ as expressed in Eq. (4). The angle θ_{ijk} in the first line indicates the bending energy for the angle with atom *i* as the apex.

	K (eV)	θ_0 (degree)	ρ_1 (Å)	ρ_2 (Å)	$r_{\min12}$ (Å)	$r_{\max12}$ (Å)	$r_{\min13}$ (Å)	$r_{\max13}$ (Å)	$r_{\min23}$ (Å)	$r_{\max23}$ (Å)
$\theta_{\text{Pd-Se-Se}}$	35.859	94.999	1.523	1.523	0.0	3.467	0.0	3.467	0.0	5.021
$\theta_{\text{Se-Pd-Pd}}$	35.859	94.999	1.523	1.523	0.0	3.467	0.0	3.467	0.0	5.021

TABLE CCLXXXI: SW potential parameters for single-layer 1T-PdSe₂ used by LAMMPS⁹ as expressed in Eqs. (9) and (10).

	ϵ (eV)	σ (Å)	a	λ	γ	$\cos \theta_0$	A_L	B_L	p	q	tol
Pd-Se ₁ -Se ₁	1.000	1.523	2.276	35.859	1.000	-0.087	10.902	3.588	4	0	0.0

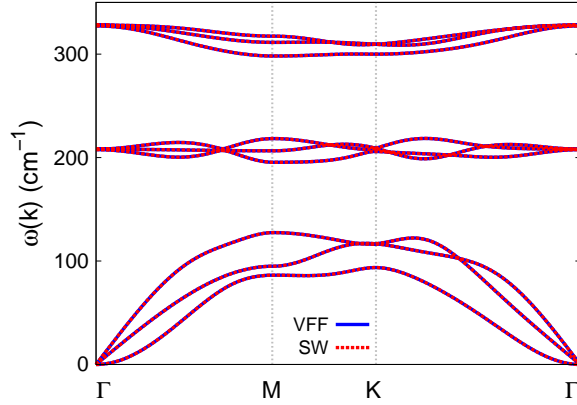


FIG. 139: (Color online) Phonon spectrum for single-layer 1T-PdSe₂ along the Γ MK Γ direction in the Brillouin zone. The phonon dispersion from the SW potential is exactly the same as that from the VFF model.

The parameters for the two-body SW potential used by GULP are shown in Tab. CCLXXIX. The parameters for the three-body SW potential used by GULP are shown in Tab. CCLXXX. Some representative parameters for the SW potential used by LAMMPS are listed in Tab. CCLXXXI.

We use LAMMPS to perform MD simulations for the mechanical behavior of the single-layer 1T-PdSe₂ under uniaxial tension at 1.0 K and 300.0 K. Fig. 138 shows the stress-strain curve for the tension of a single-layer 1T-PdSe₂ of dimension 100×100 Å. Periodic boundary conditions are applied in both armchair and zigzag directions. The single-layer 1T-PdSe₂ is stretched uniaxially along the armchair or zigzag direction. The stress is calculated without involving the actual thickness of the quasi-two-dimensional structure of the single-layer 1T-PdSe₂. The Young's modulus can be obtained by a linear fitting of the stress-strain relation in the small strain range of $[0, 0.01]$. The Young's modulus are 65.5 N/m and 65.3 N/m along the armchair and zigzag directions, respectively. The Young's modulus is essentially isotropic in the armchair and zigzag directions. The Poisson's ratio from the VFF model

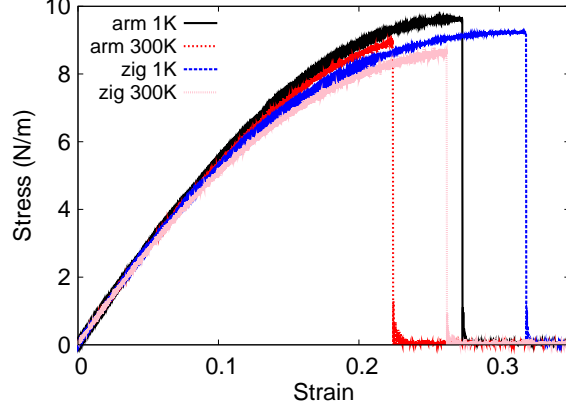


FIG. 140: (Color online) Stress-strain for single-layer 1T-PdTe₂ of dimension $100 \times 100 \text{ \AA}$ along the armchair and zigzag directions.

and the SW potential is $\nu_{xy} = \nu_{yx} = 0.21$.

There is no available value for nonlinear quantities in the single-layer 1T-PdSe₂. We have thus used the nonlinear parameter $B = 0.5d^4$ in Eq. (5), which is close to the value of B in most materials. The value of the third order nonlinear elasticity D can be extracted by fitting the stress-strain relation to the function $\sigma = E\epsilon + \frac{1}{2}D\epsilon^2$ with E as the Young's modulus. The values of D from the present SW potential are -194.7 N/m and -222.8 N/m along the armchair and zigzag directions, respectively. The ultimate stress is about 9.9 Nm^{-1} at the ultimate strain of 0.26 in the armchair direction at the low temperature of 1 K. The ultimate stress is about 9.5 Nm^{-1} at the ultimate strain of 0.31 in the zigzag direction at the low temperature of 1 K.

Fig. 139 shows that the VFF model and the SW potential give exactly the same phonon dispersion, as the SW potential is derived from the VFF model.

LXXI. 1T-PDTE₂

Most existing theoretical studies on the single-layer 1T-PdTe₂ are based on the first-principles calculations. In this section, we will develop the SW potential for the single-layer 1T-PdTe₂.

The structure for the single-layer 1T-PdTe₂ is shown in Fig. 71 (with M=Pd and X=Te). Each Pd atom is surrounded by six Te atoms. These Te atoms are categorized into the

TABLE CCLXXXII: The VFF model for single-layer 1T-PdTe₂. The second line gives an explicit expression for each VFF term. The third line is the force constant parameters. Parameters are in the unit of $\frac{\text{eV}}{\text{Å}^2}$ for the bond stretching interactions, and in the unit of eV for the angle bending interaction. The fourth line gives the initial bond length (in unit of Å) for the bond stretching interaction and the initial angle (in unit of degrees) for the angle bending interaction. The angle θ_{ijk} has atom i as the apex.

VFF type	bond stretching	angle bending	
expression	$\frac{1}{2}K_{\text{Pd-Te}}(\Delta r)^2$	$\frac{1}{2}K_{\text{Pd-Te-Te}}(\Delta\theta)^2$	$\frac{1}{2}K_{\text{Te-Pd-Pd}}(\Delta\theta)^2$
parameter	10.374	3.122	3.122
r_0 or θ_0	2.635	95.999	95.999

TABLE CCLXXXIII: Two-body SW potential parameters for single-layer 1T-PdTe₂ used by GULP⁸ as expressed in Eq. (3).

	A (eV)	ρ (Å)	B (Å ⁴)	r_{\min} (Å)	r_{\max} (Å)
Pd-Te	12.474	1.650	24.101	0.0	3.678

top group (eg. atoms 1, 3, and 5) and bottom group (eg. atoms 2, 4, and 6). Each Te atom is connected to three Pd atoms. The structural parameters are from the first-principles calculations,⁴⁸ including the lattice constant $a = 3.9162$ Å, and the bond length $d_{\text{Pd-Te}} = 2.6349$ Å, which is derived from the angle $\theta_{\text{TePdPd}} = 96^\circ$. The other angle is $\theta_{\text{PdTeTe}} = 96^\circ$ with Te atoms from the same (top or bottom) group.

Table CCLXXXII shows three VFF terms for the single-layer 1T-PdTe₂, one of which is the bond stretching interaction shown by Eq. (1) while the other two terms are the angle bending interaction shown by Eq. (2). We note that the angle bending term $K_{\text{Pd-Te-Te}}$ is

TABLE CCLXXXIV: Three-body SW potential parameters for single-layer 1T-PdTe₂ used by GULP⁸ as expressed in Eq. (4). The angle θ_{ijk} in the first line indicates the bending energy for the angle with atom i as the apex.

	K (eV)	θ_0 (degree)	ρ_1 (Å)	ρ_2 (Å)	$r_{\min12}$ (Å)	$r_{\max12}$ (Å)	$r_{\min13}$ (Å)	$r_{\max13}$ (Å)	$r_{\min23}$ (Å)	$r_{\max23}$ (Å)
$\theta_{\text{Pd-Te-Te}}$	37.406	95.999	1.650	1.650	0.0	3.678	0.0	3.678	0.0	5.350
$\theta_{\text{Te-Pd-Pd}}$	37.406	95.999	1.650	1.650	0.0	3.678	0.0	3.678	0.0	5.350

TABLE CCLXXXV: SW potential parameters for single-layer 1T-PdTe₂ used by LAMMPS⁹ as expressed in Eqs. (9) and (10).

	ϵ (eV)	σ (Å)	a	λ	γ	$\cos \theta_0$	A_L	B_L	p	q	tol
Pd-Te ₁ -Te ₁	1.000	1.650	2.229	37.406	1.000	-0.105	12.474	3.250	4	0	0.0

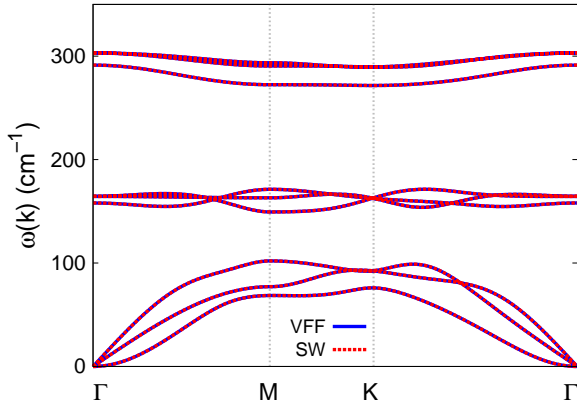


FIG. 141: (Color online) Phonon spectrum for single-layer 1T-PdTe₂ along the Γ MKT direction in the Brillouin zone. The phonon dispersion from the SW potential is exactly the same as that from the VFF model.

for the angle $\theta_{\text{Pd-Te-Te}}$ with both Te atoms from the same (top or bottom) group. We find that there are actually only two parameters in the VFF model, so we can determine their value by fitting to the Young's modulus and the Poisson's ratio of the system. The *ab initio* calculations have predicted the Young's modulus to be 63 N/m and the Poisson's ratio as 0.35.⁴⁸

The parameters for the two-body SW potential used by GULP are shown in Tab. CCLXXXIII. The parameters for the three-body SW potential used by GULP are shown in Tab. CCLXXXIV. Some representative parameters for the SW potential used by LAMMPS are listed in Tab. CCLXXXV.

We use LAMMPS to perform MD simulations for the mechanical behavior of the single-layer 1T-PdTe₂ under uniaxial tension at 1.0 K and 300.0 K. Fig. 140 shows the stress-strain curve for the tension of a single-layer 1T-PdTe₂ of dimension 100×100 Å. Periodic boundary conditions are applied in both armchair and zigzag directions. The single-layer 1T-PdTe₂ is stretched uniaxially along the armchair or zigzag direction. The stress is calculated without

TABLE CCLXXXVI: The VFF model for single-layer 1T-SnS₂. The second line gives an explicit expression for each VFF term. The third line is the force constant parameters. Parameters are in the unit of $\frac{\text{eV}}{\text{Å}^2}$ for the bond stretching interactions, and in the unit of eV for the angle bending interaction. The fourth line gives the initial bond length (in unit of Å) for the bond stretching interaction and the initial angle (in unit of degrees) for the angle bending interaction. The angle θ_{ijk} has atom i as the apex.

VFF type	bond stretching	angle bending	
expression	$\frac{1}{2}K_{\text{Sn-S}}(\Delta r)^2$	$\frac{1}{2}K_{\text{Sn-S-S}}(\Delta\theta)^2$	$\frac{1}{2}K_{\text{S-Sn-Sn}}(\Delta\theta)^2$
parameter	7.872	5.817	5.817
r_0 or θ_0	2.570	90.173	90.173

involving the actual thickness of the quasi-two-dimensional structure of the single-layer 1T-PdTe₂. The Young's modulus can be obtained by a linear fitting of the stress-strain relation in the small strain range of [0, 0.01]. The Young's modulus are 61.6 N/m and 61.4 N/m along the armchair and zigzag directions, respectively. The Young's modulus is essentially isotropic in the armchair and zigzag directions. The Poisson's ratio from the VFF model and the SW potential is $\nu_{xy} = \nu_{yx} = 0.22$.

There is no available value for nonlinear quantities in the single-layer 1T-PdTe₂. We have thus used the nonlinear parameter $B = 0.5d^4$ in Eq. (5), which is close to the value of B in most materials. The value of the third order nonlinear elasticity D can be extracted by fitting the stress-strain relation to the function $\sigma = E\epsilon + \frac{1}{2}D\epsilon^2$ with E as the Young's modulus. The values of D from the present SW potential are -178.8 N/m and -203.8 N/m along the armchair and zigzag directions, respectively. The ultimate stress is about 9.6 Nm⁻¹ at the ultimate strain of 0.27 in the armchair direction at the low temperature of 1 K. The ultimate stress is about 9.2 Nm⁻¹ at the ultimate strain of 0.32 in the zigzag direction at the low temperature of 1 K.

Fig. 141 shows that the VFF model and the SW potential give exactly the same phonon dispersion, as the SW potential is derived from the VFF model.

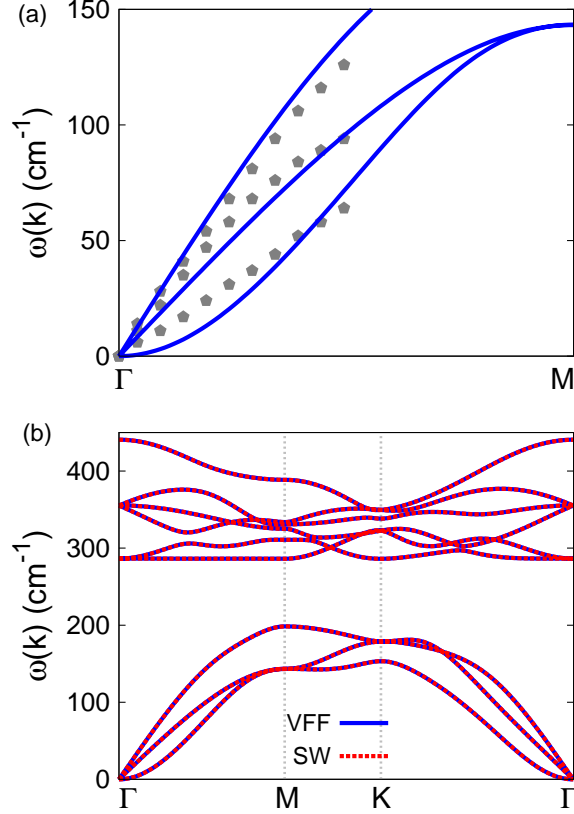


FIG. 142: (Color online) Phonon spectrum for single-layer 1T-SnS₂. (a) Phonon dispersion along the Γ M direction in the Brillouin zone. The results from the VFF model (lines) are comparable with the *ab initio* results (pentagons) from Ref. 34. (b) The phonon dispersion from the SW potential is exactly the same as that from the VFF model.

TABLE CCLXXXVII: Two-body SW potential parameters for single-layer 1T-SnS₂ used by GULP⁸ as expressed in Eq. (3).

	A (eV)	ρ (\AA)	B (\AA^4)	r_{\min} (\AA)	r_{\max} (\AA)
Sn-S	7.805	1.384	21.812	0.0	3.513

LXXII. 1T-SNS₂

Most existing theoretical studies on the single-layer 1T-SnS₂ are based on the first-principles calculations. In this section, we will develop the SW potential for the single-layer 1T-SnS₂.

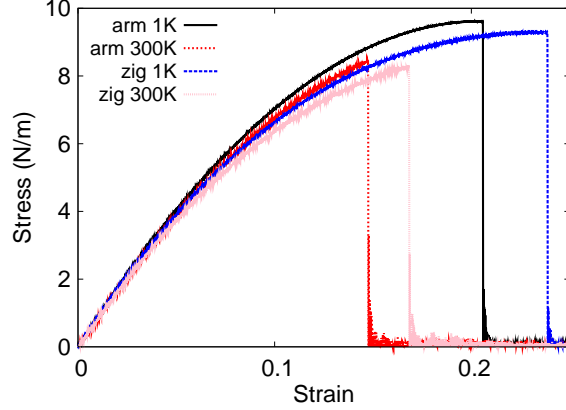


FIG. 143: (Color online) Stress-strain for single-layer 1T-SnS₂ of dimension 100 × 100 Å along the armchair and zigzag directions.

TABLE CCLXXXVIII: Three-body SW potential parameters for single-layer 1T-SnS₂ used by GULP⁸ as expressed in Eq. (4). The angle θ_{ijk} in the first line indicates the bending energy for the angle with atom *i* as the apex.

	K (eV)	θ_0 (degree)	ρ_1 (Å)	ρ_2 (Å)	$r_{\min 12}$ (Å)	$r_{\max 12}$ (Å)	$r_{\min 13}$ (Å)	$r_{\max 13}$ (Å)	$r_{\min 23}$ (Å)	$r_{\max 23}$ (Å)
$\theta_{\text{Sn-S-S}}$	54.748	90.173	1.384	1.384	0.0	3.513	0.0	3.513	0.0	4.972
$\theta_{\text{S-Sn-Sn}}$	54.748	90.173	1.384	1.384	0.0	3.513	0.0	3.513	0.0	4.972

The structure for the single-layer 1T-SnS₂ is shown in Fig. 71 (with M=Sn and X=S). Each Sn atom is surrounded by six S atoms. These S atoms are categorized into the top group (eg. atoms 1, 3, and 5) and bottom group (eg. atoms 2, 4, and 6). Each S atom is connected to three Sn atoms. The structural parameters are from the first-principles calculations,³⁴ including the lattice constant $a = 3.640$ Å, and the bond length $d_{\text{Sn-S}} = 2.570$ Å. The resultant angles are $\theta_{\text{SSnSn}} = 90.173^\circ$, and $\theta_{\text{SnSS}} = 90.173^\circ$ with S atoms from the same (top or bottom) group.

TABLE CCLXXXIX: SW potential parameters for single-layer 1T-SnS₂ used by LAMMPS⁹ as expressed in Eqs. (9) and (10).

	ϵ (eV)	σ (Å)	a	λ	γ	$\cos \theta_0$	A_L	B_L	p	q	tol
Sn-S ₁ -S ₁	1.000	1.384	2.539	54.748	1.000	-0.003	7.805	5.949	4	0	0.0

Table [CCLXXXVI](#) shows three VFF terms for the single-layer 1T-SnS₂, one of which is the bond stretching interaction shown by Eq. (1) while the other two terms are the angle bending interaction shown by Eq. (2). We note that the angle bending term $K_{\text{Sn-S-S}}$ is for the angle $\theta_{\text{Sn-S-S}}$ with both S atoms from the same (top or bottom) group. These force constant parameters are determined by fitting to the acoustic branches in the phonon dispersion along the ΓM as shown in Fig. 142 (a). The *ab initio* calculations for the phonon dispersion are from Ref. 34. The lowest acoustic branch (flexural mode) is almost linear in the *ab initio* calculations, which may due to the violation of the rigid rotational invariance.²⁰ Fig. 142 (b) shows that the VFF model and the SW potential give exactly the same phonon dispersion, as the SW potential is derived from the VFF model.

The parameters for the two-body SW potential used by GULP are shown in Tab. [CCLXXXVII](#). The parameters for the three-body SW potential used by GULP are shown in Tab. [CCLXXXVIII](#). Some representative parameters for the SW potential used by LAMMPS are listed in Tab. [CCLXXXIX](#).

We use LAMMPS to perform MD simulations for the mechanical behavior of the single-layer 1T-SnS₂ under uniaxial tension at 1.0 K and 300.0 K. Fig. 143 shows the stress-strain curve for the tension of a single-layer 1T-SnS₂ of dimension $100 \times 100 \text{ \AA}$. Periodic boundary conditions are applied in both armchair and zigzag directions. The single-layer 1T-SnS₂ is stretched uniaxially along the armchair or zigzag direction. The stress is calculated without involving the actual thickness of the quasi-two-dimensional structure of the single-layer 1T-SnS₂. The Young's modulus can be obtained by a linear fitting of the stress-strain relation in the small strain range of $[0, 0.01]$. The Young's modulus are 88.4 N/m and 87.9 N/m along the armchair and zigzag directions, respectively. The Young's modulus is essentially isotropic in the armchair and zigzag directions. The Poisson's ratio from the VFF model and the SW potential is $\nu_{xy} = \nu_{yx} = 0.13$.

There is no available value for nonlinear quantities in the single-layer 1T-SnS₂. We have thus used the nonlinear parameter $B = 0.5d^4$ in Eq. (5), which is close to the value of B in most materials. The value of the third order nonlinear elasticity D can be extracted by fitting the stress-strain relation to the function $\sigma = E\epsilon + \frac{1}{2}D\epsilon^2$ with E as the Young's modulus. The values of D from the present SW potential are -392.8 N/m and -421.6 N/m along the armchair and zigzag directions, respectively. The ultimate stress is about 9.6 Nm^{-1} at the ultimate strain of 0.20 in the armchair direction at the low temperature of 1 K. The

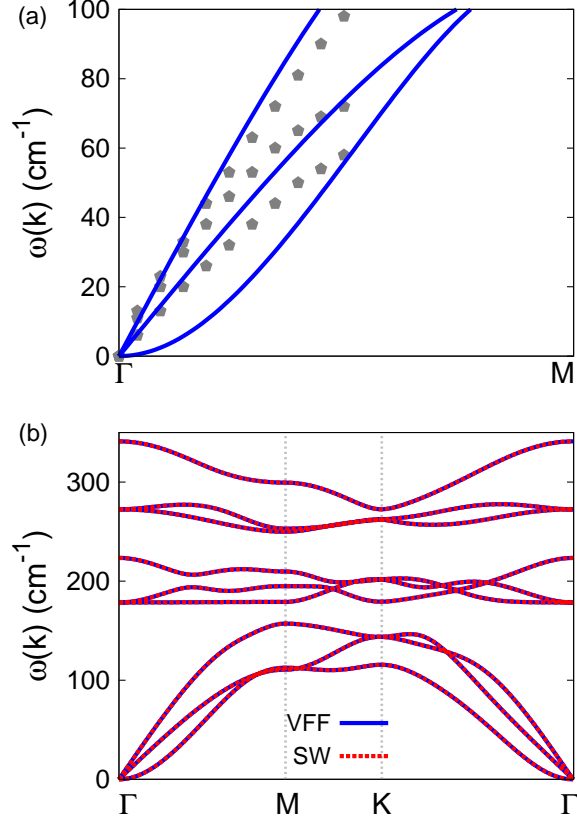


FIG. 144: (Color online) Phonon spectrum for single-layer 1T-SnSe₂. (a) Phonon dispersion along the Γ M direction in the Brillouin zone. The results from the VFF model (lines) are comparable with the *ab initio* results (pentagons) from Ref. 34. (b) The phonon dispersion from the SW potential is exactly the same as that from the VFF model.

ultimate stress is about 9.3 Nm^{-1} at the ultimate strain of 0.24 in the zigzag direction at the low temperature of 1 K.

LXXIII. 1T-SNSE₂

Most existing theoretical studies on the single-layer 1T-SnSe₂ are based on the first-principles calculations. In this section, we will develop the SW potential for the single-layer 1T-SnSe₂.

The structure for the single-layer 1T-SnSe₂ is shown in Fig. 71 (with M=Sn and X=Se). Each Sn atom is surrounded by six Se atoms. These Se atoms are categorized into the

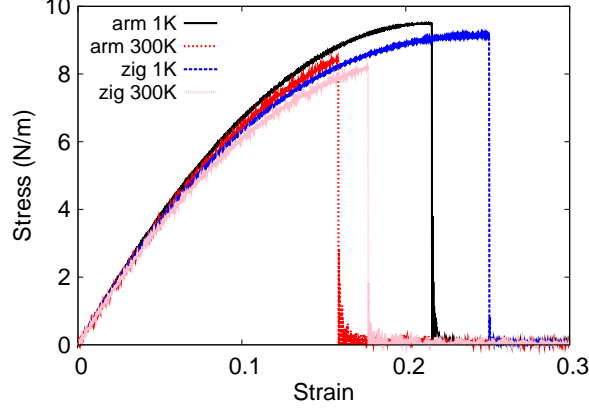


FIG. 145: (Color online) Stress-strain for single-layer 1T-SnSe₂ of dimension $100 \times 100 \text{ \AA}$ along the armchair and zigzag directions.

TABLE CCXC: The VFF model for single-layer 1T-SnSe₂. The second line gives an explicit expression for each VFF term. The third line is the force constant parameters. Parameters are in the unit of $\frac{eV}{\text{Å}^2}$ for the bond stretching interactions, and in the unit of eV for the angle bending interaction. The fourth line gives the initial bond length (in unit of Å) for the bond stretching interaction and the initial angle (in unit of degrees) for the angle bending interaction. The angle θ_{ijk} has atom *i* as the apex.

VFF type	bond stretching	angle bending	
expression	$\frac{1}{2}K_{\text{Sn-Se}}(\Delta r)^2$	$\frac{1}{2}K_{\text{Sn-Se-Se}}(\Delta\theta)^2$	$\frac{1}{2}K_{\text{Se-Sn-Sn}}(\Delta\theta)^2$
parameter	7.872	5.817	5.817
r_0 or θ_0	2.704	89.044	89.044

top group (eg. atoms 1, 3, and 5) and bottom group (eg. atoms 2, 4, and 6). Each Se atom is connected to three Sn atoms. The structural parameters are from the first-principles calculations,³⁴ including the lattice constant $a = 3.792 \text{ \AA}$, and the bond length $d_{\text{Sn-Se}} = 2.704 \text{ \AA}$. The resultant angles are $\theta_{\text{SeSnSn}} = 89.044^\circ$, and $\theta_{\text{SnSeSe}} = 89.044^\circ$ with Se atoms from the same (top or bottom) group.

Table CCXC shows three VFF terms for the single-layer 1T-SnSe₂, one of which is the bond stretching interaction shown by Eq. (1) while the other two terms are the angle bending interaction shown by Eq. (2). We note that the angle bending term $K_{\text{Sn-Se-Se}}$ is for the angle

TABLE CCXCI: Two-body SW potential parameters for single-layer 1T-SnSe₂ used by GULP⁸ as expressed in Eq. (3).

	A (eV)	ρ (Å)	B (Å ⁴)	r_{\min} (Å)	r_{\max} (Å)
Sn-Se	8.395	1.411	26.730	0.0	3.681

TABLE CCXCII: Three-body SW potential parameters for single-layer 1T-SnSe₂ used by GULP⁸ as expressed in Eq. (4). The angle θ_{ijk} in the first line indicates the bending energy for the angle with atom i as the apex.

	K (eV)	θ_0 (degree)	ρ_1 (Å)	ρ_2 (Å)	$r_{\min12}$ (Å)	$r_{\max12}$ (Å)	$r_{\min13}$ (Å)	$r_{\max13}$ (Å)	$r_{\min23}$ (Å)	$r_{\max23}$ (Å)
$\theta_{\text{Sn-Se-Se}}$	52.322	89.044	1.411	1.411	0.0	3.681	0.0	3.681	0.0	5.180
$\theta_{\text{Se-Sn-Sn}}$	52.322	89.044	1.411	1.411	0.0	3.681	0.0	3.681	0.0	5.180

$\theta_{\text{Sn-Se-Se}}$ with both Se atoms from the same (top or bottom) group. These force constant parameters are determined by fitting to the acoustic branches in the phonon dispersion along the ΓM as shown in Fig. 144 (a). The *ab initio* calculations for the phonon dispersion are from Ref. 34. The lowest acoustic branch (flexural mode) is almost linear in the *ab initio* calculations, which may due to the violation of the rigid rotational invariance.²⁰ Fig. 144 (b) shows that the VFF model and the SW potential give exactly the same phonon dispersion, as the SW potential is derived from the VFF model.

The parameters for the two-body SW potential used by GULP are shown in Tab. CCXCI. The parameters for the three-body SW potential used by GULP are shown in Tab. CCXCII. Some representative parameters for the SW potential used by LAMMPS are listed in Tab. CCXCIII.

We use LAMMPS to perform MD simulations for the mechanical behavior of the single-layer 1T-SnSe₂ under uniaxial tension at 1.0 K and 300.0 K. Fig. 145 shows the stress-strain curve for the tension of a single-layer 1T-SnSe₂ of dimension 100×100 Å. Periodic boundary

TABLE CCXCIII: SW potential parameters for single-layer 1T-SnSe₂ used by LAMMPS⁹ as expressed in Eqs. (9) and (10).

	ϵ (eV)	σ (Å)	a	λ	γ	$\cos \theta_0$	A_L	B_L	p	q	tol
Sn-Se ₁ -Se ₁	1.000	1.411	2.609	52.322	1.000	0.017	8.395	6.743	4	0	0.0

TABLE CCXCIV: The VFF model for single-layer 1T-HfS₂. The second line gives an explicit expression for each VFF term. The third line is the force constant parameters. Parameters are in the unit of $\frac{\text{eV}}{\text{\AA}^2}$ for the bond stretching interactions, and in the unit of eV for the angle bending interaction. The fourth line gives the initial bond length (in unit of \AA) for the bond stretching interaction and the initial angle (in unit of degrees) for the angle bending interaction. The angle θ_{ijk} has atom i as the apex.

VFF type	bond stretching	angle bending	
expression	$\frac{1}{2}K_{\text{Hf-S}}(\Delta r)^2$	$\frac{1}{2}K_{\text{Hf-S-S}}(\Delta\theta)^2$	$\frac{1}{2}K_{\text{S-Hf-Hf}}(\Delta\theta)^2$
parameter	7.930	4.283	4.283
r_0 or θ_0	2.550	91.078	91.078

conditions are applied in both armchair and zigzag directions. The single-layer 1T-SnSe₂ is stretched uniaxially along the armchair or zigzag direction. The stress is calculated without involving the actual thickness of the quasi-two-dimensional structure of the single-layer 1T-SnSe₂. The Young's modulus can be obtained by a linear fitting of the stress-strain relation in the small strain range of [0, 0.01]. The Young's modulus are 82.0 N/m and 81.6 N/m along the armchair and zigzag directions, respectively. The Young's modulus is essentially isotropic in the armchair and zigzag directions. The Poisson's ratio from the VFF model and the SW potential is $\nu_{xy} = \nu_{yx} = 0.15$.

There is no available value for nonlinear quantities in the single-layer 1T-SnSe₂. We have thus used the nonlinear parameter $B = 0.5d^4$ in Eq. (5), which is close to the value of B in most materials. The value of the third order nonlinear elasticity D can be extracted by fitting the stress-strain relation to the function $\sigma = E\epsilon + \frac{1}{2}D\epsilon^2$ with E as the Young's modulus. The values of D from the present SW potential are -339.2 N/m and -368.3 N/m along the armchair and zigzag directions, respectively. The ultimate stress is about 9.5 Nm⁻¹ at the ultimate strain of 0.21 in the armchair direction at the low temperature of 1 K. The ultimate stress is about 9.1 Nm⁻¹ at the ultimate strain of 0.25 in the zigzag direction at the low temperature of 1 K.

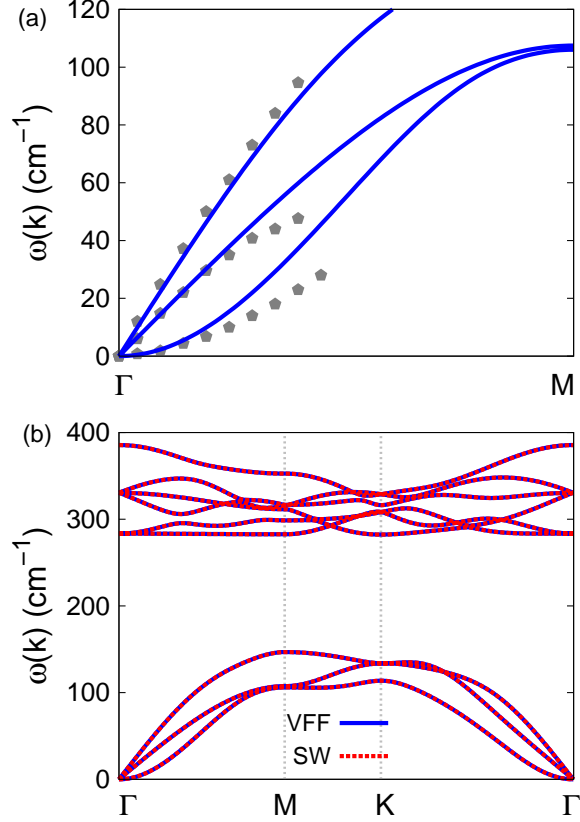


FIG. 146: (Color online) Phonon spectrum for single-layer 1T-HfS₂. (a) Phonon dispersion along the Γ M direction in the Brillouin zone. The results from the VFF model (lines) are comparable with the experiment data (pentagons) from Ref. 38. (b) The phonon dispersion from the SW potential is exactly the same as that from the VFF model.

TABLE CCXCV: Two-body SW potential parameters for single-layer 1T-HfS₂ used by GULP⁸ as expressed in Eq. (3).

	A (eV)	ρ (\AA)	B (\AA^4)	r_{\min} (\AA)	r_{\max} (\AA)
Hf-S	7.917	1.407	21.141	0.0	3.497

LXXIV. 1T-HfS₂

Most existing theoretical studies on the single-layer 1T-HfS₂ are based on the first-principles calculations. In this section, we will develop the SW potential for the single-layer 1T-HfS₂.

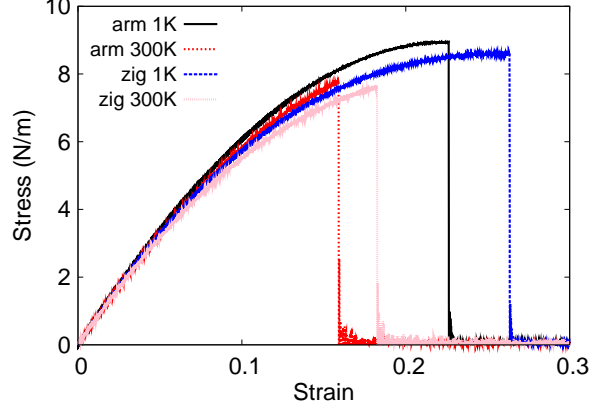


FIG. 147: (Color online) Stress-strain for single-layer 1T-HfS₂ of dimension 100 × 100 Å along the armchair and zigzag directions.

TABLE CCXCVI: Three-body SW potential parameters for single-layer 1T-HfS₂ used by GULP⁸ as expressed in Eq. (4). The angle θ_{ijk} in the first line indicates the bending energy for the angle with atom *i* as the apex.

	K (eV)	θ_0 (degree)	ρ_1 (Å)	ρ_2 (Å)	$r_{\min 12}$ (Å)	$r_{\max 12}$ (Å)	$r_{\min 13}$ (Å)	$r_{\max 13}$ (Å)	$r_{\min 23}$ (Å)	$r_{\max 23}$ (Å)
$\theta_{\text{Hf-S-S}}$	41.798	91.078	1.407	1.407	0.0	3.497	0.0	3.497	0.0	4.973
$\theta_{\text{S-Hf-Hf}}$	41.798	91.078	1.407	1.407	0.0	3.497	0.0	3.497	0.0	4.973

The structure for the single-layer 1T-HfS₂ is shown in Fig. 71 (with M=Hf and X=S). Each Hf atom is surrounded by six S atoms. These S atoms are categorized into the top group (eg. atoms 1, 3, and 5) and bottom group (eg. atoms 2, 4, and 6). Each S atom is connected to three Hf atoms. The structural parameters are from the first-principles calculations,⁵³ including the lattice constant $a = 3.64$ Å and the bond length $d_{\text{Hf-S}} = 2.55$ Å. The resultant angles are $\theta_{\text{HfSS}} = 91.078^\circ$ with S atoms from the same (top or bottom) group,

TABLE CCXCVII: SW potential parameters for single-layer 1T-HfS₂ used by LAMMPS⁹ as expressed in Eqs. (9) and (10).

	ϵ (eV)	σ (Å)	a	λ	γ	$\cos \theta_0$	A_L	B_L	p	q	tol
Hf-S-S	1.000	1.407	2.485	41.798	1.000	-0.019	7.917	5.394	4	0	0.0
S-Hf-Hf	1.000	1.407	2.485	41.798	1.000	-0.019	7.917	5.394	4	0	0.0

and $\theta_{\text{SHHf}} = 91.078^\circ$.

Table [CCXCIV](#) shows three VFF terms for the single-layer 1T-HfS₂, one of which is the bond stretching interaction shown by Eq. (1) while the other two terms are the angle bending interaction shown by Eq. (2). We note that the angle bending term $K_{\text{Hf-S-S}}$ is for the angle $\theta_{\text{Hf-S-S}}$ with both S atoms from the same (top or bottom) group. These force constant parameters are determined by fitting to the three acoustic branches in the phonon dispersion along the ΓM as shown in Fig. [146](#) (a). The *ab initio* calculations for the phonon dispersion are from Ref. 38. Similar phonon dispersion can also be found in other *ab initio* calculations.^{34,54} Fig. [146](#) (b) shows that the VFF model and the SW potential give exactly the same phonon dispersion, as the SW potential is derived from the VFF model.

The parameters for the two-body SW potential used by GULP are shown in Tab. [CCXCV](#). The parameters for the three-body SW potential used by GULP are shown in Tab. [CCXCVI](#). Some representative parameters for the SW potential used by LAMMPS are listed in Tab. [CCXCVII](#).

We use LAMMPS to perform MD simulations for the mechanical behavior of the single-layer 1T-HfS₂ under uniaxial tension at 1.0 K and 300.0 K. Fig. [147](#) shows the stress-strain curve for the tension of a single-layer 1T-HfS₂ of dimension $100 \times 100 \text{ \AA}$. Periodic boundary conditions are applied in both armchair and zigzag directions. The single-layer 1T-HfS₂ is stretched uniaxially along the armchair or zigzag direction. The stress is calculated without involving the actual thickness of the quasi-two-dimensional structure of the single-layer 1T-HfS₂. The Young's modulus can be obtained by a linear fitting of the stress-strain relation in the small strain range of $[0, 0.01]$. The Young's modulus are 73.3 N/m and 72.9 N/m along the armchair and zigzag directions, respectively. The Young's modulus is essentially isotropic in the armchair and zigzag directions. These values are close to the *ab initio* results at 0 K temperature, eg. 79.86 Nm⁻¹ in Ref. 53. The Poisson's ratio from the VFF model and the SW potential is $\nu_{xy} = \nu_{yx} = 0.16$, which agrees reasonably with the *ab initio* result⁵³ of 0.19.

There is no available value for nonlinear quantities in the single-layer 1T-HfS₂. We have thus used the nonlinear parameter $B = 0.5d^4$ in Eq. (5), which is close to the value of B in most materials. The value of the third order nonlinear elasticity D can be extracted by fitting the stress-strain relation to the function $\sigma = E\epsilon + \frac{1}{2}D\epsilon^2$ with E as the Young's modulus. The values of D from the present SW potential are -280.9 N/m and -317.2 N/m

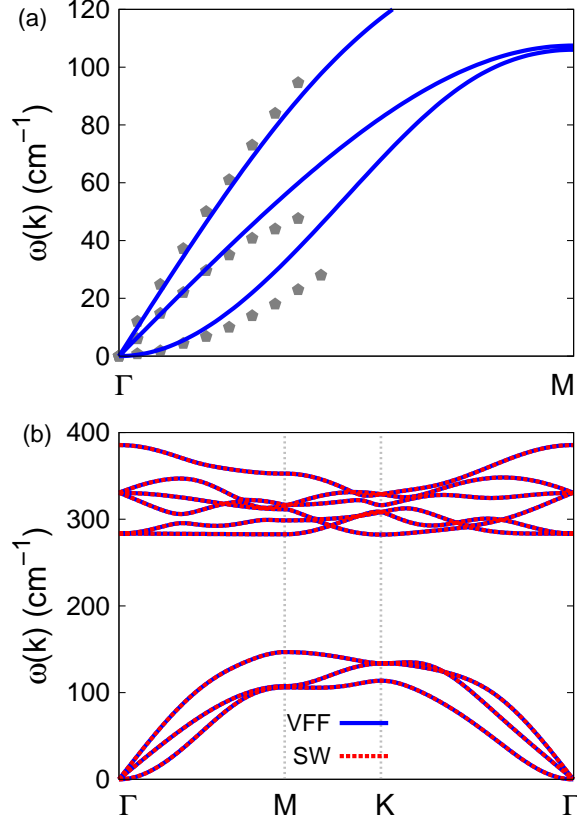


FIG. 148: (Color online) Phonon spectrum for single-layer 1T-HfSe₂. (a) Phonon dispersion along the Γ M direction in the Brillouin zone. The results from the VFF model (lines) are comparable with the experiment data (pentagons) from Ref. 50. (b) The phonon dispersion from the SW potential is exactly the same as that from the VFF model.

along the armchair and zigzag directions, respectively. The ultimate stress is about 8.9 Nm^{-1} at the ultimate strain of 0.22 in the armchair direction at the low temperature of 1 K. The ultimate stress is about 8.6 Nm^{-1} at the ultimate strain of 0.26 in the zigzag direction at the low temperature of 1 K.

LXXV. 1T-HFSE₂

Most existing theoretical studies on the single-layer 1T-HfSe₂ are based on the first-principles calculations. In this section, we will develop the SW potential for the single-layer 1T-HfSe₂.

TABLE CCXCVIII: The VFF model for single-layer 1T-HfSe₂. The second line gives an explicit expression for each VFF term. The third line is the force constant parameters. Parameters are in the unit of $\frac{\text{eV}}{\text{\AA}^2}$ for the bond stretching interactions, and in the unit of eV for the angle bending interaction. The fourth line gives the initial bond length (in unit of \AA) for the bond stretching interaction and the initial angle (in unit of degrees) for the angle bending interaction. The angle θ_{ijk} has atom i as the apex.

VFF type	bond stretching	angle bending	
expression	$\frac{1}{2}K_{\text{Hf-Se}}(\Delta r)^2$	$\frac{1}{2}K_{\text{Hf-Se-Se}}(\Delta\theta)^2$	$\frac{1}{2}K_{\text{Se-Hf-Hf}}(\Delta\theta)^2$
parameter	7.930	4.283	4.283
r_0 or θ_0	2.642	88.093	88.093

TABLE CCXCIX: Two-body SW potential parameters for single-layer 1T-HfSe₂ used by GULP⁸ as expressed in Eq. (3).

	A (eV)	ρ (\AA)	B (\AA ⁴)	r_{\min} (\AA)	r_{\max} (\AA)
Hf-Se	7.871	1.341	24.361	0.0	3.583

TABLE CCC: Three-body SW potential parameters for single-layer 1T-HfSe₂ used by GULP⁸ as expressed in Eq. (4). The angle θ_{ijk} in the first line indicates the bending energy for the angle with atom i as the apex.

	K (eV)	θ_0 (degree)	ρ_1 (\AA)	ρ_2 (\AA)	$r_{\min12}$ (\AA)	$r_{\max12}$ (\AA)	$r_{\min13}$ (\AA)	$r_{\max13}$ (\AA)	$r_{\min23}$ (\AA)	$r_{\max23}$ (\AA)
$\theta_{\text{Hf-Se-Se}}$	37.039	88.093	1.341	1.341	0.0	3.583	0.0	3.583	0.0	5.018
$\theta_{\text{Se-Hf-Hf}}$	37.039	88.093	1.341	1.341	0.0	3.583	0.0	3.583	0.0	5.018

TABLE CCCI: SW potential parameters for single-layer 1T-HfSe₂ used by LAMMPS⁹ as expressed in Eqs. (9) and (10).

	ϵ (eV)	σ (\AA)	a	λ	γ	$\cos\theta_0$	A_L	B_L	p	q	tol
Hf-Se-Se	1.000	1.341	2.672	37.039	1.000	0.033	7.871	7.533	4	0	0.0
Se-Hf-Hf	1.000	1.341	2.672	37.039	1.000	0.033	7.871	7.533	4	0	0.0

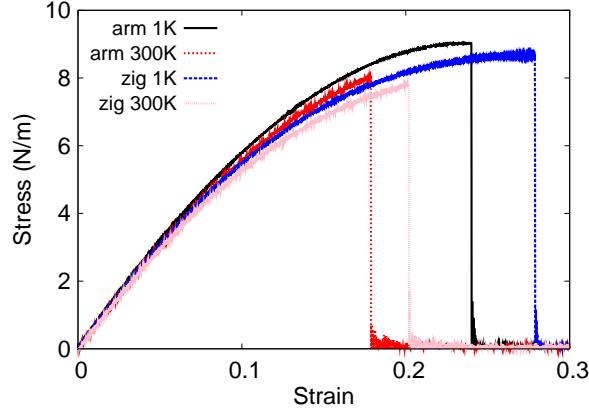


FIG. 149: (Color online) Stress-strain for single-layer 1T-HfSe₂ of dimension $100 \times 100 \text{ \AA}$ along the armchair and zigzag directions.

The structure for the single-layer 1T-HfSe₂ is shown in Fig. 71 (with M=Hf and X=Se). Each Hf atom is surrounded by six Se atoms. These Se atoms are categorized into the top group (eg. atoms 1, 3, and 5) and bottom group (eg. atoms 2, 4, and 6). Each Se atom is connected to three Hf atoms. The structural parameters are from the first-principles calculations,⁵¹ including the lattice constant $a = 3.673 \text{ \AA}$, and the position of the Se atom with respect to the Hf atomic plane $h = 1.575 \text{ \AA}$. The resultant angles are $\theta_{\text{HfSeSe}} = 88.093^\circ$ with S atoms from the same (top or bottom) group, and $\theta_{\text{SeHfHf}} = 88.093^\circ$.

Table CCXCVIII shows three VFF terms for the single-layer 1T-HfSe₂, one of which is the bond stretching interaction shown by Eq. (1) while the other two terms are the angle bending interaction shown by Eq. (2). We note that the angle bending term $K_{\text{Hf-Se-Se}}$ is for the angle $\theta_{\text{Hf-Se-Se}}$ with both Se atoms from the same (top or bottom) group. These force constant parameters are determined by fitting to the three acoustic branches in the phonon dispersion along the ΓM as shown in Fig. 148 (a). The *ab initio* calculations for the phonon dispersion are from Ref. 50. Similar phonon dispersion can also be found in other *ab initio* calculations.³⁴ Fig. 148 (b) shows that the VFF model and the SW potential give exactly the same phonon dispersion, as the SW potential is derived from the VFF model.

The parameters for the two-body SW potential used by GULP are shown in Tab. CCXCIX. The parameters for the three-body SW potential used by GULP are shown in Tab. CCC. Some representative parameters for the SW potential used by LAMMPS are listed in Tab. CCCI.

We use LAMMPS to perform MD simulations for the mechanical behavior of the single-layer 1T-HfSe₂ under uniaxial tension at 1.0 K and 300.0 K. Fig. 149 shows the stress-strain curve for the tension of a single-layer 1T-HfSe₂ of dimension 100 × 100 Å. Periodic boundary conditions are applied in both armchair and zigzag directions. The single-layer 1T-HfSe₂ is stretched uniaxially along the armchair or zigzag direction. The stress is calculated without involving the actual thickness of the quasi-two-dimensional structure of the single-layer 1T-HfSe₂. The Young's modulus can be obtained by a linear fitting of the stress-strain relation in the small strain range of [0, 0.01]. The Young's modulus are 67.3 N/m and 67.0 N/m along the armchair and zigzag directions, respectively. The Young's modulus is essentially isotropic in the armchair and zigzag directions. The Poisson's ratio from the VFF model and the SW potential is $\nu_{xy} = \nu_{yx} = 0.18$.

There is no available value for nonlinear quantities in the single-layer 1T-HfSe₂. We have thus used the nonlinear parameter $B = 0.5d^4$ in Eq. (5), which is close to the value of B in most materials. The value of the third order nonlinear elasticity D can be extracted by fitting the stress-strain relation to the function $\sigma = E\epsilon + \frac{1}{2}D\epsilon^2$ with E as the Young's modulus. The values of D from the present SW potential are -221.5 N/m and -258.6 N/m along the armchair and zigzag directions, respectively. The ultimate stress is about 9.0 Nm⁻¹ at the ultimate strain of 0.24 in the armchair direction at the low temperature of 1 K. The ultimate stress is about 8.7 Nm⁻¹ at the ultimate strain of 0.28 in the zigzag direction at the low temperature of 1 K.

LXXVI. 1T-HfTe₂

Most existing theoretical studies on the single-layer 1T-HfTe₂ are based on the first-principles calculations. In this section, we will develop the SW potential for the single-layer 1T-HfTe₂.

The structure for the single-layer 1T-HfTe₂ is shown in Fig. 71 (with M=Hf and X=Te). Each Hf atom is surrounded by six Te atoms. These Te atoms are categorized into the top group (eg. atoms 1, 3, and 5) and bottom group (eg. atoms 2, 4, and 6). Each Te atom is connected to three Hf atoms. The structural parameters are from the first-principles calculations,⁴⁸ including the lattice constant $a = 3.9606$ Å, and the bond length $d_{\text{Hf-Te}} = 2.8559$ Å, which is derived from the angle $\theta_{\text{TeHfHf}} = 87.8^\circ$. The other angle is

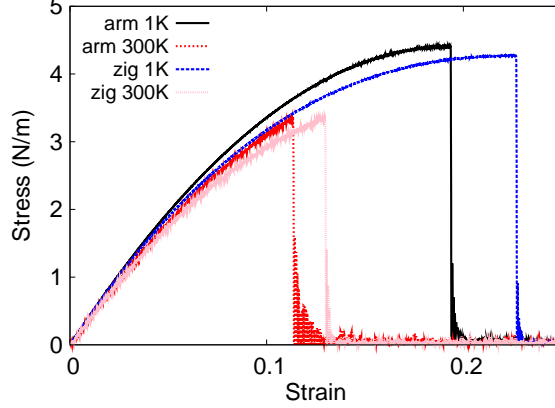


FIG. 150: (Color online) Stress-strain for single-layer 1T-HfTe₂ of dimension $100 \times 100 \text{ \AA}$ along the armchair and zigzag directions.

TABLE CCCII: The VFF model for single-layer 1T-HfTe₂. The second line gives an explicit expression for each VFF term. The third line is the force constant parameters. Parameters are in the unit of $\frac{eV}{\text{Å}^2}$ for the bond stretching interactions, and in the unit of eV for the angle bending interaction. The fourth line gives the initial bond length (in unit of Å) for the bond stretching interaction and the initial angle (in unit of degrees) for the angle bending interaction. The angle θ_{ijk} has atom i as the apex.

VFF type	bond stretching	angle bending	
expression	$\frac{1}{2}K_{\text{Hf-Te}}(\Delta r)^2$	$\frac{1}{2}K_{\text{Hf-Te-Te}}(\Delta\theta)^2$	$\frac{1}{2}K_{\text{Te-Hf-Hf}}(\Delta\theta)^2$
parameter	3.328	3.877	3.877
r_0 or θ_0	2.856	87.801	87.801

$\theta_{\text{HfTeTe}} = 87.8^\circ$ with Te atoms from the same (top or bottom) group.

Table CCCII shows three VFF terms for the single-layer 1T-HfTe₂, one of which is the bond stretching interaction shown by Eq. (1) while the other two terms are the angle bending interaction shown by Eq. (2). We note that the angle bending term $K_{\text{Hf-Te-Te}}$ is for the angle $\theta_{\text{Hf-Te-Te}}$ with both Te atoms from the same (top or bottom) group. We find that there are actually only two parameters in the VFF model, so we can determine their value by fitting to the Young's modulus and the Poisson's ratio of the system. The *ab initio* calculations have predicted the Young's modulus to be 50 N/m and the Poisson's ratio as

TABLE CCCIII: Two-body SW potential parameters for single-layer 1T-HfTe₂ used by GULP⁸ as expressed in Eq. (3).

	A (eV)	ρ (Å)	B (Å ⁴)	r_{\min} (Å)	r_{\max} (Å)
Hf-Te	3.835	1.439	33.262	0.0	3.869

TABLE CCCIV: Three-body SW potential parameters for single-layer 1T-HfTe₂ used by GULP⁸ as expressed in Eq. (4). The angle θ_{ijk} in the first line indicates the bending energy for the angle with atom i as the apex.

	K (eV)	θ_0 (degree)	ρ_1 (Å)	ρ_2 (Å)	$r_{\min12}$ (Å)	$r_{\max12}$ (Å)	$r_{\min13}$ (Å)	$r_{\max13}$ (Å)	$r_{\min23}$ (Å)	$r_{\max23}$ (Å)
$\theta_{\text{Hf-Te-Te}}$	33.196	87.801	1.439	1.439	0.0	3.869	0.0	3.869	0.0	5.410
$\theta_{\text{Te-Hf-Hf}}$	33.196	87.801	1.439	1.439	0.0	3.869	0.0	3.869	0.0	5.410

0.10.⁴⁸

The parameters for the two-body SW potential used by GULP are shown in Tab. CCCIII. The parameters for the three-body SW potential used by GULP are shown in Tab. CCCIV. Some representative parameters for the SW potential used by LAMMPS are listed in Tab. CCCV.

We use LAMMPS to perform MD simulations for the mechanical behavior of the single-layer 1T-HfTe₂ under uniaxial tension at 1.0 K and 300.0 K. Fig. 150 shows the stress-strain curve for the tension of a single-layer 1T-HfTe₂ of dimension 100×100 Å. Periodic boundary conditions are applied in both armchair and zigzag directions. The single-layer 1T-HfTe₂ is stretched uniaxially along the armchair or zigzag direction. The stress is calculated without involving the actual thickness of the quasi-two-dimensional structure of the single-layer 1T-HfTe₂. The Young's modulus can be obtained by a linear fitting of the stress-strain relation in the small strain range of $[0, 0.01]$. The Young's modulus is 43.1 N/m along the armchair and zigzag directions. The Poisson's ratio from the VFF model and the SW potential is

TABLE CCCV: SW potential parameters for single-layer 1T-HfTe₂ used by LAMMPS⁹ as expressed in Eqs. (9) and (10).

	ϵ (eV)	σ (Å)	a	λ	γ	$\cos \theta_0$	A_L	B_L	p	q	tol
Hf-Te ₁ -Te ₁	1.000	1.439	2.690	33.196	1.000	0.038	3.835	7.764	4	0	0.0

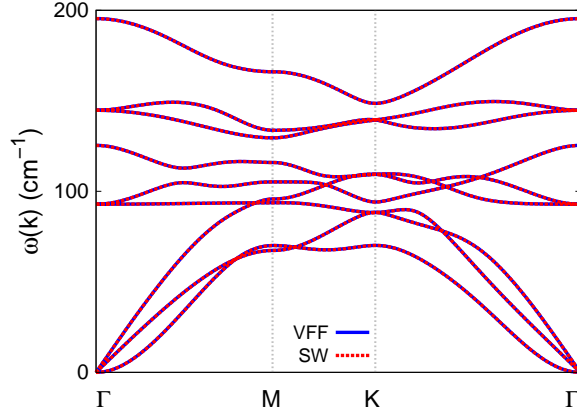


FIG. 151: (Color online) Phonon spectrum for single-layer 1T-HfTe₂ along the Γ MK Γ direction in the Brillouin zone. The phonon dispersion from the SW potential is exactly the same as that from the VFF model.

$\nu_{xy} = \nu_{yx} = 0.10$. The fitted Young's modulus value is about 10% smaller than the *ab initio* result of 50 N/m,⁴⁸ as only short-range interactions are considered in the present work. The long-range interactions are ignored, which typically leads to about 10% underestimation for the value of the Young's modulus.

There is no available value for nonlinear quantities in the single-layer 1T-HfTe₂. We have thus used the nonlinear parameter $B = 0.5d^4$ in Eq. (5), which is close to the value of B in most materials. The value of the third order nonlinear elasticity D can be extracted by fitting the stress-strain relation to the function $\sigma = E\epsilon + \frac{1}{2}D\epsilon^2$ with E as the Young's modulus. The values of D from the present SW potential are -204.3 N/m and -220.7 N/m along the armchair and zigzag directions, respectively. The ultimate stress is about 4.4 Nm⁻¹ at the ultimate strain of 0.19 in the armchair direction at the low temperature of 1 K. The ultimate stress is about 4.3 Nm⁻¹ at the ultimate strain of 0.22 in the zigzag direction at the low temperature of 1 K.

Fig. 151 shows that the VFF model and the SW potential give exactly the same phonon dispersion, as the SW potential is derived from the VFF model.

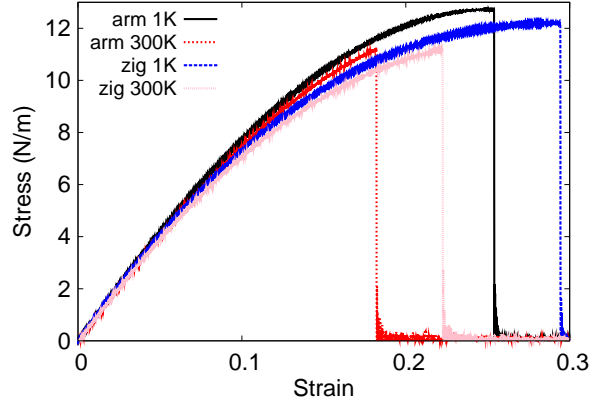


FIG. 152: (Color online) Stress-strain for single-layer 1T-TaS₂ of dimension $100 \times 100 \text{ \AA}$ along the armchair and zigzag directions.

TABLE CCCVI: The VFF model for single-layer 1T-TaS₂. The second line gives an explicit expression for each VFF term. The third line is the force constant parameters. Parameters are in the unit of $\frac{eV}{\text{Å}^2}$ for the bond stretching interactions, and in the unit of eV for the angle bending interaction. The fourth line gives the initial bond length (in unit of Å) for the bond stretching interaction and the initial angle (in unit of degrees) for the angle bending interaction. The angle θ_{ijk} has atom *i* as the apex.

VFF type	bond stretching		angle bending	
expression	$\frac{1}{2}K_{\text{Ta-S}}(\Delta r)^2$	$\frac{1}{2}K_{\text{Ta-S-S}}(\Delta\theta)^2$	$\frac{1}{2}K_{\text{S-Ta-Ta}}(\Delta\theta)^2$	
parameter	11.192	4.774	4.774	
r_0 or θ_0	2.458	85.999	85.999	

LXXVII. 1T-TAS₂

Most existing theoretical studies on the single-layer 1T-TaS₂ are based on the first-principles calculations. In this section, we will develop the SW potential for the single-layer 1T-TaS₂.

The structure for the single-layer 1T-TaS₂ is shown in Fig. 71 (with M=Ta and X=S). Each Ta atom is surrounded by six S atoms. These S atoms are categorized into the top group (eg. atoms 1, 3, and 5) and bottom group (eg. atoms 2, 4, and 6). Each S atom is connected to three Ta atoms. The structural parameters are from the first-principles calculations,⁴⁸

TABLE CCCVII: Two-body SW potential parameters for single-layer 1T-TaS₂ used by GULP⁸ as expressed in Eq. (3).

	A (eV)	ρ (Å)	B (Å ⁴)	r_{\min} (Å)	r_{\max} (Å)
Ta-S	9.110	1.174	18.246	0.0	3.307

TABLE CCCVIII: Three-body SW potential parameters for single-layer 1T-TaS₂ used by GULP⁸ as expressed in Eq. (4). The angle θ_{ijk} in the first line indicates the bending energy for the angle with atom i as the apex.

	K (eV)	θ_0 (degree)	ρ_1 (Å)	ρ_2 (Å)	$r_{\min12}$ (Å)	$r_{\max12}$ (Å)	$r_{\min13}$ (Å)	$r_{\max13}$ (Å)	$r_{\min23}$ (Å)	$r_{\max23}$ (Å)
$\theta_{\text{Ta-S-S}}$	38.092	85.999	1.174	1.174	0.0	3.307	0.0	3.307	0.0	4.579
$\theta_{\text{S-Ta-Ta}}$	38.092	85.999	1.174	1.174	0.0	3.307	0.0	3.307	0.0	4.579

including the lattice constant $a = 3.3524$ Å, and the bond length $d_{\text{Ta-S}} = 2.4578$ Å, which is derived from the angle $\theta_{\text{STaTa}} = 86^\circ$. The other angle is $\theta_{\text{TaSS}} = 86^\circ$ with S atoms from the same (top or bottom) group.

Table CCCVI shows three VFF terms for the single-layer 1T-TaS₂, one of which is the bond stretching interaction shown by Eq. (1) while the other two terms are the angle bending interaction shown by Eq. (2). We note that the angle bending term $K_{\text{Ta-S-S}}$ is for the angle $\theta_{\text{Ta-S-S}}$ with both S atoms from the same (top or bottom) group. We find that there are actually only two parameters in the VFF model, so we can determine their value by fitting to the Young's modulus and the Poisson's ratio of the system. The *ab initio* calculations have predicted the Young's modulus to be 101 N/m and the Poisson's ratio as 0.20.⁴⁸

The parameters for the two-body SW potential used by GULP are shown in Tab. CCCVII. The parameters for the three-body SW potential used by GULP are shown in Tab. CCCVIII. Some representative parameters for the SW potential used by LAMMPS are listed in Tab. CCCIX.

TABLE CCCIX: SW potential parameters for single-layer 1T-TaS₂ used by LAMMPS⁹ as expressed in Eqs. (9) and (10).

	ϵ (eV)	σ (Å)	a	λ	γ	$\cos \theta_0$	A_L	B_L	p	q	tol
Ta-S ₁ -S ₁	1.000	1.174	2.816	38.092	1.000	0.070	9.110	9.589	4	0	0.0

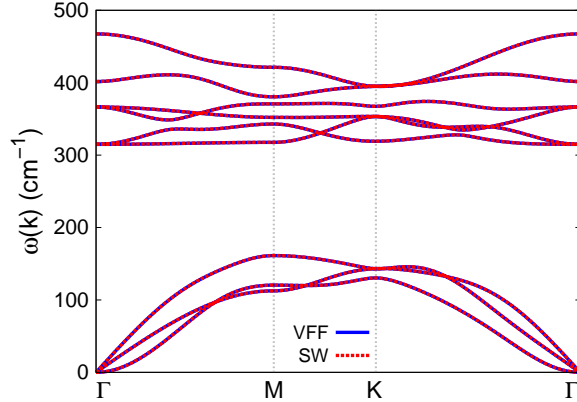


FIG. 153: (Color online) Phonon spectrum for single-layer 1T-TaS₂ along the Γ MK Γ direction in the Brillouin zone. The phonon dispersion from the SW potential is exactly the same as that from the VFF model.

We use LAMMPS to perform MD simulations for the mechanical behavior of the single-layer 1T-TaS₂ under uniaxial tension at 1.0 K and 300.0 K. Fig. 152 shows the stress-strain curve for the tension of a single-layer 1T-TaS₂ of dimension 100×100 Å. Periodic boundary conditions are applied in both armchair and zigzag directions. The single-layer 1T-TaS₂ is stretched uniaxially along the armchair or zigzag direction. The stress is calculated without involving the actual thickness of the quasi-two-dimensional structure of the single-layer 1T-TaS₂. The Young's modulus can be obtained by a linear fitting of the stress-strain relation in the small strain range of $[0, 0.01]$. The Young's modulus are 87.8 N/m and 87.4 N/m along the armchair and zigzag directions, respectively. The Young's modulus is essentially isotropic in the armchair and zigzag directions. The Poisson's ratio from the VFF model and the SW potential is $\nu_{xy} = \nu_{yx} = 0.20$. The fitted Young's modulus value is about 10% smaller than the *ab initio* result of 101 N/m,⁴⁸ as only short-range interactions are considered in the present work. The long-range interactions are ignored, which typically leads to about 10% underestimation for the value of the Young's modulus.

There is no available value for nonlinear quantities in the single-layer 1T-TaS₂. We have thus used the nonlinear parameter $B = 0.5d^4$ in Eq. (5), which is close to the value of B in most materials. The value of the third order nonlinear elasticity D can be extracted by fitting the stress-strain relation to the function $\sigma = E\epsilon + \frac{1}{2}D\epsilon^2$ with E as the Young's modulus. The values of D from the present SW potential are -276.3 N/m and -313.0 N/m along the

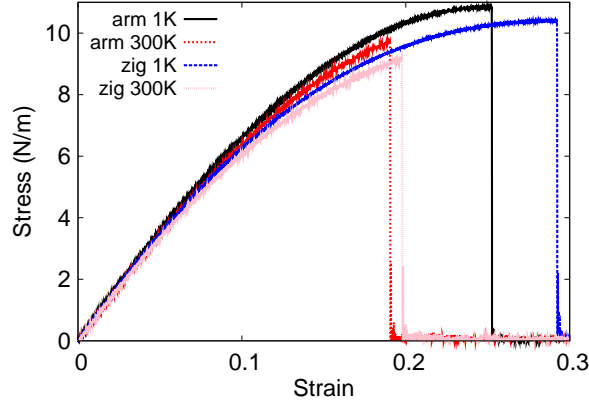


FIG. 154: (Color online) Stress-strain for single-layer 1T-TaSe₂ of dimension $100 \times 100 \text{ \AA}$ along the armchair and zigzag directions.

TABLE CCCX: The VFF model for single-layer 1T-TaSe₂. The second line gives an explicit expression for each VFF term. The third line is the force constant parameters. Parameters are in the unit of $\frac{eV}{\text{Å}^2}$ for the bond stretching interactions, and in the unit of eV for the angle bending interaction. The fourth line gives the initial bond length (in unit of Å) for the bond stretching interaction and the initial angle (in unit of degrees) for the angle bending interaction. The angle θ_{ijk} has atom *i* as the apex.

VFF type	bond stretching	angle bending	
expression	$\frac{1}{2}K_{\text{Ta-Se}}(\Delta r)^2$	$\frac{1}{2}K_{\text{Ta-Se-Se}}(\Delta\theta)^2$	$\frac{1}{2}K_{\text{Se-Ta-Ta}}(\Delta\theta)^2$
parameter	9.348	4.535	4.535
r_0 or θ_0	2.561	84.999	84.999

armchair and zigzag directions, respectively. The ultimate stress is about 12.7 Nm^{-1} at the ultimate strain of 0.25 in the armchair direction at the low temperature of 1 K. The ultimate stress is about 12.2 Nm^{-1} at the ultimate strain of 0.29 in the zigzag direction at the low temperature of 1 K.

Fig. 153 shows that the VFF model and the SW potential give exactly the same phonon dispersion, as the SW potential is derived from the VFF model.

TABLE CCCXI: Two-body SW potential parameters for single-layer 1T-TaSe₂ used by GULP⁸ as expressed in Eq. (3).

	A (eV)	ρ (Å)	B (Å ⁴)	r_{\min} (Å)	r_{\max} (Å)
Ta-Se	8.045	1.188	21.505	0.0	3.433

TABLE CCCXII: Three-body SW potential parameters for single-layer 1T-TaSe₂ used by GULP⁸ as expressed in Eq. (4). The angle θ_{ijk} in the first line indicates the bending energy for the angle with atom i as the apex.

	K (eV)	θ_0 (degree)	ρ_1 (Å)	ρ_2 (Å)	$r_{\min 12}$ (Å)	$r_{\max 12}$ (Å)	$r_{\min 13}$ (Å)	$r_{\max 13}$ (Å)	$r_{\min 23}$ (Å)	$r_{\max 23}$ (Å)
$\theta_{\text{Ta-Se-Se}}$	34.820	84.999	1.188	1.188	0.0	3.433	0.0	3.3433	0.0	4.727
$\theta_{\text{Se-Ta-Ta}}$	34.820	84.999	1.188	1.188	0.0	3.433	0.0	3.3433	0.0	4.727

LXXVIII. 1T-TASE₂

Most existing theoretical studies on the single-layer 1T-TaSe₂ are based on the first-principles calculations. In this section, we will develop the SW potential for the single-layer 1T-TaSe₂.

The structure for the single-layer 1T-TaSe₂ is shown in Fig. 71 (with M=Ta and X=Se). Each Ta atom is surrounded by six Se atoms. These Se atoms are categorized into the top group (eg. atoms 1, 3, and 5) and bottom group (eg. atoms 2, 4, and 6). Each Se atom is connected to three Ta atoms. The structural parameters are from the first-principles calculations,⁴⁸ including the lattice constant $a = 3.4602$ Å, and the bond length $d_{\text{Ta-Se}} = 2.5609$ Å, which is derived from the angle $\theta_{\text{SeTaTa}} = 85^\circ$. The other angle is $\theta_{\text{TaSeSe}} = 85^\circ$ with Se atoms from the same (top or bottom) group.

Table CCCX shows three VFF terms for the single-layer 1T-TaSe₂, one of which is the bond stretching interaction shown by Eq. (1) while the other two terms are the angle bending

TABLE CCCXIII: SW potential parameters for single-layer 1T-TaSe₂ used by LAMMPS⁹ as expressed in Eqs. (9) and (10).

	ϵ (eV)	σ (Å)	a	λ	γ	$\cos \theta_0$	A_L	B_L	p	q	tol
Ta-Se ₁ -Se ₁	1.000	1.188	2.891	34.820	1.000	0.087	8.045	10.813	4	0	0.0

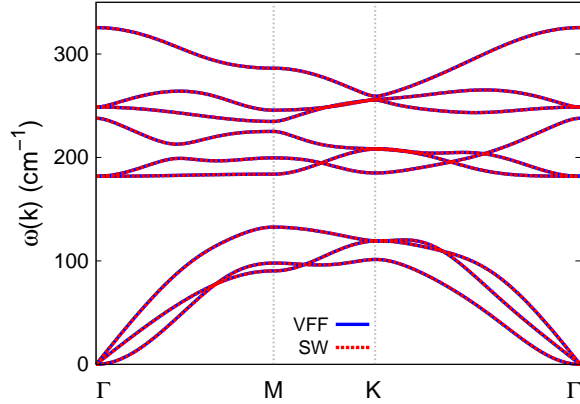


FIG. 155: (Color online) Phonon spectrum for single-layer 1T-TaSe₂ along the Γ MK Γ direction in the Brillouin zone. The phonon dispersion from the SW potential is exactly the same as that from the VFF model.

interaction shown by Eq. (2). We note that the angle bending term $K_{\text{Ta-Se-Se}}$ is for the angle $\theta_{\text{Ta-Se-Se}}$ with both Se atoms from the same (top or bottom) group. We find that there are actually only two parameters in the VFF model, so we can determine their value by fitting to the Young's modulus and the Poisson's ratio of the system. The *ab initio* calculations have predicted the Young's modulus to be 85 N/m and the Poisson's ratio as 0.20.⁴⁸

The parameters for the two-body SW potential used by GULP are shown in Tab. CCCXI. The parameters for the three-body SW potential used by GULP are shown in Tab. CCCXII. Some representative parameters for the SW potential used by LAMMPS are listed in Tab. CCCXIII.

We use LAMMPS to perform MD simulations for the mechanical behavior of the single-layer 1T-TaSe₂ under uniaxial tension at 1.0 K and 300.0 K. Fig. 154 shows the stress-strain curve for the tension of a single-layer 1T-TaSe₂ of dimension $100 \times 100 \text{ \AA}$. Periodic boundary conditions are applied in both armchair and zigzag directions. The single-layer 1T-TaSe₂ is stretched uniaxially along the armchair or zigzag direction. The stress is calculated without involving the actual thickness of the quasi-two-dimensional structure of the single-layer 1T-TaSe₂. The Young's modulus can be obtained by a linear fitting of the stress-strain relation in the small strain range of $[0, 0.01]$. The Young's modulus are 74.6 N/m and 74.4 N/m along the armchair and zigzag directions, respectively. The Young's modulus is essentially isotropic in the armchair and zigzag directions. The Poisson's ratio from the VFF model

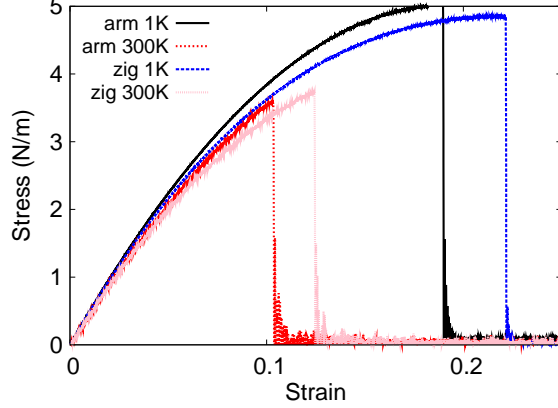


FIG. 156: (Color online) Stress-strain for single-layer 1T-TaTe₂ of dimension $100 \times 100 \text{ \AA}$ along the armchair and zigzag directions.

and the SW potential is $\nu_{xy} = \nu_{yx} = 0.20$. The fitted Young's modulus value is about 10% smaller than the *ab initio* result of 85 N/m ,⁴⁸ as only short-range interactions are considered in the present work. The long-range interactions are ignored, which typically leads to about 10% underestimation for the value of the Young's modulus.

There is no available value for nonlinear quantities in the single-layer 1T-TaSe₂. We have thus used the nonlinear parameter $B = 0.5d^4$ in Eq. (5), which is close to the value of B in most materials. The value of the third order nonlinear elasticity D can be extracted by fitting the stress-strain relation to the function $\sigma = E\epsilon + \frac{1}{2}D\epsilon^2$ with E as the Young's modulus. The values of D from the present SW potential are -231.7 N/m and -265.4 N/m along the armchair and zigzag directions, respectively. The ultimate stress is about 10.8 Nm^{-1} at the ultimate strain of 0.25 in the armchair direction at the low temperature of 1 K. The ultimate stress is about 10.4 Nm^{-1} at the ultimate strain of 0.29 in the zigzag direction at the low temperature of 1 K.

Fig. 155 shows that the VFF model and the SW potential give exactly the same phonon dispersion, as the SW potential is derived from the VFF model.

LXXIX. 1T-TATE₂

Most existing theoretical studies on the single-layer 1T-TaTe₂ are based on the first-principles calculations. In this section, we will develop the SW potential for the single-layer

TABLE CCCXIV: The VFF model for single-layer 1T-TaTe₂. The second line gives an explicit expression for each VFF term. The third line is the force constant parameters. Parameters are in the unit of $\frac{\text{eV}}{\text{\AA}^2}$ for the bond stretching interactions, and in the unit of eV for the angle bending interaction. The fourth line gives the initial bond length (in unit of \AA) for the bond stretching interaction and the initial angle (in unit of degrees) for the angle bending interaction. The angle θ_{ijk} has atom i as the apex.

VFF type	bond stretching	angle bending	
expression	$\frac{1}{2}K_{\text{Ta-Te}}(\Delta r)^2$	$\frac{1}{2}K_{\text{Ta-Te-Te}}(\Delta\theta)^2$	$\frac{1}{2}K_{\text{Te-Ta-Ta}}(\Delta\theta)^2$
parameter	3.442	4.516	4.516
r_0 or θ_0	2.770	82.999	82.999

TABLE CCCXV: Two-body SW potential parameters for single-layer 1T-TaTe₂ used by GULP⁸ as expressed in Eq. (3).

	A (eV)	ρ (\AA)	B (\AA^4)	r_{min} (\AA)	r_{max} (\AA)
Ta-Te	3.283	1.207	29.415	0.0	3.684

1T-TaTe₂.

The structure for the single-layer 1T-TaTe₂ is shown in Fig. 71 (with M=Ta and X=Te). Each Ta atom is surrounded by six Te atoms. These Te atoms are categorized into the top group (eg. atoms 1, 3, and 5) and bottom group (eg. atoms 2, 4, and 6). Each Te atom is connected to three Ta atoms. The structural parameters are from the first-principles calculations,⁴⁸ including the lattice constant $a = 3.6702 \text{ \AA}$, and the bond length $d_{\text{Ta-Te}} = 2.7695 \text{ \AA}$, which is derived from the angle $\theta_{\text{TeTaTa}} = 83^\circ$. The other angle is

TABLE CCCXVI: Three-body SW potential parameters for single-layer 1T-TaTe₂ used by GULP⁸ as expressed in Eq. (4). The angle θ_{ijk} in the first line indicates the bending energy for the angle with atom i as the apex.

	K (eV)	θ_0 (degree)	ρ_1 (\AA)	ρ_2 (\AA)	r_{min12} (\AA)	r_{max12} (\AA)	r_{min13} (\AA)	r_{max13} (\AA)	r_{min23} (\AA)	r_{max23} (\AA)
$\theta_{\text{Ta-Te-Te}}$	32.144	82.999	1.207	1.207	0.0	3.684	0.0	3.684	0.0	5.014
$\theta_{\text{Te-Ta-Ta}}$	32.144	82.999	1.207	1.207	0.0	3.684	0.0	3.684	0.0	5.014

TABLE CCCXVII: SW potential parameters for single-layer 1T-TaTe₂ used by LAMMPS⁹ as expressed in Eqs. (9) and (10).

	ϵ (eV)	σ (Å)	a	λ	γ	$\cos \theta_0$	A_L	B_L	p	q	tol
Ta-Se ₁ -Se ₁	1.000	1.188	2.891	34.820	1.000	0.087	8.045	10.813	4	0	0.0

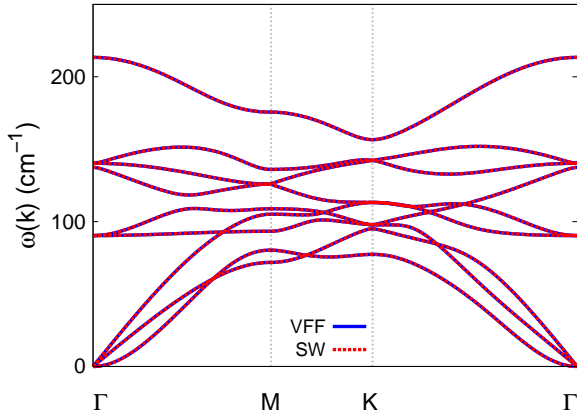


FIG. 157: (Color online) Phonon spectrum for single-layer 1T-TaTe₂ along the Γ MK Γ direction in the Brillouin zone. The phonon dispersion from the SW potential is exactly the same as that from the VFF model.

$\theta_{\text{TaTeTe}} = 83^\circ$ with Te atoms from the same (top or bottom) group.

Table CCCXIV shows three VFF terms for the single-layer 1T-TaTe₂, one of which is the bond stretching interaction shown by Eq. (1) while the other two terms are the angle bending interaction shown by Eq. (2). We note that the angle bending term $K_{\text{Ta-Te-Te}}$ is for the angle $\theta_{\text{Ta-Te-Te}}$ with both Te atoms from the same (top or bottom) group. We find that there are actually only two parameters in the VFF model, so we can determine their value by fitting to the Young's modulus and the Poisson's ratio of the system. The *ab initio* calculations have predicted the Young's modulus to be 57 N/m and the Poisson's ratio as 0.10.⁴⁸

The parameters for the two-body SW potential used by GULP are shown in Tab. CCCXV. The parameters for the three-body SW potential used by GULP are shown in Tab. CCCXVI. Some representative parameters for the SW potential used by LAMMPS are listed in Tab. CCCXVII.

We use LAMMPS to perform MD simulations for the mechanical behavior of the single-

layer 1T-TaTe₂ under uniaxial tension at 1.0 K and 300.0 K. Fig. 156 shows the stress-strain curve for the tension of a single-layer 1T-TaTe₂ of dimension 100 × 100 Å. Periodic boundary conditions are applied in both armchair and zigzag directions. The single-layer 1T-TaTe₂ is stretched uniaxially along the armchair or zigzag direction. The stress is calculated without involving the actual thickness of the quasi-two-dimensional structure of the single-layer 1T-TaTe₂. The Young's modulus can be obtained by a linear fitting of the stress-strain relation in the small strain range of [0, 0.01]. The Young's modulus are 50.3 N/m and 50.0 N/m along the armchair and zigzag directions, respectively. The Young's modulus is essentially isotropic in the armchair and zigzag directions. The Poisson's ratio from the VFF model and the SW potential is $\nu_{xy} = \nu_{yx} = 0.10$. The fitted Young's modulus value is about 10% smaller than the *ab initio* result of 57 N/m,⁴⁸ as only short-range interactions are considered in the present work. The long-range interactions are ignored, which typically leads to about 10% underestimation for the value of the Young's modulus.

There is no available value for nonlinear quantities in the single-layer 1T-TaTe₂. We have thus used the nonlinear parameter $B = 0.5d^4$ in Eq. (5), which is close to the value of B in most materials. The value of the third order nonlinear elasticity D can be extracted by fitting the stress-strain relation to the function $\sigma = E\epsilon + \frac{1}{2}D\epsilon^2$ with E as the Young's modulus. The values of D from the present SW potential are -247.1 N/m and -262.2 N/m along the armchair and zigzag directions, respectively. The ultimate stress is about 5.0 Nm⁻¹ at the ultimate strain of 0.19 in the armchair direction at the low temperature of 1 K. The ultimate stress is about 4.9 Nm⁻¹ at the ultimate strain of 0.22 in the zigzag direction at the low temperature of 1 K.

Fig. 157 shows that the VFF model and the SW potential give exactly the same phonon dispersion, as the SW potential is derived from the VFF model.

LXXX. 1T-WS₂

Most existing theoretical studies on the single-layer 1T-WS₂ are based on the first-principles calculations. In this section, we will develop the SW potential for the single-layer 1T-WS₂.

The structure for the single-layer 1T-WS₂ is shown in Fig. 71 (with M=W and X=S). Each W atom is surrounded by six S atoms. These S atoms are categorized into the top group

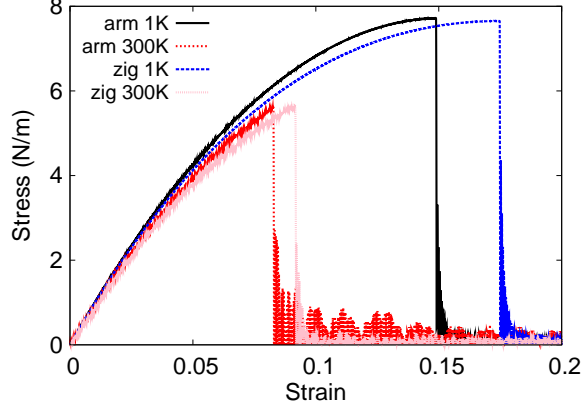


FIG. 158: (Color online) Stress-strain for single-layer 1T-WS₂ of dimension 100 × 100 Å along the armchair and zigzag directions.

TABLE CCCXVIII: The VFF model for single-layer 1T-WS₂. The second line gives an explicit expression for each VFF term. The third line is the force constant parameters. Parameters are in the unit of $\frac{\text{eV}}{\text{Å}^2}$ for the bond stretching interactions, and in the unit of eV for the angle bending interaction. The fourth line gives the initial bond length (in unit of Å) for the bond stretching interaction and the initial angle (in unit of degrees) for the angle bending interaction. The angle θ_{ijk} has atom *i* as the apex.

VFF type	bond stretching	angle bending	
expression	$\frac{1}{2}K_{\text{W-S}}(\Delta r)^2$	$\frac{1}{2}K_{\text{W-S-S}}(\Delta\theta)^2$	$\frac{1}{2}K_{\text{S-W-W}}(\Delta\theta)^2$
parameter	4.395	10.087	10.087
r_0 or θ_0	2.413	82.799	82.799

(eg. atoms 1, 3, and 5) and bottom group (eg. atoms 2, 4, and 6). Each S atom is connected to three W atoms. The structural parameters are from the first-principles calculations,⁴⁸ including the lattice constant $a = 3.1908$ Å, and the bond length $d_{\text{W-S}} = 2.4125$ Å, which is derived from the angle $\theta_{\text{SWW}} = 82.8^\circ$. The other angle is $\theta_{\text{WSS}} = 82.8^\circ$ with S atoms from the same (top or bottom) group.

Table CCCXVIII shows three VFF terms for the single-layer 1T-WS₂, one of which is the bond stretching interaction shown by Eq. (1) while the other two terms are the angle bending interaction shown by Eq. (2). We note that the angle bending term $K_{\text{W-S-S}}$ is

TABLE CCCXIX: Two-body SW potential parameters for single-layer 1T-WS₂ used by GULP⁸ as expressed in Eq. (3).

	A (eV)	ρ (Å)	B (Å ⁴)	r_{\min} (Å)	r_{\max} (Å)
W-S	3.163	1.045	16.937	0.0	3.206

TABLE CCCXX: Three-body SW potential parameters for single-layer 1T-WS₂ used by GULP⁸ as expressed in Eq. (4). The angle θ_{ijk} in the first line indicates the bending energy for the angle with atom i as the apex.

	K (eV)	θ_0 (degree)	ρ_1 (Å)	ρ_2 (Å)	$r_{\min12}$ (Å)	$r_{\max12}$ (Å)	$r_{\min13}$ (Å)	$r_{\max13}$ (Å)	$r_{\min23}$ (Å)	$r_{\max23}$ (Å)
θ_{W-S-S}	71.264	82.799	1.045	1.045	0.0	3.206	0.0	3.206	0.0	4.359
θ_{S-W-W}	71.264	82.799	1.045	1.045	0.0	3.206	0.0	3.206	0.0	4.359

for the angle θ_{W-S-S} with both S atoms from the same (top or bottom) group. We find that there are actually only two parameters in the VFF model, so we can determine their value by fitting to the Young’s modulus and the Poisson’s ratio of the system. The *ab initio* calculations have predicted the Young’s modulus to be 113 N/m and the Poisson’s ratio as -0.03.⁴⁸ The *ab initio* calculations have predicted a negative Poisson’s ratio in the 1T-WS₂, which was attributed to the orbital coupling in this material. The orbital coupling enhances the angle bending interaction in the VFF model. As a result, the value of the angle bending parameter is much larger than the bond stretching force constant parameter, which is typical in auxetic materials with negative Poisson’s ratio.⁵²

The parameters for the two-body SW potential used by GULP are shown in Tab. CCCXIX. The parameters for the three-body SW potential used by GULP are shown in Tab. CCCXX. Some representative parameters for the SW potential used by LAMMPS are listed in Tab. CCCXXI.

We use LAMMPS to perform MD simulations for the mechanical behavior of the single-

TABLE CCCXXI: SW potential parameters for single-layer 1T-WS₂ used by LAMMPS⁹ as expressed in Eqs. (9) and (10).

	ϵ (eV)	σ (Å)	a	λ	γ	$\cos \theta_0$	A_L	B_L	p	q	tol
W-S ₁ -S ₁	1.000	1.045	3.069	71.264	1.000	0.125	3.163	14.209	4	0	0.0

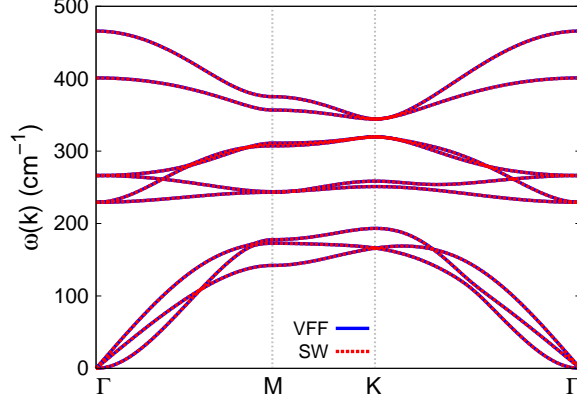


FIG. 159: (Color online) Phonon spectrum for single-layer 1T-WS₂ along the Γ MK Γ direction in the Brillouin zone. The phonon dispersion from the SW potential is exactly the same as that from the VFF model.

layer 1T-WS₂ under uniaxial tension at 1.0 K and 300.0 K. Fig. 158 shows the stress-strain curve for the tension of a single-layer 1T-WS₂ of dimension $100 \times 100 \text{ \AA}$. Periodic boundary conditions are applied in both armchair and zigzag directions. The single-layer 1T-WS₂ is stretched uniaxially along the armchair or zigzag direction. The stress is calculated without involving the actual thickness of the quasi-two-dimensional structure of the single-layer 1T-WS₂. The Young's modulus can be obtained by a linear fitting of the stress-strain relation in the small strain range of $[0, 0.01]$. The Young's modulus are 100.2 N/m and 99.5 N/m along the armchair and zigzag directions, respectively. The Young's modulus is essentially isotropic in the armchair and zigzag directions. The Poisson's ratio from the VFF model and the SW potential is $\nu_{xy} = \nu_{yx} = -0.03$. The fitted Young's modulus value is about 10% smaller than the *ab initio* result of 113 N/m,⁴⁸ as only short-range interactions are considered in the present work. The long-range interactions are ignored, which typically leads to about 10% underestimation for the value of the Young's modulus.

There is no available value for nonlinear quantities in the single-layer 1T-WS₂. We have thus used the nonlinear parameter $B = 0.5d^4$ in Eq. (5), which is close to the value of B in most materials. The value of the third order nonlinear elasticity D can be extracted by fitting the stress-strain relation to the function $\sigma = E\epsilon + \frac{1}{2}D\epsilon^2$ with E as the Young's modulus. The values of D from the present SW potential are -666.6 N/m and -660.6 N/m along the armchair and zigzag directions, respectively. The ultimate stress is about 7.7 Nm^{-1}

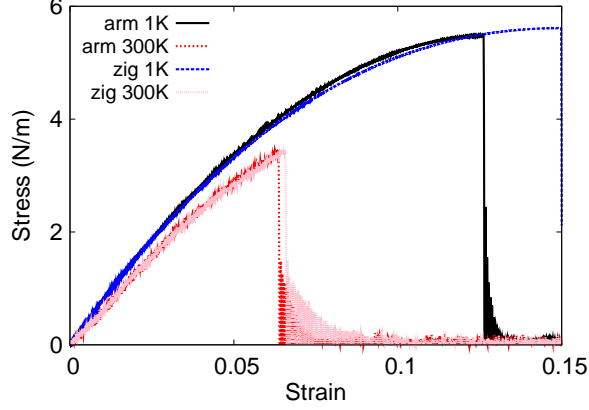


FIG. 160: (Color online) Stress-strain for single-layer 1T-WSe₂ of dimension $100 \times 100 \text{ \AA}$ along the armchair and zigzag directions.

TABLE CCCXXII: The VFF model for single-layer 1T-WSe₂. The second line gives an explicit expression for each VFF term. The third line is the force constant parameters. Parameters are in the unit of $\frac{\text{eV}}{\text{Å}^2}$ for the bond stretching interactions, and in the unit of eV for the angle bending interaction. The fourth line gives the initial bond length (in unit of Å) for the bond stretching interaction and the initial angle (in unit of degrees) for the angle bending interaction. The angle θ_{ijk} has atom *i* as the apex.

VFF type	bond stretching	angle bending	
expression	$\frac{1}{2}K_{\text{W-Se}}(\Delta r)^2$	$\frac{1}{2}K_{\text{W-Se-Se}}(\Delta\theta)^2$	$\frac{1}{2}K_{\text{Se-W-W}}(\Delta\theta)^2$
parameter	2.556	15.375	15.375
r_0 or θ_0	2.521	80.501	80.501

at the ultimate strain of 0.15 in the armchair direction at the low temperature of 1 K. The ultimate stress is about 7.7 Nm^{-1} at the ultimate strain of 0.17 in the zigzag direction at the low temperature of 1 K.

Fig. 159 shows that the VFF model and the SW potential give exactly the same phonon dispersion, as the SW potential is derived from the VFF model.

TABLE CCCXXIII: Two-body SW potential parameters for single-layer 1T-WSe₂ used by GULP⁸ as expressed in Eq. (3).

	A (eV)	ρ (Å)	B (Å ⁴)	r_{\min} (Å)	r_{\max} (Å)
W-Se	1.885	1.013	20.186	0.0	3.320

TABLE CCCXXIV: Three-body SW potential parameters for single-layer 1T-WSe₂ used by GULP⁸ as expressed in Eq. (4). The angle θ_{ijk} in the first line indicates the bending energy for the angle with atom i as the apex.

	K (eV)	θ_0 (degree)	ρ_1 (Å)	ρ_2 (Å)	$r_{\min12}$ (Å)	$r_{\max12}$ (Å)	$r_{\min13}$ (Å)	$r_{\max13}$ (Å)	$r_{\min23}$ (Å)	$r_{\max23}$ (Å)
$\theta_{W-Se-Se}$	99.800	80.501	1.013	1.013	0.0	3.320	0.0	3.320	0.0	4.450
θ_{Se-W-W}	99.800	80.501	1.013	1.013	0.0	3.320	0.0	3.320	0.0	4.450

LXXXI. 1T-WSe₂

Most existing theoretical studies on the single-layer 1T-WSe₂ are based on the first-principles calculations. In this section, we will develop the SW potential for the single-layer 1T-WSe₂.

The structure for the single-layer 1T-WSe₂ is shown in Fig. 71 (with M=W and X=Se). Each W atom is surrounded by six Se atoms. These Se atoms are categorized into the top group (eg. atoms 1, 3, and 5) and bottom group (eg. atoms 2, 4, and 6). Each Se atom is connected to three W atoms. The structural parameters are from the first-principles calculations,⁴⁸ including the lattice constant $a = 3.2574$ Å, and the bond length $d_{W-Se} = 2.5207$ Å, which is derived from the angle $\theta_{SeWW} = 80.5^\circ$. The other angle is $\theta_{WSeSe} = 80.5^\circ$ with Se atoms from the same (top or bottom) group.

Table CCCXXII shows three VFF terms for the single-layer 1T-WSe₂, one of which is the bond stretching interaction shown by Eq. (1) while the other two terms are the angle

TABLE CCCXXV: SW potential parameters for single-layer 1T-WSe₂ used by LAMMPS⁹ as expressed in Eqs. (9) and (10).

	ϵ (eV)	σ (Å)	a	λ	γ	$\cos \theta_0$	A_L	B_L	p	q	tol
W-Se ₁ -Se ₁	1.000	1.013	3.277	99.800	1.000	0.165	1.885	19.156	4	0	0.0

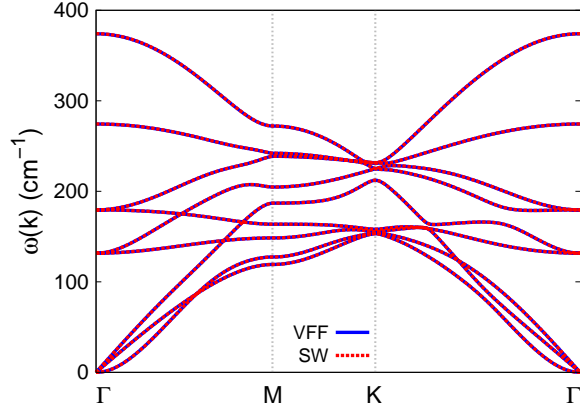


FIG. 161: (Color online) Phonon spectrum for single-layer 1T-WSe₂ along the Γ MK Γ direction in the Brillouin zone. The phonon dispersion from the SW potential is exactly the same as that from the VFF model.

bending interaction shown by Eq. (2). We note that the angle bending term $K_{\text{W-Se-Se}}$ is for the angle $\theta_{\text{W-Se-Se}}$ with both Se atoms from the same (top or bottom) group. We find that there are actually only two parameters in the VFF model, so we can determine their value by fitting to the Young's modulus and the Poisson's ratio of the system. The *ab initio* calculations have predicted the Young's modulus to be 94 N/m and the Poisson's ratio as -0.15.⁴⁸ The *ab initio* calculations have predicted a negative Poisson's ratio in the 1T-WSe₂, which was attributed to the orbital coupling in this material. The orbital coupling enhances the angle bending interaction in the VFF model. As a result, the value of the angle bending parameter is much larger than the bond stretching force constant parameter, which is typical in auxetic materials with negative Poisson's ratio.⁵²

The parameters for the two-body SW potential used by GULP are shown in Tab. CCCXXIII. The parameters for the three-body SW potential used by GULP are shown in Tab. CCCXXIV. Some representative parameters for the SW potential used by LAMMPS are listed in Tab. CCCXXV.

We use LAMMPS to perform MD simulations for the mechanical behavior of the single-layer 1T-WSe₂ under uniaxial tension at 1.0 K and 300.0 K. Fig. 160 shows the stress-strain curve for the tension of a single-layer 1T-WSe₂ of dimension $100 \times 100 \text{ \AA}$. Periodic boundary conditions are applied in both armchair and zigzag directions. The single-layer 1T-WSe₂ is stretched uniaxially along the armchair or zigzag direction. The stress is calculated without

involving the actual thickness of the quasi-two-dimensional structure of the single-layer 1T-WSe₂. The Young's modulus can be obtained by a linear fitting of the stress-strain relation in the small strain range of [0, 0.01]. The Young's modulus are 80.5 N/m and 80.3 N/m along the armchair and zigzag directions, respectively. The Young's modulus is essentially isotropic in the armchair and zigzag directions. The Poisson's ratio from the VFF model and the SW potential is $\nu_{xy} = \nu_{yx} = -0.15$. The fitted Young's modulus value is about 10% smaller than the *ab initio* result of 94 N/m,⁴⁸ as only short-range interactions are considered in the present work. The long-range interactions are ignored, which typically leads to about 10% underestimation for the value of the Young's modulus.

There is no available value for nonlinear quantities in the single-layer 1T-WSe₂. We have thus used the nonlinear parameter $B = 0.5d^4$ in Eq. (5), which is close to the value of B in most materials. The value of the third order nonlinear elasticity D can be extracted by fitting the stress-strain relation to the function $\sigma = E\epsilon + \frac{1}{2}D\epsilon^2$ with E as the Young's modulus. The values of D from the present SW potential are -666.1 N/m and -580.1 N/m along the armchair and zigzag directions, respectively. The ultimate stress is about 5.5 Nm⁻¹ at the ultimate strain of 0.13 in the armchair direction at the low temperature of 1 K. The ultimate stress is about 5.6 Nm⁻¹ at the ultimate strain of 0.15 in the zigzag direction at the low temperature of 1 K.

Fig. 161 shows that the VFF model and the SW potential give exactly the same phonon dispersion, as the SW potential is derived from the VFF model.

LXXXII. 1T-WTe₂

Most existing theoretical studies on the single-layer 1T-WTe₂ are based on the first-principles calculations. In this section, we will develop the SW potential for the single-layer 1T-WTe₂.

The structure for the single-layer 1T-WTe₂ is shown in Fig. 71 (with M=W and X=Te). Each W atom is surrounded by six Te atoms. These Te atoms are categorized into the top group (eg. atoms 1, 3, and 5) and bottom group (eg. atoms 2, 4, and 6). Each Te atom is connected to three W atoms. The structural parameters are from the first-principles calculations,⁴⁸ including the lattice constant $a = 3.4970 \text{ \AA}$, and the bond length $d_{W-Te} = 2.7202 \text{ \AA}$, which is derived from the angle $\theta_{TeWW} = 80.0^\circ$. The other angle is

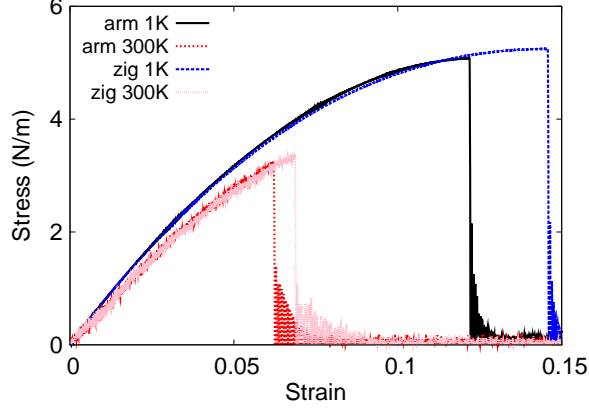


FIG. 162: (Color online) Stress-strain for single-layer 1T-WTe₂ of dimension $100 \times 100 \text{ \AA}$ along the armchair and zigzag directions.

TABLE CCCXXVI: The VFF model for single-layer 1T-WTe₂. The second line gives an explicit expression for each VFF term. The third line is the force constant parameters. Parameters are in the unit of $\frac{eV}{\text{Å}^2}$ for the bond stretching interactions, and in the unit of eV for the angle bending interaction. The fourth line gives the initial bond length (in unit of Å) for the bond stretching interaction and the initial angle (in unit of degrees) for the angle bending interaction. The angle θ_{ijk} has atom i as the apex.

VFF type	bond stretching	angle bending	
expression	$\frac{1}{2}K_{W-Te}(\Delta r)^2$	$\frac{1}{2}K_{W-Te-Te}(\Delta\theta)^2$	$\frac{1}{2}K_{Te-W-W}(\Delta\theta)^2$
parameter	2.272	19.437	19.437
r_0 or θ_0	2.720	79.999	79.999

$\theta_{WTeTe} = 80.0^\circ$ with Te atoms from the same (top or bottom) group.

Table CCCXXVI shows three VFF terms for the single-layer 1T-WTe₂, one of which is the bond stretching interaction shown by Eq. (1) while the other two terms are the angle bending interaction shown by Eq. (2). We note that the angle bending term $K_{W-Te-Te}$ is for the angle $\theta_{W-Te-Te}$ with both Te atoms from the same (top or bottom) group. We find that there are actually only two parameters in the VFF model, so we can determine their value by fitting to the Young's modulus and the Poisson's ratio of the system. The *ab initio* calculations have predicted the Young's modulus to be 88 N/m and the Poisson's ratio as

TABLE CCCXXVII: Two-body SW potential parameters for single-layer 1T-WTe₂ used by GULP⁸ as expressed in Eq. (3).

	A (eV)	ρ (Å)	B (Å ⁴)	r_{\min} (Å)	r_{\max} (Å)
W-Te	1.924	1.075	27.376	0.0	3.575

TABLE CCCXXVIII: Three-body SW potential parameters for single-layer 1T-WTe₂ used by GULP⁸ as expressed in Eq. (4). The angle θ_{ijk} in the first line indicates the bending energy for the angle with atom i as the apex.

	K (eV)	θ_0 (degree)	ρ_1 (Å)	ρ_2 (Å)	$r_{\min12}$ (Å)	$r_{\max12}$ (Å)	$r_{\min13}$ (Å)	$r_{\max13}$ (Å)	$r_{\min23}$ (Å)	$r_{\max23}$ (Å)
$\theta_{W-Te-Te}$	123.899	79.999	1.075	1.075	0.0	3.575	0.0	3.575	0.0	4.777
θ_{Te-W-W}	123.899	79.999	1.075	1.075	0.0	3.575	0.0	3.575	0.0	4.777

-0.18.⁴⁸ The *ab initio* calculations have predicted a negative Poisson's ratio in the 1T-WTe₂, which was attributed to the orbital coupling in this material. The orbital coupling enhances the angle bending interaction in the VFF model. As a result, the value of the angle bending parameter is much larger than the bond stretching force constant parameter, which is typical in auxetic materials with negative Poisson's ratio.⁵²

The parameters for the two-body SW potential used by GULP are shown in Tab. CCCXXVII. The parameters for the three-body SW potential used by GULP are shown in Tab. CCCXXVIII. Some representative parameters for the SW potential used by LAMMPS are listed in Tab. CCCXXIX.

We use LAMMPS to perform MD simulations for the mechanical behavior of the single-layer 1T-WTe₂ under uniaxial tension at 1.0 K and 300.0 K. Fig. 162 shows the stress-strain curve for the tension of a single-layer 1T-WTe₂ of dimension 100 × 100 Å. Periodic boundary conditions are applied in both armchair and zigzag directions. The single-layer 1T-WTe₂ is stretched uniaxially along the armchair or zigzag direction. The stress is calculated without

TABLE CCCXXIX: SW potential parameters for single-layer 1T-WTe₂ used by LAMMPS⁹ as expressed in Eqs. (9) and (10).

	ϵ (eV)	σ (Å)	a	λ	γ	$\cos\theta_0$	A_L	B_L	p	q	tol
W-Te ₁ -Te ₁	1.000	1.075	3.325	123.899	1.000	0.174	1.924	20.483	4	0	0.0

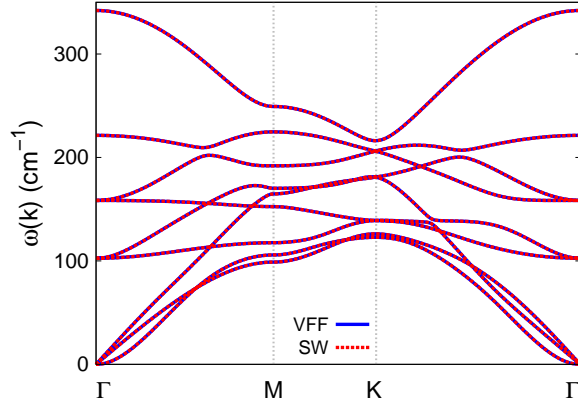


FIG. 163: (Color online) Phonon spectrum for single-layer 1T-WTe₂ along the Γ MK Γ direction in the Brillouin zone. The phonon dispersion from the SW potential is exactly the same as that from the VFF model.

involving the actual thickness of the quasi-two-dimensional structure of the single-layer 1T-WTe₂. The Young's modulus can be obtained by a linear fitting of the stress-strain relation in the small strain range of $[0, 0.01]$. The Young's modulus are 75.9 N/m and 75.8 N/m along the armchair and zigzag directions, respectively. The Young's modulus is essentially isotropic in the armchair and zigzag directions. The Poisson's ratio from the VFF model and the SW potential is $\nu_{xy} = \nu_{yx} = -0.18$. The fitted Young's modulus value is about 10% smaller than the *ab initio* result of 88 N/m,⁴⁸ as only short-range interactions are considered in the present work. The long-range interactions are ignored, which typically leads to about 10% underestimation for the value of the Young's modulus.

There is no available value for nonlinear quantities in the single-layer 1T-WTe₂. We have thus used the nonlinear parameter $B = 0.5d^4$ in Eq. (5), which is close to the value of B in most materials. The value of the third order nonlinear elasticity D can be extracted by fitting the stress-strain relation to the function $\sigma = E\epsilon + \frac{1}{2}D\epsilon^2$ with E as the Young's modulus. The values of D from the present SW potential are -546.0 N/m and -551.5 N/m along the armchair and zigzag directions, respectively. The ultimate stress is about 5.1 Nm⁻¹ at the ultimate strain of 0.12 in the armchair direction at the low temperature of 1 K. The ultimate stress is about 5.2 Nm⁻¹ at the ultimate strain of 0.14 in the zigzag direction at the low temperature of 1 K.

Fig. 163 shows that the VFF model and the SW potential give exactly the same phonon

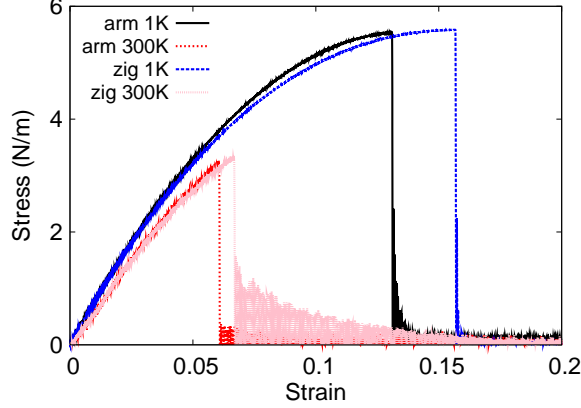


FIG. 164: (Color online) Stress-strain for single-layer 1T-ReS₂ of dimension $100 \times 100 \text{ \AA}$ along the armchair and zigzag directions.

TABLE CCCXXX: The VFF model for single-layer 1T-ReS₂. The second line gives an explicit expression for each VFF term. The third line is the force constant parameters. Parameters are in the unit of $\frac{eV}{\text{Å}^2}$ for the bond stretching interactions, and in the unit of eV for the angle bending interaction. The fourth line gives the initial bond length (in unit of Å) for the bond stretching interaction and the initial angle (in unit of degrees) for the angle bending interaction. The angle θ_{ijk} has atom *i* as the apex.

VFF type	bond stretching	angle bending	
expression	$\frac{1}{2}K_{\text{Re-S}}(\Delta r)^2$	$\frac{1}{2}K_{\text{Re-S-S}}(\Delta\theta)^2$	$\frac{1}{2}K_{\text{S-Re-Re}}(\Delta\theta)^2$
parameter	2.684	10.829	10.829
r_0 or θ_0	2.405	79.498	79.498

dispersion, as the SW potential is derived from the VFF model.

LXXXIII. 1T-RES₂

Most existing theoretical studies on the single-layer 1T-ReS₂ are based on the first-principles calculations. In this section, we will develop the SW potential for the single-layer 1T-ReS₂.

The structure for the single-layer 1T-ReS₂ is shown in Fig. 71 (with M=Re and X=S). Each Re atom is surrounded by six S atoms. These S atoms are categorized into the top group

TABLE CCCXXXI: Two-body SW potential parameters for single-layer 1T-ReS₂ used by GULP⁸ as expressed in Eq. (3).

	A (eV)	ρ (Å)	B (Å ⁴)	r_{\min} (Å)	r_{\max} (Å)
Re-S	1.751	0.934	16.714	0.0	3.154

TABLE CCCXXXII: Three-body SW potential parameters for single-layer 1T-ReS₂ used by GULP⁸ as expressed in Eq. (4). The angle θ_{ijk} in the first line indicates the bending energy for the angle with atom i as the apex.

	K (eV)	θ_0 (degree)	ρ_1 (Å)	ρ_2 (Å)	$r_{\min12}$ (Å)	$r_{\max12}$ (Å)	$r_{\min13}$ (Å)	$r_{\max13}$ (Å)	$r_{\min23}$ (Å)	$r_{\max23}$ (Å)
$\theta_{\text{Re-S-S}}$	67.797	79.498	0.934	0.934	0.0	3.154	0.0	3.154	0.0	4.201
$\theta_{\text{S-Re-Re}}$	67.797	79.498	0.934	0.934	0.0	3.154	0.0	3.154	0.0	4.201

(eg. atoms 1, 3, and 5) and bottom group (eg. atoms 2, 4, and 6). Each S atom is connected to three Re atoms. The structural parameters are from the first-principles calculations,⁴⁸ including the lattice constant $a = 3.0750$ Å, and the bond length $d_{\text{Re-S}} = 2.4045$ Å, which is derived from the angle $\theta_{\text{SReRe}} = 79.5^\circ$. The other angle is $\theta_{\text{ReSS}} = 79.5^\circ$ with S atoms from the same (top or bottom) group.

Table CCCXXX shows three VFF terms for the single-layer 1T-ReS₂, one of which is the bond stretching interaction shown by Eq. (1) while the other two terms are the angle bending interaction shown by Eq. (2). We note that the angle bending term $K_{\text{Re-S-S}}$ is for the angle $\theta_{\text{Re-S-S}}$ with both S atoms from the same (top or bottom) group. We find that there are actually only two parameters in the VFF model, so we can determine their value by fitting to the Young's modulus and the Poisson's ratio of the system. The *ab initio* calculations have predicted the Young's modulus to be 90 N/m and the Poisson's ratio as -0.11.⁴⁸ The *ab initio* calculations have predicted a negative Poisson's ratio in the 1T-ReS₂, which was attributed to the orbital coupling in this material. The orbital coupling enhances

TABLE CCCXXXIII: SW potential parameters for single-layer 1T-ReS₂ used by LAMMPS⁹ as expressed in Eqs. (9) and (10).

	ϵ (eV)	σ (Å)	a	λ	γ	$\cos \theta_0$	A_L	B_L	p	q	tol
Re-S ₁ -S ₁	1.000	0.934	3.375	67.797	1.000	0.182	1.751	21.916	4	0	0.0

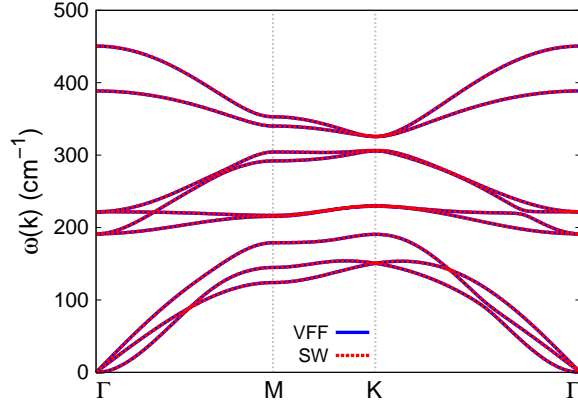


FIG. 165: (Color online) Phonon spectrum for single-layer 1T-ReS₂ along the Γ MK Γ direction in the Brillouin zone. The phonon dispersion from the SW potential is exactly the same as that from the VFF model.

the angle bending interaction in the VFF model. As a result, the value of the angle bending parameter is much larger than the bond stretching force constant parameter, which is typical in auxetic materials with negative Poisson's ratio.⁵²

The parameters for the two-body SW potential used by GULP are shown in Tab. CCCXXXI. The parameters for the three-body SW potential used by GULP are shown in Tab. CCCXXXII. Some representative parameters for the SW potential used by LAMMPS are listed in Tab. CCCXXXIII.

We use LAMMPS to perform MD simulations for the mechanical behavior of the single-layer 1T-ReS₂ under uniaxial tension at 1.0 K and 300.0 K. Fig. 164 shows the stress-strain curve for the tension of a single-layer 1T-ReS₂ of dimension 100×100 Å. Periodic boundary conditions are applied in both armchair and zigzag directions. The single-layer 1T-ReS₂ is stretched uniaxially along the armchair or zigzag direction. The stress is calculated without involving the actual thickness of the quasi-two-dimensional structure of the single-layer 1T-ReS₂. The Young's modulus can be obtained by a linear fitting of the stress-strain relation in the small strain range of $[0, 0.01]$. The Young's modulus are 78.1 N/m and 77.8 N/m along the armchair and zigzag directions, respectively. The Young's modulus is essentially isotropic in the armchair and zigzag directions. The Poisson's ratio from the VFF model and the SW potential is $\nu_{xy} = \nu_{yx} = -0.11$. The fitted Young's modulus value is about 10% smaller than the *ab initio* result of 90 N/m,⁴⁸ as only short-range interactions are considered

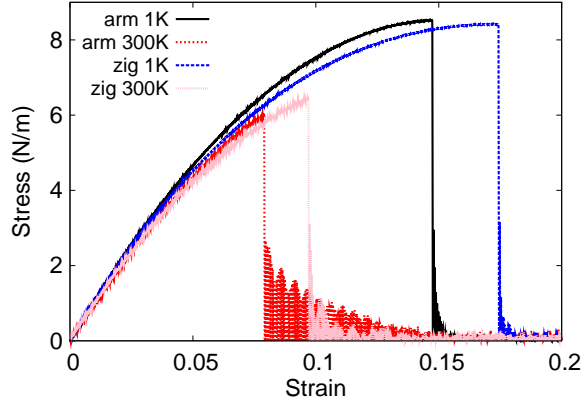


FIG. 166: (Color online) Stress-strain for single-layer 1T-ReSe₂ of dimension $100 \times 100 \text{ \AA}$ along the armchair and zigzag directions.

in the present work. The long-range interactions are ignored, which typically leads to about 10% underestimation for the value of the Young's modulus.

There is no available value for nonlinear quantities in the single-layer 1T-ReS₂. We have thus used the nonlinear parameter $B = 0.5d^4$ in Eq. (5), which is close to the value of B in most materials. The value of the third order nonlinear elasticity D can be extracted by fitting the stress-strain relation to the function $\sigma = E\epsilon + \frac{1}{2}D\epsilon^2$ with E as the Young's modulus. The values of D from the present SW potential are -537.1 N/m and -550.7 N/m along the armchair and zigzag directions, respectively. The ultimate stress is about 5.5 Nm^{-1} at the ultimate strain of 0.13 in the armchair direction at the low temperature of 1 K. The ultimate stress is about 5.6 Nm^{-1} at the ultimate strain of 0.15 in the zigzag direction at the low temperature of 1 K.

Fig. 165 shows that the VFF model and the SW potential give exactly the same phonon dispersion, as the SW potential is derived from the VFF model.

LXXXIV. 1T-RESE₂

Most existing theoretical studies on the single-layer 1T-ReSe₂ are based on the first-principles calculations. In this section, we will develop the SW potential for the single-layer 1T-ReSe₂.

The structure for the single-layer 1T-ReSe₂ is shown in Fig. 71 (with M=Re and X=Se).

TABLE CCCXXXIV: The VFF model for single-layer 1T-ReSe₂. The second line gives an explicit expression for each VFF term. The third line is the force constant parameters. Parameters are in the unit of $\frac{\text{eV}}{\text{Å}^2}$ for the bond stretching interactions, and in the unit of eV for the angle bending interaction. The fourth line gives the initial bond length (in unit of Å) for the bond stretching interaction and the initial angle (in unit of degrees) for the angle bending interaction. The angle θ_{ijk} has atom i as the apex.

VFF type	bond stretching	angle bending	
expression	$\frac{1}{2}K_{\text{Re-Se}}(\Delta r)^2$	$\frac{1}{2}K_{\text{Re-Se-Se}}(\Delta\theta)^2$	$\frac{1}{2}K_{\text{Se-Re-Re}}(\Delta\theta)^2$
parameter	4.313	12.674	12.674
r_0 or θ_0	2.515	76.999	76.999

TABLE CCCXXXV: Two-body SW potential parameters for single-layer 1T-ReSe₂ used by GULP⁸ as expressed in Eq. (3).

	A (eV)	ρ (Å)	B (Å ⁴)	r_{\min} (Å)	r_{\max} (Å)
Re-Se	2.866	0.896	20.001	0.0	3.265

Each Re atom is surrounded by six Se atoms. These Se atoms are categorized into the top group (eg. atoms 1, 3, and 5) and bottom group (eg. atoms 2, 4, and 6). Each Se atom is connected to three Re atoms. The structural parameters are from the first-principles calculations,⁴⁸ including the lattice constant $a = 3.1311$ Å, and the bond length $d_{\text{Re-Se}} = 2.5149$ Å, which is derived from the angle $\theta_{\text{SeReRe}} = 77^\circ$. The other angle is $\theta_{\text{ReSeSe}} = 77^\circ$ with Se atoms from the same (top or bottom) group.

Table CCCXXXIV shows three VFF terms for the single-layer 1T-ReSe₂, one of which

TABLE CCCXXXVI: Three-body SW potential parameters for single-layer 1T-ReSe₂ used by GULP⁸ as expressed in Eq. (4). The angle θ_{ijk} in the first line indicates the bending energy for the angle with atom i as the apex.

	K (eV)	θ_0 (degree)	ρ_1 (Å)	ρ_2 (Å)	$r_{\min12}$ (Å)	$r_{\max12}$ (Å)	$r_{\min13}$ (Å)	$r_{\max13}$ (Å)	$r_{\min23}$ (Å)	$r_{\max23}$ (Å)
$\theta_{\text{Re-Se-Se}}$	72.666	76.999	0.896	0.896	0.0	3.265	0.0	3.265	0.0	4.277
$\theta_{\text{Se-Re-Re}}$	72.666	76.999	0.896	0.896	0.0	3.265	0.0	3.265	0.0	4.277

TABLE CCCXXXVII: SW potential parameters for single-layer 1T-ReSe₂ used by LAMMPS⁹ as expressed in Eqs. (9) and (10).

	ϵ (eV)	σ (Å)	a	λ	γ	$\cos \theta_0$	A_L	B_L	p	q	tol
Re-Se ₁ -Se ₁	1.000	0.896	3.645	72.666	1.000	0.225	2.866	31.036	4	0	0.0

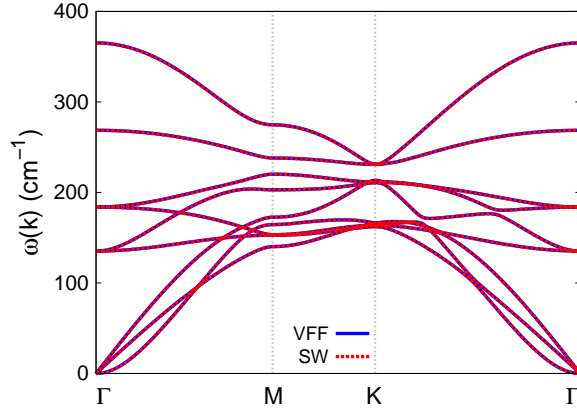


FIG. 167: (Color online) Phonon spectrum for single-layer 1T-ReSe₂ along the Γ MK Γ direction in the Brillouin zone. The phonon dispersion from the SW potential is exactly the same as that from the VFF model.

is the bond stretching interaction shown by Eq. (1) while the other two terms are the angle bending interaction shown by Eq. (2). We note that the angle bending term $K_{\text{Re-Se-Se}}$ is for the angle $\theta_{\text{Re-Se-Se}}$ with both Se atoms from the same (top or bottom) group. We find that there are actually only two parameters in the VFF model, so we can determine their value by fitting to the Young's modulus and the Poisson's ratio of the system. The *ab initio* calculations have predicted the Young's modulus to be 123 N/m and the Poisson's ratio as -0.03.⁴⁸ The *ab initio* calculations have predicted a negative Poisson's ratio in the 1T-ReSe₂, which was attributed to the orbital coupling in this material. The orbital coupling enhances the angle bending interaction in the VFF model. As a result, the value of the angle bending parameter is much larger than the bond stretching force constant parameter, which is typical in auxetic materials with negative Poisson's ratio.⁵²

The parameters for the two-body SW potential used by GULP are shown in Tab. CCCXXXV. The parameters for the three-body SW potential used by GULP are shown in Tab. CCCXXXVI. Some representative parameters for the SW potential used by

LAMMPS are listed in Tab. [CCCXXXVII](#).

We use LAMMPS to perform MD simulations for the mechanical behavior of the single-layer 1T-ReSe₂ under uniaxial tension at 1.0 K and 300.0 K. Fig. [166](#) shows the stress-strain curve for the tension of a single-layer 1T-ReSe₂ of dimension 100 × 100 Å. Periodic boundary conditions are applied in both armchair and zigzag directions. The single-layer 1T-ReSe₂ is stretched uniaxially along the armchair or zigzag direction. The stress is calculated without involving the actual thickness of the quasi-two-dimensional structure of the single-layer 1T-ReSe₂. The Young's modulus can be obtained by a linear fitting of the stress-strain relation in the small strain range of [0, 0.01]. The Young's modulus are 108.2 N/m and 107.7 N/m along the armchair and zigzag directions, respectively. The Young's modulus is essentially isotropic in the armchair and zigzag directions. The Poisson's ratio from the VFF model and the SW potential is $\nu_{xy} = \nu_{yx} = -0.03$. The fitted Young's modulus value is about 10% smaller than the *ab initio* result of 123 N/m,⁴⁸ as only short-range interactions are considered in the present work. The long-range interactions are ignored, which typically leads to about 10% underestimation for the value of the Young's modulus.

There is no available value for nonlinear quantities in the single-layer 1T-ReSe₂. We have thus used the nonlinear parameter $B = 0.5d^4$ in Eq. (5), which is close to the value of B in most materials. The value of the third order nonlinear elasticity D can be extracted by fitting the stress-strain relation to the function $\sigma = E\epsilon + \frac{1}{2}D\epsilon^2$ with E as the Young's modulus. The values of D from the present SW potential are -669.3 N/m and -699.9 N/m along the armchair and zigzag directions, respectively. The ultimate stress is about 8.5 Nm⁻¹ at the ultimate strain of 0.14 in the armchair direction at the low temperature of 1 K. The ultimate stress is about 8.4 Nm⁻¹ at the ultimate strain of 0.17 in the zigzag direction at the low temperature of 1 K.

Fig. [167](#) shows that the VFF model and the SW potential give exactly the same phonon dispersion, as the SW potential is derived from the VFF model.

LXXXV. 1T-RETE₂

Most existing theoretical studies on the single-layer 1T-ReTe₂ are based on the first-principles calculations. In this section, we will develop the SW potential for the single-layer 1T-ReTe₂.

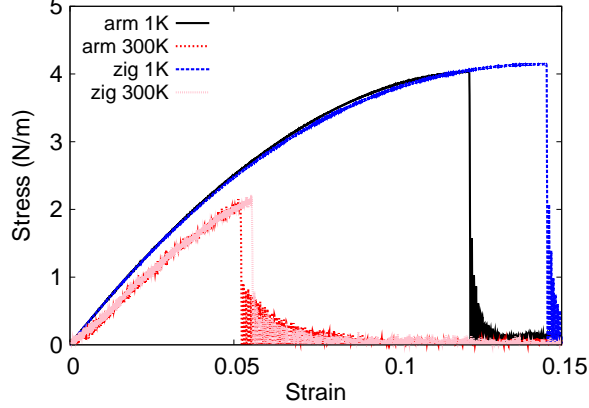


FIG. 168: (Color online) Stress-strain for single-layer 1T-ReTe₂ of dimension $100 \times 100 \text{ \AA}$ along the armchair and zigzag directions.

TABLE CCCXXXVIII: The VFF model for single-layer 1T-ReTe₂. The second line gives an explicit expression for each VFF term. The third line is the force constant parameters. Parameters are in the unit of $\frac{eV}{\text{Å}^2}$ for the bond stretching interactions, and in the unit of eV for the angle bending interaction. The fourth line gives the initial bond length (in unit of Å) for the bond stretching interaction and the initial angle (in unit of degrees) for the angle bending interaction. The angle θ_{ijk} has atom i as the apex.

VFF type	bond stretching	angle bending	
expression	$\frac{1}{2}K_{\text{Re-Te}}(\Delta r)^2$	$\frac{1}{2}K_{\text{Re-Te-Te}}(\Delta\theta)^2$	$\frac{1}{2}K_{\text{Te-Re-Re}}(\Delta\theta)^2$
parameter	1.724	14.812	14.812
r_0 or θ_0	2.703	77.501	77.501

The structure for the single-layer 1T-ReTe₂ is shown in Fig. 71 (with M=Re and X=Te). Each Re atom is surrounded by six Te atoms. These Te atoms are categorized into the top group (eg. atoms 1, 3, and 5) and bottom group (eg. atoms 2, 4, and 6). Each Te atom is connected to three Re atoms. The structural parameters are from the first-principles calculations,⁴⁸ including the lattice constant $a = 3.3834 \text{ \AA}$, and the bond length $d_{\text{Re-Te}} = 2.7027 \text{ \AA}$, which is derived from the angle $\theta_{\text{TeReRe}} = 77.5^\circ$. The other angle is $\theta_{\text{ReTeTe}} = 77.5^\circ$ with Te atoms from the same (top or bottom) group.

Table CCCXXXVIII shows three VFF terms for the single-layer 1T-ReTe₂, one of which

TABLE CCCXXXIX: Two-body SW potential parameters for single-layer 1T-ReTe₂ used by GULP⁸ as expressed in Eq. (3).

	A (eV)	ρ (Å)	B (Å ⁴)	r_{\min} (Å)	r_{\max} (Å)
Re-Te	1.343	0.980	26.678	0.0	3.517

TABLE CCCXL: Three-body SW potential parameters for single-layer 1T-ReTe₂ used by GULP⁸ as expressed in Eq. (4). The angle θ_{ijk} in the first line indicates the bending energy for the angle with atom i as the apex.

	K (eV)	θ_0 (degree)	ρ_1 (Å)	ρ_2 (Å)	$r_{\min12}$ (Å)	$r_{\max12}$ (Å)	$r_{\min13}$ (Å)	$r_{\max13}$ (Å)	$r_{\min23}$ (Å)	$r_{\max23}$ (Å)
$\theta_{\text{Re-Te-Te}}$	86.424	77.501	0.980	0.980	0.0	3.517	0.0	3.517	0.0	4.622
$\theta_{\text{Te-Re-Re}}$	86.424	77.501	0.980	0.980	0.0	3.517	0.0	3.517	0.0	4.622

is the bond stretching interaction shown by Eq. (1) while the other two terms are the angle bending interaction shown by Eq. (2). We note that the angle bending term $K_{\text{Re-Te-Te}}$ is for the angle $\theta_{\text{Re-Te-Te}}$ with both Te atoms from the same (top or bottom) group. We find that there are actually only two parameters in the VFF model, so we can determine their value by fitting to the Young's modulus and the Poisson's ratio of the system. The *ab initio* calculations have predicted the Young's modulus to be 71 N/m and the Poisson's ratio as -0.22.⁴⁸ The *ab initio* calculations have predicted a negative Poisson's ratio in the 1T-ReTe₂, which was attributed to the orbital coupling in this material. The orbital coupling enhances the angle bending interaction in the VFF model. As a result, the value of the angle bending parameter is much larger than the bond stretching force constant parameter, which is typical in auxetic materials with negative Poisson's ratio.⁵²

The parameters for the two-body SW potential used by GULP are shown in Tab. CCCXXXIX. The parameters for the three-body SW potential used by GULP are shown in Tab. CCCXL. Some representative parameters for the SW potential used by

TABLE CCCXLI: SW potential parameters for single-layer 1T-ReTe₂ used by LAMMPS⁹ as expressed in Eqs. (9) and (10).

	ϵ (eV)	σ (Å)	a	λ	γ	$\cos \theta_0$	A_L	B_L	p	q	tol
Re-Te ₁ -Te ₁	1.000	0.980	3.587	86.424	1.000	0.216	1.343	28.891	4	0	0.0

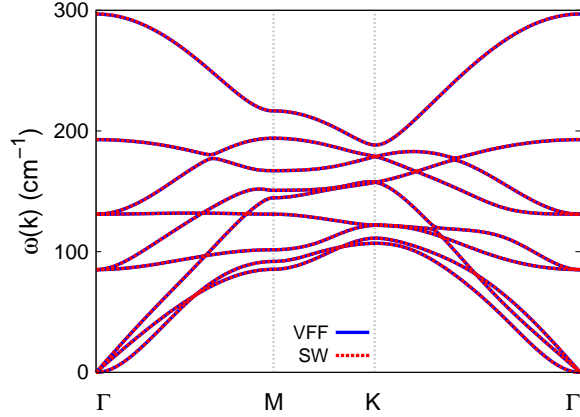


FIG. 169: (Color online) Phonon spectrum for single-layer 1T-ReTe₂ along the Γ MKT direction in the Brillouin zone. The phonon dispersion from the SW potential is exactly the same as that from the VFF model.

LAMMPS are listed in Tab. CCCXLI.

We use LAMMPS to perform MD simulations for the mechanical behavior of the single-layer 1T-ReTe₂ under uniaxial tension at 1.0 K and 300.0 K. Fig. 168 shows the stress-strain curve for the tension of a single-layer 1T-ReTe₂ of dimension $100 \times 100 \text{ \AA}$. Periodic boundary conditions are applied in both armchair and zigzag directions. The single-layer 1T-ReTe₂ is stretched uniaxially along the armchair or zigzag direction. The stress is calculated without involving the actual thickness of the quasi-two-dimensional structure of the single-layer 1T-ReTe₂. The Young's modulus can be obtained by a linear fitting of the stress-strain relation in the small strain range of $[0, 0.01]$. The Young's modulus are 59.4 N/m and 59.3 N/m along the armchair and zigzag directions, respectively. The Young's modulus is essentially isotropic in the armchair and zigzag directions. The Poisson's ratio from the VFF model and the SW potential is $\nu_{xy} = \nu_{yx} = -0.17$. The fitted Young's modulus value is about 10% smaller than the *ab initio* result of 71 N/m,⁴⁸ as only short-range interactions are considered in the present work. The long-range interactions are ignored, which typically leads to about 10% underestimation for the value of the Young's modulus.

There is no available value for nonlinear quantities in the single-layer 1T-ReTe₂. We have thus used the nonlinear parameter $B = 0.5d^4$ in Eq. (5), which is close to the value of B in most materials. The value of the third order nonlinear elasticity D can be extracted by fitting the stress-strain relation to the function $\sigma = E\epsilon + \frac{1}{2}D\epsilon^2$ with E as the Young's

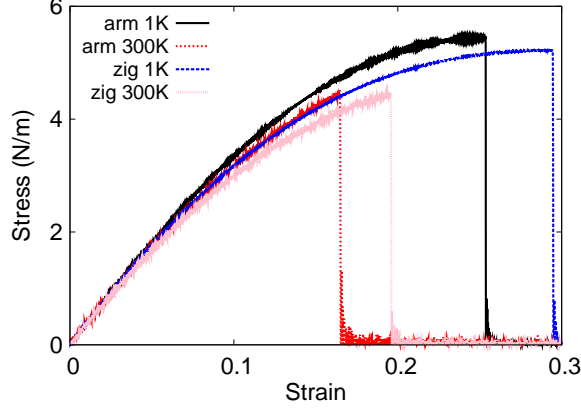


FIG. 170: (Color online) Stress-strain for single-layer 1T-IrTe₂ of dimension $100 \times 100 \text{ \AA}$ along the armchair and zigzag directions.

modulus. The values of D from the present SW potential are -416.1 N/m and -425.1 N/m along the armchair and zigzag directions, respectively. The ultimate stress is about 4.0 Nm^{-1} at the ultimate strain of 0.12 in the armchair direction at the low temperature of 1 K . The ultimate stress is about 4.1 Nm^{-1} at the ultimate strain of 0.14 in the zigzag direction at the low temperature of 1 K .

Fig. 169 shows that the VFF model and the SW potential give exactly the same phonon dispersion, as the SW potential is derived from the VFF model.

LXXXVI. 1T-IRTE₂

Most existing theoretical studies on the single-layer 1T-IrTe₂ are based on the first-principles calculations. In this section, we will develop the SW potential for the single-layer 1T-IrTe₂.

The structure for the single-layer 1T-IrTe₂ is shown in Fig. 71 (with $M=\text{Ir}$ and $X=\text{Te}$). Each Ir atom is surrounded by six Te atoms. These Te atoms are categorized into the top group (eg. atoms 1, 3, and 5) and bottom group (eg. atoms 2, 4, and 6). Each Te atom is connected to three Ir atoms. The structural parameters are from the first-principles calculations,⁴⁸ including the lattice constant $a = 3.8431 \text{ \AA}$, and the bond length $d_{\text{Ir-Te}} = 2.6490 \text{ \AA}$, which is derived from the angle $\theta_{\text{TeIrIr}} = 93^\circ$. The other angle is $\theta_{\text{IrTeTe}} = 93^\circ$ with Te atoms from the same (top or bottom) group.

TABLE CCCXLII: The VFF model for single-layer 1T-IrTe₂. The second line gives an explicit expression for each VFF term. The third line is the force constant parameters. Parameters are in the unit of $\frac{\text{eV}}{\text{\AA}^2}$ for the bond stretching interactions, and in the unit of eV for the angle bending interaction. The fourth line gives the initial bond length (in unit of \AA) for the bond stretching interaction and the initial angle (in unit of degrees) for the angle bending interaction. The angle θ_{ijk} has atom i as the apex.

VFF type	bond stretching		angle bending	
expression	$\frac{1}{2}K_{\text{Ir-Te}}(\Delta r)^2$	$\frac{1}{2}K_{\text{Ir-Te-Te}}(\Delta\theta)^2$	$\frac{1}{2}K_{\text{Te-Ir-Ir}}(\Delta\theta)^2$	
parameter	5.334	2.182	2.182	
r_0 or θ_0	2.649	93.002	93.002	

TABLE CCCXLIII: Two-body SW potential parameters for single-layer 1T-IrTe₂ used by GULP⁸ as expressed in Eq. (3).

	A (eV)	ρ (\AA)	B (\AA^4)	r_{min} (\AA)	r_{max} (\AA)
Ir-Te	6.030	1.538	24.621	0.0	3.658

Table CCCXLII shows three VFF terms for the single-layer 1T-IrTe₂, one of which is the bond stretching interaction shown by Eq. (1) while the other two terms are the angle bending interaction shown by Eq. (2). We note that the angle bending term $K_{\text{Ir-Te-Te}}$ is for the angle $\theta_{\text{Ir-Te-Te}}$ with both Te atoms from the same (top or bottom) group. We find that there are actually only two parameters in the VFF model, so we can determine their value by fitting to the Young's modulus and the Poisson's ratio of the system. The *ab initio* calculations have predicted the Young's modulus to be 45 N/m and the Poisson's ratio as 0.22.⁴⁸

TABLE CCCXLIV: Three-body SW potential parameters for single-layer 1T-IrTe₂ used by GULP⁸ as expressed in Eq. (4). The angle θ_{ijk} in the first line indicates the bending energy for the angle with atom i as the apex.

	K (eV)	θ_0 (degree)	ρ_1 (\AA)	ρ_2 (\AA)	$r_{\text{min}12}$ (\AA)	$r_{\text{max}12}$ (\AA)	$r_{\text{min}13}$ (\AA)	$r_{\text{max}13}$ (\AA)	$r_{\text{min}23}$ (\AA)	$r_{\text{max}23}$ (\AA)
$\theta_{\text{Ir-Te-Te}}$	23.056	93.002	1.538	1.538	0.0	3.658	0.0	3.658	0.0	5.250
$\theta_{\text{Te-Ir-Ir}}$	23.056	93.002	1.538	1.538	0.0	3.658	0.0	3.658	0.0	5.250

TABLE CCCXLV: SW potential parameters for single-layer 1T-IrTe₂ used by LAMMPS⁹ as expressed in Eqs. (9) and (10).

	ϵ (eV)	σ (Å)	a	λ	γ	$\cos \theta_0$	A_L	B_L	p	q	tol
Ir-Te ₁ -Te ₁	1.000	1.538	2.370	23.056	1.000	-0.052	6.030	4.398	4	0	0.0

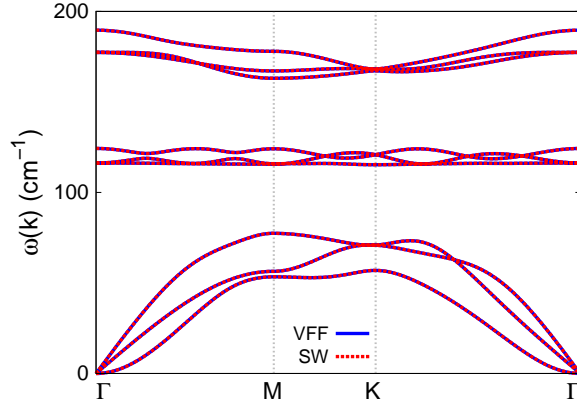


FIG. 171: (Color online) Phonon spectrum for single-layer 1T-IrTe₂ along the Γ MK Γ direction in the Brillouin zone. The phonon dispersion from the SW potential is exactly the same as that from the VFF model.

The parameters for the two-body SW potential used by GULP are shown in Tab. CCCXLIII. The parameters for the three-body SW potential used by GULP are shown in Tab. CCCXLIV. Some representative parameters for the SW potential used by LAMMPS are listed in Tab. CCCXLV.

We use LAMMPS to perform MD simulations for the mechanical behavior of the single-layer 1T-IrTe₂ under uniaxial tension at 1.0 K and 300.0 K. Fig. 170 shows the stress-strain curve for the tension of a single-layer 1T-IrTe₂ of dimension 100×100 Å. Periodic boundary conditions are applied in both armchair and zigzag directions. The single-layer 1T-IrTe₂ is stretched uniaxially along the armchair or zigzag direction. The stress is calculated without involving the actual thickness of the quasi-two-dimensional structure of the single-layer 1T-IrTe₂. The Young's modulus can be obtained by a linear fitting of the stress-strain relation in the small strain range of $[0, 0.01]$. The Young's modulus are 38.6 N/m and 38.4 N/m along the armchair and zigzag directions, respectively. The Young's modulus is essentially isotropic in the armchair and zigzag directions. The Poisson's ratio from the VFF model

TABLE CCCXLVI: The VFF model for single-layer 1T-PtS₂. The second line gives an explicit expression for each VFF term. The third line is the force constant parameters. Parameters are in the unit of $\frac{\text{eV}}{\text{Å}^2}$ for the bond stretching interactions, and in the unit of eV for the angle bending interaction. The fourth line gives the initial bond length (in unit of Å) for the bond stretching interaction and the initial angle (in unit of degrees) for the angle bending interaction. The angle θ_{ijk} has atom i as the apex.

VFF type	bond stretching	angle bending	
expression	$\frac{1}{2}K_{\text{Pt-S}}(\Delta r)^2$	$\frac{1}{2}K_{\text{Pt-S-S}}(\Delta\theta)^2$	$\frac{1}{2}K_{\text{S-Pt-Pt}}(\Delta\theta)^2$
parameter	12.128	4.975	4.975
r_0 or θ_0	2.371	96.00	96.00

and the SW potential is $\nu_{xy} = \nu_{yx} = 0.20$. The fitted Young's modulus value is about 10% smaller than the *ab initio* result of 45 N/m,⁴⁸ as only short-range interactions are considered in the present work. The long-range interactions are ignored, which typically leads to about 10% underestimation for the value of the Young's modulus.

There is no available value for nonlinear quantities in the single-layer 1T-IrTe₂. We have thus used the nonlinear parameter $B = 0.5d^4$ in Eq. (5), which is close to the value of B in most materials. The value of the third order nonlinear elasticity D can be extracted by fitting the stress-strain relation to the function $\sigma = E\epsilon + \frac{1}{2}D\epsilon^2$ with E as the Young's modulus. The values of D from the present SW potential are -127.7 N/m and -142.0 N/m along the armchair and zigzag directions, respectively. The ultimate stress is about 5.4 Nm⁻¹ at the ultimate strain of 0.25 in the armchair direction at the low temperature of 1 K. The ultimate stress is about 5.2 Nm⁻¹ at the ultimate strain of 0.29 in the zigzag direction at the low temperature of 1 K.

Fig. 171 shows that the VFF model and the SW potential give exactly the same phonon dispersion, as the SW potential is derived from the VFF model.

LXXXVII. 1T-PTS₂

Most existing theoretical studies on the single-layer 1T-PtS₂ are based on the first-principles calculations. In this section, we will develop the SW potential for the single-layer

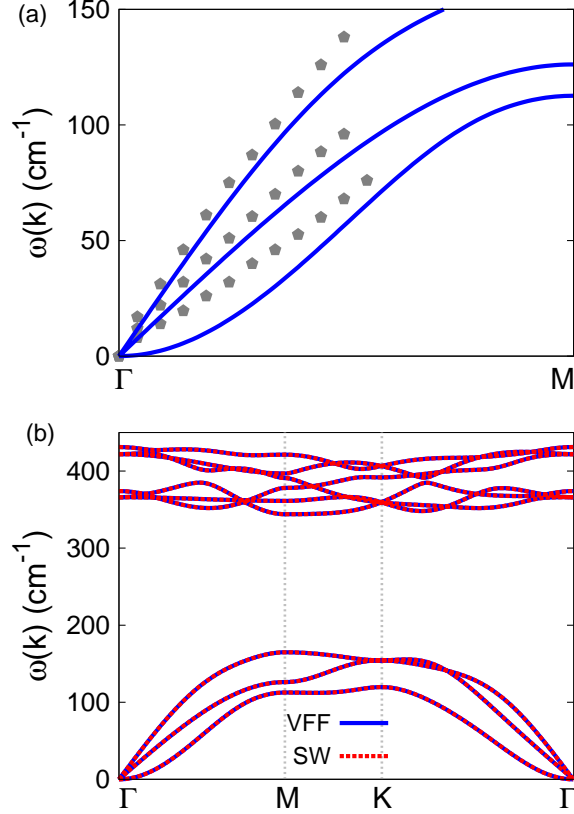


FIG. 172: (Color online) Phonon spectrum for single-layer 1T-PtS₂. (a) Phonon dispersion along the Γ M direction in the Brillouin zone. The results from the VFF model (lines) are comparable with the *ab initio* results (pentagons) from Ref. 34. (b) The phonon dispersion from the SW potential is exactly the same as that from the VFF model.

TABLE CCCXLVII: Two-body SW potential parameters for single-layer 1T-PtS₂ used by GULP⁸ as expressed in Eq. (3).

	A (eV)	ρ (\AA)	B (\AA^4)	r_{\min} (\AA)	r_{\max} (\AA)
Pt-S	11.806	1.485	15.796	0.0	3.309

1T-PtS₂.

The structure for the single-layer 1T-PtS₂ is shown in Fig. 71 (with M=Pt and X=S). Each Pt atom is surrounded by six S atoms. These S atoms are categorized into the top group (eg. atoms 1, 3, and 5) and bottom group (eg. atoms 2, 4, and 6). Each S atom is connected to three Pt atoms. The structural parameters are from the first-principles calculations,⁴⁸

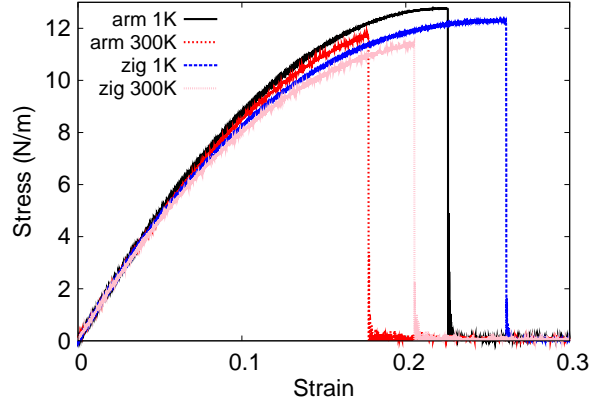


FIG. 173: (Color online) Stress-strain for single-layer 1T-PtS₂ of dimension $100 \times 100 \text{ \AA}$ along the armchair and zigzag directions.

TABLE CCCXLVIII: Three-body SW potential parameters for single-layer 1T-PtS₂ used by GULP⁸ as expressed in Eq. (4). The angle θ_{ijk} in the first line indicates the bending energy for the angle with atom i as the apex.

	K (eV)	θ_0 (degree)	ρ_1 (\AA)	ρ_2 (\AA)	$r_{\min 12}$ (\AA)	$r_{\max 12}$ (\AA)	$r_{\min 13}$ (\AA)	$r_{\max 13}$ (\AA)	$r_{\min 23}$ (\AA)	$r_{\max 23}$ (\AA)
$\theta_{\text{Pt-S-S}}$	59.607	96.00	1.485	1.485	0.0	3.309	0.0	3.309	0.0	4.813
$\theta_{\text{S-Pt-Pt}}$	59.607	96.00	1.485	1.485	0.0	3.309	0.0	3.309	0.0	4.813

including the lattice constant $a = 3.5237 \text{ \AA}$, and the bond length $d_{\text{Pt-S}} = 2.3708 \text{ \AA}$, which is derived from the angle $\theta_{\text{SPtPt}} = 96^\circ$. The other angle is $\theta_{\text{PtSS}} = 96^\circ$ with S atoms from the same (top or bottom) group.

Table CCCXLVI shows three VFF terms for the single-layer 1T-PtS₂, one of which is the bond stretching interaction shown by Eq. (1) while the other two terms are the angle bending interaction shown by Eq. (2). We note that the angle bending term $K_{\text{Pt-S-S}}$ is for the angle $\theta_{\text{Pt-S-S}}$ with both S atoms from the same (top or bottom) group. These force

TABLE CCCXLIX: SW potential parameters for single-layer 1T-PtS₂ used by LAMMPS⁹ as expressed in Eqs. (9) and (10).

	ϵ (eV)	σ (\AA)	a	λ	γ	$\cos \theta_0$	A_L	B_L	p	q	tol
Pt-S ₁ -S ₁	1.000	1.485	2.229	59.607	1.000	-0.105	11.806	3.250	4	0	0.0

constant parameters are determined by fitting to the three acoustic branches in the phonon dispersion along the Γ M as shown in Fig. 172 (a). The *ab initio* calculations for the phonon dispersion are from Ref. 34. The lowest acoustic branch (flexural mode) is almost linear in the *ab initio* calculations, which may be due to the violation of the rigid rotational invariance.²⁰ Fig. 172 (b) shows that the VFF model and the SW potential give exactly the same phonon dispersion, as the SW potential is derived from the VFF model.

The parameters for the two-body SW potential used by GULP are shown in Tab. CCCXLVII. The parameters for the three-body SW potential used by GULP are shown in Tab. CCCXLVIII. Some representative parameters for the SW potential used by LAMMPS are listed in Tab. CCCXLIX.

We use LAMMPS to perform MD simulations for the mechanical behavior of the single-layer 1T-PtS₂ under uniaxial tension at 1.0 K and 300.0 K. Fig. 173 shows the stress-strain curve for the tension of a single-layer 1T-PtS₂ of dimension 100 × 100 Å. Periodic boundary conditions are applied in both armchair and zigzag directions. The single-layer 1T-PtS₂ is stretched uniaxially along the armchair or zigzag direction. The stress is calculated without involving the actual thickness of the quasi-two-dimensional structure of the single-layer 1T-PtS₂. The Young's modulus can be obtained by a linear fitting of the stress-strain relation in the small strain range of [0, 0.01]. The Young's modulus are 105.9 N/m and 105.4 N/m along the armchair and zigzag directions, respectively. The Young's modulus is essentially isotropic in the armchair and zigzag directions. The Poisson's ratio from the VFF model and the SW potential is $\nu_{xy} = \nu_{yx} = 0.16$.

There is no available value for nonlinear quantities in the single-layer 1T-PtS₂. We have thus used the nonlinear parameter $B = 0.5d^4$ in Eq. (5), which is close to the value of B in most materials. The value of the third order nonlinear elasticity D can be extracted by fitting the stress-strain relation to the function $\sigma = E\epsilon + \frac{1}{2}D\epsilon^2$ with E as the Young's modulus. The values of D from the present SW potential are -420.6 N/m and -457.1 N/m along the armchair and zigzag directions, respectively. The ultimate stress is about 12.8 Nm⁻¹ at the ultimate strain of 0.22 in the armchair direction at the low temperature of 1 K. The ultimate stress is about 12.3 Nm⁻¹ at the ultimate strain of 0.26 in the zigzag direction at the low temperature of 1 K.

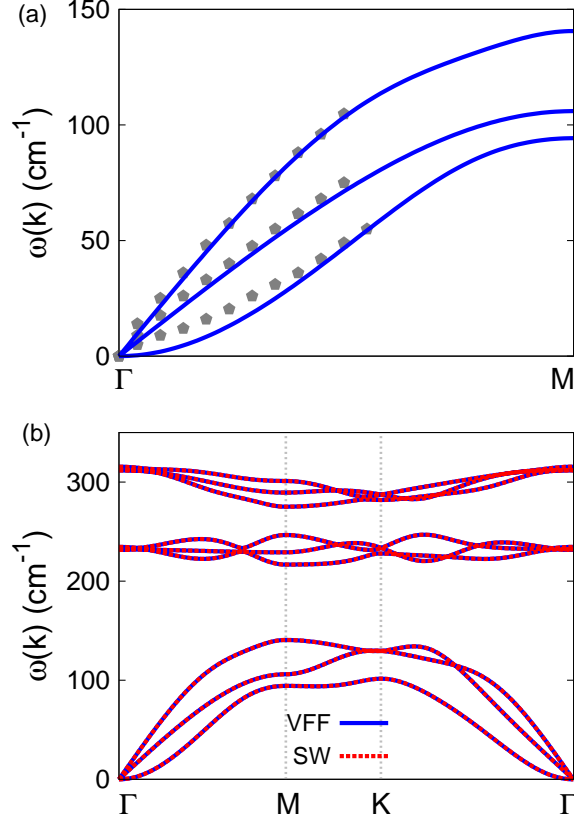


FIG. 174: (Color online) Phonon spectrum for single-layer 1T-PtSe₂. (a) Phonon dispersion along the Γ M direction in the Brillouin zone. The results from the VFF model (lines) are comparable with the *ab initio* results (pentagons) from Ref. 34. (b) The phonon dispersion from the SW potential is exactly the same as that from the VFF model.

LXXXVIII. 1T-PTSE₂

Most existing theoretical studies on the single-layer 1T-PtSe₂ are based on the first-principles calculations. In this section, we will develop the SW potential for the single-layer 1T-PtSe₂.

The structure for the single-layer 1T-PtSe₂ is shown in Fig. 71 (with M=Pt and X=Se). Each Pt atom is surrounded by six Se atoms. These Se atoms are categorized into the top group (eg. atoms 1, 3, and 5) and bottom group (eg. atoms 2, 4, and 6). Each Se atom is connected to three Pt atoms. The structural parameters are from the first-principles calculations,⁴⁸ including the lattice constant $a = 3.6662 \text{ \AA}$, and the bond length

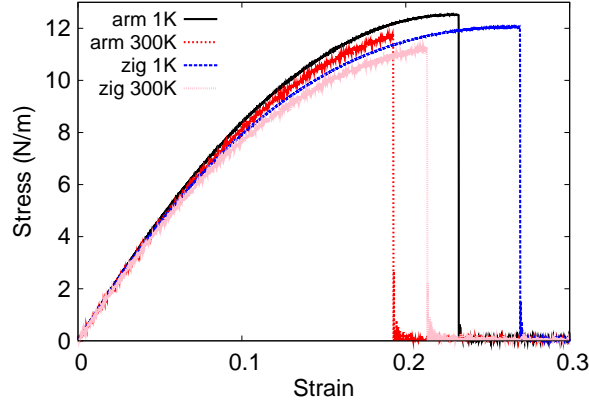


FIG. 175: (Color online) Stress-strain for single-layer 1T-PtSe₂ of dimension $100 \times 100 \text{ \AA}$ along the armchair and zigzag directions.

TABLE CCCL: The VFF model for single-layer 1T-PtSe₂. The second line gives an explicit expression for each VFF term. The third line is the force constant parameters. Parameters are in the unit of $\frac{\text{eV}}{\text{A}^2}$ for the bond stretching interactions, and in the unit of eV for the angle bending interaction. The fourth line gives the initial bond length (in unit of \AA) for the bond stretching interaction and the initial angle (in unit of degrees) for the angle bending interaction. The angle θ_{ijk} has atom i as the apex.

VFF type	bond stretching	angle bending	
expression	$\frac{1}{2}K_{\text{Pt-Se}}(\Delta r)^2$	$\frac{1}{2}K_{\text{Pt-Se-Se}}(\Delta\theta)^2$	$\frac{1}{2}K_{\text{Se-Pt-Pt}}(\Delta\theta)^2$
parameter	12.128	4.975	4.975
r_0 or θ_0	2.467	95.999	95.999

$d_{\text{Pt-Se}} = 2.4667 \text{ \AA}$, which is derived from the angle $\theta_{\text{SePtPt}} = 96^\circ$. The other angle is $\theta_{\text{PtSeSe}} = 96^\circ$ with Se atoms from the same (top or bottom) group.

Table CCCL shows three VFF terms for the single-layer 1T-PtSe₂, one of which is the bond stretching interaction shown by Eq. (1) while the other two terms are the angle bending interaction shown by Eq. (2). We note that the angle bending term $K_{\text{Pt-Se-Se}}$ is for the angle $\theta_{\text{Pt-Se-Se}}$ with both Se atoms from the same (top or bottom) group. These force constant parameters are determined by fitting to the three acoustic branches in the phonon dispersion along the ΓM as shown in Fig. 174 (a). The *ab initio* calculations for the phonon dispersion

TABLE CCCLI: Two-body SW potential parameters for single-layer 1T-PtSe₂ used by GULP⁸ as expressed in Eq. (3).

	A (eV)	ρ (Å)	B (Å ⁴)	r_{\min} (Å)	r_{\max} (Å)
Pt-Se	12.781	1.545	18.511	0.0	3.443

TABLE CCCLII: Three-body SW potential parameters for single-layer 1T-PtSe₂ used by GULP⁸ as expressed in Eq. (4). The angle θ_{ijk} in the first line indicates the bending energy for the angle with atom i as the apex.

	K (eV)	θ_0 (degree)	ρ_1 (Å)	ρ_2 (Å)	$r_{\min12}$ (Å)	$r_{\max12}$ (Å)	$r_{\min13}$ (Å)	$r_{\max13}$ (Å)	$r_{\min23}$ (Å)	$r_{\max23}$ (Å)
$\theta_{\text{Pt-Se-Se}}$	59.608	95.999	1.545	1.545	0.0	3.443	0.0	3.443	0.0	5.008
$\theta_{\text{Se-Pt-Pt}}$	59.608	95.999	1.545	1.545	0.0	3.443	0.0	3.443	0.0	5.008

are from Ref. 34. The lowest acoustic branch (flexural mode) is almost linear in the *ab initio* calculations, which may due to the violation of the rigid rotational invariance.²⁰ Fig. 174 (b) shows that the VFF model and the SW potential give exactly the same phonon dispersion, as the SW potential is derived from the VFF model.

The parameters for the two-body SW potential used by GULP are shown in Tab. CCCLI. The parameters for the three-body SW potential used by GULP are shown in Tab. CCCLII. Some representative parameters for the SW potential used by LAMMPS are listed in Tab. CCCLIII.

We use LAMMPS to perform MD simulations for the mechanical behavior of the single-layer 1T-PtSe₂ under uniaxial tension at 1.0 K and 300.0 K. Fig. 175 shows the stress-strain curve for the tension of a single-layer 1T-PtSe₂ of dimension 100×100 Å. Periodic boundary conditions are applied in both armchair and zigzag directions. The single-layer 1T-PtSe₂ is stretched uniaxially along the armchair or zigzag direction. The stress is calculated without involving the actual thickness of the quasi-two-dimensional structure of the single-layer 1T-

TABLE CCCLIII: SW potential parameters for single-layer 1T-PtSe₂ used by LAMMPS⁹ as expressed in Eqs. (9) and (10).

	ϵ (eV)	σ (Å)	a	λ	γ	$\cos \theta_0$	A_L	B_L	p	q	tol
Pt-Se ₁ -Se ₁	1.000	1.545	2.229	59.608	1.000	-0.105	12.781	3.250	4	0	0.0

TABLE CCCLIV: The VFF model for single-layer 1T-PtTe₂. The second line gives an explicit expression for each VFF term. The third line is the force constant parameters. Parameters are in the unit of $\frac{\text{eV}}{\text{Å}^2}$ for the bond stretching interactions, and in the unit of eV for the angle bending interaction. The fourth line gives the initial bond length (in unit of Å) for the bond stretching interaction and the initial angle (in unit of degrees) for the angle bending interaction. The angle θ_{ijk} has atom i as the apex.

VFF type	bond stretching	angle bending	
expression	$\frac{1}{2}K_{\text{Pt-Te}}(\Delta r)^2$	$\frac{1}{2}K_{\text{Pt-Te-Te}}(\Delta\theta)^2$	$\frac{1}{2}K_{\text{Te-Pt-Pt}}(\Delta\theta)^2$
parameter	12.128	4.975	4.975
r_0 or θ_0	2.661	95.998	95.998

PtSe₂. The Young's modulus can be obtained by a linear fitting of the stress-strain relation in the small strain range of [0, 0.01]. The Young's modulus are 101.1 N/m and 100.5 N/m along the armchair and zigzag directions, respectively. The Young's modulus is essentially isotropic in the armchair and zigzag directions. The Poisson's ratio from the VFF model and the SW potential is $\nu_{xy} = \nu_{yx} = 0.17$.

There is no available value for nonlinear quantities in the single-layer 1T-PtSe₂. We have thus used the nonlinear parameter $B = 0.5d^4$ in Eq. (5), which is close to the value of B in most materials. The value of the third order nonlinear elasticity D can be extracted by fitting the stress-strain relation to the function $\sigma = E\epsilon + \frac{1}{2}D\epsilon^2$ with E as the Young's modulus. The values of D from the present SW potential are -391.4 N/m and -424.0 N/m along the armchair and zigzag directions, respectively. The ultimate stress is about 12.5 Nm⁻¹ at the ultimate strain of 0.23 in the armchair direction at the low temperature of 1 K. The ultimate stress is about 12.1 Nm⁻¹ at the ultimate strain of 0.27 in the zigzag direction at the low temperature of 1 K.

LXXXIX. 1T-PTTE₂

Most existing theoretical studies on the single-layer 1T-PtTe₂ are based on the first-principles calculations. In this section, we will develop the SW potential for the single-layer 1T-PtTe₂.

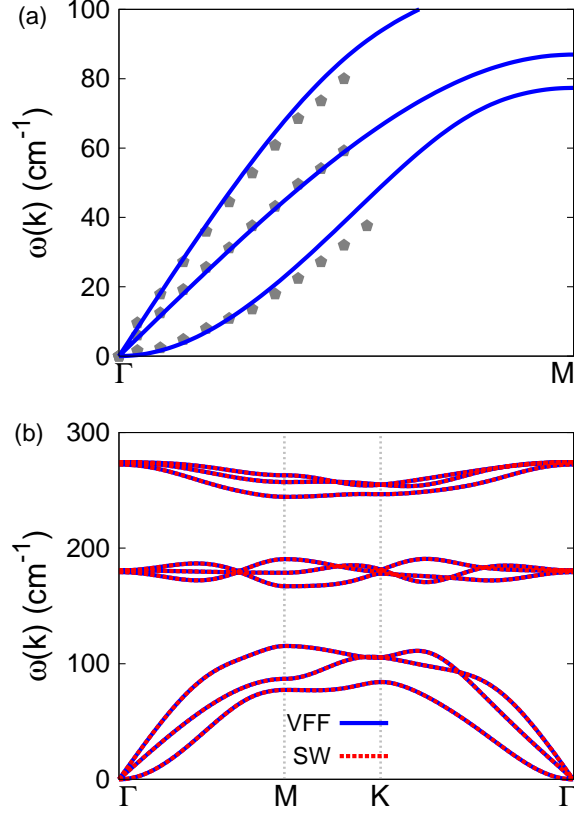


FIG. 176: (Color online) Phonon spectrum for single-layer 1T-PtTe₂. (a) Phonon dispersion along the Γ M direction in the Brillouin zone. The results from the VFF model (lines) are comparable with the *ab initio* results (pentagons) from Ref. 34. (b) The phonon dispersion from the SW potential is exactly the same as that from the VFF model.

TABLE CCCLV: Two-body SW potential parameters for single-layer 1T-PtTe₂ used by GULP⁸ as expressed in Eq. (3).

	A (eV)	ρ (\AA)	B (\AA^4)	r_{\min} (\AA)	r_{\max} (\AA)
Pt-Te	14.877	1.667	25.081	0.0	3.714

The structure for the single-layer 1T-PtTe₂ is shown in Fig. 71 (with M=Pt and X=Te). Each Pt atom is surrounded by six Te atoms. These Te atoms are categorized into the top group (eg. atoms 1, 3, and 5) and bottom group (eg. atoms 2, 4, and 6). Each Te atom is connected to three Pt atoms. The structural parameters are from the first-principles calculations,⁴⁸ including the lattice constant $a = 3.9554 \text{ \AA}$, and the bond length

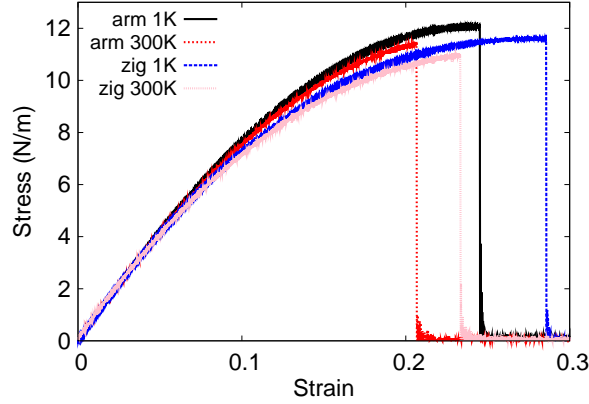


FIG. 177: (Color online) Stress-strain for single-layer 1T-PtTe₂ of dimension $100 \times 100 \text{ \AA}$ along the armchair and zigzag directions.

TABLE CCCLVI: Three-body SW potential parameters for single-layer 1T-PtTe₂ used by GULP⁸ as expressed in Eq. (4). The angle θ_{ijk} in the first line indicates the bending energy for the angle with atom i as the apex.

	K (eV)	θ_0 (degree)	ρ_1 (Å)	ρ_2 (Å)	$r_{\min 12}$ (Å)	$r_{\max 12}$ (Å)	$r_{\min 13}$ (Å)	$r_{\max 13}$ (Å)	$r_{\min 23}$ (Å)	$r_{\max 23}$ (Å)
$\theta_{\text{Pt-Te-Te}}$	59.607	95.998	1.667	1.667	0.0	3.714	0.0	3.714	0.0	5.403
$\theta_{\text{Te-Pt-Pt}}$	59.607	95.998	1.667	1.667	0.0	3.714	0.0	3.714	0.0	5.403

$d_{\text{Pt-Te}} = 2.6613 \text{ \AA}$, which is derived from the angle $\theta_{\text{TePtPt}} = 96^\circ$. The other angle is $\theta_{\text{PtTeTe}} = 96^\circ$ with Te atoms from the same (top or bottom) group.

Table CCCLIV shows three VFF terms for the single-layer 1T-PtTe₂, one of which is the bond stretching interaction shown by Eq. (1) while the other two terms are the angle bending interaction shown by Eq. (2). We note that the angle bending term $K_{\text{Pt-Te-Te}}$ is for the angle $\theta_{\text{Pt-Te-Te}}$ with both Te atoms from the same (top or bottom) group. These force constant parameters are determined by fitting to the three acoustic branches in the

TABLE CCCLVII: SW potential parameters for single-layer 1T-PtTe₂ used by LAMMPS⁹ as expressed in Eqs. (9) and (10).

	ϵ (eV)	σ (Å)	a	λ	γ	$\cos \theta_0$	A_L	B_L	p	q	tol
Pt-Te ₁ -Te ₁	1.000	1.667	2.229	59.607	1.000	-0.104	14.877	3.250	4	0	0.0

phonon dispersion along the Γ M as shown in Fig. 176 (a). The *ab initio* calculations for the phonon dispersion are from Ref. 34. Fig. 176 (b) shows that the VFF model and the SW potential give exactly the same phonon dispersion, as the SW potential is derived from the VFF model.

The parameters for the two-body SW potential used by GULP are shown in Tab. CCCLV. The parameters for the three-body SW potential used by GULP are shown in Tab. CCCLVI. Some representative parameters for the SW potential used by LAMMPS are listed in Tab. CCCLVII.

We use LAMMPS to perform MD simulations for the mechanical behavior of the single-layer 1T-PtTe₂ under uniaxial tension at 1.0 K and 300.0 K. Fig. 177 shows the stress-strain curve for the tension of a single-layer 1T-PtTe₂ of dimension 100×100 Å. Periodic boundary conditions are applied in both armchair and zigzag directions. The single-layer 1T-PtTe₂ is stretched uniaxially along the armchair or zigzag direction. The stress is calculated without involving the actual thickness of the quasi-two-dimensional structure of the single-layer 1T-PtTe₂. The Young's modulus can be obtained by a linear fitting of the stress-strain relation in the small strain range of $[0, 0.01]$. The Young's modulus are 89.1 N/m and 88.7 N/m along the armchair and zigzag directions, respectively. The Young's modulus is essentially isotropic in the armchair and zigzag directions. The Poisson's ratio from the VFF model and the SW potential is $\nu_{xy} = \nu_{yx} = 0.19$.

There is no available value for nonlinear quantities in the single-layer 1T-PtTe₂. We have thus used the nonlinear parameter $B = 0.5d^4$ in Eq. (5), which is close to the value of B in most materials. The value of the third order nonlinear elasticity D can be extracted by fitting the stress-strain relation to the function $\sigma = E\epsilon + \frac{1}{2}D\epsilon^2$ with E as the Young's modulus. The values of D from the present SW potential are -306.8 N/m and -340.9 N/m along the armchair and zigzag directions, respectively. The ultimate stress is about 12.1 Nm^{-1} at the ultimate strain of 0.24 in the armchair direction at the low temperature of 1 K. The ultimate stress is about 11.6 Nm^{-1} at the ultimate strain of 0.28 in the zigzag direction at the low temperature of 1 K.

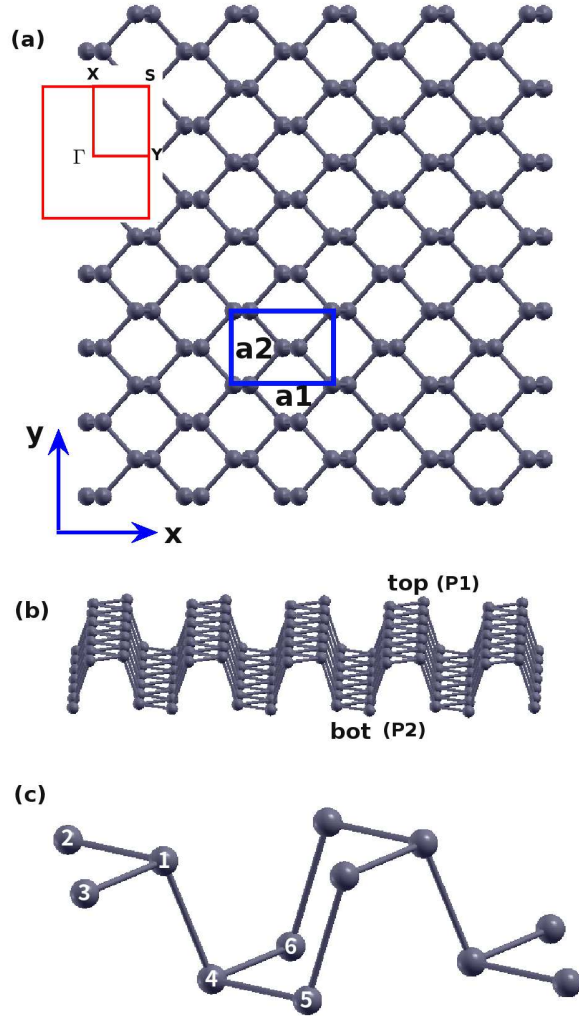


FIG. 178: (Color online) Structure for single-layer black phosphorus. (a) Top view. The armchair direction is along the x-axis, while the zigzag direction is along the y-axis. Inset shows the first Brillouin zone. (b) Perspective view illustrates the puckered configuration. The pucker is perpendicular to the x-axis and is parallel with the y-axis. Atoms are divided into the top (denoted by P_1) and the bottom (denoted by P_2) groups. (c) Atomic configuration.

XC. BLACK PHOSPHORUS

The black phosphorus is also named the α phosphorus. There are several empirical potentials available for the atomic interaction in the black phosphorus. A VFF model was proposed for the single-layer black phosphorus in 1982.⁵⁶ One of the present author (J.W.J.) simplified this VFF model by ignoring some angle-angle crossing terms, and use the

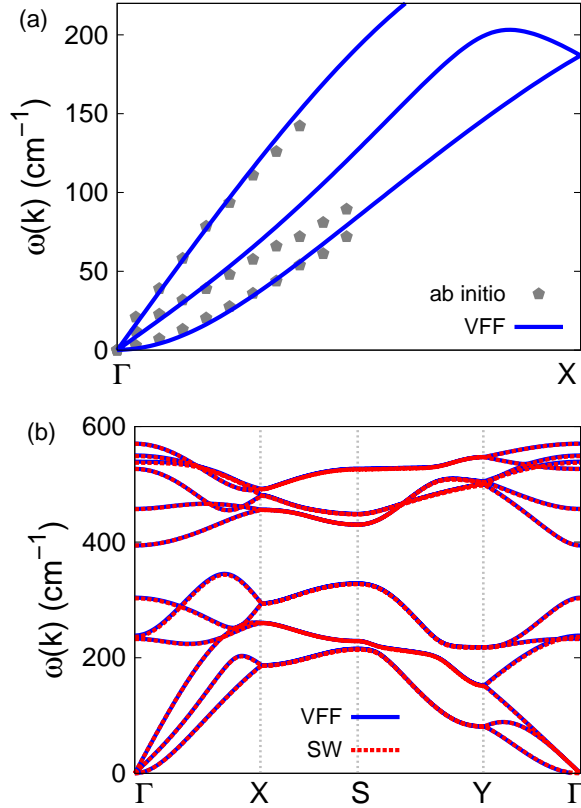


FIG. 179: (Color online) Phonon dispersion for the single-layer black phosphorus. (a) The VFF model is fitted to the three acoustic branches in the long wave limit along the ΓX direction. The *ab initio* results (gray pentagons) are from Ref. 55. (b) The VFF model (blue lines) and the SW potential (red lines) give the same phonon dispersion for the black phosphorus along $\Gamma XSYT$.

simplified VFF model to develop the SW potential for the black phosphorus.⁷ However, the mechanical properties from this SW potential are smaller than first-principles calculations, as some angle-angle crossing VFF terms can not be implemented in the SW potential. We will thus propose a new set of SW potential for the single-layer black phosphorus in this section.

The structure of the single-layer black phosphorus is shown in Fig. 178, with structural parameters from the *ab initio* calculations.⁵⁷ The black phosphorus has a puckered configuration as shown in Fig. 178 (b), where the pucker is perpendicular to the x-direction. The bases for the rectangular unit cell are $a_1 = 4.422 \text{ \AA}$ and $a_2 = 3.348 \text{ \AA}$. For bulk black phosphorus, the basis lattice vector in the third direction is $a_3 = 10.587 \text{ \AA}$. There are

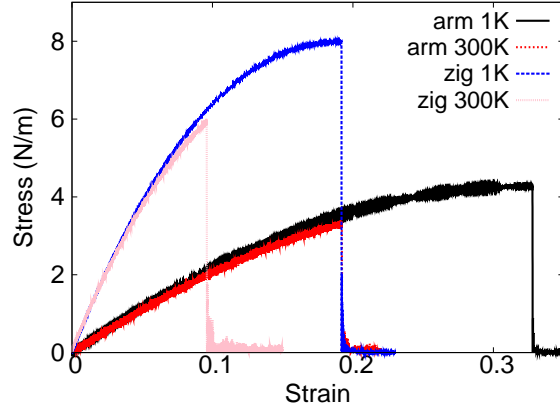


FIG. 180: (Color online) Stress-strain relations for the black phosphorus of size $100 \times 100 \text{ \AA}$. The black phosphorus is uniaxially stretched along the armchair or zigzag directions at temperatures 1 K and 300 K.

TABLE CCCLVIII: The VFF model for black phosphorus. The second line gives an explicit expression for each VFF term, where atom indexes are from Fig. 178 (c). The third line is the force constant parameters. Parameters are in the unit of $\frac{eV}{\text{\AA}^2}$ for the bond stretching interactions, and in the unit of eV for the angle bending interaction. The fourth line gives the initial bond length (in unit of \AA) for the bond stretching interaction and the initial angle (in unit of degrees) for the angle bending interaction. The angle θ_{ijk} has atom i as the apex.

VFF type	bond stretching		angle bending	
expression	$\frac{1}{2}K_{12}(\Delta r_{12})^2$	$\frac{1}{2}K_{14}(\Delta r_{14})^2$	$\frac{1}{2}K_{123}(\Delta\theta_{123})^2$	$\frac{1}{2}K_{134}(\Delta\theta_{134})^2$
parameter	10.542	10.542	7.048	7.048
r_0 or θ_0	2.238	2.260	96.581	102.307

four phosphorus atoms in the basic unit cell, and their relative coordinates are $(-u, 0, -v)$, $(u, 0, v)$, $(0.5 - u, 0.5, v)$, and $(0.5 + u, 0.5, -v)$ with $u = 0.0821$ and $v = 0.1011$. Atoms are categorized into the top and bottom groups. Atoms in the top group are denoted by P_1 , while atoms in the bottom group are denoted by P_2 .

Table CCCLVIII shows four VFF terms for the single-layer black phosphorus, two of which are the bond stretching interactions shown by Eq. (1) while the other two terms are the angle bending interaction shown by Eq. (2). The force constant parameters are reasonably chosen to be the same for the two bond stretching terms denoted by r_{12} and r_{14} ,

TABLE CCCLIX: Two-body SW potential parameters for black phosphorus used by GULP,⁸ as expressed in Eq. (3). The quantity (r_{ij}) in the first line lists one representative term for the two-body SW potential between atoms i and j . Atom indexes are from Fig. 178 (c).

	A (eV)	ρ (Å)	B (Å ⁴)	r_{\min} (Å)	r_{\max} (Å)
r_{12}	4.172	0.551	12.543	0.0	2.793
r_{14}	4.976	0.685	13.044	0.0	2.882

TABLE CCCLX: Three-body SW potential parameters for black phosphorus used by GULP,⁸ as expressed in Eq. (4). The first line (θ_{ijk}) presents one representative term for the three-body SW potential. The angle θ_{ijk} has the atom i as the apex. Atom indexes are from Fig. 178 (c).

	K (eV)	θ_0 (degree)	ρ_1 (Å)	ρ_2 (Å)	$r_{\min 12}$ (Å)	$r_{\max 12}$ (Å)	$r_{\min 13}$ (Å)	$r_{\max 13}$ (Å)	$r_{\min 23}$ (Å)	$r_{\max 23}$ (Å)
θ_{123}	25.965	96.581	0.551	0.551	0.0	2.793	0.0	2.793	2.793	3.365
θ_{134}	29.932	102.307	0.551	0.685	0.0	2.793	0.0	2.882	2.882	3.772

as these two bonds have very close bond length value. The force constant parameters are the same for the two angle bending terms θ_{123} and θ_{134} , which have very similar chemical environment. These force constant parameters are determined by fitting to the three acoustic branches in the phonon dispersion along the ΓX as shown in Fig. 179 (a). The *ab initio* calculations for the phonon dispersion are from Ref. 55. Similar phonon dispersion can also be found in other *ab initio* calculations.⁵⁸⁻⁶⁴ Fig. 179 (b) shows that the VFF model and the SW potential give exactly the same phonon dispersion, as the SW potential is derived from the VFF model.

The parameters for the two-body SW potential used by GULP are shown in

TABLE CCCLXI: SW potential parameters for black phosphorus used by LAMMPS,⁹ as expressed in Eqs. (9) and (10). Atom types (P_1 and P_2) in the first column are displayed in Fig. 178.

	ϵ (eV)	σ (Å)	a	λ	γ	$\cos \theta_0$	A_L	B_L	p	q	tol
P_1 - P_1 - P_1	1.000	0.551	5.069	25.965	1.000	-0.115	4.172	136.080	4	0	0.0
P_1 - P_2 - P_2	1.000	0.685	4.207	0.000	1.000	0.000	4.976	59.245	4	0	0.0
P_1 - P_1 - P_2	1.000	0.000	0.000	29.932	1.000	-0.213	0.000	0.000	4	0	0.0

Tab. CCCLIX. The parameters for the three-body SW potential used by GULP are shown in Tab. CCCLX. Parameters for the SW potential used by LAMMPS are listed in Tab. CCCLXI.

Fig. 180 shows the stress strain relations for the black phosphorus of size $100 \times 100 \text{ \AA}$. The structure is uniaxially stretched in the armchair or zigzag directions at 1 K and 300 K. The Young's modulus is 24.3 Nm^{-1} and 90.5 Nm^{-1} in the armchair and zigzag directions respectively at 1 K, which are obtained by linear fitting of the stress strain relations in $[0, 0.01]$. These values agree quite well with previously reported *ab initio* results, eg. 28.9 Nm^{-1} and 101.6 Nm^{-1} from Ref. 65, or 24.4 Nm^{-1} and 92.1 Nm^{-1} from Ref. 66, or 24.3 Nm^{-1} and 80.2 Nm^{-1} from Ref. 58. The ultimate stress is about 4.27 Nm^{-1} at the critical strain of 0.33 in the armchair direction at the low temperature of 1 K. The ultimate stress is about 8.0 Nm^{-1} at the critical strain of 0.19 in the zigzag direction at the low temperature of 1 K. These values agree quite well with the *ab initio* results at 0 K.⁶⁶

It should be noted that the Poisson's ratios from the VFF model and the SW potential are $\nu_{xy} = 0.058$ and $\nu_{yx} = 0.22$. These values are obviously smaller than first-principles calculations results, eg. 0.4 and 0.93 from Ref. 67, or 0.17 and 0.62 from Ref. 58, or 0.24 and 0.81 from Ref. 59. The Poisson's ratio can not be obtained correctly by the VFF model proposed in 1982⁵⁶ and the SW potential⁷ either.⁶⁸ These failures are due to the missing of one angle-angle crossing term,⁶⁹ which has not been implemented in the package LAMMPS and is not included in the present work.

XCI. P-ARSENENE

Present studies on the puckered (p-) arsenene, also named α arsenene, are based on first-principles calculations, and no empirical potential has been proposed for the p-arsenene. We will thus parametrize a set of VFF model for the single-layer p-arsenene in this section. We will also derive the SW potential based on the VFF model for the single-layer p-arsenene.

The structure of the single-layer p-arsenene is exactly the same as that of the black phosphorus as shown in Fig. 178. Structural parameters for p-arsenene are from the *ab initio* calculations.⁷⁰ The pucker of the p-arsenene is perpendicular to the x (armchair)-direction. The bases for the rectangular unit cell are $a_1 = 4.77 \text{ \AA}$ and $a_2 = 3.68 \text{ \AA}$. There are four As atoms in the basic unit cell, and their relative coordinates are $(-u, 0, -v)$,

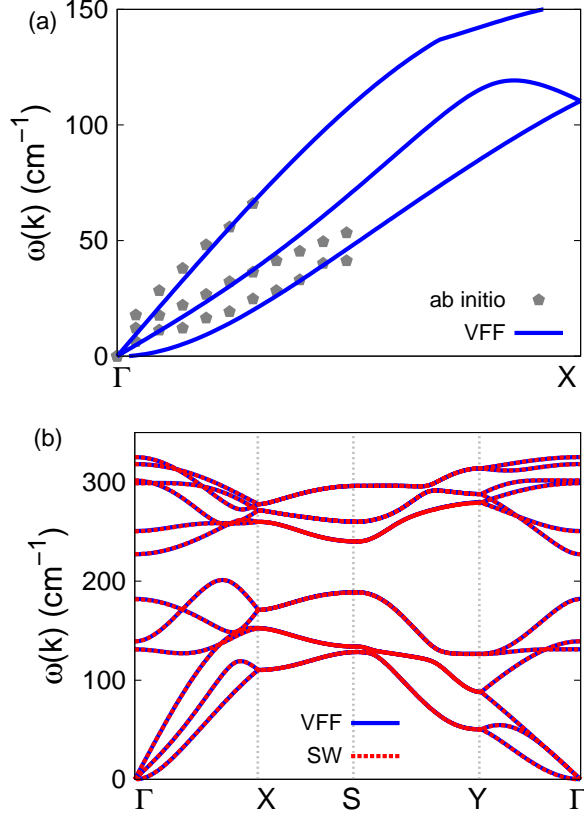


FIG. 181: (Color online) Phonon dispersion for the single-layer p-arsenene. (a) The VFF model is fitted to the three acoustic branches in the long wave limit along the ΓX direction. The *ab initio* results (gray pentagons) are from Ref. 70. (b) The VFF model (blue lines) and the SW potential (red lines) give the same phonon dispersion for the p-arsenene along $\Gamma XSYT$.

$(u, , v)$, $(0.5 - u, 0.5, v)$, and $(0.5 + u, 0.5, -v)$ with $u = 0.0714$ and $v = 0.108$. The value of the dimensionless parameter u is extracted from the geometrical parameters provided in Ref. 70. The other dimensionless parameter v is a ratio based on the lattice constant in the out-of-plane z -direction, so the other basis $a_3 = 11.11 \text{ \AA}$ from Ref. 71 is also adopted in extracting the value of v . We note that the main purpose of the usage of u and v in representing atomic coordinates is to follow the same convention for all puckered structures. The resultant atomic coordinates are the same as that in Ref. 70.

Table CCCLXII shows four VFF terms for the single-layer p-arsenene, two of which are the bond stretching interactions shown by Eq. (1) while the other two terms are the angle bending interaction shown by Eq. (2). The force constant parameters are reasonably chosen

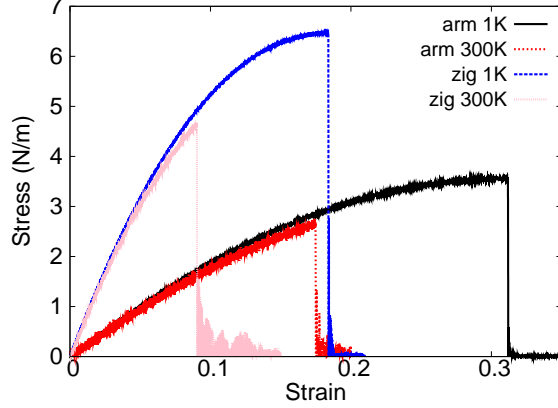


FIG. 182: (Color online) Stress-strain relations for the p-arsenene of size $100 \times 100 \text{ \AA}$. The p-arsenene is uniaxially stretched along the armchair or zigzag directions at temperatures 1 K and 300 K.

TABLE CCCLXII: The VFF model for p-arsenene. The second line gives an explicit expression for each VFF term, where atom indexes are from Fig. 178 (c). The third line is the force constant parameters. Parameters are in the unit of $\frac{eV}{\text{Å}^2}$ for the bond stretching interactions, and in the unit of eV for the angle bending interaction. The fourth line gives the initial bond length (in unit of Å) for the bond stretching interaction and the initial angle (in unit of degrees) for the angle bending interaction. The angle θ_{ijk} has atom i as the apex.

VFF type	bond stretching		angle bending	
expression	$\frac{1}{2}K_{12}(\Delta r_{12})^2$	$\frac{1}{2}K_{14}(\Delta r_{14})^2$	$\frac{1}{2}K_{123}(\Delta\theta_{123})^2$	$\frac{1}{2}K_{134}(\Delta\theta_{134})^2$
parameter	7.936	7.936	7.456	7.456
r_0 or θ_0	2.508	2.495	94.400	100.692

to be the same for the two bond stretching terms denoted by r_{12} and r_{14} , as these two bonds have very close bond length value. The force constant parameters happen to be the same for the two angle bending terms θ_{123} and θ_{134} . These force constant parameters are determined by fitting to the three acoustic branches in the phonon dispersion along the ΓX as shown in Fig. 181 (a). The *ab initio* calculations for the phonon dispersion are from Ref. 70. Similar phonon dispersion can also be found in other *ab initio* calculations.^{64,72–74} We note that the lowest-frequency branch around the Γ point from the VFF model is lower than the *ab initio* results. This branch is the flexural branch, which should be a quadratic dispersion.

TABLE CCCLXIII: Two-body SW potential parameters for p-arsenene used by GULP,⁸ as expressed in Eq. (3). The quantity (r_{ij}) in the first line lists one representative term for the two-body SW potential between atoms i and j . Atom indexes are from Fig. 178 (c).

	A (eV)	ρ (Å)	B (Å ⁴)	r_{\min} (Å)	r_{\max} (Å)
r_{12}	3.180	0.455	19.782	0.0	3.042
r_{14}	4.477	0.737	19.375	0.0	3.173

TABLE CCCLXIV: Three-body SW potential parameters for p-arsenene used by GULP,⁸ as expressed in Eq. (4). The first line (θ_{ijk}) presents one representative term for the three-body SW potential. The angle θ_{ijk} has the atom i as the apex. Atom indexes are from Fig. 178 (c).

	K (eV)	θ_0 (degree)	ρ_1 (Å)	ρ_2 (Å)	$r_{\min 12}$ (Å)	$r_{\max 12}$ (Å)	$r_{\min 13}$ (Å)	$r_{\max 13}$ (Å)	$r_{\min 23}$ (Å)	$r_{\max 23}$ (Å)
θ_{123}	20.597	94.400	0.455	0.455	0.0	3.042	0.0	3.042	3.628	4.225
θ_{134}	26.831	100.692	0.455	0.737	0.0	3.042	0.0	3.173	3.173	4.149

However, the *ab initio* calculations give a linear dispersion for the flexural branch due to the violation of the rigid rotational invariance in the first-principles package,²⁰ so *ab initio* calculations typically overestimate the frequency of this branch. Fig. 181 (b) shows that the VFF model and the SW potential give exactly the same phonon dispersion, as the SW potential is derived from the VFF model.

The parameters for the two-body SW potential used by GULP are shown in Tab. CCCLXIII. The parameters for the three-body SW potential used by GULP are shown in Tab. CCCLXIV. Parameters for the SW potential used by LAMMPS are listed in

TABLE CCCLXV: SW potential parameters for p-arsenene used by LAMMPS,⁹ as expressed in Eqs. (9) and (10). Atom types in the first column are displayed in Fig. 178 (b), with element symbol P substituted by As.

	ϵ (eV)	σ (Å)	a	λ	γ	$\cos \theta_0$	A_L	B_L	p	q	tol
As ₁ -As ₁ -As ₁	1.000	0.455	6.686	20.597	1.000	-0.077	3.180	461.556	4	0	0.0
As ₁ -As ₂ -As ₂	1.000	0.737	4.305	0.000	1.000	0.000	4.477	65.671	4	0	0.0
As ₁ -As ₁ -As ₂	1.000	0.000	0.000	26.831	1.000	-0.186	0.000	0.000	4	0	0.0

TABLE CCCLXVI: The VFF model for p-antimonene. The second line gives an explicit expression for each VFF term, where atom indexes are from Fig. 183 (c). The third line is the force constant parameters. Parameters are in the unit of $\frac{\text{eV}}{\text{\AA}^2}$ for the bond stretching interactions, and in the unit of eV for the angle bending interaction. The fourth line gives the initial bond length (in unit of \AA) for the bond stretching interaction and the initial angle (in unit of degrees) for the angle bending interaction. The angle θ_{ijk} has atom i as the apex.

VFF type	bond stretching		angle bending		
expression	$\frac{1}{2}K_{12}(\Delta r_{12})^2$	$\frac{1}{2}K_{14}(\Delta r_{14})^2$	$\frac{1}{2}K_{123}(\Delta\theta_{123})^2$	$\frac{1}{2}K_{134}(\Delta\theta_{134})^2$	$\frac{1}{2}K_{415}(\Delta\theta_{415})^2$
parameter	7.675	7.675	6.534	12.068	12.068
r_0 or θ_0	2.950	2.870	95.380	88.300	102.800

Tab. CCCLXV.

Fig. 182 shows the stress strain relations for the p-arsenene of size $100 \times 100 \text{ \AA}$. The structure is uniaxially stretched in the armchair or zigzag directions at 1 K and 300 K. The Young's modulus is 20.7 Nm^{-1} and 73.0 Nm^{-1} in the armchair and zigzag directions respectively at 1 K, which are obtained by linear fitting of the stress strain relations in $[0, 0.01]$. The third-order nonlinear elastic constant D can be obtained by fitting the stress-strain relation to $\sigma = E\epsilon + \frac{1}{2}D\epsilon^2$ with E as the Young's modulus. The values of D are -56.4 N/m and -415.5 N/m at 1 K along the armchair and zigzag directions, respectively. The ultimate stress is about 3.5 Nm^{-1} at the critical strain of 0.31 in the armchair direction at the low temperature of 1 K. The ultimate stress is about 6.5 Nm^{-1} at the critical strain of 0.18 in the zigzag direction at the low temperature of 1 K.

XCII. P-ANTIMONENE

Present studies on the puckered (p-) antimonene, also named α antimonene, are based on first-principles calculations, and no empirical potential has been proposed for the p-antimonene. We will thus parametrize a set of VFF model for the single-layer p-antimonene in this section. We will also derive the SW potential based on the VFF model for the single-layer p-antimonene.

The structure of the single-layer p-antimonene is shown in Fig. 183, which is similar as

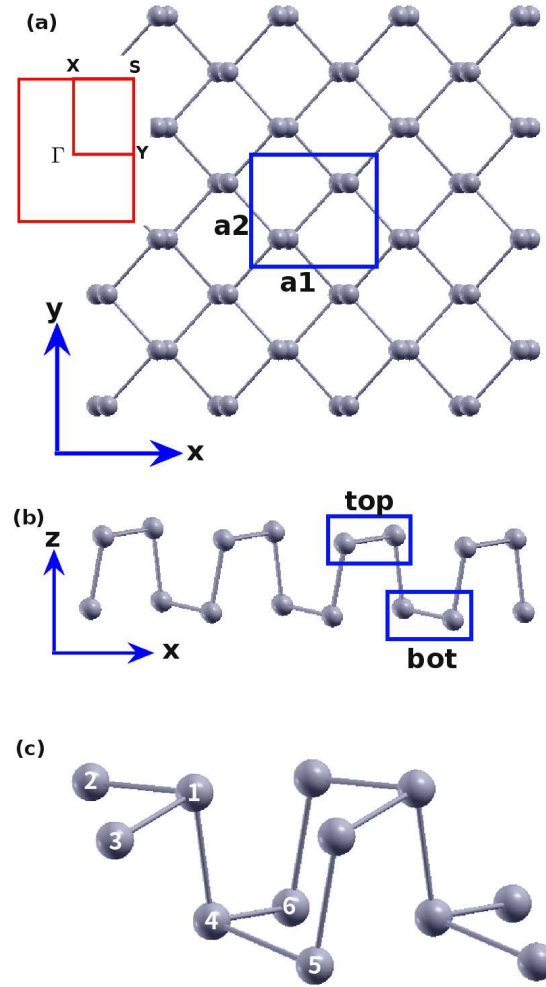


FIG. 183: (Color online) Structure for single-layer p-antimonene. (a) Top view. The armchair direction is along the x-axis, while the zigzag direction is along the y-axis. The first Brillouin zone is shown in the inset. (b) Side view illustrates the puckered configuration. The pucker is perpendicular to the x-axis and is parallel with the y-axis. Sb atoms in the top/bottom group have different z-coordinates. (c) Atomic configuration.

that of the black phosphorus as shown in Fig. 178. Structural parameters for p-antimonene are from the *ab initio* calculations.⁷⁰ The pucker of the p-antimonene is perpendicular to the x (armchair)-direction. The bases for the rectangular unit cell are $a_1 = 4.73 \text{ \AA}$ and $a_2 = 4.36 \text{ \AA}$. There are four Sb atoms in the basic unit cell, and their relative coordinates are $(-u, 0, -v)$, $(u, 0, v)$, $(0.5 - u, 0.5, v + w)$, and $(0.5 + u, 0.5, -v + w)$ with $u = 0.044$, $v = 0.128$ and $w = 0.0338$. The value of the dimensionless parameter u is extracted from

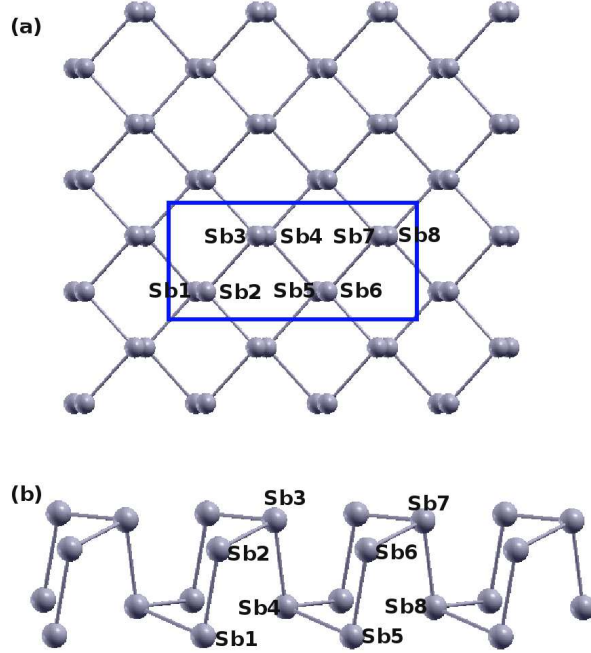


FIG. 184: (Color online) Eight atom types are introduced for the Sb atoms in the p-antimonene. (a) Top view. (b) Side view.

TABLE CCCLXVII: Two-body SW potential parameters for p-antimonene used by GULP,⁸ as expressed in Eq. (3). The quantity (r_{ij}) in the first line lists one representative term for the two-body SW potential between atoms i and j . Atom indexes are from Fig. 183 (c).

	A (eV)	ρ (\AA)	B (\AA^4)	r_{\min} (\AA)	r_{\max} (\AA)
r_{12}	1.750	0.122	37.867	0.0	3.250
r_{14}	11.221	1.843	33.923	0.0	4.020

the geometrical parameters (bond lengths and bond angles) provided in Ref. 70. The dimensionless parameters v and w are ratios based on the lattice constant in the out-of-plane z -direction, so an arbitrary value of $a_3 = 11.11 \text{ \AA}$ is adopted in extracting the values of v and w . The value of a_3 has no effect on the actual position of each Sb atom. We note that the main purpose of the usage of u , v , and w in representing atomic coordinates is to follow the same convention of black phosphorus. The resultant atomic coordinates are the same as that in Ref. 70.

As shown in Fig. 183 (b), a specific feature in the puckered configuration of the p-

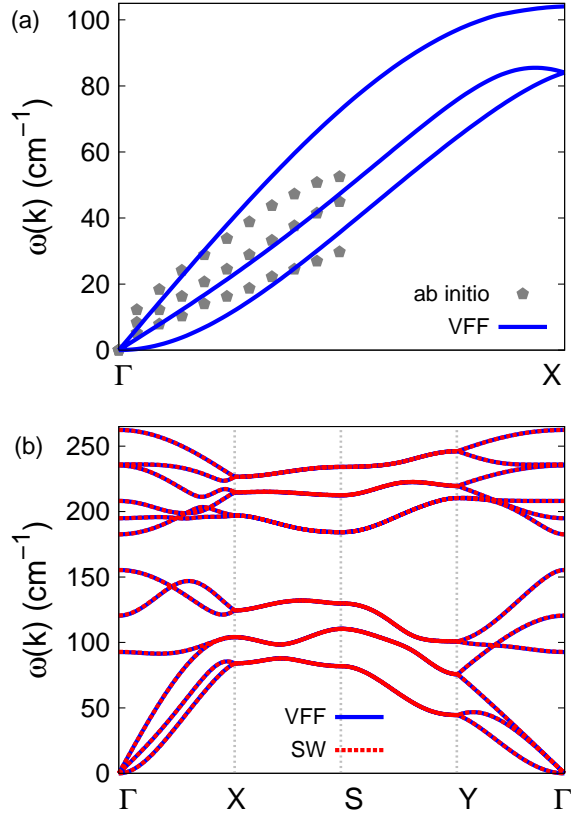


FIG. 185: (Color online) Phonon dispersion for the single-layer p-antimonene. (a) The VFF model is fitted to the three acoustic branches in the long wave limit along the ΓX direction. The *ab initio* results (gray pentagons) are from Ref. 70. (b) The VFF model (blue lines) and the SW potential (red lines) give the same phonon dispersion for the p-antimonene along $\Gamma XSYT$.

antimonene is that Sb atoms in the top/bottom group are further divided into two subgroups with different z -coordinates. Specifically, in Fig. 183 (c), there is a difference of wa_3 between the z -coordinate of atom 1 and the z -coordinates of atoms 2 and 3. Similarly, atom 4 is higher than atoms 5 and 6 for wa_3 along the z -direction. As a result of the nonzero value of w , there are two different inter-group angles, i.e., $\theta_{134} = 88.3^\circ$ and $\theta_{415} = 102.8^\circ$. We have $w = 0$ for the ideal puckered configuration of the black phosphorus.

Table CCCLXVI shows five VFF terms for the single-layer p-antimonene, two of which are the bond stretching interactions shown by Eq. (1) while the other three terms are the angle bending interaction shown by Eq. (2). The force constant parameters are reasonably chosen to be the same for the two bond stretching terms denoted by r_{12} and r_{14} , as these two

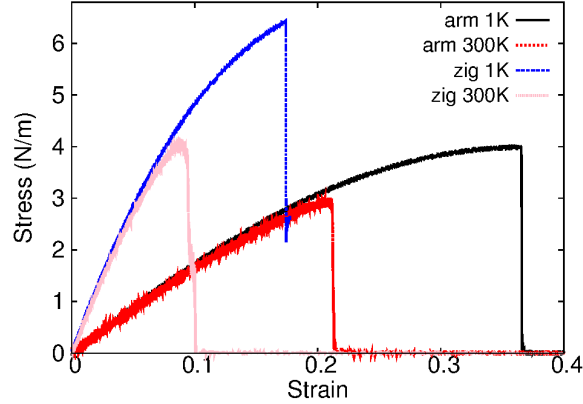


FIG. 186: (Color online) Stress-strain relations for the p-antimonene of size $100 \times 100 \text{ \AA}$. The p-antimonene is uniaxially stretched along the armchair or zigzag directions at temperatures 1 K and 300 K.

TABLE CCCLXVIII: Three-body SW potential parameters for p-antimonene used by GULP,⁸ as expressed in Eq. (4). The first line (θ_{ijk}) presents one representative term for the three-body SW potential. The angle θ_{ijk} has the atom i as the apex. Atom indexes are from Fig. 183 (c).

	K (eV)	θ_0 (degree)	ρ_1 (\AA)	ρ_2 (\AA)	$r_{\min 12}$ (\AA)	$r_{\max 12}$ (\AA)	$r_{\min 13}$ (\AA)	$r_{\max 13}$ (\AA)	$r_{\min 23}$ (\AA)	$r_{\max 23}$ (\AA)
θ_{123}	7.435	95.380	0.122	0.122	0.0	3.250	0.0	3.250	0.0	4.545
θ_{134}	45.054	88.380	1.843	0.122	0.0	4.020	0.0	3.250	0.0	5.715
θ_{415}	47.338	102.800	1.843	0.122	0.0	4.020	0.0	3.250	0.0	6.105

bonds have very close bond length value. The force constant parameters are the same for the two angle bending terms θ_{134} and θ_{415} , which have the same arm lengths. As a result, there are only three force constant parameters, i.e., $K_{12} = K_{14}$, K_{123} , and $K_{134} = K_{415}$. These three force constant parameters are determined by fitting to the three acoustic branches in the phonon dispersion along the ΓX as shown in Fig. 185 (a). The *ab initio* calculations for the phonon dispersion are from Ref. 70. Similar phonon dispersion can also be found in other *ab initio* calculations.^{64,75,76} We note that the lowest-frequency branch around the Γ point from the VFF model is lower than the *ab initio* results. This branch is the flexural branch, which should be a quadratic dispersion. However, the *ab initio* calculations give a linear dispersion for the flexural branch due to the violation of the rigid rotational invariance in the first-principles package,²⁰ so *ab initio* calculations typically overestimate the frequency

TABLE CCCLXIX: SW potential parameters for p-antimonene used by LAMMPS,⁹ as expressed in Eqs. (9) and (10). Atom types in the first column are displayed in Fig. 184.

	ϵ (eV)	σ (Å)	a	λ	γ	$\cos \theta_0$	A_L	B_L	p	q	tol
Sb ₅ -Sb ₄ -Sb ₄	1.000	5.103	0.958	635.059	1.000	-0.094	38.498	0.056	4	0	0.0
Sb ₁ -Sb ₂ -Sb ₂	1.000	1.924	2.102	0.000	1.000	0.000	11.708	2.476	4	0	0.0
Sb ₅ -Sb ₄ -Sb ₆	1.000	0.000	0.000	431.139	1.000	0.030	0.000	0.000	4	0	0.0
Sb ₂ -Sb ₃ -Sb ₁	1.000	0.000	0.000	452.994	1.000	-0.222	0.000	0.000	4	0	0.0

of this branch. Fig. 185 (b) shows that the VFF model and the SW potential give exactly the same phonon dispersion, as the SW potential is derived from the VFF model.

The parameters for the two-body SW potential used by GULP are shown in Tab. CCCLXVII. The parameters for the three-body SW potential used by GULP are shown in Tab. CCCLXVIII. Parameters for the SW potential used by LAMMPS are listed in Tab. CCCLXIX. Eight atom types have been introduced for writing the SW potential script used by LAMMPS as shown in Fig. 184, which technically increases the cutoff for the bond stretching interaction between atom 1 and atom 2 in Fig. 183 (c).

Fig. 186 shows the stress strain relations for the p-antimonene of size 100×100 Å. The structure is uniaxially stretched in the armchair or zigzag directions at 1 K and 300 K. The Young's modulus is 18.3 Nm^{-1} and 65.2 Nm^{-1} in the armchair and zigzag directions respectively at 1 K, which are obtained by linear fitting of the stress strain relations in $[0, 0.01]$. The Poisson's ratios from the VFF model and the SW potential are $\nu_{xy} = 0.08$ and $\nu_{yx} = 0.29$. The third-order nonlinear elastic constant D can be obtained by fitting the stress-strain relation to $\sigma = E\epsilon + \frac{1}{2}D\epsilon^2$ with E as the Young's modulus. The values of D are -22.1 N/m and -354.1 N/m at 1 K along the armchair and zigzag directions, respectively. The ultimate stress is about 3.7 Nm^{-1} at the critical strain of 0.37 in the armchair direction at the low temperature of 1 K. The ultimate stress is about 6.4 Nm^{-1} at the critical strain of 0.17 in the zigzag direction at the low temperature of 1 K.

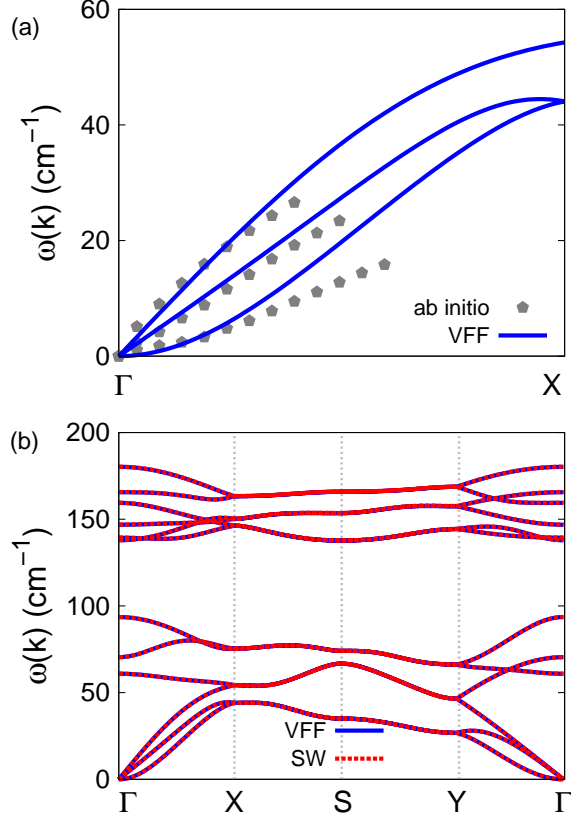


FIG. 187: (Color online) Phonon dispersion for the single-layer p-bismuthene. (a) The VFF model is fitted to the three acoustic branches in the long wave limit along the ΓX direction. The *ab initio* results (gray pentagons) are from Ref. 77. (b) The VFF model (blue lines) and the SW potential (red lines) give the same phonon dispersion for the p-bismuthene along $\Gamma XSY\Gamma$.

XCI. P-BISMUTHENE

Present studies on the puckered (p-) bismuthene, which is also named α bismuthene, are based on first-principles calculations, and no empirical potential has been proposed for the p-bismuthene. We will thus parametrize a set of VFF model for the single-layer p-bismuthene in this section. We will also derive the SW potential based on the VFF model for the single-layer p-bismuthene.

The structure of the single-layer p-bismuthene is the same as p-antimonene as shown in Fig. 183. Structural parameters for p-bismuthene are from the *ab initio* calculations.⁷⁷ The pucker of the p-bismuthene is perpendicular to the x (armchair)-direction. The bases for

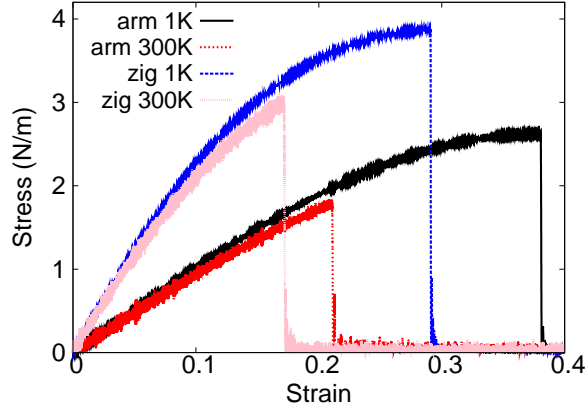


FIG. 188: (Color online) Stress-strain relations for the p-bismuthene of size $100 \times 100 \text{ \AA}$. The p-bismuthene is uniaxially stretched along the armchair or zigzag directions at temperatures 1 K and 300 K.

TABLE CCCLXX: The VFF model for p-bismuthene. The second line gives an explicit expression for each VFF term, where atom indexes are from Fig. 183 (c). The third line is the force constant parameters. Parameters are in the unit of $\frac{eV}{\text{Å}^2}$ for the bond stretching interactions, and in the unit of eV for the angle bending interaction. The fourth line gives the initial bond length (in unit of Å) for the bond stretching interaction and the initial angle (in unit of degrees) for the angle bending interaction. The angle θ_{ijk} has atom i as the apex.

VFF type	bond stretching		angle bending		
expression	$\frac{1}{2}K_{12}(\Delta r_{12})^2$	$\frac{1}{2}K_{14}(\Delta r_{14})^2$	$\frac{1}{2}K_{123}(\Delta\theta_{123})^2$	$\frac{1}{2}K_{134}(\Delta\theta_{134})^2$	$\frac{1}{2}K_{415}(\Delta\theta_{415})^2$
parameter	7.675	7.675	2.267	8.347	8.347
r_0 or θ_0	3.110	3.097	94.018	86.486	103.491

the rectangular unit cell are $a_1 = 4.94 \text{ \AA}$ and $a_2 = 4.55 \text{ \AA}$. There are four Bi atoms in the basic unit cell, and their relative coordinates are $(-u, 0, -v)$, $(u, 0, v)$, $(0.5 - u, 0.5, v + w)$, and $(0.5 + u, 0.5, -v + w)$ with $u = 0.0405$, $v = 0.130$ and $w = 0.0391$. The value of the dimensionless parameter u is extracted from the geometrical parameters provided in Ref. 77. The dimensionless parameters v and w are ratios based on the lattice constant in the out-of-plane z -direction, so an arbitrary value of $a_3 = 11.81 \text{ \AA}$ is adopted in extracting the values of v and w . The value of a_3 has no effect on the actual position of each Bi atom. We note that the main purpose of the usage of u , v , and w in representing atomic coordinates is to

TABLE CCCLXXI: Two-body SW potential parameters for p-bismuthene used by GULP,⁸ as expressed in Eq. (3). The quantity (r_{ij}) in the first line lists one representative term for the two-body SW potential between atoms i and j . Atom indexes are from Fig. 183 (c).

	A (eV)	ρ (Å)	B (Å ⁴)	r_{\min} (Å)	r_{\max} (Å)
r_{12}	1.777	0.109	46.775	0.0	3.401
r_{14}	12.322	1.872	45.998	0.0	4.301

TABLE CCCLXXII: Three-body SW potential parameters for p-bismuthene used by GULP,⁸ as expressed in Eq. (4). The first line (θ_{ijk}) presents one representative term for the three-body SW potential. The angle θ_{ijk} has the atom i as the apex. Atom indexes are from Fig. 183 (c).

	K (eV)	θ_0 (degree)	ρ_1 (Å)	ρ_2 (Å)	$r_{\min12}$ (Å)	$r_{\max12}$ (Å)	$r_{\min13}$ (Å)	$r_{\max13}$ (Å)	$r_{\min23}$ (Å)	$r_{\max23}$ (Å)
θ_{123}	2.408	94.018	0.109	0.109	0.0	3.401	0.0	3.401	0.0	4.745
θ_{134}	28.842	86.486	1.872	0.109	0.0	4.301	0.0	3.401	0.0	5.982
θ_{415}	30.388	103.491	1.872	0.109	0.0	4.301	0.0	3.401	0.0	6.473

follow the same convention of black phosphorus. The resultant atomic coordinates are the same as that in Ref. 77.

As shown in Fig. 183 (b), a specific feature in the puckered configuration of the p-bismuthene is that Bi atoms in the top/bottom group are further divided into two subgroups with different z -coordinates. Specifically, in Fig. 183 (c), there is a difference of wa_3 between the z -coordinate of atom 1 and the z -coordinates of atoms 2 and 3. Similarly, atom 4 is

TABLE CCCLXXIII: SW potential parameters for p-bismuthene used by LAMMPS,⁹ as expressed in Eqs. (9) and (10). Atom types in the first column are displayed in Fig. 184 with elemental symbol Sb substituted by Bi.

	ϵ (eV)	σ (Å)	a	λ	γ	$\cos \theta_0$	A_L	B_L	p	q	tol
Bi ₁ -Bi ₈ -Bi ₈	1.000	2.737	1.571	112.813	1.000	-0.070	18.974	1.000	4	0	0.0
Bi ₁ -Bi ₂ -Bi ₂	1.000	2.808	1.532	0.000	1.000	0.000	19.577	0.888	4	0	0.0
Bi ₁ -Bi ₈ -Bi ₂	1.000	0.000	0.000	429.598	1.000	0.061	0.000	0.000	4	0	0.0
Bi ₂ -Bi ₃ -Bi ₁	1.000	0.000	0.000	452.618	1.000	-0.233	0.000	0.000	4	0	0.0

higher than atoms 5 and 6 for wa_3 along the z-direction. As a result of the nonzero value of w , there are two different inter-group angles, i.e., $\theta_{134} = 86.486^\circ$ and $\theta_{415} = 103.491^\circ$. We have $w = 0$ for the ideal puckered configuration of the black phosphorus.

Table CCCLXX shows five VFF terms for the single-layer p-bismuthene, two of which are the bond stretching interactions shown by Eq. (1) while the other three terms are the angle bending interaction shown by Eq. (2). The force constant parameters are reasonably chosen to be the same for the two bond stretching terms denoted by r_{12} and r_{14} , as these two bonds have very close bond length value. The force constant parameters are the same for the two angle bending terms θ_{134} and θ_{415} , which have the same arm lengths. As a result, there are only three force constant parameters, i.e., $K_{12} = K_{14}$, K_{123} , and $K_{134} = K_{415}$. These three force constant parameters are determined by fitting to the three acoustic branches in the phonon dispersion along the ΓX as shown in Fig. 187 (a). The *ab initio* calculations for the phonon dispersion are from Ref. 77. Similar phonon dispersion can also be found in other *ab initio* calculations.⁶⁴ Fig. 187 (b) shows that the VFF model and the SW potential give exactly the same phonon dispersion, as the SW potential is derived from the VFF model.

The parameters for the two-body SW potential used by GULP are shown in Tab. CCCLXXI. The parameters for the three-body SW potential used by GULP are shown in Tab. CCCLXXII. Parameters for the SW potential used by LAMMPS are listed in Tab. CCCLXXIII. Eight atom types have been introduced for writing the SW potential script used by LAMMPS as shown in Fig. 184, which helps to increase the cutoff for the bond stretching interaction between atoms like 1 and 2 in Fig. 183 (c).

Fig. 188 shows the stress strain relations for the p-bismuthene of size $100 \times 100 \text{ \AA}$. The structure is uniaxially stretched in the armchair or zigzag directions at 1 K and 300 K. The Young's modulus is 10.2 Nm^{-1} and 26.2 Nm^{-1} in the armchair and zigzag directions respectively at 1 K, which are obtained by linear fitting of the stress strain relations in $[0, 0.01]$. The Poisson's ratios from the VFF model and the SW potential are $\nu_{xy} = 0.24$ and $\nu_{yx} = 0.61$. These values are very close to the *ab initio* calculations, eg. $\nu_{xy} = 0.261$ and $\nu_{yx} = 0.648$ in Ref. 77. The third-order nonlinear elastic constant D can be obtained by fitting the stress-strain relation to $\sigma = E\epsilon + \frac{1}{2}D\epsilon^2$ with E as the Young's modulus. The values of D are -12.4 N/m and -86.4 N/m at 1 K along the armchair and zigzag directions, respectively. The ultimate stress is about 2.6 Nm^{-1} at the critical strain of 0.38 in the armchair direction at the low temperature of 1 K. The ultimate stress is about 3.9 Nm^{-1} at

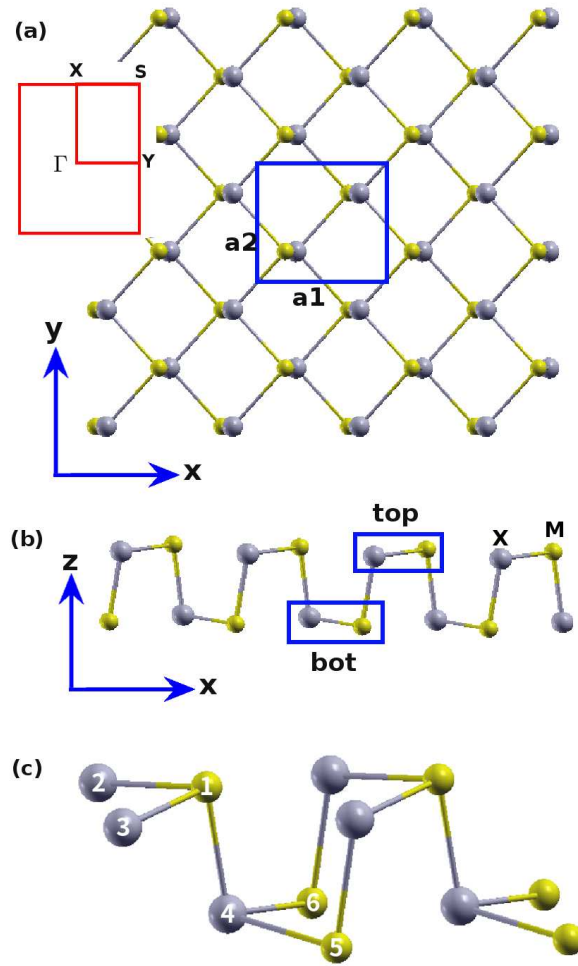


FIG. 189: (Color online) Structure for single-layer p-MX, with M from group IV and X from group VI. (a) Top view. The armchair direction is along the x-axis, while the zigzag direction is along the y-axis. Red inset shows the first Brillouin zone. (b) Side view illustrates the puckered configuration. The pucker is perpendicular to the x-axis and is parallel with the y-axis. (c) Atomic configuration. Atom M (X) is represented by yellow smaller (gray larger) balls.

the critical strain of 0.29 in the zigzag direction at the low temperature of 1 K.

XCIV. P-SiO

Present studies on the puckered (p-) SiO are based on first-principles calculations, and no empirical potential has been proposed for the p-SiO. We will thus parametrize the SW potential for the single-layer p-SiO in this section.

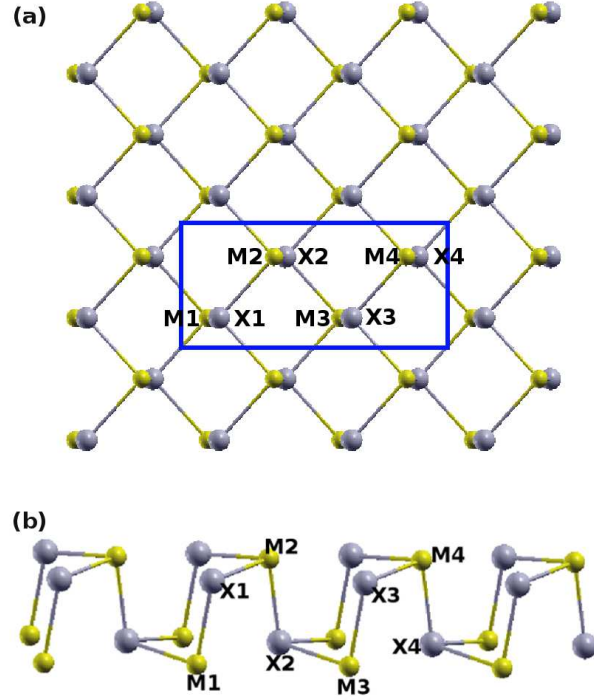


FIG. 190: (Color online) Eight atom types are introduced for atoms in the p-MX, with M from group IV and X from group VI. (a) Top view. (b) Side view.

The structure of the single-layer p-SiO is shown in Fig. 189, with M=Si and X=O. Structural parameters for p-SiO are from the *ab initio* calculations.⁷⁸ There are four atoms in the unit cell with relative coordinates as $(-u, 0, -v)$, $(u, 0, v)$, $(0.5 - u, 0.5, v + w)$, and $(0.5 + u, 0.5, -v + w)$ with $u = 0.1501$, $v = 0.0605$ and $w = 0.0800$. The value of these dimensionless parameters are extracted from the geometrical parameters provided in Ref. 78, including lattice constants $a_1 = 4.701 \text{ \AA}$ and $a_2 = 2.739 \text{ \AA}$, bond lengths $d_{12} = 1.843 \text{ \AA}$ and $d_{14} = 2.859 \text{ \AA}$, and the angle $\theta_{145} = 96.0^\circ$. The dimensionless parameters v and w are ratios based on the lattice constant in the out-of-plane z -direction, which is arbitrarily chosen as $a_3 = 10.0 \text{ \AA}$. We note that the main purpose of the usage of u , v , and w in representing atomic coordinates is to follow the same convention for all puckered structures in the present work. The resultant atomic coordinates are the same as that in Ref. 78.

As shown in Fig. 189, a specific feature in the puckered configuration of the p-SiO is that there is a small difference of wa_3 between the z -coordinate of atom 1 and the z -coordinates of atoms 2 and 3. Similarly, atom 4 is higher than atoms 5 and 6 for wa_3 along the z -direction.

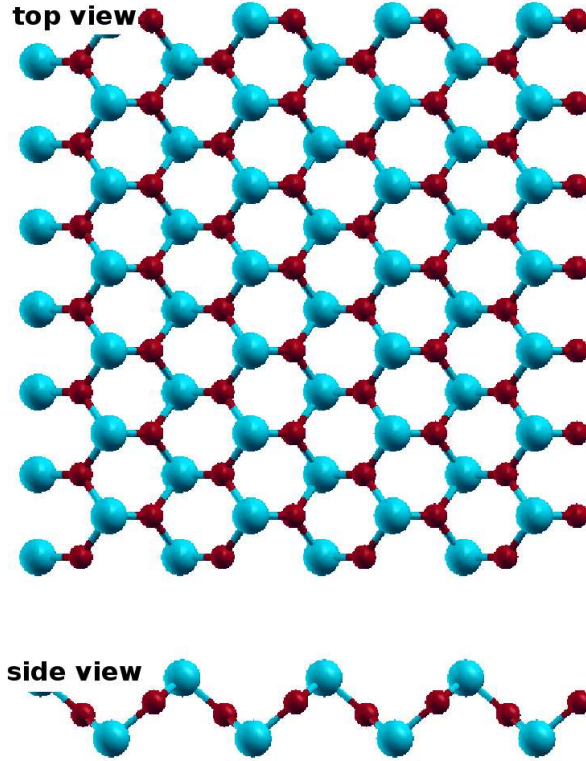


FIG. 191: (Color online) Zigzag configuration of single-layer p-MX, with M from group IV and X=O. Atom M (O) is represented by purple larger (red smaller) balls.

The sign of w determines which types of atoms take the out-most positions, e.g., atoms 1, 5, and 6 are the out-most atoms if $w > 0$ in Fig. 189 (c), while atoms 2, 3, and 4 will take the out-most positions for $w < 0$. The p-SiO has a zigzag configuration as shown in Fig. 191, which is a specific case of the puckered structure shown in Fig. 189.

Table CCCLXXIV shows five VFF terms for the single-layer p-SiO, two of which are the bond stretching interactions shown by Eq. (1) while the other three terms are the angle bending interaction shown by Eq. (2). The force constant parameters are the same for the two angle bending terms θ_{134} and θ_{415} , which have the same arm lengths. All force constant parameters are determined by fitting to the acoustic branches in the phonon dispersion along the ΓX as shown in Fig. 192 (a). The *ab initio* calculations for the phonon dispersion are calculated from the SIESTA package.⁷⁹ The generalized gradients approximation is applied to account for the exchange-correlation function with Perdew, Burke, and Ernzerhof parameterization,⁸⁰ and the double- ζ orbital basis set is adopted. Fig. 192 (b) shows that

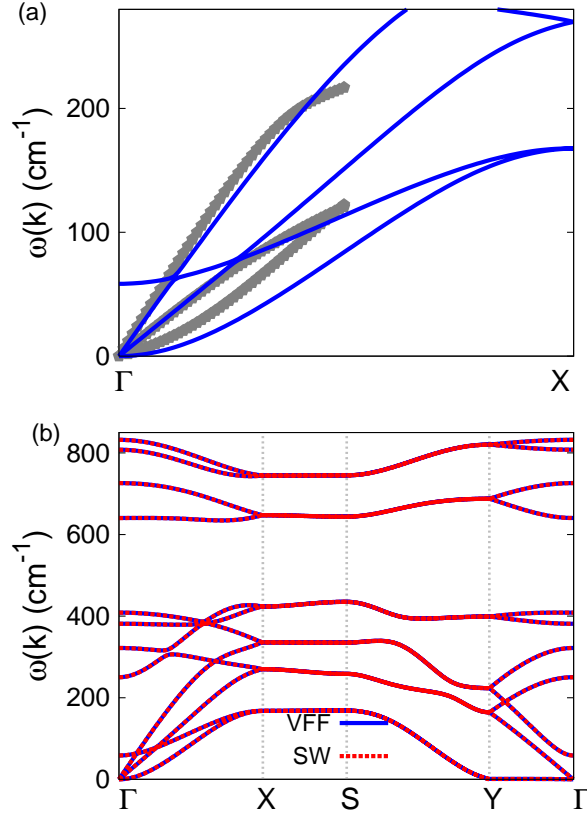


FIG. 192: (Color online) Phonon dispersion for the single-layer p-SiO. (a) The VFF model is fitted to the acoustic branches in the long wave limit along the ΓX direction. The *ab initio* calculations are calculated from SIESTA. (b) The VFF model (blue lines) and the SW potential (red lines) give the same phonon dispersion for the p-SiO along $\Gamma XSYT$.

the VFF model and the SW potential give exactly the same phonon dispersion.

The parameters for the two-body SW potential used by GULP are shown in Tab. CCCLXXV. The parameters for the three-body SW potential used by GULP are shown in Tab. CCCLXXVI. Parameters for the SW potential used by LAMMPS are listed in Tab. CCCLXXVII.

Fig. 193 shows the stress strain relations for the single-layer p-SiO of size $100 \times 100 \text{ \AA}$. The structure is uniaxially stretched in the armchair or zigzag directions at 1 K and 300 K. The structure of p-SiO is so soft along the armchair direction that the Young's modulus is almost zero in the armchair direction. The Young's modulus is 81.3 Nm^{-1} in the zigzag direction at 1 K, which is obtained by linear fitting of the stress strain relations in $[0, 0.01]$.

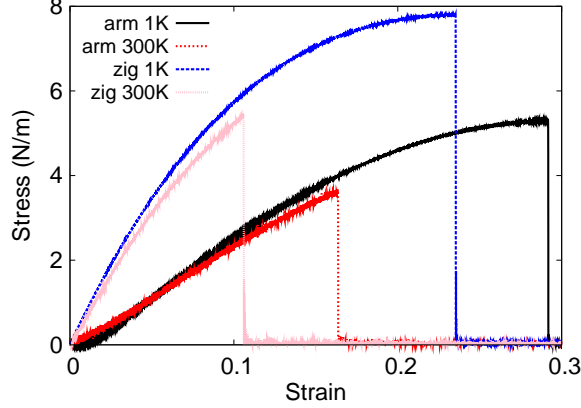


FIG. 193: (Color online) Stress-strain relations for the single-layer p-SiO of size $100 \times 100 \text{ \AA}$. The single-layer p-SiO is uniaxially stretched along the armchair or zigzag directions at temperatures 1 K and 300 K.

TABLE CCCLXXIV: The VFF model for the single-layer p-SiO. The second line gives an explicit expression for each VFF term, where atom indexes are from Fig. 189 (c). The third line is the force constant parameters. Parameters are in the unit of $\frac{eV}{\text{Å}^2}$ for the bond stretching interactions, and in the unit of eV for the angle bending interaction. The fourth line gives the initial bond length (in unit of Å) for the bond stretching interaction and the initial angle (in unit of degrees) for the angle bending interaction. The angle θ_{ijk} has atom i as the apex.

VFF type	bond stretching		angle bending		
expression	$\frac{1}{2}K_{12} (\Delta r_{12})^2$	$\frac{1}{2}K_{14} (\Delta r_{14})^2$	$\frac{1}{2}K_{123} (\Delta \theta_{123})^2$	$\frac{1}{2}K_{134} (\Delta \theta_{134})^2$	$\frac{1}{2}K_{415} (\Delta \theta_{415})^2$
parameter	12.191	12.191	4.817	3.123	3.123
r_0 or θ_0	1.843	1.859	95.989	96.000	132.005

The third-order nonlinear elastic constant D can be obtained by fitting the stress-strain relation to $\sigma = E\epsilon + \frac{1}{2}D\epsilon^2$ with E as the Young's modulus. The value of D is -432.4 Nm^{-1} at 1 K along the zigzag direction. The ultimate stress is about 5.3 Nm^{-1} at the critical strain of 0.29 in the armchair direction at the low temperature of 1 K. The ultimate stress is about 7.8 Nm^{-1} at the critical strain of 0.23 in the zigzag direction at the low temperature of 1 K.

TABLE CCCLXXV: Two-body SW potential parameters for the single-layer p-SiO used by GULP,⁸ as expressed in Eq. (3). The quantity (r_{ij}) in the first line lists one representative term for the two-body SW potential between atoms i and j. Atom indexes are from Fig. 189 (c).

	A (eV)	ρ (Å)	B (Å ⁴)	r_{\min} (Å)	r_{\max} (Å)
r_{12}	19.127	2.720	5.769	0.0	2.962
r_{14}	7.105	1.133	5.972	0.0	2.585

TABLE CCCLXXVI: Three-body SW potential parameters for the single-layer p-SiO used by GULP,⁸ as expressed in Eq. (4). The first line (θ_{ijk}) presents one representative term for the three-body SW potential. The angle θ_{ijk} has the atom i as the apex. Atom indexes are from Fig. 189 (c).

	K (eV)	θ_0 (degree)	ρ_1 (Å)	ρ_2 (Å)	$r_{\min12}$ (Å)	$r_{\max12}$ (Å)	$r_{\min13}$ (Å)	$r_{\max13}$ (Å)	$r_{\min23}$ (Å)	$r_{\max23}$ (Å)
θ_{123}	314.008	95.989	2.720	2.720	0.0	2.962	0.0	2.962	0.0	3.720
θ_{134}	85.406	96.000	1.133	2.720	0.0	2.585	0.0	2.962	0.0	3.875
θ_{415}	152.982	132.005	1.133	2.720	0.0	2.585	0.0	2.962	0.0	4.194

XCV. P-GEO

Present studies on the puckered (p-) GeO are based on first-principles calculations, and no empirical potential has been proposed for the p-GeO. We will thus parametrize the SW potential for the single-layer p-GeO in this section.

The structure of the single-layer p-GeO is shown in Fig. 189, with M=Ge and X=O. Structural parameters for p-GeO are from the *ab initio* calculations.⁷⁸ There are four atoms

TABLE CCCLXXVII: SW potential parameters for p-SiO used by LAMMPS,⁹ as expressed in Eqs. (9) and (10). Atom types in the first column are displayed in Fig. 190, with M=Si and X=O.

	ϵ (eV)	σ (Å)	a	λ	γ	$\cos \theta_0$	A_L	B_L	p	q	tol
Si ₁ -O ₂ -O ₂	1.000	2.720	1.089	314.008	1.000	-0.104	19.127	0.105	4	0	0.0
Si ₁ -O ₁ -O ₁	1.000	1.133	2.282	0.000	1.000	0.000	7.105	3.630	4	0	0.0
Si ₁ -O ₁ -O ₂	1.000	0.000	0.000	85.406	1.000	-0.105	0.000	0.000	4	0	0.0
O ₁ -Si ₁ -Si ₂	1.000	0.000	0.000	152.982	1.000	-0.669	0.000	0.000	4	0	0.0

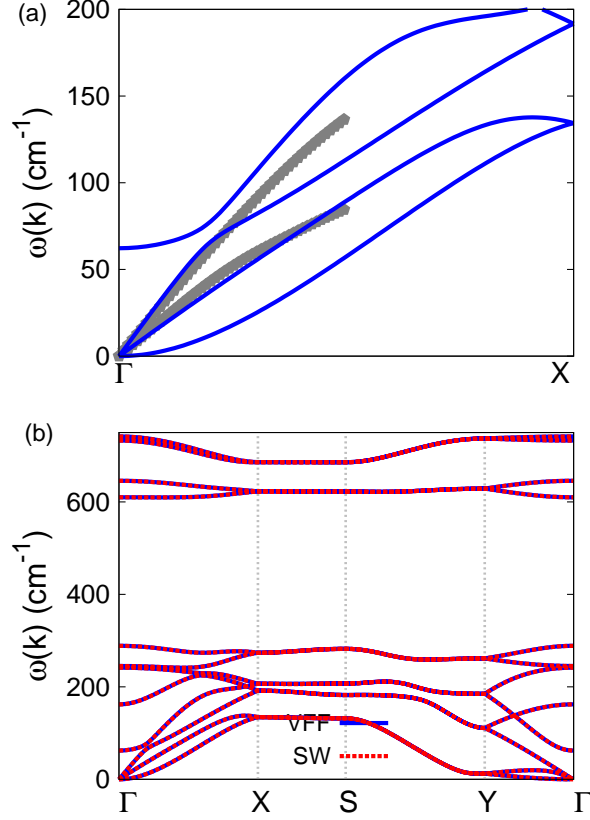


FIG. 194: (Color online) Phonon dispersion for the single-layer p-GeO. (a) The VFF model is fitted to the acoustic branches in the long wave limit along the ΓX direction. The *ab initio* calculations are calculated from SIESTA. (b) The VFF model (blue lines) and the SW potential (red lines) give the same phonon dispersion for the p-GeO along $\Gamma XSYT$.

in the unit cell with relative coordinates as $(-u, 0, -v)$, $(u, 0, v)$, $(0.5 - u, 0.5, v + w)$, and $(0.5 + u, 0.5, -v + w)$ with $u = 0.1622$, $v = 0.0616$ and $w = 0.0884$. The value of these dimensionless parameters are extracted from the geometrical parameters provided in Ref. 78, including lattice constants $a_1 = 4.801 \text{ \AA}$ and $a_2 = 3.055 \text{ \AA}$, bond lengths $d_{12} = 1.956 \text{ \AA}$ and $d_{14} = 1.986 \text{ \AA}$, and the angle $\theta_{145} = 93.3^\circ$. The dimensionless parameters v and w are ratios based on the lattice constant in the out-of-plane z -direction, which is arbitrarily chosen as $a_3 = 10.0 \text{ \AA}$. We note that the main purpose of the usage of u , v , and w in representing atomic coordinates is to follow the same convention for all puckered structures in the present work. The resultant atomic coordinates are the same as that in Ref. 78.

As shown in Fig. 189, a specific feature in the puckered configuration of the p-GeO is that

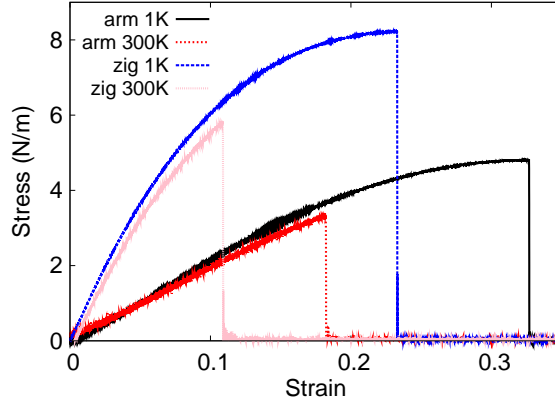


FIG. 195: (Color online) Stress-strain relations for the single-layer p-GeO of size $100 \times 100 \text{ \AA}$. The single-layer p-GeO is uniaxially stretched along the armchair or zigzag directions at temperatures 1 K and 300 K.

TABLE CCCLXXVIII: The VFF model for the single-layer p-GeO. The second line gives an explicit expression for each VFF term, where atom indexes are from Fig. 189 (c). The third line is the force constant parameters. Parameters are in the unit of $\frac{eV}{\text{Å}^2}$ for the bond stretching interactions, and in the unit of eV for the angle bending interaction. The fourth line gives the initial bond length (in unit of Å) for the bond stretching interaction and the initial angle (in unit of degrees) for the angle bending interaction. The angle θ_{ijk} has atom i as the apex.

VFF type	bond stretching		angle bending		
expression	$\frac{1}{2}K_{12}(\Delta r_{12})^2$	$\frac{1}{2}K_{14}(\Delta r_{14})^2$	$\frac{1}{2}K_{123}(\Delta\theta_{123})^2$	$\frac{1}{2}K_{134}(\Delta\theta_{134})^2$	$\frac{1}{2}K_{415}(\Delta\theta_{415})^2$
parameter	12.191	12.191	4.817	3.123	3.123
r_0 or θ_0	1.956	1.986	102.692	93.300	128.213

there is a small difference of wa_3 between the z-coordinate of atom 1 and the z-coordinates of atoms 2 and 3. Similarly, atom 4 is higher than atoms 5 and 6 for wa_3 along the z-direction. The sign of w determines which types of atoms take the out-most positions, e.g., atoms 1, 5, and 6 are the out-most atoms if $w > 0$ in Fig. 189 (c), while atoms 2, 3, and 4 will take the out-most positions for $w < 0$. The p-GeO has a zigzag configuration as shown in Fig. 191, which is a specific case of the puckered structure shown in Fig. 189.

Table CCCLXXVIII shows five VFF terms for the single-layer p-GeO, two of which are the bond stretching interactions shown by Eq. (1) while the other three terms are the angle

TABLE CCCLXXIX: Two-body SW potential parameters for the single-layer p-GeO used by GULP,⁸ as expressed in Eq. (3). The quantity (r_{ij}) in the first line lists one representative term for the two-body SW potential between atoms i and j. Atom indexes are from Fig. 189 (c).

	A (eV)	ρ (\AA)	B (\AA^4)	r_{\min} (\AA)	r_{\max} (\AA)
r_{12}	21.562	2.889	7.319	0.0	3.144
r_{14}	9.258	1.384	7.778	0.0	2.815

TABLE CCCLXXX: Three-body SW potential parameters for the single-layer p-GeO used by GULP,⁸ as expressed in Eq. (4). The first line (θ_{ijk}) presents one representative term for the three-body SW potential. The angle θ_{ijk} has the atom i as the apex. Atom indexes are from Fig. 189 (c).

	K (eV)	θ_0 (degree)	ρ_1 (\AA)	ρ_2 (\AA)	$r_{\min 12}$ (\AA)	$r_{\max 12}$ (\AA)	$r_{\min 13}$ (\AA)	$r_{\max 13}$ (\AA)	$r_{\min 23}$ (\AA)	$r_{\max 23}$ (\AA)
θ_{123}	326.824	102.692	2.889	2.889	0.0	3.144	0.0	3.144	0.0	3.928
θ_{134}	94.550	93.300	1.384	2.889	0.0	2.815	0.0	3.144	0.0	3.933
θ_{415}	152.646	128.213	1.384	2.889	0.0	2.815	0.0	3.144	0.0	4.284

bending interaction shown by Eq. (2). The force constant parameters are the same for the two angle bending terms θ_{134} and θ_{415} , which have the same arm lengths. All force constant parameters are determined by fitting to the acoustic branches in the phonon dispersion along the ΓX as shown in Fig. 194 (a). The *ab initio* calculations for the phonon dispersion are calculated from the SIESTA package.⁷⁹ The generalized gradients approximation is applied to account for the exchange-correlation function with Perdew, Burke, and Ernzerhof

TABLE CCCLXXXI: SW potential parameters for p-GeO used by LAMMPS,⁹ as expressed in Eqs. (9) and (10). Atom types in the first column are displayed in Fig. 190, with M=Ge and X=O.

	ϵ (eV)	σ (\AA)	a	λ	γ	$\cos \theta_0$	A_L	B_L	p	q	tol
Ge ₁ -O ₂ -O ₂	1.000	2.889	1.089	326.824	1.000	-0.220	21.562	0.105	4	0	0.0
Ge ₁ -O ₁ -O ₁	1.000	1.384	2.034	0.000	1.000	0.000	9.258	2.119	4	0	0.0
Ge ₁ -O ₁ -O ₂	1.000	0.000	0.000	94.550	1.000	-0.058	0.000	0.000	4	0	0.0
O ₁ -Ge ₁ -Ge ₂	1.000	0.000	0.000	152.646	1.000	-0.619	0.000	0.000	4	0	0.0

parameterization,⁸⁰ and the double- ζ orbital basis set is adopted. Fig. 194 (b) shows that the VFF model and the SW potential give exactly the same phonon dispersion.

The parameters for the two-body SW potential used by GULP are shown in Tab. CCCLXXIX. The parameters for the three-body SW potential used by GULP are shown in Tab. CCCLXXX. Parameters for the SW potential used by LAMMPS are listed in Tab. CCCLXXXI.

Fig. 195 shows the stress strain relations for the single-layer p-GeO of size $100 \times 100 \text{ \AA}$. The structure is uniaxially stretched in the armchair or zigzag directions at 1 K and 300 K. The structure of p-GeO is so soft along the armchair direction that the Young's modulus is almost zero in the armchair direction. The Young's modulus is 14.5 Nm^{-1} and 78.9 Nm^{-1} in the armchair and zigzag directions at 1 K, which are obtained by linear fitting of the stress strain relations in $[0, 0.01]$. The Poisson's ratios from the VFF model and the SW potential are $\nu_{xy} = 0.09$ and $\nu_{yx} = 0.65$. The third-order nonlinear elastic constant D can be obtained by fitting the stress-strain relation to $\sigma = E\epsilon + \frac{1}{2}D\epsilon^2$ with E as the Young's modulus. The values of D are 22.0 Nm^{-1} and -383.3 Nm^{-1} at 1 K along the armchair and zigzag directions, respectively. The ultimate stress is about 4.8 Nm^{-1} at the critical strain of 0.32 in the armchair direction at the low temperature of 1 K. The ultimate stress is about 8.2 Nm^{-1} at the critical strain of 0.23 in the zigzag direction at the low temperature of 1 K.

XCVI. P-SNO

Present studies on the puckered (p-) SnO are based on first-principles calculations, and no empirical potential has been proposed for the p-SnO. We will thus parametrize the SW potential for the single-layer p-SnO in this section.

The structure of the single-layer p-SnO is shown in Fig. 189, with $M=\text{Sn}$ and $X=\text{O}$. Structural parameters for p-SnO are from the *ab initio* calculations.⁷⁸ There are four atoms in the unit cell with relative coordinates as $(-u, 0, -v)$, $(u, 0, v)$, $(0.5 - u, 0.5, v + w)$, and $(0.5 + u, 0.5, -v + w)$ with $u = 0.1485$, $v = 0.0818$ and $w = 0.0836$. The value of these dimensionless parameters are extracted from the geometrical parameters provided in Ref. 78, including lattice constants $a_1 = 4.764 \text{ \AA}$ and $a_2 = 3.400 \text{ \AA}$, bond lengths $d_{12} = 2.127 \text{ \AA}$ and $d_{14} = 2.163 \text{ \AA}$, and the angle $\theta_{145} = 90.0^\circ$. The dimensionless parameters v and w are ratios based on the lattice constant in the out-of-plane z-direction, which is arbitrarily chosen as

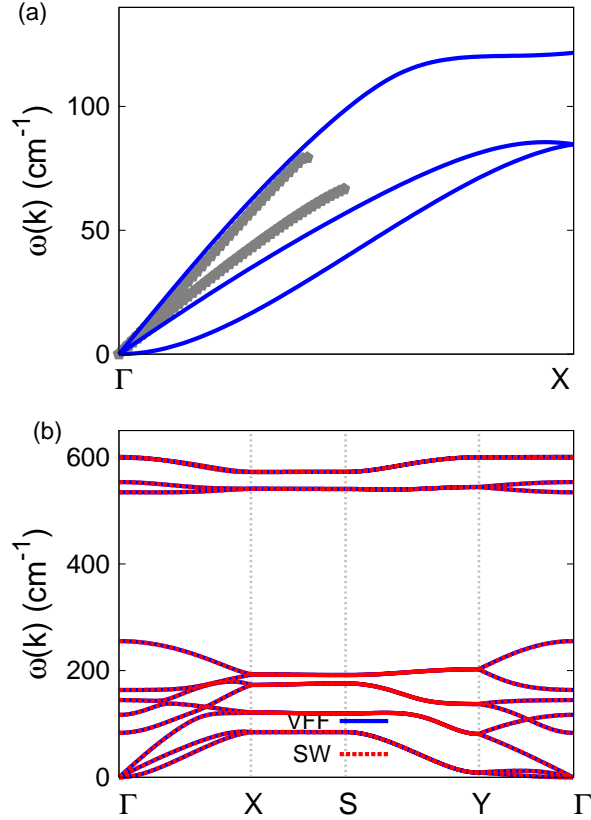


FIG. 196: (Color online) Phonon dispersion for the single-layer p-SnO. (a) The VFF model is fitted to the acoustic branches in the long wave limit along the ΓX direction. The *ab initio* calculations are calculated from SIESTA. (b) The VFF model (blue lines) and the SW potential (red lines) give the same phonon dispersion for the p-SnO along $\Gamma XSYT$.

$a_3 = 10.0 \text{ \AA}$. We note that the main purpose of the usage of u , v , and w in representing atomic coordinates is to follow the same convention for all puckered structures in the present work. The resultant atomic coordinates are the same as that in Ref. 78.

As shown in Fig. 189, a specific feature in the puckered configuration of the p-SnO is that there is a small difference of wa_3 between the z-coordinate of atom 1 and the z-coordinates of atoms 2 and 3. Similarly, atom 4 is higher than atoms 5 and 6 for wa_3 along the z-direction. The sign of w determines which types of atoms take the out-most positions, e.g., atoms 1, 5, and 6 are the out-most atoms if $w > 0$ in Fig. 189 (c), while atoms 2, 3, and 4 will take the out-most positions for $w < 0$. The p-SnO has a zigzag configuration as shown in Fig. 191, which is a specific case of the puckered structure shown in Fig. 189.

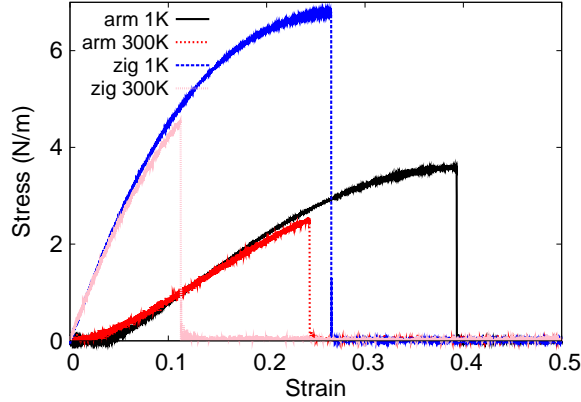


FIG. 197: (Color online) Stress-strain relations for the single-layer p-SnO of size $100 \times 100 \text{ \AA}$. The single-layer p-SnO is uniaxially stretched along the armchair or zigzag directions at temperatures 1 K and 300 K.

TABLE CCCLXXXII: The VFF model for the single-layer p-SnO. The second line gives an explicit expression for each VFF term, where atom indexes are from Fig. 189 (c). The third line is the force constant parameters. Parameters are in the unit of $\frac{eV}{\text{Å}^2}$ for the bond stretching interactions, and in the unit of eV for the angle bending interaction. The fourth line gives the initial bond length (in unit of Å) for the bond stretching interaction and the initial angle (in unit of degrees) for the angle bending interaction. The angle θ_{ijk} has atom i as the apex.

VFF type	bond stretching		angle bending		
expression	$\frac{1}{2}K_{12}(\Delta r_{12})^2$	$\frac{1}{2}K_{14}(\Delta r_{14})^2$	$\frac{1}{2}K_{123}(\Delta\theta_{123})^2$	$\frac{1}{2}K_{134}(\Delta\theta_{134})^2$	$\frac{1}{2}K_{415}(\Delta\theta_{415})^2$
parameter	9.208	9.208	2.835	3.023	3.023
r_0 or θ_0	2.127	2.163	106.117	90.000	126.496

Table CCCLXXXII shows five VFF terms for the single-layer p-SnO, two of which are the bond stretching interactions shown by Eq. (1) while the other three terms are the angle bending interaction shown by Eq. (2). The force constant parameters are the same for the two angle bending terms θ_{134} and θ_{415} , which have the same arm lengths. All force constant parameters are determined by fitting to the acoustic branches in the phonon dispersion along the ΓX as shown in Fig. 196 (a). The *ab initio* calculations for the phonon dispersion are calculated from the SIESTA package.⁷⁹ The generalized gradients approximation is applied to account for the exchange-correlation function with Perdew, Burke, and Ernzerhof

TABLE CCCLXXXIII: Two-body SW potential parameters for the single-layer p-SnO used by GULP,⁸ as expressed in Eq. (3). The quantity (r_{ij}) in the first line lists one representative term for the two-body SW potential between atoms i and j. Atom indexes are from Fig. 189 (c).

	A (eV)	ρ (\AA)	B (\AA^4)	r_{\min} (\AA)	r_{\max} (\AA)
r_{12}	11.711	2.107	10.234	0.0	3.185
r_{14}	8.879	1.612	10.945	0.0	3.096

TABLE CCCLXXXIV: Three-body SW potential parameters for the single-layer p-SnO used by GULP,⁸ as expressed in Eq. (4). The first line (θ_{ijk}) presents one representative term for the three-body SW potential. The angle θ_{ijk} has the atom i as the apex. Atom indexes are from Fig. 189 (c).

	K (eV)	θ_0 (degree)	ρ_1 (\AA)	ρ_2 (\AA)	$r_{\min12}$ (\AA)	$r_{\max12}$ (\AA)	$r_{\min13}$ (\AA)	$r_{\max13}$ (\AA)	$r_{\min23}$ (\AA)	$r_{\max23}$ (\AA)
θ_{123}	82.293	106.117	2.107	2.107	0.0	3.185	0.0	3.185	0.0	4.082
θ_{134}	62.178	90.000	1.612	2.107	0.0	3.096	0.0	3.185	0.0	4.017
θ_{415}	96.214	126.496	1.612	2.107	0.0	3.096	0.0	3.185	0.0	4.426

parameterization,⁸⁰ and the double- ζ orbital basis set is adopted. Fig. 196 (b) shows that the VFF model and the SW potential give exactly the same phonon dispersion.

The parameters for the two-body SW potential used by GULP are shown in Tab. CCCLXXXIII. The parameters for the three-body SW potential used by GULP are shown in Tab. CCCLXXXIV. Parameters for the SW potential used by LAMMPS are listed in Tab. CCCLXXXV.

TABLE CCCLXXXV: SW potential parameters for p-SnO used by LAMMPS,⁹ as expressed in Eqs. (9) and (10). Atom types in the first column are displayed in Fig. 190, with M=Sn and X=O.

	ϵ (eV)	σ (\AA)	a	λ	γ	$\cos \theta_0$	A_L	B_L	p	q	tol
Sn ₁ -O ₂ -O ₂	1.000	2.107	1.512	82.293	1.000	-0.278	11.711	0.519	4	0	0.0
Sn ₁ -O ₁ -O ₁	1.000	1.612	1.921	0.000	1.000	0.000	8.879	1.623	4	0	0.0
Sn ₁ -O ₁ -O ₂	1.000	0.000	0.000	62.178	1.000	0.000	0.000	0.000	4	0	0.0
O ₁ -Sn ₁ -Sn ₂	1.000	0.000	0.000	96.214	1.000	-0.595	0.000	0.000	4	0	0.0

TABLE CCCLXXXVI: The VFF model for the single-layer p-CS. The second line gives an explicit expression for each VFF term, where atom indexes are from Fig. 189 (c). The third line is the force constant parameters. Parameters are in the unit of $\frac{\text{eV}}{\text{\AA}^2}$ for the bond stretching interactions, and in the unit of eV for the angle bending interaction. The fourth line gives the initial bond length (in unit of \AA) for the bond stretching interaction and the initial angle (in unit of degrees) for the angle bending interaction. The angle θ_{ijk} has atom i as the apex.

VFF type	bond stretching		angle bending		
expression	$\frac{1}{2}K_{12}(\Delta r_{12})^2$	$\frac{1}{2}K_{14}(\Delta r_{14})^2$	$\frac{1}{2}K_{123}(\Delta\theta_{123})^2$	$\frac{1}{2}K_{134}(\Delta\theta_{134})^2$	$\frac{1}{2}K_{415}(\Delta\theta_{415})^2$
parameter	9.291	9.291	3.933	3.075	3.075
r_0 or θ_0	1.757	1.849	105.384	118.100	104.288

Fig. 197 shows the stress strain relations for the single-layer p-SnO of size $100 \times 100 \text{\AA}$. The structure is uniaxially stretched in the armchair or zigzag directions at 1 K and 300 K. The structure of p-SnO is so soft along the armchair direction that the Young's modulus is almost zero in the armchair direction. The Young's modulus is 52.8 Nm^{-1} in the zigzag direction at 1 K, which is obtained by linear fitting of the stress strain relations in $[0, 0.01]$. The third-order nonlinear elastic constant D can be obtained by fitting the stress-strain relation to $\sigma = E\epsilon + \frac{1}{2}D\epsilon^2$ with E as the Young's modulus. The value of D is -204.5 Nm^{-1} at 1 K along the zigzag direction. The ultimate stress is about 3.8 Nm^{-1} at the critical strain of 0.38 in the armchair direction at the low temperature of 1 K. The ultimate stress is about 6.8 Nm^{-1} at the critical strain of 0.26 in the zigzag direction at the low temperature of 1 K.

XCVII. P-CS

Present studies on the puckered (p-) CS are based on first-principles calculations, and no empirical potential has been proposed for the p-CS. We will thus parametrize the SW potential for the single-layer p-CS in this section.

The structure of the single-layer p-CS is shown in Fig. 189, with $M=C$ and $X=S$. Structural parameters for p-CS are from the *ab initio* calculations.⁷⁸ There are four atoms in the unit cell with relative coordinates as $(-u, 0, -v)$, $(u, 0, v)$, $(0.5 - u, 0.5, v + w)$, and

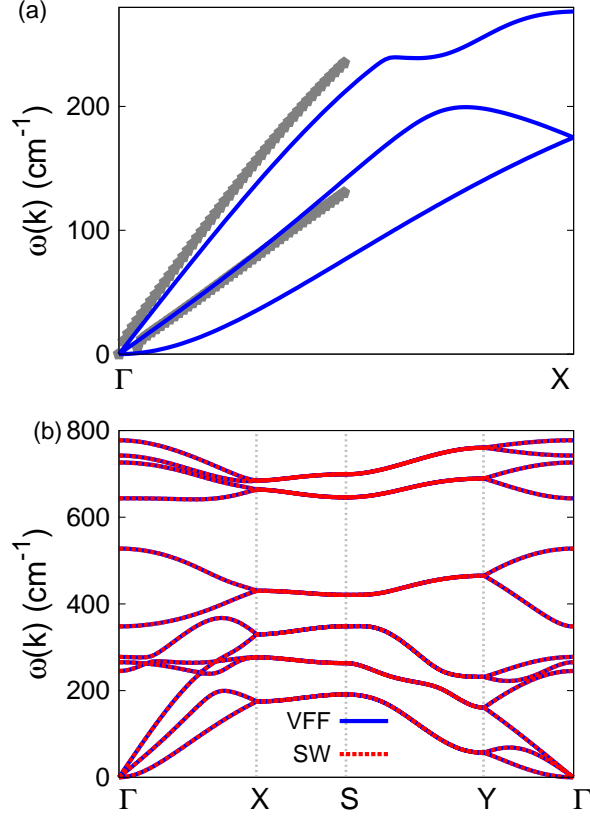


FIG. 198: (Color online) Phonon dispersion for the single-layer p-CS. (a) The VFF model is fitted to the acoustic branches in the long wave limit along the ΓX direction. The *ab initio* calculations are calculated from SIESTA. (b) The VFF model (blue lines) and the SW potential (red lines) give the same phonon dispersion for the p-CS along $\Gamma XSYT$.

$(0.5 + u, 0.5, -v + w)$ with $u = 0.1302$, $v = 0.0733$ and $w = -0.0248$. The value of these dimensionless parameters are extracted from the geometrical parameters provided in Ref. 78, including lattice constants $a_1 = 4.323 \text{ \AA}$ and $a_2 = 2.795 \text{ \AA}$, bond lengths $d_{12} = 1.757 \text{ \AA}$ and $d_{14} = 1.849 \text{ \AA}$, and the angle $\theta_{145} = 118.1^\circ$. The dimensionless parameters v and w are ratios based on the lattice constant in the out-of-plane z -direction, which is arbitrarily chosen as $a_3 = 10.0 \text{ \AA}$. We note that the main purpose of the usage of u , v , and w in representing atomic coordinates is to follow the same convention for all puckered structures in the present work. The resultant atomic coordinates are the same as that in Ref. 78.

As shown in Fig. 189, a specific feature in the puckered configuration of the p-CS is that there is a small difference of wa_3 between the z -coordinate of atom 1 and the z -coordinates of

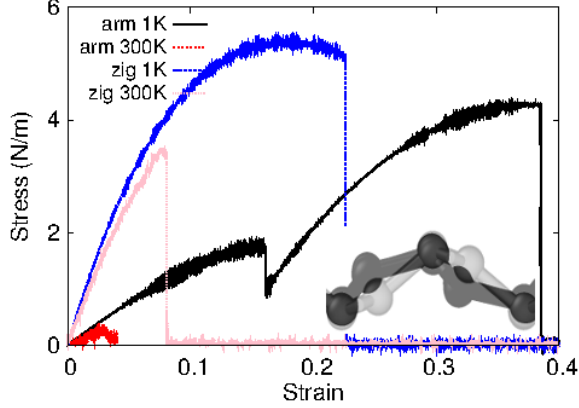


FIG. 199: (Color online) Stress-strain relations for the single-layer p-CS of size $100 \times 100 \text{ \AA}$. The single-layer p-CS is uniaxially stretched along the armchair or zigzag directions at temperatures 1 K and 300 K. Inset shows the structure before (light) and after (dark) the structural transition around 0.16.

TABLE CCCLXXXVII: Two-body SW potential parameters for the single-layer p-CS used by GULP,⁸ as expressed in Eq. (3). The quantity (r_{ij}) in the first line lists one representative term for the two-body SW potential between atoms i and j . Atom indexes are from Fig. 189 (c).

	A (eV)	ρ (\AA)	B (\AA^4)	r_{\min} (\AA)	r_{\max} (\AA)
r_{12}	8.898	1.894	4.765	0.0	2.669
r_{14}	5.791	1.220	5.844	0.0	2.600

atoms 2 and 3. Similarly, atom 4 is higher than atoms 5 and 6 for wa_3 along the z-direction. The sign of w determines which types of atoms take the out-most positions, e.g., atoms 1, 5, and 6 are the out-most atoms if $w > 0$ in Fig. 189 (c), while atoms 2, 3, and 4 will take the out-most positions for $w < 0$.

Table CCCLXXXVI shows five VFF terms for the single-layer p-CS, two of which are the bond stretching interactions shown by Eq. (1) while the other three terms are the angle bending interaction shown by Eq. (2). The force constant parameters are the same for the two angle bending terms θ_{134} and θ_{415} , which have the same arm lengths. All force constant parameters are determined by fitting to the acoustic branches in the phonon dispersion along the ΓX as shown in Fig. 198 (a). The *ab initio* calculations for the phonon dispersion are calculated from the SIESTA package.⁷⁹ The generalized gradients approximation is ap-

TABLE CCCLXXXVIII: Three-body SW potential parameters for the single-layer p-CS used by GULP,⁸ as expressed in Eq. (4). The first line (θ_{ijk}) presents one representative term for the three-body SW potential. The angle θ_{ijk} has the atom i as the apex. Atom indexes are from Fig. 189 (c).

	K (eV)	θ_0 (degree)	ρ_1 (Å)	ρ_2 (Å)	$r_{\min 12}$ (Å)	$r_{\max 12}$ (Å)	$r_{\min 13}$ (Å)	$r_{\max 13}$ (Å)	$r_{\min 23}$ (Å)	$r_{\max 23}$ (Å)
θ_{123}	134.527	105.384	1.894	1.894	0.0	2.669	0.0	2.669	0.0	3.559
θ_{134}	79.992	118.100	1.220	1.894	0.0	2.600	0.0	2.669	0.0	4.046
θ_{415}	66.283	104.288	1.220	1.894	0.0	2.600	0.0	2.669	0.0	3.921

TABLE CCCLXXXIX: SW potential parameters for p-CS used by LAMMPS,⁹ as expressed in Eqs. (9) and (10). Atom types in the first column are displayed in Fig. 190, with M=C and X=S.

	ϵ (eV)	σ (Å)	a	λ	γ	$\cos \theta_0$	A_L	B_L	p	q	tol
C ₁ -S ₂ -S ₂	1.000	1.894	1.410	134.527	1.000	-0.265	8.898	0.371	4	0	0.0
C ₁ -S ₁ -S ₁	1.000	1.220	2.131	0.000	1.000	0.000	5.791	2.637	4	0	0.0
C ₁ -S ₁ -S ₂	1.000	0.000	0.000	79.992	1.000	-0.471	0.000	0.000	4	0	0.0
S ₁ -C ₁ -C ₂	1.000	0.000	0.000	66.283	1.000	-0.247	0.000	0.000	4	0	0.0

plied to account for the exchange-correlation function with Perdew, Burke, and Ernzerhof parameterization,⁸⁰ and the double- ζ orbital basis set is adopted. Fig. 198 (b) shows that the VFF model and the SW potential give exactly the same phonon dispersion.

The parameters for the two-body SW potential used by GULP are shown in Tab. CCCLXXXVII. The parameters for the three-body SW potential used by GULP are shown in Tab. CCCLXXXVIII. Parameters for the SW potential used by LAMMPS are listed in Tab. CCCLXXXIX.

Fig. 199 shows the stress strain relations for the single-layer p-CS of size 100×100 Å. The structure is uniaxially stretched in the armchair or zigzag directions at 1 K and 300 K. There is a structural transition around 0.16 at 1 K, where the C atom is twisted. The Young's modulus is 16.2 Nm^{-1} and 70.5 Nm^{-1} in the armchair and zigzag directions respectively at 1 K, which are obtained by linear fitting of the stress strain relations in $[0, 0.01]$. The Poisson's ratios from the VFF model and the SW potential are $\nu_{xy} = -0.06$ and $\nu_{yx} = -0.27$. The third-order nonlinear elastic constant D can be obtained by fitting the stress-strain

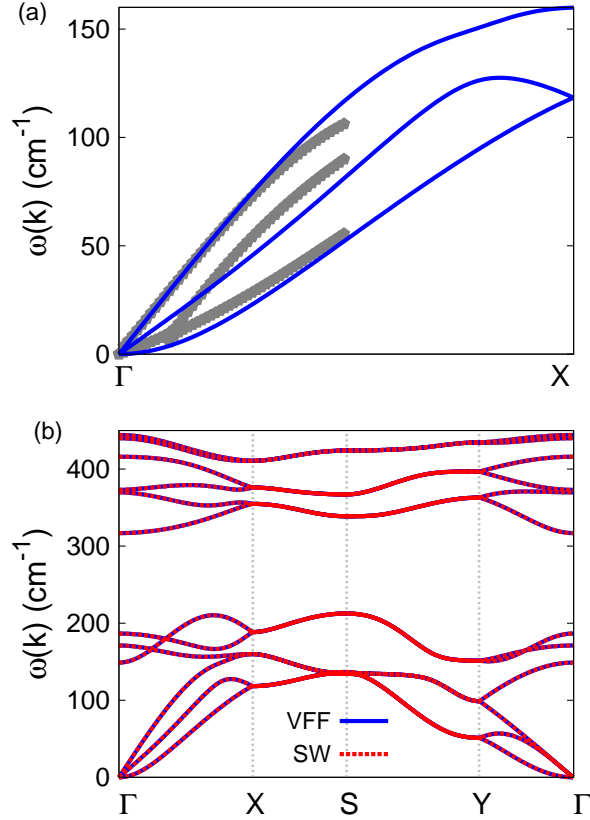


FIG. 200: (Color online) Phonon dispersion for the single-layer p-SiS. (a) The VFF model is fitted to the acoustic branches in the long wave limit along the ΓX direction. The *ab initio* calculations are calculated from SIESTA. (b) The VFF model (blue lines) and the SW potential (red lines) give the same phonon dispersion for the p-SiS along $\Gamma XSYT$.

relation to $\sigma = E\epsilon + \frac{1}{2}D\epsilon^2$ with E as the Young's modulus. The values of D are -27.3 Nm^{-1} and -447.2 Nm^{-1} at 1 K along the armchair and zigzag directions, respectively. The ultimate stress is about 4.3 Nm^{-1} at the critical strain of 0.38 in the armchair direction at the low temperature of 1 K. The ultimate stress is about 5.2 Nm^{-1} at the critical strain of 0.22 in the zigzag direction at the low temperature of 1 K.

XCVIII. P-SIS

Present studies on the puckered (p-) SiS are based on first-principles calculations, and no empirical potential has been proposed for the p-SiS. We will thus parametrize the SW

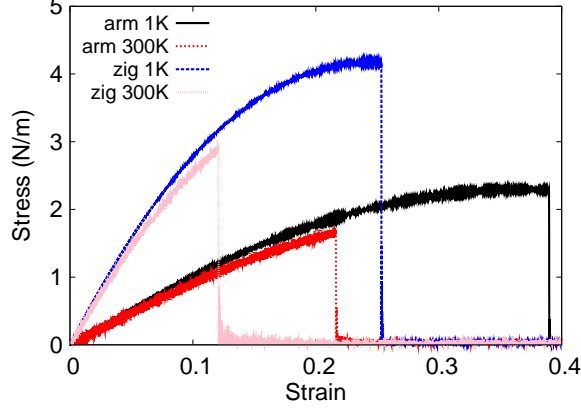


FIG. 201: (Color online) Stress-strain relations for the single-layer p-SiS of size $100 \times 100 \text{ \AA}$. The single-layer p-SiS is uniaxially stretched along the armchair or zigzag directions at temperatures 1 K and 300 K.

TABLE CCCXC: The VFF model for the single-layer p-SiS. The second line gives an explicit expression for each VFF term, where atom indexes are from Fig. 189 (c). The third line is the force constant parameters. Parameters are in the unit of $\frac{eV}{\text{Å}^2}$ for the bond stretching interactions, and in the unit of eV for the angle bending interaction. The fourth line gives the initial bond length (in unit of Å) for the bond stretching interaction and the initial angle (in unit of degrees) for the angle bending interaction. The angle θ_{ijk} has atom i as the apex.

VFF type	bond stretching		angle bending		
expression	$\frac{1}{2}K_{12}(\Delta r_{12})^2$	$\frac{1}{2}K_{14}(\Delta r_{14})^2$	$\frac{1}{2}K_{123}(\Delta\theta_{123})^2$	$\frac{1}{2}K_{134}(\Delta\theta_{134})^2$	$\frac{1}{2}K_{415}(\Delta\theta_{415})^2$
parameter	7.135	7.135	2.512	2.922	2.922
r_0 or θ_0	2.300	2.344	93.554	96.500	111.710

potential for the single-layer p-SiS in this section.

The structure of the single-layer p-SiS is shown in Fig. 189, with $M=\text{Si}$ and $X=\text{S}$. Structural parameters for p-SiS are from the *ab initio* calculations.⁷⁸ There are four atoms in the unit cell with relative coordinates as $(-u, 0, -v)$, $(u, 0, v)$, $(0.5 - u, 0.5, v + w)$, and $(0.5 + u, 0.5, -v + w)$ with $u = 0.0884$, $v = 0.1093$ and $w = 0.0316$. The value of these dimensionless parameters are extracted from the geometrical parameters provided in Ref. 78, including lattice constants $a_1 = 4.774 \text{ \AA}$ and $a_2 = 3.352 \text{ \AA}$, bond lengths $d_{12} = 2.300 \text{ \AA}$ and $d_{14} = 2.344 \text{ \AA}$, and the angle $\theta_{145} = 96.5^\circ$. The dimensionless parameters v and w are ratios

TABLE CCCXCI: Two-body SW potential parameters for the single-layer p-SiS used by GULP,⁸ as expressed in Eq. (3). The quantity (r_{ij}) in the first line lists one representative term for the two-body SW potential between atoms i and j . Atom indexes are from Fig. 189 (c).

	A (eV)	ρ (Å)	B (Å ⁴)	r_{\min} (Å)	r_{\max} (Å)
r_{12}	3.878	0.797	13.992	0.0	2.977
r_{14}	6.051	1.301	15.094	0.0	3.217

TABLE CCCXCII: Three-body SW potential parameters for the single-layer p-SiS used by GULP,⁸ as expressed in Eq. (4). The first line (θ_{ijk}) presents one representative term for the three-body SW potential. The angle θ_{ijk} has the atom i as the apex. Atom indexes are from Fig. 189 (c).

	K (eV)	θ_0 (degree)	ρ_1 (Å)	ρ_2 (Å)	$r_{\min12}$ (Å)	$r_{\max12}$ (Å)	$r_{\min13}$ (Å)	$r_{\max13}$ (Å)	$r_{\min23}$ (Å)	$r_{\max23}$ (Å)
θ_{123}	13.284	93.554	0.797	0.797	0.0	2.977	0.0	2.977	0.0	4.063
θ_{134}	21.310	96.500	1.301	0.797	0.0	3.217	0.0	2.977	0.0	4.232
θ_{415}	24.372	111.710	1.301	0.797	0.0	3.217	0.0	2.977	0.0	4.423

based on the lattice constant in the out-of-plane z -direction, which is arbitrarily chosen as $a_3 = 10.0$ Å. We note that the main purpose of the usage of u , v , and w in representing atomic coordinates is to follow the same convention for all puckered structures in the present work. The resultant atomic coordinates are the same as that in Ref. 78.

As shown in Fig. 189, a specific feature in the puckered configuration of the p-SiS is that there is a small difference of wa_3 between the z -coordinate of atom 1 and the z -coordinates of atoms 2 and 3. Similarly, atom 4 is higher than atoms 5 and 6 for wa_3 along the z -direction.

TABLE CCCXCIII: SW potential parameters for p-SiS used by LAMMPS,⁹ as expressed in Eqs. (9) and (10). Atom types in the first column are displayed in Fig. 190, with M=Si and X=S.

	ϵ (eV)	σ (Å)	a	λ	γ	$\cos \theta_0$	A_L	B_L	p	q	tol
Si ₁ -S ₂ -S ₂	1.000	0.797	3.735	13.284	1.000	-0.062	3.878	34.661	4	0	0.0
Si ₁ -S ₁ -S ₁	1.000	1.301	2.474	0.000	1.000	0.000	6.051	5.276	4	0	0.0
Si ₁ -S ₁ -S ₂	1.000	0.000	0.000	21.310	1.000	-0.113	0.000	0.000	4	0	0.0
S ₁ -Si ₁ -Si ₂	1.000	0.000	0.000	24.372	1.000	-0.370	0.000	0.000	4	0	0.0

The sign of w determines which types of atoms take the out-most positions, e.g., atoms 1, 5, and 6 are the out-most atoms if $w > 0$ in Fig. 189 (c), while atoms 2, 3, and 4 will take the out-most positions for $w < 0$.

Table CCCXC shows five VFF terms for the single-layer p-SiS, two of which are the bond stretching interactions shown by Eq. (1) while the other three terms are the angle bending interaction shown by Eq. (2). The force constant parameters are the same for the two angle bending terms θ_{134} and θ_{415} , which have the same arm lengths. All force constant parameters are determined by fitting to the acoustic branches in the phonon dispersion along the ΓX as shown in Fig. 200 (a). The *ab initio* calculations for the phonon dispersion are calculated from the SIESTA package.⁷⁹ The generalized gradients approximation is applied to account for the exchange-correlation function with Perdew, Burke, and Ernzerhof parameterization,⁸⁰ and the double- ζ orbital basis set is adopted. Fig. 200 (b) shows that the VFF model and the SW potential give exactly the same phonon dispersion.

The parameters for the two-body SW potential used by GULP are shown in Tab. CCCXCI. The parameters for the three-body SW potential used by GULP are shown in Tab. CCCXCII. Parameters for the SW potential used by LAMMPS are listed in Tab. CCCXCIII.

Fig. 201 shows the stress strain relations for the single-layer p-SiS of size $100 \times 100 \text{ \AA}$. The structure is uniaxially stretched in the armchair or zigzag directions at 1 K and 300 K. The Young's modulus is 10.9 Nm^{-1} and 34.8 Nm^{-1} in the armchair and zigzag directions respectively at 1 K, which are obtained by linear fitting of the stress strain relations in $[0, 0.01]$. The Poisson's ratios from the VFF model and the SW potential are $\nu_{xy} = 0.04$ and $\nu_{yx} = 0.12$. The third-order nonlinear elastic constant D can be obtained by fitting the stress-strain relation to $\sigma = E\epsilon + \frac{1}{2}D\epsilon^2$ with E as the Young's modulus. The values of D are -24.1 Nm^{-1} and -145.2 Nm^{-1} at 1 K along the armchair and zigzag directions, respectively. The ultimate stress is about 2.3 Nm^{-1} at the critical strain of 0.39 in the armchair direction at the low temperature of 1 K. The ultimate stress is about 4.2 Nm^{-1} at the critical strain of 0.25 in the zigzag direction at the low temperature of 1 K.

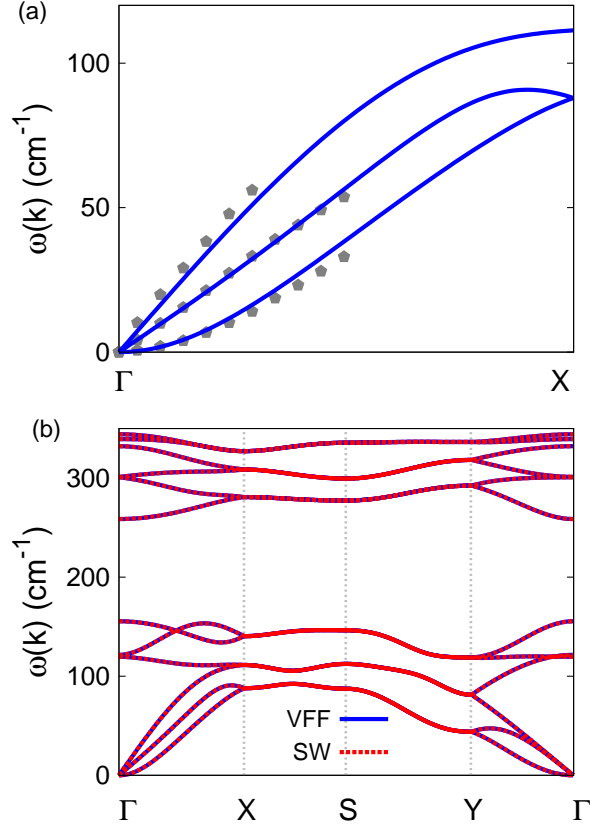


FIG. 202: (Color online) Phonon dispersion for the single-layer p-GeS. (a) The VFF model is fitted to the acoustic branches in the long wave limit along the Γ X direction. The *ab initio* calculations are from Ref. 81. (b) The VFF model (blue lines) and the SW potential (red lines) give the same phonon dispersion for the p-GeS along Γ XSY Γ .

XCIX. P-GeS

Present studies on the puckered (p-) GeS are based on first-principles calculations, and no empirical potential has been proposed for the p-GeS. We will thus parametrize the SW potential for the single-layer p-GeS in this section.

The structure of the single-layer p-GeS is shown in Fig. 189, with $M=\text{Ge}$ and $X=\text{S}$. Structural parameters for p-GeS are from the *ab initio* calculations.⁷⁸ There are four atoms in the unit cell with relative coordinates as $(-u, 0, -v)$, $(u, 0, v)$, $(0.5 - u, 0.5, v + w)$, and $(0.5 + u, 0.5, -v + w)$ with $u = 0.0673$, $v = 0.1173$ and $w = 0.0228$. The value of these dimensionless parameters are extracted from the geometrical parameters provided in Ref. 78,

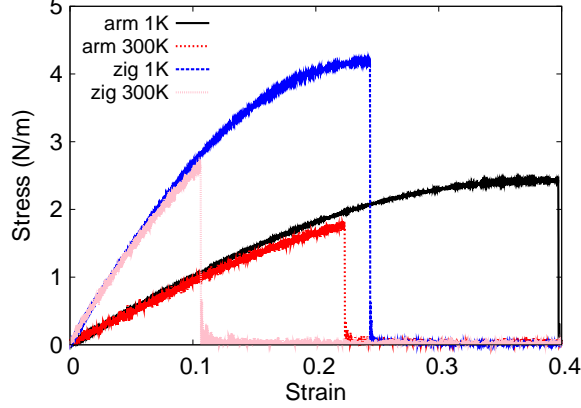


FIG. 203: (Color online) Stress-strain relations for the single-layer p-GeS of size $100 \times 100 \text{ \AA}$. The single-layer p-GeS is uniaxially stretched along the armchair or zigzag directions at temperatures 1 K and 300 K.

TABLE CCCXCIV: The VFF model for the single-layer p-GeS. The second line gives an explicit expression for each VFF term, where atom indexes are from Fig. 189 (c). The third line is the force constant parameters. Parameters are in the unit of $\frac{eV}{\text{Å}^2}$ for the bond stretching interactions, and in the unit of eV for the angle bending interaction. The fourth line gives the initial bond length (in unit of Å) for the bond stretching interaction and the initial angle (in unit of degrees) for the angle bending interaction. The angle θ_{ijk} has atom i as the apex.

VFF type	bond stretching		angle bending		
expression	$\frac{1}{2}K_{12}(\Delta r_{12})^2$	$\frac{1}{2}K_{14}(\Delta r_{14})^2$	$\frac{1}{2}K_{123}(\Delta\theta_{123})^2$	$\frac{1}{2}K_{134}(\Delta\theta_{134})^2$	$\frac{1}{2}K_{415}(\Delta\theta_{415})^2$
parameter	6.364	6.364	2.153	3.896	3.896
r_0 or θ_0	2.462	2.423	95.402	94.400	104.837

including lattice constants $a_1 = 4.492 \text{ \AA}$ and $a_2 = 3.642 \text{ \AA}$, bond lengths $d_{12} = 2.462 \text{ \AA}$ and $d_{14} = 2.423 \text{ \AA}$, and the angle $\theta_{145} = 94.4^\circ$. The dimensionless parameters v and w are ratios based on the lattice constant in the out-of-plane z -direction, which is arbitrarily chosen as $a_3 = 10.0 \text{ \AA}$. We note that the main purpose of the usage of u , v , and w in representing atomic coordinates is to follow the same convention for all puckered structures in the present work. The resultant atomic coordinates are the same as that in Ref. 78.

As shown in Fig. 189, a specific feature in the puckered configuration of the p-GeS is that there is a small difference of wa_3 between the z -coordinate of atom 1 and the z -coordinates of

TABLE CCCXCV: Two-body SW potential parameters for the single-layer p-GeS used by GULP,⁸ as expressed in Eq. (3). The quantity (r_{ij}) in the first line lists one representative term for the two-body SW potential between atoms i and j. Atom indexes are from Fig. 189 (c).

	A (eV)	ρ (Å)	B (Å ⁴)	r_{\min} (Å)	r_{\max} (Å)
r_{12}	2.096	0.351	18.371	0.0	2.926
r_{14}	6.694	1.571	17.234	0.0	3.398

TABLE CCCXCVI: Three-body SW potential parameters for the single-layer p-GeS used by GULP,⁸ as expressed in Eq. (4). The first line (θ_{ijk}) presents one representative term for the three-body SW potential. The angle θ_{ijk} has the atom i as the apex. Atom indexes are from Fig. 189 (c).

	K (eV)	θ_0 (degree)	ρ_1 (Å)	ρ_2 (Å)	$r_{\min12}$ (Å)	$r_{\max12}$ (Å)	$r_{\min13}$ (Å)	$r_{\max13}$ (Å)	$r_{\min23}$ (Å)	$r_{\max23}$ (Å)
θ_{123}	4.905	95.402	0.350	0.350	0.0	2.926	0.0	2.926	0.0	4.067
θ_{134}	20.842	94.400	1.571	0.350	0.0	3.398	0.0	2.926	0.0	4.292
θ_{415}	22.173	104.837	1.571	0.350	0.0	3.398	0.0	2.296	0.0	4.438

atoms 2 and 3. Similarly, atom 4 is higher than atoms 5 and 6 for wa_3 along the z-direction. The sign of w determines which types of atoms take the out-most positions, e.g., atoms 1, 5, and 6 are the out-most atoms if $w > 0$ in Fig. 189 (c), while atoms 2, 3, and 4 will take the out-most positions for $w < 0$.

Table CCCXCIV shows five VFF terms for the single-layer p-GeS, two of which are the bond stretching interactions shown by Eq. (1) while the other three terms are the angle

TABLE CCCXCVII: SW potential parameters for p-GeS used by LAMMPS,⁹ as expressed in Eqs. (9) and (10). Atom types in the first column are displayed in Fig. 190, with M=Ge and X=S.

	ϵ (eV)	σ (Å)	a	λ	γ	$\cos \theta_0$	A_L	B_L	p	q	tol
Ge ₁ -S ₄ -S ₄	1.000	0.351	8.332	4.905	1.000	-0.094	2.096	1227.130	4	0	0.0
Ge ₁ -S ₁ -S ₁	1.000	1.571	2.163	0.000	1.000	0.000	6.694	2.830	4	0	0.0
Ge ₁ -S ₁ -S ₄	1.000	0.000	0.000	20.842	1.000	-0.077	0.000	0.000	4	0	0.0
S ₁ -Ge ₁ -Ge ₂	1.000	0.000	0.000	22.173	1.000	-0.256	0.000	0.000	4	0	0.0

bending interaction shown by Eq. (2). The force constant parameters are the same for the two angle bending terms θ_{134} and θ_{415} , which have the same arm lengths. All force constant parameters are determined by fitting to the acoustic branches in the phonon dispersion along the ΓX as shown in Fig. 202 (a). The *ab initio* calculations are from Ref. 81. Fig. 202 (b) shows that the VFF model and the SW potential give exactly the same phonon dispersion.

The parameters for the two-body SW potential used by GULP are shown in Tab. CCCXCV. The parameters for the three-body SW potential used by GULP are shown in Tab. CCCXCVI. Parameters for the SW potential used by LAMMPS are listed in Tab. CCCXCVII. Eight atom types have been introduced for writing the SW potential script used by LAMMPS as shown in Fig. 190 with M=Ge and X=S, which helps to increase the cutoff for the bond stretching interaction between atom 1 and atom 2 in Fig. 189 (c).

Fig. 203 shows the stress strain relations for the single-layer p-GeS of size $100 \times 100 \text{ \AA}$. The structure is uniaxially stretched in the armchair or zigzag directions at 1 K and 300 K. The Young's modulus is 10.6 Nm^{-1} and 32.1 Nm^{-1} in the armchair and zigzag directions respectively at 1 K, which are obtained by linear fitting of the stress strain relations in $[0, 0.01]$. The Poisson's ratios from the VFF model and the SW potential are $\nu_{xy} = 0.10$ and $\nu_{yx} = 0.29$. The third-order nonlinear elastic constant D can be obtained by fitting the stress-strain relation to $\sigma = E\epsilon + \frac{1}{2}D\epsilon^2$ with E as the Young's modulus. The values of D are -20.4 Nm^{-1} and -118.8 Nm^{-1} at 1 K along the armchair and zigzag directions, respectively. The ultimate stress is about 2.4 Nm^{-1} at the critical strain of 0.39 in the armchair direction at the low temperature of 1 K. The ultimate stress is about 4.2 Nm^{-1} at the critical strain of 0.24 in the zigzag direction at the low temperature of 1 K.

C. P-SNS

Present studies on the puckered (p-) SnS are based on first-principles calculations, and no empirical potential has been proposed for the p-SnS. We will thus parametrize the SW potential for the single-layer p-SnS in this section.

The structure of the single-layer p-SnS is shown in Fig. 189, with M=Sn and X=S. Structural parameters for p-SnS are from the *ab initio* calculations.⁷⁸ There are four atoms in the unit cell with relative coordinates as $(-u, 0, -v)$, $(u, 0, v)$, $(0.5 - u, 0.5, v + w)$, and $(0.5 + u, 0.5, -v + w)$ with $u = 0.0426$, $v = 0.1284$ and $w = 0.0308$. The value of these

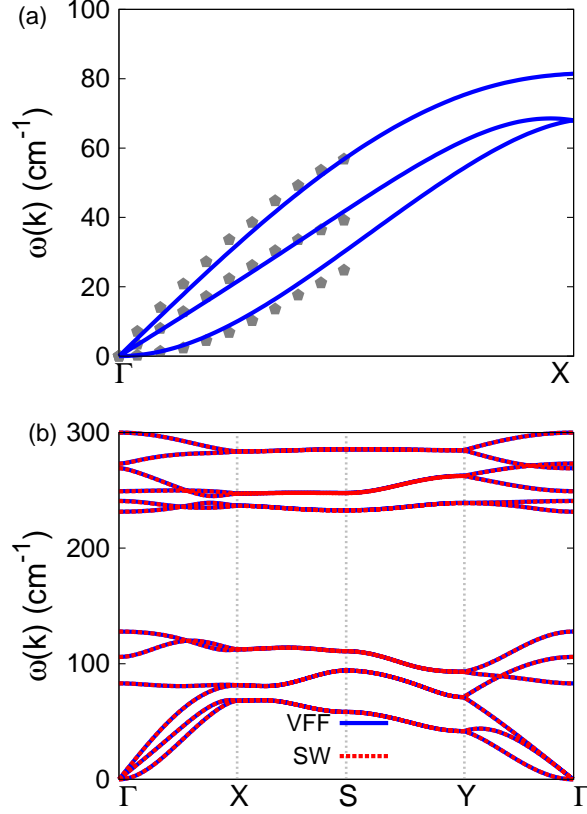


FIG. 204: (Color online) Phonon dispersion for the single-layer p-SnS. (a) The VFF model is fitted to the acoustic branches in the long wave limit along the ΓX direction. The *ab initio* calculations are from Ref. 81. (b) The VFF model (blue lines) and the SW potential (red lines) give the same phonon dispersion for the p-SnS along $\Gamma X S Y T$.

dimensionless parameters are extracted from the geometrical parameters provided in Ref. 78, including lattice constants $a_1 = 4.347 \text{ \AA}$ and $a_2 = 4.047 \text{ \AA}$, bond lengths $d_{12} = 2.728 \text{ \AA}$ and $d_{14} = 2.595 \text{ \AA}$, and the angle $\theta_{145} = 89.0^\circ$. The dimensionless parameters v and w are ratios based on the lattice constant in the out-of-plane z -direction, which is arbitrarily chosen as $a_3 = 10.0 \text{ \AA}$. We note that the main purpose of the usage of u , v , and w in representing atomic coordinates is to follow the same convention for all puckered structures in the present work. The resultant atomic coordinates are the same as that in Ref. 78.

As shown in Fig. 189, a specific feature in the puckered configuration of the p-SnS is that there is a small difference of wa_3 between the z -coordinate of atom 1 and the z -coordinates of atoms 2 and 3. Similarly, atom 4 is higher than atoms 5 and 6 for wa_3 along the z -direction.

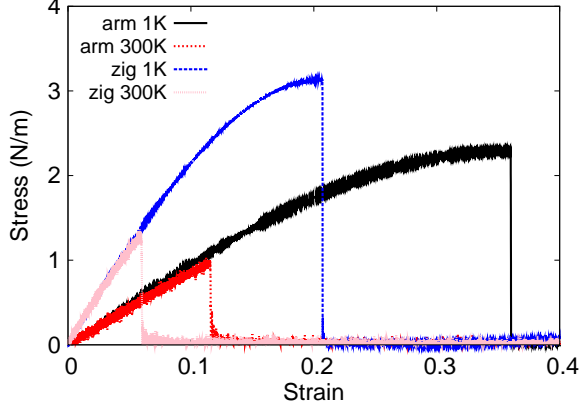


FIG. 205: (Color online) Stress-strain relations for the single-layer p-SnS of size $100 \times 100 \text{ \AA}$. The single-layer p-SnS is uniaxially stretched along the armchair or zigzag directions at temperatures 1 K and 300 K.

TABLE CCCXCVIII: The VFF model for the single-layer p-SnS. The second line gives an explicit expression for each VFF term, where atom indexes are from Fig. 189 (c). The third line is the force constant parameters. Parameters are in the unit of $\frac{eV}{\text{\AA}^2}$ for the bond stretching interactions, and in the unit of eV for the angle bending interaction. The fourth line gives the initial bond length (in unit of \AA) for the bond stretching interaction and the initial angle (in unit of degrees) for the angle bending interaction. The angle θ_{ijk} has atom i as the apex.

VFF type	bond stretching		angle bending		
expression	$\frac{1}{2}K_{12}(\Delta r_{12})^2$	$\frac{1}{2}K_{14}(\Delta r_{14})^2$	$\frac{1}{2}K_{123}(\Delta\theta_{123})^2$	$\frac{1}{2}K_{134}(\Delta\theta_{134})^2$	$\frac{1}{2}K_{415}(\Delta\theta_{415})^2$
parameter	4.163	4.163	1.776	5.841	5.841
r_0 or θ_0	2.728	2.595	95.762	89.000	101.887

The sign of w determines which types of atoms take the out-most positions, e.g., atoms 1, 5, and 6 are the out-most atoms if $w > 0$ in Fig. 189 (c), while atoms 2, 3, and 4 will take the out-most positions for $w < 0$.

Table CCCXCVIII shows five VFF terms for the single-layer p-SnS, two of which are the bond stretching interactions shown by Eq. (1) while the other three terms are the angle bending interaction shown by Eq. (2). The force constant parameters are the same for the two angle bending terms θ_{134} and θ_{415} , which have the same arm lengths. All force constant parameters are determined by fitting to the acoustic branches in the phonon dispersion along

TABLE CCCXCIX: Two-body SW potential parameters for the single-layer p-SnS used by GULP,⁸ as expressed in Eq. (3). The quantity (r_{ij}) in the first line lists one representative term for the two-body SW potential between atoms i and j. Atom indexes are from Fig. 189 (c).

	A (eV)	ρ (\AA)	B (\AA^4)	r_{\min} (\AA)	r_{\max} (\AA)
r_{12}	0.782	0.106	27.692	0.0	2.997
r_{14}	5.636	1.887	22.674	0.0	3.702

TABLE CD: Three-body SW potential parameters for the single-layer p-SnS used by GULP,⁸ as expressed in Eq. (4). The first line (θ_{ijk}) presents one representative term for the three-body SW potential. The angle θ_{ijk} has the atom i as the apex. Atom indexes are from Fig. 189 (c).

	K (eV)	θ_0 (degree)	ρ_1 (\AA)	ρ_2 (\AA)	$r_{\min 12}$ (\AA)	$r_{\max 12}$ (\AA)	$r_{\min 13}$ (\AA)	$r_{\max 13}$ (\AA)	$r_{\min 23}$ (\AA)	$r_{\max 23}$ (\AA)
θ_{123}	1.968	95.762	0.106	0.106	0.0	2.997	0.0	2.997	0.0	4.197
θ_{134}	23.839	89.000	1.887	0.106	0.0	3.702	0.0	2.997	0.0	4.366
θ_{415}	24.888	101.887	1.887	0.106	0.0	3.702	0.0	2.997	0.0	4.566

the GX as shown in Fig. 204 (a). The *ab initio* calculations are from Ref. 81. Fig. 204 (b) shows that the VFF model and the SW potential give exactly the same phonon dispersion.

The parameters for the two-body SW potential used by GULP are shown in Tab. CCCXCIX. The parameters for the three-body SW potential used by GULP are shown in Tab. CD. Parameters for the SW potential used by LAMMPS are listed in Tab. CDI. Eight atom types have been introduced for writing the SW potential script used by LAMMPS as shown in Fig. 190 with M=Sn and X=S, which helps to increase the cutoff for the bond

TABLE CDI: SW potential parameters for p-SnS used by LAMMPS,⁹ as expressed in Eqs. (9) and (10). Atom types in the first column are displayed in Fig. 190, with M=Sn and X=S.

	ϵ (eV)	σ (\AA)	a	λ	γ	$\cos \theta_0$	A_L	B_L	p	q	tol
Sn ₁ -S ₄ -S ₄	1.000	0.106	28.347	1.971	1.000	-0.100	0.783	221784.222	4	0	0.0
Sn ₁ -S ₁ -S ₁	1.000	1.887	1.961	0.000	1.000	0.000	5.636	1.787	4	0	0.0
Sn ₁ -S ₁ -S ₄	1.000	0.000	0.000	23.839	1.000	0.017	0.000	0.000	4	0	0.0
S ₁ -Sn ₁ -Sn ₂	1.000	0.000	0.000	24.888	1.000	-0.206	0.000	0.000	4	0	0.0

TABLE CDII: The VFF model for the single-layer p-CSe. The second line gives an explicit expression for each VFF term, where atom indexes are from Fig. 189 (c). The third line is the force constant parameters. Parameters are in the unit of $\frac{\text{eV}}{\text{\AA}^2}$ for the bond stretching interactions, and in the unit of eV for the angle bending interaction. The fourth line gives the initial bond length (in unit of \AA) for the bond stretching interaction and the initial angle (in unit of degrees) for the angle bending interaction. The angle θ_{ijk} has atom i as the apex.

VFF type	bond stretching		angle bending		
expression	$\frac{1}{2}K_{12}(\Delta r_{12})^2$	$\frac{1}{2}K_{14}(\Delta r_{14})^2$	$\frac{1}{2}K_{123}(\Delta\theta_{123})^2$	$\frac{1}{2}K_{134}(\Delta\theta_{134})^2$	$\frac{1}{2}K_{415}(\Delta\theta_{415})^2$
parameter	10.120	10.120	4.505	3.910	3.910
r_0 or θ_0	1.961	2.014	101.354	113.000	100.563

stretching interaction between atom 1 and atom 2 in Fig. 189 (c).

Fig. 205 shows the stress strain relations for the single-layer p-SnS of size $100 \times 100 \text{ \AA}$. The structure is uniaxially stretched in the armchair or zigzag directions at 1 K and 300 K. The Young's modulus is 9.6 Nm^{-1} and 24.5 Nm^{-1} in the armchair and zigzag directions respectively at 1 K, which are obtained by linear fitting of the stress strain relations in $[0, 0.01]$. The Poisson's ratios from the VFF model and the SW potential are $\nu_{xy} = 0.18$ and $\nu_{yx} = 0.47$. The third-order nonlinear elastic constant D can be obtained by fitting the stress-strain relation to $\sigma = E\epsilon + \frac{1}{2}D\epsilon^2$ with E as the Young's modulus. The values of D are -14.7 Nm^{-1} and -80.3 Nm^{-1} at 1 K along the armchair and zigzag directions, respectively. The ultimate stress is about 2.3 Nm^{-1} at the critical strain of 0.36 in the armchair direction at the low temperature of 1 K. The ultimate stress is about 3.1 Nm^{-1} at the critical strain of 0.20 in the zigzag direction at the low temperature of 1 K.

CI. P-CSE

Present studies on the puckered (p-) CSe are based on first-principles calculations, and no empirical potential has been proposed for the p-CSe. We will thus parametrize the SW potential for the single-layer p-CSe in this section.

The structure of the single-layer p-CSe is shown in Fig. 189, with $M=C$ and $X=Se$. Structural parameters for p-CSe are from the *ab initio* calculations.⁷⁸ There are four atoms

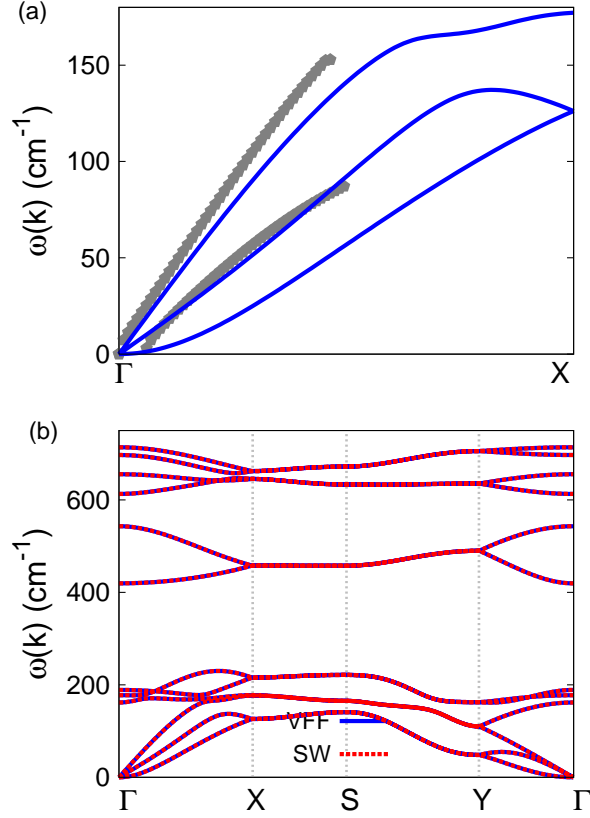


FIG. 206: (Color online) Phonon dispersion for the single-layer p-CSe. (a) The VFF model is fitted to the acoustic branches in the long wave limit along the ΓX direction. The *ab initio* calculations are calculated from SIESTA. (b) The VFF model (blue lines) and the SW potential (red lines) give the same phonon dispersion for the p-CSe along $\Gamma XSYT$.

in the unit cell with relative coordinates as $(-u, 0, -v)$, $(u, 0, v)$, $(0.5 - u, 0.5, v + w)$, and $(0.5 + u, 0.5, -v + w)$ with $u = 0.1079$, $v = 0.0894$ and $w = -0.0229$. The value of these dimensionless parameters are extracted from the geometrical parameters provided in Ref. 78, including lattice constants $a_1 = 4.299 \text{ \AA}$ and $a_2 = 3.034 \text{ \AA}$, bond lengths $d_{12} = 1.961 \text{ \AA}$ and $d_{14} = 2.014 \text{ \AA}$, and the angle $\theta_{145} = 113.0^\circ$. The dimensionless parameters v and w are ratios based on the lattice constant in the out-of-plane z -direction, which is arbitrarily chosen as $a_3 = 10.0 \text{ \AA}$. We note that the main purpose of the usage of u , v , and w in representing atomic coordinates is to follow the same convention for all puckered structures in the present work. The resultant atomic coordinates are the same as that in Ref. 78.

As shown in Fig. 189, a specific feature in the puckered configuration of the p-CSe is that

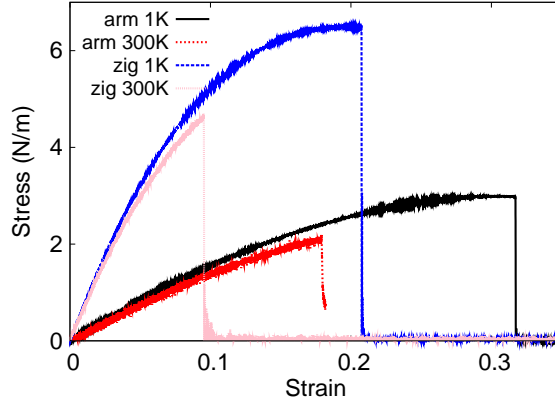


FIG. 207: (Color online) Stress-strain relations for the single-layer p-CSe of size $100 \times 100 \text{ \AA}$. The single-layer p-CSe is uniaxially stretched along the armchair or zigzag directions at temperatures 1 K and 300 K.

TABLE CDIII: Two-body SW potential parameters for the single-layer p-CSe used by GULP,⁸ as expressed in Eq. (3). The quantity (r_{ij}) in the first line lists one representative term for the two-body SW potential between atoms i and j . Atom indexes are from Fig. 189 (c).

	A (eV)	ρ (\AA)	B (\AA^4)	r_{\min} (\AA)	r_{\max} (\AA)
r_{12}	6.141	1.114	7.394	0.0	2.700
r_{14}	7.411	1.316	8.226	0.0	2.828

there is a small difference of wa_3 between the z -coordinate of atom 1 and the z -coordinates of atoms 2 and 3. Similarly, atom 4 is higher than atoms 5 and 6 for wa_3 along the z -direction. The sign of w determines which types of atoms take the out-most positions, e.g., atoms 1, 5, and 6 are the out-most atoms if $w > 0$ in Fig. 189 (c), while atoms 2, 3, and 4 will take the out-most positions for $w < 0$.

Table CDII shows five VFF terms for the single-layer p-CSe, two of which are the bond stretching interactions shown by Eq. (1) while the other three terms are the angle bending interaction shown by Eq. (2). The force constant parameters are the same for the two angle bending terms θ_{134} and θ_{415} , which have the same arm lengths. All force constant parameters are determined by fitting to the acoustic branches in the phonon dispersion along the ΓX as shown in Fig. 206 (a). The *ab initio* calculations for the phonon dispersion are calculated from the SIESTA package.⁷⁹ The generalized gradients approximation is applied to account

TABLE CDIV: Three-body SW potential parameters for the single-layer p-CSe used by GULP,⁸ as expressed in Eq. (4). The first line (θ_{ijk}) presents one representative term for the three-body SW potential. The angle θ_{ijk} has the atom i as the apex. Atom indexes are from Fig. 189 (c).

	K (eV)	θ_0 (degree)	ρ_1 (Å)	ρ_2 (Å)	$r_{\min 12}$ (Å)	$r_{\max 12}$ (Å)	$r_{\min 13}$ (Å)	$r_{\max 13}$ (Å)	$r_{\min 23}$ (Å)	$r_{\max 23}$ (Å)
θ_{123}	47.768	101.354	1.114	1.114	0.0	2.700	0.0	2.700	0.0	3.667
θ_{134}	52.464	113.000	1.316	1.114	0.0	2.828	0.0	2.700	0.0	4.157
θ_{415}	46.000	100.563	1.316	1.114	0.0	2.828	0.0	2.700	0.0	4.032

TABLE CDV: SW potential parameters for p-CSe used by LAMMPS,⁹ as expressed in Eqs. (9) and (10). Atom types in the first column are displayed in Fig. 190, with $M=C$ and $X=Se$.

	ϵ (eV)	σ (Å)	a	λ	γ	$\cos \theta_0$	A_L	B_L	p	q	tol
$C_1-Se_4-Se_4$	1.000	1.114	2.424	47.768	1.000	-0.197	6.141	4.802	4	0	0.0
$C_1-Se_1-Se_1$	1.000	1.316	2.149	0.000	1.000	0.000	7.411	2.743	4	0	0.0
$C_1-Se_1-Se_4$	1.000	0.000	0.000	52.464	1.000	-0.391	0.000	0.000	4	0	0.0
$Se_1-C_1-C_2$	1.000	0.000	0.000	46.000	1.000	-0.183	0.000	0.000	4	0	0.0

for the exchange-correlation function with Perdew, Burke, and Ernzerhof parameterization,⁸⁰ and the double- ζ orbital basis set is adopted. Fig. 206 (b) shows that the VFF model and the SW potential give exactly the same phonon dispersion.

The parameters for the two-body SW potential used by GULP are shown in Tab. CDIII. The parameters for the three-body SW potential used by GULP are shown in Tab. CDIV. Parameters for the SW potential used by LAMMPS are listed in Tab. CDV. Eight atom types have been introduced for writing the SW potential script used by LAMMPS as shown in Fig. 190 with $M=C$ and $X=Se$, which helps to increase the cutoff for the bond stretching interaction between atom 1 and atom 2 in Fig. 189 (c).

Fig. 207 shows the stress strain relations for the single-layer p-CSe of size 100×100 Å. The structure is uniaxially stretched in the armchair or zigzag directions at 1 K and 300 K. The Young's modulus is 17.2 Nm^{-1} and 75.4 Nm^{-1} in the armchair and zigzag directions respectively at 1 K, which are obtained by linear fitting of the stress strain relations in $[0, 0.01]$. The Poisson's ratios from the VFF model and the SW potential are $\nu_{xy} = -0.02$ and $\nu_{yx} = -0.11$. The third-order nonlinear elastic constant D can be obtained by fitting the

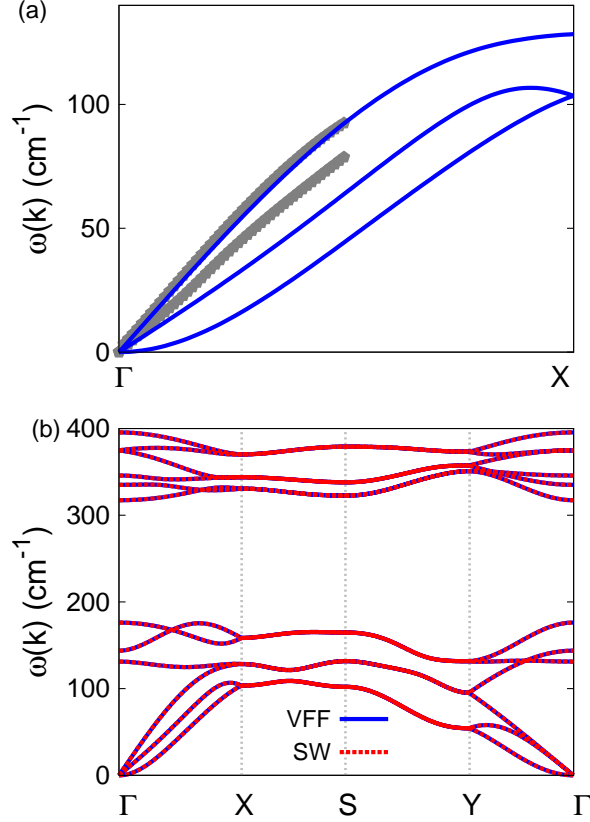


FIG. 208: (Color online) Phonon dispersion for the single-layer p-SiSe. (a) The VFF model is fitted to the acoustic branches in the long wave limit along the Γ X direction. The *ab initio* calculations are calculated from SIESTA. (b) The VFF model (blue lines) and the SW potential (red lines) give the same phonon dispersion for the p-SiSe along Γ XSYT.

stress-strain relation to $\sigma = E\epsilon + \frac{1}{2}D\epsilon^2$ with E as the Young's modulus. The values of D are -46.3 Nm^{-1} and -442.0 Nm^{-1} at 1 K along the armchair and zigzag directions, respectively. The ultimate stress is about 3.0 Nm^{-1} at the critical strain of 0.31 in the armchair direction at the low temperature of 1 K. The ultimate stress is about 6.5 Nm^{-1} at the critical strain of 0.20 in the zigzag direction at the low temperature of 1 K.

CII. P-SISE

Present studies on the puckered (p-) SiSe are based on first-principles calculations, and no empirical potential has been proposed for the p-SiSe. We will thus parametrize the SW

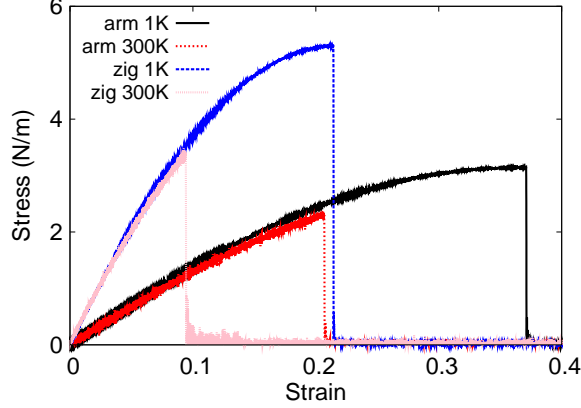


FIG. 209: (Color online) Stress-strain relations for the single-layer p-SiSe of size $100 \times 100 \text{ \AA}$. The single-layer p-SiSe is uniaxially stretched along the armchair or zigzag directions at temperatures 1 K and 300 K.

TABLE CDVI: The VFF model for the single-layer p-SiSe. The second line gives an explicit expression for each VFF term, where atom indexes are from Fig. 189 (c). The third line is the force constant parameters. Parameters are in the unit of $\frac{eV}{\text{Å}^2}$ for the bond stretching interactions, and in the unit of eV for the angle bending interaction. The fourth line gives the initial bond length (in unit of Å) for the bond stretching interaction and the initial angle (in unit of degrees) for the angle bending interaction. The angle θ_{ijk} has atom i as the apex.

VFF type	bond stretching		angle bending		
expression	$\frac{1}{2}K_{12}(\Delta r_{12})^2$	$\frac{1}{2}K_{14}(\Delta r_{14})^2$	$\frac{1}{2}K_{123}(\Delta\theta_{123})^2$	$\frac{1}{2}K_{134}(\Delta\theta_{134})^2$	$\frac{1}{2}K_{415}(\Delta\theta_{415})^2$
parameter	7.192	7.192	3.222	5.890	5.890
r_0 or θ_0	2.524	2.448	95.513	98.200	97.686

potential for the single-layer p-SiSe in this section.

The structure of the single-layer p-SiSe is shown in Fig. 189, with $M=\text{Si}$ and $X=\text{Se}$. Structural parameters for p-SiSe are from the *ab initio* calculations.⁷⁸ There are four atoms in the unit cell with relative coordinates as $(-u, 0, -v)$, $(u, 0, v)$, $(0.5 - u, 0.5, v + w)$, and $(0.5 + u, 0.5, -v + w)$ with $u = 0.0572$, $v = 0.1198$ and $w = -0.0011$. The value of these dimensionless parameters are extracted from the geometrical parameters provided in Ref. 78, including lattice constants $a_1 = 4.400 \text{ \AA}$ and $a_2 = 3.737 \text{ \AA}$, bond lengths $d_{12} = 2.524 \text{ \AA}$ and $d_{14} = 2.448 \text{ \AA}$, and the angle $\theta_{145} = 98.2^\circ$. The dimensionless parameters v and w are ratios

TABLE CDVII: Two-body SW potential parameters for the single-layer p-SiSe used by GULP,⁸ as expressed in Eq. (3). The quantity (r_{ij}) in the first line lists one representative term for the two-body SW potential between atoms i and j . Atom indexes are from Fig. 189 (c).

	A (eV)	ρ (\AA)	B (\AA^4)	r_{\min} (\AA)	r_{\max} (\AA)
r_{12}	1.883	0.230	20.292	0.0	2.905
r_{14}	8.098	1.665	17.956	0.0	3.457

TABLE CDVIII: Three-body SW potential parameters for the single-layer p-SiSe used by GULP,⁸ as expressed in Eq. (4). The first line (θ_{ijk}) presents one representative term for the three-body SW potential. The angle θ_{ijk} has the atom i as the apex. Atom indexes are from Fig. 189 (c).

	K (eV)	θ_0 (degree)	ρ_1 (\AA)	ρ_2 (\AA)	$r_{\min12}$ (\AA)	$r_{\max12}$ (\AA)	$r_{\min13}$ (\AA)	$r_{\max13}$ (\AA)	$r_{\min23}$ (\AA)	$r_{\max23}$ (\AA)
θ_{123}	5.440	95.513	0.230	0.230	0.0	2.905	0.0	2.905	0.0	4.069
θ_{134}	28.616	98.200	1.665	0.230	0.0	3.457	0.0	2.905	0.0	4.379
θ_{415}	28.545	97.686	1.665	0.230	0.0	3.457	0.0	2.905	0.0	4.369

based on the lattice constant in the out-of-plane z -direction, which is arbitrarily chosen as $a_3 = 10.0 \text{ \AA}$. We note that the main purpose of the usage of u , v , and w in representing atomic coordinates is to follow the same convention for all puckered structures in the present work. The resultant atomic coordinates are the same as that in Ref. 78.

As shown in Fig. 189, a specific feature in the puckered configuration of the p-SiSe is that there is a small difference of wa_3 between the z -coordinate of atom 1 and the z -coordinates of atoms 2 and 3. Similarly, atom 4 is higher than atoms 5 and 6 for wa_3 along the z -direction.

TABLE CDIX: SW potential parameters for p-SiSe used by LAMMPS,⁹ as expressed in Eqs. (9) and (10). Atom types in the first column are displayed in Fig. 190, with M=Si and X=Se.

	ϵ (eV)	σ (\AA)	a	λ	γ	$\cos \theta_0$	A_L	B_L	p	q	tol
Si ₁ -Se ₄ -Se ₄	1.000	0.230	12.628	5.440	1.000	-0.096	1.883	7245.111	4	0	0.0
Si ₁ -Se ₁ -Se ₁	1.000	1.665	2.076	0.000	1.000	0.000	8.098	2.335	4	0	0.0
Si ₁ -Se ₁ -Se ₄	1.000	0.000	0.000	28.616	1.000	-0.143	0.000	0.000	4	0	0.0
Se ₁ -Si ₁ -Si ₂	1.000	0.000	0.000	28.545	1.000	-0.134	0.000	0.000	4	0	0.0

The sign of w determines which types of atoms take the out-most positions, e.g., atoms 1, 5, and 6 are the out-most atoms if $w > 0$ in Fig. 189 (c), while atoms 2, 3, and 4 will take the out-most positions for $w < 0$.

Table CDVI shows five VFF terms for the single-layer p-SiSe, two of which are the bond stretching interactions shown by Eq. (1) while the other three terms are the angle bending interaction shown by Eq. (2). The force constant parameters are the same for the two angle bending terms θ_{134} and θ_{415} , which have the same arm lengths. All force constant parameters are determined by fitting to the acoustic branches in the phonon dispersion along the ΓX as shown in Fig. 208 (a). The *ab initio* calculations for the phonon dispersion are calculated from the SIESTA package.⁷⁹ The generalized gradients approximation is applied to account for the exchange-correlation function with Perdew, Burke, and Ernzerhof parameterization,⁸⁰ and the double- ζ orbital basis set is adopted. Fig. 208 (b) shows that the VFF model and the SW potential give exactly the same phonon dispersion.

The parameters for the two-body SW potential used by GULP are shown in Tab. CDVII. The parameters for the three-body SW potential used by GULP are shown in Tab. CDVIII. Parameters for the SW potential used by LAMMPS are listed in Tab. CDIX. Eight atom types have been introduced for writing the SW potential script used by LAMMPS as shown in Fig. 190 with M=Si and X=Se, which helps to increase the cutoff for the bond stretching interaction between atom 1 and atom 2 in Fig. 189 (c).

Fig. 209 shows the stress strain relations for the single-layer p-SiSe of size $100 \times 100 \text{ \AA}$. The structure is uniaxially stretched in the armchair or zigzag directions at 1 K and 300 K. The Young's modulus is 14.4 Nm^{-1} and 44.6 Nm^{-1} in the armchair and zigzag directions respectively at 1 K, which are obtained by linear fitting of the stress strain relations in $[0, 0.01]$. The Poisson's ratios from the VFF model and the SW potential are $\nu_{xy} = 0.09$ and $\nu_{yx} = 0.30$. The third-order nonlinear elastic constant D can be obtained by fitting the stress-strain relation to $\sigma = E\epsilon + \frac{1}{2}D\epsilon^2$ with E as the Young's modulus. The values of D are -28.8 Nm^{-1} and -176.6 Nm^{-1} at 1 K along the armchair and zigzag directions, respectively. The ultimate stress is about 3.1 Nm^{-1} at the critical strain of 0.37 in the armchair direction at the low temperature of 1 K. The ultimate stress is about 5.3 Nm^{-1} at the critical strain of 0.21 in the zigzag direction at the low temperature of 1 K.

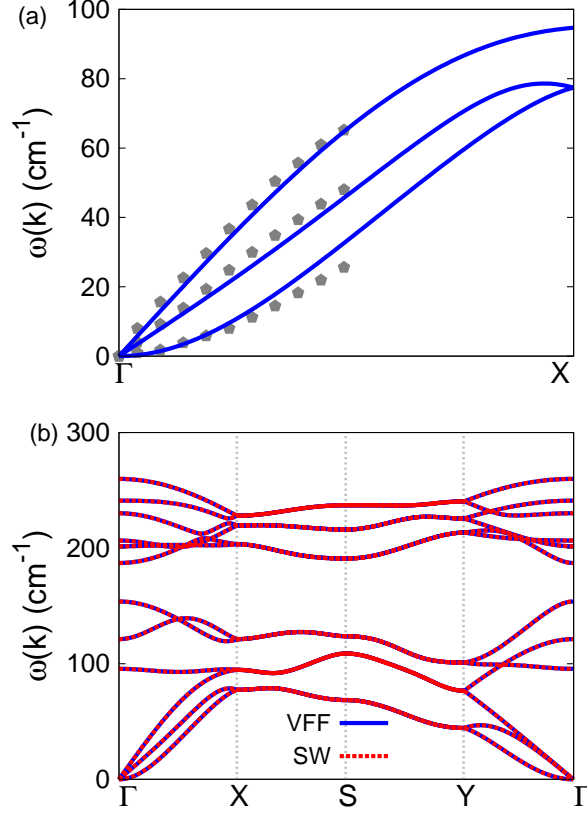


FIG. 210: (Color online) Phonon dispersion for the single-layer p-GeSe. (a) The VFF model is fitted to the acoustic branches in the long wave limit along the Γ X direction. The *ab initio* calculations are from Ref. 81. (b) The VFF model (blue lines) and the SW potential (red lines) give the same phonon dispersion for the p-GeSe along Γ XSY Γ .

CIII. P-GESE

Present studies on the puckered (p-) GeSe are based on first-principles calculations, and no empirical potential has been proposed for the p-GeSe. We will thus parametrize the SW potential for the single-layer p-GeSe in this section.

The structure of the single-layer p-GeSe is shown in Fig. 189, with M=Ge and X=Se. Structural parameters for p-GeSe are from the *ab initio* calculations.⁷⁸ There are four atoms in the unit cell with relative coordinates as $(-u, 0, -v)$, $(u, 0, v)$, $(0.5 - u, 0.5, v + w)$, and $(0.5 + u, 0.5, -v + w)$ with $u = 0.0439$, $v = 0.1258$ and $w = -0.0080$. The value of these dimensionless parameters are extracted from the geometrical parameters provided in Ref. 78,

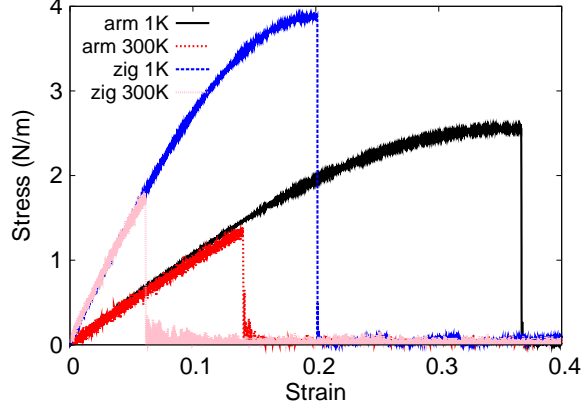


FIG. 211: (Color online) Stress-strain relations for the single-layer p-GeSe of size $100 \times 100 \text{ \AA}$. The single-layer p-GeSe is uniaxially stretched along the armchair or zigzag directions at temperatures 1 K and 300 K.

TABLE CDX: The VFF model for the single-layer p-GeSe. The second line gives an explicit expression for each VFF term, where atom indexes are from Fig. 189 (c). The third line is the force constant parameters. Parameters are in the unit of $\frac{eV}{\text{\AA}^2}$ for the bond stretching interactions, and in the unit of eV for the angle bending interaction. The fourth line gives the initial bond length (in unit of \AA) for the bond stretching interaction and the initial angle (in unit of degrees) for the angle bending interaction. The angle θ_{ijk} has atom i as the apex.

VFF type	bond stretching		angle bending		
expression	$\frac{1}{2}K_{12}(\Delta r_{12})^2$	$\frac{1}{2}K_{14}(\Delta r_{14})^2$	$\frac{1}{2}K_{123}(\Delta\theta_{123})^2$	$\frac{1}{2}K_{134}(\Delta\theta_{134})^2$	$\frac{1}{2}K_{415}(\Delta\theta_{415})^2$
parameter	5.063	5.063	2.249	5.927	5.927
r_0 or θ_0	2.661	2.544	96.322	97.000	93.964

including lattice constants $a_1 = 4.302 \text{ \AA}$ and $a_2 = 3.965 \text{ \AA}$, bond lengths $d_{12} = 2.661 \text{ \AA}$ and $d_{14} = 2.544 \text{ \AA}$, and the angle $\theta_{145} = 97.4^\circ$. The dimensionless parameters v and w are ratios based on the lattice constant in the out-of-plane z -direction, which is arbitrarily chosen as $a_3 = 10.0 \text{ \AA}$. We note that the main purpose of the usage of u , v , and w in representing atomic coordinates is to follow the same convention for all puckered structures in the present work. The resultant atomic coordinates are the same as that in Ref. 78.

As shown in Fig. 189, a specific feature in the puckered configuration of the p-GeSe is that there is a small difference of wa_3 between the z -coordinate of atom 1 and the z -coordinates of

TABLE CDXI: Two-body SW potential parameters for the single-layer p-GeSe used by GULP,⁸ as expressed in Eq. (3). The quantity (r_{ij}) in the first line lists one representative term for the two-body SW potential between atoms i and j . Atom indexes are from Fig. 189 (c).

	A (eV)	ρ (Å)	B (Å ⁴)	r_{\min} (Å)	r_{\max} (Å)
r_{12}	0.962	0.115	25.070	0.0	2.938
r_{14}	6.572	1.846	20.943	0.0	3.628

TABLE CDXII: Three-body SW potential parameters for the single-layer p-GeSe used by GULP,⁸ as expressed in Eq. (4). The first line (θ_{ijk}) presents one representative term for the three-body SW potential. The angle θ_{ijk} has the atom i as the apex. Atom indexes are from Fig. 189 (c).

	K (eV)	θ_0 (degree)	ρ_1 (Å)	ρ_2 (Å)	$r_{\min12}$ (Å)	$r_{\max12}$ (Å)	$r_{\min13}$ (Å)	$r_{\max13}$ (Å)	$r_{\min23}$ (Å)	$r_{\max23}$ (Å)
θ_{123}	2.614	96.322	0.115	0.115	0.0	2.938	0.0	2.938	0.0	4.133
θ_{134}	25.087	97.400	1.846	0.115	0.0	3.628	0.0	2.938	0.0	4.455
θ_{415}	24.789	93.964	1.846	0.155	0.0	3.628	0.0	2.938	0.0	4.404

atoms 2 and 3. Similarly, atom 4 is higher than atoms 5 and 6 for wa_3 along the z-direction. The sign of w determines which types of atoms take the out-most positions, e.g., atoms 1, 5, and 6 are the out-most atoms if $w > 0$ in Fig. 189 (c), while atoms 2, 3, and 4 will take the out-most positions for $w < 0$.

Table CDX shows five VFF terms for the single-layer p-GeSe, two of which are the bond stretching interactions shown by Eq. (1) while the other three terms are the angle bending interaction shown by Eq. (2). The force constant parameters are the same for the two angle

TABLE CDXIII: SW potential parameters for p-GeSe used by LAMMPS,⁹ as expressed in Eqs. (9) and (10). Atom types in the first column are displayed in Fig. 190, with M=Ge and X=Se.

	ϵ (eV)	σ (Å)	a	λ	γ	$\cos \theta_0$	A_L	B_L	p	q	tol
Ge ₁ -Se ₄ -Se ₄	1.000	0.115	25.561	2.614	1.000	-0.110	0.962	143723.555	4	0	0.0
Ge ₁ -Se ₁ -Se ₁	1.000	1.846	1.965	0.000	1.000	0.000	6.572	1.804	4	0	0.0
Ge ₁ -Se ₁ -Se ₄	1.000	0.000	0.000	25.087	1.000	-0.129	0.000	0.000	4	0	0.0
Se ₁ -Ge ₁ -Ge ₂	1.000	0.000	0.000	24.789	1.000	-0.069	0.000	0.000	4	0	0.0

bending terms θ_{134} and θ_{415} , which have the same arm lengths. All force constant parameters are determined by fitting to the acoustic branches in the phonon dispersion along the ΓX as shown in Fig. 210 (a). The *ab initio* calculations are from Ref. 81. Fig. 210 (b) shows that the VFF model and the SW potential give exactly the same phonon dispersion.

The parameters for the two-body SW potential used by GULP are shown in Tab. CDXI. The parameters for the three-body SW potential used by GULP are shown in Tab. CDXII. Parameters for the SW potential used by LAMMPS are listed in Tab. CDXIII. Eight atom types have been introduced for writing the SW potential script used by LAMMPS as shown in Fig. 190 with M=Ge and X=Se, which helps to increase the cutoff for the bond stretching interaction between atom 1 and atom 2 in Fig. 189 (c).

Fig. 211 shows the stress strain relations for the single-layer p-GeSe of size $100 \times 100 \text{ \AA}$. The structure is uniaxially stretched in the armchair or zigzag directions at 1 K and 300 K. The Young's modulus is 11.1 Nm^{-1} and 32.0 Nm^{-1} in the armchair and zigzag directions respectively at 1 K, which are obtained by linear fitting of the stress strain relations in $[0, 0.01]$. The Poisson's ratios from the VFF model and the SW potential are $\nu_{xy} = 0.14$ and $\nu_{yx} = 0.42$. The third-order nonlinear elastic constant D can be obtained by fitting the stress-strain relation to $\sigma = E\epsilon + \frac{1}{2}D\epsilon^2$ with E as the Young's modulus. The values of D are -19.3 Nm^{-1} and -114.7 Nm^{-1} at 1 K along the armchair and zigzag directions, respectively. The ultimate stress is about 2.6 Nm^{-1} at the critical strain of 0.36 in the armchair direction at the low temperature of 1 K. The ultimate stress is about 3.9 Nm^{-1} at the critical strain of 0.20 in the zigzag direction at the low temperature of 1 K.

CIV. P-SNSE

Present studies on the puckered (p-) SnSe are based on first-principles calculations, and no empirical potential has been proposed for the p-SnSe. We will thus parametrize the SW potential for the single-layer p-SnSe in this section.

The structure of the single-layer p-SnSe is shown in Fig. 189, with M=Sn and X=Se. Structural parameters for p-SnSe are from the *ab initio* calculations.⁷⁸ There are four atoms in the unit cell with relative coordinates as $(-u, 0, -v)$, $(u, 0, v)$, $(0.5 - u, 0.5, v + w)$, and $(0.5 + u, 0.5, -v + w)$ with $u = 0.0313$, $v = 0.1358$ and $w = 0.0074$. The value of these dimensionless parameters are extracted from the geometrical parameters provided in Ref. 78,

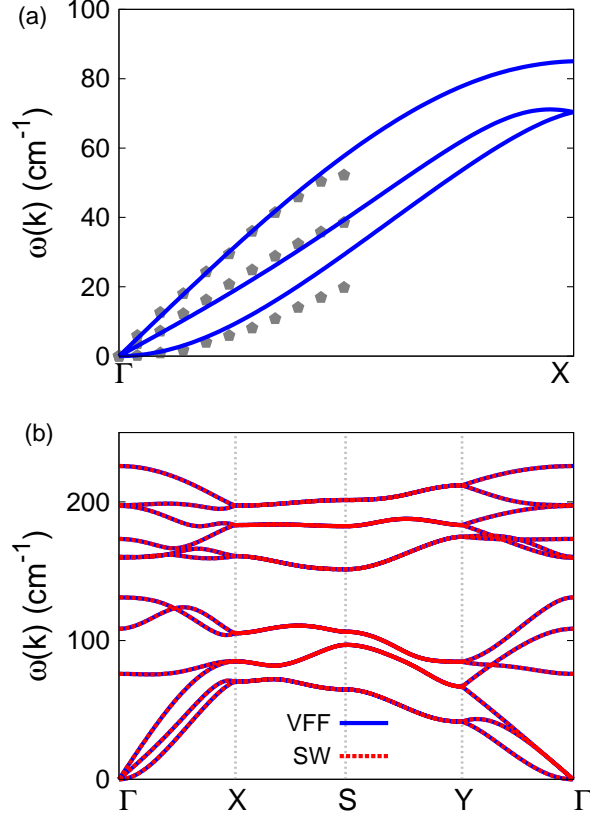


FIG. 212: (Color online) Phonon dispersion for the single-layer p-SnSe. (a) The VFF model is fitted to the acoustic branches in the long wave limit along the Γ X direction. The *ab initio* calculations are from Ref. 82. (b) The VFF model (blue lines) and the SW potential (red lines) give the same phonon dispersion for the p-SnSe along Γ XSY Γ .

including lattice constants $a_1 = 4.453 \text{ \AA}$ and $a_2 = 4.260 \text{ \AA}$, bond lengths $d_{12} = 2.887 \text{ \AA}$ and $d_{14} = 2.730 \text{ \AA}$, and the angle $\theta_{145} = 92.5^\circ$. The dimensionless parameters v and w are ratios based on the lattice constant in the out-of-plane z-direction, which is arbitrarily chosen as $a_3 = 10.0 \text{ \AA}$. We note that the main purpose of the usage of u , v , and w in representing atomic coordinates is to follow the same convention for all puckered structures in the present work. The resultant atomic coordinates are the same as that in Ref. 78.

As shown in Fig. 189, a specific feature in the puckered configuration of the p-SnSe is that there is a small difference of wa_3 between the z-coordinate of atom 1 and the z-coordinates of atoms 2 and 3. Similarly, atom 4 is higher than atoms 5 and 6 for wa_3 along the z-direction. The sign of w determines which types of atoms take the out-most positions, e.g., atoms 1,

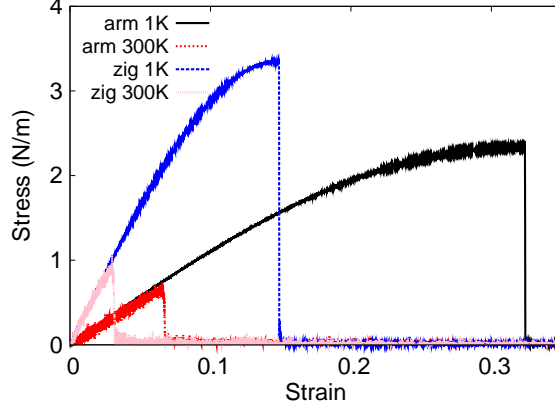


FIG. 213: (Color online) Stress-strain relations for the single-layer p-SnSe of size $100 \times 100 \text{ \AA}$. The single-layer p-SnSe is uniaxially stretched along the armchair or zigzag directions at temperatures 1 K and 300 K.

TABLE CDXIV: The VFF model for the single-layer p-SnSe. The second line gives an explicit expression for each VFF term, where atom indexes are from Fig. 189 (c). The third line is the force constant parameters. Parameters are in the unit of $\frac{eV}{\text{Å}^2}$ for the bond stretching interactions, and in the unit of eV for the angle bending interaction. The fourth line gives the initial bond length (in unit of Å) for the bond stretching interaction and the initial angle (in unit of degrees) for the angle bending interaction. The angle θ_{ijk} has atom i as the apex.

VFF type	bond stretching		angle bending		
expression	$\frac{1}{2}K_{12}(\Delta r_{12})^2$	$\frac{1}{2}K_{14}(\Delta r_{14})^2$	$\frac{1}{2}K_{123}(\Delta\theta_{123})^2$	$\frac{1}{2}K_{134}(\Delta\theta_{134})^2$	$\frac{1}{2}K_{415}(\Delta\theta_{415})^2$
parameter	3.872	3.872	3.157	7.674	7.674
r_0 or θ_0	2.887	2.730	95.087	92.500	95.411

5, and 6 are the out-most atoms if $w > 0$ in Fig. 189 (c), while atoms 2, 3, and 4 will take the out-most positions for $w < 0$.

Table CDXIV shows five VFF terms for the single-layer p-SnSe, two of which are the bond stretching interactions shown by Eq. (1) while the other three terms are the angle bending interaction shown by Eq. (2). The force constant parameters are the same for the two angle bending terms θ_{134} and θ_{415} , which have the same arm lengths. All force constant parameters are determined by fitting to the acoustic branches in the phonon dispersion along the ΓX as shown in Fig. 212 (a). The *ab initio* calculations are from Ref. 82. Fig. 212 (b)

TABLE CDXV: Two-body SW potential parameters for the single-layer p-SnSe used by GULP,⁸ as expressed in Eq. (3). The quantity (r_{ij}) in the first line lists one representative term for the two-body SW potential between atoms i and j . Atom indexes are from Fig. 189 (c).

	A (eV)	ρ (Å)	B (Å ⁴)	r_{\min} (Å)	r_{\max} (Å)
r_{12}	0.565	0.056	34.734	0.0	3.088
r_{14}	5.811	1.989	27.773	0.0	3.895

TABLE CDXVI: Three-body SW potential parameters for the single-layer p-SnSe used by GULP,⁸ as expressed in Eq. (4). The first line (θ_{ijk}) presents one representative term for the three-body SW potential. The angle θ_{ijk} has the atom i as the apex. Atom indexes are from Fig. 189 (c).

	K (eV)	θ_0 (degree)	ρ_1 (Å)	ρ_2 (Å)	$r_{\min12}$ (Å)	$r_{\max12}$ (Å)	$r_{\min13}$ (Å)	$r_{\max13}$ (Å)	$r_{\min23}$ (Å)	$r_{\max23}$ (Å)
θ_{123}	2.777	95.087	0.056	0.056	0.0	3.088	0.0	3.088	0.0	4.357
θ_{134}	27.996	92.500	1.989	0.056	0.0	3.895	0.0	3.088	0.0	4.530
θ_{415}	28.193	95.411	1.989	0.056	0.0	3.895	0.0	3.088	0.0	4.576

shows that the VFF model and the SW potential give exactly the same phonon dispersion.

The parameters for the two-body SW potential used by GULP are shown in Tab. CDXV. The parameters for the three-body SW potential used by GULP are shown in Tab. CDXVI. Parameters for the SW potential used by LAMMPS are listed in Tab. CDXVII. Eight atom types have been introduced for writing the SW potential script used by LAMMPS as shown in Fig. 190 with M=Sn and X=Se, which helps to increase the cutoff for the bond stretching interaction between atom 1 and atom 2 in Fig. 189 (c).

TABLE CDXVII: SW potential parameters for p-SnSe used by LAMMPS,⁹ as expressed in Eqs. (9) and (10). Atom types in the first column are displayed in Fig. 190, with M=Sn and X=Se.

	ϵ (eV)	σ (Å)	a	λ	γ	$\cos \theta_0$	A_L	B_L	p	q	tol
Sn ₁ -Se ₄ -Se ₄	1.000	0.056	55.166	2.777	1.000	-0.089	0.565	3537820.961	4	0	0.0
Sn ₁ -Se ₁ -Se ₁	1.000	1.989	1.959	0.000	1.000	0.000	5.811	1.776	4	0	0.0
Sn ₁ -Se ₁ -Se ₄	1.000	0.000	0.000	27.996	1.000	-0.044	0.000	0.000	4	0	0.0
Se ₁ -Sn ₁ -Sn ₂	1.000	0.000	0.000	28.193	1.000	-0.094	0.000	0.000	4	0	0.0

TABLE CDXVIII: The VFF model for the single-layer p-CTe. The second line gives an explicit expression for each VFF term, where atom indexes are from Fig. 189 (c). The third line is the force constant parameters. Parameters are in the unit of $\frac{\text{eV}}{\text{\AA}^2}$ for the bond stretching interactions, and in the unit of eV for the angle bending interaction. The fourth line gives the initial bond length (in unit of \AA) for the bond stretching interaction and the initial angle (in unit of degrees) for the angle bending interaction. The angle θ_{ijk} has atom i as the apex.

VFF type	bond stretching		angle bending		
expression	$\frac{1}{2}K_{12}(\Delta r_{12})^2$	$\frac{1}{2}K_{14}(\Delta r_{14})^2$	$\frac{1}{2}K_{123}(\Delta\theta_{123})^2$	$\frac{1}{2}K_{134}(\Delta\theta_{134})^2$	$\frac{1}{2}K_{415}(\Delta\theta_{415})^2$
parameter	13.235	13.235	4.210	3.901	3.901
r_0 or θ_0	2.164	2.181	103.122	110.000	90.854

Fig. 213 shows the stress strain relations for the single-layer p-SnSe of size $100 \times 100 \text{\AA}$. The structure is uniaxially stretched in the armchair or zigzag directions at 1 K and 300 K. The Young's modulus is 11.4 Nm^{-1} and 34.1 Nm^{-1} in the armchair and zigzag directions respectively at 1 K, which are obtained by linear fitting of the stress strain relations in $[0, 0.01]$. The Poisson's ratios from the VFF model and the SW potential are $\nu_{xy} = 0.11$ and $\nu_{yx} = 0.33$. The third-order nonlinear elastic constant D can be obtained by fitting the stress-strain relation to $\sigma = E\epsilon + \frac{1}{2}D\epsilon^2$ with E as the Young's modulus. The values of D are -22.0 Nm^{-1} and -128.8 Nm^{-1} at 1 K along the armchair and zigzag directions, respectively. The ultimate stress is about 2.3 Nm^{-1} at the critical strain of 0.32 in the armchair direction at the low temperature of 1 K. The ultimate stress is about 3.3 Nm^{-1} at the critical strain of 0.15 in the zigzag direction at the low temperature of 1 K.

CV. P-CTE

Present studies on the puckered (p-) CTe are based on first-principles calculations, and no empirical potential has been proposed for the p-CTe. We will thus parametrize the SW potential for the single-layer p-CTe in this section.

The structure of the single-layer p-CTe is shown in Fig. 189, with $M=C$ and $X=Te$. Structural parameters for p-CTe are from the *ab initio* calculations.⁷⁸ There are four atoms in the unit cell with relative coordinates as $(-u, 0, -v)$, $(u, 0, v)$, $(0.5 - u, 0.5, v + w)$, and

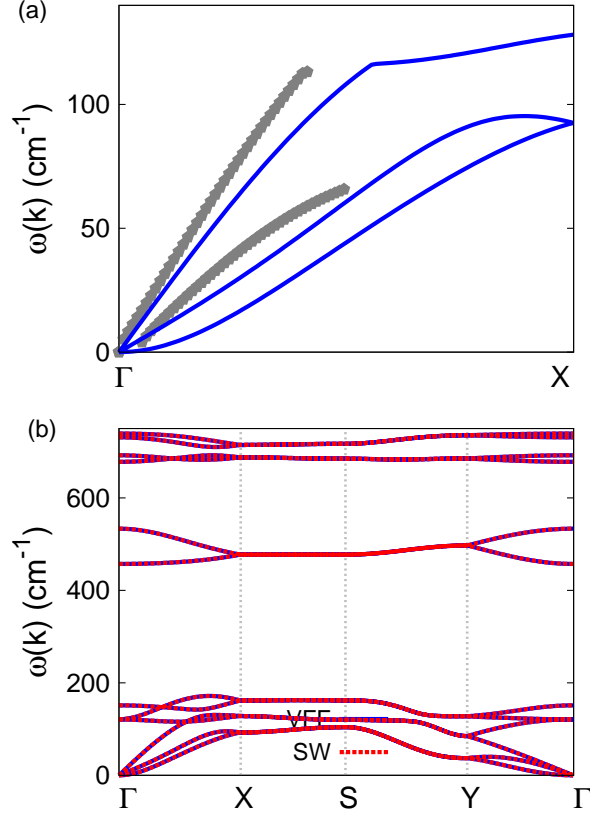


FIG. 214: (Color online) Phonon dispersion for the single-layer p-CTe. (a) The VFF model is fitted to the acoustic branches in the long wave limit along the ΓX direction. The *ab initio* calculations are calculated from SIESTA. (b) The VFF model (blue lines) and the SW potential (red lines) give the same phonon dispersion for the p-CTe along $\Gamma XSYT$.

$(0.5 + u, 0.5, -v + w)$ with $u = 0.0837$, $v = 0.1041$ and $w = -0.0371$. The value of these dimensionless parameters are extracted from the geometrical parameters provided in Ref. 78, including lattice constants $a_1 = 3.889 \text{ \AA}$ and $a_2 = 3.390 \text{ \AA}$, bond lengths $d_{12} = 2.164 \text{ \AA}$ and $d_{14} = 2.181 \text{ \AA}$, and the angle $\theta_{145} = 110.0^\circ$. The dimensionless parameters v and w are ratios based on the lattice constant in the out-of-plane z -direction, which is arbitrarily chosen as $a_3 = 10.0 \text{ \AA}$. We note that the main purpose of the usage of u , v , and w in representing atomic coordinates is to follow the same convention for all puckered structures in the present work. The resultant atomic coordinates are the same as that in Ref. 78.

As shown in Fig. 189, a specific feature in the puckered configuration of the p-CTe is that there is a small difference of wa_3 between the z -coordinate of atom 1 and the z -coordinates of

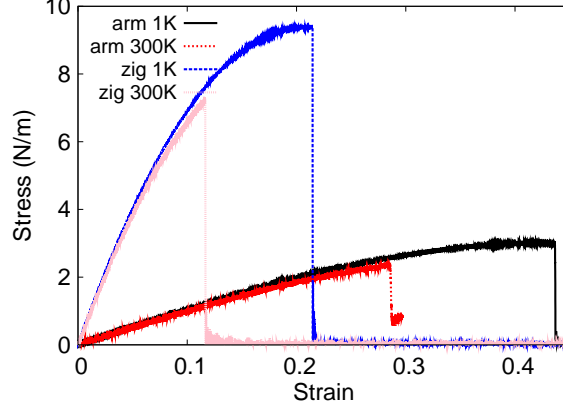


FIG. 215: (Color online) Stress-strain relations for the single-layer p-C7E of size $100 \times 100 \text{ \AA}$. The single-layer p-C7E is uniaxially stretched along the armchair or zigzag directions at temperatures 1 K and 300 K.

TABLE CDXIX: Two-body SW potential parameters for the single-layer p-C7E used by GULP,⁸ as expressed in Eq. (3). The quantity (r_{ij}) in the first line lists one representative term for the two-body SW potential between atoms i and j . Atom indexes are from Fig. 189 (c).

	A (eV)	ρ (\AA)	B (\AA^4)	r_{\min} (\AA)	r_{\max} (\AA)
r_{12}	4.165	0.424	10.965	0.0	2.643
r_{14}	12.519	1.569	11.313	0.0	3.106

atoms 2 and 3. Similarly, atom 4 is higher than atoms 5 and 6 for wa_3 along the z-direction. The sign of w determines which types of atoms take the out-most positions, e.g., atoms 1, 5, and 6 are the out-most atoms if $w > 0$ in Fig. 189 (c), while atoms 2, 3, and 4 will take the out-most positions for $w < 0$.

Table CDXVIII shows five VFF terms for the single-layer p-C7E, two of which are the bond stretching interactions shown by Eq. (1) while the other three terms are the angle bending interaction shown by Eq. (2). The force constant parameters are the same for the two angle bending terms θ_{134} and θ_{415} , which have the same arm lengths. All force constant parameters are determined by fitting to the acoustic branches in the phonon dispersion along the ΓX as shown in Fig. 214 (a). The *ab initio* calculations for the phonon dispersion are calculated from the SIESTA package.⁷⁹ The generalized gradients approximation is applied to account for the exchange-correlation function with Perdew, Burke, and Ernzerhof

TABLE CDXX: Three-body SW potential parameters for the single-layer p-C₂Te used by GULP,⁸ as expressed in Eq. (4). The first line (θ_{ijk}) presents one representative term for the three-body SW potential. The angle θ_{ijk} has the atom *i* as the apex. Atom indexes are from Fig. 189 (c).

	K (eV)	θ_0 (degree)	ρ_1 (Å)	ρ_2 (Å)	$r_{\min 12}$ (Å)	$r_{\max 12}$ (Å)	$r_{\min 13}$ (Å)	$r_{\max 13}$ (Å)	$r_{\min 23}$ (Å)	$r_{\max 23}$ (Å)
θ_{123}	13.040	103.122	0.424	0.424	0.0	2.643	0.0	2.643	0.0	3.639
θ_{134}	29.206	110.000	1.569	0.424	0.0	3.106	0.0	2.643	0.0	4.280
θ_{415}	25.795	90.854	1.569	0.424	0.0	3.106	0.0	2.643	0.0	4.043

TABLE CDXXI: SW potential parameters for p-C₂Te used by LAMMPS,⁹ as expressed in Eqs. (9) and (10). Atom types in the first column are displayed in Fig. 190, with M=C and X=Te.

	ϵ (eV)	σ (Å)	a	λ	γ	$\cos \theta_0$	A_L	B_L	p	q	tol
C ₁ -Te ₄ -Te ₄	1.000	0.424	6.232	13.040	1.000	-0.227	4.165	338.925	4	0	0.0
C ₁ -Te ₁ -Te ₁	1.000	1.569	1.979	0.000	1.000	0.000	12.519	1.866	4	0	0.0
C ₁ -Te ₁ -Te ₄	1.000	0.000	0.000	29.206	1.000	-0.342	0.000	0.000	4	0	0.0
Te ₁ -C ₁ -C ₂	1.000	0.000	0.000	25.795	1.000	-0.015	0.000	0.000	4	0	0.0

parameterization,⁸⁰ and the double- ζ orbital basis set is adopted. Fig. 214 (b) shows that the VFF model and the SW potential give exactly the same phonon dispersion.

The parameters for the two-body SW potential used by GULP are shown in Tab. CDXIX. The parameters for the three-body SW potential used by GULP are shown in Tab. CDXX. Parameters for the SW potential used by LAMMPS are listed in Tab. CDXXI. Eight atom types have been introduced for writing the SW potential script used by LAMMPS as shown in Fig. 190 with M=C and X=Te, which helps to increase the cutoff for the bond stretching interaction between atom 1 and atom 2 in Fig. 189 (c).

Fig. 215 shows the stress strain relations for the single-layer p-C₂Te of size 100×100 Å. The structure is uniaxially stretched in the armchair or zigzag directions at 1 K and 300 K. The Young's modulus is 10.8 Nm^{-1} and 89.1 Nm^{-1} in the armchair and zigzag directions respectively at 1 K, which are obtained by linear fitting of the stress strain relations in $[0, 0.01]$. The Poisson's ratios from the VFF model and the SW potential are $\nu_{xy} = 0.02$ and $\nu_{yx} = 0.20$. The third-order nonlinear elastic constant D can be obtained by fitting the stress-strain relation to $\sigma = E\epsilon + \frac{1}{2}D\epsilon^2$ with E as the Young's modulus. The values of D are

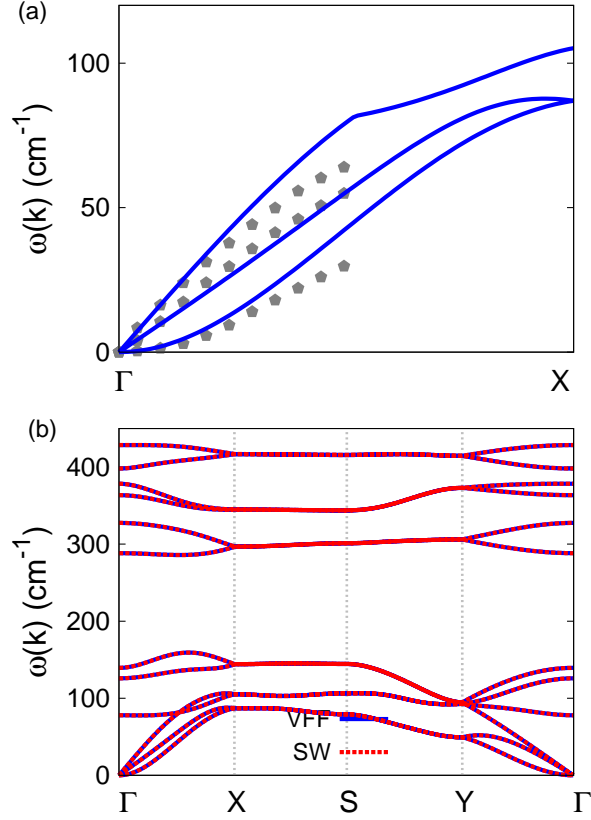


FIG. 216: (Color online) Phonon dispersion for the single-layer p-SiTe. (a) The VFF model is fitted to the acoustic branches in the long wave limit along the ΓX direction. The *ab initio* calculations are from Ref. 83. (b) The VFF model (blue lines) and the SW potential (red lines) give the same phonon dispersion for the p-SiTe along $\Gamma XSY\Gamma$.

-15.3 Nm^{-1} and -419.6 Nm^{-1} at 1 K along the armchair and zigzag directions, respectively. The ultimate stress is about 3.0 Nm^{-1} at the critical strain of 0.43 in the armchair direction at the low temperature of 1 K. The ultimate stress is about 9.4 Nm^{-1} at the critical strain of 0.21 in the zigzag direction at the low temperature of 1 K.

CVI. P-SITE

Present studies on the puckered (p-) SiTe are based on first-principles calculations, and no empirical potential has been proposed for the p-SiTe. We will thus parametrize the SW potential for the single-layer p-SiTe in this section.

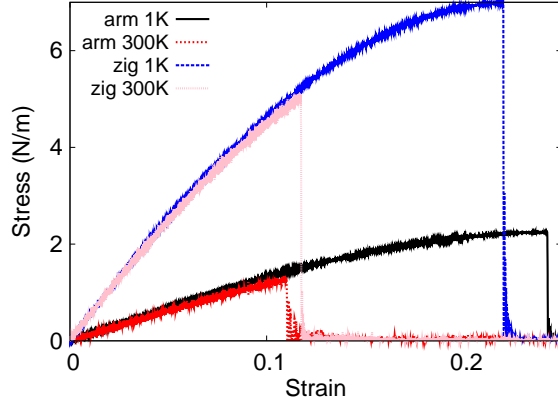


FIG. 217: (Color online) Stress-strain relations for the single-layer p-SiTe of size $100 \times 100 \text{ \AA}$. The single-layer p-SiTe is uniaxially stretched along the armchair or zigzag directions at temperatures 1 K and 300 K.

TABLE CDXXII: The VFF model for the single-layer p-SiTe. The second line gives an explicit expression for each VFF term, where atom indexes are from Fig. 189 (c). The third line is the force constant parameters. Parameters are in the unit of $\frac{eV}{\text{Å}^2}$ for the bond stretching interactions, and in the unit of eV for the angle bending interaction. The fourth line gives the initial bond length (in unit of Å) for the bond stretching interaction and the initial angle (in unit of degrees) for the angle bending interaction. The angle θ_{ijk} has atom i as the apex.

VFF type	bond stretching		angle bending		
expression	$\frac{1}{2}K_{12}(\Delta r_{12})^2$	$\frac{1}{2}K_{14}(\Delta r_{14})^2$	$\frac{1}{2}K_{123}(\Delta\theta_{123})^2$	$\frac{1}{2}K_{134}(\Delta\theta_{134})^2$	$\frac{1}{2}K_{415}(\Delta\theta_{415})^2$
parameter	9.479	2.892	3.145	10.111	10.111
r_0 or θ_0	2.641	2.772	102.142	100.200	92.760

The structure of the single-layer p-SiTe is shown in Fig. 189, with M=Si and X=Te. Structural parameters for p-SiTe are from the *ab initio* calculations.⁷⁸ There are four atoms in the unit cell with relative coordinates as $(-u, 0, -v)$, $(u, 0, v)$, $(0.5 - u, 0.5, v + w)$, and $(0.5 + u, 0.5, -v + w)$ with $u = 0.0581$, $v = 0.1363$ and $w = -0.0173$. The value of these dimensionless parameters are extracted from the geometrical parameters provided in Ref. 78, including lattice constants $a_1 = 4.300 \text{ \AA}$ and $a_2 = 4.109 \text{ \AA}$, bond lengths $d_{12} = 2.641 \text{ \AA}$ and $d_{14} = 2.772 \text{ \AA}$, and the angle $\theta_{145} = 100.200^\circ$. The dimensionless parameters v and w are ratios based on the lattice constant in the out-of-plane z -direction, which is arbitrarily chosen

TABLE CDXXIII: Two-body SW potential parameters for the single-layer p-SiTe used by GULP,⁸ as expressed in Eq. (3). The quantity (r_{ij}) in the first line lists one representative term for the two-body SW potential between atoms i and j. Atom indexes are from Fig. 189 (c).

	A (eV)	ρ (Å)	B (Å ⁴)	r_{\min} (Å)	r_{\max} (Å)
r_{12}	2.394	0.194	24.324	0.0	2.999
r_{14}	3.818	1.722	29.522	0.0	3.864

TABLE CDXXIV: Three-body SW potential parameters for the single-layer p-SiTe used by GULP,⁸ as expressed in Eq. (4). The first line (θ_{ijk}) presents one representative term for the three-body SW potential. The angle θ_{ijk} has the atom i as the apex. Atom indexes are from Fig. 189 (c).

	K (eV)	θ_0 (degree)	ρ_1 (Å)	ρ_2 (Å)	$r_{\min12}$ (Å)	$r_{\max12}$ (Å)	$r_{\min13}$ (Å)	$r_{\max13}$ (Å)	$r_{\min23}$ (Å)	$r_{\max23}$ (Å)
θ_{123}	4.868	102.142	0.194	0.194	0.0	2.999	0.0	2.999	0.0	4.204
θ_{134}	43.419	100.200	1.722	0.194	0.0	3.864	0.0	2.999	0.0	4.577
θ_{415}	42.155	92.760	1.722	0.194	0.0	3.864	0.0	2.999	0.0	4.289

as $a_3 = 10.0$ Å. We note that the main purpose of the usage of u , v , and w in representing atomic coordinates is to follow the same convention for all puckered structures in the present work. The resultant atomic coordinates are the same as that in Ref. 78.

As shown in Fig. 189, a specific feature in the puckered configuration of the p-SiTe is that there is a small difference of wa_3 between the z-coordinate of atom 1 and the z-coordinates of atoms 2 and 3. Similarly, atom 4 is higher than atoms 5 and 6 for wa_3 along the z-direction. The sign of w determines which types of atoms take the out-most positions, e.g., atoms 1,

TABLE CDXXV: SW potential parameters for p-SiTe used by LAMMPS,⁹ as expressed in Eqs. (9) and (10). Atom types in the first column are displayed in Fig. 190, with M=Si and X=Te.

	ϵ (eV)	σ (Å)	a	λ	γ	$\cos \theta_0$	A_L	B_L	p	q	tol
Si ₁ -Te ₄ -Te ₄	1.000	0.194	15.442	4.868	1.000	-0.210	2.394	17093.960	4	0	0.0
Si ₁ -Te ₁ -Te ₁	1.000	1.722	2.245	0.000	1.000	0.000	3.818	3.360	4	0	0.0
Si ₁ -Te ₁ -Te ₄	1.000	0.000	0.000	43.419	1.000	-0.177	0.000	0.000	4	0	0.0
Te ₁ -Si ₁ -Si ₂	1.000	0.000	0.000	42.155	1.000	-0.048	0.000	0.000	4	0	0.0

5, and 6 are the out-most atoms if $w > 0$ in Fig. 189 (c), while atoms 2, 3, and 4 will take the out-most positions for $w < 0$.

Table CDXXII shows five VFF terms for the single-layer p-SiTe, two of which are the bond stretching interactions shown by Eq. (1) while the other three terms are the angle bending interaction shown by Eq. (2). The force constant parameters are the same for the two angle bending terms θ_{134} and θ_{415} , which have the same arm lengths. All force constant parameters are determined by fitting to the acoustic branches in the phonon dispersion along the ΓX as shown in Fig. 216 (a). The *ab initio* calculations are from Ref. 83. Fig. 216 (b) shows that the VFF model and the SW potential give exactly the same phonon dispersion.

The parameters for the two-body SW potential used by GULP are shown in Tab. CDXXIII. The parameters for the three-body SW potential used by GULP are shown in Tab. CDXXIV. Parameters for the SW potential used by LAMMPS are listed in Tab. CDXXV. Eight atom types have been introduced for writing the SW potential script used by LAMMPS as shown in Fig. 190 with M=Si and X=Te, which helps to increase the cutoff for the bond stretching interaction between atom 1 and atom 2 in Fig. 189 (c).

Fig. 217 shows the stress strain relations for the single-layer p-SiTe of size $100 \times 100 \text{ \AA}$. The structure is uniaxially stretched in the armchair or zigzag directions at 1 K and 300 K. The Young's modulus is 14.0 Nm^{-1} and 53.6 Nm^{-1} in the armchair and zigzag directions respectively at 1 K, which are obtained by linear fitting of the stress strain relations in $[0, 0.01]$. The Poisson's ratios from the VFF model and the SW potential are $\nu_{xy} = 0.12$ and $\nu_{yx} = 0.47$. The third-order nonlinear elastic constant D can be obtained by fitting the stress-strain relation to $\sigma = E\epsilon + \frac{1}{2}D\epsilon^2$ with E as the Young's modulus. The values of D are -32.9 Nm^{-1} and -183.2 Nm^{-1} at 1 K along the armchair and zigzag directions, respectively. The ultimate stress is about 2.2 Nm^{-1} at the critical strain of 0.24 in the armchair direction at the low temperature of 1 K. The ultimate stress is about 7.0 Nm^{-1} at the critical strain of 0.22 in the zigzag direction at the low temperature of 1 K.

CVII. P-GETE

Present studies on the puckered (p-) GeTe are based on first-principles calculations, and no empirical potential has been proposed for the p-GeTe. We will thus parametrize the SW potential for the single-layer p-GeTe in this section.

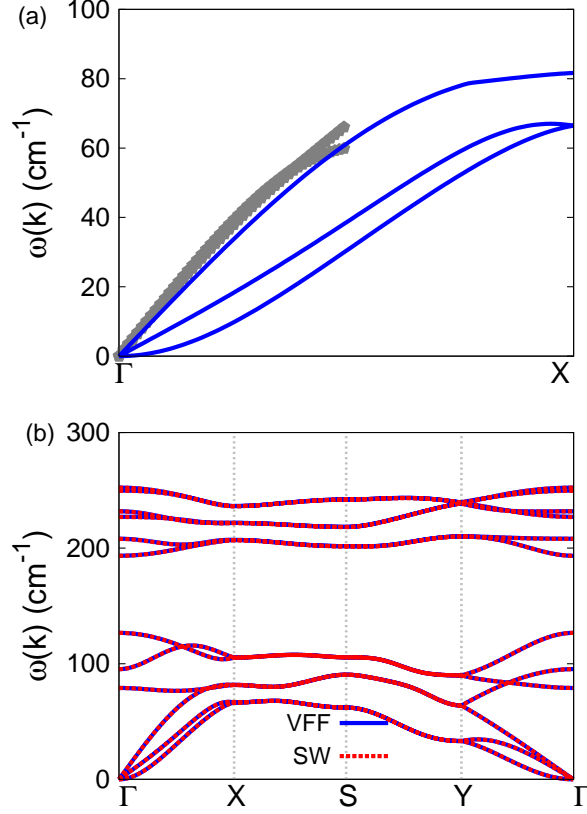


FIG. 218: (Color online) Phonon dispersion for the single-layer p-GeTe. (a) The VFF model is fitted to the acoustic branches in the long wave limit along the Γ X direction. The *ab initio* calculations are calculated from SIESTA. (b) The VFF model (blue lines) and the SW potential (red lines) give the same phonon dispersion for the p-GeTe along Γ XSYT.

The structure of the single-layer p-GeTe is shown in Fig. 189, with M=Ge and X=Te. Structural parameters for p-GeTe are from the *ab initio* calculations.⁷⁸ There are four atoms in the unit cell with relative coordinates as $(-u, 0, -v)$, $(u, 0, v)$, $(0.5 - u, 0.5, v + w)$, and $(0.5 + u, 0.5, -v + w)$ with $u = 0.0538$, $v = 0.1422$ and $w = -0.0216$. The value of these dimensionless parameters are extracted from the geometrical parameters provided in Ref. 78, including lattice constants $a_1 = 4.376 \text{ \AA}$ and $a_2 = 4.238 \text{ \AA}$, bond lengths $d_{12} = 2.736 \text{ \AA}$ and $d_{14} = 2.883 \text{ \AA}$, and the angle $\theta_{145} = 100.4^\circ$. The dimensionless parameters v and w are ratios based on the lattice constant in the out-of-plane z-direction, which is arbitrarily chosen as $a_3 = 10.0 \text{ \AA}$. We note that the main purpose of the usage of u , v , and w in representing atomic coordinates is to follow the same convention for all puckered structures in the present

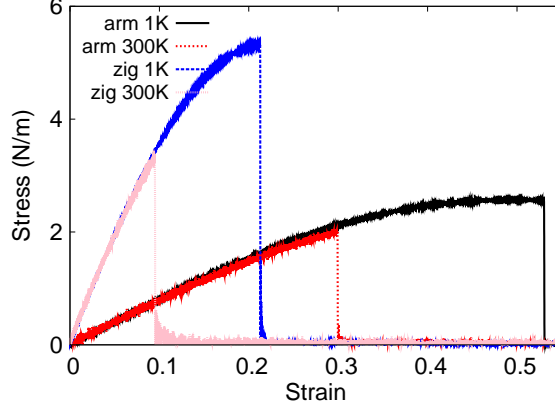


FIG. 219: (Color online) Stress-strain relations for the single-layer p-GeTe of size $100 \times 100 \text{ \AA}$. The single-layer p-GeTe is uniaxially stretched along the armchair or zigzag directions at temperatures 1 K and 300 K.

TABLE CDXXVI: The VFF model for the single-layer p-GeTe. The second line gives an explicit expression for each VFF term, where atom indexes are from Fig. 189 (c). The third line is the force constant parameters. Parameters are in the unit of $\frac{eV}{\text{Å}^2}$ for the bond stretching interactions, and in the unit of eV for the angle bending interaction. The fourth line gives the initial bond length (in unit of Å) for the bond stretching interaction and the initial angle (in unit of degrees) for the angle bending interaction. The angle θ_{ijk} has atom i as the apex.

VFF type	bond stretching		angle bending		
expression	$\frac{1}{2}K_{12}(\Delta r_{12})^2$	$\frac{1}{2}K_{14}(\Delta r_{14})^2$	$\frac{1}{2}K_{123}(\Delta\theta_{123})^2$	$\frac{1}{2}K_{134}(\Delta\theta_{134})^2$	$\frac{1}{2}K_{415}(\Delta\theta_{415})^2$
parameter	7.074	7.074	2.611	5.876	5.876
r_0 or θ_0	2.736	2.883	101.517	100.400	91.402

work. The resultant atomic coordinates are the same as that in Ref. 78.

As shown in Fig. 189, a specific feature in the puckered configuration of the p-GeTe is that there is a small difference of wa_3 between the z-coordinate of atom 1 and the z-coordinates of atoms 2 and 3. Similarly, atom 4 is higher than atoms 5 and 6 for wa_3 along the z-direction. The sign of w determines which types of atoms take the out-most positions, e.g., atoms 1, 5, and 6 are the out-most atoms if $w > 0$ in Fig. 189 (c), while atoms 2, 3, and 4 will take the out-most positions for $w < 0$.

Table CDXXVI shows five VFF terms for the single-layer p-GeTe, two of which are the

TABLE CDXXVII: Two-body SW potential parameters for the single-layer p-GeTe used by GULP,⁸ as expressed in Eq. (3). The quantity (r_{ij}) in the first line lists one representative term for the two-body SW potential between atoms i and j. Atom indexes are from Fig. 189 (c).

	A (eV)	ρ (Å)	B (Å ⁴)	r_{\min} (Å)	r_{\max} (Å)
r_{12}	1.708	0.165	28.018	0.0	3.072
r_{14}	9.854	1.745	34.542	0.0	4.005

TABLE CDXXVIII: Three-body SW potential parameters for the single-layer p-GeTe used by GULP,⁸ as expressed in Eq. (4). The first line (θ_{ijk}) presents one representative term for the three-body SW potential. The angle θ_{ijk} has the atom i as the apex. Atom indexes are from Fig. 189 (c).

	K (eV)	θ_0 (degree)	ρ_1 (Å)	ρ_2 (Å)	$r_{\min12}$ (Å)	$r_{\max12}$ (Å)	$r_{\min13}$ (Å)	$r_{\max13}$ (Å)	$r_{\min23}$ (Å)	$r_{\max23}$ (Å)
θ_{123}	3.626	101.517	0.165	0.165	0.0	3.072	0.0	3.072	0.0	4.307
θ_{134}	23.509	100.400	1.745	0.165	0.0	4.005	0.0	3.072	0.0	4.659
θ_{415}	22.756	91.402	1.745	0.165	0.0	4.005	0.0	3.072	0.0	4.434

bond stretching interactions shown by Eq. (1) while the other three terms are the angle bending interaction shown by Eq. (2). The force constant parameters are the same for the two angle bending terms θ_{134} and θ_{415} , which have the same arm lengths. All force constant parameters are determined by fitting to the acoustic branches in the phonon dispersion along the ΓX as shown in Fig. 218 (a). The *ab initio* calculations for the phonon dispersion

TABLE CDXXIX: SW potential parameters for p-GeTe used by LAMMPS,⁹ as expressed in Eqs. (9) and (10). Atom types in the first column are displayed in Fig. 190, with M=Ge and X=Te.

	ϵ (eV)	σ (Å)	a	λ	γ	$\cos \theta_0$	A_L	B_L	p	q	tol
Ge ₁ -Te ₄ -Te ₄	1.000	0.165	18.665	3.626	1.000	-0.200	1.708	38204.858	4	0	0.0
Ge ₁ -Te ₁ -Te ₁	1.000	1.745	2.295	0.000	1.000	0.000	9.854	3.725	4	0	0.0
Ge ₁ -Te ₁ -Te ₄	1.000	0.000	0.000	23.509	1.000	-0.181	0.000	0.000	4	0	0.0
Te ₁ -Ge ₁ -Ge ₂	1.000	0.000	0.000	22.756	1.000	-0.024	0.000	0.000	4	0	0.0

are calculated from the SIESTA package.⁷⁹ The generalized gradients approximation is applied to account for the exchange-correlation function with Perdew, Burke, and Ernzerhof parameterization,⁸⁰ and the double- ζ orbital basis set is adopted. Fig. 218 (b) shows that the VFF model and the SW potential give exactly the same phonon dispersion.

The parameters for the two-body SW potential used by GULP are shown in Tab. CDXXVII. The parameters for the three-body SW potential used by GULP are shown in Tab. CDXXVIII. Parameters for the SW potential used by LAMMPS are listed in Tab. CDXXIX. Eight atom types have been introduced for writing the SW potential script used by LAMMPS as shown in Fig. 190 with M=Ge and X=Te, which helps to increase the cutoff for the bond stretching interaction between atom 1 and atom 2 in Fig. 189 (c).

Fig. 219 shows the stress strain relations for the single-layer p-GeTe of size $100 \times 100 \text{ \AA}$. The structure is uniaxially stretched in the armchair or zigzag directions at 1 K and 300 K. The Young's modulus is 8.1 Nm^{-1} and 41.6 Nm^{-1} in the armchair and zigzag directions respectively at 1 K, which are obtained by linear fitting of the stress strain relations in $[0, 0.01]$. The Poisson's ratios from the VFF model and the SW potential are $\nu_{xy} = 0.09$ and $\nu_{yx} = 0.49$. The third-order nonlinear elastic constant D can be obtained by fitting the stress-strain relation to $\sigma = E\epsilon + \frac{1}{2}D\epsilon^2$ with E as the Young's modulus. The values of D are -10.5 Nm^{-1} and -143.7 Nm^{-1} at 1 K along the armchair and zigzag directions, respectively. The ultimate stress is about 2.6 Nm^{-1} at the critical strain of 0.53 in the armchair direction at the low temperature of 1 K. The ultimate stress is about 5.3 Nm^{-1} at the critical strain of 0.21 in the zigzag direction at the low temperature of 1 K.

CVIII. P-SNTE

Present studies on the puckered (p-) SnTe are based on first-principles calculations, and no empirical potential has been proposed for the p-SnTe. We will thus parametrize the SW potential for the single-layer p-SnTe in this section.

The structure of the single-layer p-SnTe is shown in Fig. 189, with M=Sn and X=Te. Structural parameters for p-SnTe are from the *ab initio* calculations.⁷⁸ There are four atoms in the unit cell with relative coordinates as $(-u, 0, -v)$, $(u, 0, v)$, $(0.5 - u, 0.5, v + w)$, and $(0.5 + u, 0.5, -v + w)$ with $u = 0.0478$, $v = 0.1567$ and $w = -0.0050$. The value of these dimensionless parameters are extracted from the geometrical parameters provided in Ref. 78,

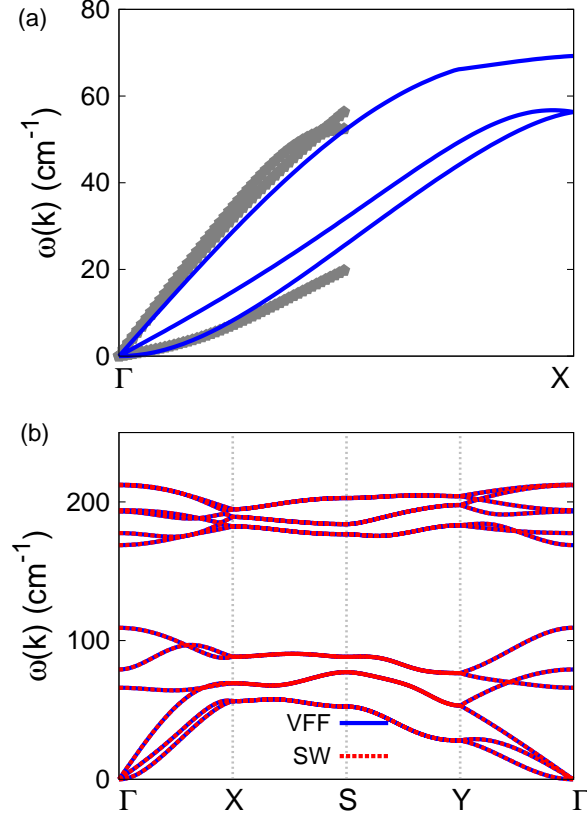


FIG. 220: (Color online) Phonon dispersion for the single-layer p-SnTe. (a) The VFF model is fitted to the acoustic branches in the long wave limit along the Γ X direction. The *ab initio* calculations are calculated from SIESTA. (b) The VFF model (blue lines) and the SW potential (red lines) give the same phonon dispersion for the p-SnTe along Γ XSY Γ .

including lattice constants $a_1 = 4.581 \text{ \AA}$ and $a_2 = 4.542 \text{ \AA}$, bond lengths $d_{12} = 2.931 \text{ \AA}$ and $d_{14} = 3.164 \text{ \AA}$, and the angle $\theta_{145} = 96.0^\circ$. The dimensionless parameters v and w are ratios based on the lattice constant in the out-of-plane z-direction, which is arbitrarily chosen as $a_3 = 10.0 \text{ \AA}$. We note that the main purpose of the usage of u , v , and w in representing atomic coordinates is to follow the same convention for all puckered structures in the present work. The resultant atomic coordinates are the same as that in Ref. 78.

As shown in Fig. 189, a specific feature in the puckered configuration of the p-SnTe is that there is a small difference of wa_3 between the z-coordinate of atom 1 and the z-coordinates of atoms 2 and 3. Similarly, atom 4 is higher than atoms 5 and 6 for wa_3 along the z-direction. The sign of w determines which types of atoms take the out-most positions, e.g., atoms 1,

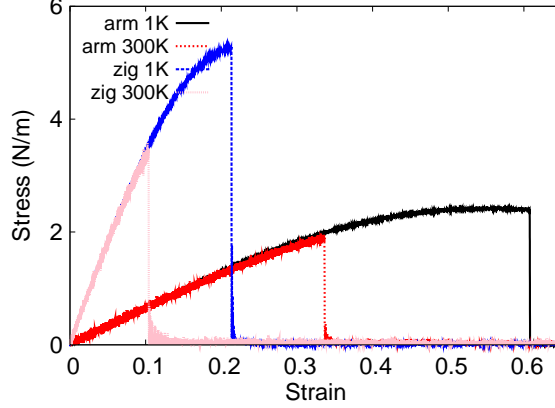


FIG. 221: (Color online) Stress-strain relations for the single-layer p-SnTe of size $100 \times 100 \text{ \AA}$. The single-layer p-SnTe is uniaxially stretched along the armchair or zigzag directions at temperatures 1 K and 300 K.

TABLE CDXXX: The VFF model for the single-layer p-SnTe. The second line gives an explicit expression for each VFF term, where atom indexes are from Fig. 189 (c). The third line is the force constant parameters. Parameters are in the unit of $\frac{eV}{\text{Å}^2}$ for the bond stretching interactions, and in the unit of eV for the angle bending interaction. The fourth line gives the initial bond length (in unit of Å) for the bond stretching interaction and the initial angle (in unit of degrees) for the angle bending interaction. The angle θ_{ijk} has atom i as the apex.

VFF type	bond stretching		angle bending		
expression	$\frac{1}{2}K_{12}(\Delta r_{12})^2$	$\frac{1}{2}K_{14}(\Delta r_{14})^2$	$\frac{1}{2}K_{123}(\Delta\theta_{123})^2$	$\frac{1}{2}K_{134}(\Delta\theta_{134})^2$	$\frac{1}{2}K_{415}(\Delta\theta_{415})^2$
parameter	7.074	7.074	2.611	2.611	5.876
r_0 or θ_0	2.931	3.164	101.578	96.000	94.045

5, and 6 are the out-most atoms if $w > 0$ in Fig. 189 (c), while atoms 2, 3, and 4 will take the out-most positions for $w < 0$.

Table CDXXX shows five VFF terms for the single-layer p-SnTe, two of which are the bond stretching interactions shown by Eq. (1) while the other three terms are the angle bending interaction shown by Eq. (2). The force constant parameters are the same for the two angle bending terms θ_{134} and θ_{415} , which have the same arm lengths. All force constant parameters are determined by fitting to the acoustic branches in the phonon dispersion along the ΓX as shown in Fig. 220 (a). The *ab initio* calculations for the phonon dispersion

TABLE CDXXXI: Two-body SW potential parameters for the single-layer p-SnTe used by GULP,⁸ as expressed in Eq. (3). The quantity (r_{ij}) in the first line lists one representative term for the two-body SW potential between atoms i and j . Atom indexes are from Fig. 189 (c).

	A (eV)	ρ (Å)	B (Å ⁴)	r_{\min} (Å)	r_{\max} (Å)
r_{12}	1.662	0.131	36.901	0.0	3.241
r_{14}	11.054	1.777	50.109	0.0	4.349

TABLE CDXXXII: Three-body SW potential parameters for the single-layer p-SnTe used by GULP,⁸ as expressed in Eq. (4). The first line (θ_{ijk}) presents one representative term for the three-body SW potential. The angle θ_{ijk} has the atom i as the apex. Atom indexes are from Fig. 189 (c).

	K (eV)	θ_0 (degree)	ρ_1 (Å)	ρ_2 (Å)	$r_{\min12}$ (Å)	$r_{\max12}$ (Å)	$r_{\min13}$ (Å)	$r_{\max13}$ (Å)	$r_{\min23}$ (Å)	$r_{\max23}$ (Å)
θ_{123}	3.170	101.578	0.131	0.131	0.0	3.241	0.0	3.241	0.0	4.562
θ_{134}	20.298	96.000	1.777	0.131	0.0	4.349	0.0	3.241	0.0	4.766
θ_{415}	20.176	94.045	1.777	0.131	0.0	4.349	0.0	3.241	0.0	4.595

are calculated from the SIESTA package.⁷⁹ The generalized gradients approximation is applied to account for the exchange-correlation function with Perdew, Burke, and Ernzerhof parameterization,⁸⁰ and the double- ζ orbital basis set is adopted. Fig. 220 (b) shows that the VFF model and the SW potential give exactly the same phonon dispersion.

The parameters for the two-body SW potential used by GULP are shown in

TABLE CDXXXIII: SW potential parameters for p-SnTe used by LAMMPS,⁹ as expressed in Eqs. (9) and (10). Atom types in the first column are displayed in Fig. 190, with M=Sn and X=Te.

	ϵ (eV)	σ (Å)	a	λ	γ	$\cos \theta_0$	A_L	B_L	p	q	tol
Sn ₁ -Te ₄ -Te ₄	1.000	0.131	24.712	3.170	1.000	-0.201	1.662	124727.735	4	0	0.0
Sn ₁ -Te ₁ -Te ₁	1.000	1.777	2.448	0.000	1.000	0.000	11.054	5.028	4	0	0.0
Sn ₁ -Te ₁ -Te ₄	1.000	0.000	0.000	20.298	1.000	-0.105	0.000	0.000	4	0	0.0
Te ₁ -Sn ₁ -Sn ₂	1.000	0.000	0.000	20.176	1.000	-0.071	0.000	0.000	4	0	0.0

TABLE CDXXXIV: The VFF model for silicene. The second line gives an explicit expression for each VFF term. The third line is the force constant parameters. Parameters are in the unit of $\frac{\text{eV}}{\text{\AA}^2}$ for the bond stretching interactions, and in the unit of eV for the angle bending interaction. The fourth line gives the initial bond length (in unit of \AA) for the bond stretching interaction and the initial angle (in unit of degrees) for the angle bending interaction.

VFF type	bond stretching	angle bending
expression	$\frac{1}{2}K_r (\Delta r)^2$	$\frac{1}{2}K_\theta (\Delta\theta)^2$
parameter	18.387	3.465
r_0 or θ_0	2.279	116.218

Tab. CDXXXI. The parameters for the three-body SW potential used by GULP are shown in Tab. CDXXXII. Parameters for the SW potential used by LAMMPS are listed in Tab. CDXXXIII. Eight atom types have been introduced for writing the SW potential script used by LAMMPS as shown in Fig. 190 with M=Sn and X=Te, which helps to increase the cutoff for the bond stretching interaction between atom 1 and atom 2 in Fig. 189 (c).

Fig. 221 shows the stress strain relations for the single-layer p-SnTe of size $100 \times 100 \text{ \AA}$. The structure is uniaxially stretched in the armchair or zigzag directions at 1 K and 300 K. The Young's modulus is 6.6 Nm^{-1} and 38.5 Nm^{-1} in the armchair and zigzag directions respectively at 1 K, which are obtained by linear fitting of the stress strain relations in $[0, 0.01]$. The Poisson's ratios from the VFF model and the SW potential are $\nu_{xy} = 0.10$ and $\nu_{yx} = 0.57$. The third-order nonlinear elastic constant D can be obtained by fitting the stress-strain relation to $\sigma = E\epsilon + \frac{1}{2}D\epsilon^2$ with E as the Young's modulus. The values of D are -7.2 Nm^{-1} and -114.5 Nm^{-1} at 1 K along the armchair and zigzag directions, respectively. The ultimate stress is about 2.4 Nm^{-1} at the critical strain of 0.61 in the armchair direction at the low temperature of 1 K. The ultimate stress is about 5.3 Nm^{-1} at the critical strain of 0.21 in the zigzag direction at the low temperature of 1 K.

CIX. SILICENE

There have been several empirical potentials available for the silicene. A many-body potential based on the Lennard-Jones and Axilrod-Teller functions was used to describe the

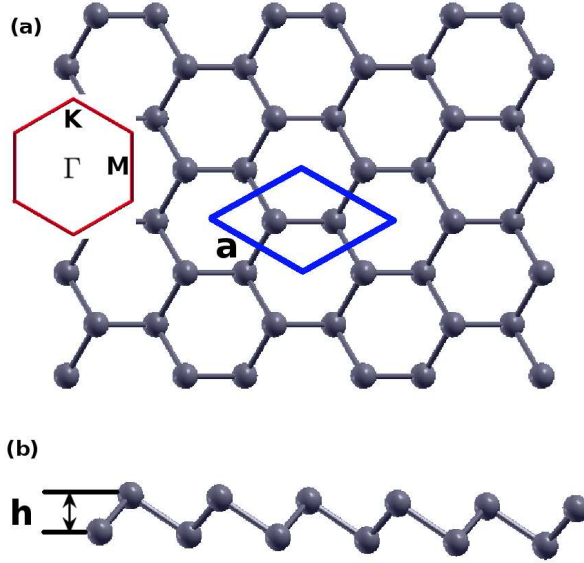


FIG. 222: (Color online) Structure for the buckled M, with M from group V. (a) Top view. The armchair direction is along the horizontal direction, while the zigzag direction is along the vertical direction. The unit cell is displayed by the blue rhombus. Inset shows the first Brillouin zone. (b) Side view illustrates the buckled configuration of height h .

TABLE CDXXXV: Two-body SW potential parameters for silicene used by GULP,⁸ as expressed in Eq. (3).

	A (eV)	ρ (\AA)	B (\AA^4)	r_{\min} (\AA)	r_{\max} (\AA)
Si-Si	19.343	1.668	16.186	0.0	3.075

interaction within the single-layer silicene.⁸⁵ The modified embedded-atom potential⁸⁶ was used by Pei et al to simulate the thermal transport in the single-layer silicene in 2013.⁸⁷ The environment-dependent interatomic potential⁸⁸ was also used to simulate the silicene.⁸⁹ In particular, the original set of SW parameters⁴ for the silicon were found to be not suitable for

TABLE CDXXXVI: Three-body SW potential parameters for silicene used by GULP,⁸ as expressed in Eq. (4).

	K (eV)	θ_0 (degree)	ρ_1 (\AA)	ρ_2 (\AA)	$r_{\min12}$ (\AA)	$r_{\max12}$ (\AA)	$r_{\min13}$ (\AA)	$r_{\max13}$ (\AA)	$r_{\min23}$ (\AA)	$r_{\max23}$ (\AA)
Si-Si-Si	142.310	116.218	1.668	1.668	0.0	3.075	0.0	3.075	3.075	4.181

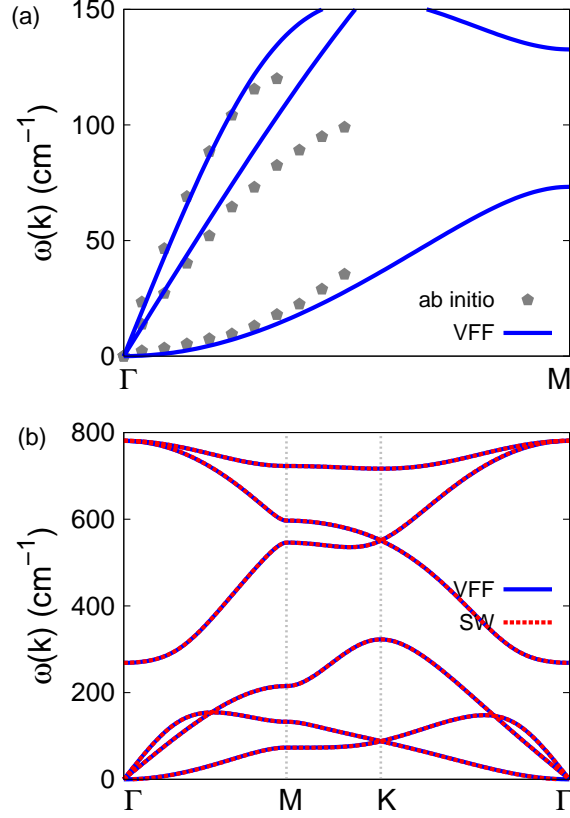


FIG. 223: (Color online) Phonon dispersion for the silicene. (a) The VFF model is fitted to the three acoustic branches in the long wave limit along the ΓM direction. The *ab initio* results (gray pentagons) are from Ref. 84. (b) The VFF model (blue lines) and the SW potential (red lines) give the same phonon dispersion for the silicene along $\Gamma M K \Gamma$.

TABLE CDXXXVII: SW potential parameters for silicene used by LAMMPS,⁹ as expressed in Eqs. (9) and (10).

	ϵ (eV)	σ (Å)	a	λ	γ	$\cos \theta_0$	A_L	B_L	p	q	tol
Si-Si-Si	1.000	1.668	1.844	142.310	1.000	-0.442	19.343	2.091	4	0	0.0

the planar silicene, so two sets of optimized parameters for the SW potential were proposed to simulate the thermal conductivity in the single-layer silicene in 2014.⁹⁰ We will develop a new SW potential to describe the interaction within the silicene in this section, with specific focus on the mechanical properties of the silicene.

The structure of the silicene is shown in Fig. 222, with structural parameters from the

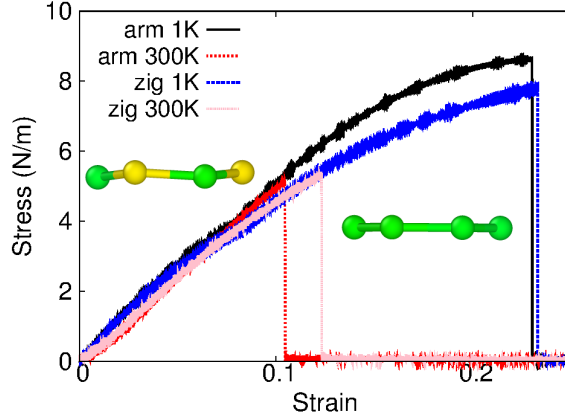


FIG. 224: (Color online) Stress-strain relations for the silicene of size $100 \times 100 \text{ \AA}$. The silicene is uniaxially stretched along the armchair or zigzag directions at temperatures 1 K and 300 K. Left inset shows the buckled configuration for the silicene at the uniaxial strain 0.07 at 1 K along the armchair direction. Right inset: the buckled configuration becomes planar for the silicene at the uniaxial strain of 0.08 at 1 K along the armchair direction.

ab initio calculations.⁸⁴ The silicene has a buckled configuration as shown in Fig. 222 (b), where the buckle is along the zigzag direction. The height of the buckle is $h = 0.45 \text{ \AA}$ and the lattice constant is 3.87 \AA , which results in a bond length of 2.279 \AA .

Table CDXXXIV shows the VFF model for the silicene. The force constant parameters are determined by fitting to the three acoustic branches in the phonon dispersion along the ΓM as shown in Fig. 223 (a). The *ab initio* calculations for the phonon dispersion are from Ref. 84. Similar phonon dispersion can also be found in other *ab initio* calculations.^{84,91–102} Fig. 223 (b) shows that the VFF model and the SW potential give exactly the same phonon dispersion, as the SW potential is derived from the VFF model.

We note that the present SW potential is fitted perfectly to the three acoustic phonon branches, so it can give a nice description for the elastic deformation of the silicene. As a trade off, the optical phonons are overestimated by the present SW potential. Hence, the present SW potential is in particular suitable for the simulation of mechanical or thermal processes which are dominated by acoustic phonons, while the present SW potential may cause a systematic error for the optical absorption process which mainly involves the optical phonons. One can introduce the long-range interactions (eg. the second-nearest-neighboring interaction) to give a good description for both acoustic and optical phonon branches, see

one such example for borophene in Ref. 14. It is because the long-range interaction mainly contributes to the acoustic phonon branches, while it makes only neglectable contribution to the optical phonon branches. As another solution, the SW potential can give reasonable descriptions for the optical phonon branches by reducing its accuracy in describing acoustic phonon branches as done in Ref. 90.

The parameters for the two-body SW potential used by GULP are shown in Tab. CDXXXV. The parameters for the three-body SW potential used by GULP are shown in Tab. CDXXXVI. Parameters for the SW potential used by LAMMPS are listed in Tab. CDXXXVII.

Fig. 224 shows the stress strain relations for the silicene of size $100 \times 100 \text{ \AA}$. The structure is uniaxially stretched in the armchair or zigzag directions at 1 K and 300 K. The Young's modulus is 63.3 Nm^{-1} in both armchair and zigzag directions at 1 K, which are obtained by linear fitting of the stress strain relations in $[0, 0.01]$. The Young's modulus is isotropic for the silicene. The value of the Young's modulus agrees with the value of 63.8 Nm^{-1} from the *ab initio* calculations.¹⁰³ The Poisson's ratios from the VFF model and the SW potential are $\nu_{xy} = \nu_{yx} = 0.15$, which are smaller but comparable with the *ab initio* results of 0.325.¹⁰³ The third-order nonlinear elastic constant D can be obtained by fitting the stress-strain relation to $\sigma = E\epsilon + \frac{1}{2}D\epsilon^2$ with E as the Young's modulus. The values of D are -212.5 Nm^{-1} and -267.5 Nm^{-1} at 1 K along the armchair and zigzag directions, respectively. The ultimate stress is about 8.6 Nm^{-1} at the critical strain of 0.23 in the armchair direction at the low temperature of 1 K. The ultimate stress is about 7.8 Nm^{-1} at the critical strain of 0.23 in the zigzag direction at the low temperature of 1 K.

The stress-strain curves shown in Fig. 224 disclose a structural transition at the strain around 0.076 for the silicene at the low temperature of 1 K. The buckled configuration of the silicene is flattened during this structural transition, which can be seen from these two insets in Fig. 224. This structural transition was also observed in the *ab initio* calculations,⁹⁵ where the critical strain for the structural transition is 0.2. At temperatures above 300 K, this structural transition is blurred by stronger thermal vibrations; i.e., the buckled configuration of the silicene can be strongly disturbed by the thermal vibration at higher temperatures.

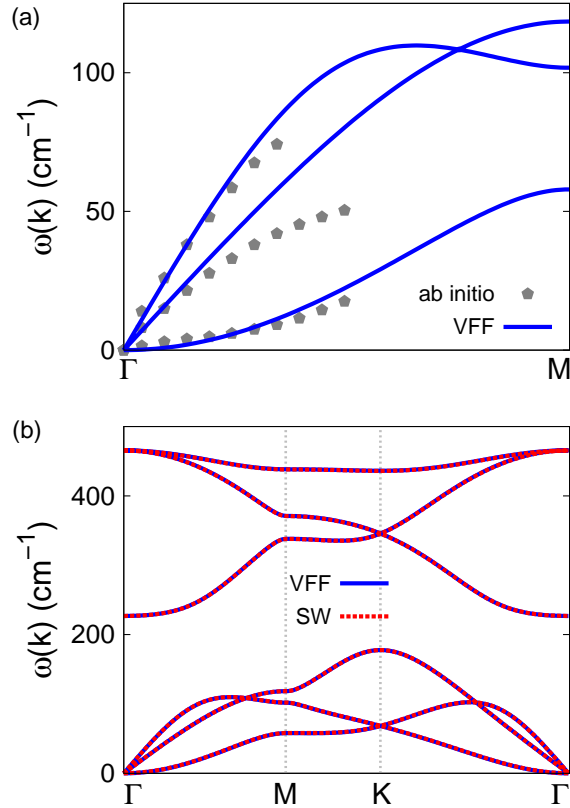


FIG. 225: (Color online) Phonon dispersion for the germanene. (a) The VFF model is fitted to the three acoustic branches in the long wave limit along the ΓM direction. The *ab initio* results (gray pentagons) are from Ref. 84. (b) The VFF model (blue lines) and the SW potential (red lines) give the same phonon dispersion for the germanene along $\Gamma M K \Gamma$.

CX. GERMANENE

In a recent work, the Tersoff potential was applied to simulate the thermal conductivity of the germanene nanoribbon.¹⁰⁴ We will provide the SW potential to describe the interaction within the germanene in this section.

The structure of the germanene is shown in Fig. 222, with structural parameters from the *ab initio* calculations.⁸⁴ The germanene has a buckled configuration as shown in Fig. 222 (b), where the buckle is along the zigzag direction. The height of the buckle is $h = 0.69 \text{ \AA}$ and the lattice constant is 4.06 \AA , which results in a bond length of 2.443 \AA .

Table CDXXXVIII shows the VFF model for the germanene. The force constant pa-

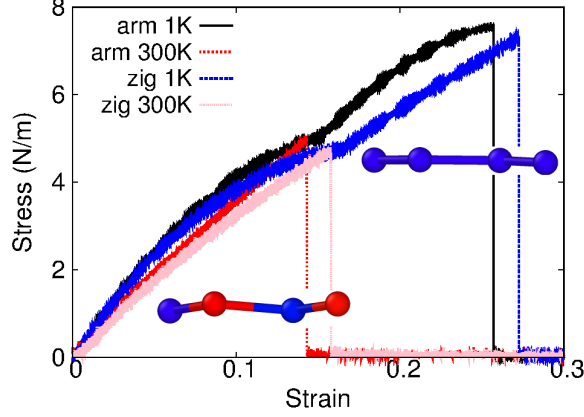


FIG. 226: (Color online) Stress-strain relations for the germanene of size $100 \times 100 \text{ \AA}$. The germanene is uniaxially stretched along the armchair or zigzag directions at temperatures 1 K and 300 K. Left bottom inset shows the buckled configuration for the germanene at the uniaxial strain 0.14 at 1 K along the armchair direction. Right top inset: the buckled configuration becomes planar for the germanene at the uniaxial strain of 0.16 at 1 K along the armchair direction.

TABLE CDXXXVIII: The VFF model for germanene. The second line gives an explicit expression for each VFF term. The third line is the force constant parameters. Parameters are in the unit of $\frac{\text{eV}}{\text{\AA}^2}$ for the bond stretching interactions, and in the unit of eV for the angle bending interaction. The fourth line gives the initial bond length (in unit of \AA) for the bond stretching interaction and the initial angle (in unit of degrees) for the angle bending interaction.

VFF type	bond stretching	angle bending
expression	$\frac{1}{2}K_r (\Delta r)^2$	$\frac{1}{2}K_\theta (\Delta \theta)^2$
parameter	18.387	3.465
r_0 or θ_0	2.443	112.358

Parameters are determined by fitting to the three acoustic branches in the phonon dispersion along the ΓM as shown in Fig. 225 (a). The *ab initio* calculations for the phonon dispersion are from Ref. 84. Similar phonon dispersion can also be found in other *ab initio* calculations.^{84,92,93,98,101,102,105} Fig. 225 (b) shows that the VFF model and the SW potential give exactly the same phonon dispersion, as the SW potential is derived from the VFF model.

TABLE CDXXXIX: Two-body SW potential parameters for germanene used by GULP,⁸ as expressed in Eq. (3).

	A (eV)	ρ (Å)	B (Å ⁴)	r_{\min} (Å)	r_{\max} (Å)
Ge-Ge	19.570	1.607	21.372	0.0	3.252

TABLE CDXL: Three-body SW potential parameters for germanene used by GULP,⁸ as expressed in Eq. (4).

	K (eV)	θ_0 (degree)	ρ_1 (Å)	ρ_2 (Å)	$r_{\min12}$ (Å)	$r_{\max12}$ (Å)	$r_{\min13}$ (Å)	$r_{\max13}$ (Å)	$r_{\min23}$ (Å)	$r_{\max23}$ (Å)
Ge-Ge-Ge	107.735	112.358	1.607	1.607	0.0	3.252	0.0	3.252	3.252	4.4

The parameters for the two-body SW potential used by GULP are shown in Tab. CDXXXIX. The parameters for the three-body SW potential used by GULP are shown in Tab. CDXL. Parameters for the SW potential used by LAMMPS are listed in Tab. CDXLI.

Fig. 226 shows the stress strain relations for the germanene of size 100×100 Å. The structure is uniaxially stretched in the armchair or zigzag directions at 1 K and 300 K. The Young's modulus is 53.2 Nm^{-1} in both armchair and zigzag directions at 1 K, which are obtained by linear fitting of the stress strain relations in $[0, 0.01]$. The Young's modulus is isotropic for the germanene. The Poisson's ratios from the VFF model and the SW potential are $\nu_{xy} = \nu_{yx} = 0.19$. The third-order nonlinear elastic constant D can be obtained by fitting the stress-strain relation to $\sigma = E\epsilon + \frac{1}{2}D\epsilon^2$ with E as the Young's modulus. The values of D are -229.2 Nm^{-1} and -278.2 Nm^{-1} at 1 K along the armchair and zigzag directions, respectively. The ultimate stress is about 7.5 Nm^{-1} at the critical strain of 0.26 in the armchair direction at the low temperature of 1 K. The ultimate stress is about 7.3 Nm^{-1} at the critical strain of 0.27 in the zigzag direction at the low temperature of 1 K.

The stress-strain curves shown in Fig. 226 disclose a structural transition for the germanene at the low temperature of 1 K. The critical strains for the structural transition are

TABLE CDXLI: SW potential parameters for germanene used by LAMMPS,⁹ as expressed in Eqs. (9) and (10).

	ϵ (eV)	σ (Å)	a	λ	γ	$\cos \theta_0$	A_L	B_L	p	q	tol
Ge-Ge-Ge	1.000	1.607	2.024	107.735	1.000	-0.380	19.570	3.205	4	0	0.0

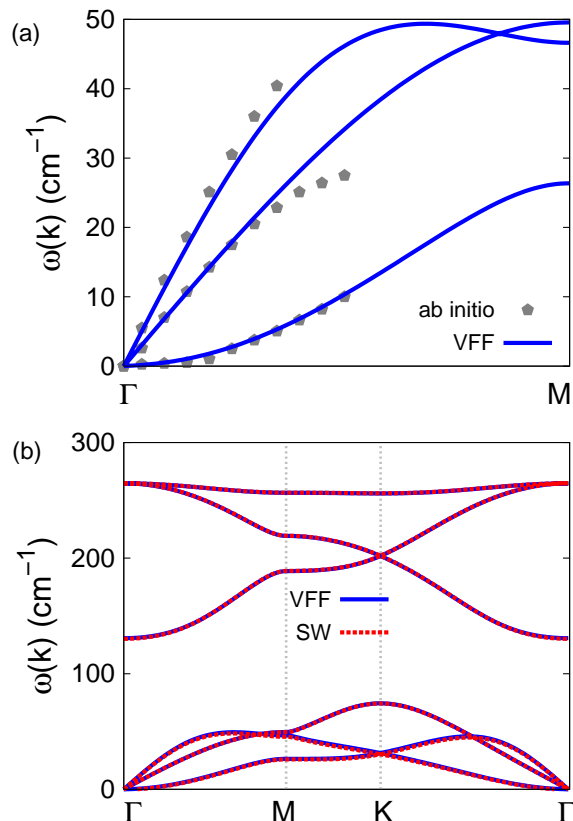


FIG. 227: (Color online) Phonon dispersion for the stanene. (a) The VFF model is fitted to the three acoustic branches in the long wave limit along the Γ M direction. The *ab initio* results (gray pentagons) are from Ref. 105. (b) The VFF model (blue lines) and the SW potential (red lines) give the same phonon dispersion for the stanene along Γ MKT.

0.15 and 0.16 along the armchair and zigzag directions, respectively. The buckled configuration of the germanene is flattened during this structural transition, which can be seen from these two insets in Fig. 226. At temperatures above 300 K, this structural transition is blurred by stronger thermal vibrations; i.e., the buckled configuration of the germanene can be strongly disturbed by the thermal vibration at higher temperatures.

CXI. STANENE

There are several available empirical potentials for the description of the interaction within the stanene. The modified embedded atom method potential was applied to simulate

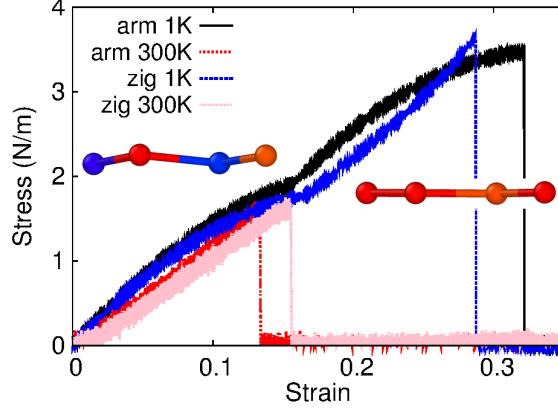


FIG. 228: (Color online) Stress-strain relations for the stanene of size $100 \times 100 \text{ \AA}$. The stanene is uniaxially stretched along the armchair or zigzag directions at temperatures 1 K and 300 K. Left inset: the buckled configuration for the stanene at the uniaxial strain 0.14 at 1 K along the armchair direction. Right inset: the buckled configuration becomes planar for the stanene at the uniaxial strain of 0.16 at 1 K along the armchair direction.

TABLE CDXLII: The VFF model for stanene. The second line gives an explicit expression for each VFF term. The third line is the force constant parameters. Parameters are in the unit of $\frac{eV}{\text{\AA}^2}$ for the bond stretching interactions, and in the unit of eV for the angle bending interaction. The fourth line gives the initial bond length (in unit of \AA) for the bond stretching interaction and the initial angle (in unit of degrees) for the angle bending interaction.

VFF type	bond stretching	angle bending
expression	$\frac{1}{2}K_r (\Delta r)^2$	$\frac{1}{2}K_\theta (\Delta \theta)^2$
parameter	10.489	1.372
r_0 or θ_0	2.836	111.224

mechanical properties for the stanene.¹⁰⁶ A VFF model was fitted for the stanene in 2015.¹⁰⁷ The Tersoff potential was parameterized to describe the interaction for stanene.¹⁰⁸ In this section, we will develop the SW potential for the stanene.

The structure of the stanene is shown in Fig. 222, with structural parameters from the *ab initio* calculations.¹⁰⁵ The stanene has a buckled configuration as shown in Fig. 222 (b), where the buckle is along the zigzag direction. The height of the buckle is $h = 0.86 \text{ \AA}$ and

TABLE CDXLIII: Two-body SW potential parameters for stanene used by GULP,⁸ as expressed in Eq. (3).

	A (eV)	ρ (Å)	B (Å ⁴)	r_{\min} (Å)	r_{\max} (Å)
Sn-Sn	19.542	2.227	42.047	0.0	3.758

TABLE CDXLIV: Three-body SW potential parameters for stanene used by GULP,⁸ as expressed in Eq. (4).

	K (eV)	θ_0 (degree)	ρ_1 (Å)	ρ_2 (Å)	$r_{\min12}$ (Å)	$r_{\max12}$ (Å)	$r_{\min13}$ (Å)	$r_{\max13}$ (Å)	$r_{\min23}$ (Å)	$r_{\max23}$ (Å)
Sn-Sn-Sn	98.863	111.224	2.227	2.227	0.0	3.758	0.0	3.758	3.758	5.076

the lattice constant is 4.68 Å, which results in a bond length of 2.836 Å.

Table CDXLII shows the VFF model for the stanene. The force constant parameters are determined by fitting to the three acoustic branches in the phonon dispersion along the ΓM as shown in Fig. 227 (a). The *ab initio* calculations for the phonon dispersion are from Ref. 105 with the spin-orbit coupling effect. Similar phonon dispersion can also be found in other *ab initio* calculations.^{101,102,105,109–111} Fig. 227 (b) shows that the VFF model and the SW potential give exactly the same phonon dispersion, as the SW potential is derived from the VFF model.

The parameters for the two-body SW potential used by GULP are shown in Tab. CDXLIII. The parameters for the three-body SW potential used by GULP are shown in Tab. CDXLIV. Parameters for the SW potential used by LAMMPS are listed in Tab. CDXLV.

Fig. 228 shows the stress strain relations for the stanene of size 100×100 Å. The structure is uniaxially stretched in the armchair or zigzag directions at 1 K and 300 K. The Young's modulus is 17.0 Nm^{-1} in both armchair and zigzag directions at 1 K, which are obtained by linear fitting of the stress strain relations in $[0, 0.01]$. The Young's modulus is isotropic

TABLE CDXLV: SW potential parameters for stanene used by LAMMPS,⁹ as expressed in Eqs. (9) and (10).

	ϵ (eV)	σ (Å)	a	λ	γ	$\cos \theta_0$	A_L	B_L	p	q	tol
Sn-Sn-Sn	1.000	2.227	1.687	98.863	1.000	-0.362	19.542	1.709	4	0	0.0

TABLE CDXLVI: The VFF model for indiene. The second line gives an explicit expression for each VFF term. The third line is the force constant parameters. Parameters are in the unit of $\frac{\text{eV}}{\text{\AA}^2}$ for the bond stretching interactions, and in the unit of eV for the angle bending interaction. The fourth line gives the initial bond length (in unit of \AA) for the bond stretching interaction and the initial angle (in unit of degrees) for the angle bending interaction.

VFF type	bond stretching	angle bending
expression	$\frac{1}{2}K_r (\Delta r)^2$	$\frac{1}{2}K_\theta (\Delta\theta)^2$
parameter	2.128	1.175
r_0 or θ_0	2.890	94.372

for the stanene. The Poisson's ratios from the VFF model and the SW potential are $\nu_{xy} = \nu_{yx} = 0.29$. The third-order nonlinear elastic constant D can be obtained by fitting the stress-strain relation to $\sigma = E\epsilon + \frac{1}{2}D\epsilon^2$ with E as the Young's modulus. The values of D are -37.2 Nm^{-1} and -69.4 Nm^{-1} at 1 K along the armchair and zigzag directions, respectively. The ultimate stress is about 3.5 Nm^{-1} at the critical strain of 0.32 in the armchair direction at the low temperature of 1 K. The ultimate stress is about 3.6 Nm^{-1} at the critical strain of 0.29 in the zigzag direction at the low temperature of 1 K.

The stress-strain curves shown in Fig. 228 disclose a structural transition for the stanene at the low temperature of 1 K. The critical strain for the structural transition is about 0.15 along the armchair and zigzag directions. The buckled configuration of the stanene is flattened during this structural transition, which can be seen from these two insets in Fig. 228. At temperatures above 300 K, this structural transition is blurred by stronger thermal vibrations; i.e., the buckled configuration of the stanene can be strongly disturbed by the thermal vibration at higher temperatures.

CXII. INDIENE

In this section, we will develop the SW potential for the indiene, i.e., the single layer of Indium atoms. The structure of the indiene is shown in Fig. 222, with structural parameters from the *ab initio* calculations.¹¹² The indiene has a buckled configuration as shown in Fig. 222 (b), where the buckle is along the zigzag direction. The lattice constant is 4.24 \AA

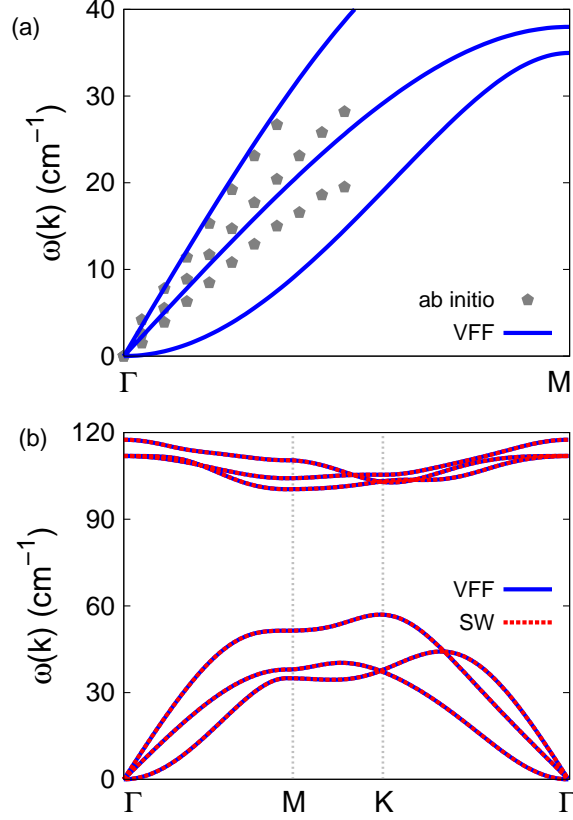


FIG. 229: (Color online) Phonon dispersion for the indiene. (a) The VFF model is fitted to the three acoustic branches in the long wave limit along the ΓM direction. The *ab initio* results (gray pentagons) are from Ref. 112. (b) The VFF model (blue lines) and the SW potential (red lines) give the same phonon dispersion for the indiene along $\Gamma\text{MK}\Gamma$.

TABLE CDXLVII: Two-body SW potential parameters for indiene used by GULP,⁸ as expressed in Eq. (3).

	A (eV)	ρ (\AA)	B (\AA^4)	r_{\min} (\AA)	r_{\max} (\AA)
In-In	1.537	0.946	41.855	0.0	3.565

and the bond length is 2.89 \AA , which results in the buckling height of $h = 1.536 \text{ \AA}$.

Table CDXLVI shows the VFF model for the indiene. The force constant parameters are determined by fitting to the three acoustic branches in the phonon dispersion along the ΓM as shown in Fig. 229 (a). The *ab initio* calculations for the phonon dispersion are from Ref. 112. We note that the lowest-frequency branch around the Γ point from the

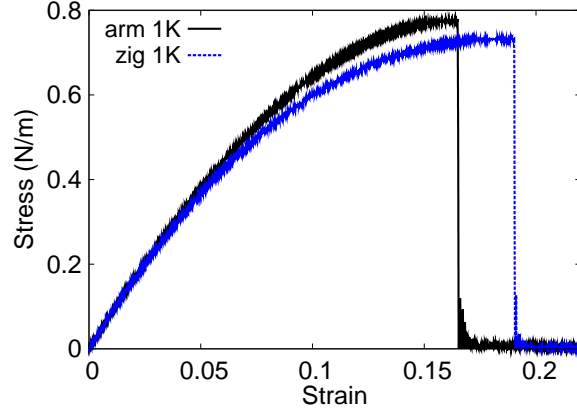


FIG. 230: (Color online) Stress-strain relations for the indiene of size $100 \times 100 \text{ \AA}$. The indiene is uniaxially stretched along the armchair or zigzag directions at temperatures 1 K.

TABLE CDXLVIII: Three-body SW potential parameters for indiene used by GULP,⁸ as expressed in Eq. (4).

	K (eV)	θ_0 (degree)	ρ_1 (\AA)	ρ_2 (\AA)	$r_{\min 12}$ (\AA)	$r_{\max 12}$ (\AA)	$r_{\min 13}$ (\AA)	$r_{\max 13}$ (\AA)	$r_{\min 23}$ (\AA)	$r_{\max 23}$ (\AA)
In-In-In	9.745	94.372	0.946	0.946	0.0	3.565	0.0	4.565	3.565	4.686

VFF model is lower than the *ab initio* results. This branch is the flexural branch, which should be a quadratic dispersion. However, the *ab initio* calculations give a linear dispersion for the flexural branch due to the violation of the rigid rotational invariance in the first-principles package,²⁰ so *ab initio* calculations typically overestimate the frequency of this branch. Fig. 229 (b) shows that the VFF model and the SW potential give exactly the same phonon dispersion, as the SW potential is derived from the VFF model.

The parameters for the two-body SW potential used by GULP are shown in Tab. CDXLVII. The parameters for the three-body SW potential used by GULP are shown in Tab. CDXLVIII. Parameters for the SW potential used by LAMMPS are listed in

TABLE CDXLIX: SW potential parameters for indiene used by LAMMPS,⁹ as expressed in Eqs. (9) and (10).

	ϵ (eV)	σ (\AA)	a	λ	γ	$\cos \theta_0$	A_L	B_L	p	q	tol
In-In-In	1.000	0.946	3.768	9.745	1.000	-0.076	1.537	52.262	4	0	0.0

TABLE CDL: The VFF model for blue phosphorus. The second line gives an explicit expression for each VFF term. The third line is the force constant parameters. Parameters are in the unit of $\frac{\text{eV}}{\text{\AA}^2}$ for the bond stretching interactions, and in the unit of eV for the angle bending interaction. The fourth line gives the initial bond length (in unit of \AA) for the bond stretching interaction and the initial angle (in unit of degrees) for the angle bending interaction.

VFF type	bond stretching	angle bending
expression	$\frac{1}{2}K_r (\Delta r)^2$	$\frac{1}{2}K_\theta (\Delta\theta)^2$
parameter	15.372	5.138
r_0 or θ_0	2.270	94.209

TABLE CDLI: Two-body SW potential parameters for blue phosphorus used by GULP,⁸ as expressed in Eq. (3).

	A (eV)	ρ (\AA)	B (\AA^4)	r_{\min} (\AA)	r_{\max} (\AA)
P-P	5.706	0.491	13.276	0.0	2.798

Tab. CDXLIX.

Fig. 230 shows the stress strain relations for the indiene of size $100 \times 100 \text{\AA}$. The structure is uniaxially stretched in the armchair or zigzag directions at 1 K. The Young's modulus is 8.4 Nm^{-1} in both armchair and zigzag directions at 1 K, which are obtained by linear fitting of the stress strain relations in $[0, 0.01]$. The Young's modulus of the indiene is very small; i.e., the indiene is very soft. As a result, we find that the structure becomes unstable at room temperature. The Poisson's ratios from the VFF model and the SW potential are $\nu_{xy} = \nu_{yx} = 0.18$. The third-order nonlinear elastic constant D can be obtained by fitting the stress-strain relation to $\sigma = E\epsilon + \frac{1}{2}D\epsilon^2$ with E as the Young's modulus. The values of D are -42.0 Nm^{-1} and -50.2 Nm^{-1} at 1 K along the armchair and zigzag directions, respectively. The ultimate stress is about 0.77 Nm^{-1} at the critical strain of 0.16 in the armchair direction at the low temperature of 1 K. The ultimate stress is about 0.73 Nm^{-1} at the critical strain of 0.19 in the zigzag direction at the low temperature of 1 K.

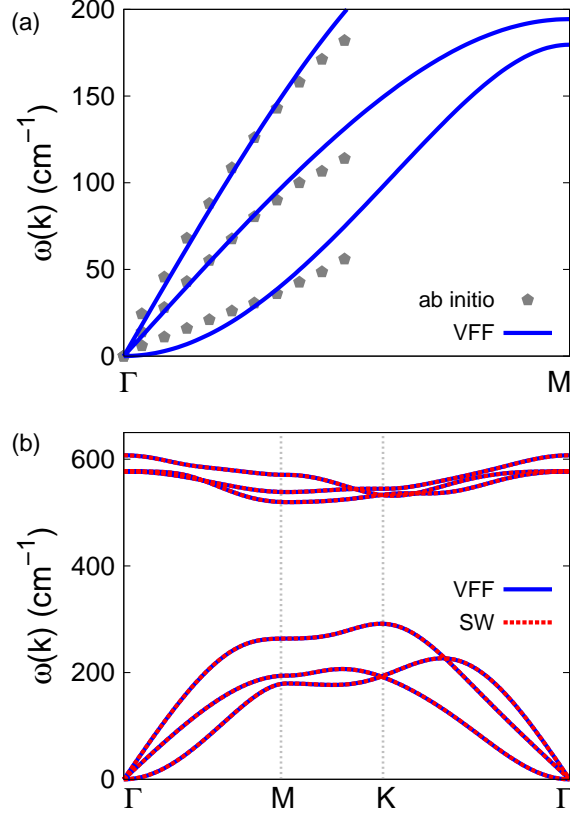


FIG. 231: (Color online) Phonon dispersion for the single-layer blue phosphorus. (a) The VFF model is fitted to the three acoustic branches in the long wave limit along the Γ M direction. The *ab initio* results (gray pentagons) are from Ref. 55. (b) The VFF model (blue lines) and the SW potential (red lines) give the same phonon dispersion for the blue phosphorus along Γ MKT.

TABLE CDLII: Three-body SW potential parameters for blue phosphorus used by GULP,⁸ as expressed in Eq. (4).

	K (eV)	θ_0 (degree)	ρ_1 (\AA)	ρ_2 (\AA)	$r_{\min 12}$ (\AA)	$r_{\max 12}$ (\AA)	$r_{\min 13}$ (\AA)	$r_{\max 13}$ (\AA)	$r_{\min 23}$ (\AA)	$r_{\max 23}$ (\AA)
P-P-P	16.605	94.209	0.491	0.491	0.0	2.798	0.0	2.798	2.798	3.677

CXIII. BLUE PHOSPHORUS

The blue phosphorus is also named β -phosphorus. Present studies on the blue phosphorus are based on first-principles calculations, and no empirical potential has been proposed for the blue phosphorus. We will thus parametrize a set of VFF model for the single-layer blue

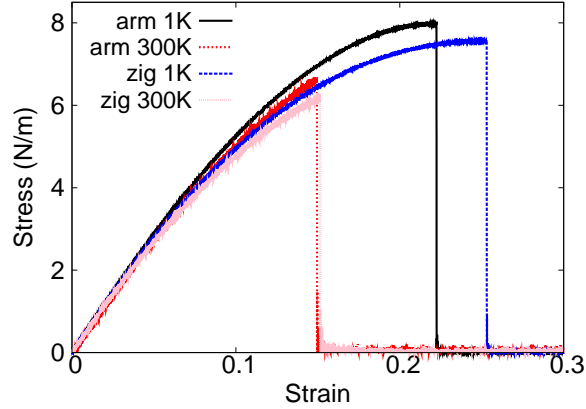


FIG. 232: (Color online) Stress-strain relations for the blue phosphorus of size $100 \times 100 \text{ \AA}$. The blue phosphorus is uniaxially stretched along the armchair or zigzag directions at temperatures 1 K and 300 K.

TABLE CDLIII: SW potential parameters for blue phosphorus used by LAMMPS,⁹ as expressed in Eqs. (9) and (10).

	ϵ (eV)	σ (\AA)	a	λ	γ	$\cos \theta_0$	A_L	B_L	p	q	tol
P-P-P	1.000	0.491	5.699	16.605	1.000	-0.073	5.706	228.424	4	0	0.0

phosphorus in this section. We will also derive the SW potential based on the VFF model for the single-layer blue phosphorus.

The structure of the single-layer blue phosphorus is shown in Fig. 222, with structural parameters from the *ab initio* calculations.⁵⁵ The blue phosphorus has a buckled configuration as shown in Fig. 222 (b), where the buckle is along the zigzag direction. The height of the buckle is $h = 1.211 \text{ \AA}$. The lattice constant is 3.326 \AA , and the bond length is 2.270 \AA .

Table CDL shows the VFF model for the single-layer blue phosphorus. The force constant parameters are determined by fitting to the three acoustic branches in the phonon dispersion along the Γ M as shown in Fig. 231 (a). The *ab initio* calculations for the phonon dispersion are from Ref. 55. Similar phonon dispersion can also be found in other *ab initio* calculations.^{61,64,84} Fig. 231 (b) shows that the VFF model and the SW potential give exactly the same phonon dispersion, as the SW potential is derived from the VFF model.

The parameters for the two-body SW potential used by GULP are shown in Tab. CDLI. The parameters for the three-body SW potential used by GULP are shown in Tab. CDLII.

TABLE CDLIV: The VFF model for b-arsenene. The second line gives an explicit expression for each VFF term. The third line is the force constant parameters. Parameters are in the unit of $\frac{\text{eV}}{\text{\AA}^2}$ for the bond stretching interactions, and in the unit of eV for the angle bending interaction. The fourth line gives the initial bond length (in unit of \AA) for the bond stretching interaction and the initial angle (in unit of degrees) for the angle bending interaction.

VFF type	bond stretching	angle bending
expression	$\frac{1}{2}K_r (\Delta r)^2$	$\frac{1}{2}K_\theta (\Delta\theta)^2$
parameter	15.372	5.138
r_0 or θ_0	2.510	91.964

TABLE CDLV: Two-body SW potential parameters for b-arsenene used by GULP,⁸ as expressed in Eq. (3).

	A (eV)	ρ (\AA)	B (\AA^4)	r_{\min} (\AA)	r_{\max} (\AA)
As-As	6.418	0.482	19.846	0.0	3.060

Parameters for the SW potential used by LAMMPS are listed in Tab. CDLIII.

Fig. 232 shows the stress strain relations for the single-layer blue phosphorus of size $100 \times 100 \text{\AA}$. The structure is uniaxially stretched in the armchair or zigzag directions at 1 K and 300 K. The Young's modulus is 60.5 Nm^{-1} and 60.6 Nm^{-1} in the armchair and zigzag directions respectively at 1 K, which are obtained by linear fitting of the stress strain relations in $[0, 0.01]$. The Young's modulus is isotropic for the blue phosphorus. The Poisson's ratios from the VFF model and the SW potential are $\nu_{xy} = \nu_{yx} = 0.18$. The third-order nonlinear elastic constant D can be obtained by fitting the stress-strain relation to $\sigma = E\epsilon + \frac{1}{2}D\epsilon^2$ with E as the Young's modulus. The values of D are -195.3 Nm^{-1} and -237.0 Nm^{-1} at 1 K along the armchair and zigzag directions, respectively. The ultimate stress is about 8.0 Nm^{-1} at the critical strain of 0.22 in the armchair direction at the low temperature of 1 K. The ultimate stress is about 7.6 Nm^{-1} at the critical strain of 0.25 in the zigzag direction at the low temperature of 1 K.

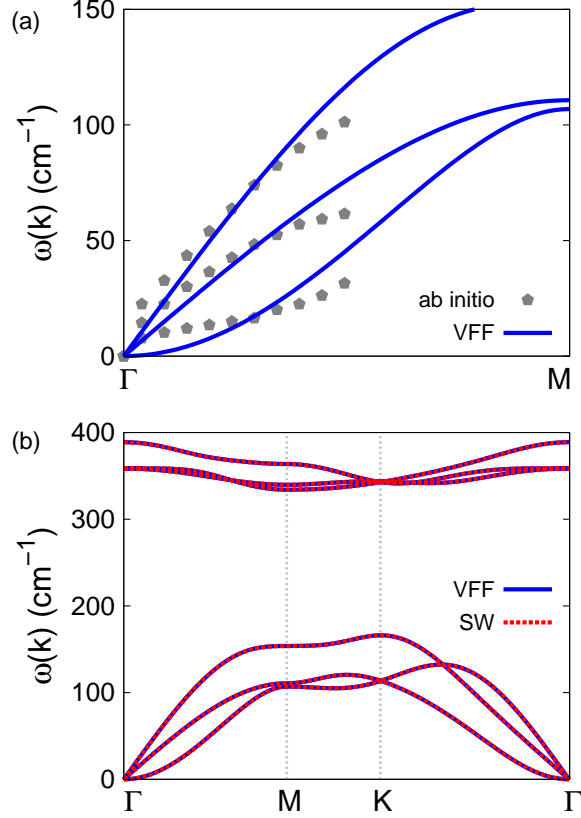


FIG. 233: (Color online) Phonon dispersion for the single-layer b-arsenene. (a) The VFF model is fitted to the three acoustic branches in the long wave limit along the Γ M direction. The *ab initio* results (gray pentagons) are from Ref. 70. (b) The VFF model (blue lines) and the SW potential (red lines) give the same phonon dispersion for the b-arsenene along Γ MK Γ .

TABLE CDLVI: Three-body SW potential parameters for b-arsenene used by GULP,⁸ as expressed in Eq. (4).

	K (eV)	θ_0 (degree)	ρ_1 (\AA)	ρ_2 (\AA)	$r_{\min 12}$ (\AA)	$r_{\max 12}$ (\AA)	$r_{\min 13}$ (\AA)	$r_{\max 13}$ (\AA)	$r_{\min 23}$ (\AA)	$r_{\max 23}$ (\AA)
As-As-As	14.845	91.964	0.482	0.482	0.0	3.060	0.0	3.060	3.060	4.004

CXIV. B-ARSENENE

Present studies on the buckled (b-) arsenene, which is also named β arsenene, are based on first-principles calculations, and no empirical potential has been proposed for the b-arsenene. We will thus parametrize a set of VFF model for the single-layer b-arsenene in this section.

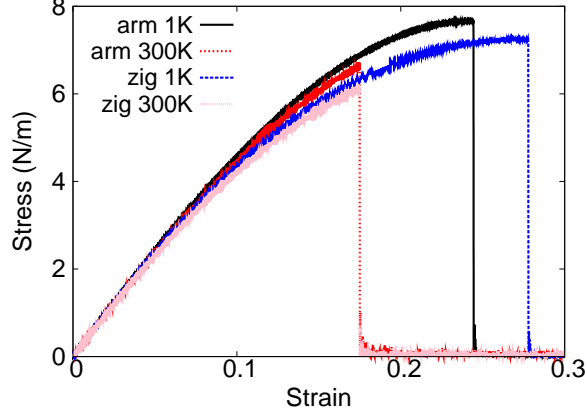


FIG. 234: (Color online) Stress-strain relations for the b-arsenene of size $100 \times 100 \text{ \AA}$. The b-arsenene is uniaxially stretched along the armchair or zigzag directions at temperatures 1 K and 300 K.

TABLE CDLVII: SW potential parameters for b-arsenene used by LAMMPS,⁹ as expressed in Eqs. (9) and (10).

	ϵ (eV)	σ (\AA)	a	λ	γ	$\cos \theta_0$	A_L	B_L	p	q	tol
As-As-As	1.000	0.482	6.349	14.845	1.000	-0.034	6.418	367.693	4	0	0.0

We will also derive the SW potential based on the VFF model for the single-layer b-arsenene.

The structure of the single-layer b-arsenene is shown in Fig. 222, with structural parameters from the *ab initio* calculations.⁷⁰ The b-arsenene has a buckled configuration as shown in Fig. 222 (b), where the buckle is along the zigzag direction. The height of the buckle is $h = 1.40 \text{ \AA}$. The lattice constant is 3.61 \AA , and the bond length is 2.51 \AA .

Table CDLIV shows the VFF model for the single-layer b-arsenene. The force constant parameters are determined by fitting to the three acoustic branches in the phonon dispersion along the ΓM as shown in Fig. 233 (a). The *ab initio* calculations for the phonon dispersion are from Ref. 70. Similar phonon dispersion can also be found in other *ab initio* calculations.^{64,72,73} We note that the lowest-frequency branch around the Γ point from the VFF model is lower than the *ab initio* results. This branch is the flexural branch, which should be a quadratic dispersion. However, the *ab initio* calculations give a linear dispersion for the flexural branch due to the violation of the rigid rotational invariance in the first-principles package,²⁰ so *ab initio* calculations typically overestimate the frequency of this

TABLE CDLVIII: The VFF model for b-antimonene. The second line gives an explicit expression for each VFF term. The third line is the force constant parameters. Parameters are in the unit of $\frac{\text{eV}}{\text{\AA}^2}$ for the bond stretching interactions, and in the unit of eV for the angle bending interaction. The fourth line gives the initial bond length (in unit of \AA) for the bond stretching interaction and the initial angle (in unit of degrees) for the angle bending interaction.

VFF type	bond stretching	angle bending
expression	$\frac{1}{2}K_r (\Delta r)^2$	$\frac{1}{2}K_\theta (\Delta\theta)^2$
parameter	15.372	5.138
r_0 or θ_0	2.890	90.927

branch. Fig. 233 (b) shows that the VFF model and the SW potential give exactly the same phonon dispersion, as the SW potential is derived from the VFF model.

The parameters for the two-body SW potential used by GULP are shown in Tab. CDLV. The parameters for the three-body SW potential used by GULP are shown in Tab. CDLVI. Parameters for the SW potential used by LAMMPS are listed in Tab. CDLVII.

Fig. 234 shows the stress strain relations for the single-layer b-arsenene of size $100 \times 100 \text{\AA}$. The structure is uniaxially stretched in the armchair or zigzag directions at 1 K and 300 K. The Young's modulus is 50.8 Nm^{-1} and 49.9 Nm^{-1} in the armchair and zigzag directions respectively at 1 K, which are obtained by linear fitting of the stress strain relations in $[0, 0.01]$. The Young's modulus is isotropic for the b-arsenene. The Poisson's ratios from the VFF model and the SW potential are $\nu_{xy} = \nu_{yx} = 0.21$. The third-order nonlinear elastic constant D can be obtained by fitting the stress-strain relation to $\sigma = E\epsilon + \frac{1}{2}D\epsilon^2$ with E as the Young's modulus. The values of D are -127.6 Nm^{-1} and -153.6 Nm^{-1} at 1 K along the armchair and zigzag directions, respectively. The ultimate stress is about 7.6 Nm^{-1} at the critical strain of 0.24 in the armchair direction at the low temperature of 1 K. The ultimate stress is about 7.2 Nm^{-1} at the critical strain of 0.28 in the zigzag direction at the low temperature of 1 K.

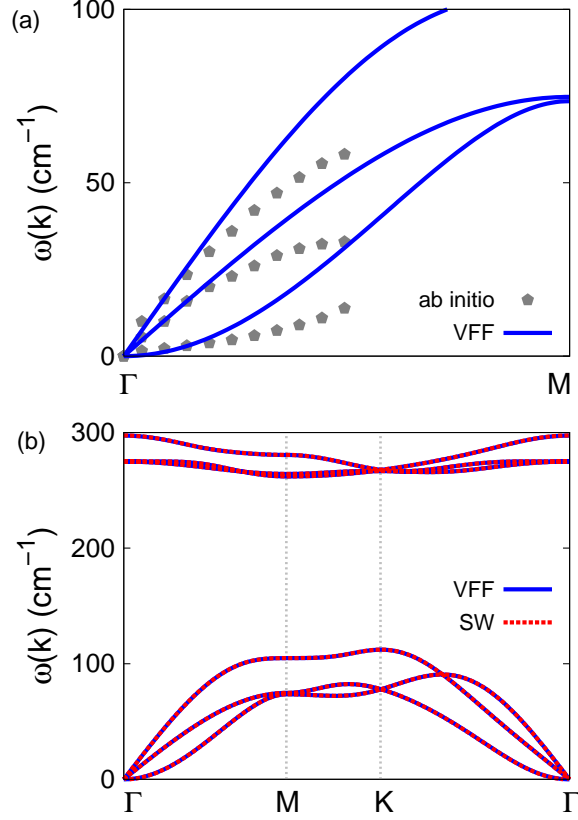


FIG. 235: (Color online) Phonon dispersion for the single-layer b-antimonene. (a) The VFF model is fitted to the three acoustic branches in the long wave limit along the ΓM direction. The *ab initio* results (gray pentagons) are from Ref. 70. (b) The VFF model (blue lines) and the SW potential (red lines) give the same phonon dispersion for the b-antimonene along $\Gamma\text{MKT}\Gamma$.

TABLE CDLIX: Two-body SW potential parameters for b-antimonene used by GULP,⁸ as expressed in Eq. (3).

	A (eV)	ρ (\AA)	B (\AA^4)	r_{min} (\AA)	r_{max} (\AA)
Sb-Sb	8.173	0.523	34.879	0.0	3.505

CXV. B-ANTIMONENE

The buckled (b-) antimonene is a Sb allotrope, which is also named β antimonene. Present studies on the b-antimonene are based on first-principles calculations, and no empirical potential has been proposed for the b-antimonene. We will thus parametrize a set of VFF

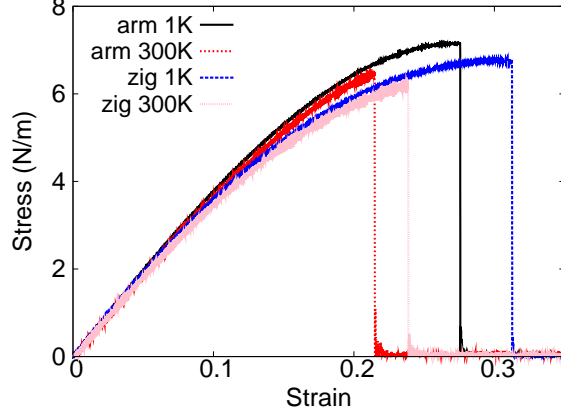


FIG. 236: (Color online) Stress-strain relations for the b-antimonene of size $100 \times 100 \text{ \AA}$. The b-antimonene is uniaxially stretched along the armchair or zigzag directions at temperatures 1 K and 300 K.

TABLE CDLX: Three-body SW potential parameters for b-antimonene used by GULP,⁸ as expressed in Eq. (4).

	K (eV)	θ_0 (degree)	ρ_1 (\AA)	ρ_2 (\AA)	$r_{\min 12}$ (\AA)	$r_{\max 12}$ (\AA)	$r_{\min 13}$ (\AA)	$r_{\max 13}$ (\AA)	$r_{\min 23}$ (\AA)	$r_{\max 23}$ (\AA)
Sb-Sb-Sb	14.100	90.927	0.523	0.523	0.0	3.505	0.0	3.503	3.505	4.577

model for the single-layer b-antimonene in this section. We will also derive the SW potential based on the VFF model for the single-layer b-antimonene.

The structure of the single-layer b-antimonene is shown in Fig. 222, with structural parameters from the *ab initio* calculations.⁷⁰ The b-antimonene has a buckled configuration as shown in Fig. 222 (b), where the buckle is along the zigzag direction. The height of the buckle is $h = 1.65 \text{ \AA}$. The lattice constant is 4.12 \AA , and the bond length is 2.89 \AA .

Table CDLVIII shows the VFF model for the single-layer b-antimonene. The force constant parameters are determined by fitting to the three acoustic branches in the phonon

TABLE CDLXI: SW potential parameters for b-antimonene used by LAMMPS,⁹ as expressed in Eqs. (9) and (10).

	ϵ (eV)	σ (\AA)	a	λ	γ	$\cos \theta_0$	A_L	B_L	p	q	tol
Sb-Sb-Sb	1.000	0.523	6.702	14.100	1.000	-0.016	8.173	466.184	4	0	0.0

TABLE CDLXII: The VFF model for b-bismuthene. The second line gives an explicit expression for each VFF term. The third line is the force constant parameters. Parameters are in the unit of $\frac{\text{eV}}{\text{\AA}^2}$ for the bond stretching interactions, and in the unit of eV for the angle bending interaction. The fourth line gives the initial bond length (in unit of \AA) for the bond stretching interaction and the initial angle (in unit of degrees) for the angle bending interaction.

VFF type	bond stretching	angle bending
expression	$\frac{1}{2}K_r (\Delta r)^2$	$\frac{1}{2}K_\theta (\Delta\theta)^2$
parameter	11.529	3.853
r_0 or θ_0	3.045	90.901

dispersion along the ΓM as shown in Fig. 235 (a). The *ab initio* calculations for the phonon dispersion are from Ref. 70. Similar phonon dispersion can also be found in other *ab initio* calculations.^{64,72,73} Fig. 235 (b) shows that the VFF model and the SW potential give exactly the same phonon dispersion, as the SW potential is derived from the VFF model.

The parameters for the two-body SW potential used by GULP are shown in Tab. CDLIX. The parameters for the three-body SW potential used by GULP are shown in Tab. CDLX. Parameters for the SW potential used by LAMMPS are listed in Tab. CDLXI.

Fig. 236 shows the stress strain relations for the single-layer b-antimonene of size $100 \times 100 \text{\AA}$. The structure is uniaxially stretched in the armchair or zigzag directions at 1 K and 300 K. The Young's modulus is 39.6 Nm^{-1} in both armchair and zigzag directions at 1 K, which are obtained by linear fitting of the stress strain relations in $[0, 0.01]$. The Young's modulus is isotropic for the b-antimonene. The Poisson's ratios from the VFF model and the SW potential are $\nu_{xy} = \nu_{yx} = 0.24$. The third-order nonlinear elastic constant D can be obtained by fitting the stress-strain relation to $\sigma = E\epsilon + \frac{1}{2}D\epsilon^2$ with E as the Young's modulus. The values of D are -62.6 Nm^{-1} and -91.5 Nm^{-1} at 1 K along the armchair and zigzag directions, respectively. The ultimate stress is about 7.1 Nm^{-1} at the critical strain of 0.28 in the armchair direction at the low temperature of 1 K. The ultimate stress is about 6.7 Nm^{-1} at the critical strain of 0.31 in the zigzag direction at the low temperature of 1 K.

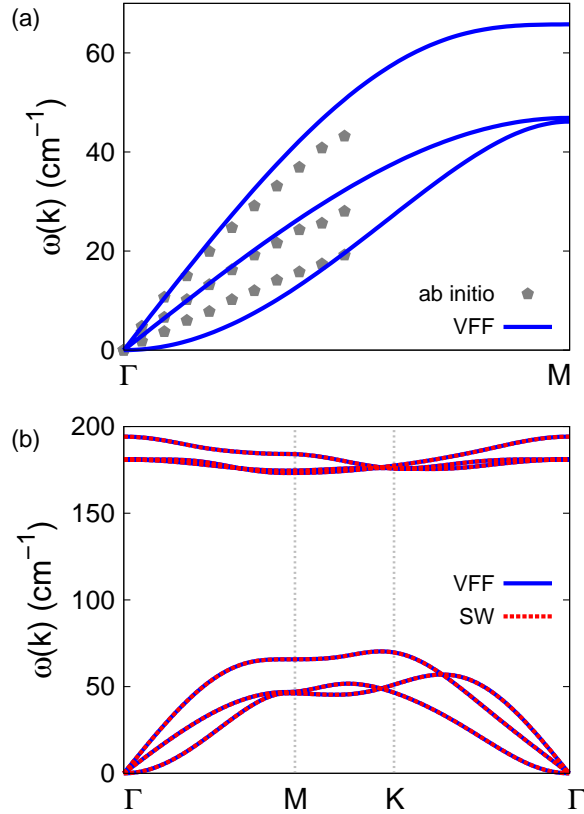


FIG. 237: (Color online) Phonon dispersion for the single-layer b-bismuthene. (a) The VFF model is fitted to the three acoustic branches in the long wave limit along the ΓM direction. The *ab initio* results (gray pentagons) are from Ref. 64. (b) The VFF model (blue lines) and the SW potential (red lines) give the same phonon dispersion for the b-bismuthene along $\Gamma M K \Gamma$.

TABLE CDLXIII: Two-body SW potential parameters for b-bismuthene used by GULP,⁸ as expressed in Eq. (3).

	A (eV)	ρ (\AA)	B (\AA^4)	r_{\min} (\AA)	r_{\max} (\AA)
Bi-Bi	6.805	0.552	42.985	0.0	3.693

CXVI. B-BISMUTHENE

The buckled (b-) bismuthene is a Bi allotrope, which is also named *beta* bismuthene. Most studies on the b-bismuthene are based on first-principles calculations, while a modified Morse potential was proposed for the b-bismuthene in 2013.¹¹³ We will parametrize a set of VFF

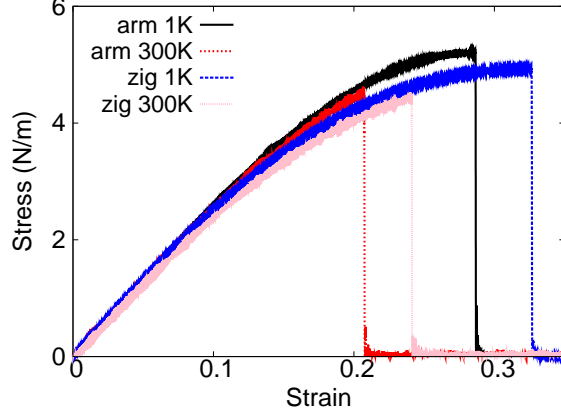


FIG. 238: (Color online) Stress-strain relations for the b-bismuthene of size $100 \times 100 \text{ \AA}$. The b-bismuthene is uniaxially stretched along the armchair or zigzag directions at temperatures 1 K and 300 K.

TABLE CDLXIV: Three-body SW potential parameters for b-bismuthene used by GULP,⁸ as expressed in Eq. (4).

	K (eV)	θ_0 (degree)	ρ_1 (\AA)	ρ_2 (\AA)	$r_{\min 12}$ (\AA)	$r_{\max 12}$ (\AA)	$r_{\min 13}$ (\AA)	$r_{\max 13}$ (\AA)	$r_{\min 23}$ (\AA)	$r_{\max 23}$ (\AA)
Bi-Bi-Bi	10.574	90.901	0.552	0.552	0.0	3.693	0.0	3.693	3.693	4.821

model for the single-layer b-bismuthene in this section. We will also derive the SW potential based on the VFF model for the single-layer b-bismuthene.

The structure of the single-layer b-bismuthene is shown in Fig. 222, with structural parameters from the *ab initio* calculations.⁷⁰ The b-bismuthene has a buckled configuration as shown in Fig. 222 (b), where the buckle is along the zigzag direction. The height of the buckle is $h = 1.73 \text{ \AA}$. The lattice constant is 4.34 \AA , and the bond length is 3.045 \AA .

Table CDLXII shows the VFF model for the single-layer b-bismuthene. The force constant parameters are determined by fitting to the three acoustic branches in the phonon

TABLE CDLXV: SW potential parameters for b-bismuthene used by LAMMPS,⁹ as expressed in Eqs. (9) and (10).

	ϵ (eV)	σ (\AA)	a	λ	γ	$\cos \theta_0$	A_L	B_L	p	q	tol
Bi-Bi-Bi	1.000	0.552	6.690	10.574	1.000	-0.016	6.805	462.978	4	0	0.0

dispersion along the Γ M as shown in Fig. 237 (a). The *ab initio* calculations for the phonon dispersion are from Ref. 64. Similar phonon dispersion can also be found in other *ab initio* calculations.⁷⁷ We note that the lowest-frequency branch around the Γ point from the VFF model is lower than the *ab initio* results. This branch is the flexural branch, which should be a quadratic dispersion. However, the *ab initio* calculations give a linear dispersion for the flexural branch due to the violation of the rigid rotational invariance in the first-principles package,²⁰ so *ab initio* calculations typically overestimate the frequency of this branch. Fig. 237 (b) shows that the VFF model and the SW potential give exactly the same phonon dispersion, as the SW potential is derived from the VFF model.

The parameters for the two-body SW potential used by GULP are shown in Tab. CDLXIII. The parameters for the three-body SW potential used by GULP are shown in Tab. CDLXIV. Parameters for the SW potential used by LAMMPS are listed in Tab. CDLXV.

Fig. 238 shows the stress strain relations for the single-layer b-bismuthene of size 100×100 Å. The structure is uniaxially stretched in the armchair or zigzag directions at 1 K and 300 K. The Young's modulus is 27.0 Nm^{-1} in both armchair and zigzag directions at 1 K, which are obtained by linear fitting of the stress strain relations in $[0, 0.01]$. The Young's modulus is isotropic for the b-bismuthene. The value of the Young's modulus is close to the value of 23.9 Nm^{-1} from the *ab initio* calculations.⁷⁷ The Poisson's ratios from the VFF model and the SW potential are $\nu_{xy} = \nu_{yx} = 0.25$, which are comparable with the *ab initio* results of 0.327.⁷⁷ The third-order nonlinear elastic constant D can be obtained by fitting the stress-strain relation to $\sigma = E\epsilon + \frac{1}{2}D\epsilon^2$ with E as the Young's modulus. The values of D are -34.3 Nm^{-1} and -54.5 Nm^{-1} at 1 K along the armchair and zigzag directions, respectively. The ultimate stress is about 5.2 Nm^{-1} at the critical strain of 0.29 in the armchair direction at the low temperature of 1 K. The ultimate stress is about 4.9 Nm^{-1} at the critical strain of 0.33 in the zigzag direction at the low temperature of 1 K.

CXVII. B-CO

Present studies on the buckled (b-) CO are based on first-principles calculations, and no empirical potential has been proposed for the b-CO. We will thus parametrize a set of SW potential for the single-layer b-CO in this section.

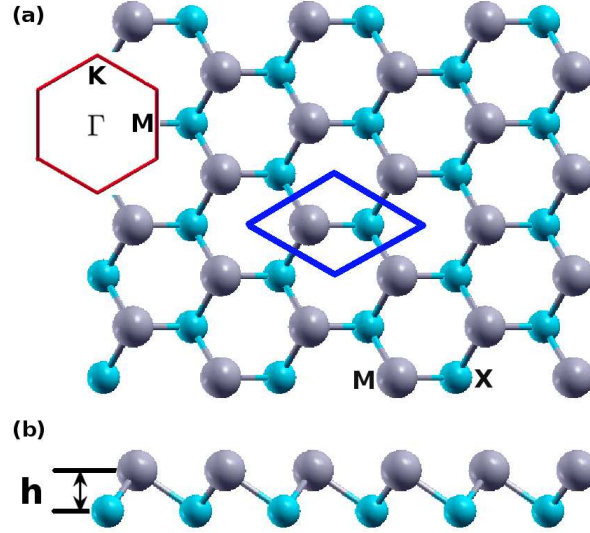


FIG. 239: (Color online) Structure for single-layer buckled MX (b-MX), with M from group IV and X from group VI, or both M and X from group IV, or M from group III and X from group V. (a) Top view. The armchair direction is along the horizontal direction, while the zigzag direction is along the vertical direction. The unit cell is displayed by the blue rhombus. Inset shows the first Brillouin zone. (b) Side view illustrates the buckled configuration of height h .

TABLE CDLXVI: The VFF model for b-CO. The second line gives an explicit expression for each VFF term. The third line is the force constant parameters. Parameters are in the unit of $\frac{\text{eV}}{\text{\AA}^2}$ for the bond stretching interactions, and in the unit of eV for the angle bending interaction. The fourth line gives the initial bond length (in unit of \AA) for the bond stretching interaction and the initial angle (in unit of degrees) for the angle bending interaction.

VFF type	bond stretching	angle bending
expression	$\frac{1}{2}K_r (\Delta r)^2$	$\frac{1}{2}K_\theta (\Delta \theta)^2$
parameter	16.063	5.221
r_0 or θ_0	1.636	97.181

The structure of the single-layer b-CO is shown in Fig. 239. The structural parameters are from the *ab initio* calculations.⁷⁸ The b-CO has a buckled configuration as shown in Fig. 239 (b), where the buckle is along the zigzag direction. This structure can be determined by two independent geometrical parameters, including the lattice constant 2.454 \AA and the

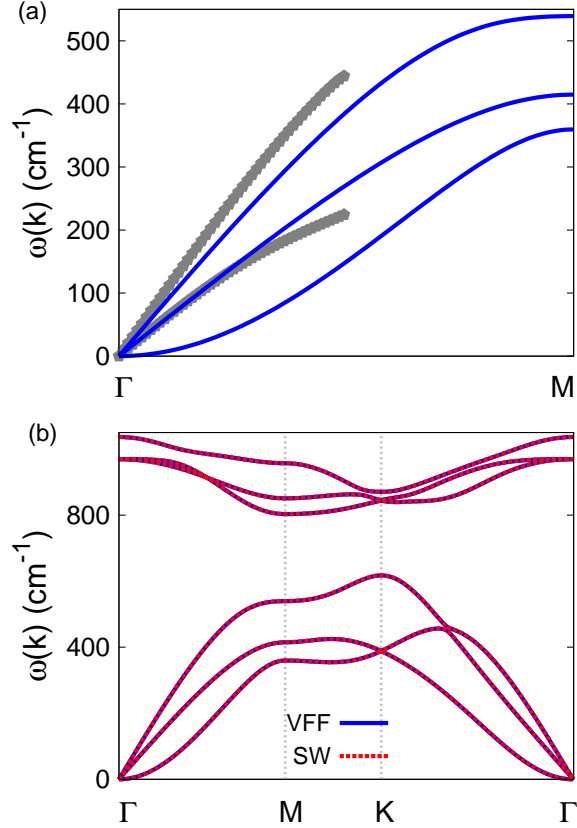


FIG. 240: (Color online) Phonon dispersion for the single-layer b-CO. (a) The VFF model is fitted to the two in-plane acoustic branches in the long wave limit along the Γ M direction. The *ab initio* results (gray pentagons) are calculated from SIESTA. (b) The VFF model (blue lines) and the SW potential (red lines) give the same phonon dispersion for the b-CO along Γ MK Γ .

TABLE CDLXVII: Two-body SW potential parameters for b-CO used by GULP,⁸ as expressed in Eq. (3).

	A (eV)	ρ (\AA)	B (\AA^4)	r_{\min} (\AA)	r_{\max} (\AA)
C-O	7.656	1.054	3.582	0.0	2.293

bond length 1.636 \AA .

Table CDLXVI shows the VFF model for the single-layer b-CO. The force constant parameters are determined by fitting to the acoustic branches in the phonon dispersion along the Γ M as shown in Fig. 240 (a). The *ab initio* calculations for the phonon dispersion are calculated from the SIESTA package.⁷⁹ The generalized gradients approximation is ap-

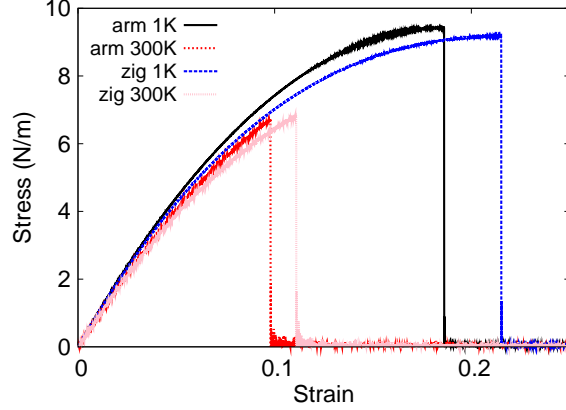


FIG. 241: (Color online) Stress-strain relations for the b-CO of size $100 \times 100 \text{ \AA}$. The b-CO is uniaxially stretched along the armchair or zigzag directions at temperatures 1 K and 300 K.

TABLE CDLXVIII: Three-body SW potential parameters for b-CO used by GULP,⁸ as expressed in Eq. (4).

	K (eV)	θ_0 (degree)	ρ_1 (\AA)	ρ_2 (\AA)	$r_{\min 12}$ (\AA)	$r_{\max 12}$ (\AA)	$r_{\min 13}$ (\AA)	$r_{\max 13}$ (\AA)	$r_{\min 23}$ (\AA)	$r_{\max 23}$ (\AA)
C-O-O	65.778	97.181	1.054	1.054	0.0	2.293	0.0	2.293	0.0	3.352
O-C-C	65.778	97.181	1.054	1.054	0.0	2.293	0.0	2.293	0.0	3.352

plied to account for the exchange-correlation function with Perdew, Burke, and Ernzerhof parameterization,⁸⁰ and the double- ζ orbital basis set is adopted. Fig. 240 (b) shows that the VFF model and the SW potential give exactly the same phonon dispersion, as the SW potential is derived from the VFF model.

The parameters for the two-body SW potential used by GULP are shown in Tab. CDLXVII. The parameters for the three-body SW potential used by GULP are shown in Tab. CDLXVIII. Parameters for the SW potential used by LAMMPS are listed in

TABLE CDLXIX: SW potential parameters for b-CO used by LAMMPS,⁹ as expressed in Eqs. (9) and (10).

	ϵ (eV)	σ (\AA)	a	λ	γ	$\cos \theta_0$	A_L	B_L	p	q	tol
C-O-O	1.000	1.054	2.175	65.778	1.000	-0.125	7.812	2.900	4	0	0.0
O-C-C	1.000	1.054	2.175	65.778	1.000	-0.125	7.812	2.900	4	0	0.0

Tab. CDLXIX.

We use LAMMPS to perform MD simulations for the mechanical behavior of the single-layer b-CO under uniaxial tension at 1.0 K and 300.0 K. Fig. 241 shows the stress-strain curve for the tension of a single-layer b-CO of dimension $100 \times 100 \text{ \AA}$. Periodic boundary conditions are applied in both armchair and zigzag directions. The single-layer b-CO is stretched uniaxially along the armchair or zigzag direction. The stress is calculated without involving the actual thickness of the quasi-two-dimensional structure of the single-layer b-CO. The Young's modulus can be obtained by a linear fitting of the stress-strain relation in the small strain range of $[0, 0.01]$. The Young's modulus are 99.1 N/m and 98.8 N/m along the armchair and zigzag directions, respectively. The Young's modulus is essentially isotropic in the armchair and zigzag directions. The Poisson's ratio from the VFF model and the SW potential is $\nu_{xy} = \nu_{yx} = 0.08$.

There is no available value for nonlinear quantities in the single-layer b-CO. We have thus used the nonlinear parameter $B = 0.5d^4$ in Eq. (5), which is close to the value of B in most materials. The value of the third order nonlinear elasticity D can be extracted by fitting the stress-strain relation to the function $\sigma = E\epsilon + \frac{1}{2}D\epsilon^2$ with E as the Young's modulus. The values of D from the present SW potential are -513.8 N/m and -542.0 N/m along the armchair and zigzag directions, respectively. The ultimate stress is about 9.4 Nm^{-1} at the ultimate strain of 0.18 in the armchair direction at the low temperature of 1 K. The ultimate stress is about 9.2 Nm^{-1} at the ultimate strain of 0.21 in the zigzag direction at the low temperature of 1 K.

CXVIII. B-CS

Present studies on the buckled (b-) CS are based on first-principles calculations, and no empirical potential has been proposed for the b-CS. We will thus parametrize a set of SW potential for the single-layer b-CS in this section.

The structure of the single-layer b-CS is shown in Fig. 239. The structural parameters are from the *ab initio* calculations.⁷⁸ The b-CS has a buckled configuration as shown in Fig. 239 (b), where the buckle is along the zigzag direction. This structure can be determined by two independent geometrical parameters, including the lattice constant 2.836 \AA and the bond length 1.880 \AA .

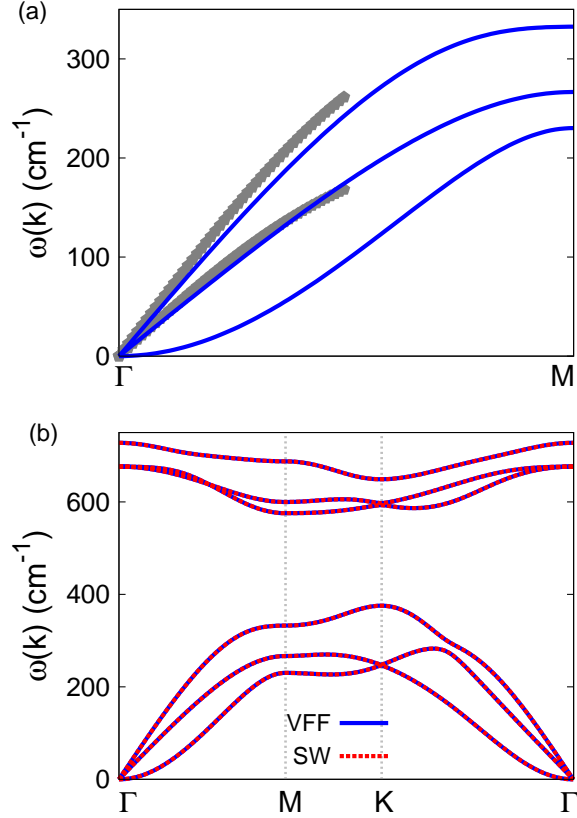


FIG. 242: (Color online) Phonon dispersion for the single-layer b-CS. (a) The VFF model is fitted to the two in-plane acoustic branches in the long wave limit along the Γ M direction. The *ab initio* results (gray pentagons) are calculated from SIESTA. (b) The VFF model (blue lines) and the SW potential (red lines) give the same phonon dispersion for the b-CS along Γ MK Γ .

Table CDLXX shows the VFF model for the single-layer b-CS. The force constant parameters are determined by fitting to the acoustic branches in the phonon dispersion along the Γ M as shown in Fig. 242 (a). The *ab initio* calculations for the phonon dispersion are calculated from the SIESTA package.⁷⁹ The generalized gradients approximation is applied to account for the exchange-correlation function with Perdew, Burke, and Ernzerhof parameterization,⁸⁰ and the double- ζ orbital basis set is adopted. Fig. 242 (b) shows that the VFF model and the SW potential give exactly the same phonon dispersion, as the SW potential is derived from the VFF model.

The parameters for the two-body SW potential used by GULP are shown in Tab. CDLXXI. The parameters for the three-body SW potential used by GULP are shown

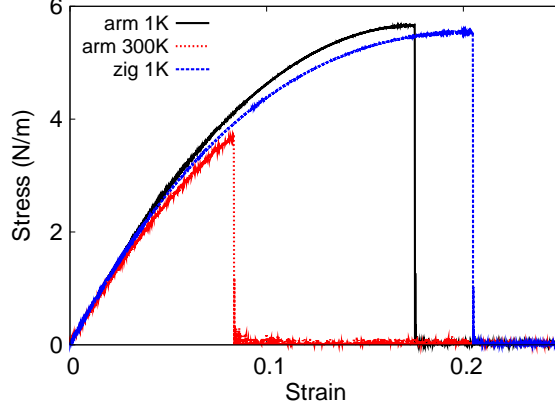


FIG. 243: (Color online) Stress-strain relations for the b-CS of size $100 \times 100 \text{ \AA}$. The b-CS is uniaxially stretched along the armchair or zigzag directions at temperatures 1 K and 300 K.

TABLE CDLXX: The VFF model for b-CS. The second line gives an explicit expression for each VFF term. The third line is the force constant parameters. Parameters are in the unit of $\frac{\text{eV}}{\text{\AA}^2}$ for the bond stretching interactions, and in the unit of eV for the angle bending interaction. The fourth line gives the initial bond length (in unit of \AA) for the bond stretching interaction and the initial angle (in unit of degrees) for the angle bending interaction.

VFF type	bond stretching	angle bending
expression	$\frac{1}{2}K_r(\Delta r)^2$	$\frac{1}{2}K_\theta(\Delta\theta)^2$
parameter	9.390	4.722
r_0 or θ_0	1.880	97.921

in Tab. CDLXXII. Parameters for the SW potential used by LAMMPS are listed in Tab. CDLXXIII.

We use LAMMPS to perform MD simulations for the mechanical behavior of the single-layer b-CS under uniaxial tension at 1.0 K and 300.0 K. Fig. 243 shows the stress-strain

TABLE CDLXXI: Two-body SW potential parameters for b-CS used by GULP,⁸ as expressed in Eq. (3).

	A (eV)	ρ (\AA)	B (\AA^4)	r_{\min} (\AA)	r_{\max} (\AA)
C-S	6.014	1.233	6.246	0.0	2.641

TABLE CDLXXII: Three-body SW potential parameters for b-CS used by GULP,⁸ as expressed in Eq. (4).

	K (eV)	θ_0 (degree)	ρ_1 (Å)	ρ_2 (Å)	$r_{\min 12}$ (Å)	$r_{\max 12}$ (Å)	$r_{\min 13}$ (Å)	$r_{\max 13}$ (Å)	$r_{\min 23}$ (Å)	$r_{\max 23}$ (Å)
C-S-S	61.413	97.921	1.233	1.233	0.0	2.641	0.0	2.641	0.0	3.874
S-C-C	61.413	97.921	1.233	1.233	0.0	2.641	0.0	2.641	0.0	3.874

TABLE CDLXXIII: SW potential parameters for b-CS used by LAMMPS,⁹ as expressed in Eqs. (9) and (10).

	ϵ (eV)	σ (Å)	a	λ	γ	$\cos \theta_0$	A_L	B_L	p	q	tol
C-S-S	1.000	1.233	2.142	61.413	1.000	-0.138	6.014	2.703	4	0	0.0
S-C-C	1.000	1.233	2.142	61.413	1.000	-0.138	6.014	2.703	4	0	0.0

curve for the tension of a single-layer b-CS of dimension 100×100 Å. Periodic boundary conditions are applied in both armchair and zigzag directions. The single-layer b-CS is stretched uniaxially along the armchair or zigzag direction. The stress is calculated without involving the actual thickness of the quasi-two-dimensional structure of the single-layer b-CS. The Young's modulus can be obtained by a linear fitting of the stress-strain relation in the small strain range of $[0, 0.01]$. The Young's modulus are 63.5 N/m and 63.6 N/m along the armchair and zigzag directions, respectively. The Young's modulus is essentially isotropic in the armchair and zigzag directions. The Poisson's ratio from the VFF model and the SW potential is $\nu_{xy} = \nu_{yx} = 0.05$.

There is no available value for nonlinear quantities in the single-layer b-CS. We have thus used the nonlinear parameter $B = 0.5d^4$ in Eq. (5), which is close to the value of B in most materials. The value of the third order nonlinear elasticity D can be extracted by fitting the stress-strain relation to the function $\sigma = E\epsilon + \frac{1}{2}D\epsilon^2$ with E as the Young's modulus. The values of D from the present SW potential are -352.5 N/m and -372.0 N/m along the armchair and zigzag directions, respectively. The ultimate stress is about 5.7 Nm^{-1} at the ultimate strain of 0.17 in the armchair direction at the low temperature of 1 K. The ultimate stress is about 5.5 Nm^{-1} at the ultimate strain of 0.20 in the zigzag direction at the low temperature of 1 K.

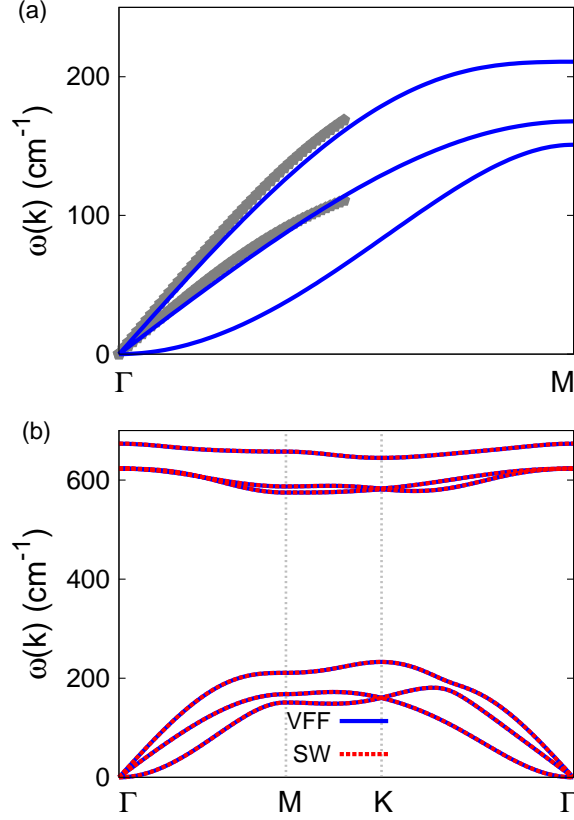


FIG. 244: (Color online) Phonon dispersion for the single-layer b-CSe. (a) The VFF model is fitted to the two in-plane acoustic branches in the long wave limit along the Γ M direction. The *ab initio* results (gray pentagons) are calculated from SIESTA. (b) The VFF model (blue lines) and the SW potential (red lines) give the same phonon dispersion for the b-CSe along Γ MK Γ .

CXIX. B-CSE

Present studies on the buckled (b-) CSe are based on first-principles calculations, and no empirical potential has been proposed for the b-CSe. We will thus parametrize a set of SW potential for the single-layer b-CSe in this section.

The structure of the single-layer b-CSe is shown in Fig. 239. The structural parameters are from the *ab initio* calculations.⁷⁸ The b-CSe has a buckled configuration as shown in Fig. 239 (b), where the buckle is along the zigzag direction. This structure can be determined by two independent geometrical parameters, including the lattice constant 3.063 \AA and the bond length 2.055 \AA .

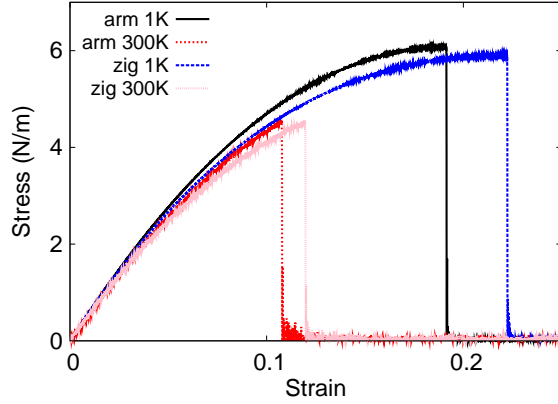


FIG. 245: (Color online) Stress-strain relations for the b-CSe of size $100 \times 100 \text{ \AA}$. The b-CSe is uniaxially stretched along the armchair or zigzag directions at temperatures 1 K and 300 K.

TABLE CDLXXIV: The VFF model for b-CSe. The second line gives an explicit expression for each VFF term. The third line is the force constant parameters. Parameters are in the unit of $\frac{eV}{\text{\AA}^2}$ for the bond stretching interactions, and in the unit of eV for the angle bending interaction. The fourth line gives the initial bond length (in unit of \AA) for the bond stretching interaction and the initial angle (in unit of degrees) for the angle bending interaction.

VFF type	bond stretching	angle bending
expression	$\frac{1}{2}K_r(\Delta r)^2$	$\frac{1}{2}K_\theta(\Delta\theta)^2$
parameter	10.425	5.031
r_0 or θ_0	2.055	96.362

Table CDLXXIV shows the VFF model for the single-layer b-CSe. The force constant parameters are determined by fitting to the acoustic branches in the phonon dispersion along the ΓM as shown in Fig. 244 (a). The *ab initio* calculations for the phonon dispersion are calculated from the SIESTA package.⁷⁹ The generalized gradients approximation is ap-

TABLE CDLXXV: Two-body SW potential parameters for b-CSe used by GULP,⁸ as expressed in Eq. (3).

	A (eV)	ρ (\AA)	B (\AA^4)	r_{\min} (\AA)	r_{\max} (\AA)
C-Se	7.691	1.298	8.917	0.0	2.872

TABLE CDLXXVI: Three-body SW potential parameters for b-CSe used by GULP,⁸ as expressed in Eq. (4).

	K (eV)	θ_0 (degree)	ρ_1 (Å)	ρ_2 (Å)	$r_{\min 12}$ (Å)	$r_{\max 12}$ (Å)	$r_{\min 13}$ (Å)	$r_{\max 13}$ (Å)	$r_{\min 23}$ (Å)	$r_{\max 23}$ (Å)
C-Se-Se	61.215	96.362	1.298	1.298	0.0	2.872	0.0	2.872	0.0	4.184
Se-C-C	61.215	96.362	1.298	1.298	0.0	2.872	0.0	2.872	0.0	4.184

TABLE CDLXXVII: SW potential parameters for b-CSe used by LAMMPS,⁹ as expressed in Eqs. (9) and (10).

	ϵ (eV)	σ (Å)	a	λ	γ	$\cos \theta_0$	A_L	B_L	p	q	tol
C-Se-Se	1.000	1.298	2.212	61.215	1.000	-0.111	7.691	3.137	4	0	0.0
Se-C-C	1.000	1.298	2.212	61.215	1.000	-0.111	7.691	3.137	4	0	0.0

plied to account for the exchange-correlation function with Perdew, Burke, and Ernzerhof parameterization,⁸⁰ and the double- ζ orbital basis set is adopted. Fig. 244 (b) shows that the VFF model and the SW potential give exactly the same phonon dispersion, as the SW potential is derived from the VFF model.

The parameters for the two-body SW potential used by GULP are shown in Tab. CDLXXV. The parameters for the three-body SW potential used by GULP are shown in Tab. CDLXXVI. Parameters for the SW potential used by LAMMPS are listed in Tab. CDLXXVII.

We use LAMMPS to perform MD simulations for the mechanical behavior of the single-layer b-CSe under uniaxial tension at 1.0 K and 300.0 K. Fig. 245 shows the stress-strain curve for the tension of a single-layer b-CSe of dimension 100×100 Å. Periodic boundary conditions are applied in both armchair and zigzag directions. The single-layer b-CSe is stretched uniaxially along the armchair or zigzag direction. The stress is calculated without involving the actual thickness of the quasi-two-dimensional structure of the single-layer b-CSe. The Young's modulus can be obtained by a linear fitting of the stress-strain relation in the small strain range of $[0, 0.01]$. The Young's modulus are 61.6 N/m and 61.4 N/m along the armchair and zigzag directions, respectively. The Young's modulus is essentially isotropic in the armchair and zigzag directions. The Poisson's ratio from the VFF model and the SW potential is $\nu_{xy} = \nu_{yx} = 0.09$.

TABLE CDLXXVIII: The VFF model for b-CTe. The second line gives an explicit expression for each VFF term. The third line is the force constant parameters. Parameters are in the unit of $\frac{\text{eV}}{\text{\AA}^2}$ for the bond stretching interactions, and in the unit of eV for the angle bending interaction. The fourth line gives the initial bond length (in unit of \AA) for the bond stretching interaction and the initial angle (in unit of degrees) for the angle bending interaction.

VFF type	bond stretching	angle bending
expression	$\frac{1}{2}K_r (\Delta r)^2$	$\frac{1}{2}K_\theta (\Delta \theta)^2$
parameter	9.367	4.311
r_0 or θ_0	2.231	97.239

TABLE CDLXXIX: Two-body SW potential parameters for b-CTe used by GULP,⁸ as expressed in Eq. (3).

	A (eV)	ρ (\AA)	B (\AA^4)	r_{\min} (\AA)	r_{\max} (\AA)
C-Te	8.314	1.440	12.387	0.0	3.127

There is no available value for nonlinear quantities in the single-layer b-CSe. We have thus used the nonlinear parameter $B = 0.5d^4$ in Eq. (5), which is close to the value of B in most materials. The value of the third order nonlinear elasticity D can be extracted by fitting the stress-strain relation to the function $\sigma = E\epsilon + \frac{1}{2}D\epsilon^2$ with E as the Young's modulus. The values of D from the present SW potential are -306.6 N/m and -324.9 N/m along the armchair and zigzag directions, respectively. The ultimate stress is about 6.1 Nm^{-1} at the ultimate strain of 0.19 in the armchair direction at the low temperature of 1 K. The ultimate stress is about 5.9 Nm^{-1} at the ultimate strain of 0.22 in the zigzag direction at the low temperature of 1 K.

CXX. B-CTE

Present studies on the buckled (b-) CTe are based on first-principles calculations, and no empirical potential has been proposed for the b-CTe. We will thus parametrize a set of SW potential for the single-layer b-CTe in this section.

The structure of the single-layer b-CTe is shown in Fig. 239. The structural parameters

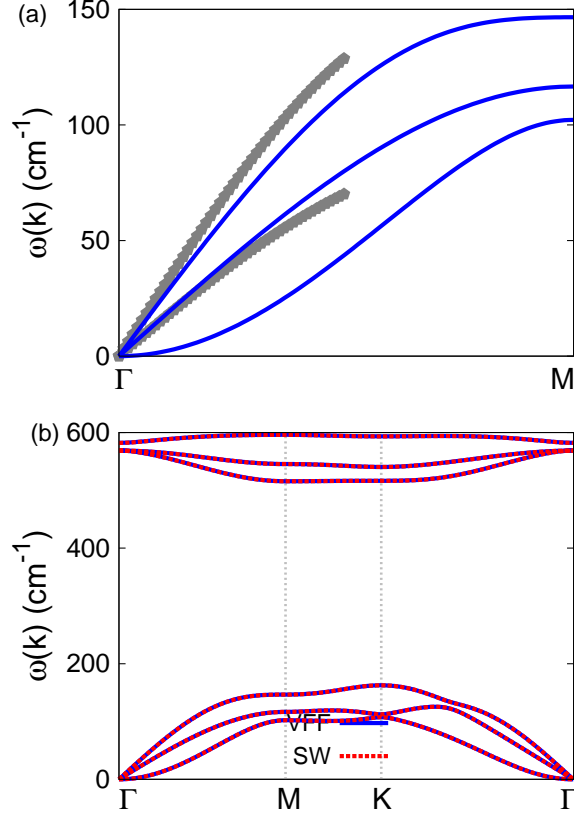


FIG. 246: (Color online) Phonon dispersion for the single-layer b-CTe. (a) The VFF model is fitted to the two in-plane acoustic branches in the long wave limit along the Γ M direction. The *ab initio* results (gray pentagons) are calculated from SIESTA. (b) The VFF model (blue lines) and the SW potential (red lines) give the same phonon dispersion for the b-CTe along Γ MKT.

TABLE CDLXXX: Three-body SW potential parameters for b-CTe used by GULP,⁸ as expressed in Eq. (4).

	K (eV)	θ_0 (degree)	ρ_1 (\AA)	ρ_2 (\AA)	$r_{\min 12}$ (\AA)	$r_{\max 12}$ (\AA)	$r_{\min 13}$ (\AA)	$r_{\max 13}$ (\AA)	$r_{\min 23}$ (\AA)	$r_{\max 23}$ (\AA)
C-Te-Te	54.451	97.239	1.440	1.440	0.0	3.127	0.0	3.127	0.0	4.573
Te-C-C	54.451	97.239	1.440	1.440	0.0	3.127	0.0	3.127	0.0	4.573

are from the *ab initio* calculations.⁷⁸ The b-CTe has a buckled configuration as shown in Fig. 239 (b), where the buckle is along the zigzag direction. This structure can be determined by two independent geometrical parameters, including the lattice constant 3.348 \AA and the bond length 2.231 \AA .

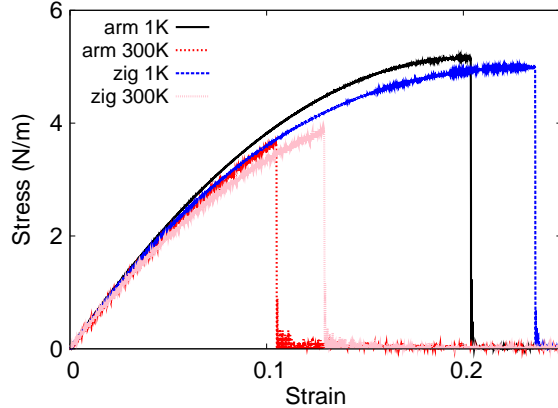


FIG. 247: (Color online) Stress-strain relations for the b-CTe of size $100 \times 100 \text{ \AA}$. The b-CTe is uniaxially stretched along the armchair or zigzag directions at temperatures 1 K and 300 K.

TABLE CDLXXXI: SW potential parameters for b-CTe used by LAMMPS,⁹ as expressed in Eqs. (9) and (10).

	ϵ (eV)	σ (\AA)	a	λ	γ	$\cos \theta_0$	A_L	B_L	p	q	tol
C-Te-Te	1.000	1.440	2.172	54.451	1.000	-0.126	8.314	2.883	4	0	0.0
Te-C-C	1.000	1.440	2.172	54.451	1.000	-0.126	8.314	2.883	4	0	0.0

Table CDLXXVIII shows the VFF model for the single-layer b-CTe. The force constant parameters are determined by fitting to the acoustic branches in the phonon dispersion along the Γ M as shown in Fig. 246 (a). The *ab initio* calculations for the phonon dispersion are calculated from the SIESTA package.⁷⁹ The generalized gradients approximation is applied to account for the exchange-correlation function with Perdew, Burke, and Ernzerhof parameterization,⁸⁰ and the double- ζ orbital basis set is adopted. Fig. 246 (b) shows that the VFF model and the SW potential give exactly the same phonon dispersion, as the SW potential is derived from the VFF model.

The parameters for the two-body SW potential used by GULP are shown in Tab. CDLXXIX. The parameters for the three-body SW potential used by GULP are shown in Tab. CDLXXX. Parameters for the SW potential used by LAMMPS are listed in Tab. CDLXXXI.

We use LAMMPS to perform MD simulations for the mechanical behavior of the single-layer b-CTe under uniaxial tension at 1.0 K and 300.0 K. Fig. 247 shows the stress-strain

TABLE CDLXXXII: The VFF model for b-SiO. The second line gives an explicit expression for each VFF term. The third line is the force constant parameters. Parameters are in the unit of $\frac{\text{eV}}{\text{\AA}^2}$ for the bond stretching interactions, and in the unit of eV for the angle bending interaction. The fourth line gives the initial bond length (in unit of \AA) for the bond stretching interaction and the initial angle (in unit of degrees) for the angle bending interaction.

VFF type	bond stretching	angle bending
expression	$\frac{1}{2}K_r (\Delta r)^2$	$\frac{1}{2}K_\theta (\Delta\theta)^2$
parameter	9.315	3.300
r_0 or θ_0	1.884	96.676

curve for the tension of a single-layer b-CTe of dimension $100 \times 100 \text{ \AA}$. Periodic boundary conditions are applied in both armchair and zigzag directions. The single-layer b-CTe is stretched uniaxially along the armchair or zigzag direction. The stress is calculated without involving the actual thickness of the quasi-two-dimensional structure of the single-layer b-CTe. The Young's modulus can be obtained by a linear fitting of the stress-strain relation in the small strain range of $[0, 0.01]$. The Young's modulus are 48.8 N/m and 48.3 N/m along the armchair and zigzag directions, respectively. The Young's modulus is essentially isotropic in the armchair and zigzag directions. The Poisson's ratio from the VFF model and the SW potential is $\nu_{xy} = \nu_{yx} = 0.12$.

There is no available value for nonlinear quantities in the single-layer b-CTe. We have thus used the nonlinear parameter $B = 0.5d^4$ in Eq. (5), which is close to the value of B in most materials. The value of the third order nonlinear elasticity D can be extracted by fitting the stress-strain relation to the function $\sigma = E\epsilon + \frac{1}{2}D\epsilon^2$ with E as the Young's modulus. The values of D from the present SW potential are -306.6 N/m and -324.9 N/m along the armchair and zigzag directions, respectively. The ultimate stress is about 5.2 Nm^{-1} at the ultimate strain of 0.20 in the armchair direction at the low temperature of 1 K. The ultimate stress is about 5.0 Nm^{-1} at the ultimate strain of 0.23 in the zigzag direction at the low temperature of 1 K.

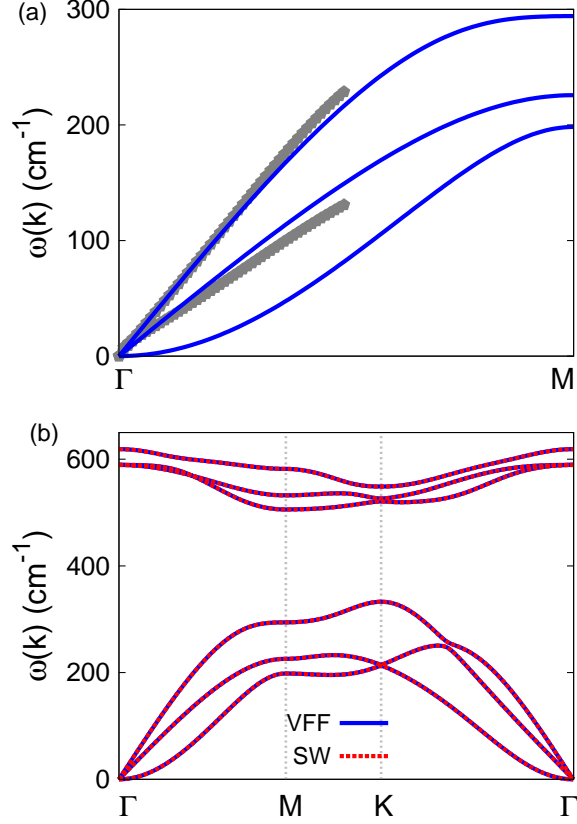


FIG. 248: (Color online) Phonon dispersion for the single-layer b-SiO. (a) The VFF model is fitted to the two in-plane acoustic branches in the long wave limit along the ΓM direction. The *ab initio* results (gray pentagons) are calculated from SIESTA. (b) The VFF model (blue lines) and the SW potential (red lines) give the same phonon dispersion for the b-SiO along $\Gamma MK\Gamma$.

TABLE CDLXXXIII: Two-body SW potential parameters for b-SiO used by GULP,⁸ as expressed in Eq. (3).

	A (eV)	ρ (\AA)	B (\AA^4)	r_{\min} (\AA)	r_{\max} (\AA)
Si-O	5.819	1.200	6.299	0.0	2.636

CXXI. B-SiO

Present studies on the buckled (b-) SiO are based on first-principles calculations, and no empirical potential has been proposed for the b-SiO. We will thus parametrize a set of SW potential for the single-layer b-SiO in this section.

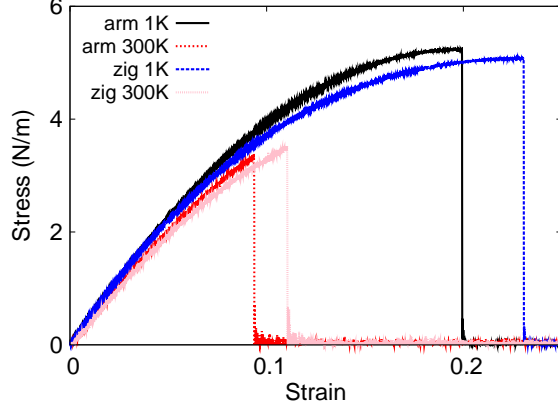


FIG. 249: (Color online) Stress-strain relations for the b-SiO of size $100 \times 100 \text{ \AA}$. The b-SiO is uniaxially stretched along the armchair or zigzag directions at temperatures 1 K and 300 K.

TABLE CDLXXXIV: Three-body SW potential parameters for b-SiO used by GULP,⁸ as expressed in Eq. (4).

	K (eV)	θ_0 (degree)	ρ_1 (\AA)	ρ_2 (\AA)	$r_{\min 12}$ (\AA)	$r_{\max 12}$ (\AA)	$r_{\min 13}$ (\AA)	$r_{\max 13}$ (\AA)	$r_{\min 23}$ (\AA)	$r_{\max 23}$ (\AA)
Si-O-O	40.695	96.676	1.200	1.200	0.0	2.636	0.0	2.636	0.0	3.845
O-Si-Si	40.695	96.676	1.200	1.200	0.0	2.636	0.0	2.636	0.0	3.845

The structure of the single-layer b-SiO is shown in Fig. 239. The structural parameters are from the *ab initio* calculations.⁷⁸ The b-SiO has a buckled configuration as shown in Fig. 239 (b), where the buckle is along the zigzag direction. This structure can be determined by two independent geometrical parameters, including the lattice constant 2.815 \AA and the bond length 1.884 \AA .

Table CDLXXXII shows the VFF model for the single-layer b-SiO. The force constant parameters are determined by fitting to the acoustic branches in the phonon dispersion

TABLE CDLXXXV: SW potential parameters for b-SiO used by LAMMPS,⁹ as expressed in Eqs. (9) and (10).

	ϵ (eV)	σ (\AA)	a	λ	γ	$\cos \theta_0$	A_L	B_L	p	q	tol
Si-O-O	1.000	1.200	2.197	40.695	1.000	-0.116	5.819	3.043	4	0	0.0
O-Si-Si	1.000	1.200	2.197	40.695	1.000	-0.116	5.819	3.043	4	0	0.0

along the Γ M as shown in Fig. 248 (a). The *ab initio* calculations for the phonon dispersion are calculated from the SIESTA package.⁷⁹ The generalized gradients approximation is applied to account for the exchange-correlation function with Perdew, Burke, and Ernzerhof parameterization,⁸⁰ and the double- ζ orbital basis set is adopted. Fig. 248 (b) shows that the VFF model and the SW potential give exactly the same phonon dispersion, as the SW potential is derived from the VFF model.

The parameters for the two-body SW potential used by GULP are shown in Tab. CDLXXXIII. The parameters for the three-body SW potential used by GULP are shown in Tab. CDLXXXIV. Parameters for the SW potential used by LAMMPS are listed in Tab. CDLXXXV.

We use LAMMPS to perform MD simulations for the mechanical behavior of the single-layer b-SiO under uniaxial tension at 1.0 K and 300.0 K. Fig. 249 shows the stress-strain curve for the tension of a single-layer b-SiO of dimension 100×100 Å. Periodic boundary conditions are applied in both armchair and zigzag directions. The single-layer b-SiO is stretched uniaxially along the armchair or zigzag direction. The stress is calculated without involving the actual thickness of the quasi-two-dimensional structure of the single-layer b-SiO. The Young's modulus can be obtained by a linear fitting of the stress-strain relation in the small strain range of $[0, 0.01]$. The Young's modulus are 51.3 N/m and 50.3 N/m along the armchair and zigzag directions, respectively. The Young's modulus is essentially isotropic in the armchair and zigzag directions. The Poisson's ratio from the VFF model and the SW potential is $\nu_{xy} = \nu_{yx} = 0.11$.

There is no available value for nonlinear quantities in the single-layer b-SiO. We have thus used the nonlinear parameter $B = 0.5d^4$ in Eq. (5), which is close to the value of B in most materials. The value of the third order nonlinear elasticity D can be extracted by fitting the stress-strain relation to the function $\sigma = E\epsilon + \frac{1}{2}D\epsilon^2$ with E as the Young's modulus. The values of D from the present SW potential are -247.8 N/m and -253.6 N/m along the armchair and zigzag directions, respectively. The ultimate stress is about 5.2 Nm^{-1} at the ultimate strain of 0.20 in the armchair direction at the low temperature of 1 K. The ultimate stress is about 5.1 Nm^{-1} at the ultimate strain of 0.23 in the zigzag direction at the low temperature of 1 K.

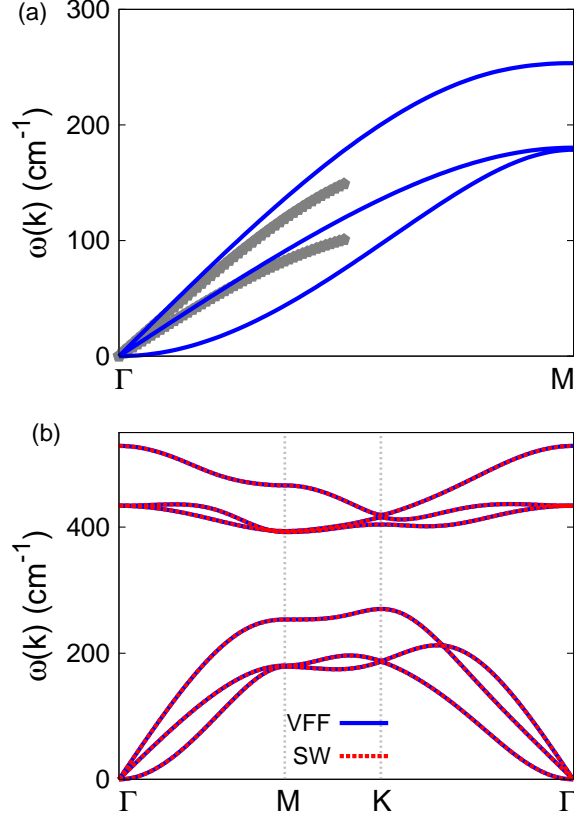


FIG. 250: (Color online) Phonon dispersion for the single-layer b-SiS. (a) The VFF model is fitted to the two in-plane acoustic branches in the long wave limit along the Γ M direction. The *ab initio* results (gray pentagons) are calculated from SIESTA. (b) The VFF model (blue lines) and the SW potential (red lines) give the same phonon dispersion for the b-SiS along Γ MK Γ .

CXXII. B-SIS

Present studies on the buckled (b-) SiS are based on first-principles calculations, and no empirical potential has been proposed for the b-SiS. We will thus parametrize a set of SW potential for the single-layer b-SiS in this section.

The structure of the single-layer b-SiS is shown in Fig. 239. The structural parameters are from the *ab initio* calculations.⁷⁸ The b-SiS has a buckled configuration as shown in Fig. 239 (b), where the buckle is along the zigzag direction. This structure can be determined by two independent geometrical parameters, including the lattice constant 3.299 Å and the bond length 2.321 Å.

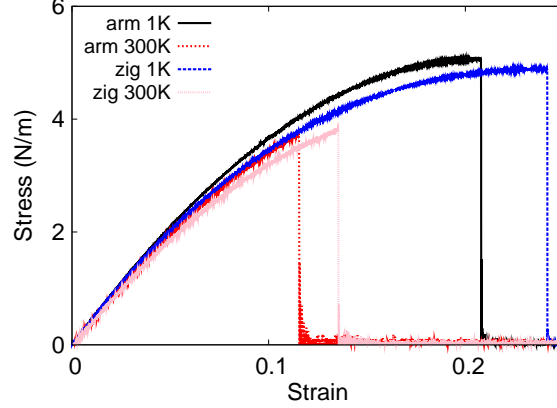


FIG. 251: (Color online) Stress-strain relations for the b-SiS of size $100 \times 100 \text{ \AA}$. The b-SiS is uniaxially stretched along the armchair or zigzag directions at temperatures 1 K and 300 K.

TABLE CDLXXXVI: The VFF model for b-SiS. The second line gives an explicit expression for each VFF term. The third line is the force constant parameters. Parameters are in the unit of $\frac{\text{eV}}{\text{\AA}^2}$ for the bond stretching interactions, and in the unit of eV for the angle bending interaction. The fourth line gives the initial bond length (in unit of \AA) for the bond stretching interaction and the initial angle (in unit of degrees) for the angle bending interaction.

VFF type	bond stretching	angle bending
expression	$\frac{1}{2}K_r(\Delta r)^2$	$\frac{1}{2}K_\theta(\Delta\theta)^2$
parameter	8.441	4.802
r_0 or θ_0	2.321	90.581

Table CDLXXXVI shows the VFF model for the single-layer b-SiS. The force constant parameters are determined by fitting to the acoustic branches in the phonon dispersion along the ΓM as shown in Fig. 250 (a). The *ab initio* calculations for the phonon dispersion are calculated from the SIESTA package.⁷⁹ The generalized gradients approximation is ap-

TABLE CDLXXXVII: Two-body SW potential parameters for b-SiS used by GULP,⁸ as expressed in Eq. (3).

	A (eV)	ρ (\AA)	B (\AA^4)	r_{min} (\AA)	r_{max} (\AA)
Si-S	6.897	1.264	14.510	0.0	3.177

TABLE CDLXXXVIII: Three-body SW potential parameters for b-SiS used by GULP,⁸ as expressed in Eq. (4).

	K (eV)	θ_0 (degree)	ρ_1 (Å)	ρ_2 (Å)	$r_{\min 12}$ (Å)	$r_{\max 12}$ (Å)	$r_{\min 13}$ (Å)	$r_{\max 13}$ (Å)	$r_{\min 23}$ (Å)	$r_{\max 23}$ (Å)
Si-S-S	45.954	90.581	1.264	1.264	0.0	3.177	0.0	3.177	0.0	4.506
S-Si-Si	45.954	90.581	1.264	1.264	0.0	3.177	0.0	3.177	0.0	4.506

TABLE CDLXXXIX: SW potential parameters for b-SiS used by LAMMPS,⁹ as expressed in Eqs. (9) and (10).

	ϵ (eV)	σ (Å)	a	λ	γ	$\cos \theta_0$	A_L	B_L	p	q	tol
Si-S-S	1.000	1.264	2.514	45.954	1.000	-0.010	6.897	5.687	4	0	0.0
S-Si-Si	1.000	1.264	2.514	45.954	1.000	-0.010	6.897	5.687	4	0	0.0

plied to account for the exchange-correlation function with Perdew, Burke, and Ernzerhof parameterization,⁸⁰ and the double- ζ orbital basis set is adopted. Fig. 250 (b) shows that the VFF model and the SW potential give exactly the same phonon dispersion, as the SW potential is derived from the VFF model.

The parameters for the two-body SW potential used by GULP are shown in Tab. CDLXXXVII. The parameters for the three-body SW potential used by GULP are shown in Tab. CDLXXXVIII. Parameters for the SW potential used by LAMMPS are listed in Tab. CDLXXXIX.

We use LAMMPS to perform MD simulations for the mechanical behavior of the single-layer b-SiS under uniaxial tension at 1.0 K and 300.0 K. Fig. 251 shows the stress-strain curve for the tension of a single-layer b-SiS of dimension 100×100 Å. Periodic boundary conditions are applied in both armchair and zigzag directions. The single-layer b-SiS is stretched uniaxially along the armchair or zigzag direction. The stress is calculated without involving the actual thickness of the quasi-two-dimensional structure of the single-layer b-SiS. The Young's modulus can be obtained by a linear fitting of the stress-strain relation in the small strain range of $[0, 0.01]$. The Young's modulus are 45.5 N/m and 45.8 N/m along the armchair and zigzag directions, respectively. The Young's modulus is essentially isotropic in the armchair and zigzag directions. The Poisson's ratio from the VFF model and the SW potential is $\nu_{xy} = \nu_{yx} = 0.13$.

TABLE CDXC: The VFF model for b-SiSe. The second line gives an explicit expression for each VFF term. The third line is the force constant parameters. Parameters are in the unit of $\frac{\text{eV}}{\text{\AA}^2}$ for the bond stretching interactions, and in the unit of eV for the angle bending interaction. The fourth line gives the initial bond length (in unit of \AA) for the bond stretching interaction and the initial angle (in unit of degrees) for the angle bending interaction.

VFF type	bond stretching	angle bending
expression	$\frac{1}{2}K_r (\Delta r)^2$	$\frac{1}{2}K_\theta (\Delta\theta)^2$
parameter	8.441	4.802
r_0 or θ_0	2.477	90.590

TABLE CDXCI: Two-body SW potential parameters for b-SiSe used by GULP,⁸ as expressed in Eq. (3).

	A (eV)	ρ (\AA)	B (\AA^4)	r_{\min} (\AA)	r_{\max} (\AA)
Si-Se	7.857	1.349	18.822	0.0	3.391

There is no available value for nonlinear quantities in the single-layer b-SiS. We have thus used the nonlinear parameter $B = 0.5d^4$ in Eq. (5), which is close to the value of B in most materials. The value of the third order nonlinear elasticity D can be extracted by fitting the stress-strain relation to the function $\sigma = E\epsilon + \frac{1}{2}D\epsilon^2$ with E as the Young's modulus. The values of D from the present SW potential are -196.4 N/m and -217.9 N/m along the armchair and zigzag directions, respectively. The ultimate stress is about 5.1 Nm^{-1} at the ultimate strain of 0.21 in the armchair direction at the low temperature of 1 K. The ultimate stress is about 4.9 Nm^{-1} at the ultimate strain of 0.24 in the zigzag direction at the low temperature of 1 K.

CXXIII. B-SISE

Present studies on the buckled (b-) SiSe are based on first-principles calculations, and no empirical potential has been proposed for the b-SiSe. We will thus parametrize a set of SW potential for the single-layer b-SiSe in this section.

The structure of the single-layer b-SiSe is shown in Fig. 239. The structural parameters

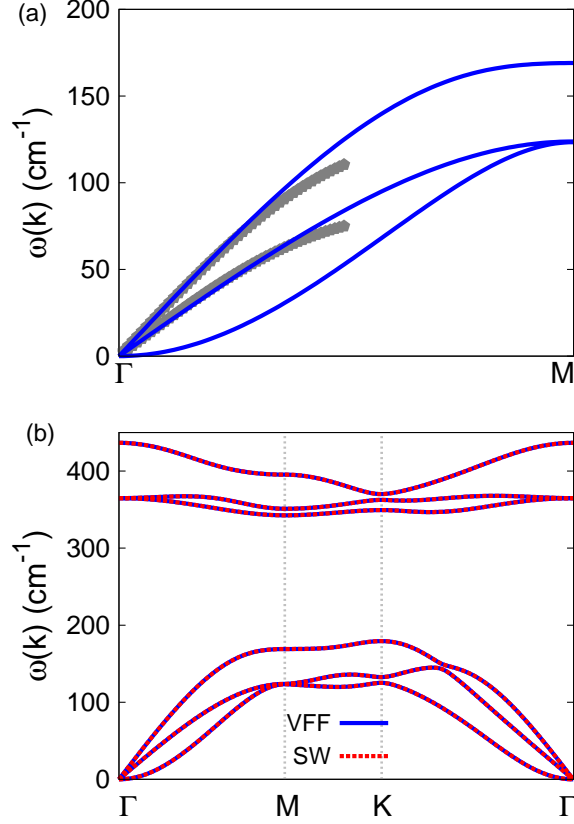


FIG. 252: (Color online) Phonon dispersion for the single-layer b-SiSe. (a) The VFF model is fitted to the two in-plane acoustic branches in the long wave limit along the ΓM direction. The *ab initio* results (gray pentagons) are calculated from SIESTA. (b) The VFF model (blue lines) and the SW potential (red lines) give the same phonon dispersion for the b-SiSe along $\Gamma M K T$.

TABLE CDXCII: Three-body SW potential parameters for b-SiSe used by GULP,⁸ as expressed in Eq. (4).

	K (eV)	θ_0 (degree)	ρ_1 (\AA)	ρ_2 (\AA)	$r_{\min 12}$ (\AA)	$r_{\max 12}$ (\AA)	$r_{\min 13}$ (\AA)	$r_{\max 13}$ (\AA)	$r_{\min 23}$ (\AA)	$r_{\max 23}$ (\AA)
Si-Se-Se	45.968	90.590	1.349	1.349	0.0	3.391	0.0	3.391	0.0	4.810
Se-Si-Si	45.968	90.590	1.349	1.349	0.0	3.391	0.0	3.391	0.0	4.810

are from the *ab initio* calculations.⁷⁸ The b-SiSe has a buckled configuration as shown in Fig. 239 (b), where the buckle is along the zigzag direction. This structure can be determined by two independent geometrical parameters, including the lattice constant 3.521 \AA and the bond length 2.477 \AA .

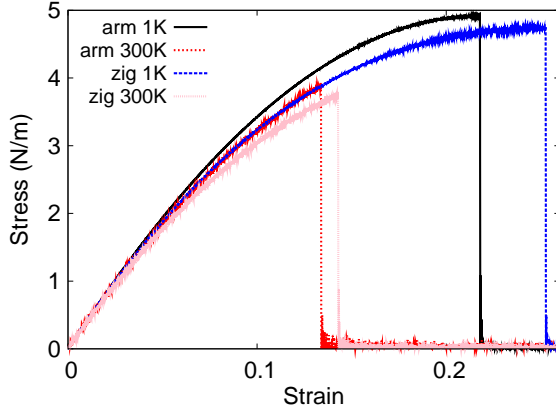


FIG. 253: (Color online) Stress-strain relations for the b-SiSe of size $100 \times 100 \text{ \AA}$. The b-SiSe is uniaxially stretched along the armchair or zigzag directions at temperatures 1 K and 300 K.

TABLE CDXCIII: SW potential parameters for b-SiSe used by LAMMPS,⁹ as expressed in Eqs. (9) and (10).

	ϵ (eV)	σ (\AA)	a	λ	γ	$\cos \theta_0$	A_L	B_L	p	q	tol
Si-Se-Se	1.000	1.349	2.514	45.968	1.000	-0.010	7.857	5.6683	4	0	0.0
Se-Si-Si	1.000	1.349	2.514	45.968	1.000	-0.010	7.857	5.6683	4	0	0.0

Table CDXC shows the VFF model for the single-layer b-SiSe. The force constant parameters are determined by fitting to the acoustic branches in the phonon dispersion along the ΓM as shown in Fig. 252 (a). The *ab initio* calculations for the phonon dispersion are calculated from the SIESTA package.⁷⁹ The generalized gradients approximation is applied to account for the exchange-correlation function with Perdew, Burke, and Ernzerhof parameterization,⁸⁰ and the double- ζ orbital basis set is adopted. Fig. 252 (b) shows that the VFF model and the SW potential give exactly the same phonon dispersion, as the SW potential is derived from the VFF model.

The parameters for the two-body SW potential used by GULP are shown in Tab. CDXCI. The parameters for the three-body SW potential used by GULP are shown in Tab. CDXCII. Parameters for the SW potential used by LAMMPS are listed in Tab. CDXCIII.

We use LAMMPS to perform MD simulations for the mechanical behavior of the single-layer b-SiSe under uniaxial tension at 1.0 K and 300.0 K. Fig. 253 shows the stress-strain curve for the tension of a single-layer b-SiSe of dimension $100 \times 100 \text{ \AA}$. Periodic boundary

TABLE CDXCIV: The VFF model for b-SiTe. The second line gives an explicit expression for each VFF term. The third line is the force constant parameters. Parameters are in the unit of $\frac{\text{eV}}{\text{\AA}^2}$ for the bond stretching interactions, and in the unit of eV for the angle bending interaction. The fourth line gives the initial bond length (in unit of \AA) for the bond stretching interaction and the initial angle (in unit of degrees) for the angle bending interaction.

VFF type	bond stretching	angle bending
expression	$\frac{1}{2}K_r (\Delta r)^2$	$\frac{1}{2}K_\theta (\Delta\theta)^2$
parameter	8.418	4.349
r_0 or θ_0	2.690	90.779

conditions are applied in both armchair and zigzag directions. The single-layer b-SiSe is stretched uniaxially along the armchair or zigzag direction. The stress is calculated without involving the actual thickness of the quasi-two-dimensional structure of the single-layer b-SiSe. The Young's modulus can be obtained by a linear fitting of the stress-strain relation in the small strain range of $[0, 0.01]$. The Young's modulus are 41.8 N/m and 41.9 N/m along the armchair and zigzag directions, respectively. The Young's modulus is essentially isotropic in the armchair and zigzag directions. The Poisson's ratio from the VFF model and the SW potential is $\nu_{xy} = \nu_{yx} = 0.15$.

There is no available value for nonlinear quantities in the single-layer b-SiSe. We have thus used the nonlinear parameter $B = 0.5d^4$ in Eq. (5), which is close to the value of B in most materials. The value of the third order nonlinear elasticity D can be extracted by fitting the stress-strain relation to the function $\sigma = E\epsilon + \frac{1}{2}D\epsilon^2$ with E as the Young's modulus. The values of D from the present SW potential are -169.9 N/m and -188.0 N/m along the armchair and zigzag directions, respectively. The ultimate stress is about 4.9 Nm^{-1} at the ultimate strain of 0.22 in the armchair direction at the low temperature of 1 K. The ultimate stress is about 4.7 Nm^{-1} at the ultimate strain of 0.25 in the zigzag direction at the low temperature of 1 K.

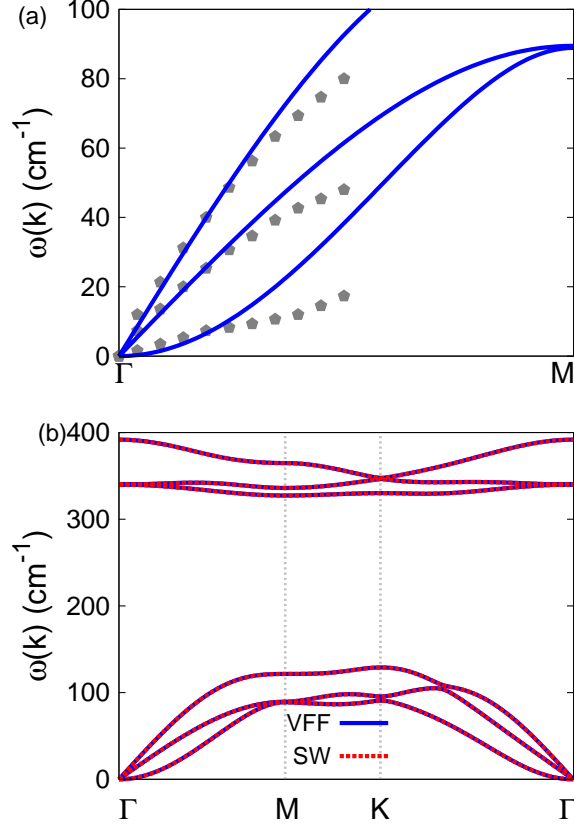


FIG. 254: (Color online) Phonon dispersion for the single-layer b-SiTe. (a) The VFF model is fitted to the three acoustic branches in the long wave limit along the Γ M direction. The *ab initio* results (gray pentagons) are from Ref. 83. (b) The VFF model (blue lines) and the SW potential (red lines) give the same phonon dispersion for the b-SiTe along Γ MK Γ .

TABLE CDXCV: Two-body SW potential parameters for b-SiTe used by GULP,⁸ as expressed in Eq. (3).

	A (eV)	ρ (\AA)	B (\AA^4)	r_{\min} (\AA)	r_{\max} (\AA)
Si-Te	9.285	1.473	26.181	0.0	3.685

CXXIV. B-SITE

Present studies on the buckled (b-) SiTe are based on first-principles calculations, and no empirical potential has been proposed for the b-SiTe. We will thus parametrize a set of SW potential for the single-layer b-SiTe in this section.

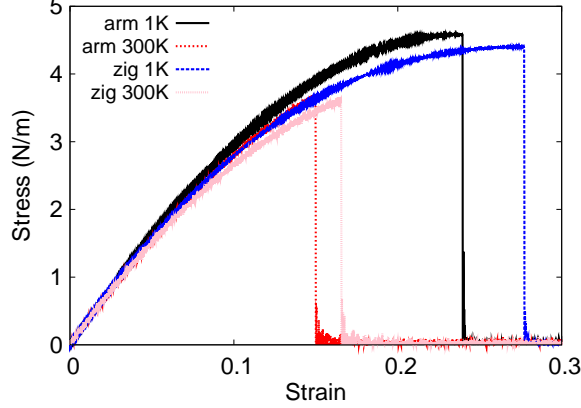


FIG. 255: (Color online) Stress-strain relations for the b-SiTe of size $100 \times 100 \text{ \AA}$. The b-SiTe is uniaxially stretched along the armchair or zigzag directions at temperatures 1 K and 300 K.

TABLE CDXCVI: Three-body SW potential parameters for b-SiTe used by GULP,⁸ as expressed in Eq. (4).

	K (eV)	θ_0 (degree)	ρ_1 (\AA)	ρ_2 (\AA)	$r_{\min 12}$ (\AA)	$r_{\max 12}$ (\AA)	$r_{\min 13}$ (\AA)	$r_{\max 13}$ (\AA)	$r_{\min 23}$ (\AA)	$r_{\max 23}$ (\AA)
Si-Te-Te	41.952	90.779	1.473	1.473	0.0	3.685	0.0	3.685	0.0	5.232
Te-Si-Si	41.952	90.779	1.473	1.473	0.0	3.685	0.0	3.685	0.0	5.232

The structure of the single-layer b-SiTe is shown in Fig. 239. The structural parameters are from the *ab initio* calculations.⁸³ The b-SiTe has a buckled configuration as shown in Fig. 239 (b), where the buckle is along the zigzag direction. This structure can be determined by two independent geometrical parameters, eg. the lattice constant 3.83 \AA and the bond length 2.689 \AA . The resultant height of the buckle is $h = 1.53 \text{ \AA}$.

Table CDXCIV shows the VFF model for the single-layer b-SiTe. The force constant parameters are determined by fitting to the acoustic branches in the phonon dispersion

TABLE CDXCVII: SW potential parameters for b-SiTe used by LAMMPS,⁹ as expressed in Eqs. (9) and (10).

	ϵ (eV)	σ (\AA)	a	λ	γ	$\cos \theta_0$	A_L	B_L	p	q	tol
Si-Te-Te	1.000	0.725	4.497	27.653	1.000	-0.014	4.428	113.714	4	0	0.0
Te-Si-Si	1.000	0.725	4.497	27.653	1.000	-0.014	4.428	113.714	4	0	0.0

along the Γ M as shown in Fig. 254 (a). The *ab initio* calculations for the phonon dispersion are from Ref. 83. Fig. 254 (b) shows that the VFF model and the SW potential give exactly the same phonon dispersion, as the SW potential is derived from the VFF model.

The parameters for the two-body SW potential used by GULP are shown in Tab. CDXCV. The parameters for the three-body SW potential used by GULP are shown in Tab. CDXCVI. Parameters for the SW potential used by LAMMPS are listed in Tab. CDXCVII.

We use LAMMPS to perform MD simulations for the mechanical behavior of the single-layer b-SiTe under uniaxial tension at 1.0 K and 300.0 K. Fig. 255 shows the stress-strain curve for the tension of a single-layer b-SiTe of dimension 100×100 Å. Periodic boundary conditions are applied in both armchair and zigzag directions. The single-layer b-SiTe is stretched uniaxially along the armchair or zigzag direction. The stress is calculated without involving the actual thickness of the quasi-two-dimensional structure of the single-layer b-SiTe. The Young's modulus can be obtained by a linear fitting of the stress-strain relation in the small strain range of $[0, 0.01]$. The Young's modulus are 34.3 N/m and 34.6 N/m along the armchair and zigzag directions, respectively. The Young's modulus is essentially isotropic in the armchair and zigzag directions. These values agrees with the *ab initio* result at 0 K temperature, eg. 34.1 Nm^{-1} in Ref. 83. The Poisson's ratio from the VFF model and the SW potential is $\nu_{xy} = \nu_{yx} = 0.18$, which agrees with the *ab initio* result⁸³ of 0.18.

There is no available value for nonlinear quantities in the single-layer b-SiTe. We have thus used the nonlinear parameter $B = 0.5d^4$ in Eq. (5), which is close to the value of B in most materials. The value of the third order nonlinear elasticity D can be extracted by fitting the stress-strain relation to the function $\sigma = E\epsilon + \frac{1}{2}D\epsilon^2$ with E as the Young's modulus. The values of D from the present SW potential are -119.3 N/m and -137.2 N/m along the armchair and zigzag directions, respectively. The ultimate stress is about 4.6 Nm^{-1} at the ultimate strain of 0.24 in the armchair direction at the low temperature of 1 K. The ultimate stress is about 4.4 Nm^{-1} at the ultimate strain of 0.27 in the zigzag direction at the low temperature of 1 K.

CXXV. B-GeO

Present studies on the buckled (b-) GeO are based on first-principles calculations, and no empirical potential has been proposed for the b-GeO. We will thus parametrize a set of

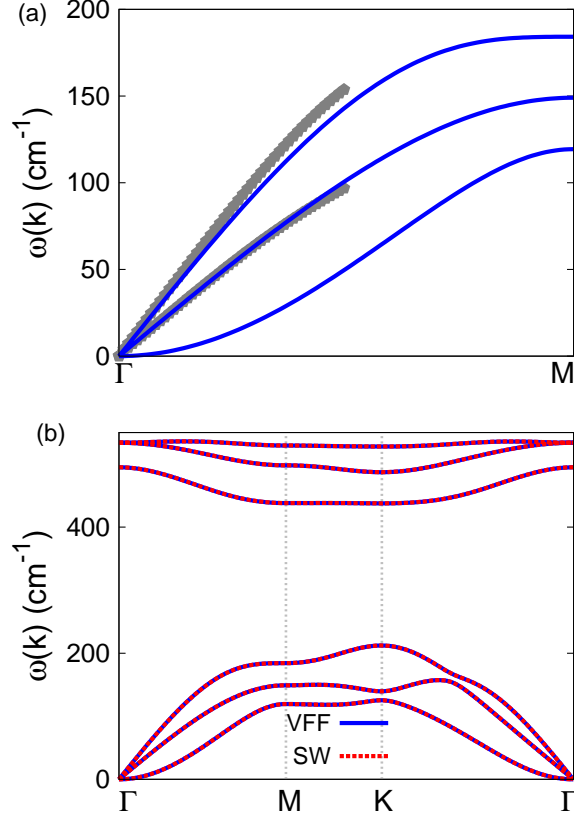


FIG. 256: (Color online) Phonon dispersion for the single-layer b-GeO. (a) The VFF model is fitted to the two in-plane acoustic branches in the long wave limit along the ΓM direction. The *ab initio* results (gray pentagons) are calculated from SIESTA. (b) The VFF model (blue lines) and the SW potential (red lines) give the same phonon dispersion for the b-GeO along $\Gamma MK\Gamma$.

SW potential for the single-layer b-GeO in this section.

The structure of the single-layer b-GeO is shown in Fig. 239. The structural parameters are from the *ab initio* calculations.⁷⁸ The b-GeO has a buckled configuration as shown in Fig. 239 (b), where the buckle is along the zigzag direction. This structure can be determined by two independent geometrical parameters, including the lattice constant 3.124 \AA and the bond length 2.032 \AA .

Table CDXCVIII shows the VFF model for the single-layer b-GeO. The force constant parameters are determined by fitting to the acoustic branches in the phonon dispersion along the ΓM as shown in Fig. 256 (a). The *ab initio* calculations for the phonon dispersion are calculated from the SIESTA package.⁷⁹ The generalized gradients approximation is ap-

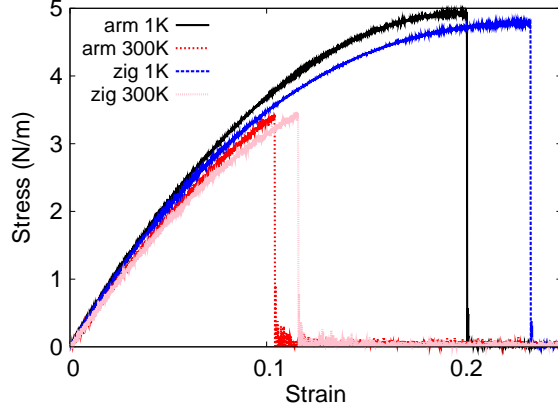


FIG. 257: (Color online) Stress-strain relations for the b-GeO of size $100 \times 100 \text{ \AA}$. The b-GeO is uniaxially stretched along the armchair or zigzag directions at temperatures 1 K and 300 K.

TABLE CDXCVIII: The VFF model for b-GeO. The second line gives an explicit expression for each VFF term. The third line is the force constant parameters. Parameters are in the unit of $\frac{eV}{\text{\AA}^2}$ for the bond stretching interactions, and in the unit of eV for the angle bending interaction. The fourth line gives the initial bond length (in unit of \AA) for the bond stretching interaction and the initial angle (in unit of degrees) for the angle bending interaction.

VFF type	bond stretching	angle bending
expression	$\frac{1}{2}K_r(\Delta r)^2$	$\frac{1}{2}K_\theta(\Delta\theta)^2$
parameter	9.315	3.300
r_0 or θ_0	2.032	100.475

plied to account for the exchange-correlation function with Perdew, Burke, and Ernzerhof parameterization,⁸⁰ and the double- ζ orbital basis set is adopted. Fig. 256 (b) shows that the VFF model and the SW potential give exactly the same phonon dispersion, as the SW potential is derived from the VFF model.

TABLE CDXCIX: Two-body SW potential parameters for b-GeO used by GULP,⁸ as expressed in Eq. (3).

	A (eV)	ρ (\AA)	B (\AA^4)	r_{\min} (\AA)	r_{\max} (\AA)
Ge-O	7.390	1.413	8.524	0.0	2.879

TABLE D: Three-body SW potential parameters for b-GeO used by GULP,⁸ as expressed in Eq. (4).

	K (eV)	θ_0 (degree)	ρ_1 (Å)	ρ_2 (Å)	$r_{\min 12}$ (Å)	$r_{\max 12}$ (Å)	$r_{\min 13}$ (Å)	$r_{\max 13}$ (Å)	$r_{\min 23}$ (Å)	$r_{\max 23}$ (Å)
Ge-O-O	47.962	100.475	1.413	1.413	0.0	2.879	0.0	2.879	0.0	4.267
O-Ge-Ge	47.962	100.475	1.413	1.413	0.0	2.879	0.0	2.879	0.0	4.267

TABLE DI: SW potential parameters for b-GeO used by LAMMPS,⁹ as expressed in Eqs. (9) and (10).

	ϵ (eV)	σ (Å)	a	λ	γ	$\cos \theta_0$	A_L	B_L	p	q	tol
Ge-O-O	1.000	1.413	2.037	47.962	1.000	-0.182	7.390	2.136	4	0	0.0
O-Ge-Ge	1.000	1.413	2.037	47.962	1.000	-0.182	7.390	2.136	4	0	0.0

The parameters for the two-body SW potential used by GULP are shown in Tab. CDXCIX. The parameters for the three-body SW potential used by GULP are shown in Tab. D. Parameters for the SW potential used by LAMMPS are listed in Tab. DI.

We use LAMMPS to perform MD simulations for the mechanical behavior of the single-layer b-GeO under uniaxial tension at 1.0 K and 300.0 K. Fig. 257 shows the stress-strain curve for the tension of a single-layer b-GeO of dimension 100×100 Å. Periodic boundary conditions are applied in both armchair and zigzag directions. The single-layer b-GeO is stretched uniaxially along the armchair or zigzag direction. The stress is calculated without involving the actual thickness of the quasi-two-dimensional structure of the single-layer b-GeO. The Young's modulus can be obtained by a linear fitting of the stress-strain relation in the small strain range of $[0, 0.01]$. The Young's modulus are 47.5 N/m and 46.8 N/m along the armchair and zigzag directions, respectively. The Young's modulus is essentially isotropic in the armchair and zigzag directions. The Poisson's ratio from the VFF model and the SW potential is $\nu_{xy} = \nu_{yx} = 0.11$.

There is no available value for nonlinear quantities in the single-layer b-GeO. We have thus used the nonlinear parameter $B = 0.5d^4$ in Eq. (5), which is close to the value of B in most materials. The value of the third order nonlinear elasticity D can be extracted by fitting the stress-strain relation to the function $\sigma = E\epsilon + \frac{1}{2}D\epsilon^2$ with E as the Young's modulus. The values of D from the present SW potential are -224.6 N/m and -232.8 N/m along the armchair and zigzag directions, respectively. The ultimate stress is about 4.9 Nm^{-1}

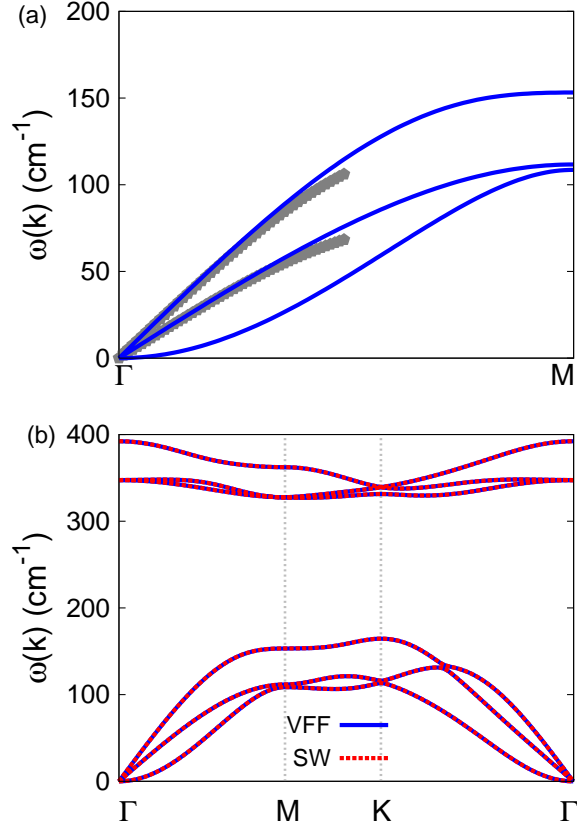


FIG. 258: (Color online) Phonon dispersion for the single-layer b-GeS. (a) The VFF model is fitted to the two in-plane acoustic branches in the long wave limit along the Γ M direction. The *ab initio* results (gray pentagons) are calculated from SIESTA. (b) The VFF model (blue lines) and the SW potential (red lines) give the same phonon dispersion for the b-GeS along Γ MK Γ .

at the ultimate strain of 0.20 in the armchair direction at the low temperature of 1 K. The ultimate stress is about 4.8 Nm^{-1} at the ultimate strain of 0.23 in the zigzag direction at the low temperature of 1 K.

CXXVI. B-GES

Present studies on the buckled (b-) GeS are based on first-principles calculations, and no empirical potential has been proposed for the b-GeS. We will thus parametrize a set of SW potential for the single-layer b-GeS in this section.

The structure of the single-layer b-GeS is shown in Fig. 239. The structural parameters

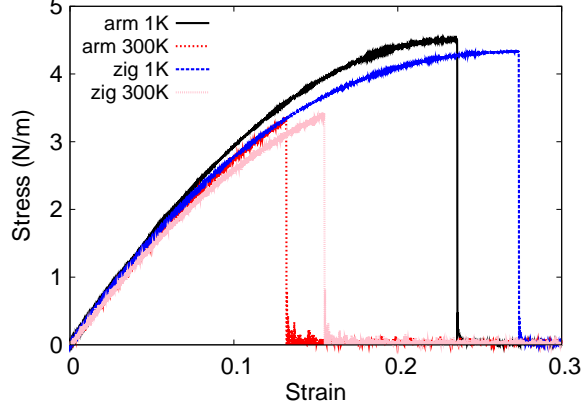


FIG. 259: (Color online) Stress-strain relations for the b-GeS of size $100 \times 100 \text{ \AA}$. The b-GeS is uniaxially stretched along the armchair or zigzag directions at temperatures 1 K and 300 K.

TABLE DII: The VFF model for b-GeS. The second line gives an explicit expression for each VFF term. The third line is the force constant parameters. Parameters are in the unit of $\frac{eV}{\text{\AA}^2}$ for the bond stretching interactions, and in the unit of eV for the angle bending interaction. The fourth line gives the initial bond length (in unit of \AA) for the bond stretching interaction and the initial angle (in unit of degrees) for the angle bending interaction.

VFF type	bond stretching	angle bending
expression	$\frac{1}{2}K_r(\Delta r)^2$	$\frac{1}{2}K_\theta(\Delta\theta)^2$
parameter	8.322	3.516
r_0 or θ_0	2.428	91.725

are from the *ab initio* calculations.⁷⁸ The b-GeS has a buckled configuration as shown in Fig. 239 (b), where the buckle is along the zigzag direction. This structure can be determined by two independent geometrical parameters, including the lattice constant 3.485 \AA and the bond length 2.428 \AA .

TABLE DIII: Two-body SW potential parameters for b-GeS used by GULP,⁸ as expressed in Eq. (3).

	A (eV)	ρ (\AA)	B (\AA^4)	r_{\min} (\AA)	r_{\max} (\AA)
Ge-S	7.657	1.363	17.377	0.0	3.338

TABLE DIV: Three-body SW potential parameters for b-GeS used by GULP,⁸ as expressed in Eq. (4).

	K (eV)	θ_0 (degree)	ρ_1 (Å)	ρ_2 (Å)	$r_{\min 12}$ (Å)	$r_{\max 12}$ (Å)	$r_{\min 13}$ (Å)	$r_{\max 13}$ (Å)	$r_{\min 23}$ (Å)	$r_{\max 23}$ (Å)
Ge-S-S	35.249	91.725	1.363	1.363	0.0	3.338	0.0	3.338	0.0	4.761
S-Ge-Ge	35.249	91.725	1.363	1.363	0.0	3.338	0.0	3.338	0.0	4.761

TABLE DV: SW potential parameters for b-GeS used by LAMMPS,⁹ as expressed in Eqs. (9) and (10).

	ϵ (eV)	σ (Å)	a	λ	γ	$\cos \theta_0$	A_L	B_L	p	q	tol
Ge-S-S	1.000	1.363	2.448	35.249	1.000	-0.030	7.657	5.030	4	0	0.0
S-Ge-Ge	1.000	1.363	2.448	35.249	1.000	-0.030	7.657	5.030	4	0	0.0

Table DII shows the VFF model for the single-layer b-GeS. The force constant parameters are determined by fitting to the acoustic branches in the phonon dispersion along the ΓM as shown in Fig. 258 (a). The *ab initio* calculations for the phonon dispersion are calculated from the SIESTA package.⁷⁹ The generalized gradients approximation is applied to account for the exchange-correlation function with Perdew, Burke, and Ernzerhof parameterization,⁸⁰ and the double- ζ orbital basis set is adopted. Fig. 258 (b) shows that the VFF model and the SW potential give exactly the same phonon dispersion, as the SW potential is derived from the VFF model.

The parameters for the two-body SW potential used by GULP are shown in Tab. DIII. The parameters for the three-body SW potential used by GULP are shown in Tab. DIV. Parameters for the SW potential used by LAMMPS are listed in Tab. DV.

We use LAMMPS to perform MD simulations for the mechanical behavior of the single-layer b-GeS under uniaxial tension at 1.0 K and 300.0 K. Fig. 259 shows the stress-strain curve for the tension of a single-layer b-GeS of dimension 100×100 Å. Periodic boundary conditions are applied in both armchair and zigzag directions. The single-layer b-GeS is stretched uniaxially along the armchair or zigzag direction. The stress is calculated without involving the actual thickness of the quasi-two-dimensional structure of the single-layer b-GeS. The Young's modulus can be obtained by a linear fitting of the stress-strain relation in the small strain range of $[0, 0.01]$. The Young's modulus are 34.9 N/m and 34.1 N/m

TABLE DVI: The VFF model for b-GeSe. The second line gives an explicit expression for each VFF term. The third line is the force constant parameters. Parameters are in the unit of $\frac{eV}{\text{\AA}^2}$ for the bond stretching interactions, and in the unit of eV for the angle bending interaction. The fourth line gives the initial bond length (in unit of \AA) for the bond stretching interaction and the initial angle (in unit of degrees) for the angle bending interaction.

VFF type	bond stretching	angle bending
expression	$\frac{1}{2}K_r (\Delta r)^2$	$\frac{1}{2}K_\theta (\Delta\theta)^2$
parameter	8.322	3.516
r_0 or θ_0	2.568	91.406

TABLE DVII: Two-body SW potential parameters for b-GeSe used by GULP,⁸ as expressed in Eq. (3).

	A (eV)	ρ (\AA)	B (\AA^4)	r_{\min} (\AA)	r_{\max} (\AA)
Ge-Se	8.498	1.430	21.745	0.0	3.526

along the armchair and zigzag directions, respectively. The Young's modulus is essentially isotropic in the armchair and zigzag directions. The Poisson's ratio from the VFF model and the SW potential is $\nu_{xy} = \nu_{yx} = 0.18$.

There is no available value for nonlinear quantities in the single-layer b-GeS. We have thus used the nonlinear parameter $B = 0.5d^4$ in Eq. (5), which is close to the value of B in most materials. The value of the third order nonlinear elasticity D can be extracted by fitting the stress-strain relation to the function $\sigma = E\epsilon + \frac{1}{2}D\epsilon^2$ with E as the Young's modulus. The values of D from the present SW potential are -128.1 N/m and -135.0 N/m along the armchair and zigzag directions, respectively. The ultimate stress is about 4.5 Nm^{-1} at the ultimate strain of 0.23 in the armchair direction at the low temperature of 1 K. The ultimate stress is about 4.3 Nm^{-1} at the ultimate strain of 0.27 in the zigzag direction at the low temperature of 1 K.

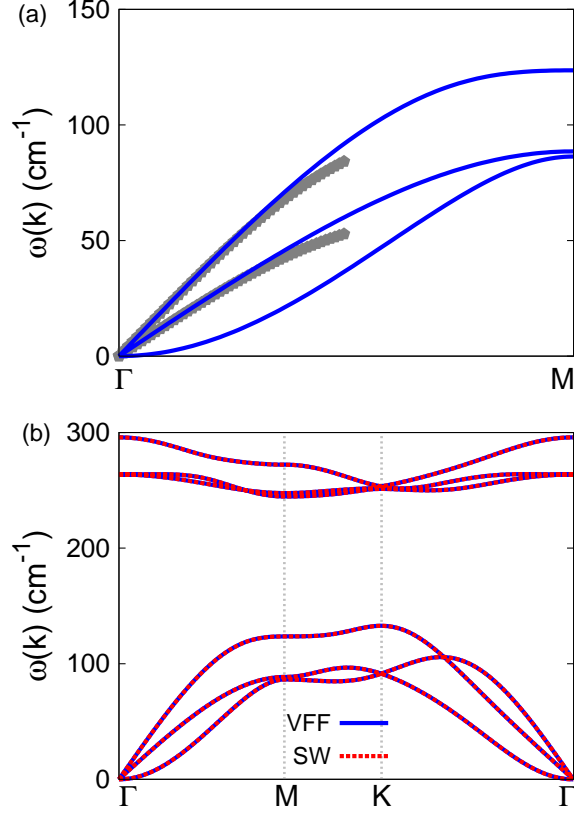


FIG. 260: (Color online) Phonon dispersion for the single-layer b-GeSe. (a) The VFF model is fitted to the two in-plane acoustic branches in the long wave limit along the ΓM direction. The *ab initio* results (gray pentagons) are calculated from SIESTA. (b) The VFF model (blue lines) and the SW potential (red lines) give the same phonon dispersion for the b-GeSe along $\Gamma MK\Gamma$.

TABLE DVIII: Three-body SW potential parameters for b-GeSe used by GULP,⁸ as expressed in Eq. (4).

	K (eV)	θ_0 (degree)	ρ_1 (\AA)	ρ_2 (\AA)	$r_{\min 12}$ (\AA)	$r_{\max 12}$ (\AA)	$r_{\min 13}$ (\AA)	$r_{\max 13}$ (\AA)	$r_{\min 23}$ (\AA)	$r_{\max 23}$ (\AA)
Ge-Se-Se	34.791	91.406	1.430	1.430	0.0	3.526	0.0	3.526	0.0	5.021
Se-Ge-Ge	34.791	91.406	1.430	1.430	0.0	3.526	0.0	3.526	0.0	5.021

CXXVII. B-GESE

Present studies on the buckled (b-) GeSe are based on first-principles calculations, and no empirical potential has been proposed for the b-GeSe. We will thus parametrize a set of

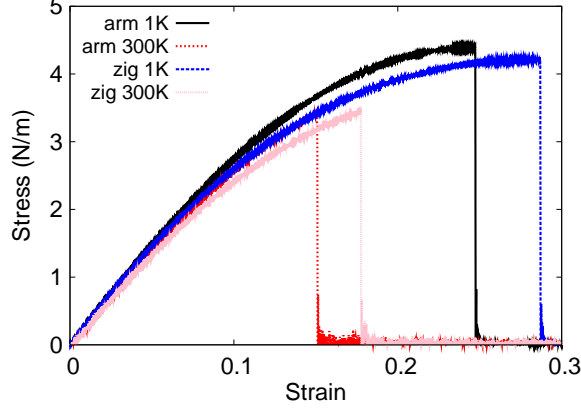


FIG. 261: (Color online) Stress-strain relations for the b-GeSe of size $100 \times 100 \text{ \AA}$. The b-GeSe is uniaxially stretched along the armchair or zigzag directions at temperatures 1 K and 300 K.

TABLE DIX: SW potential parameters for b-GeSe used by LAMMPS,⁹ as expressed in Eqs. (9) and (10).

	ϵ (eV)	σ (\AA)	a	λ	γ	$\cos \theta_0$	A_L	B_L	p	q	tol
Ge-Se-Se	1.000	1.430	2.466	34.791	1.000	-0.025	8.498	5.205	4	0	0.0
Se-Ge-Ge	1.000	1.430	2.466	34.791	1.000	-0.025	8.498	5.205	4	0	0.0

SW potential for the single-layer b-GeSe in this section.

The structure of the single-layer b-GeSe is shown in Fig. 239. The structural parameters are from the *ab initio* calculations.⁷⁸ The b-GeSe has a buckled configuration as shown in Fig. 239 (b), where the buckle is along the zigzag direction. This structure can be determined by two independent geometrical parameters, including the lattice constant 3.676 \AA and the bond length 2.568 \AA .

Table DVI shows the VFF model for the single-layer b-GeSe. The force constant parameters are determined by fitting to the acoustic branches in the phonon dispersion along the ΓM as shown in Fig. 260 (a). The *ab initio* calculations for the phonon dispersion are calculated from the SIESTA package.⁷⁹ The generalized gradients approximation is applied to account for the exchange-correlation function with Perdew, Burke, and Ernzerhof parameterization,⁸⁰ and the double- ζ orbital basis set is adopted. Fig. 260 (b) shows that the VFF model and the SW potential give exactly the same phonon dispersion, as the SW potential is derived from the VFF model.

The parameters for the two-body SW potential used by GULP are shown in Tab. DVII. The parameters for the three-body SW potential used by GULP are shown in Tab. DVIII. Parameters for the SW potential used by LAMMPS are listed in Tab. DIX.

We use LAMMPS to perform MD simulations for the mechanical behavior of the single-layer b-GeSe under uniaxial tension at 1.0 K and 300.0 K. Fig. 261 shows the stress-strain curve for the tension of a single-layer b-GeSe of dimension $100 \times 100 \text{ \AA}$. Periodic boundary conditions are applied in both armchair and zigzag directions. The single-layer b-GeSe is stretched uniaxially along the armchair or zigzag direction. The stress is calculated without involving the actual thickness of the quasi-two-dimensional structure of the single-layer b-GeSe. The Young's modulus can be obtained by a linear fitting of the stress-strain relation in the small strain range of $[0, 0.01]$. The Young's modulus are 31.6 N/m and 31.5 N/m along the armchair and zigzag directions, respectively. The Young's modulus is essentially isotropic in the armchair and zigzag directions. The Poisson's ratio from the VFF model and the SW potential is $\nu_{xy} = \nu_{yx} = 0.19$.

There is no available value for nonlinear quantities in the single-layer b-GeSe. We have thus used the nonlinear parameter $B = 0.5d^4$ in Eq. (5), which is close to the value of B in most materials. The value of the third order nonlinear elasticity D can be extracted by fitting the stress-strain relation to the function $\sigma = E\epsilon + \frac{1}{2}D\epsilon^2$ with E as the Young's modulus. The values of D from the present SW potential are -105.2 N/m and -118.3 N/m along the armchair and zigzag directions, respectively. The ultimate stress is about 4.4 Nm^{-1} at the ultimate strain of 0.24 in the armchair direction at the low temperature of 1 K. The ultimate stress is about 4.2 Nm^{-1} at the ultimate strain of 0.28 in the zigzag direction at the low temperature of 1 K.

CXXVIII. B-GETE

Present studies on the buckled (b-) GeTe are based on first-principles calculations, and no empirical potential has been proposed for the b-GeTe. We will thus parametrize a set of SW potential for the single-layer b-GeTe in this section.

The structure of the single-layer b-GeTe is shown in Fig. 239. The structural parameters are from the *ab initio* calculations.⁷⁸ The b-GeTe has a buckled configuration as shown in Fig. 239 (b), where the buckle is along the zigzag direction. This structure can be determined

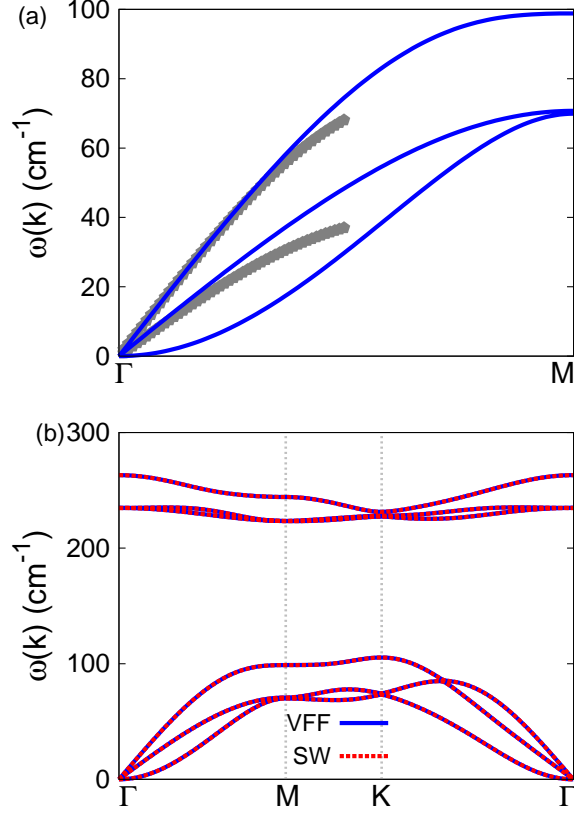


FIG. 262: (Color online) Phonon dispersion for the single-layer b-GeTe. (a) The VFF model is fitted to the two in-plane acoustic branches in the long wave limit along the Γ M direction. The *ab initio* results (gray pentagons) are calculated from SIESTA. (b) The VFF model (blue lines) and the SW potential (red lines) give the same phonon dispersion for the b-GeTe along Γ MKT.

by two independent geometrical parameters, including the lattice constant 3.939 \AA and the bond length 2.768 \AA .

Table DX shows the VFF model for the single-layer b-GeTe. The force constant parameters are determined by fitting to the acoustic branches in the phonon dispersion along the Γ M as shown in Fig. 262 (a). The *ab initio* calculations for the phonon dispersion are calculated from the SIESTA package.⁷⁹ The generalized gradients approximation is applied to account for the exchange-correlation function with Perdew, Burke, and Ernzerhof parameterization,⁸⁰ and the double- ζ orbital basis set is adopted. Fig. 262 (b) shows that the VFF model and the SW potential give exactly the same phonon dispersion, as the SW potential is derived from the VFF model.

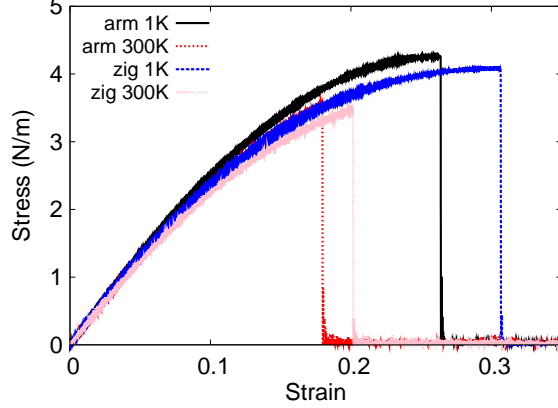


FIG. 263: (Color online) Stress-strain relations for the b-GeTe of size $100 \times 100 \text{ \AA}$. The b-GeTe is uniaxially stretched along the armchair or zigzag directions at temperatures 1 K and 300 K.

TABLE DX: The VFF model for b-GeTe. The second line gives an explicit expression for each VFF term. The third line is the force constant parameters. Parameters are in the unit of $\frac{\text{eV}}{\text{\AA}^2}$ for the bond stretching interactions, and in the unit of eV for the angle bending interaction. The fourth line gives the initial bond length (in unit of \AA) for the bond stretching interaction and the initial angle (in unit of degrees) for the angle bending interaction.

VFF type	bond stretching	angle bending
expression	$\frac{1}{2}K_r(\Delta r)^2$	$\frac{1}{2}K_\theta(\Delta\theta)^2$
parameter	8.322	3.516
r_0 or θ_0	2.768	90.718

The parameters for the two-body SW potential used by GULP are shown in Tab. DXI. The parameters for the three-body SW potential used by GULP are shown in Tab. DXII. Parameters for the SW potential used by LAMMPS are listed in Tab. DXIII.

We use LAMMPS to perform MD simulations for the mechanical behavior of the single-

TABLE DXI: Two-body SW potential parameters for b-GeTe used by GULP,⁸ as expressed in Eq. (3).

	A (eV)	ρ (\AA)	B (\AA^4)	r_{\min} (\AA)	r_{\max} (\AA)
Ge-Te	9.704	1.513	29.352	0.0	3.791

TABLE DXII: Three-body SW potential parameters for b-GeTe used by GULP,⁸ as expressed in Eq. (4).

	K (eV)	θ_0 (degree)	ρ_1 (Å)	ρ_2 (Å)	$r_{\min 12}$ (Å)	$r_{\max 12}$ (Å)	$r_{\min 13}$ (Å)	$r_{\max 13}$ (Å)	$r_{\min 23}$ (Å)	$r_{\max 23}$ (Å)
Ge-Te-Te	33.832	90.718	1.513	1.513	0.0	3.791	0.0	3.791	0.0	5.381
Te-Ge-Ge	33.832	90.718	1.513	1.513	0.0	3.791	0.0	3.791	0.0	5.381

TABLE DXIII: SW potential parameters for b-GeTe used by LAMMPS,⁹ as expressed in Eqs. (9) and (10).

	ϵ (eV)	σ (Å)	a	λ	γ	$\cos \theta_0$	A_L	B_L	p	q	tol
Ge-Te-Te	1.000	1.513	2.506	33.832	1.000	-0.013	9.704	5.605	4	0	0.0
Te-Ge-Ge	1.000	1.513	2.506	33.832	1.000	-0.013	9.704	5.605	4	0	0.0

layer b-GeTe under uniaxial tension at 1.0 K and 300.0 K. Fig. 263 shows the stress-strain curve for the tension of a single-layer b-GeTe of dimension 100×100 Å. Periodic boundary conditions are applied in both armchair and zigzag directions. The single-layer b-GeTe is stretched uniaxially along the armchair or zigzag direction. The stress is calculated without involving the actual thickness of the quasi-two-dimensional structure of the single-layer b-GeTe. The Young's modulus can be obtained by a linear fitting of the stress-strain relation in the small strain range of $[0, 0.01]$. The Young's modulus are 27.7 N/m and 28.0 N/m along the armchair and zigzag directions, respectively. The Young's modulus is essentially isotropic in the armchair and zigzag directions. The Poisson's ratio from the VFF model and the SW potential is $\nu_{xy} = \nu_{yx} = 0.21$.

There is no available value for nonlinear quantities in the single-layer b-GeTe. We have thus used the nonlinear parameter $B = 0.5d^4$ in Eq. (5), which is close to the value of B in most materials. The value of the third order nonlinear elasticity D can be extracted by fitting the stress-strain relation to the function $\sigma = E\epsilon + \frac{1}{2}D\epsilon^2$ with E as the Young's modulus. The values of D from the present SW potential are -80.4 N/m and -95.9 N/m along the armchair and zigzag directions, respectively. The ultimate stress is about 4.3 Nm^{-1} at the ultimate strain of 0.26 in the armchair direction at the low temperature of 1 K. The ultimate stress is about 4.1 Nm^{-1} at the ultimate strain of 0.30 in the zigzag direction at the low temperature of 1 K.

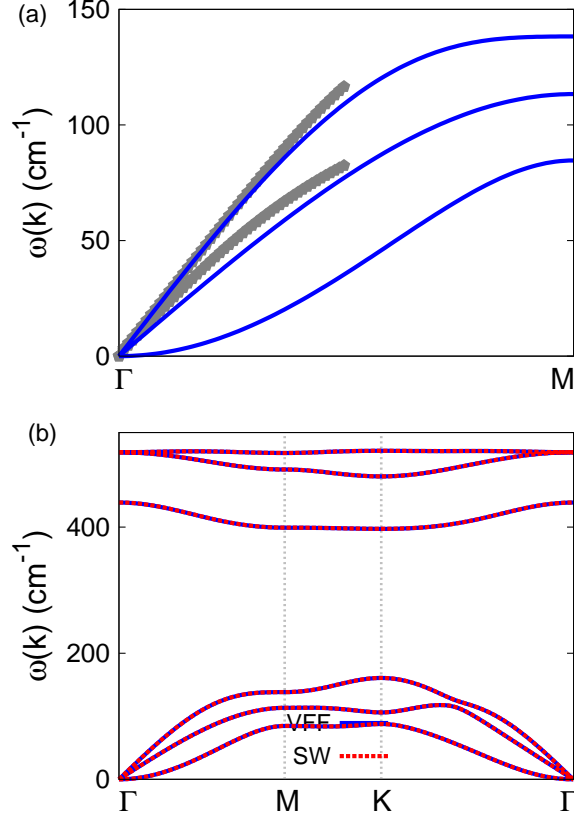


FIG. 264: (Color online) Phonon dispersion for the single-layer b-SnO. (a) The VFF model is fitted to the two in-plane acoustic branches in the long wave limit along the Γ M direction. The *ab initio* results (gray pentagons) are calculated from SIESTA. (b) The VFF model (blue lines) and the SW potential (red lines) give the same phonon dispersion for the b-SnO along Γ MK Γ .

CXXIX. B-SNO

Present studies on the buckled (b-) SnO are based on first-principles calculations, and no empirical potential has been proposed for the b-SnO. We will thus parametrize a set of SW potential for the single-layer b-SnO in this section.

The structure of the single-layer b-SnO is shown in Fig. 239. The structural parameters are from the *ab initio* calculations.⁷⁸ The b-SnO has a buckled configuration as shown in Fig. 239 (b), where the buckle is along the zigzag direction. This structure can be determined by two independent geometrical parameters, including the lattice constant 3.442 \AA and the bond length 2.204 \AA .

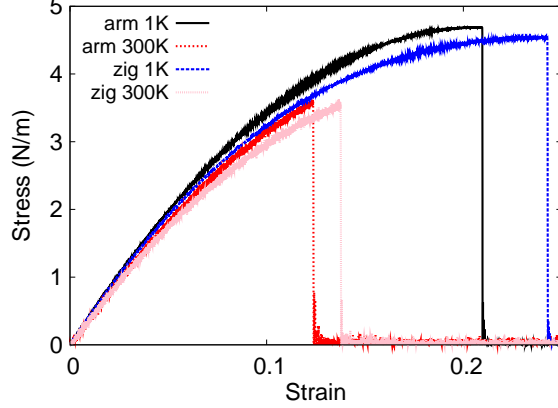


FIG. 265: (Color online) Stress-strain relations for the b-SnO of size $100 \times 100 \text{ \AA}$. The b-SnO is uniaxially stretched along the armchair or zigzag directions at temperatures 1 K and 300 K.

TABLE DXIV: The VFF model for b-SnO. The second line gives an explicit expression for each VFF term. The third line is the force constant parameters. Parameters are in the unit of $\frac{\text{eV}}{\text{\AA}^2}$ for the bond stretching interactions, and in the unit of eV for the angle bending interaction. The fourth line gives the initial bond length (in unit of \AA) for the bond stretching interaction and the initial angle (in unit of degrees) for the angle bending interaction.

VFF type	bond stretching	angle bending
expression	$\frac{1}{2}K_r(\Delta r)^2$	$\frac{1}{2}K_\theta(\Delta\theta)^2$
parameter	9.315	3.300
r_0 or θ_0	2.204	102.677

Table DXIV shows the VFF model for the single-layer b-SnO. The force constant parameters are determined by fitting to the acoustic branches in the phonon dispersion along the ΓM as shown in Fig. 264 (a). The *ab initio* calculations for the phonon dispersion are calculated from the SIESTA package.⁷⁹ The generalized gradients approximation is ap-

TABLE DXV: Two-body SW potential parameters for b-SnO used by GULP,⁸ as expressed in Eq. (3).

	A (eV)	ρ (\AA)	B (\AA^4)	r_{min} (\AA)	r_{max} (\AA)
Sn-O	9.133	1.609	11.798	0.0	3.146

TABLE DXVI: Three-body SW potential parameters for b-SnO used by GULP,⁸ as expressed in Eq. (4).

	K (eV)	θ_0 (degree)	ρ_1 (Å)	ρ_2 (Å)	$r_{\min 12}$ (Å)	$r_{\max 12}$ (Å)	$r_{\min 13}$ (Å)	$r_{\max 13}$ (Å)	$r_{\min 23}$ (Å)	$r_{\max 23}$ (Å)
Sn-O-O	52.875	102.677	1.609	1.609	0.0	3.146	0.0	3.146	0.0	4.702
O-Sn-Sn	52.875	102.677	1.609	1.609	0.0	3.146	0.0	3.146	0.0	4.702

TABLE DXVII: SW potential parameters for b-SnO used by LAMMPS,⁹ as expressed in Eqs. (9) and (10).

	ϵ (eV)	σ (Å)	a	λ	γ	$\cos \theta_0$	A_L	B_L	p	q	tol
Sn-O-O	1.000	1.609	1.955	52.875	1.000	-0.219	9.133	1.760	4	0	0.0
O-Sn-Sn	1.000	1.609	1.955	52.875	1.000	-0.219	9.133	1.760	4	0	0.0

plied to account for the exchange-correlation function with Perdew, Burke, and Ernzerhof parameterization,⁸⁰ and the double- ζ orbital basis set is adopted. Fig. 264 (b) shows that the VFF model and the SW potential give exactly the same phonon dispersion, as the SW potential is derived from the VFF model.

The parameters for the two-body SW potential used by GULP are shown in Tab. DXV. The parameters for the three-body SW potential used by GULP are shown in Tab. DXVI. Parameters for the SW potential used by LAMMPS are listed in Tab. DXVII.

We use LAMMPS to perform MD simulations for the mechanical behavior of the single-layer b-SnO under uniaxial tension at 1.0 K and 300.0 K. Fig. 265 shows the stress-strain curve for the tension of a single-layer b-SnO of dimension 100×100 Å. Periodic boundary conditions are applied in both armchair and zigzag directions. The single-layer b-SnO is stretched uniaxially along the armchair or zigzag direction. The stress is calculated without involving the actual thickness of the quasi-two-dimensional structure of the single-layer b-SnO. The Young's modulus can be obtained by a linear fitting of the stress-strain relation in the small strain range of $[0, 0.01]$. The Young's modulus are 43.7 N/m and 43.8 N/m along the armchair and zigzag directions, respectively. The Young's modulus is essentially isotropic in the armchair and zigzag directions. The Poisson's ratio from the VFF model and the SW potential is $\nu_{xy} = \nu_{yx} = 0.12$.

There is no available value for nonlinear quantities in the single-layer b-SnO. We have

TABLE DXVIII: The VFF model for b-SnS. The second line gives an explicit expression for each VFF term. The third line is the force constant parameters. Parameters are in the unit of $\frac{\text{eV}}{\text{\AA}^2}$ for the bond stretching interactions, and in the unit of eV for the angle bending interaction. The fourth line gives the initial bond length (in unit of \AA) for the bond stretching interaction and the initial angle (in unit of degrees) for the angle bending interaction.

VFF type	bond stretching	angle bending
expression	$\frac{1}{2}K_r (\Delta r)^2$	$\frac{1}{2}K_\theta (\Delta \theta)^2$
parameter	6.909	2.710
r_0 or θ_0	2.616	91.793

TABLE DXIX: Two-body SW potential parameters for b-SnS used by GULP,⁸ as expressed in Eq. (3).

	A (eV)	ρ (\AA)	B (\AA^4)	r_{\min} (\AA)	r_{\max} (\AA)
Sn-S	7.392	1.472	23.416	0.0	3.597

thus used the nonlinear parameter $B = 0.5d^4$ in Eq. (5), which is close to the value of B in most materials. The value of the third order nonlinear elasticity D can be extracted by fitting the stress-strain relation to the function $\sigma = E\epsilon + \frac{1}{2}D\epsilon^2$ with E as the Young's modulus. The values of D from the present SW potential are -199.9 N/m and -215.1 N/m along the armchair and zigzag directions, respectively. The ultimate stress is about 4.7 Nm^{-1} at the ultimate strain of 0.21 in the armchair direction at the low temperature of 1 K. The ultimate stress is about 4.5 Nm^{-1} at the ultimate strain of 0.24 in the zigzag direction at the low temperature of 1 K.

CXXX. B-SNS

Present studies on the buckled (b-) SnS are based on first-principles calculations, and no empirical potential has been proposed for the b-SnS. We will thus parametrize a set of SW potential for the single-layer b-SnS in this section.

The structure of the single-layer b-SnS is shown in Fig. 239. The structural parameters are from the *ab initio* calculations.⁷⁸ The b-SnS has a buckled configuration as shown in

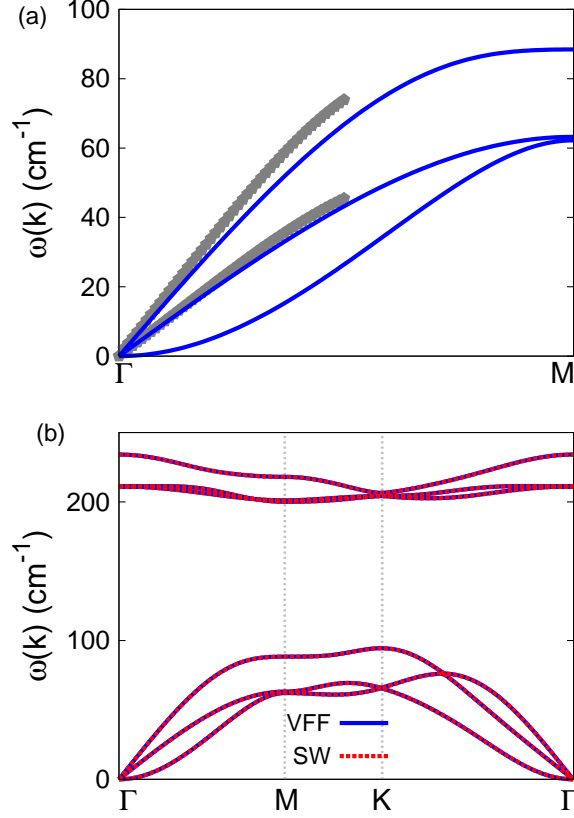


FIG. 266: (Color online) Phonon dispersion for the single-layer b-SnS. (a) The VFF model is fitted to the two in-plane acoustic branches in the long wave limit along the Γ M direction. The *ab initio* results (gray pentagons) are calculated from SIESTA. (b) The VFF model (blue lines) and the SW potential (red lines) give the same phonon dispersion for the b-SnS along Γ MKT.

TABLE DXX: Three-body SW potential parameters for b-SnS used by GULP,⁸ as expressed in Eq. (4).

	K (eV)	θ_0 (degree)	ρ_1 (\AA)	ρ_2 (\AA)	$r_{\min 12}$ (\AA)	$r_{\max 12}$ (\AA)	$r_{\min 13}$ (\AA)	$r_{\max 13}$ (\AA)	$r_{\min 23}$ (\AA)	$r_{\max 23}$ (\AA)
Sn-S-S	27.243	91.793	1.472	1.472	0.0	3.597	0.0	3.597	0.0	5.132
S-Sn-Sn	27.243	91.793	1.472	1.472	0.0	3.597	0.0	3.597	0.0	5.132

Fig. 239 (b), where the buckle is along the zigzag direction. This structure can be determined by two independent geometrical parameters, including the lattice constant 3.757 \AA and the bond length 2.616 \AA .

Table DXVIII shows the VFF model for the single-layer b-SnS. The force constant pa-

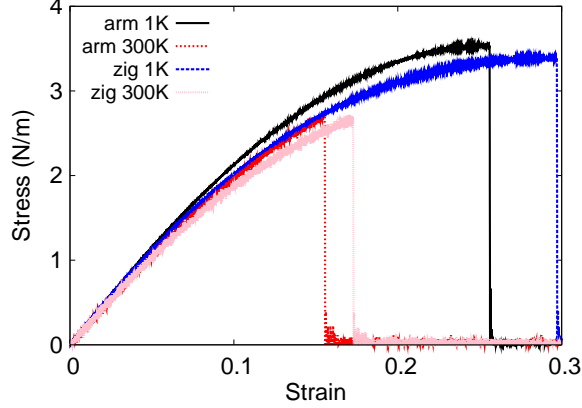


FIG. 267: (Color online) Stress-strain relations for the b-SnS of size $100 \times 100 \text{ \AA}$. The b-SnS is uniaxially stretched along the armchair or zigzag directions at temperatures 1 K and 300 K.

TABLE DXXI: SW potential parameters for b-SnS used by LAMMPS,⁹ as expressed in Eqs. (9) and (10).

	ϵ (eV)	σ (\AA)	a	λ	γ	$\cos \theta_0$	A_L	B_L	p	q	tol
Sn-S-S	1.000	1.472	2.444	27.243	1.000	-0.031	7.392	4.994	4	0	0.0
S-Sn-Sn	1.000	1.472	2.444	27.243	1.000	-0.031	7.392	4.994	4	0	0.0

parameters are determined by fitting to the acoustic branches in the phonon dispersion along the Γ M as shown in Fig. 266 (a). The *ab initio* calculations for the phonon dispersion are calculated from the SIESTA package.⁷⁹ The generalized gradients approximation is applied to account for the exchange-correlation function with Perdew, Burke, and Ernzerhof parameterization,⁸⁰ and the double- ζ orbital basis set is adopted. Fig. 266 (b) shows that the VFF model and the SW potential give exactly the same phonon dispersion, as the SW potential is derived from the VFF model.

The parameters for the two-body SW potential used by GULP are shown in Tab. DXIX. The parameters for the three-body SW potential used by GULP are shown in Tab. DXX. Parameters for the SW potential used by LAMMPS are listed in Tab. DXXI.

We use LAMMPS to perform MD simulations for the mechanical behavior of the single-layer b-SnS under uniaxial tension at 1.0 K and 300.0 K. Fig. 267 shows the stress-strain curve for the tension of a single-layer b-SnS of dimension $100 \times 100 \text{ \AA}$. Periodic boundary conditions are applied in both armchair and zigzag directions. The single-layer b-SnS is

TABLE DXXII: The VFF model for b-SnSe. The second line gives an explicit expression for each VFF term. The third line is the force constant parameters. Parameters are in the unit of $\frac{eV}{\text{\AA}^2}$ for the bond stretching interactions, and in the unit of eV for the angle bending interaction. The fourth line gives the initial bond length (in unit of \AA) for the bond stretching interaction and the initial angle (in unit of degrees) for the angle bending interaction.

VFF type	bond stretching	angle bending
expression	$\frac{1}{2}K_r (\Delta r)^2$	$\frac{1}{2}K_\theta (\Delta\theta)^2$
parameter	6.909	2.710
r_0 or θ_0	2.747	90.923

stretched uniaxially along the armchair or zigzag direction. The stress is calculated without involving the actual thickness of the quasi-two-dimensional structure of the single-layer b-SnS. The Young's modulus can be obtained by a linear fitting of the stress-strain relation in the small strain range of $[0, 0.01]$. The Young's modulus are 23.8 N/m and 24.4 N/m along the armchair and zigzag directions, respectively. The Young's modulus is essentially isotropic in the armchair and zigzag directions. The Poisson's ratio from the VFF model and the SW potential is $\nu_{xy} = \nu_{yx} = 0.20$.

There is no available value for nonlinear quantities in the single-layer b-SnS. We have thus used the nonlinear parameter $B = 0.5d^4$ in Eq. (5), which is close to the value of B in most materials. The value of the third order nonlinear elasticity D can be extracted by fitting the stress-strain relation to the function $\sigma = E\epsilon + \frac{1}{2}D\epsilon^2$ with E as the Young's modulus. The values of D from the present SW potential are -71.8 N/m and -88.3 N/m along the armchair and zigzag directions, respectively. The ultimate stress is about 3.5 Nm^{-1} at the ultimate strain of 0.25 in the armchair direction at the low temperature of 1 K. The ultimate stress is about 3.4 Nm^{-1} at the ultimate strain of 0.29 in the zigzag direction at the low temperature of 1 K.

CXXXI. B-SNSE

Present studies on the buckled (b-) SnSe are based on first-principles calculations, and no empirical potential has been proposed for the b-SnSe. We will thus parametrize a set of

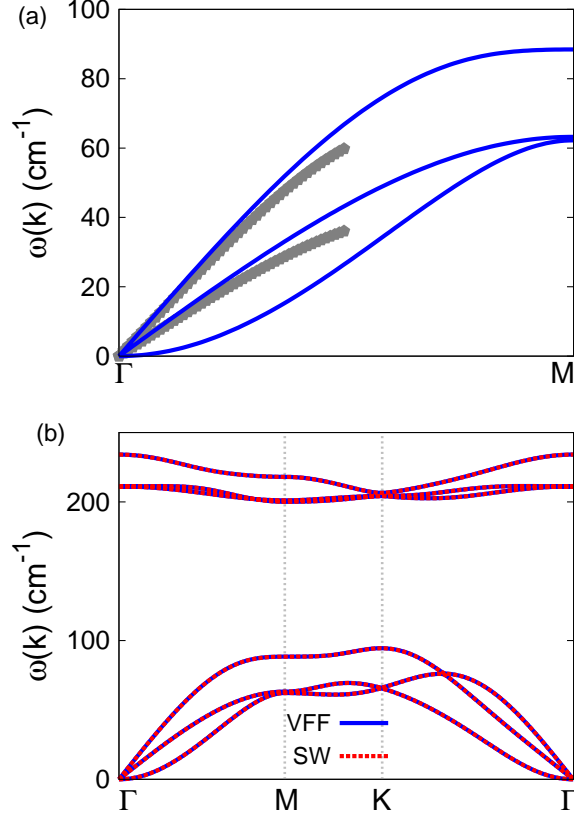


FIG. 268: (Color online) Phonon dispersion for the single-layer b-SnSe. (a) The VFF model is fitted to the two in-plane acoustic branches in the long wave limit along the ΓM direction. The *ab initio* results (gray pentagons) are calculated from SIESTA. (b) The VFF model (blue lines) and the SW potential (red lines) give the same phonon dispersion for the b-SnSe along $\Gamma MK\Gamma$.

TABLE DXXIII: Two-body SW potential parameters for b-SnSe used by GULP,⁸ as expressed in Eq. (3).

	A (eV)	ρ (\AA)	B (\AA^4)	r_{\min} (\AA)	r_{\max} (\AA)
Si-Se	7.976	1.510	28.471	0.0	3.765

SW potential for the single-layer b-SnSe in this section.

The structure of the single-layer b-SnSe is shown in Fig. 239. The structural parameters are from the *ab initio* calculations.⁷⁸ The b-SnSe has a buckled configuration as shown in Fig. 239 (b), where the buckle is along the zigzag direction. This structure can be determined by two independent geometrical parameters, including the lattice constant 3.916 \AA and the

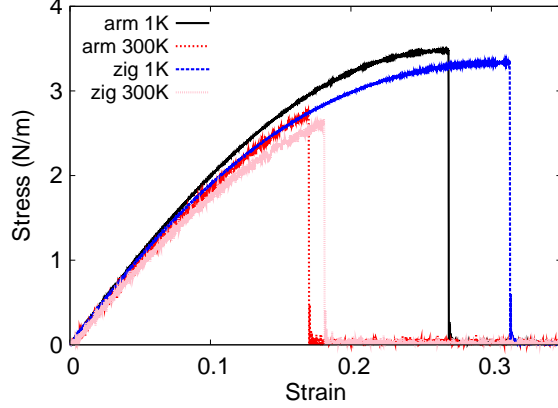


FIG. 269: (Color online) Stress-strain relations for the b-SnSe of size $100 \times 100 \text{ \AA}$. The b-SnSe is uniaxially stretched along the armchair or zigzag directions at temperatures 1 K and 300 K.

TABLE DXXIV: Three-body SW potential parameters for b-SnSe used by GULP,⁸ as expressed in Eq. (4).

	K (eV)	θ_0 (degree)	ρ_1 (\AA)	ρ_2 (\AA)	$r_{\min 12}$ (\AA)	$r_{\max 12}$ (\AA)	$r_{\min 13}$ (\AA)	$r_{\max 13}$ (\AA)	$r_{\min 23}$ (\AA)	$r_{\max 23}$ (\AA)
Sn-Se-Se	26.294	90.923	1.510	1.510	0.0	3.765	0.0	3.765	0.0	5.349
Se-Sn-Sn	26.294	90.923	1.510	1.510	0.0	3.765	0.0	3.765	0.0	5.349

bond length 2.747 \AA .

Table DXXII shows the VFF model for the single-layer b-SnSe. The force constant parameters are determined by fitting to the acoustic branches in the phonon dispersion along the ΓM as shown in Fig. 268 (a). The *ab initio* calculations for the phonon dispersion are calculated from the SIESTA package.⁷⁹ The generalized gradients approximation is applied to account for the exchange-correlation function with Perdew, Burke, and Ernzerhof parameterization,⁸⁰ and the double- ζ orbital basis set is adopted. Fig. 268 (b) shows that

TABLE DXXV: SW potential parameters for b-SnSe used by LAMMPS,⁹ as expressed in Eqs. (9) and (10).

	ϵ (eV)	σ (\AA)	a	λ	γ	$\cos \theta_0$	A_L	B_L	p	q	tol
Sn-Se-Se	1.000	1.510	2.494	26.294	1.000	-0.016	7.976	5.482	4	0	0.0
Se-Sn-Sn	1.000	1.510	2.494	26.294	1.000	-0.016	7.976	5.482	4	0	0.0

the VFF model and the SW potential give exactly the same phonon dispersion, as the SW potential is derived from the VFF model.

The parameters for the two-body SW potential used by GULP are shown in Tab. [DXXIII](#). The parameters for the three-body SW potential used by GULP are shown in Tab. [DXXIV](#). Parameters for the SW potential used by LAMMPS are listed in Tab. [DXXV](#).

We use LAMMPS to perform MD simulations for the mechanical behavior of the single-layer b-SnSe under uniaxial tension at 1.0 K and 300.0 K. Fig. [269](#) shows the stress-strain curve for the tension of a single-layer b-SnSe of dimension 100×100 Å. Periodic boundary conditions are applied in both armchair and zigzag directions. The single-layer b-SnSe is stretched uniaxially along the armchair or zigzag direction. The stress is calculated without involving the actual thickness of the quasi-two-dimensional structure of the single-layer b-SnSe. The Young's modulus can be obtained by a linear fitting of the stress-strain relation in the small strain range of $[0, 0.01]$. The Young's modulus are 22.0 N/m and 22.2 N/m along the armchair and zigzag directions, respectively. The Young's modulus is essentially isotropic in the armchair and zigzag directions. The Poisson's ratio from the VFF model and the SW potential is $\nu_{xy} = \nu_{yx} = 0.22$.

There is no available value for nonlinear quantities in the single-layer b-SnSe. We have thus used the nonlinear parameter $B = 0.5d^4$ in Eq. (5), which is close to the value of B in most materials. The value of the third order nonlinear elasticity D can be extracted by fitting the stress-strain relation to the function $\sigma = E\epsilon + \frac{1}{2}D\epsilon^2$ with E as the Young's modulus. The values of D from the present SW potential are -61.6 N/m and -73.69 N/m along the armchair and zigzag directions, respectively. The ultimate stress is about 3.5 Nm^{-1} at the ultimate strain of 0.27 in the armchair direction at the low temperature of 1 K. The ultimate stress is about 3.3 Nm^{-1} at the ultimate strain of 0.31 in the zigzag direction at the low temperature of 1 K.

CXXXII. B-SNTE

Present studies on the buckled (b-) SnTe are based on first-principles calculations, and no empirical potential has been proposed for the b-SnTe. We will thus parametrize a set of SW potential for the single-layer b-SnTe in this section.

The structure of the single-layer b-SnTe is shown in Fig. [239](#). The structural parameters

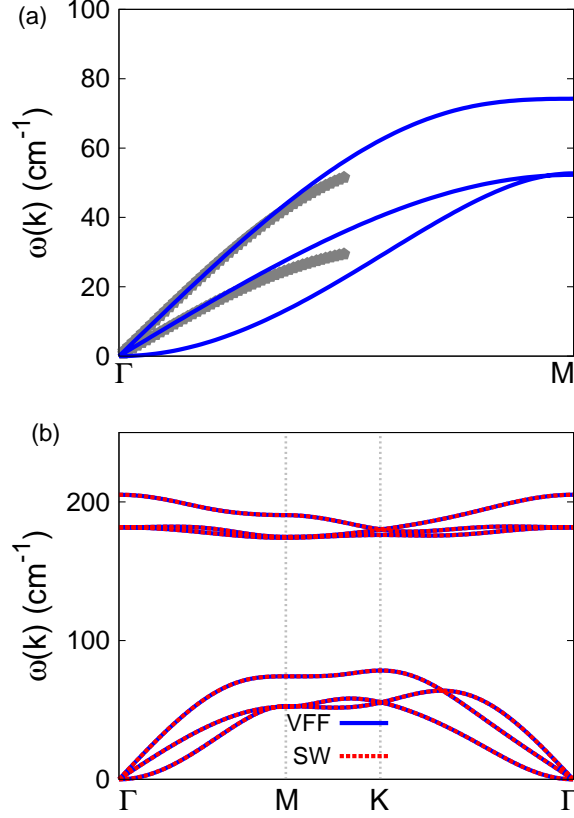


FIG. 270: (Color online) Phonon dispersion for the single-layer b-SnTe. (a) The VFF model is fitted to the two in-plane acoustic branches in the long wave limit along the ΓM direction. The *ab initio* results (gray pentagons) are calculated from SIESTA. (b) The VFF model (blue lines) and the SW potential (red lines) give the same phonon dispersion for the b-SnTe along $\Gamma MK\Gamma$.

are from the *ab initio* calculations.⁷⁸ The b-SnTe has a buckled configuration as shown in Fig. 239 (b), where the buckle is along the zigzag direction. This structure can be determined by two independent geometrical parameters, including the lattice constant 4.151 \AA and the bond length 2.947 \AA .

Table DXXVI shows the VFF model for the single-layer b-SnTe. The force constant parameters are determined by fitting to the acoustic branches in the phonon dispersion along the ΓM as shown in Fig. 270 (a). The *ab initio* calculations for the phonon dispersion are calculated from the SIESTA package.⁷⁹ The generalized gradients approximation is applied to account for the exchange-correlation function with Perdew, Burke, and Ernzerhof parameterization,⁸⁰ and the double- ζ orbital basis set is adopted. Fig. 270 (b) shows that

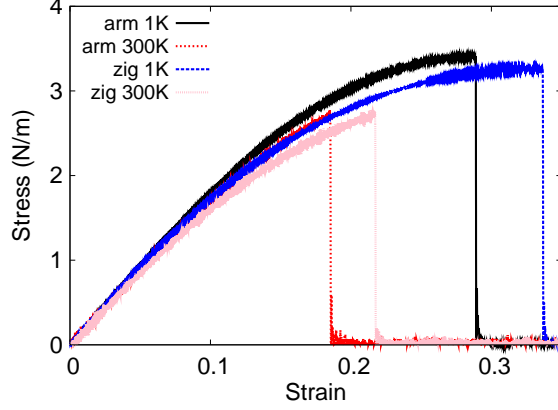


FIG. 271: (Color online) Stress-strain relations for the b-SnTe of size $100 \times 100 \text{ \AA}$. The b-SnTe is uniaxially stretched along the armchair or zigzag directions at temperatures 1 K and 300 K.

TABLE DXXVI: The VFF model for b-SnTe. The second line gives an explicit expression for each VFF term. The third line is the force constant parameters. Parameters are in the unit of $\frac{\text{eV}}{\text{\AA}^2}$ for the bond stretching interactions, and in the unit of eV for the angle bending interaction. The fourth line gives the initial bond length (in unit of \AA) for the bond stretching interaction and the initial angle (in unit of degrees) for the angle bending interaction.

VFF type	bond stretching	angle bending
expression	$\frac{1}{2}K_r (\Delta r)^2$	$\frac{1}{2}K_\theta (\Delta \theta)^2$
parameter	6.909	2.710
r_0 or θ_0	2.947	89.542

the VFF model and the SW potential give exactly the same phonon dispersion, as the SW potential is derived from the VFF model.

The parameters for the two-body SW potential used by GULP are shown in Tab. DXXVII. The parameters for the three-body SW potential used by GULP are shown in Tab. DXXVIII.

TABLE DXXVII: Two-body SW potential parameters for b-SnTe used by GULP,⁸ as expressed in Eq. (3).

	A (eV)	ρ (\AA)	B (\AA^4)	r_{\min} (\AA)	r_{\max} (\AA)
Sn-Te	8.864	1.559	37.713	0.0	4.019

TABLE DXXVIII: Three-body SW potential parameters for b-SnTe used by GULP,⁸ as expressed in Eq. (4).

	K (eV)	θ_0 (degree)	ρ_1 (Å)	ρ_2 (Å)	$r_{\min 12}$ (Å)	$r_{\max 12}$ (Å)	$r_{\min 13}$ (Å)	$r_{\max 13}$ (Å)	$r_{\min 23}$ (Å)	$r_{\max 23}$ (Å)
Sn-Te-Te	24.867	89.542	1.559	1.559	0.0	4.019	0.0	4.019	0.0	5.670
Te-Sn-Sn	24.867	89.542	1.559	1.559	0.0	4.019	0.0	4.019	0.0	5.670

TABLE DXXIX: SW potential parameters for b-SnTe used by LAMMPS,⁹ as expressed in Eqs. (9) and (10).

	ϵ (eV)	σ (Å)	a	λ	γ	$\cos \theta_0$	A_L	B_L	p	q	tol
Sn-Te-Te	1.000	1.559	2.577	24.867	1.000	0.008	8.864	6.378	4	0	0.0
Te-Sn-Sn	1.000	1.559	2.577	24.867	1.000	0.008	8.864	6.378	4	0	0.0

Parameters for the SW potential used by LAMMPS are listed in Tab. DXXIX.

We use LAMMPS to perform MD simulations for the mechanical behavior of the single-layer b-SnTe under uniaxial tension at 1.0 K and 300.0 K. Fig. 271 shows the stress-strain curve for the tension of a single-layer b-SnTe of dimension 100×100 Å. Periodic boundary conditions are applied in both armchair and zigzag directions. The single-layer b-SnTe is stretched uniaxially along the armchair or zigzag direction. The stress is calculated without involving the actual thickness of the quasi-two-dimensional structure of the single-layer b-SnTe. The Young's modulus can be obtained by a linear fitting of the stress-strain relation in the small strain range of $[0, 0.01]$. The Young's modulus are 19.6 N/m and 19.1 N/m along the armchair and zigzag directions, respectively. The Young's modulus is essentially isotropic in the armchair and zigzag directions. The Poisson's ratio from the VFF model and the SW potential is $\nu_{xy} = \nu_{yx} = 0.23$.

There is no available value for nonlinear quantities in the single-layer b-SnTe. We have thus used the nonlinear parameter $B = 0.5d^4$ in Eq. (5), which is close to the value of B in most materials. The value of the third order nonlinear elasticity D can be extracted by fitting the stress-strain relation to the function $\sigma = E\epsilon + \frac{1}{2}D\epsilon^2$ with E as the Young's modulus. The values of D from the present SW potential are -48.7 N/m and -54.3 N/m along the armchair and zigzag directions, respectively. The ultimate stress is about 3.4 Nm^{-1} at the ultimate strain of 0.29 in the armchair direction at the low temperature of 1 K. The

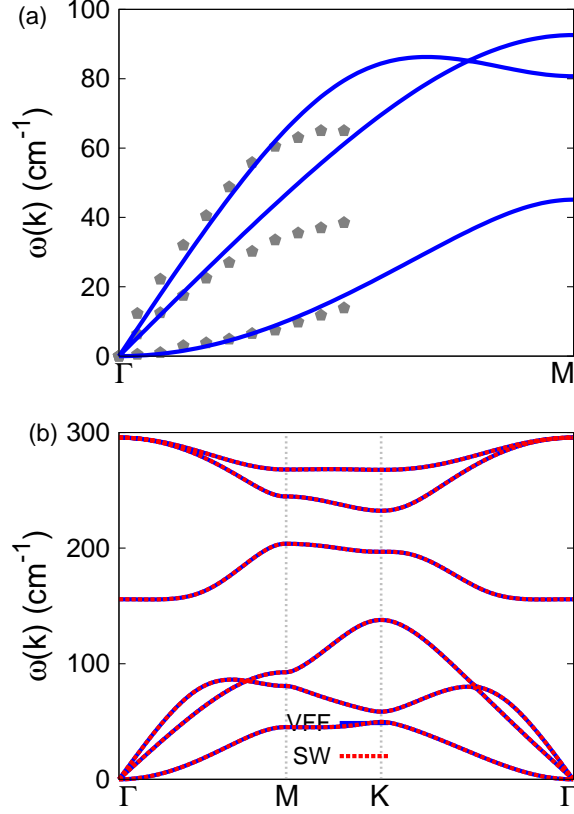


FIG. 272: (Color online) Phonon dispersion for the single-layer b-SnGe. (a) The VFF model is fitted to the three acoustic branches in the long wave limit along the Γ M direction. The *ab initio* results (gray pentagons) are from Ref. 114. (b) The VFF model (blue lines) and the SW potential (red lines) give the same phonon dispersion for the b-SnGe along Γ MK Γ .

ultimate stress is about 3.3 Nm^{-1} at the ultimate strain of 0.33 in the zigzag direction at the low temperature of 1 K.

CXXXIII. B-SNGE

Present studies on the buckled SnGe (b-SnGe) are based on first-principles calculations, and no empirical potential has been proposed for the b-SnGe. We will thus parametrize a set of SW potential for the single-layer b-SnGe in this section.

The structure of the single-layer b-SnGe is shown in Fig. 239. The structural parameters are from the *ab initio* calculations.¹¹⁴ The b-SnGe has a buckled configuration as shown in

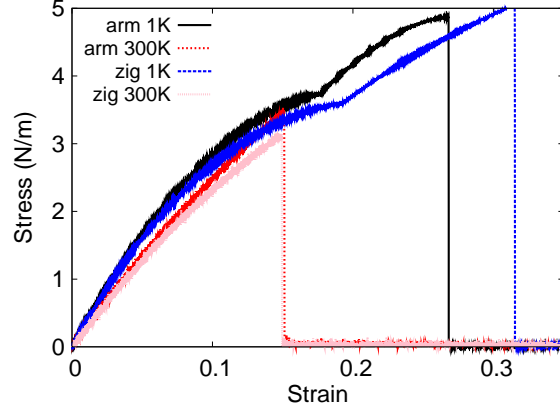


FIG. 273: (Color online) Stress-strain relations for the b-SnGe of size $100 \times 100 \text{ \AA}$. The b-SnGe is uniaxially stretched along the armchair or zigzag directions at temperatures 1 K and 300 K.

TABLE DXXX: The VFF model for b-SnGe. The second line gives an explicit expression for each VFF term. The third line is the force constant parameters. Parameters are in the unit of $\frac{\text{eV}}{\text{\AA}^2}$ for the bond stretching interactions, and in the unit of eV for the angle bending interaction. The fourth line gives the initial bond length (in unit of \AA) for the bond stretching interaction and the initial angle (in unit of degrees) for the angle bending interaction.

VFF type	bond stretching	angle bending
expression	$\frac{1}{2}K_r(\Delta r)^2$	$\frac{1}{2}K_\theta(\Delta\theta)^2$
parameter	8.390	3.112
r_0 or θ_0	2.570	112.350

Fig. 239 (b), where the buckle is along the zigzag direction. This structure can be determined by two independent geometrical parameters, eg. the lattice constant 4.27 \AA and the bond length 2.57 \AA . The resultant height of the buckle is $h = 0.73 \text{ \AA}$.

Table DXXX shows the VFF model for the single-layer b-SnGe. The force constant

TABLE DXXXI: Two-body SW potential parameters for b-SnGe used by GULP,⁸ as expressed in Eq. (3).

	A (eV)	ρ (\AA)	B (\AA^4)	r_{\min} (\AA)	r_{\max} (\AA)
Sn-Ge	13.674	2.267	21.812	0.0	3.777

TABLE DXXXII: Three-body SW potential parameters for b-SnGe used by GULP,⁸ as expressed in Eq. (4).

	K (eV)	θ_0 (degree)	ρ_1 (Å)	ρ_2 (Å)	$r_{\min 12}$ (Å)	$r_{\max 12}$ (Å)	$r_{\min 13}$ (Å)	$r_{\max 13}$ (Å)	$r_{\min 23}$ (Å)	$r_{\max 23}$ (Å)
Sn-Ge-Ge	77.881	112.350	2.267	2.267	0.0	3.777	0.0	3.777	0.0	5.833
Ge-Sn-Sn	77.881	112.350	2.267	2.267	0.0	3.777	0.0	3.777	0.0	5.833

TABLE DXXXIII: SW potential parameters for b-SnGe used by LAMMPS,⁹ as expressed in Eqs. (9) and (10).

	ϵ (eV)	σ (Å)	a	λ	γ	$\cos \theta_0$	A_L	B_L	p	q	tol
Sn-Ge-Ge	1.000	2.267	1.666	77.881	1.000	-0.380	13.674	0.826	4	0	0.0
Ge-Sn-Sn	1.000	2.267	1.666	77.881	1.000	-0.380	13.674	0.826	4	0	0.0

parameters are determined by fitting to the acoustic branches in the phonon dispersion along the ΓM as shown in Fig. 272 (a). The *ab initio* calculations for the phonon dispersion are from Ref. 114. Fig. 272 (b) shows that the VFF model and the SW potential give exactly the same phonon dispersion, as the SW potential is derived from the VFF model.

The parameters for the two-body SW potential used by GULP are shown in Tab. DXXXI. The parameters for the three-body SW potential used by GULP are shown in Tab. DXXXII. Parameters for the SW potential used by LAMMPS are listed in Tab. DXXXIII.

We use LAMMPS to perform MD simulations for the mechanical behavior of the single-layer b-SnGe under uniaxial tension at 1.0 K and 300.0 K. Fig. 273 shows the stress-strain curve for the tension of a single-layer b-SnGe of dimension 100×100 Å. Periodic boundary conditions are applied in both armchair and zigzag directions. The single-layer b-SnGe is stretched uniaxially along the armchair or zigzag direction. The stress is calculated without involving the actual thickness of the quasi-two-dimensional structure of the single-layer b-SnGe. The Young's modulus can be obtained by a linear fitting of the stress-strain relation in the small strain range of $[0, 0.01]$. The Young's modulus is 36.8 N/m along both armchair and zigzag directions. The Poisson's ratio from the VFF model and the SW potential is $\nu_{xy} = \nu_{yx} = 0.11$.

There is no available value for nonlinear quantities in the single-layer b-SnGe. We have thus used the nonlinear parameter $B = 0.5d^4$ in Eq. (5), which is close to the value of B

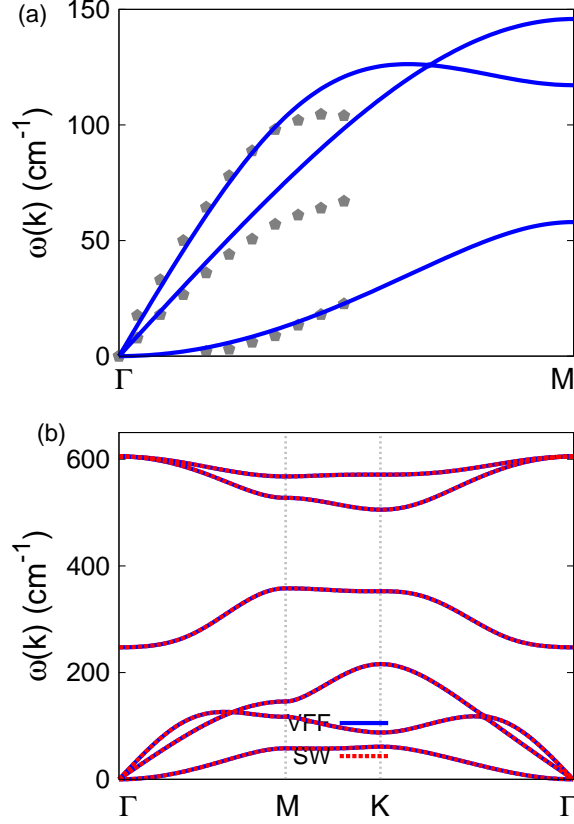


FIG. 274: (Color online) Phonon dispersion for the single-layer b-SiGe. (a) The VFF model is fitted to the three acoustic branches in the long wave limit along the Γ M direction. The *ab initio* results (gray pentagons) are from Ref. 114. (b) The VFF model (blue lines) and the SW potential (red lines) give the same phonon dispersion for the b-SiGe along Γ MK Γ .

in most materials. The value of the third order nonlinear elasticity D can be extracted by fitting the stress-strain relation to the function $\sigma = E\epsilon + \frac{1}{2}D\epsilon^2$ with E as the Young's modulus. The values of D from the present SW potential are -171.6 N/m and -197.0 N/m along the armchair and zigzag directions, respectively. The ultimate stress is about 4.9 Nm^{-1} at the ultimate strain of 0.27 in the armchair direction at the low temperature of 1 K. The ultimate stress is about 5.0 Nm^{-1} at the ultimate strain of 0.31 in the zigzag direction at the low temperature of 1 K.

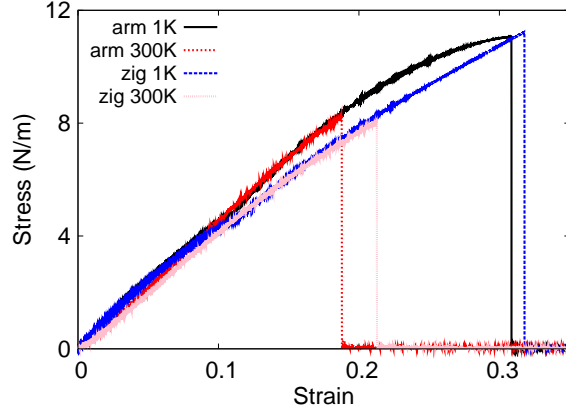


FIG. 275: (Color online) Stress-strain relations for the b-SiGe of size $100 \times 100 \text{ \AA}$. The b-SiGe is uniaxially stretched along the armchair or zigzag directions at temperatures 1 K and 300 K.

TABLE DXXXIV: The VFF model for b-SiGe. The second line gives an explicit expression for each VFF term. The third line is the force constant parameters. Parameters are in the unit of $\frac{\text{eV}}{\text{\AA}^2}$ for the bond stretching interactions, and in the unit of eV for the angle bending interaction. The fourth line gives the initial bond length (in unit of \AA) for the bond stretching interaction and the initial angle (in unit of degrees) for the angle bending interaction.

VFF type	bond stretching	angle bending
expression	$\frac{1}{2}K_r(\Delta r)^2$	$\frac{1}{2}K_\theta(\Delta\theta)^2$
parameter	16.390	3.112
r_0 or θ_0	2.310	114.702

CXXXIV. B-SIGE

Present studies on the buckled SiGe (b-SiGe) are based on first-principles calculations, and no empirical potential has been proposed for the b-SiGe. We will thus parametrize a

TABLE DXXXV: Two-body SW potential parameters for b-SiGe used by GULP,⁸ as expressed in Eq. (3).

	A (eV)	ρ (\AA)	B (\AA^4)	r_{\min} (\AA)	r_{\max} (\AA)
Si-Ge	22.576	2.122	14.237	0.0	3.417

TABLE DXXXVI: Three-body SW potential parameters for b-SiGe used by GULP,⁸ as expressed in Eq. (4).

	K (eV)	θ_0 (degree)	ρ_1 (Å)	ρ_2 (Å)	$r_{\min 12}$ (Å)	$r_{\max 12}$ (Å)	$r_{\min 13}$ (Å)	$r_{\max 13}$ (Å)	$r_{\min 23}$ (Å)	$r_{\max 23}$ (Å)
Si-Ge-Ge	87.197	114.702	2.122	2.122	0.0	3.417	0.0	3.417	0.0	5.314
Ge-Si-Si	87.197	114.702	2.122	2.122	0.0	3.417	0.0	3.417	0.0	5.314

TABLE DXXXVII: SW potential parameters for b-SiGe used by LAMMPS,⁹ as expressed in Eqs. (9) and (10).

	ϵ (eV)	σ (Å)	a	λ	γ	$\cos \theta_0$	A_L	B_L	p	q	tol
Si-Ge-Ge	1.000	2.122	1.610	87.197	1.000	-0.418	22.576	0.702	4	0	0.0
Ge-Si-Si	1.000	2.122	1.610	87.197	1.000	-0.418	22.576	0.702	4	0	0.0

set of SW potential for the single-layer b-SiGe in this section.

The structure of the single-layer b-SiGe is shown in Fig. 239. The structural parameters are from the *ab initio* calculations.¹¹⁴ The b-SiGe has a buckled configuration as shown in Fig. 239 (b), where the buckle is along the zigzag direction. This structure can be determined by two independent geometrical parameters, eg. the lattice constant 3.89 Å and the bond length 2.31 Å. The resultant height of the buckle is $h = 0.55$ Å.

Table DXXXIV shows the VFF model for the single-layer b-SiGe. The force constant parameters are determined by fitting to the acoustic branches in the phonon dispersion along the ΓM as shown in Fig. 274 (a). The *ab initio* calculations for the phonon dispersion are from Ref. 114. Fig. 274 (b) shows that the VFF model and the SW potential give exactly the same phonon dispersion, as the SW potential is derived from the VFF model.

The parameters for the two-body SW potential used by GULP are shown in Tab. DXXXV. The parameters for the three-body SW potential used by GULP are shown in Tab. DXXXVI. Parameters for the SW potential used by LAMMPS are listed in Tab. DXXXVII.

We use LAMMPS to perform MD simulations for the mechanical behavior of the single-layer b-SiGe under uniaxial tension at 1.0 K and 300.0 K. Fig. 275 shows the stress-strain curve for the tension of a single-layer b-SiGe of dimension 100×100 Å. Periodic boundary conditions are applied in both armchair and zigzag directions. The single-layer b-SiGe is stretched uniaxially along the armchair or zigzag direction. The stress is calculated without

TABLE DXXXVIII: The VFF model for b-SnSi. The second line gives an explicit expression for each VFF term. The third line is the force constant parameters. Parameters are in the unit of $\frac{eV}{\text{Å}^2}$ for the bond stretching interactions, and in the unit of eV for the angle bending interaction. The fourth line gives the initial bond length (in unit of Å) for the bond stretching interaction and the initial angle (in unit of degrees) for the angle bending interaction.

VFF type	bond stretching	angle bending
expression	$\frac{1}{2}K_r (\Delta r)^2$	$\frac{1}{2}K_\theta (\Delta \theta)^2$
parameter	10.315	2.880
r_0 or θ_0	2.520	113.298

involving the actual thickness of the quasi-two-dimensional structure of the single-layer b-SiGe. The Young's modulus can be obtained by a linear fitting of the stress-strain relation in the small strain range of $[0, 0.01]$. The Young's modulus is 54.6 N/m and 54.3 N/m along the armchair and zigzag directions, respectively. The Poisson's ratio from the VFF model and the SW potential is $\nu_{xy} = \nu_{yx} = 0.16$.

There is no available value for nonlinear quantities in the single-layer b-SiGe. We have thus used the nonlinear parameter $B = 0.5d^4$ in Eq. (5), which is close to the value of B in most materials. The value of the third order nonlinear elasticity D can be extracted by fitting the stress-strain relation to the function $\sigma = E\epsilon + \frac{1}{2}D\epsilon^2$ with E as the Young's modulus. The values of D from the present SW potential are -186.7 N/m and -233.5 N/m along the armchair and zigzag directions, respectively. The ultimate stress is about 11.0 Nm^{-1} at the ultimate strain of 0.31 in the armchair direction at the low temperature of 1 K. The ultimate stress is about 11.2 Nm^{-1} at the ultimate strain of 0.31 in the zigzag direction at the low temperature of 1 K.

CXXXV. B-SNSI

Present studies on the buckled SnSi (b-SnSi) are based on first-principles calculations, and no empirical potential has been proposed for the b-SnSi. We will thus parametrize a set of SW potential for the single-layer b-SnSi in this section.

The structure of the single-layer b-SnSi is shown in Fig. 239. The structural parameters

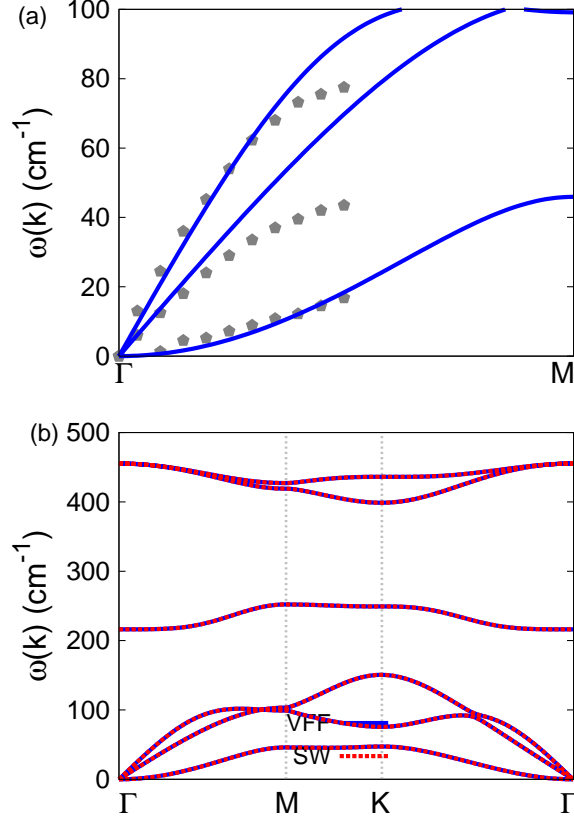


FIG. 276: (Color online) Phonon dispersion for the single-layer b-SnSi. (a) The VFF model is fitted to the three acoustic branches in the long wave limit along the Γ M direction. The *ab initio* results (gray pentagons) are from Ref. 114. (b) The VFF model (blue lines) and the SW potential (red lines) give the same phonon dispersion for the b-SnSi along Γ MKT Γ .

TABLE DXXXIX: Two-body SW potential parameters for b-SnSi used by GULP,⁸ as expressed in Eq. (3).

	A (eV)	ρ (\AA)	B (\AA^4)	r_{\min} (\AA)	r_{\max} (\AA)
Sn-Si	16.463	2.260	20.164	0.0	3.713

are from the *ab initio* calculations.¹¹⁴ The b-SnSi has a buckled configuration as shown in Fig. 239 (b), where the buckle is along the zigzag direction. This structure can be determined by two independent geometrical parameters, eg. the lattice constant 4.21 \AA and the bond length 2.52 \AA . The resultant height of the buckle is $h = 0.67 \text{ \AA}$.

Table DXXXVIII shows the VFF model for the single-layer b-SnSi. The force constant

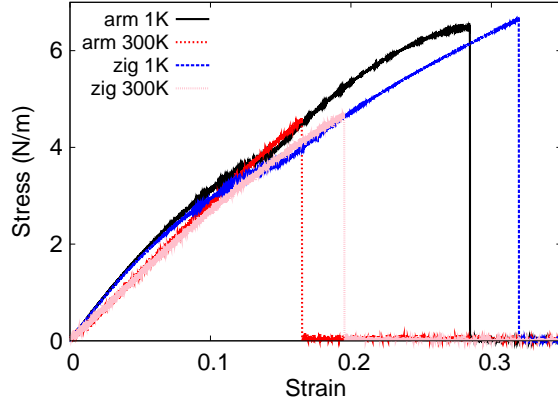


FIG. 277: (Color online) Stress-strain relations for the b-SnSi of size $100 \times 100 \text{ \AA}$. The b-SnSi is uniaxially stretched along the armchair or zigzag directions at temperatures 1 K and 300 K.

TABLE DXL: Three-body SW potential parameters for b-SnSi used by GULP,⁸ as expressed in Eq. (4).

	K (eV)	θ_0 (degree)	ρ_1 (\AA)	ρ_2 (\AA)	$r_{\min 12}$ (\AA)	$r_{\max 12}$ (\AA)	$r_{\min 13}$ (\AA)	$r_{\max 13}$ (\AA)	$r_{\min 23}$ (\AA)	$r_{\max 23}$ (\AA)
Sn-Si-Si	75.415	113.298	2.260	2.260	0.0	3.713	0.0	3.713	0.0	5.751
Si-Sn-Sn	75.415	113.298	2.260	2.260	0.0	3.713	0.0	3.713	0.0	5.751

parameters are determined by fitting to the acoustic branches in the phonon dispersion along the ΓM as shown in Fig. 276 (a). The *ab initio* calculations for the phonon dispersion are from Ref. 114. Fig. 276 (b) shows that the VFF model and the SW potential give exactly the same phonon dispersion, as the SW potential is derived from the VFF model.

The parameters for the two-body SW potential used by GULP are shown in Tab. DXXXIX. The parameters for the three-body SW potential used by GULP are shown in Tab. DXL. Parameters for the SW potential used by LAMMPS are listed in Tab. DXLI.

TABLE DXLI: SW potential parameters for b-SnSi used by LAMMPS,⁹ as expressed in Eqs. (9) and (10).

	ϵ (eV)	σ (\AA)	a	λ	γ	$\cos \theta_0$	A_L	B_L	p	q	tol
Sn-Si-Si	1.000	2.260	1.643	75.415	1.000	-0.396	16.463	0.773	4	0	0.0
Si-Sn-Sn	1.000	2.260	1.643	75.415	1.000	-0.396	16.463	0.773	4	0	0.0

We use LAMMPS to perform MD simulations for the mechanical behavior of the single-layer b-SnSi under uniaxial tension at 1.0 K and 300.0 K. Fig. 277 shows the stress-strain curve for the tension of a single-layer b-SnSi of dimension $100 \times 100 \text{ \AA}$. Periodic boundary conditions are applied in both armchair and zigzag directions. The single-layer b-SnSi is stretched uniaxially along the armchair or zigzag direction. The stress is calculated without involving the actual thickness of the quasi-two-dimensional structure of the single-layer b-SnSi. The Young's modulus can be obtained by a linear fitting of the stress-strain relation in the small strain range of $[0, 0.01]$. The Young's modulus is 39.0 N/m and 38.4 N/m along the armchair and zigzag directions, respectively. The Poisson's ratio from the VFF model and the SW potential is $\nu_{xy} = \nu_{yx} = 0.14$.

There is no available value for nonlinear quantities in the single-layer b-SnSi. We have thus used the nonlinear parameter $B = 0.5d^4$ in Eq. (5), which is close to the value of B in most materials. The value of the third order nonlinear elasticity D can be extracted by fitting the stress-strain relation to the function $\sigma = E\epsilon + \frac{1}{2}D\epsilon^2$ with E as the Young's modulus. The values of D from the present SW potential are -150.5 N/m and -174.8 N/m along the armchair and zigzag directions, respectively. The ultimate stress is about 6.5 Nm^{-1} at the ultimate strain of 0.28 in the armchair direction at the low temperature of 1 K. The ultimate stress is about 6.6 Nm^{-1} at the ultimate strain of 0.32 in the zigzag direction at the low temperature of 1 K.

CXXXVI. B-INP

Present studies on the buckled InP (b-InP) are based on first-principles calculations, and no empirical potential has been proposed for the b-InP. We will thus parametrize a set of SW potential for the single-layer b-InP in this section.

The structure of the single-layer b-InP is shown in Fig. 239. The structural parameters are from the *ab initio* calculations.¹¹⁴ The b-InP has a buckled configuration as shown in Fig. 239 (b), where the buckle is along the zigzag direction. This structure can be determined by two independent geometrical parameters, eg. the lattice constant 4.17 \AA and the bond length 2.46 \AA . The resultant height of the buckle is $h = 0.51 \text{ \AA}$.

Table DXLII shows the VFF model for the single-layer b-InP. The force constant parameters are determined by fitting to the acoustic branches in the phonon dispersion along the

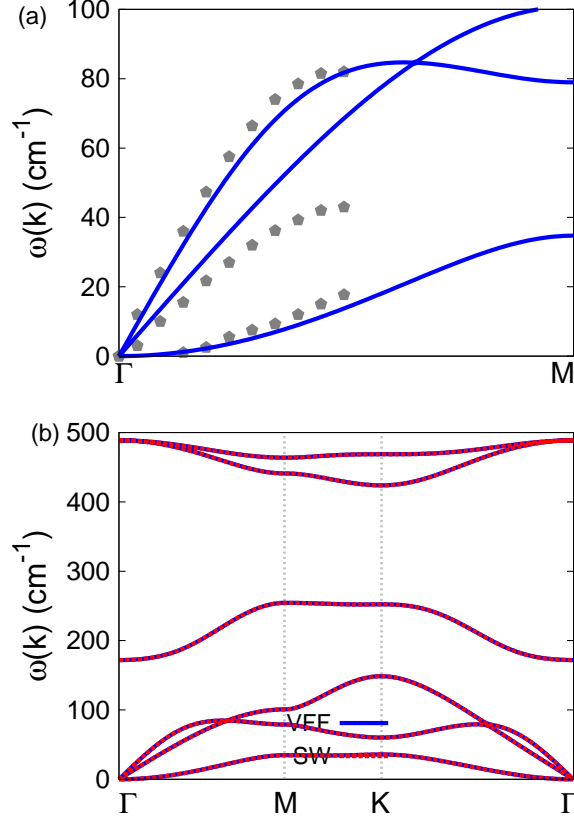


FIG. 278: (Color online) Phonon dispersion for the single-layer b-InP. (a) The VFF model is fitted to the three acoustic branches in the long wave limit along the ΓM direction. The *ab initio* results (gray pentagons) are from Ref. 114. (b) The VFF model (blue lines) and the SW potential (red lines) give the same phonon dispersion for the b-InP along $\Gamma\text{MKT}\Gamma$.

ΓM as shown in Fig. 278 (a). The *ab initio* calculations for the phonon dispersion are from Ref. 114. Fig. 278 (b) shows that the VFF model and the SW potential give exactly the same phonon dispersion, as the SW potential is derived from the VFF model.

The parameters for the two-body SW potential used by GULP are shown in Tab. DXLIII. The parameters for the three-body SW potential used by GULP are shown in Tab. DXLIV. Parameters for the SW potential used by LAMMPS are listed in Tab. DXLV.

We use LAMMPS to perform MD simulations for the mechanical behavior of the single-layer b-InP under uniaxial tension at 1.0 K and 300.0 K. Fig. 279 shows the stress-strain curve for the tension of a single-layer b-InP of dimension $100 \times 100 \text{ \AA}$. Periodic boundary conditions are applied in both armchair and zigzag directions. The single-layer b-InP is

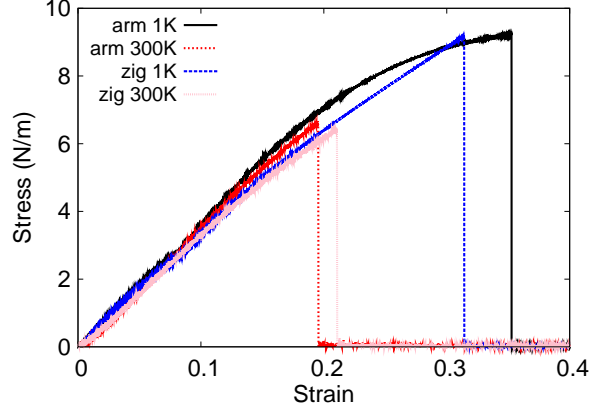


FIG. 279: (Color online) Stress-strain relations for the b-InP of size $100 \times 100 \text{ \AA}$. The b-InP is uniaxially stretched along the armchair or zigzag directions at temperatures 1 K and 300 K.

TABLE DXLII: The VFF model for b-InP. The second line gives an explicit expression for each VFF term. The third line is the force constant parameters. Parameters are in the unit of $\frac{\text{eV}}{\text{\AA}^2}$ for the bond stretching interactions, and in the unit of eV for the angle bending interaction. The fourth line gives the initial bond length (in unit of \AA) for the bond stretching interaction and the initial angle (in unit of degrees) for the angle bending interaction.

VFF type	bond stretching	angle bending
expression	$\frac{1}{2}K_r(\Delta r)^2$	$\frac{1}{2}K_\theta(\Delta\theta)^2$
parameter	12.903	2.384
r_0 or θ_0	2.460	115.895

stretched uniaxially along the armchair or zigzag direction. The stress is calculated without involving the actual thickness of the quasi-two-dimensional structure of the single-layer b-InP. The Young's modulus can be obtained by a linear fitting of the stress-strain relation in the small strain range of $[0, 0.01]$. The Young's modulus is 39.3 N/m and 38.3 N/m along

TABLE DXLIII: Two-body SW potential parameters for b-InP used by GULP,⁸ as expressed in Eq. (3).

	A (eV)	ρ (\AA)	B (\AA^4)	r_{\min} (\AA)	r_{\max} (\AA)
In-P	20.610	2.306	18.311	0.0	3.651

TABLE DXLIV: Three-body SW potential parameters for b-InP used by GULP,⁸ as expressed in Eq. (4).

	K (eV)	θ_0 (degree)	ρ_1 (Å)	ρ_2 (Å)	$r_{\min 12}$ (Å)	$r_{\max 12}$ (Å)	$r_{\min 13}$ (Å)	$r_{\max 13}$ (Å)	$r_{\min 23}$ (Å)	$r_{\max 23}$ (Å)
In-P-P	70.782	115.895	2.306	2.306	0.0	3.651	0.0	3.651	0.0	5.696
P-In-In	70.782	115.895	2.306	2.306	0.0	3.651	0.0	3.651	0.0	5.696

TABLE DXLV: SW potential parameters for b-InP used by LAMMPS,⁹ as expressed in Eqs. (9) and (10).

	ϵ (eV)	σ (Å)	a	λ	γ	$\cos \theta_0$	A_L	B_L	p	q	tol
In-P-P	1.000	2.306	1.583	70.782	1.000	-0.437	20.610	0.648	4	0	0.0
P-In-In	1.000	2.306	1.583	70.782	1.000	-0.437	20.610	0.648	4	0	0.0

the armchair and zigzag directions, respectively. The Poisson's ratio from the VFF model and the SW potential is $\nu_{xy} = \nu_{yx} = 0.17$.

There is no available value for nonlinear quantities in the single-layer b-InP. We have thus used the nonlinear parameter $B = 0.5d^4$ in Eq. (5), which is close to the value of B in most materials. The value of the third order nonlinear elasticity D can be extracted by fitting the stress-strain relation to the function $\sigma = E\epsilon + \frac{1}{2}D\epsilon^2$ with E as the Young's modulus. The values of D from the present SW potential are -119.3 N/m and -132.0 N/m along the armchair and zigzag directions, respectively. The ultimate stress is about 9.2 Nm^{-1} at the ultimate strain of 0.35 in the armchair direction at the low temperature of 1 K. The ultimate stress is about 9.1 Nm^{-1} at the ultimate strain of 0.31 in the zigzag direction at the low temperature of 1 K.

CXXXVII. B-INAs

Present studies on the buckled InAs (b-InAs) are based on first-principles calculations, and no empirical potential has been proposed for the b-InAs. We will thus parametrize a set of SW potential for the single-layer b-InAs in this section.

The structure of the single-layer b-InAs is shown in Fig. 239. The structural parameters are from the *ab initio* calculations.¹¹⁴ The b-InAs has a buckled configuration as shown in

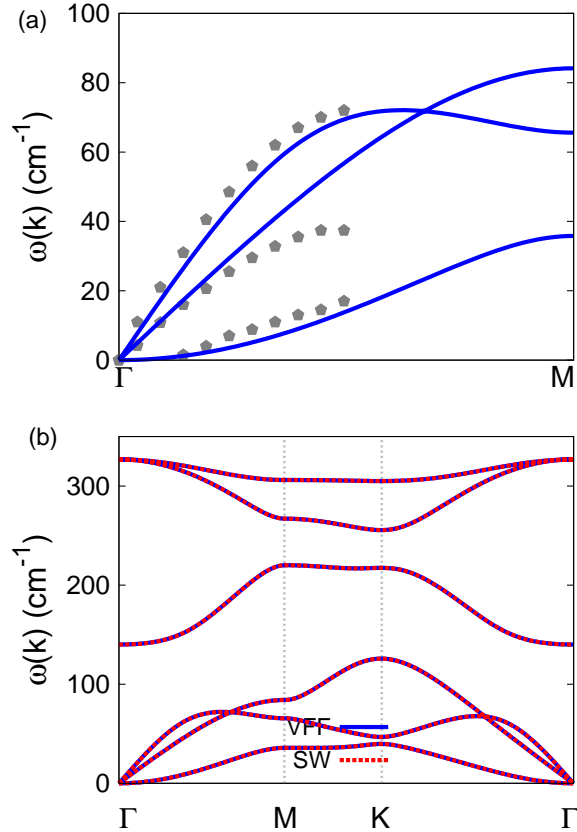


FIG. 280: (Color online) Phonon dispersion for the single-layer b-InAs. (a) The VFF model is fitted to the three acoustic branches in the long wave limit along the Γ M direction. The *ab initio* results (gray pentagons) are from Ref. 114. (b) The VFF model (blue lines) and the SW potential (red lines) give the same phonon dispersion for the b-InAs along Γ MK Γ .

Fig. 239 (b), where the buckle is along the zigzag direction. This structure can be determined by two independent geometrical parameters, eg. the lattice constant 4.28 \AA and the bond length 2.55 \AA . The resultant height of the buckle is $h = 0.62 \text{ \AA}$.

Table DXLVI shows the VFF model for the single-layer b-InAs. The force constant parameters are determined by fitting to the acoustic branches in the phonon dispersion along the Γ M as shown in Fig. 280 (a). The *ab initio* calculations for the phonon dispersion are from Ref. 114. Fig. 280 (b) shows that the VFF model and the SW potential give exactly the same phonon dispersion, as the SW potential is derived from the VFF model.

The parameters for the two-body SW potential used by GULP are shown in Tab. DXLVII. The parameters for the three-body SW potential used by GULP are shown in Tab. DXLVIII.

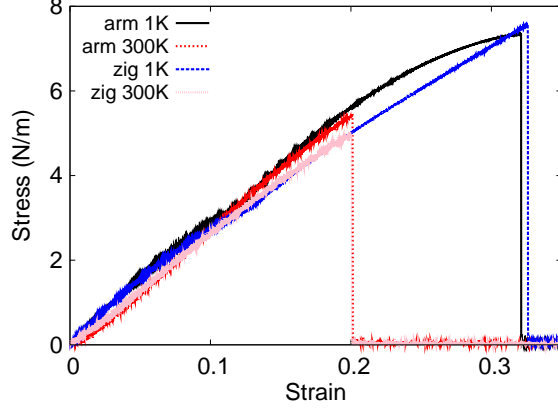


FIG. 281: (Color online) Stress-strain relations for the b-InAs of size $100 \times 100 \text{ \AA}$. The b-InAs is uniaxially stretched along the armchair or zigzag directions at temperatures 1 K and 300 K.

TABLE DXLVI: The VFF model for b-InAs. The second line gives an explicit expression for each VFF term. The third line is the force constant parameters. Parameters are in the unit of $\frac{\text{eV}}{\text{\AA}^2}$ for the bond stretching interactions, and in the unit of eV for the angle bending interaction. The fourth line gives the initial bond length (in unit of \AA) for the bond stretching interaction and the initial angle (in unit of degrees) for the angle bending interaction.

VFF type	bond stretching	angle bending
expression	$\frac{1}{2}K_r(\Delta r)^2$	$\frac{1}{2}K_\theta(\Delta\theta)^2$
parameter	10.903	2.384
r_0 or θ_0	2.550	114.115

Parameters for the SW potential used by LAMMPS are listed in Tab. [DXLIX](#).

We use LAMMPS to perform MD simulations for the mechanical behavior of the single-layer b-InAs under uniaxial tension at 1.0 K and 300.0 K. Fig. [281](#) shows the stress-strain curve for the tension of a single-layer b-InAs of dimension $100 \times 100 \text{ \AA}$. Periodic boundary

TABLE DXLVII: Two-body SW potential parameters for b-InAs used by GULP,⁸ as expressed in Eq. (3).

	A (eV)	ρ (\AA)	B (\AA^4)	r_{\min} (\AA)	r_{\max} (\AA)
In-As	18.099	2.320	21.141	0.0	3.766

TABLE DXLVIII: Three-body SW potential parameters for b-InAs used by GULP,⁸ as expressed in Eq. (4).

	K (eV)	θ_0 (degree)	ρ_1 (Å)	ρ_2 (Å)	$r_{\min 12}$ (Å)	$r_{\max 12}$ (Å)	$r_{\min 13}$ (Å)	$r_{\max 13}$ (Å)	$r_{\min 23}$ (Å)	$r_{\max 23}$ (Å)
In-As-As	64.931	114.115	2.320	2.320	0.0	3.766	0.0	3.766	0.0	5.847
As-In-In	64.931	114.115	2.320	2.320	0.0	3.766	0.0	3.766	0.0	5.847

TABLE DXLIX: SW potential parameters for b-InAs used by LAMMPS,⁹ as expressed in Eqs. (9) and (10).

	ϵ (eV)	σ (Å)	a	λ	γ	$\cos \theta_0$	A_L	B_L	p	q	tol
In-As-As	1.000	2.320	1.624	64.931	1.000	-0.409	18.099	0.730	4	0	0.0
As-In-In	1.000	2.320	1.624	64.931	1.000	-0.409	18.099	0.730	4	0	0.0

conditions are applied in both armchair and zigzag directions. The single-layer b-InAs is stretched uniaxially along the armchair or zigzag direction. The stress is calculated without involving the actual thickness of the quasi-two-dimensional structure of the single-layer b-InAs. The Young's modulus can be obtained by a linear fitting of the stress-strain relation in the small strain range of $[0, 0.01]$. The Young's modulus is 33.9 N/m and 34.2 N/m along the armchair and zigzag directions, respectively. The Poisson's ratio from the VFF model and the SW potential is $\nu_{xy} = \nu_{yx} = 0.17$.

There is no available value for nonlinear quantities in the single-layer b-InAs. We have thus used the nonlinear parameter $B = 0.5d^4$ in Eq. (5), which is close to the value of B in most materials. The value of the third order nonlinear elasticity D can be extracted by fitting the stress-strain relation to the function $\sigma = E\epsilon + \frac{1}{2}D\epsilon^2$ with E as the Young's modulus. The values of D from the present SW potential are -85.0 N/m and -130.2 N/m along the armchair and zigzag directions, respectively. The ultimate stress is about 7.3 Nm^{-1} at the ultimate strain of 0.32 in the armchair direction at the low temperature of 1 K. The ultimate stress is about 7.5 Nm^{-1} at the ultimate strain of 0.32 in the zigzag direction at the low temperature of 1 K.

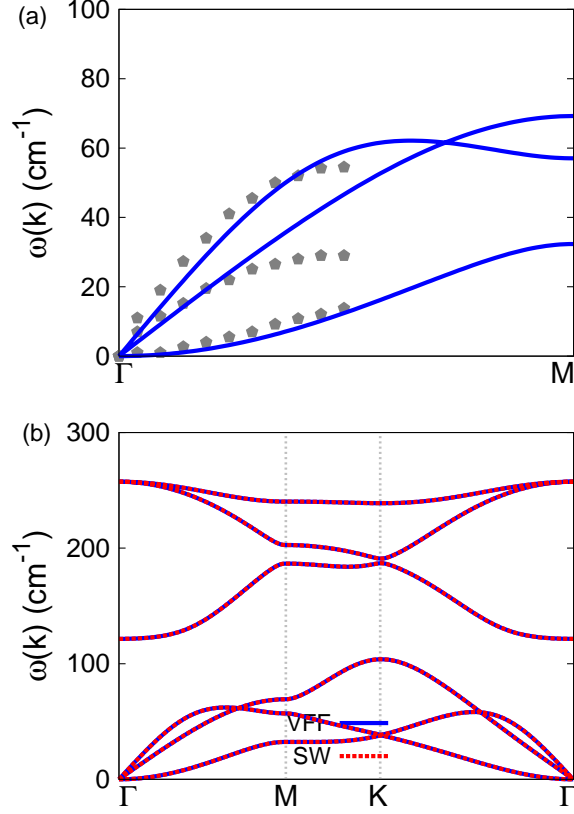


FIG. 282: (Color online) Phonon dispersion for the single-layer b-InSb. (a) The VFF model is fitted to the three acoustic branches in the long wave limit along the Γ M direction. The *ab initio* results (gray pentagons) are from Ref. 114. (b) The VFF model (blue lines) and the SW potential (red lines) give the same phonon dispersion for the b-InSb along Γ MKT.

CXXXVIII. B-INSB

Present studies on the buckled InSb (b-InSb) are based on first-principles calculations, and no empirical potential has been proposed for the b-InSb. We will thus parametrize a set of SW potential for the single-layer b-InSb in this section.

The structure of the single-layer b-InSb is shown in Fig. 239. The structural parameters are from the *ab initio* calculations.¹¹⁴ The b-InSb has a buckled configuration as shown in Fig. 239 (b), where the buckle is along the zigzag direction. This structure can be determined by two independent geometrical parameters, eg. the lattice constant 4.57 \AA and the bond length 2.74 \AA . The resultant height of the buckle is $h = 0.73 \text{ \AA}$.

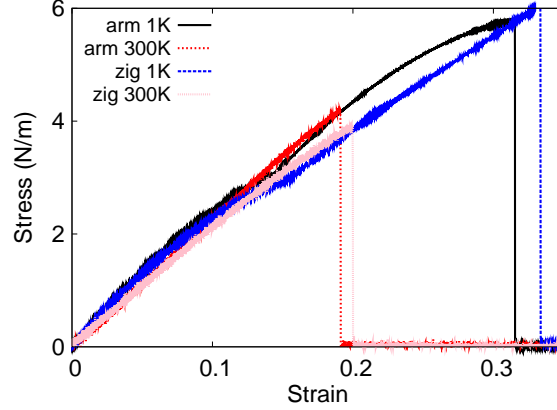


FIG. 283: (Color online) Stress-strain relations for the b-InSb of size $100 \times 100 \text{ \AA}$. The b-InSb is uniaxially stretched along the armchair or zigzag directions at temperatures 1 K and 300 K.

TABLE DL: The VFF model for b-InSb. The second line gives an explicit expression for each VFF term. The third line is the force constant parameters. Parameters are in the unit of $\frac{eV}{\text{\AA}^2}$ for the bond stretching interactions, and in the unit of eV for the angle bending interaction. The fourth line gives the initial bond length (in unit of \AA) for the bond stretching interaction and the initial angle (in unit of degrees) for the angle bending interaction.

VFF type	bond stretching	angle bending
expression	$\frac{1}{2}K_r(\Delta r)^2$	$\frac{1}{2}K_\theta(\Delta\theta)^2$
parameter	8.903	2.384
r_0 or θ_0	2.740	113.012

Table DL shows the VFF model for the single-layer b-InSb. The force constant parameters are determined by fitting to the acoustic branches in the phonon dispersion along the ΓM as shown in Fig. 282 (a). The *ab initio* calculations for the phonon dispersion are from Ref. 114. Fig. 282 (b) shows that the VFF model and the SW potential give exactly the

TABLE DLI: Two-body SW potential parameters for b-InSb used by GULP,⁸ as expressed in Eq. (3).

	A (eV)	ρ (\AA)	B (\AA^4)	r_{\min} (\AA)	r_{\max} (\AA)
In-Sb	16.706	2.445	28.182	0.0	4.034

TABLE DLII: Three-body SW potential parameters for b-InSb used by GULP,⁸ as expressed in Eq. (4).

	K (eV)	θ_0 (degree)	ρ_1 (Å)	ρ_2 (Å)	$r_{\min 12}$ (Å)	$r_{\max 12}$ (Å)	$r_{\min 13}$ (Å)	$r_{\max 13}$ (Å)	$r_{\min 23}$ (Å)	$r_{\max 23}$ (Å)
In-Sb-Sb	61.578	113.012	2.445	2.445	0.0	4.034	0.0	4.034	0.0	6.243
Sb-In-In	61.578	113.012	2.445	2.445	0.0	4.034	0.0	4.034	0.0	6.243

TABLE DLIII: SW potential parameters for b-InSb used by LAMMPS,⁹ as expressed in Eqs. (9) and (10).

	ϵ (eV)	σ (Å)	a	λ	γ	$\cos \theta_0$	A_L	B_L	p	q	tol
In-Sb-Sb	1.000	2.445	1.650	61.578	1.000	-0.391	16.706	0.788	4	0	0.0
Sb-In-In	1.000	2.445	1.650	61.578	1.000	-0.391	16.706	0.788	4	0	0.0

same phonon dispersion, as the SW potential is derived from the VFF model.

The parameters for the two-body SW potential used by GULP are shown in Tab. DLI. The parameters for the three-body SW potential used by GULP are shown in Tab. DLII. Parameters for the SW potential used by LAMMPS are listed in Tab. DLIII.

We use LAMMPS to perform MD simulations for the mechanical behavior of the single-layer b-InSb under uniaxial tension at 1.0 K and 300.0 K. Fig. 283 shows the stress-strain curve for the tension of a single-layer b-InSb of dimension 100×100 Å. Periodic boundary conditions are applied in both armchair and zigzag directions. The single-layer b-InSb is stretched uniaxially along the armchair or zigzag direction. The stress is calculated without involving the actual thickness of the quasi-two-dimensional structure of the single-layer b-InSb. The Young's modulus can be obtained by a linear fitting of the stress-strain relation in the small strain range of $[0, 0.01]$. The Young's modulus is 28.6 N/m and 28.9 N/m along the armchair and zigzag directions, respectively. The Poisson's ratio from the VFF model and the SW potential is $\nu_{xy} = \nu_{yx} = 0.17$.

There is no available value for nonlinear quantities in the single-layer b-InSb. We have thus used the nonlinear parameter $B = 0.5d^4$ in Eq. (5), which is close to the value of B in most materials. The value of the third order nonlinear elasticity D can be extracted by fitting the stress-strain relation to the function $\sigma = E\epsilon + \frac{1}{2}D\epsilon^2$ with E as the Young's modulus. The values of D from the present SW potential are -85.4 N/m and -121.0 N/m

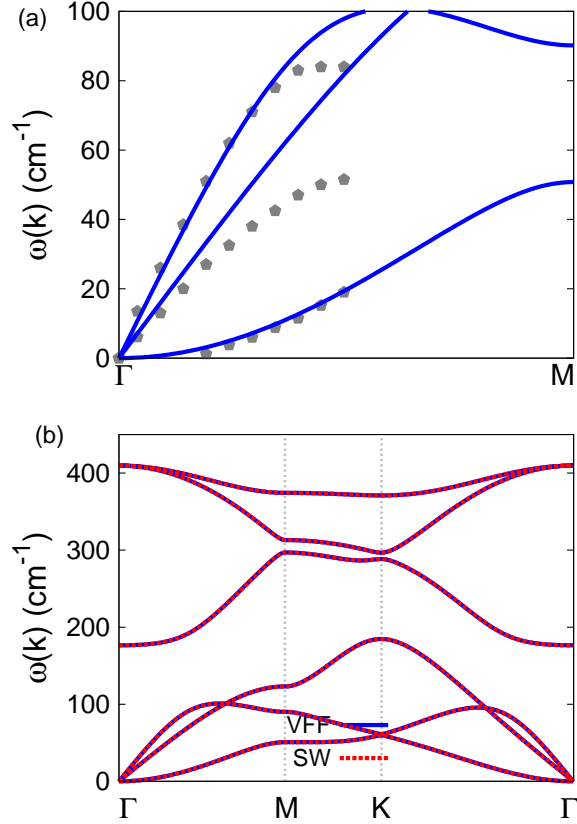


FIG. 284: (Color online) Phonon dispersion for the single-layer b-GaAs. (a) The VFF model is fitted to the three acoustic branches in the long wave limit along the Γ M direction. The *ab initio* results (gray pentagons) are from Ref. 114. (b) The VFF model (blue lines) and the SW potential (red lines) give the same phonon dispersion for the b-GaAs along Γ MK Γ .

along the armchair and zigzag directions, respectively. The ultimate stress is about 5.8 Nm^{-1} at the ultimate strain of 0.31 in the armchair direction at the low temperature of 1 K. The ultimate stress is about 6.0 Nm^{-1} at the ultimate strain of 0.33 in the zigzag direction at the low temperature of 1 K.

CXXXIX. B-GAAS

Present studies on the buckled GaAs (b-GaAs) are based on first-principles calculations, and no empirical potential has been proposed for the b-GaAs. We will thus parametrize a set of SW potential for the single-layer b-GaAs in this section.

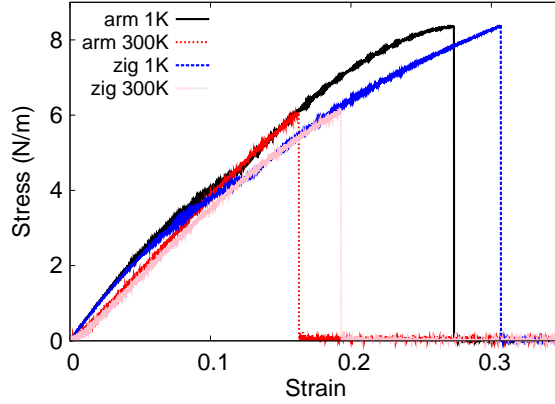


FIG. 285: (Color online) Stress-strain relations for the b-GaAs of size $100 \times 100 \text{ \AA}$. The b-GaAs is uniaxially stretched along the armchair or zigzag directions at temperatures 1 K and 300 K.

TABLE DLIV: The VFF model for b-GaAs. The second line gives an explicit expression for each VFF term. The third line is the force constant parameters. Parameters are in the unit of $\frac{\text{eV}}{\text{\AA}^2}$ for the bond stretching interactions, and in the unit of eV for the angle bending interaction. The fourth line gives the initial bond length (in unit of \AA) for the bond stretching interaction and the initial angle (in unit of degrees) for the angle bending interaction.

VFF type	bond stretching	angle bending
expression	$\frac{1}{2}K_r(\Delta r)^2$	$\frac{1}{2}K_\theta(\Delta\theta)^2$
parameter	12.903	3.284
r_0 or θ_0	2.360	114.513

The structure of the single-layer b-GaAs is shown in Fig. 239. The structural parameters are from the *ab initio* calculations.¹¹⁴ The b-GaAs has a buckled configuration as shown in Fig. 239 (b), where the buckle is along the zigzag direction. This structure can be determined by two independent geometrical parameters, eg. the lattice constant 3.97 \AA and the bond

TABLE DLV: Two-body SW potential parameters for b-GaAs used by GULP,⁸ as expressed in Eq. (3).

	A (eV)	ρ (\AA)	B (\AA^4)	r_{\min} (\AA)	r_{\max} (\AA)
Ga-As	18.485	2.161	15.510	0.0	3.489

TABLE DLVI: Three-body SW potential parameters for b-GaAs used by GULP,⁸ as expressed in Eq. (4).

	K (eV)	θ_0 (degree)	ρ_1 (Å)	ρ_2 (Å)	$r_{\min 12}$ (Å)	$r_{\max 12}$ (Å)	$r_{\min 13}$ (Å)	$r_{\max 13}$ (Å)	$r_{\min 23}$ (Å)	$r_{\max 23}$ (Å)
Ga-As-As	91.177	114.513	2.161	2.161	0.0	3.489	0.0	3.489	0.0	5.423
As-Ga-Ga	91.177	114.513	2.161	2.161	0.0	3.489	0.0	3.489	0.0	5.423

TABLE DLVII: SW potential parameters for b-GaAs used by LAMMPS,⁹ as expressed in Eqs. (9) and (10).

	ϵ (eV)	σ (Å)	a	λ	γ	$\cos \theta_0$	A_L	B_L	p	q	tol
Ga-As-As	1.000	2.161	1.614	91.177	1.000	-0.415	18.485	0.711	4	0	0.0
As-Ga-Ga	1.000	2.161	1.614	91.177	1.000	-0.415	18.485	0.711	4	0	0.0

length 2.36 Å. The resultant height of the buckle is $h = 0.55$ Å.

Table DLIV shows the VFF model for the single-layer b-GaAs. The force constant parameters are determined by fitting to the acoustic branches in the phonon dispersion along the Γ M as shown in Fig. 284 (a). The *ab initio* calculations for the phonon dispersion are from Ref. 114. Fig. 284 (b) shows that the VFF model and the SW potential give exactly the same phonon dispersion, as the SW potential is derived from the VFF model.

The parameters for the two-body SW potential used by GULP are shown in Tab. DLV. The parameters for the three-body SW potential used by GULP are shown in Tab. DLVI. Parameters for the SW potential used by LAMMPS are listed in Tab. DLVII.

We use LAMMPS to perform MD simulations for the mechanical behavior of the single-layer b-GaAs under uniaxial tension at 1.0 K and 300.0 K. Fig. 285 shows the stress-strain curve for the tension of a single-layer b-GaAs of dimension 100×100 Å. Periodic boundary conditions are applied in both armchair and zigzag directions. The single-layer b-GaAs is stretched uniaxially along the armchair or zigzag direction. The stress is calculated without involving the actual thickness of the quasi-two-dimensional structure of the single-layer b-GaAs. The Young's modulus can be obtained by a linear fitting of the stress-strain relation in the small strain range of $[0, 0.01]$. The Young's modulus is 50.5 N/m and 50.9 N/m along the armchair and zigzag directions, respectively. The Poisson's ratio from the VFF model and the SW potential is $\nu_{xy} = \nu_{yx} = 0.13$.

TABLE DLVIII: The VFF model for b-GaP. The second line gives an explicit expression for each VFF term. The third line is the force constant parameters. Parameters are in the unit of $\frac{\text{eV}}{\text{\AA}^2}$ for the bond stretching interactions, and in the unit of eV for the angle bending interaction. The fourth line gives the initial bond length (in unit of \AA) for the bond stretching interaction and the initial angle (in unit of degrees) for the angle bending interaction.

VFF type	bond stretching	angle bending
expression	$\frac{1}{2}K_r (\Delta r)^2$	$\frac{1}{2}K_\theta (\Delta\theta)^2$
parameter	16.050	3.022
r_0 or θ_0	2.250	117.152

TABLE DLIX: Two-body SW potential parameters for b-GaP used by GULP,⁸ as expressed in Eq. (3).

	A (eV)	ρ (\AA)	B (\AA^4)	r_{\min} (\AA)	r_{\max} (\AA)
Ga-P	21.948	2.152	12.814	0.0	3.350

There is no available value for nonlinear quantities in the single-layer b-GaAs. We have thus used the nonlinear parameter $B = 0.5d^4$ in Eq. (5), which is close to the value of B in most materials. The value of the third order nonlinear elasticity D can be extracted by fitting the stress-strain relation to the function $\sigma = E\epsilon + \frac{1}{2}D\epsilon^2$ with E as the Young's modulus. The values of D from the present SW potential are -199.5 N/m and -258.6 N/m along the armchair and zigzag directions, respectively. The ultimate stress is about 8.3 Nm^{-1} at the ultimate strain of 0.27 in the armchair direction at the low temperature of 1 K. The ultimate stress is about 8.3 Nm^{-1} at the ultimate strain of 0.30 in the zigzag direction at the low temperature of 1 K.

CXL. B-GAP

Present studies on the buckled GaP (b-GaP) are based on first-principles calculations, and no empirical potential has been proposed for the b-GaP. We will thus parametrize a set of SW potential for the single-layer b-GaP in this section.

The structure of the single-layer b-GaP is shown in Fig. 239. The structural parameters

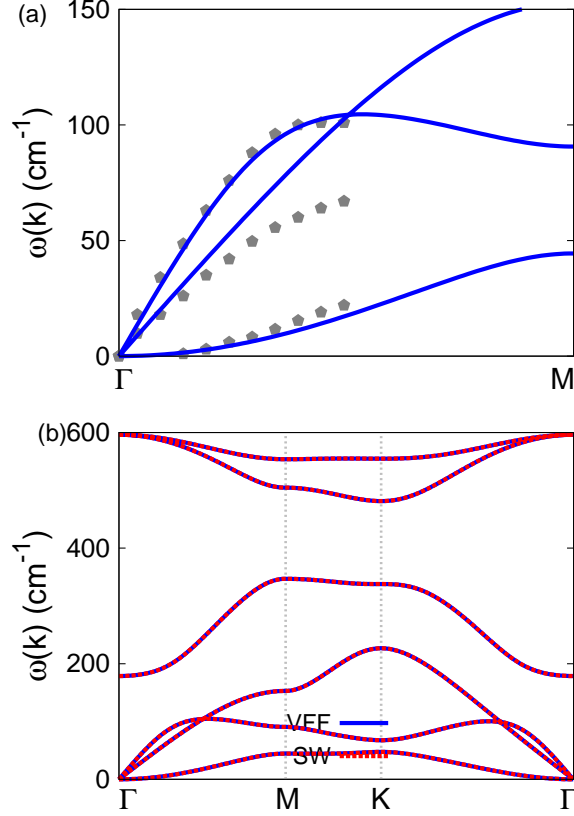


FIG. 286: (Color online) Phonon dispersion for the single-layer b-GaP. (a) The VFF model is fitted to the three acoustic branches in the long wave limit along the ΓM direction. The *ab initio* results (gray pentagons) are from Ref. 114. (b) The VFF model (blue lines) and the SW potential (red lines) give the same phonon dispersion for the b-GaP along $\Gamma\text{MK}\Gamma$.

TABLE DLX: Three-body SW potential parameters for b-GaP used by GULP,⁸ as expressed in Eq. (4).

	K (eV)	θ_0 (degree)	ρ_1 (\AA)	ρ_2 (\AA)	$r_{\text{min}12}$ (\AA)	$r_{\text{max}12}$ (\AA)	$r_{\text{min}13}$ (\AA)	$r_{\text{max}13}$ (\AA)	$r_{\text{min}23}$ (\AA)	$r_{\text{max}23}$ (\AA)
Ga-P-P	95.438	117.152	2.152	2.152	0.0	3.350	0.0	3.350	0.0	5.246
P-Ga-Ga	95.438	117.152	2.152	2.152	0.0	3.350	0.0	3.350	0.0	5.246

are from the *ab initio* calculations.¹¹⁴ The b-GaP has a buckled configuration as shown in Fig. 239 (b), where the buckle is along the zigzag direction. This structure can be determined by two independent geometrical parameters, eg. the lattice constant 3.84 \AA and the bond length 2.25 \AA . The resultant height of the buckle is $h = 0.40 \text{\AA}$.

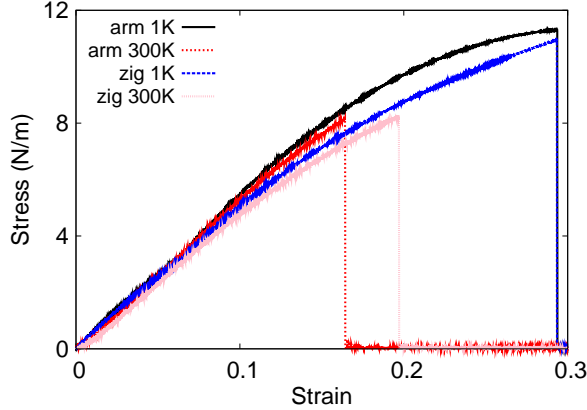


FIG. 287: (Color online) Stress-strain relations for the b-GaP of size $100 \times 100 \text{ \AA}$. The b-GaP is uniaxially stretched along the armchair or zigzag directions at temperatures 1 K and 300 K.

TABLE DLXI: SW potential parameters for b-GaP used by LAMMPS,⁹ as expressed in Eqs. (9) and (10).

	ϵ (eV)	σ (\AA)	a	λ	γ	$\cos \theta_0$	A_L	B_L	p	q	tol
Ga-P-P	1.000	2.152	1.557	95.438	1.000	-0.456	21.948	0.597	4	0	0.0
P-Ga-Ga	1.000	2.152	1.557	95.438	1.000	-0.456	21.948	0.597	4	0	0.0

Table DLVIII shows the VFF model for the single-layer b-GaP. The force constant parameters are determined by fitting to the acoustic branches in the phonon dispersion along the Γ M as shown in Fig. 286 (a). The *ab initio* calculations for the phonon dispersion are from Ref. 114. Fig. 286 (b) shows that the VFF model and the SW potential give exactly the same phonon dispersion, as the SW potential is derived from the VFF model.

The parameters for the two-body SW potential used by GULP are shown in Tab. DLIX. The parameters for the three-body SW potential used by GULP are shown in Tab. DLX. Parameters for the SW potential used by LAMMPS are listed in Tab. DLXI.

We use LAMMPS to perform MD simulations for the mechanical behavior of the single-layer b-GaP under uniaxial tension at 1.0 K and 300.0 K. Fig. 287 shows the stress-strain curve for the tension of a single-layer b-GaP of dimension $100 \times 100 \text{ \AA}$. Periodic boundary conditions are applied in both armchair and zigzag directions. The single-layer b-GaP is stretched uniaxially along the armchair or zigzag direction. The stress is calculated without involving the actual thickness of the quasi-two-dimensional structure of the single-layer b-

TABLE DLXII: The VFF model for b-AlSb. The second line gives an explicit expression for each VFF term. The third line is the force constant parameters. Parameters are in the unit of $\frac{eV}{\text{\AA}^2}$ for the bond stretching interactions, and in the unit of eV for the angle bending interaction. The fourth line gives the initial bond length (in unit of \AA) for the bond stretching interaction and the initial angle (in unit of degrees) for the angle bending interaction.

VFF type	bond stretching	angle bending
expression	$\frac{1}{2}K_r (\Delta r)^2$	$\frac{1}{2}K_\theta (\Delta\theta)^2$
parameter	12.050	3.022
r_0 or θ_0	2.570	114.791

TABLE DLXIII: Two-body SW potential parameters for b-AlSb used by GULP,⁸ as expressed in Eq. (3).

	A (eV)	ρ (\AA)	B (\AA^4)	r_{\min} (\AA)	r_{\max} (\AA)
Al-Sb	20.580	2.365	21.812	0.0	3.803

GaP. The Young's modulus can be obtained by a linear fitting of the stress-strain relation in the small strain range of $[0, 0.01]$. The Young's modulus is 57.2 N/m and 57.4 N/m along the armchair and zigzag directions, respectively. The Poisson's ratio from the VFF model and the SW potential is $\nu_{xy} = \nu_{yx} = 0.14$.

There is no available value for nonlinear quantities in the single-layer b-GaP. We have thus used the nonlinear parameter $B = 0.5d^4$ in Eq. (5), which is close to the value of B in most materials. The value of the third order nonlinear elasticity D can be extracted by fitting the stress-strain relation to the function $\sigma = E\epsilon + \frac{1}{2}D\epsilon^2$ with E as the Young's modulus. The values of D from the present SW potential are -186.4 N/m and -261.6 N/m along the armchair and zigzag directions, respectively. The ultimate stress is about 11.3 Nm^{-1} at the ultimate strain of 0.29 in the armchair direction at the low temperature of 1 K. The ultimate stress is about 10.9 Nm^{-1} at the ultimate strain of 0.29 in the zigzag direction at the low temperature of 1 K.

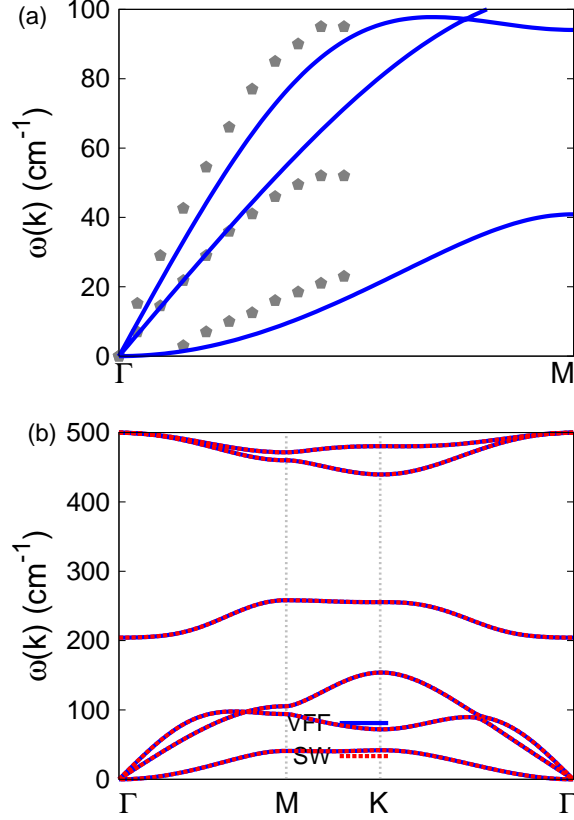


FIG. 288: (Color online) Phonon dispersion for the single-layer b-AlSb. (a) The VFF model is fitted to the three acoustic branches in the long wave limit along the Γ M direction. The *ab initio* results (gray pentagons) are from Ref. 114. (b) The VFF model (blue lines) and the SW potential (red lines) give the same phonon dispersion for the b-AlSb along Γ MK Γ .

TABLE DLXIV: Three-body SW potential parameters for b-AlSb used by GULP,⁸ as expressed in Eq. (4).

	K (eV)	θ_0 (degree)	ρ_1 (\AA)	ρ_2 (\AA)	$r_{\min 12}$ (\AA)	$r_{\max 12}$ (\AA)	$r_{\min 13}$ (\AA)	$r_{\max 13}$ (\AA)	$r_{\min 23}$ (\AA)	$r_{\max 23}$ (\AA)
Al-Sb-Sb	85.046	114.791	2.365	2.365	0.0	3.803	0.0	3.803	0.0	5.915
Sb-Al-Al	85.046	114.791	2.365	2.365	0.0	3.803	0.0	3.803	0.0	5.915

CXLI. B-ALSB

Present studies on the buckled AlSb (b-AlSb) are based on first-principles calculations, and no empirical potential has been proposed for the b-AlSb. We will thus parametrize a

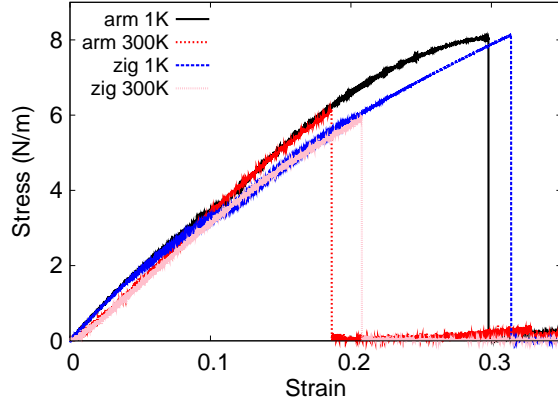


FIG. 289: (Color online) Stress-strain relations for the b-AlSb of size $100 \times 100 \text{ \AA}$. The b-AlSb is uniaxially stretched along the armchair or zigzag directions at temperatures 1 K and 300 K.

TABLE DLXV: SW potential parameters for b-AlSb used by LAMMPS,⁹ as expressed in Eqs. (9) and (10).

	ϵ (eV)	σ (\AA)	a	λ	γ	$\cos \theta_0$	A_L	B_L	p	q	tol
Al-Sb-Sb	1.000	2.365	1.608	85.046	1.000	-0.419	20.580	0.697	4	0	0.0
Sb-Al-Al	1.000	2.365	1.608	85.046	1.000	-0.419	20.580	0.697	4	0	0.0

set of SW potential for the single-layer b-AlSb in this section.

The structure of the single-layer b-AlSb is shown in Fig. 239. The structural parameters are from the *ab initio* calculations.¹¹⁴ The b-AlSb has a buckled configuration as shown in Fig. 239 (b), where the buckle is along the zigzag direction. This structure can be determined by two independent geometrical parameters, eg. the lattice constant 4.33 \AA and the bond length 2.57 \AA . The resultant height of the buckle is $h = 0.60 \text{ \AA}$.

Table DLXII shows the VFF model for the single-layer b-AlSb. The force constant parameters are determined by fitting to the acoustic branches in the phonon dispersion along the ΓM as shown in Fig. 288 (a). The *ab initio* calculations for the phonon dispersion are from Ref. 114. Fig. 288 (b) shows that the VFF model and the SW potential give exactly the same phonon dispersion, as the SW potential is derived from the VFF model.

The parameters for the two-body SW potential used by GULP are shown in Tab. DLXIII. The parameters for the three-body SW potential used by GULP are shown in Tab. DLXIV. Parameters for the SW potential used by LAMMPS are listed in Tab. DLXV.

We use LAMMPS to perform MD simulations for the mechanical behavior of the single-layer b-ALSb under uniaxial tension at 1.0 K and 300.0 K. Fig. 289 shows the stress-strain curve for the tension of a single-layer b-ALSb of dimension $100 \times 100 \text{ \AA}$. Periodic boundary conditions are applied in both armchair and zigzag directions. The single-layer b-ALSb is stretched uniaxially along the armchair or zigzag direction. The stress is calculated without involving the actual thickness of the quasi-two-dimensional structure of the single-layer b-ALSb. The Young's modulus can be obtained by a linear fitting of the stress-strain relation in the small strain range of $[0, 0.01]$. The Young's modulus is 41.7 N/m and 42.0 N/m along the armchair and zigzag directions, respectively. The Poisson's ratio from the VFF model and the SW potential is $\nu_{xy} = \nu_{yx} = 0.15$.

There is no available value for nonlinear quantities in the single-layer b-ALSb. We have thus used the nonlinear parameter $B = 0.5d^4$ in Eq. (5), which is close to the value of B in most materials. The value of the third order nonlinear elasticity D can be extracted by fitting the stress-strain relation to the function $\sigma = E\epsilon + \frac{1}{2}D\epsilon^2$ with E as the Young's modulus. The values of D from the present SW potential are -142.4 N/m and -190.8 N/m along the armchair and zigzag directions, respectively. The ultimate stress is about 8.1 Nm^{-1} at the ultimate strain of 0.29 in the armchair direction at the low temperature of 1 K. The ultimate stress is about 8.1 Nm^{-1} at the ultimate strain of 0.31 in the zigzag direction at the low temperature of 1 K.

CXLII. BO

Present studies on the BO are based on first-principles calculations, and no empirical potential has been proposed for the BO. We will thus parametrize a set of SW potential for the single-layer BO in this section.

The structure of the single-layer BO is shown in Fig. 290 with M=B and X=O. The structural parameters are from the *ab initio* calculations.¹¹⁵ The BO has a bi-buckled configuration as shown in Fig. 290 (b), where the buckle is along the zigzag direction. Two buckling layers are symmetrically integrated through the interior B-B bonds, forming a bi-buckled configuration. This structure can be determined by three independent geometrical parameters, eg. the lattice constant 2.44 \AA , the bond length $d_{\text{B-O}} = 1.52 \text{ \AA}$, and the bond length $d_{\text{B-B}} = 1.77 \text{ \AA}$.

TABLE DLXVI: The VFF model for BO. The second line gives an explicit expression for each VFF term. The third line is the force constant parameters. Parameters are in the unit of $\frac{\text{eV}}{\text{\AA}^2}$ for the bond stretching interactions, and in the unit of eV for the angle bending interaction. The fourth line gives the initial bond length (in unit of \AA) for the bond stretching interaction and the initial angle (in unit of degrees) for the angle bending interaction.

VFF type	bond stretching		angle bending	
expression	$\frac{1}{2}K_{\text{B-O}}(\Delta r)^2$	$\frac{1}{2}K_{\text{B-B}}(\Delta r)^2$	$\frac{1}{2}K_{\text{BOO}}(\Delta\theta)^2$	$\frac{1}{2}K_{\text{BBO}}(\Delta\theta)^2$
parameter	23.030	15.512	5.577	6.209
r_0 or θ_0	1.520	1.770	106.764	112.059

TABLE DLXVII: Two-body SW potential parameters for BO used by GULP,⁸ as expressed in Eq. (3).

	A (eV)	ρ (\AA)	B (\AA^4)	r_{min} (\AA)	r_{max} (\AA)
B ₁ -O ₁	11.725	1.207	2.669	0.0	2.197
B ₁ -B ₂	6.749	0.875	4.908	0.0	2.392

TABLE DLXVIII: Three-body SW potential parameters for BO used by GULP,⁸ as expressed in Eq. (4).

	K (eV)	θ_0 (degree)	ρ_1 (\AA)	ρ_2 (\AA)	r_{min12} (\AA)	r_{max12} (\AA)	r_{min13} (\AA)	r_{max13} (\AA)	r_{min23} (\AA)	r_{max23} (\AA)
B ₁ -O ₁ -O ₁	107.486	106.764	1.207	1.207	0.0	2.197	0.0	2.197	0.0	3.333
B ₁ -B ₂ -O ₁	87.662	112.059	0.875	1.207	0.0	2.392	0.0	2.197	0.0	3.198

TABLE DLXIX: SW potential parameters for BO used by LAMMPS,⁹ as expressed in Eqs. (9) and (10).

	ϵ (eV)	σ (\AA)	a	λ	γ	$\cos\theta_0$	A_L	B_L	p	q	tol
B ₁ -O ₁ -O ₁	1.000	1.207	1.820	107.486	1.000	-0.288	11.725	1.256	4	0	0.0
B ₁ -B ₂ -B ₂	1.000	0.875	2.734	0.000	1.000	0.000	6.749	8.377	4	0	0.0
B ₁ -B ₂ -O ₁	1.000	0.000	0.000	87.662	1.000	-0.376	0.000	0.000	4	0	0.0

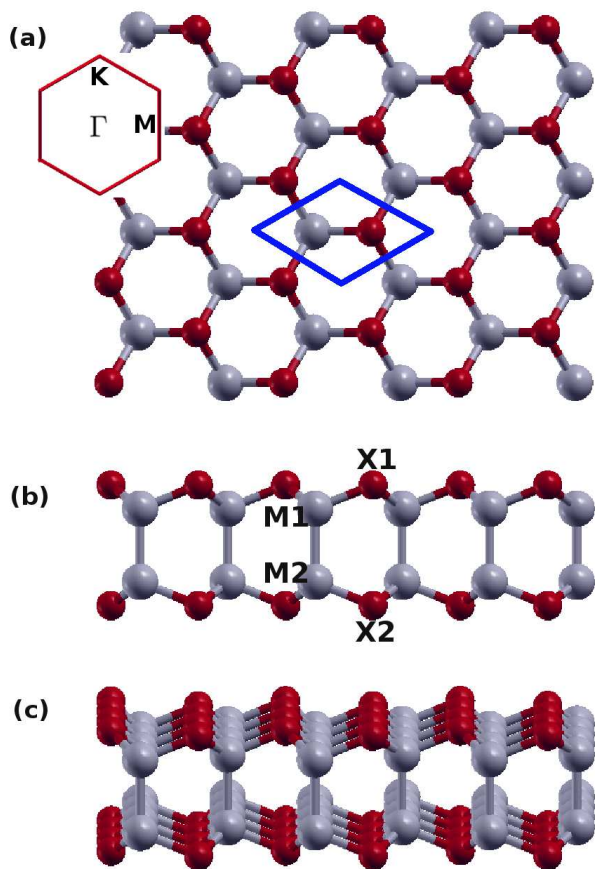


FIG. 290: (Color online) Structure of bi-buckled MX crystal, with M from group III and X from group VI. (a) Top view. The unit cell is highlighted by a blue parallelogram. Inset shows the first Brillouin zone of the reciprocal lattice space. (b) Side view displays the bi-buckled configuration. (c) Perspective view. M atoms are represented by larger gray balls. X atoms are represented by smaller red balls.

Table [DLXVI](#) shows the VFF model for the single-layer BO. The force constant parameters are determined by fitting to the six low-frequency branches in the phonon dispersion along the Γ M as shown in Fig. [291](#) (a). The *ab initio* calculations for the phonon dispersion are from Ref. 115. Fig. [291](#) (b) shows that the VFF model and the SW potential give exactly the same phonon dispersion, as the SW potential is derived from the VFF model.

The parameters for the two-body SW potential used by GULP are shown in Tab. [DLXVII](#). The parameters for the three-body SW potential used by GULP are shown in Tab. [DLXVIII](#). Parameters for the SW potential used by LAMMPS are listed in Tab. [DLXIX](#).

We use LAMMPS to perform MD simulations for the mechanical behavior of the single-

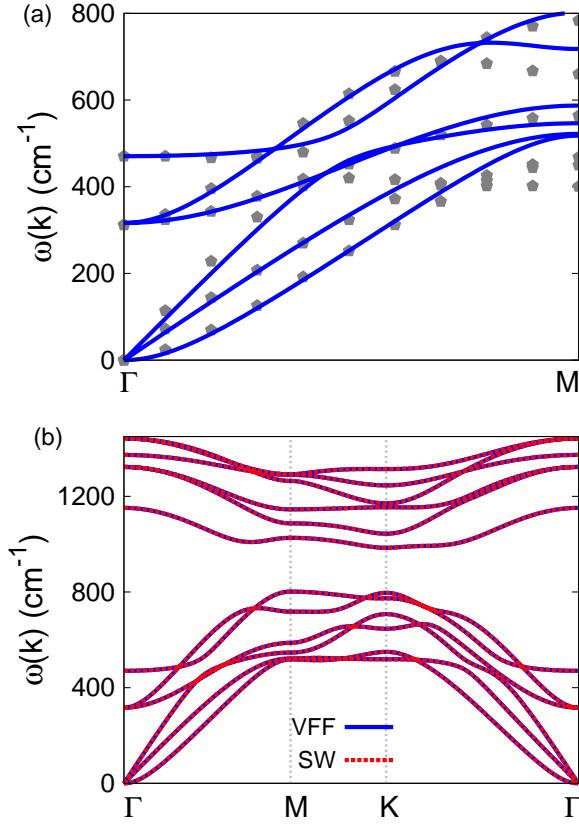


FIG. 291: (Color online) Phonon dispersion for the single-layer BO. (a) The VFF model is fitted to the six low-frequency branches along the Γ M direction. The *ab initio* results (gray pentagons) are from Ref. 115. (b) The VFF model (blue lines) and the SW potential (red lines) give the same phonon dispersion for the BO along Γ MKT Γ .

layer BO under uniaxial tension at 1.0 K and 300.0 K. Fig. 292 shows the stress-strain curve for the tension of a single-layer BO of dimension $100 \times 100 \text{ \AA}$. Periodic boundary conditions are applied in both armchair and zigzag directions. The single-layer BO is stretched uniaxially along the armchair or zigzag direction. The stress is calculated without involving the actual thickness of the quasi-two-dimensional structure of the single-layer BO. The Young's modulus can be obtained by a linear fitting of the stress-strain relation in the small strain range of $[0, 0.01]$. The Young's modulus is 299.6 N/m and 297.7 N/m along the armchair and zigzag directions, respectively. The Poisson's ratio from the VFF model and the SW potential is $\nu_{xy} = \nu_{yx} = 0.11$.

There is no available value for nonlinear quantities in the single-layer BO. We have thus

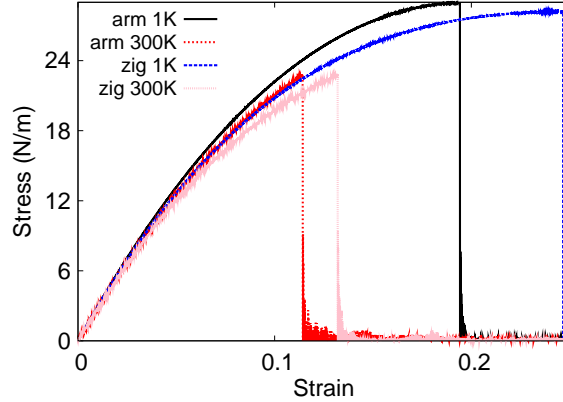


FIG. 292: (Color online) Stress-strain relations for the BO of size $100 \times 100 \text{ \AA}$. The BO is uniaxially stretched along the armchair or zigzag directions at temperatures 1 K and 300 K.

used the nonlinear parameter $B = 0.5d^4$ in Eq. (5), which is close to the value of B in most materials. The value of the third order nonlinear elasticity D can be extracted by fitting the stress-strain relation to the function $\sigma = E\epsilon + \frac{1}{2}D\epsilon^2$ with E as the Young's modulus. The values of D from the present SW potential are -1554.7 N/m and -1585.2 N/m along the armchair and zigzag directions, respectively. The ultimate stress is about 28.9 Nm^{-1} at the ultimate strain of 0.19 in the armchair direction at the low temperature of 1 K. The ultimate stress is about 28.2 Nm^{-1} at the ultimate strain of 0.24 in the zigzag direction at the low temperature of 1 K.

CXLIII. ALO

Present studies on the AIO are based on first-principles calculations, and no empirical potential has been proposed for the AIO. We will thus parametrize a set of SW potential for the single-layer AIO in this section.

The structure of the single-layer AIO is shown in Fig. 290 with $M=\text{Al}$ and $X=\text{O}$. The structural parameters are from the *ab initio* calculations.¹¹⁵ The AIO has a bi-buckled configuration as shown in Fig. 290 (b), where the buckle is along the zigzag direction. Two buckling layers are symmetrically integrated through the interior Al-Al bonds, forming a bi-buckled configuration. This structure can be determined by three independent geometrical parameters, eg. the lattice constant 2.96 \AA , the bond length $d_{\text{Al-O}} = 1.83 \text{ \AA}$, and the bond

TABLE DLXX: The VFF model for AlO. The second line gives an explicit expression for each VFF term. The third line is the force constant parameters. Parameters are in the unit of $\frac{\text{eV}}{\text{\AA}^2}$ for the bond stretching interactions, and in the unit of eV for the angle bending interaction. The fourth line gives the initial bond length (in unit of \AA) for the bond stretching interaction and the initial angle (in unit of degrees) for the angle bending interaction.

VFF type	bond stretching		angle bending	
expression	$\frac{1}{2}K_{\text{Al-O}}(\Delta r)^2$	$\frac{1}{2}K_{\text{Al-Al}}(\Delta r)^2$	$\frac{1}{2}K_{\text{AlOO}}(\Delta\theta)^2$	$\frac{1}{2}K_{\text{AlAlO}}(\Delta\theta)^2$
parameter	18.189	6.410	3.182	1.318
r_0 or θ_0	1.830	2.620	107.947	110.956

TABLE DLXXI: Two-body SW potential parameters for AlO used by GULP,⁸ as expressed in Eq. (3).

	A (eV)	ρ (\AA)	B (\AA^4)	r_{\min} (\AA)	r_{\max} (\AA)
Al ₁ -O ₁	13.758	1.488	5.608	0.0	2.655
Al ₁ -Al ₂	3.609	0.678	23.560	0.0	3.287

TABLE DLXXII: Three-body SW potential parameters for AlO used by GULP,⁸ as expressed in Eq. (4).

	K (eV)	θ_0 (degree)	ρ_1 (\AA)	ρ_2 (\AA)	$r_{\min12}$ (\AA)	$r_{\max12}$ (\AA)	$r_{\min13}$ (\AA)	$r_{\max13}$ (\AA)	$r_{\min23}$ (\AA)	$r_{\max23}$ (\AA)
Al ₁ -O ₁ -O ₁	64.759	107.947	1.488	1.488	0.0	2.655	0.0	2.655	0.0	4.043
Al ₁ -O ₁ -Al ₂	12.688	110.956	1.488	0.678	0.0	2.655	0.0	3.287	0.0	4.213

TABLE DLXXIII: SW potential parameters for AlO used by LAMMPS,⁹ as expressed in Eqs. (9) and (10).

	ϵ (eV)	σ (\AA)	a	λ	γ	$\cos\theta_0$	A_L	B_L	p	q	tol
Al ₁ -O ₁ -O ₁	1.000	1.488	1.785	64.759	1.000	-0.308	13.758	1.145	4	0	0.0
Al ₁ -Al ₂ -Al ₂	1.000	0.678	4.846	0.000	1.000	0.000	3.609	111.363	4	0	0.0
Al ₁ -Al ₂ -O ₁	1.000	0.000	0.000	12.688	1.000	-0.358	0.000	0.000	4	0	0.0

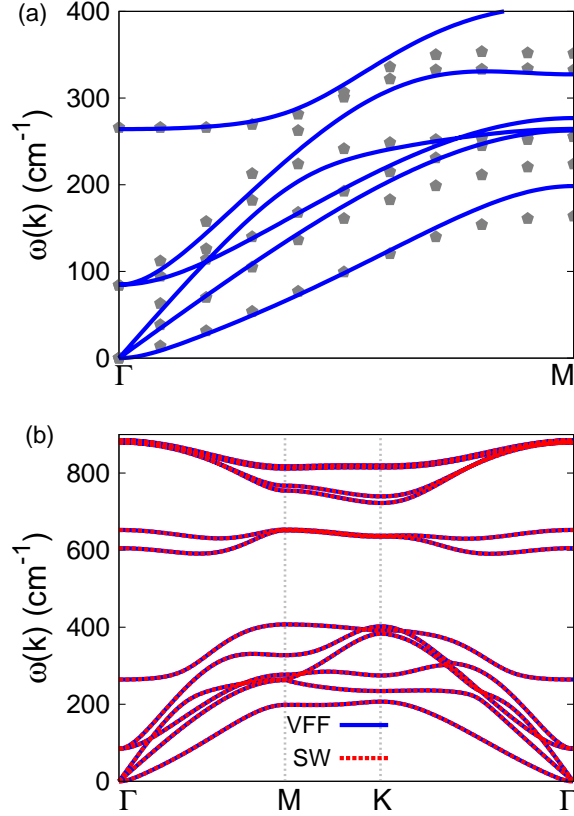


FIG. 293: (Color online) Phonon dispersion for the single-layer AlO. (a) The VFF model is fitted to the six low-frequency branches along the Γ M direction. The *ab initio* results (gray pentagons) are from Ref. 115. (b) The VFF model (blue lines) and the SW potential (red lines) give the same phonon dispersion for the AlO along Γ MKT.

length $d_{\text{Al-Al}} = 2.62 \text{ \AA}$.

Table DLXX shows the VFF model for the single-layer AlO. The force constant parameters are determined by fitting to the six low-frequency branches in the phonon dispersion along the Γ M as shown in Fig. 293 (a). The *ab initio* calculations for the phonon dispersion are from Ref. 115. Fig. 293 (b) shows that the VFF model and the SW potential give exactly the same phonon dispersion, as the SW potential is derived from the VFF model.

The parameters for the two-body SW potential used by GULP are shown in Tab. DLXXI. The parameters for the three-body SW potential used by GULP are shown in Tab. DLXXII. Parameters for the SW potential used by LAMMPS are listed in Tab. DLXXIII.

We use LAMMPS to perform MD simulations for the mechanical behavior of the single-

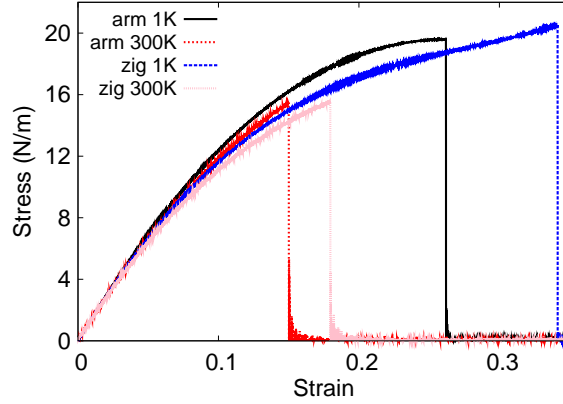


FIG. 294: (Color online) Stress-strain relations for the AlO of size $100 \times 100 \text{ \AA}$. The AlO is uniaxially stretched along the armchair or zigzag directions at temperatures 1 K and 300 K.

layer AlO under uniaxial tension at 1.0 K and 300.0 K. Fig. 294 shows the stress-strain curve for the tension of a single-layer AlO of dimension $100 \times 100 \text{ \AA}$. Periodic boundary conditions are applied in both armchair and zigzag directions. The single-layer AlO is stretched uniaxially along the armchair or zigzag direction. The stress is calculated without involving the actual thickness of the quasi-two-dimensional structure of the single-layer AlO. The Young's modulus can be obtained by a linear fitting of the stress-strain relation in the small strain range of $[0, 0.01]$. The Young's modulus is 149.3 N/m and 148.2 N/m along the armchair and zigzag directions, respectively. The Poisson's ratio from the VFF model and the SW potential is $\nu_{xy} = \nu_{yx} = 0.19$.

There is no available value for nonlinear quantities in the single-layer AlO. We have thus used the nonlinear parameter $B = 0.5d^4$ in Eq. (5), which is close to the value of B in most materials. The value of the third order nonlinear elasticity D can be extracted by fitting the stress-strain relation to the function $\sigma = E\epsilon + \frac{1}{2}D\epsilon^2$ with E as the Young's modulus. The values of D from the present SW potential are -563.9 N/m and -565.6 N/m along the armchair and zigzag directions, respectively. The ultimate stress is about 19.6 Nm^{-1} at the ultimate strain of 0.26 in the armchair direction at the low temperature of 1 K. The ultimate stress is about 20.4 Nm^{-1} at the ultimate strain of 0.34 in the zigzag direction at the low temperature of 1 K.

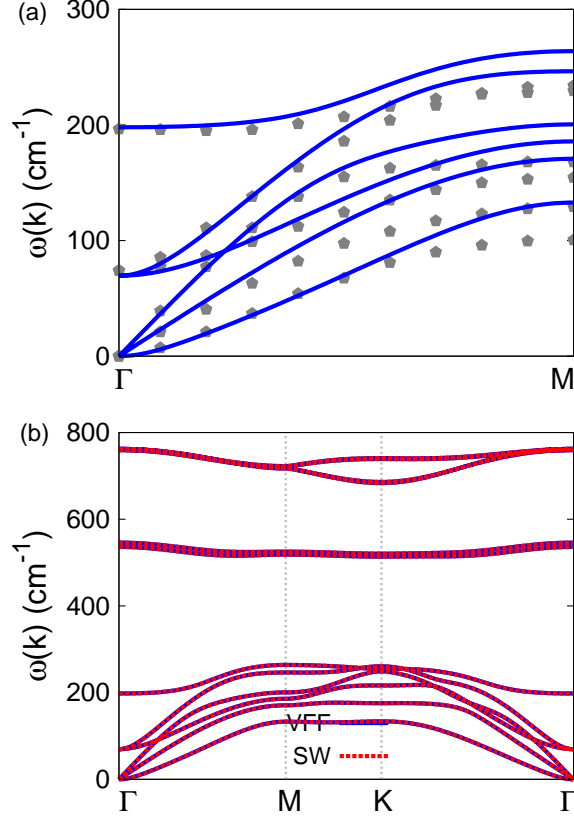


FIG. 295: (Color online) Phonon dispersion for the single-layer GaO. (a) The VFF model is fitted to the six low-frequency branches along the Γ M direction. The *ab initio* results (gray pentagons) are from Ref. 115. (b) The VFF model (blue lines) and the SW potential (red lines) give the same phonon dispersion for the GaO along Γ MKT Γ .

CXLIV. GAO

Present studies on the GaO are based on first-principles calculations, and no empirical potential has been proposed for the GaO. We will thus parametrize a set of SW potential for the single-layer GaO in this section.

The structure of the single-layer GaO is shown in Fig. 290 with M=Ga and X=O. The structural parameters are from the *ab initio* calculations.¹¹⁵ The GaO has a bi-buckled configuration as shown in Fig. 290 (b), where the buckle is along the zigzag direction. Two buckling layers are symmetrically integrated through the interior Ga-Ga bonds, forming a bi-buckled configuration. This structure can be determined by three independent geometrical

TABLE DLXXIV: The VFF model for GaO. The second line gives an explicit expression for each VFF term. The third line is the force constant parameters. Parameters are in the unit of $\frac{eV}{\text{\AA}^2}$ for the bond stretching interactions, and in the unit of eV for the angle bending interaction. The fourth line gives the initial bond length (in unit of \AA) for the bond stretching interaction and the initial angle (in unit of degrees) for the angle bending interaction.

VFF type	bond stretching		angle bending	
expression	$\frac{1}{2}K_{\text{Ga-O}}(\Delta r)^2$	$\frac{1}{2}K_{\text{Ga-Ga}}(\Delta r)^2$	$\frac{1}{2}K_{\text{GaOO}}(\Delta\theta)^2$	$\frac{1}{2}K_{\text{GaGaO}}(\Delta\theta)^2$
parameter	18.189	6.410	3.182	1.628
r_0 or θ_0	1.940	2.510	107.051	111.794

TABLE DLXXV: Two-body SW potential parameters for GaO used by GULP,⁸ as expressed in Eq. (3).

	A (eV)	ρ (\AA)	B (\AA^4)	r_{\min} (\AA)	r_{\max} (\AA)
Ga ₁ -O ₁	15.178	1.550	7.082	0.0	2.807
Ga ₁ -Ga ₂	4.225	0.890	19.846	0.0	3.257

TABLE DLXXVI: Three-body SW potential parameters for GaO used by GULP,⁸ as expressed in Eq. (4).

	K (eV)	θ_0 (degree)	ρ_1 (\AA)	ρ_2 (\AA)	$r_{\min12}$ (\AA)	$r_{\max12}$ (\AA)	$r_{\min13}$ (\AA)	$r_{\max13}$ (\AA)	$r_{\min23}$ (\AA)	$r_{\max23}$ (\AA)
Ga ₁ -O ₁ -O ₁	62.149	107.051	1.550	1.550	0.0	2.807	0.0	2.807	0.0	4.262
Ga ₁ -O ₁ -Ga ₂	18.443	111.794	1.550	0.890	0.0	2.807	0.0	3.257	0.0	4.269

TABLE DLXXVII: SW potential parameters for GaO used by LAMMPS,⁹ as expressed in Eqs. (9) and (10).

	ϵ (eV)	σ (\AA)	a	λ	γ	$\cos\theta_0$	A_L	B_L	p	q	tol
Ga ₁ -O ₁ -O ₁	1.000	1.550	1.811	62.149	1.000	-0.293	15.178	1.227	4	0	0.0
Ga ₁ -Ga ₂ -Ga ₂	1.000	0.890	3.661	0.000	1.000	0.000	4.225	31.685	4	0	0.0
Ga ₁ -Ga ₂ -O ₁	1.000	0.000	0.000	18.443	1.000	-0.371	0.000	0.000	4	0	0.0

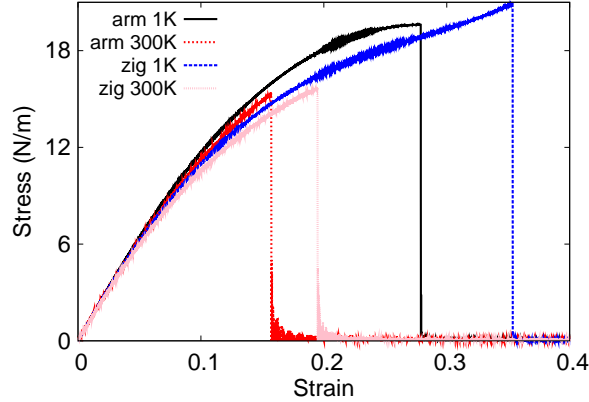


FIG. 296: (Color online) Stress-strain relations for the GaO of size $100 \times 100 \text{ \AA}$. The GaO is uniaxially stretched along the armchair or zigzag directions at temperatures 1 K and 300 K.

parameters, eg. the lattice constant 3.12 \AA , the bond length $d_{\text{Ga-O}} = 1.94 \text{ \AA}$, and the bond length $d_{\text{Ga-Ga}} = 2.51 \text{ \AA}$.

Table DLXXIV shows the VFF model for the single-layer GaO. The force constant parameters are determined by fitting to the six low-frequency branches in the phonon dispersion along the ΓM as shown in Fig. 295 (a). The *ab initio* calculations for the phonon dispersion are from Ref. 115. Fig. 295 (b) shows that the VFF model and the SW potential give exactly the same phonon dispersion, as the SW potential is derived from the VFF model.

The parameters for the two-body SW potential used by GULP are shown in Tab. DLXXV. The parameters for the three-body SW potential used by GULP are shown in Tab. DLXXVI. Parameters for the SW potential used by LAMMPS are listed in Tab. DLXXVII.

We use LAMMPS to perform MD simulations for the mechanical behavior of the single-layer GaO under uniaxial tension at 1.0 K and 300.0 K. Fig. 296 shows the stress-strain curve for the tension of a single-layer GaO of dimension $100 \times 100 \text{ \AA}$. Periodic boundary conditions are applied in both armchair and zigzag directions. The single-layer GaO is stretched uniaxially along the armchair or zigzag direction. The stress is calculated without involving the actual thickness of the quasi-two-dimensional structure of the single-layer GaO. The Young's modulus can be obtained by a linear fitting of the stress-strain relation in the small strain range of $[0, 0.01]$. The Young's modulus is 137.2 N/m and 136.6 N/m along the armchair and zigzag directions, respectively. The Poisson's ratio from the VFF model and the SW potential is $\nu_{xy} = \nu_{yx} = 0.22$.

TABLE DLXXVIII: The VFF model for InO. The second line gives an explicit expression for each VFF term. The third line is the force constant parameters. Parameters are in the unit of $\frac{eV}{\text{\AA}^2}$ for the bond stretching interactions, and in the unit of eV for the angle bending interaction. The fourth line gives the initial bond length (in unit of \AA) for the bond stretching interaction and the initial angle (in unit of degrees) for the angle bending interaction.

VFF type	bond stretching		angle bending	
expression	$\frac{1}{2}K_{\text{In-O}}(\Delta r)^2$	$\frac{1}{2}K_{\text{In-In}}(\Delta r)^2$	$\frac{1}{2}K_{\text{InOO}}(\Delta\theta)^2$	$\frac{1}{2}K_{\text{InInO}}(\Delta\theta)^2$
parameter	16.916	4.250	2.171	1.138
r_0 or θ_0	2.160	2.860	107.328	111.538

TABLE DLXXIX: Two-body SW potential parameters for InO used by GULP,⁸ as expressed in Eq. (3).

	A (eV)	ρ (\AA)	B (\AA^4)	r_{min} (\AA)	r_{max} (\AA)
In ₁ -O ₁	17.600	1.735	10.884	0.0	3.128
In ₁ -In ₂	3.440	0.945	33.453	0.0	3.682

There is no available value for nonlinear quantities in the single-layer GaO. We have thus used the nonlinear parameter $B = 0.5d^4$ in Eq. (5), which is close to the value of B in most materials. The value of the third order nonlinear elasticity D can be extracted by fitting the stress-strain relation to the function $\sigma = E\epsilon + \frac{1}{2}D\epsilon^2$ with E as the Young's modulus. The values of D from the present SW potential are -467.5 N/m and -529.6 N/m along the armchair and zigzag directions, respectively. The ultimate stress is about 19.6 Nm^{-1} at the ultimate strain of 0.28 in the armchair direction at the low temperature of 1 K. The ultimate stress is about 20.8 Nm^{-1} at the ultimate strain of 0.35 in the zigzag direction at the low temperature of 1 K.

CXLV. INO

Present studies on the InO are based on first-principles calculations, and no empirical potential has been proposed for the InO. We will thus parametrize a set of SW potential for the single-layer InO in this section.

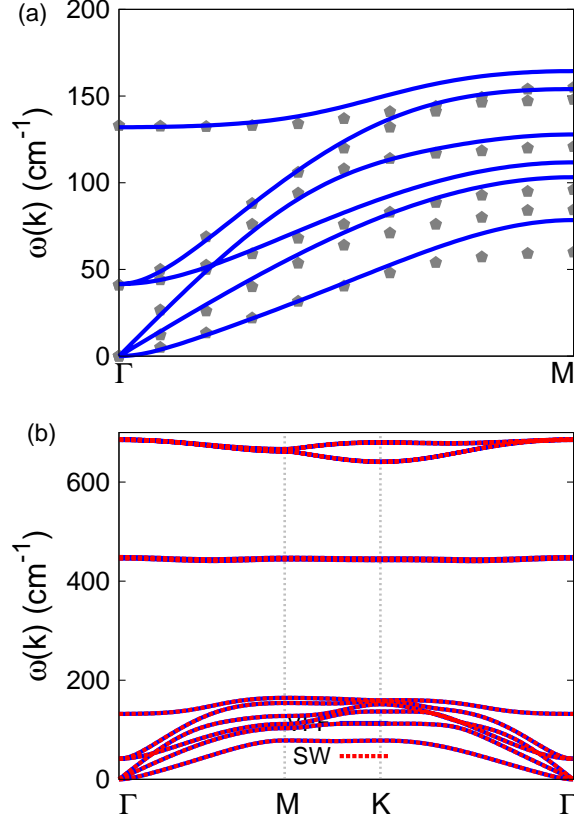


FIG. 297: (Color online) Phonon dispersion for the single-layer InO. (a) The VFF model is fitted to the six low-frequency branches along the Γ M direction. The *ab initio* results (gray pentagons) are from Ref. 115. (b) The VFF model (blue lines) and the SW potential (red lines) give the same phonon dispersion for the InO along Γ MKT Γ .

TABLE DLXXX: Three-body SW potential parameters for InO used by GULP,⁸ as expressed in Eq. (4).

	K (eV)	θ_0 (degree)	ρ_1 (\AA)	ρ_2 (\AA)	$r_{\min 12}$ (\AA)	$r_{\max 12}$ (\AA)	$r_{\min 13}$ (\AA)	$r_{\max 13}$ (\AA)	$r_{\min 23}$ (\AA)	$r_{\max 23}$ (\AA)
In ₁ -O ₁ -O ₁	42.946	107.328	1.735	1.735	0.0	3.128	0.0	3.128	0.0	4.754
In ₁ -O ₁ -In ₂	12.470	111.538	1.735	0.945	0.0	3.128	0.0	3.682	0.0	4.800

The structure of the single-layer InO is shown in Fig. 290 with M=In and X=O. The structural parameters are from the *ab initio* calculations.¹¹⁵ The InO has a bi-buckled configuration as shown in Fig. 290 (b), where the buckle is along the zigzag direction. Two buckling layers are symmetrically integrated through the interior In-In bonds, forming a bi-

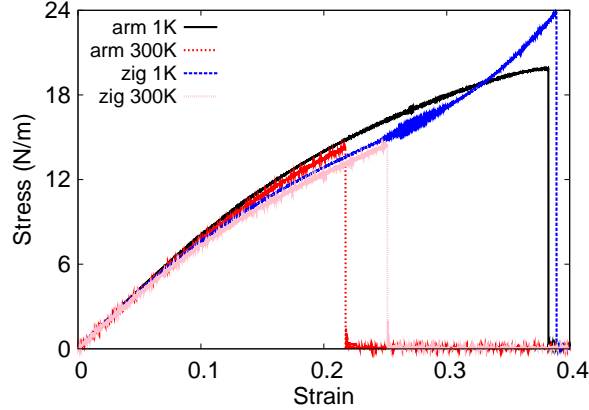


FIG. 298: (Color online) Stress-strain relations for the InO of size $100 \times 100 \text{ \AA}$. The InO is uniaxially stretched along the armchair or zigzag directions at temperatures 1 K and 300 K.

TABLE DLXXXI: SW potential parameters for InO used by LAMMPS,⁹ as expressed in Eqs. (9) and (10).

	ϵ (eV)	σ (\AA)	a	λ	γ	$\cos \theta_0$	A_L	B_L	p	q	tol
In ₁ -O ₁ -O ₁	1.000	1.735	1.803	42.946	1.000	-0.298	17.600	1.201	4	0	0.0
In ₁ -In ₂ -In ₂	1.000	0.945	3.895	0.000	1.000	0.000	3.440	41.864	4	0	0.0
In ₁ -In ₂ -O ₁	1.000	0.000	0.000	12.470	1.000	-0.367	0.000	0.000	4	0	0.0

buckled configuration. This structure can be determined by three independent geometrical parameters, eg. the lattice constant 3.48 \AA , the bond length $d_{\text{In-O}} = 2.16 \text{ \AA}$, and the bond length $d_{\text{In-In}} = 2.86 \text{ \AA}$.

Table DLXXVIII shows the VFF model for the single-layer InO. The force constant parameters are determined by fitting to the six low-frequency branches in the phonon dispersion along the ΓM as shown in Fig. 297 (a). The *ab initio* calculations for the phonon dispersion are from Ref. 115. Fig. 297 (b) shows that the VFF model and the SW potential give exactly the same phonon dispersion, as the SW potential is derived from the VFF model.

The parameters for the two-body SW potential used by GULP are shown in Tab. DLXXIX. The parameters for the three-body SW potential used by GULP are shown in Tab. DLXXX. Parameters for the SW potential used by LAMMPS are listed in Tab. DLXXXI.

We use LAMMPS to perform MD simulations for the mechanical behavior of the single-

TABLE DLXXXII: The VFF model for BS. The second line gives an explicit expression for each VFF term. The third line is the force constant parameters. Parameters are in the unit of $\frac{eV}{\text{\AA}^2}$ for the bond stretching interactions, and in the unit of eV for the angle bending interaction. The fourth line gives the initial bond length (in unit of \AA) for the bond stretching interaction and the initial angle (in unit of degrees) for the angle bending interaction.

VFF type	bond stretching		angle bending	
expression	$\frac{1}{2}K_{B-S}(\Delta r)^2$	$\frac{1}{2}K_{B-B}(\Delta r)^2$	$\frac{1}{2}K_{BSS}(\Delta\theta)^2$	$\frac{1}{2}K_{BBS}(\Delta\theta)^2$
parameter	17.138	16.385	5.144	3.861
r_0 or θ_0	1.940	1.720	102.691	115.613

layer InO under uniaxial tension at 1.0 K and 300.0 K. Fig. 298 shows the stress-strain curve for the tension of a single-layer InO of dimension $100 \times 100 \text{\AA}$. Periodic boundary conditions are applied in both armchair and zigzag directions. The single-layer InO is stretched uniaxially along the armchair or zigzag direction. The stress is calculated without involving the actual thickness of the quasi-two-dimensional structure of the single-layer InO. The Young's modulus can be obtained by a linear fitting of the stress-strain relation in the small strain range of $[0, 0.01]$. The Young's modulus is 85.7 N/m along the armchair and zigzag directions. The Poisson's ratio from the VFF model and the SW potential is $\nu_{xy} = \nu_{yx} = 0.29$.

There is no available value for nonlinear quantities in the single-layer InO. We have thus used the nonlinear parameter $B = 0.5d^4$ in Eq. (5), which is close to the value of B in most materials. The value of the third order nonlinear elasticity D can be extracted by fitting the stress-strain relation to the function $\sigma = E\epsilon + \frac{1}{2}D\epsilon^2$ with E as the Young's modulus. The values of D from the present SW potential are -157.3 N/m and -210.9 N/m along the armchair and zigzag directions, respectively. The ultimate stress is about 19.9 Nm^{-1} at the ultimate strain of 0.38 in the armchair direction at the low temperature of 1 K. The ultimate stress is about 23.6 Nm^{-1} at the ultimate strain of 0.39 in the zigzag direction at the low temperature of 1 K.

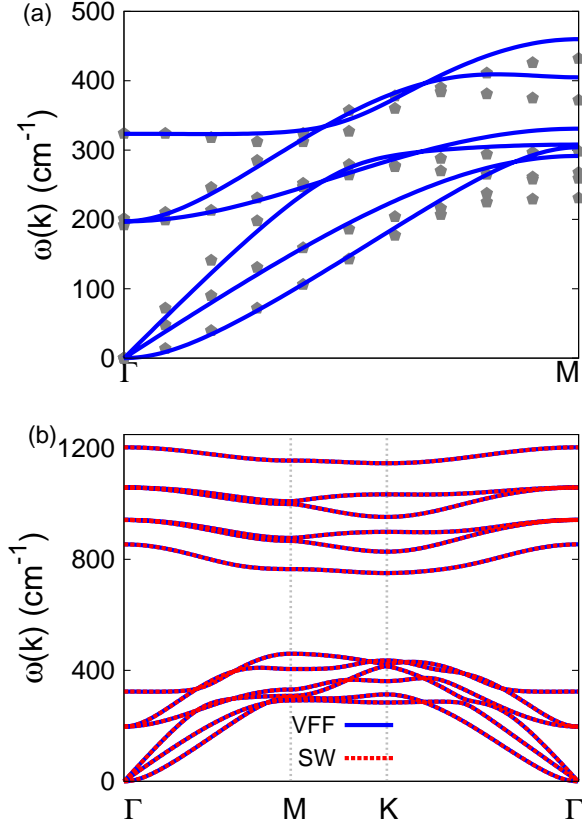


FIG. 299: (Color online) Phonon dispersion for the single-layer BS. (a) The VFF model is fitted to the six low-frequency branches along the Γ M direction. The *ab initio* results (gray pentagons) are from Ref. 115. (b) The VFF model (blue lines) and the SW potential (red lines) give the same phonon dispersion for the BS along Γ MKT.

TABLE DLXXXIII: Two-body SW potential parameters for BS used by GULP,⁸ as expressed in Eq. (3).

	A (eV)	ρ (\AA)	B (\AA^4)	r_{\min} (\AA)	r_{\max} (\AA)
B ₁ -S ₁	13.021	1.417	7.082	0.0	2.769
B ₁ -B ₂	14.613	1.809	4.376	0.0	2.602

CXLVI. BS

Present studies on the BS are based on first-principles calculations, and no empirical potential has been proposed for the BS. We will thus parametrize a set of SW potential for

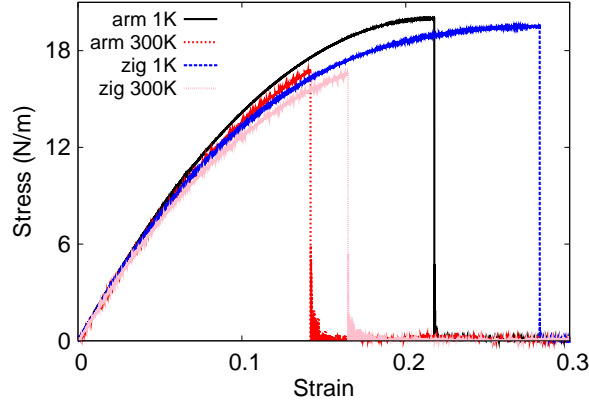


FIG. 300: (Color online) Stress-strain relations for the BS of size $100 \times 100 \text{ \AA}$. The BS is uniaxially stretched along the armchair or zigzag directions at temperatures 1 K and 300 K.

TABLE DLXXXIV: Three-body SW potential parameters for BS used by GULP,⁸ as expressed in Eq. (4).

	K (eV)	θ_0 (degree)	ρ_1 (\AA)	ρ_2 (\AA)	$r_{\min 12}$ (\AA)	$r_{\max 12}$ (\AA)	$r_{\min 13}$ (\AA)	$r_{\max 13}$ (\AA)	$r_{\min 23}$ (\AA)	$r_{\max 23}$ (\AA)
B ₁ -S ₁ -S ₁	82.459	102.691	1.417	1.417	0.0	2.769	0.0	2.769	0.0	4.139
B ₁ -B ₂ -S ₁	102.002	115.613	1.809	1.417	0.0	2.602	0.0	2.769	0.0	3.717

the single-layer BS in this section.

The structure of the single-layer BS is shown in Fig. 290 with M=B and X=S. The structural parameters are from the *ab initio* calculations.¹¹⁵ The BS has a bi-buckled configuration as shown in Fig. 290 (b), where the buckle is along the zigzag direction. Two buckling layers are symmetrically integrated through the interior B-B bonds, forming a bi-buckled configuration. This structure can be determined by three independent geometrical

TABLE DLXXXV: SW potential parameters for BS used by LAMMPS,⁹ as expressed in Eqs. (9) and (10).

	ϵ (eV)	σ (\AA)	a	λ	γ	$\cos \theta_0$	A_L	B_L	p	q	tol
B ₁ -S ₁ -S ₁	1.000	1.417	1.955	82.459	1.000	-0.220	13.021	1.758	4	0	0.0
B ₁ -B ₂ -B ₂	1.000	1.809	1.438	0.000	1.000	0.000	14.613	0.408	4	0	0.0
B ₁ -B ₂ -S ₁	1.000	0.000	0.000	102.002	1.000	-0.432	0.000	0.000	4	0	0.0

parameters, eg. the lattice constant 3.03 Å, the bond length $d_{B-S} = 1.94$ Å, and the bond length $d_{B-B} = 1.72$ Å.

Table DLXXXII shows the VFF model for the single-layer BS. The force constant parameters are determined by fitting to the six low-frequency branches in the phonon dispersion along the ΓM as shown in Fig. 299 (a). The *ab initio* calculations for the phonon dispersion are from Ref. 115. Fig. 299 (b) shows that the VFF model and the SW potential give exactly the same phonon dispersion, as the SW potential is derived from the VFF model.

The parameters for the two-body SW potential used by GULP are shown in Tab. DLXXXIII. The parameters for the three-body SW potential used by GULP are shown in Tab. DLXXXIV. Parameters for the SW potential used by LAMMPS are listed in Tab. DLXXXV.

We use LAMMPS to perform MD simulations for the mechanical behavior of the single-layer BS under uniaxial tension at 1.0 K and 300.0 K. Fig. 300 shows the stress-strain curve for the tension of a single-layer BS of dimension 100×100 Å. Periodic boundary conditions are applied in both armchair and zigzag directions. The single-layer BS is stretched uniaxially along the armchair or zigzag direction. The stress is calculated without involving the actual thickness of the quasi-two-dimensional structure of the single-layer BS. The Young's modulus can be obtained by a linear fitting of the stress-strain relation in the small strain range of $[0, 0.01]$. The Young's modulus is 179.4 N/m and 178.5 N/m along the armchair and zigzag directions, respectively. The Poisson's ratio from the VFF model and the SW potential is $\nu_{xy} = \nu_{yx} = 0.16$.

There is no available value for nonlinear quantities in the single-layer BS. We have thus used the nonlinear parameter $B = 0.5d^4$ in Eq. (5), which is close to the value of B in most materials. The value of the third order nonlinear elasticity D can be extracted by fitting the stress-strain relation to the function $\sigma = E\epsilon + \frac{1}{2}D\epsilon^2$ with E as the Young's modulus. The values of D from the present SW potential are -793.2 N/m and -823.2 N/m along the armchair and zigzag directions, respectively. The ultimate stress is about 20.0 Nm^{-1} at the ultimate strain of 0.21 in the armchair direction at the low temperature of 1 K. The ultimate stress is about 19.5 Nm^{-1} at the ultimate strain of 0.28 in the zigzag direction at the low temperature of 1 K.

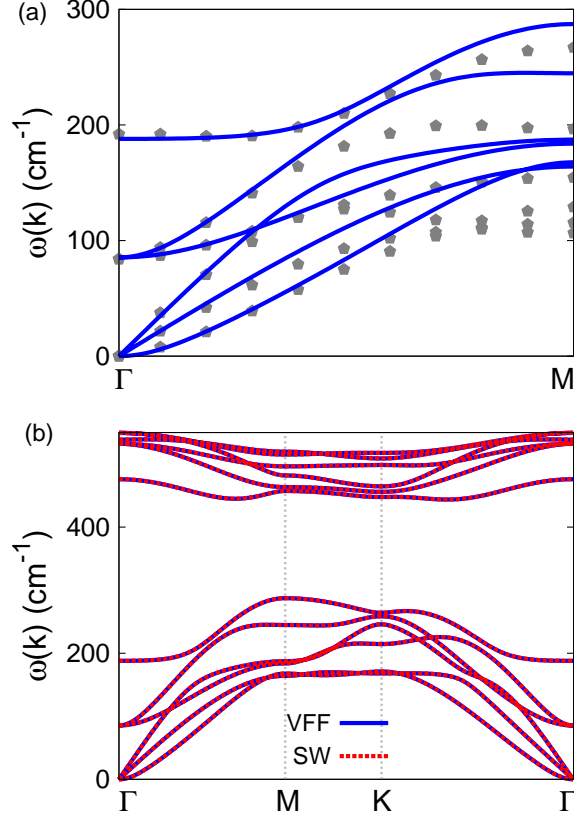


FIG. 301: (Color online) Phonon dispersion for the single-layer AIS. (a) The VFF model is fitted to the six low-frequency branches along the Γ M direction. The *ab initio* results (gray pentagons) are from Ref. 115. (b) The VFF model (blue lines) and the SW potential (red lines) give the same phonon dispersion for the AIS along Γ MKT Γ .

CXLVII. ALS

Present studies on the AIS are based on first-principles calculations, and no empirical potential has been proposed for the AIS. We will thus parametrize a set of SW potential for the single-layer AIS in this section.

The structure of the single-layer AIS is shown in Fig. 290 with M=Al and X=S. The structural parameters are from the *ab initio* calculations.¹¹⁵ The AIS has a bi-buckled configuration as shown in Fig. 290 (b), where the buckle is along the zigzag direction. Two buckling layers are symmetrically integrated through the interior Al-Al bonds, forming a bi-buckled configuration. This structure can be determined by three independent geometrical

TABLE DLXXXVI: The VFF model for AIS. The second line gives an explicit expression for each VFF term. The third line is the force constant parameters. Parameters are in the unit of $\frac{eV}{\text{\AA}^2}$ for the bond stretching interactions, and in the unit of eV for the angle bending interaction. The fourth line gives the initial bond length (in unit of \AA) for the bond stretching interaction and the initial angle (in unit of degrees) for the angle bending interaction.

VFF type	bond stretching		angle bending	
expression	$\frac{1}{2}K_{\text{Al-S}}(\Delta r)^2$	$\frac{1}{2}K_{\text{Al-Al}}(\Delta r)^2$	$\frac{1}{2}K_{\text{AlSS}}(\Delta\theta)^2$	$\frac{1}{2}K_{\text{AlAIS}}(\Delta\theta)^2$
parameter	11.065	4.912	3.210	1.900
r_0 or θ_0	2.320	2.590	100.600	117.324

TABLE DLXXXVII: Two-body SW potential parameters for AIS used by GULP,⁸ as expressed in Eq. (3).

	A (eV)	ρ (\AA)	B (\AA^4)	r_{\min} (\AA)	r_{\max} (\AA)
Al ₁ -S ₁	11.476	1.618	14.485	0.0	3.289
Al ₁ -Al ₂	4.575	1.280	22.499	0.0	3.500

TABLE DLXXXVIII: Three-body SW potential parameters for AIS used by GULP,⁸ as expressed in Eq. (4).

	K (eV)	θ_0 (degree)	ρ_1 (\AA)	ρ_2 (\AA)	$r_{\min12}$ (\AA)	$r_{\max12}$ (\AA)	$r_{\min13}$ (\AA)	$r_{\max13}$ (\AA)	$r_{\min23}$ (\AA)	$r_{\max23}$ (\AA)
Al ₁ -S ₁ -S ₁	46.910	100.600	1.618	1.618	0.0	3.289	0.0	3.289	0.0	4.877
Al ₁ -S ₁ -Al ₂	26.090	117.324	1.280	1.618	0.0	3.500	0.0	3.289	0.0	4.853

TABLE DLXXXIX: SW potential parameters for AIS used by LAMMPS,⁹ as expressed in Eqs. (9) and (10).

	ϵ (eV)	σ (\AA)	a	λ	γ	$\cos\theta_0$	A_L	B_L	p	q	tol
Al ₁ -S ₁ -S ₁	1.000	1.618	2.032	46.910	1.000	-0.184	11.476	2.112	4	0	0.0
Al ₁ -Al ₂ -Al ₂	1.000	1.280	2.735	0.000	1.000	0.000	4.575	8.388	4	0	0.0
Al ₁ -Al ₂ -S ₁	1.000	0.000	0.000	26.090	1.000	-0.459	0.000	0.000	4	0	0.0

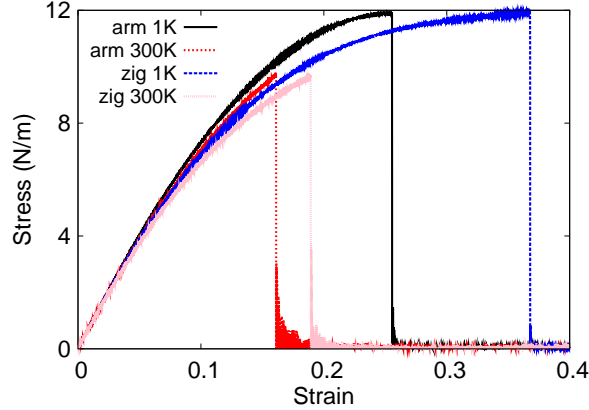


FIG. 302: (Color online) Stress-strain relations for the AIS of size $100 \times 100 \text{ \AA}$. The AIS is uniaxially stretched along the armchair or zigzag directions at temperatures 1 K and 300 K.

parameters, eg. the lattice constant 3.57 \AA , the bond length $d_{\text{Al-S}} = 2.32 \text{ \AA}$, and the bond length $d_{\text{Al-Al}} = 2.59 \text{ \AA}$.

Table DLXXXVI shows the VFF model for the single-layer AIS. The force constant parameters are determined by fitting to the six low-frequency branches in the phonon dispersion along the ΓM as shown in Fig. 301 (a). The *ab initio* calculations for the phonon dispersion are from Ref. 115. Fig. 301 (b) shows that the VFF model and the SW potential give exactly the same phonon dispersion, as the SW potential is derived from the VFF model.

The parameters for the two-body SW potential used by GULP are shown in Tab. DLXXXVII. The parameters for the three-body SW potential used by GULP are shown in Tab. DLXXXVIII. Parameters for the SW potential used by LAMMPS are listed in Tab. DLXXXIX.

We use LAMMPS to perform MD simulations for the mechanical behavior of the single-layer AIS under uniaxial tension at 1.0 K and 300.0 K. Fig. 302 shows the stress-strain curve for the tension of a single-layer AIS of dimension $100 \times 100 \text{ \AA}$. Periodic boundary conditions are applied in both armchair and zigzag directions. The single-layer AIS is stretched uniaxially along the armchair or zigzag direction. The stress is calculated without involving the actual thickness of the quasi-two-dimensional structure of the single-layer AIS. The Young's modulus can be obtained by a linear fitting of the stress-strain relation in the small strain range of $[0, 0.01]$. The Young's modulus is 85.2 N/m and 84.6 N/m along the armchair and zigzag directions, respectively. The Poisson's ratio from the VFF model and the SW

TABLE DXC: The VFF model for GaS. The second line gives an explicit expression for each VFF term. The third line is the force constant parameters. Parameters are in the unit of $\frac{\text{eV}}{\text{\AA}^2}$ for the bond stretching interactions, and in the unit of eV for the angle bending interaction. The fourth line gives the initial bond length (in unit of \AA) for the bond stretching interaction and the initial angle (in unit of degrees) for the angle bending interaction.

VFF type	bond stretching		angle bending	
expression	$\frac{1}{2}K_{\text{Ga-S}}(\Delta r)^2$	$\frac{1}{2}K_{\text{Ga-Ga}}(\Delta r)^2$	$\frac{1}{2}K_{\text{GaSS}}(\Delta\theta)^2$	$\frac{1}{2}K_{\text{GaGaS}}(\Delta\theta)^2$
parameter	10.014	6.133	2.925	1.900
r_0 or θ_0	2.360	2.470	100.921	117.065

TABLE DXCI: Two-body SW potential parameters for GaS used by GULP,⁸ as expressed in Eq. (3).

	A (eV)	ρ (\AA)	B (\AA^4)	r_{\min} (\AA)	r_{\max} (\AA)
Ga ₁ -S ₁	10.825	1.658	15.510	0.0	3.349
Ga ₁ -Ga ₂	6.316	1.506	18.610	0.0	3.434

potential is $\nu_{xy} = \nu_{yx} = 0.22$.

There is no available value for nonlinear quantities in the single-layer ALS. We have thus used the nonlinear parameter $B = 0.5d^4$ in Eq. (5), which is close to the value of B in most materials. The value of the third order nonlinear elasticity D can be extracted by fitting the stress-strain relation to the function $\sigma = E\epsilon + \frac{1}{2}D\epsilon^2$ with E as the Young's modulus. The values of D from the present SW potential are -289.7 N/m and -302.4 N/m along the armchair and zigzag directions, respectively. The ultimate stress is about 11.9 Nm^{-1} at the ultimate strain of 0.25 in the armchair direction at the low temperature of 1 K. The ultimate stress is about 11.9 Nm^{-1} at the ultimate strain of 0.36 in the zigzag direction at the low temperature of 1 K.

CXLVIII. GAS

Present studies on the GaS are based on first-principles calculations, and no empirical potential has been proposed for the GaS. We will thus parametrize a set of SW potential

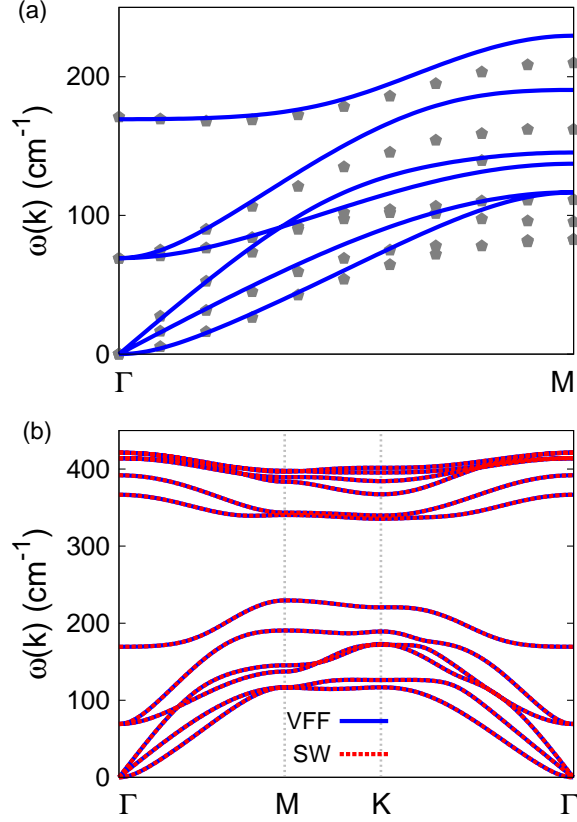


FIG. 303: (Color online) Phonon dispersion for the single-layer GaS. (a) The VFF model is fitted to the six low-frequency branches along the Γ M direction. The *ab initio* results (gray pentagons) are from Ref. 115. (b) The VFF model (blue lines) and the SW potential (red lines) give the same phonon dispersion for the GaS along Γ MKT.

TABLE DXCII: Three-body SW potential parameters for GaS used by GULP,⁸ as expressed in Eq. (4).

	K (eV)	θ_0 (degree)	ρ_1 (Å)	ρ_2 (Å)	$r_{\min 12}$ (Å)	$r_{\max 12}$ (Å)	$r_{\min 13}$ (Å)	$r_{\max 13}$ (Å)	$r_{\min 23}$ (Å)	$r_{\max 23}$ (Å)
Ga ₁ -S ₁ -S ₁	43.355	100.921	1.658	1.658	0.0	3.349	0.0	3.349	0.0	4.972
Ga ₁ -S ₁ -Ga ₂	30.536	117.065	1.658	1.506	0.0	3.349	0.0	3.434	0.0	4.809

for the single-layer GaS in this section.

The structure of the single-layer GaS is shown in Fig. 290 with M=Ga and X=S. The structural parameters are from the *ab initio* calculations.¹¹⁵ The GaS has a bi-buckled configuration as shown in Fig. 290 (b), where the buckle is along the zigzag direction. Two

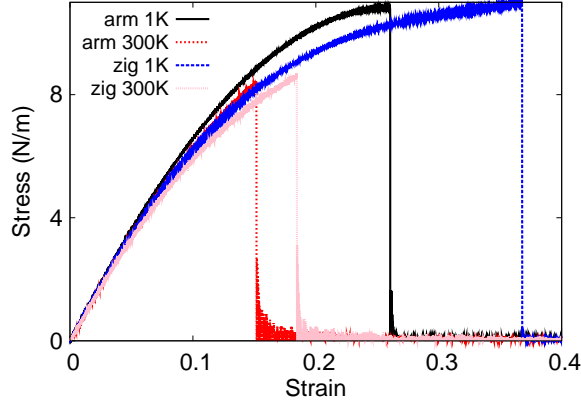


FIG. 304: (Color online) Stress-strain relations for the GaS of size $100 \times 100 \text{ \AA}$. The GaS is uniaxially stretched along the armchair or zigzag directions at temperatures 1 K and 300 K.

TABLE DXCIII: SW potential parameters for GaS used by LAMMPS,⁹ as expressed in Eqs. (9) and (10).

	ϵ (eV)	σ (\AA)	a	λ	γ	$\cos \theta_0$	A_L	B_L	p	q	tol
Ga ₁ -S ₁ -S ₁	1.000	1.658	2.020	43.355	1.000	-0.189	10.825	2.052	4	0	0.0
Ga ₁ -Ga ₂ -Ga ₂	1.000	1.506	2.280	0.000	1.000	0.000	6.316	3.615	4	0	0.0
Ga ₁ -Ga ₂ -S ₁	1.000	0.000	0.000	30.536	1.000	-0.455	0.000	0.000	4	0	0.0

buckling layers are symmetrically integrated through the interior Ga-Ga bonds, forming a bi-buckled configuration. This structure can be determined by three independent geometrical parameters, eg. the lattice constant 3.64 \AA , the bond length $d_{\text{Ga-S}} = 2.36 \text{ \AA}$, and the bond length $d_{\text{Ga-Ga}} = 2.47 \text{ \AA}$.

Table DXC shows the VFF model for the single-layer GaS. The force constant parameters are determined by fitting to the six low-frequency branches in the phonon dispersion along the ΓM as shown in Fig. 303 (a). The *ab initio* calculations for the phonon dispersion are from Ref. 115. Fig. 303 (b) shows that the VFF model and the SW potential give exactly the same phonon dispersion, as the SW potential is derived from the VFF model.

The parameters for the two-body SW potential used by GULP are shown in Tab. DXCI. The parameters for the three-body SW potential used by GULP are shown in Tab. DXCII. Parameters for the SW potential used by LAMMPS are listed in Tab. DXCIII.

We use LAMMPS to perform MD simulations for the mechanical behavior of the single-

TABLE DXCIV: The VFF model for InS. The second line gives an explicit expression for each VFF term. The third line is the force constant parameters. Parameters are in the unit of $\frac{\text{eV}}{\text{\AA}^2}$ for the bond stretching interactions, and in the unit of eV for the angle bending interaction. The fourth line gives the initial bond length (in unit of \AA) for the bond stretching interaction and the initial angle (in unit of degrees) for the angle bending interaction.

VFF type	bond stretching		angle bending	
expression	$\frac{1}{2}K_{\text{In-S}}(\Delta r)^2$	$\frac{1}{2}K_{\text{In-In}}(\Delta r)^2$	$\frac{1}{2}K_{\text{InSS}}(\Delta\theta)^2$	$\frac{1}{2}K_{\text{InInS}}(\Delta\theta)^2$
parameter	10.014	4.533	2.179	1.412
r_0 or θ_0	2.560	2.820	100.624	117.305

layer GaS under uniaxial tension at 1.0 K and 300.0 K. Fig. 304 shows the stress-strain curve for the tension of a single-layer GaS of dimension $100 \times 100 \text{ \AA}$. Periodic boundary conditions are applied in both armchair and zigzag directions. The single-layer GaS is stretched uniaxially along the armchair or zigzag direction. The stress is calculated without involving the actual thickness of the quasi-two-dimensional structure of the single-layer GaS. The Young's modulus can be obtained by a linear fitting of the stress-strain relation in the small strain range of $[0, 0.01]$. The Young's modulus is 76.2 N/m along the armchair and zigzag directions. The Poisson's ratio from the VFF model and the SW potential is $\nu_{xy} = \nu_{yx} = 0.23$.

There is no available value for nonlinear quantities in the single-layer GaS. We have thus used the nonlinear parameter $B = 0.5d^4$ in Eq. (5), which is close to the value of B in most materigas. The value of the third order nonlinear elasticity D can be extracted by fitting the stress-strain relation to the function $\sigma = E\epsilon + \frac{1}{2}D\epsilon^2$ with E as the Young's modulus. The values of D from the present SW potential are -254.5 N/m and -269.8 N/m along the armchair and zigzag directions, respectively. The ultimate stress is about 10.8 Nm^{-1} at the ultimate strain of 0.26 in the armchair direction at the low temperature of 1 K. The ultimate stress is about 11.0 Nm^{-1} at the ultimate strain of 0.36 in the zigzag direction at the low temperature of 1 K.

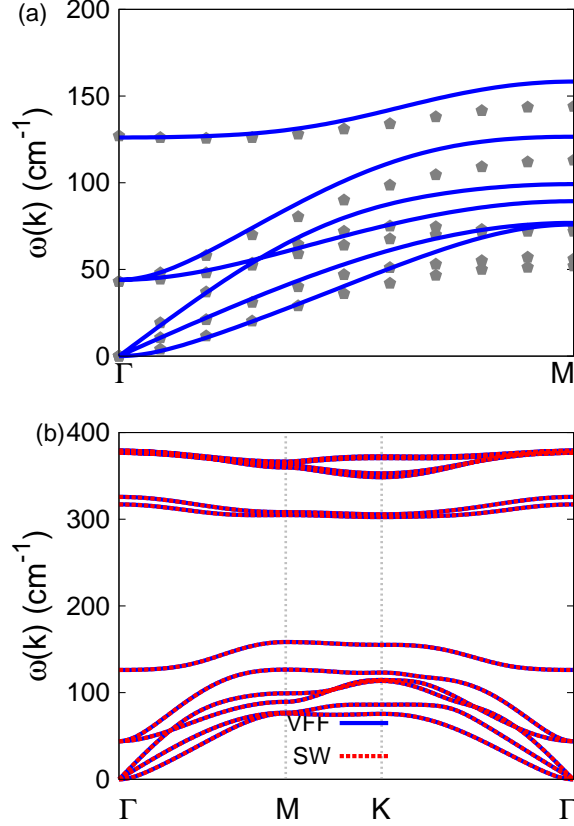


FIG. 305: (Color online) Phonon dispersion for the single-layer InS. (a) The VFF model is fitted to the six low-frequency branches along the Γ M direction. The *ab initio* results (gray pentagons) are from Ref. 115. (b) The VFF model (blue lines) and the SW potential (red lines) give the same phonon dispersion for the InS along Γ MK Γ .

TABLE DXCV: Two-body SW potential parameters for InS used by GULP,⁸ as expressed in Eq. (3).

	A (eV)	ρ (\AA)	B (\AA^4)	r_{\min} (\AA)	r_{\max} (\AA)
In ₁ -S ₁	12.652	1.787	21.475	0.0	3.629
In ₁ -In ₂	5.202	1.454	31.620	0.0	3.833

CXLIX. INS

Present studies on the InS are based on first-principles calculations, and no empirical potential has been proposed for the InS. We will thus parametrize a set of SW potential for

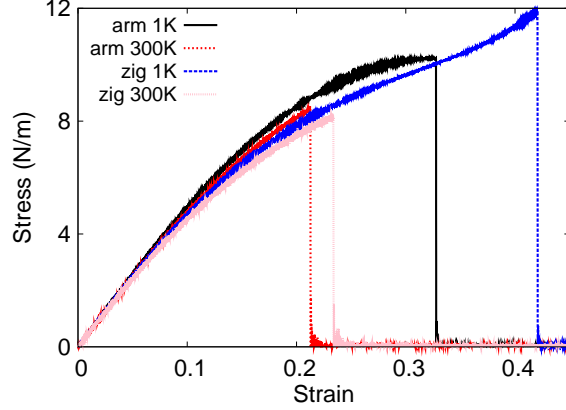


FIG. 306: (Color online) Stress-strain relations for the InS of size $100 \times 100 \text{ \AA}$. The InS is uniaxially stretched along the armchair or zigzag directions at temperatures 1 K and 300 K.

TABLE DXCVI: Three-body SW potential parameters for InS used by GULP,⁸ as expressed in Eq. (4).

	K (eV)	θ_0 (degree)	ρ_1 (\AA)	ρ_2 (\AA)	$r_{\min 12}$ (\AA)	$r_{\max 12}$ (\AA)	$r_{\min 13}$ (\AA)	$r_{\max 13}$ (\AA)	$r_{\min 23}$ (\AA)	$r_{\max 23}$ (\AA)
In ₁ -S ₁ -S ₁	31.876	100.624	1.787	1.787	0.0	3.629	0.0	3.629	0.0	5.382
In ₁ -S ₁ -In ₂	19.900	117.305	1.787	1.454	0.0	3.629	0.0	3.833	0.0	5.325

the single-layer InS in this section.

The structure of the single-layer InS is shown in Fig. 290 with M=In and X=S. The structural parameters are from the *ab initio* calculations.¹¹⁵ The InS has a bi-buckled configuration as shown in Fig. 290 (b), where the buckle is along the zigzag direction. Two buckling layers are symmetrically integrated through the interior In-In bonds, forming a bi-buckled configuration. This structure can be determined by three independent geometrical

TABLE DXCVII: SW potential parameters for InS used by LAMMPS,⁹ as expressed in Eqs. (9) and (10).

	ϵ (eV)	σ (\AA)	a	λ	γ	$\cos \theta_0$	A_L	B_L	p	q	tol
In ₁ -S ₁ -S ₁	1.000	1.787	2.031	31.876	1.000	-0.184	12.652	2.108	4	0	0.0
In ₁ -In ₂ -In ₂	1.000	1.454	2.635	0.000	1.000	0.000	5.202	7.067	4	0	0.0
In ₁ -In ₂ -S ₁	1.000	0.000	0.000	19.990	1.000	-0.459	0.000	0.000	4	0	0.0

parameters, eg. the lattice constant 3.94 Å, the bond length $d_{\text{In-S}} = 2.56$ Å, and the bond length $d_{\text{In-In}} = 2.82$ Å.

Table [DXCIV](#) shows the VFF model for the single-layer InS. The force constant parameters are determined by fitting to the six low-frequency branches in the phonon dispersion along the Γ M as shown in Fig. [305](#) (a). The *ab initio* calculations for the phonon dispersion are from Ref. 115. Fig. [305](#) (b) shows that the VFF model and the SW potential give exactly the same phonon dispersion, as the SW potential is derived from the VFF model.

The parameters for the two-body SW potential used by GULP are shown in Tab. [DXCV](#). The parameters for the three-body SW potential used by GULP are shown in Tab. [DXCVI](#). Parameters for the SW potential used by LAMMPS are listed in Tab. [DXCVII](#).

We use LAMMPS to perform MD simulations for the mechanical behavior of the single-layer InS under uniaxial tension at 1.0 K and 300.0 K. Fig. [306](#) shows the stress-strain curve for the tension of a single-layer InS of dimension 100×100 Å. Periodic boundary conditions are applied in both armchair and zigzag directions. The single-layer InS is stretched uniaxially along the armchair or zigzag direction. The stress is calculated without involving the actual thickness of the quasi-two-dimensional structure of the single-layer InS. The Young's modulus can be obtained by a linear fitting of the stress-strain relation in the small strain range of $[0, 0.01]$. The Young's modulus is 52.9 N/m and 53.2 N/m along the armchair and zigzag directions, respectively. The Poisson's ratio from the VFF model and the SW potential is $\nu_{xy} = \nu_{yx} = 0.29$.

There is no available value for nonlinear quantities in the single-layer InS. We have thus used the nonlinear parameter $B = 0.5d^4$ in Eq. (5), which is close to the value of B in most materials. The value of the third order nonlinear elasticity D can be extracted by fitting the stress-strain relation to the function $\sigma = E\epsilon + \frac{1}{2}D\epsilon^2$ with E as the Young's modulus. The values of D from the present SW potential are -115.9 N/m and -141.1 N/m along the armchair and zigzag directions, respectively. The ultimate stress is about 10.2 Nm^{-1} at the ultimate strain of 0.32 in the armchair direction at the low temperature of 1 K. The ultimate stress is about 11.8 Nm^{-1} at the ultimate strain of 0.42 in the zigzag direction at the low temperature of 1 K.

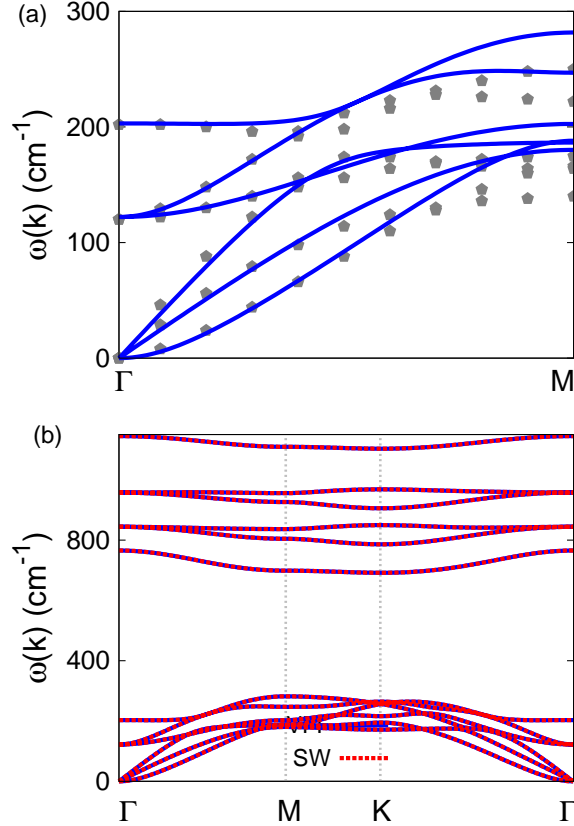


FIG. 307: (Color online) Phonon dispersion for the single-layer BSe. (a) The VFF model is fitted to the six low-frequency branches along the ΓM direction. The *ab initio* results (gray pentagons) are from Ref. 115. (b) The VFF model (blue lines) and the SW potential (red lines) give the same phonon dispersion for the BSe along $\Gamma M K \Gamma$.

CL. BSE

Present studies on the BSe are based on first-principles calculations, and no empirical potential has been proposed for the BSe. We will thus parametrize a set of SW potential for the single-layer BSe in this section.

The structure of the single-layer BSe is shown in Fig. 290 with $M=B$ and $X=Se$. The structural parameters are from the *ab initio* calculations.¹¹⁵ The BSe has a bi-buckled configuration as shown in Fig. 290 (b), where the buckle is along the zigzag direction. Two buckling layers are symmetrically integrated through the interior B-B bonds, forming a bi-buckled configuration. This structure can be determined by three independent geometrical

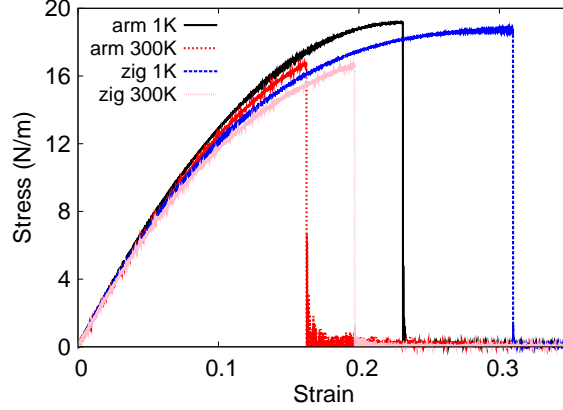


FIG. 308: (Color online) Stress-strain relations for the BSe of size $100 \times 100 \text{ \AA}$. The BSe is uniaxially stretched along the armchair or zigzag directions at temperatures 1 K and 300 K.

TABLE DXCVIII: The VFF model for BSe. The second line gives an explicit expression for each VFF term. The third line is the force constant parameters. Parameters are in the unit of $\frac{\text{eV}}{\text{\AA}^2}$ for the bond stretching interactions, and in the unit of eV for the angle bending interaction. The fourth line gives the initial bond length (in unit of \AA) for the bond stretching interaction and the initial angle (in unit of degrees) for the angle bending interaction.

VFF type	bond stretching		angle bending	
expression	$\frac{1}{2}K_{\text{B-Se}}(\Delta r)^2$	$\frac{1}{2}K_{\text{B-B}}(\Delta r)^2$	$\frac{1}{2}K_{\text{BSeSe}}(\Delta\theta)^2$	$\frac{1}{2}K_{\text{BBSe}}(\Delta\theta)^2$
parameter	17.138	15.227	5.144	3.113
r_0 or θ_0	2.100	1.710	101.394	116.681

parameters, eg. the lattice constant 3.25 \AA , the bond length $d_{\text{B-Se}} = 2.10 \text{ \AA}$, and the bond length $d_{\text{B-B}} = 1.71 \text{ \AA}$.

Table DXCVIII shows the VFF model for the single-layer BSe. The force constant parameters are determined by fitting to the six low-frequency branches in the phonon dispersion along the ΓM as shown in Fig. 307 (a). The *ab initio* calculations for the phonon dispersion are from Ref. 115. Fig. 307 (b) shows that the VFF model and the SW potential give exactly the same phonon dispersion, as the SW potential is derived from the VFF model.

The parameters for the two-body SW potential used by GULP are shown in Tab. DXCIX. The parameters for the three-body SW potential used by GULP are shown in Tab. DC. Parameters for the SW potential used by LAMMPS are listed in Tab. DCI.

TABLE DXCIX: Two-body SW potential parameters for BSe used by GULP,⁸ as expressed in Eq. (3).

	A (eV)	ρ (Å)	B (Å ⁴)	r_{\min} (Å)	r_{\max} (Å)
B ₁ -Se ₁	14.825	1.491	9.724	0.0	2.985
B ₁ -B ₂	17.700	2.252	4.275	0.0	2.691

TABLE DC: Three-body SW potential parameters for BSe used by GULP,⁸ as expressed in Eq. (4).

	K (eV)	θ_0 (degree)	ρ_1 (Å)	ρ_2 (Å)	$r_{\min12}$ (Å)	$r_{\max12}$ (Å)	$r_{\min13}$ (Å)	$r_{\max13}$ (Å)	$r_{\min23}$ (Å)	$r_{\max23}$ (Å)
B ₁ -S ₁ -Se ₁	77.850	101.394	1.491	1.491	0.0	2.985	0.0	2.985	0.0	4.440
B ₁ -B ₂ -Se ₁	104.372	116.681	2.252	1.491	0.0	2.691	0.0	2.985	0.0	3.923

We use LAMMPS to perform MD simulations for the mechanical behavior of the single-layer BSe under uniaxial tension at 1.0 K and 300.0 K. Fig. 308 shows the stress-strain curve for the tension of a single-layer BSe of dimension 100×100 Å. Periodic boundary conditions are applied in both armchair and zigzag directions. The single-layer BSe is stretched uniaxially along the armchair or zigzag direction. The stress is calculated without involving the actual thickness of the quasi-two-dimensional structure of the single-layer BSe. The Young's modulus can be obtained by a linear fitting of the stress-strain relation in the small strain range of $[0, 0.01]$. The Young's modulus is 157.3 N/m and 156.4 N/m along the armchair and zigzag directions, respectively. The Poisson's ratio from the VFF model and the SW potential is $\nu_{xy} = \nu_{yx} = 0.19$.

There is no available value for nonlinear quantities in the single-layer BSe. We have thus used the nonlinear parameter $B = 0.5d^4$ in Eq. (5), which is close to the value of B in most materials. The value of the third order nonlinear elasticity D can be extracted by fitting

TABLE DCI: SW potential parameters for BSe used by LAMMPS,⁹ as expressed in Eqs. (9) and (10).

	ϵ (eV)	σ (Å)	a	λ	γ	$\cos \theta_0$	A_L	B_L	p	q	tol
B ₁ -Se ₁ -Se ₁	1.000	1.491	2.002	77.850	1.000	-0.198	14.825	1.968	4	0	0.0
B ₁ -B ₂ -B ₂	1.000	2.252	1.195	0.000	1.000	0.000	17.700	0.166	4	0	0.0
B ₁ -B ₂ -Se ₁	1.000	0.000	0.000	104.372	1.000	-0.449	0.000	0.000	4	0	0.0

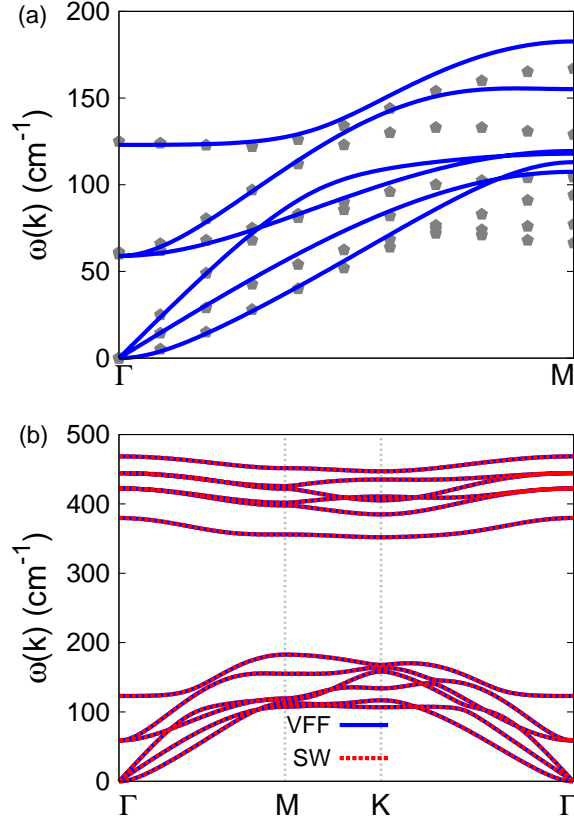


FIG. 309: (Color online) Phonon dispersion for the single-layer AlSe. (a) The VFF model is fitted to the six low-frequency branches along the Γ M direction. The *ab initio* results (gray pentagons) are from Ref. 115. (b) The VFF model (blue lines) and the SW potential (red lines) give the same phonon dispersion for the AlSe along Γ MK Γ .

the stress-strain relation to the function $\sigma = E\epsilon + \frac{1}{2}D\epsilon^2$ with E as the Young's modulus. The values of D from the present SW potential are -627.0 N/m and -655.6 N/m along the armchair and zigzag directions, respectively. The ultimate stress is about 19.2 Nm^{-1} at the ultimate strain of 0.23 in the armchair direction at the low temperature of 1 K. The ultimate stress is about 18.7 Nm^{-1} at the ultimate strain of 0.31 in the zigzag direction at the low temperature of 1 K.

TABLE DCII: The VFF model for AlSe. The second line gives an explicit expression for each VFF term. The third line is the force constant parameters. Parameters are in the unit of $\frac{\text{eV}}{\text{\AA}^2}$ for the bond stretching interactions, and in the unit of eV for the angle bending interaction. The fourth line gives the initial bond length (in unit of \AA) for the bond stretching interaction and the initial angle (in unit of degrees) for the angle bending interaction.

VFF type	bond stretching		angle bending	
expression	$\frac{1}{2}K_{Al-Se}(\Delta r)^2$	$\frac{1}{2}K_{Al-Al}(\Delta r)^2$	$\frac{1}{2}K_{AlSeSe}(\Delta\theta)^2$	$\frac{1}{2}K_{AlAlSe}(\Delta\theta)^2$
parameter	9.831	4.487	2.916	1.659
r_0 or θ_0	2.470	2.570	99.846	117.926

TABLE DCIII: Two-body SW potential parameters for AlSe used by GULP,⁸ as expressed in Eq. (3).

	A (eV)	ρ (\AA)	B (\AA^4)	r_{\min} (\AA)	r_{\max} (\AA)
Al ₁ -Se ₁	11.362	1.694	18.610	0.0	3.493
Al ₁ -Al ₂	4.974	1.558	21.812	0.0	3.570

TABLE DCIV: Three-body SW potential parameters for AlSe used by GULP,⁸ as expressed in Eq. (4).

	K (eV)	θ_0 (degree)	ρ_1 (\AA)	ρ_2 (\AA)	$r_{\min12}$ (\AA)	$r_{\max12}$ (\AA)	$r_{\min13}$ (\AA)	$r_{\max13}$ (\AA)	$r_{\min23}$ (\AA)	$r_{\max23}$ (\AA)
Al ₁ -Se ₁ -Se ₁	41.235	99.846	1.694	1.694	0.0	3.493	0.0	3.493	0.0	5.164
Al ₁ -Se ₁ -Al ₂	26.418	117.926	1.558	1.694	0.0	3.570	0.0	3.493	0.0	5.029

TABLE DCV: SW potential parameters for AlSe used by LAMMPS,⁹ as expressed in Eqs. (9) and (10).

	ϵ (eV)	σ (\AA)	a	λ	γ	$\cos\theta_0$	A_L	B_L	p	q	tol
Al ₁ -Se ₁ -Se ₁	1.000	1.694	2.062	41.235	1.000	-0.171	11.362	2.260	4	0	0.0
Al ₁ -Al ₂ -Al ₂	1.000	1.558	2.292	0.000	1.000	0.000	4.974	3.704	4	0	0.0
Al ₁ -Al ₂ -Se ₁	1.000	0.000	0.000	26.418	1.000	-0.468	0.000	0.000	4	0	0.0

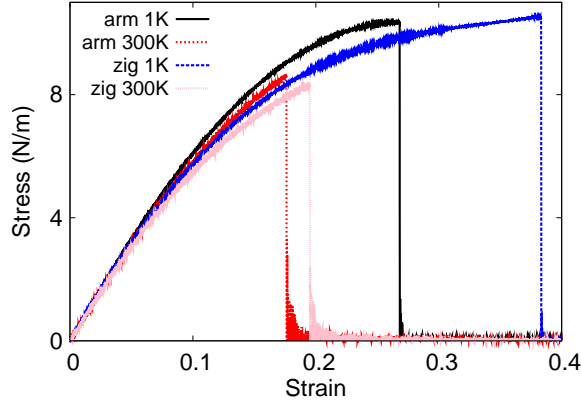


FIG. 310: (Color online) Stress-strain relations for the AlSe of size $100 \times 100 \text{ \AA}$. The AlSe is uniaxially stretched along the armchair or zigzag directions at temperatures 1 K and 300 K.

CLI. ALSE

Present studies on the AlSe are based on first-principles calculations, and no empirical potential has been proposed for the AlSe. We will thus parametrize a set of SW potential for the single-layer AlSe in this section.

The structure of the single-layer AlSe is shown in Fig. 290 with $M=\text{Al}$ and $X=\text{Se}$. The structural parameters are from the *ab initio* calculations.¹¹⁵ The AlSe has a bi-buckled configuration as shown in Fig. 290 (b), where the buckle is along the zigzag direction. Two buckling layers are symmetrically integrated through the interior Al-Al bonds, forming a bi-buckled configuration. This structure can be determined by three independent geometrical parameters, eg. the lattice constant 3.78 \AA , the bond length $d_{\text{Al-Se}} = 2.47 \text{ \AA}$, and the bond length $d_{\text{Al-Al}} = 2.57 \text{ \AA}$.

Table DCII shows the VFF model for the single-layer AlSe. The force constant parameters are determined by fitting to the six low-frequency branches in the phonon dispersion along the ΓM as shown in Fig. 309 (a). The *ab initio* calculations for the phonon dispersion are from Ref. 115. Fig. 309 (b) shows that the VFF model and the SW potential give exactly the same phonon dispersion, as the SW potential is derived from the VFF model.

The parameters for the two-body SW potential used by GULP are shown in Tab. DCIII. The parameters for the three-body SW potential used by GULP are shown in Tab. DCIV. Parameters for the SW potential used by LAMMPS are listed in Tab. DCV.

We use LAMMPS to perform MD simulations for the mechanical behavior of the single-layer AlSe under uniaxial tension at 1.0 K and 300.0 K. Fig. 310 shows the stress-strain curve for the tension of a single-layer AlSe of dimension $100 \times 100 \text{ \AA}$. Periodic boundary conditions are applied in both armchair and zigzag directions. The single-layer AlSe is stretched uniaxially along the armchair or zigzag direction. The stress is calculated without involving the actual thickness of the quasi-two-dimensional structure of the single-layer AlSe. The Young's modulus can be obtained by a linear fitting of the stress-strain relation in the small strain range of $[0, 0.01]$. The Young's modulus is 69.4 N/m and 69.2 N/m along the armchair and zigzag directions, respectively. The Poisson's ratio from the VFF model and the SW potential is $\nu_{xy} = \nu_{yx} = 0.24$.

There is no available value for nonlinear quantities in the single-layer AlSe. We have thus used the nonlinear parameter $B = 0.5d^4$ in Eq. (5), which is close to the value of B in most materials. The value of the third order nonlinear elasticity D can be extracted by fitting the stress-strain relation to the function $\sigma = E\epsilon + \frac{1}{2}D\epsilon^2$ with E as the Young's modulus. The values of D from the present SW potential are -217.3 N/m and -231.9 N/m along the armchair and zigzag directions, respectively. The ultimate stress is about 10.4 Nm^{-1} at the ultimate strain of 0.27 in the armchair direction at the low temperature of 1 K. The ultimate stress is about 10.5 Nm^{-1} at the ultimate strain of 0.38 in the zigzag direction at the low temperature of 1 K.

CLII. GASE

Present studies on the GaSe are based on first-principles calculations, and no empirical potential has been proposed for the GaSe. We will thus parametrize a set of SW potential for the single-layer GaSe in this section.

The structure of the single-layer GaSe is shown in Fig. 290 with $M=\text{Ga}$ and $X=\text{Se}$. The structural parameters are from the *ab initio* calculations.¹¹⁵ The GaSe has a bi-buckled configuration as shown in Fig. 290 (b), where the buckle is along the zigzag direction. Two buckling layers are symmetrically integrated through the interior Ga-Ga bonds, forming a bi-buckled configuration. This structure can be determined by three independent geometrical parameters, eg. the lattice constant 3.82 \AA , the bond length $d_{\text{Ga-Se}} = 2.50 \text{ \AA}$, and the bond length $d_{\text{Ga-Ga}} = 2.46 \text{ \AA}$.

TABLE DCVI: The VFF model for GaSe. The second line gives an explicit expression for each VFF term. The third line is the force constant parameters. Parameters are in the unit of $\frac{eV}{\text{\AA}^2}$ for the bond stretching interactions, and in the unit of eV for the angle bending interaction. The fourth line gives the initial bond length (in unit of \AA) for the bond stretching interaction and the initial angle (in unit of degrees) for the angle bending interaction.

VFF type	bond stretching		angle bending	
expression	$\frac{1}{2}K_{\text{Ga-Se}}(\Delta r)^2$	$\frac{1}{2}K_{\text{Ga-Ga}}(\Delta r)^2$	$\frac{1}{2}K_{\text{GaSeSe}}(\Delta\theta)^2$	$\frac{1}{2}K_{\text{GaGaSe}}(\Delta\theta)^2$
parameter	10.014	5.400	2.925	1.701
r_0 or θ_0	2.500	2.460	99.636	118.092

TABLE DCVII: Two-body SW potential parameters for GaSe used by GULP,⁸ as expressed in Eq. (3).

	A (eV)	ρ (\AA)	B (\AA^4)	r_{\min} (\AA)	r_{\max} (\AA)
Ga ₁ -Se ₁	11.798	1.706	19.531	0.0	3.533
Ga ₁ -Ga ₂	6.479	1.765	18.311	0.0	3.502

TABLE DCVIII: Three-body SW potential parameters for GaSe used by GULP,⁸ as expressed in Eq. (4).

	K (eV)	θ_0 (degree)	ρ_1 (\AA)	ρ_2 (\AA)	$r_{\min12}$ (\AA)	$r_{\max12}$ (\AA)	$r_{\min13}$ (\AA)	$r_{\max13}$ (\AA)	$r_{\min23}$ (\AA)	$r_{\max23}$ (\AA)
Ga ₁ -Se ₁ -Se ₁	40.978	99.636	1.706	1.706	0.0	3.533	0.0	3.533	0.0	5.218
Ga ₁ -Se ₁ -Ga ₂	31.031	118.092	1.765	1.706	0.0	3.502	0.0	3.533	0.0	4.985

TABLE DCIX: SW potential parameters for GaSe used by LAMMPS,⁹ as expressed in Eqs. (9) and (10).

	ϵ (eV)	σ (\AA)	a	λ	γ	$\cos\theta_0$	A_L	B_L	p	q	tol
Ga ₁ -Se ₁ -Se ₁	1.000	1.706	2.070	40.978	1.000	-0.167	11.798	2.305	4	0	0.0
Ga ₁ -Ga ₂ -Ga ₂	1.000	1.765	1.984	0.000	1.000	0.000	6.479	1.888	4	0	0.0
Ga ₁ -Ga ₂ -Se ₁	1.000	0.000	0.000	31.031	1.000	-0.471	0.000	0.000	4	0	0.0

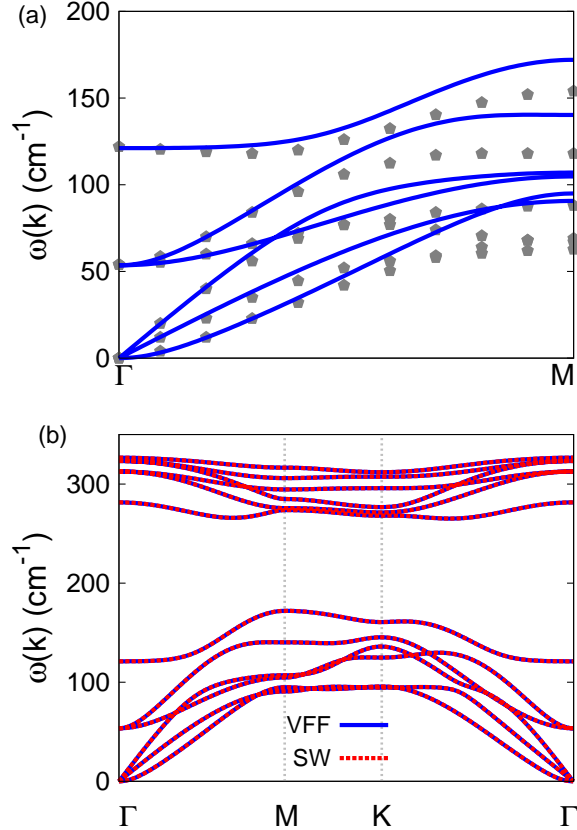


FIG. 311: (Color online) Phonon dispersion for the single-layer GaSe. (a) The VFF model is fitted to the six low-frequency branches along the Γ M direction. The *ab initio* results (gray pentagons) are from Ref. 115. (b) The VFF model (blue lines) and the SW potential (red lines) give the same phonon dispersion for the GaSe along Γ MK Γ .

Table DCVI shows the VFF model for the single-layer GaSe. The force constant parameters are determined by fitting to the six low-frequency branches in the phonon dispersion along the Γ M as shown in Fig. 311 (a). The *ab initio* calculations for the phonon dispersion are from Ref. 115. Fig. 311 (b) shows that the VFF model and the SW potential give exactly the same phonon dispersion, as the SW potential is derived from the VFF model.

The parameters for the two-body SW potential used by GULP are shown in Tab. DCVII. The parameters for the three-body SW potential used by GULP are shown in Tab. DCVIII. Parameters for the SW potential used by LAMMPS are listed in Tab. DCIX.

We use LAMMPS to perform MD simulations for the mechanical behavior of the single-layer GaSe under uniaxial tension at 1.0 K and 300.0 K. Fig. 312 shows the stress-strain

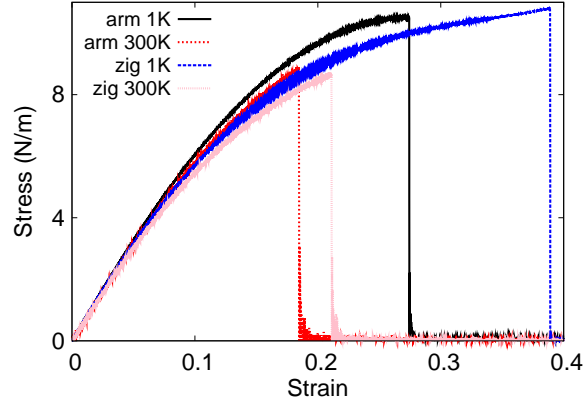


FIG. 312: (Color online) Stress-strain relations for the GaSe of size $100 \times 100 \text{ \AA}$. The GaSe is uniaxially stretched along the armchair or zigzag directions at temperatures 1 K and 300 K.

curve for the tension of a single-layer GaSe of dimension $100 \times 100 \text{ \AA}$. Periodic boundary conditions are applied in both armchair and zigzag directions. The single-layer GaSe is stretched uniaxially along the armchair or zigzag direction. The stress is calculated without involving the actual thickness of the quasi-two-dimensional structure of the single-layer GaSe. The Young's modulus can be obtained by a linear fitting of the stress-strain relation in the small strain range of $[0, 0.01]$. The Young's modulus is 68.3 N/m and 67.9 N/m along the armchair and zigzag directions, respectively. The Poisson's ratio from the VFF model and the SW potential is $\nu_{xy} = \nu_{yx} = 0.25$.

There is no available value for nonlinear quantities in the single-layer GaSe. We have thus used the nonlinear parameter $B = 0.5d^4$ in Eq. (5), which is close to the value of B in most materials. The value of the third order nonlinear elasticity D can be extracted by fitting the stress-strain relation to the function $\sigma = E\epsilon + \frac{1}{2}D\epsilon^2$ with E as the Young's modulus. The values of D from the present SW potential are -206.1 N/m and -219.8 N/m along the armchair and zigzag directions, respectively. The ultimate stress is about 10.5 Nm^{-1} at the ultimate strain of 0.27 in the armchair direction at the low temperature of 1 K. The ultimate stress is about 10.8 Nm^{-1} at the ultimate strain of 0.39 in the zigzag direction at the low temperature of 1 K.

TABLE DCX: The VFF model for InSe. The second line gives an explicit expression for each VFF term. The third line is the force constant parameters. Parameters are in the unit of $\frac{\text{eV}}{\text{\AA}^2}$ for the bond stretching interactions, and in the unit of eV for the angle bending interaction. The fourth line gives the initial bond length (in unit of \AA) for the bond stretching interaction and the initial angle (in unit of degrees) for the angle bending interaction.

VFF type	bond stretching		angle bending	
expression	$\frac{1}{2}K_{\text{In-Se}}(\Delta r)^2$	$\frac{1}{2}K_{\text{In-In}}(\Delta r)^2$	$\frac{1}{2}K_{\text{InSeSe}}(\Delta\theta)^2$	$\frac{1}{2}K_{\text{InInSe}}(\Delta\theta)^2$
parameter	9.812	4.185	2.090	1.227
r_0 or θ_0	2.690	2.810	99.296	118.361

TABLE DCXI: Two-body SW potential parameters for InSe used by GULP,⁸ as expressed in Eq. (3).

	A (eV)	ρ (\AA)	B (\AA^4)	r_{\min} (\AA)	r_{\max} (\AA)
In ₁ -Se ₁	13.281	1.822	26.181	0.0	3.797
In ₁ -In ₂	5.414	1.661	31.174	0.0	2.890

TABLE DCXII: Three-body SW potential parameters for InSe used by GULP,⁸ as expressed in Eq. (4).

	K (eV)	θ_0 (degree)	ρ_1 (\AA)	ρ_2 (\AA)	$r_{\min12}$ (\AA)	$r_{\max12}$ (\AA)	$r_{\min13}$ (\AA)	$r_{\max13}$ (\AA)	$r_{\min23}$ (\AA)	$r_{\max23}$ (\AA)
In ₁ -Se ₁ -Se ₁	28.853	99.296	1.822	1.822	0.0	3.797	0.0	3.797	0.0	5.601
In ₁ -Se ₁ -In ₂	19.120	118.361	1.822	1.661	0.0	3.797	0.0	3.890	0.0	5.489

TABLE DCXIII: SW potential parameters for InSe used by LAMMPS,⁹ as expressed in Eqs. (9) and (10).

	ϵ (eV)	σ (\AA)	a	λ	γ	$\cos\theta_0$	A_L	B_L	p	q	tol
In ₁ -Se ₁ -Se ₁	1.000	1.822	2.084	28.853	1.000	-0.162	13.281	2.377	4	0	0.0
In ₁ -In ₂ -In ₂	1.000	1.661	2.342	0.000	1.000	0.000	5.414	4.094	4	0	0.0
In ₁ -In ₂ -Se ₁	1.000	0.000	0.000	19.120	1.000	-0.475	0.000	0.000	4	0	0.0

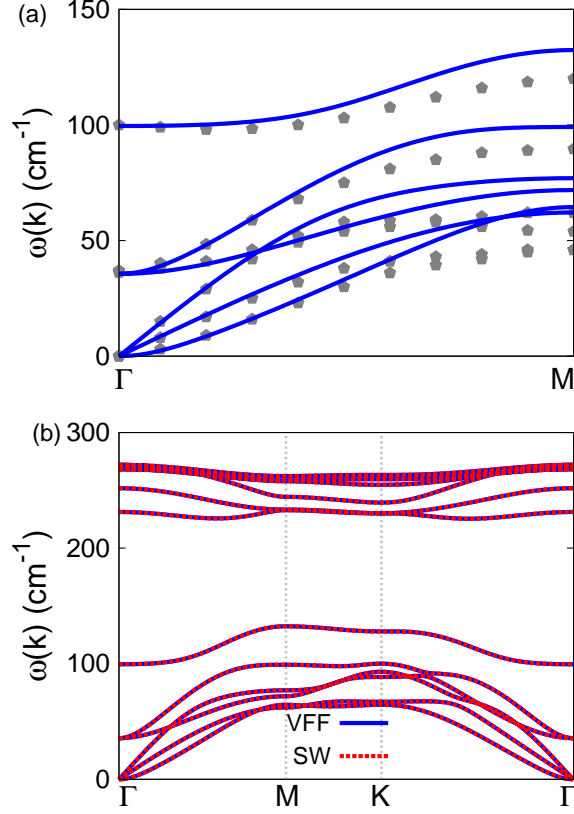


FIG. 313: (Color online) Phonon dispersion for the single-layer InSe. (a) The VFF model is fitted to the six low-frequency branches along the ΓM direction. The *ab initio* results (gray pentagons) are from Ref. 115. (b) The VFF model (blue lines) and the SW potential (red lines) give the same phonon dispersion for the InSe along $\Gamma M K \Gamma$.

CLIII. INSE

Present studies on the InSe are based on first-principles calculations, and no empirical potential has been proposed for the InSe. We will thus parametrize a set of SW potential for the single-layer InSe in this section.

The structure of the single-layer InSe is shown in Fig. 290 with $M=\text{In}$ and $X=\text{Se}$. The structural parameters are from the *ab initio* calculations.¹¹⁵ The InSe has a bi-buckled configuration as shown in Fig. 290 (b), where the buckle is along the zigzag direction. Two buckling layers are symmetrically integrated through the interior In-In bonds, forming a bi-buckled configuration. This structure can be determined by three independent geometrical

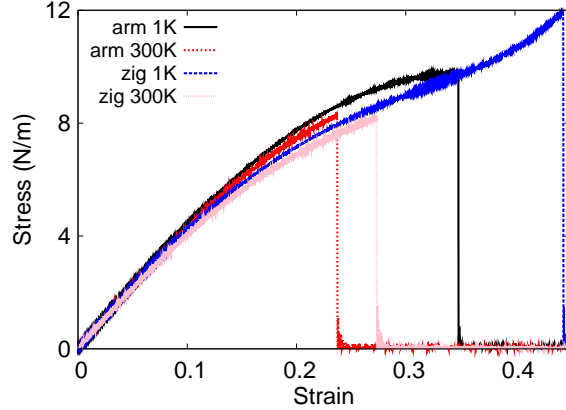


FIG. 314: (Color online) Stress-strain relations for the InSe of size $100 \times 100 \text{ \AA}$. The InSe is uniaxially stretched along the armchair or zigzag directions at temperatures 1 K and 300 K.

parameters, eg. the lattice constant 4.10 \AA , the bond length $d_{\text{In-Se}} = 2.69 \text{ \AA}$, and the bond length $d_{\text{In-In}} = 2.81 \text{ \AA}$.

Table DCX shows the VFF model for the single-layer InSe. The force constant parameters are determined by fitting to the six low-frequency branches in the phonon dispersion along the ΓM as shown in Fig. 313 (a). The *ab initio* calculations for the phonon dispersion are from Ref. 115. Fig. 313 (b) shows that the VFF model and the SW potential give exactly the same phonon dispersion, as the SW potential is derived from the VFF model.

The parameters for the two-body SW potential used by GULP are shown in Tab. DCXI. The parameters for the three-body SW potential used by GULP are shown in Tab. DCXII. Parameters for the SW potential used by LAMMPS are listed in Tab. DCXIII.

We use LAMMPS to perform MD simulations for the mechanical behavior of the single-layer InSe under uniaxial tension at 1.0 K and 300.0 K. Fig. 314 shows the stress-strain curve for the tension of a single-layer InSe of dimension $100 \times 100 \text{ \AA}$. Periodic boundary conditions are applied in both armchair and zigzag directions. The single-layer InSe is stretched uniaxially along the armchair or zigzag direction. The stress is calculated without involving the actual thickness of the quasi-two-dimensional structure of the single-layer InSe. The Young's modulus can be obtained by a linear fitting of the stress-strain relation in the small strain range of $[0, 0.01]$. The Young's modulus is 45.7 N/m and 45.8 N/m along the armchair and zigzag directions, respectively. The Poisson's ratio from the VFF model and the SW potential is $\nu_{xy} = \nu_{yx} = 0.30$.

TABLE DCXIV: The VFF model for BTe. The second line gives an explicit expression for each VFF term. The third line is the force constant parameters. Parameters are in the unit of $\frac{eV}{\text{\AA}^2}$ for the bond stretching interactions, and in the unit of eV for the angle bending interaction. The fourth line gives the initial bond length (in unit of \AA) for the bond stretching interaction and the initial angle (in unit of degrees) for the angle bending interaction.

VFF type	bond stretching		angle bending	
expression	$\frac{1}{2}K_{B-\text{Te}}(\Delta r)^2$	$\frac{1}{2}K_{B-B}(\Delta r)^2$	$\frac{1}{2}K_{B\text{TeTe}}(\Delta\theta)^2$	$\frac{1}{2}K_{BB\text{Te}}(\Delta\theta)^2$
parameter	13.287	14.502	5.466	2.515
r_0 or θ_0	2.310	1.710	100.809	117.156

TABLE DCXV: Two-body SW potential parameters for BTe used by GULP,⁸ as expressed in Eq. (3).

	A (eV)	ρ (\AA)	B (\AA^4)	r_{\min} (\AA)	r_{\max} (\AA)
B ₁ -Te ₁	13.727	1.619	14.237	0.0	3.277
B ₁ -B ₂	24.140	2.933	4.275	0.0	2.830

There is no available value for nonlinear quantities in the single-layer InSe. We have thus used the nonlinear parameter $B = 0.5d^4$ in Eq. (5), which is close to the value of B in most materials. The value of the third order nonlinear elasticity D can be extracted by fitting the stress-strain relation to the function $\sigma = E\epsilon + \frac{1}{2}D\epsilon^2$ with E as the Young's modulus. The values of D from the present SW potential are -81.6 N/m and -103.5 N/m along the armchair and zigzag directions, respectively. The ultimate stress is about 9.8 Nm^{-1} at the ultimate strain of 0.35 in the armchair direction at the low temperature of 1 K. The ultimate stress is about 11.9 Nm^{-1} at the ultimate strain of 0.44 in the zigzag direction at the low temperature of 1 K.

CLIV. BTE

Present studies on the BTe are based on first-principles calculations, and no empirical potential has been proposed for the BTe. We will thus parametrize a set of SW potential for the single-layer BTe in this section.

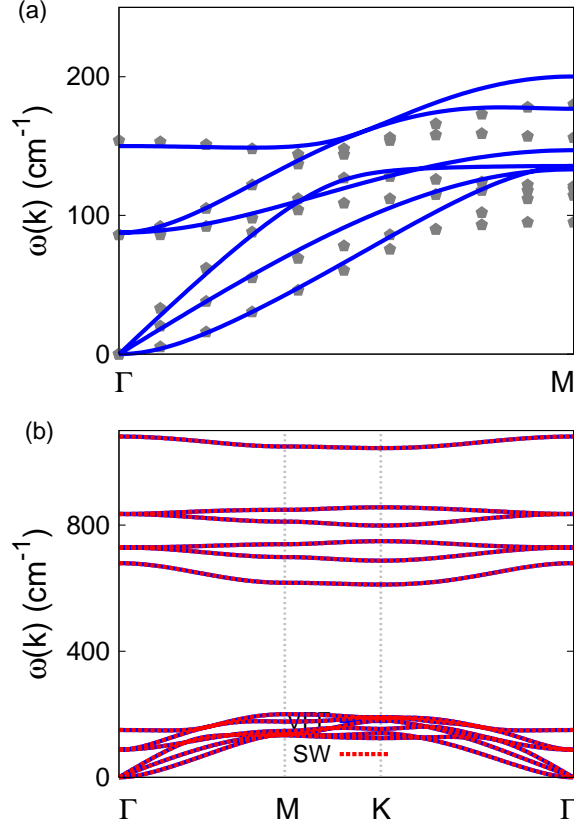


FIG. 315: (Color online) Phonon dispersion for the single-layer BTe. (a) The VFF model is fitted to the six low-frequency branches along the ΓM direction. The *ab initio* results (gray pentagons) are from Ref. 115. (b) The VFF model (blue lines) and the SW potential (red lines) give the same phonon dispersion for the BTe along $\Gamma MK\Gamma$.

TABLE DCXVI: Three-body SW potential parameters for BTe used by GULP,⁸ as expressed in Eq. (4).

	K (eV)	θ_0 (degree)	ρ_1 (\AA)	ρ_2 (\AA)	$r_{\min 12}$ (\AA)	$r_{\max 12}$ (\AA)	$r_{\min 13}$ (\AA)	$r_{\max 13}$ (\AA)	$r_{\min 23}$ (\AA)	$r_{\max 23}$ (\AA)
B ₁ -Te ₁ -Te ₁	80.622	100.809	1.619	1.619	0.0	3.277	0.0	3.277	0.0	4.863
B ₁ -B ₂ -Te ₁	116.3301	117.156	2.933	1.619	0.0	2.830	0.0	3.277	0.0	4.199

The structure of the single-layer BTe is shown in Fig. 290 with M=B and X=Te. The structural parameters are from the *ab initio* calculations.¹¹⁵ The BTe has a bi-buckled configuration as shown in Fig. 290 (b), where the buckle is along the zigzag direction. Two buckling layers are symmetrically integrated through the interior B-B bonds, forming a bi-

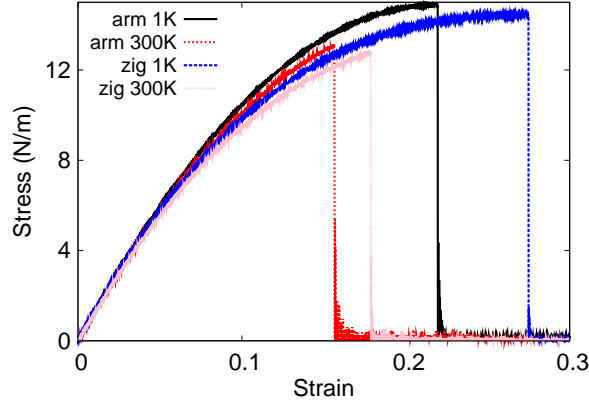


FIG. 316: (Color online) Stress-strain relations for the BTe of size $100 \times 100 \text{ \AA}$. The BTe is uniaxially stretched along the armchair or zigzag directions at temperatures 1 K and 300 K.

TABLE DCXVII: SW potential parameters for BTe used by LAMMPS,⁹ as expressed in Eqs. (9) and (10).

	ϵ (eV)	σ (\AA)	a	λ	γ	$\cos \theta_0$	A_L	B_L	p	q	tol
B ₁ -Te ₁ -Te ₁	1.000	1.619	2.024	80.622	1.000	-0.188	13.727	2.073	4	0	0.0
B ₁ -B ₂ -B ₂	1.000	2.933	0.965	0.000	1.000	0.000	24.140	0.058	4	0	0.0
B ₁ -B ₂ -Te ₁	1.000	0.000	0.000	116.301	1.000	-0.456	0.000	0.000	4	0	0.0

buckled configuration. This structure can be determined by three independent geometrical parameters, eg. the lattice constant 3.56 \AA , the bond length $d_{\text{B-Te}} = 2.31 \text{ \AA}$, and the bond length $d_{\text{B-B}} = 1.71 \text{ \AA}$.

Table DCXIV shows the VFF model for the single-layer BTe. The force constant parameters are determined by fitting to the six low-frequency branches in the phonon dispersion along the ΓM as shown in Fig. 315 (a). The *ab initio* calculations for the phonon dispersion are from Ref. 115. Fig. 315 (b) shows that the VFF model and the SW potential give exactly the same phonon dispersion, as the SW potential is derived from the VFF model.

The parameters for the two-body SW potential used by GULP are shown in Tab. DCXV. The parameters for the three-body SW potential used by GULP are shown in Tab. DCXVI. Parameters for the SW potential used by LAMMPS are listed in Tab. DCXVII.

We use LAMMPS to perform MD simulations for the mechanical behavior of the single-layer BTe under uniaxial tension at 1.0 K and 300.0 K. Fig. 316 shows the stress-strain

TABLE DCXVIII: The VFF model for AlTe. The second line gives an explicit expression for each VFF term. The third line is the force constant parameters. Parameters are in the unit of $\frac{eV}{\text{\AA}^2}$ for the bond stretching interactions, and in the unit of eV for the angle bending interaction. The fourth line gives the initial bond length (in unit of \AA) for the bond stretching interaction and the initial angle (in unit of degrees) for the angle bending interaction.

VFF type	bond stretching		angle bending	
expression	$\frac{1}{2}K_{\text{Al-Te}}(\Delta r)^2$	$\frac{1}{2}K_{\text{Al-Al}}(\Delta r)^2$	$\frac{1}{2}K_{\text{AlTeTe}}(\Delta\theta)^2$	$\frac{1}{2}K_{\text{AlAlTe}}(\Delta\theta)^2$
parameter	8.077	3.859	2.820	1.518
r_0 or θ_0	2.700	2.580	99.124	118.495

curve for the tension of a single-layer BTe of dimension $100 \times 100 \text{ \AA}$. Periodic boundary conditions are applied in both armchair and zigzag directions. The single-layer BTe is stretched uniaxially along the armchair or zigzag direction. The stress is calculated without involving the actual thickness of the quasi-two-dimensional structure of the single-layer BTe. The Young's modulus can be obtained by a linear fitting of the stress-strain relation in the small strain range of $[0, 0.01]$. The Young's modulus is 130.6 N/m and 129.7 N/m along the armchair and zigzag directions, respectively. The Poisson's ratio from the VFF model and the SW potential is $\nu_{xy} = \nu_{yx} = 0.16$.

There is no available value for nonlinear quantities in the single-layer BTe. We have thus used the nonlinear parameter $B = 0.5d^4$ in Eq. (5), which is close to the value of B in most materials. The value of the third order nonlinear elasticity D can be extracted by fitting the stress-strain relation to the function $\sigma = E\epsilon + \frac{1}{2}D\epsilon^2$ with E as the Young's modulus. The values of D from the present SW potential are -560.4 N/m and -588.7 N/m along the armchair and zigzag directions, respectively. The ultimate stress is about 14.9 Nm^{-1} at the ultimate strain of 0.22 in the armchair direction at the low temperature of 1 K. The ultimate stress is about 14.4 Nm^{-1} at the ultimate strain of 0.27 in the zigzag direction at the low temperature of 1 K.

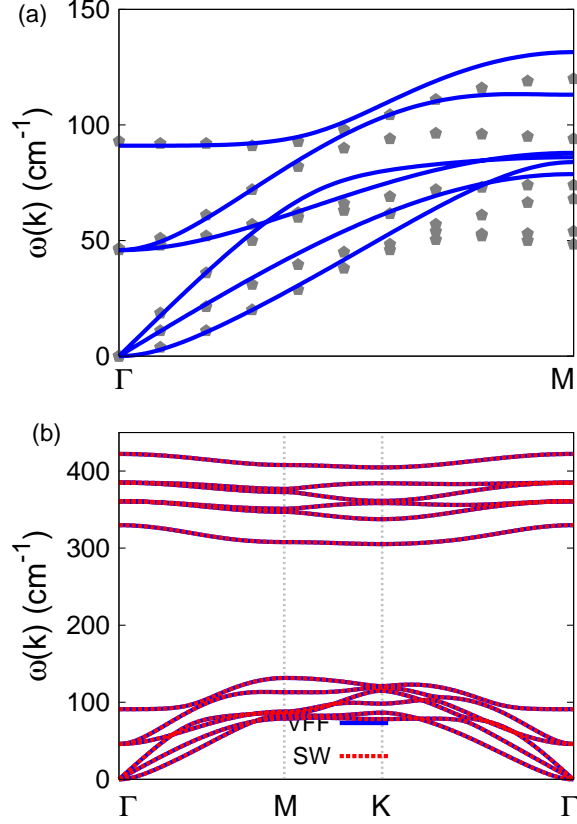


FIG. 317: (Color online) Phonon dispersion for the single-layer AlTe. (a) The VFF model is fitted to the six low-frequency branches along the Γ M direction. The *ab initio* results (gray pentagons) are from Ref. 115. (b) The VFF model (blue lines) and the SW potential (red lines) give the same phonon dispersion for the AlTe along Γ MK Γ .

TABLE DCXIX: Two-body SW potential parameters for AlTe used by GULP,⁸ as expressed in Eq. (3).

	A (eV)	ρ (\AA)	B (\AA^4)	r_{\min} (\AA)	r_{\max} (\AA)
Al ₁ -Te ₁	10.971	1.821	26.572	0.0	3.809
Al ₁ -Al ₂	5.523	2.002	22.154	0.0	3.716

CLV. ALTE

Present studies on the AlTe are based on first-principles calculations, and no empirical potential has been proposed for the AlTe. We will thus parametrize a set of SW potential

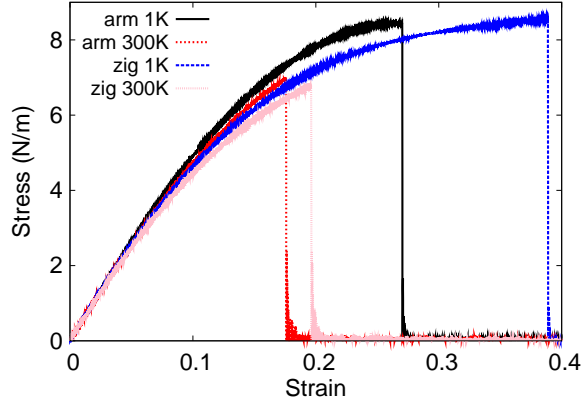


FIG. 318: (Color online) Stress-strain relations for the AlTe of size $100 \times 100 \text{ \AA}$. The AlTe is uniaxially stretched along the armchair or zigzag directions at temperatures 1 K and 300 K.

TABLE DCXX: Three-body SW potential parameters for AlTe used by GULP,⁸ as expressed in Eq. (4).

	K (eV)	θ_0 (degree)	ρ_1 (\AA)	ρ_2 (\AA)	$r_{\min 12}$ (\AA)	$r_{\max 12}$ (\AA)	$r_{\min 13}$ (\AA)	$r_{\max 13}$ (\AA)	$r_{\min 23}$ (\AA)	$r_{\max 23}$ (\AA)
Al ₁ -Te ₁ -Te ₁	38.638	99.124	1.821	1.821	0.0	3.809	0.0	3.809	0.0	5.614
Al ₁ -Te ₁ -Al ₂	29.574	118.495	2.002	1.821	0.0	3.716	0.0	3.809	0.0	5.330

for the single-layer AlTe in this section.

The structure of the single-layer AlTe is shown in Fig. 290 with M=Al and X=Te. The structural parameters are from the *ab initio* calculations.¹¹⁵ The AlTe has a bi-buckled configuration as shown in Fig. 290 (b), where the buckle is along the zigzag direction. Two buckling layers are symmetrically integrated through the interior Al-Al bonds, forming a bi-buckled configuration. This structure can be determined by three independent geometrical

TABLE DCXXI: SW potential parameters for AlTe used by LAMMPS,⁹ as expressed in Eqs. (9) and (10).

	ϵ (eV)	σ (\AA)	a	λ	γ	$\cos \theta_0$	A_L	B_L	p	q	tol
Al ₁ -Te ₁ -Te ₁	1.000	1.821	2.091	38.638	1.000	-0.159	10.971	2.415	4	0	0.0
Al ₁ -Al ₂ -Al ₂	1.000	2.002	1.856	0.000	1.000	0.000	5.523	1.379	4	0	0.0
Al ₁ -Al ₂ -Te ₁	1.000	0.000	0.000	29.574	1.000	-0.477	0.000	0.000	4	0	0.0

parameters, eg. the lattice constant 4.11 Å, the bond length $d_{\text{Al-Te}} = 2.70$ Å, and the bond length $d_{\text{Al-Al}} = 2.58$ Å.

Table DCXVIII shows the VFF model for the single-layer AlTe. The force constant parameters are determined by fitting to the six low-frequency branches in the phonon dispersion along the ΓM as shown in Fig. 317 (a). The *ab initio* calculations for the phonon dispersion are from Ref. 115. Fig. 317 (b) shows that the VFF model and the SW potential give exactly the same phonon dispersion, as the SW potential is derived from the VFF model.

The parameters for the two-body SW potential used by GULP are shown in Tab. DCXIX. The parameters for the three-body SW potential used by GULP are shown in Tab. DCXX. Parameters for the SW potential used by LAMMPS are listed in Tab. DCXXI.

We use LAMMPS to perform MD simulations for the mechanical behavior of the single-layer AlTe under uniaxial tension at 1.0 K and 300.0 K. Fig. 318 shows the stress-strain curve for the tension of a single-layer AlTe of dimension 100×100 Å. Periodic boundary conditions are applied in both armchair and zigzag directions. The single-layer AlTe is stretched uniaxially along the armchair or zigzag direction. The stress is calculated without involving the actual thickness of the quasi-two-dimensional structure of the single-layer AlTe. The Young's modulus can be obtained by a linear fitting of the stress-strain relation in the small strain range of $[0, 0.01]$. The Young's modulus is 55.8 N/m and 54.9 N/m along the armchair and zigzag directions, respectively. The Poisson's ratio from the VFF model and the SW potential is $\nu_{xy} = \nu_{yx} = 0.24$.

There is no available value for nonlinear quantities in the single-layer AlTe. We have thus used the nonlinear parameter $B = 0.5d^4$ in Eq. (5), which is close to the value of B in most materials. The value of the third order nonlinear elasticity D can be extracted by fitting the stress-strain relation to the function $\sigma = E\epsilon + \frac{1}{2}D\epsilon^2$ with E as the Young's modulus. The values of D from the present SW potential are -171.4 N/m and -179.0 N/m along the armchair and zigzag directions, respectively. The ultimate stress is about 8.4 Nm^{-1} at the ultimate strain of 0.27 in the armchair direction at the low temperature of 1 K. The ultimate stress is about 8.6 Nm^{-1} at the ultimate strain of 0.39 in the zigzag direction at the low temperature of 1 K.

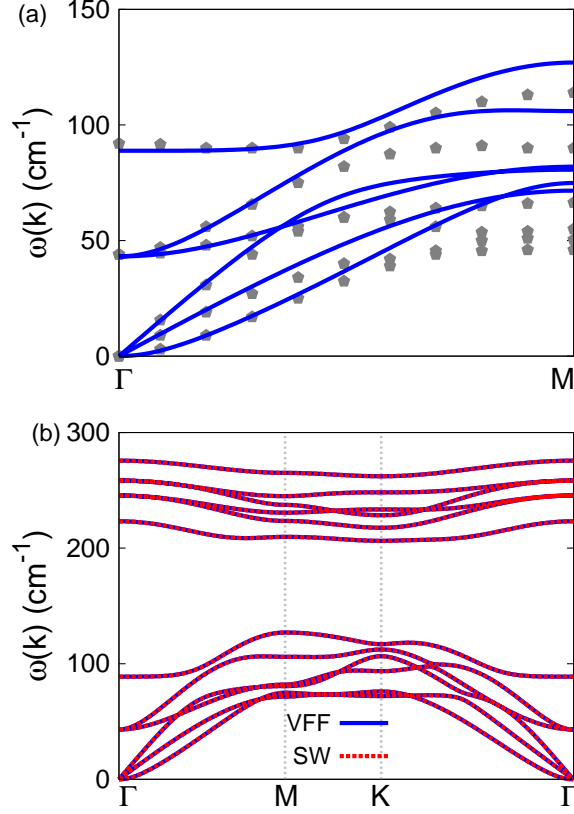


FIG. 319: (Color online) Phonon dispersion for the single-layer GaTe. (a) The VFF model is fitted to the six low-frequency branches along the Γ M direction. The *ab initio* results (gray pentagons) are from Ref. 115. (b) The VFF model (blue lines) and the SW potential (red lines) give the same phonon dispersion for the GaTe along Γ MKT.

CLVI. GATE

Present studies on the GaTe are based on first-principles calculations, and no empirical potential has been proposed for the GaTe. We will thus parametrize a set of SW potential for the single-layer GaTe in this section.

The structure of the single-layer GaTe is shown in Fig. 290 with M=Ga and X=Te. The structural parameters are from the *ab initio* calculations.¹¹⁵ The GaTe has a bi-buckled configuration as shown in Fig. 290 (b), where the buckle is along the zigzag direction. Two buckling layers are symmetrically integrated through the interior Ga-Ga bonds, forming a bi-buckled configuration. This structure can be determined by three independent geometrical

TABLE DCXXII: The VFF model for GaTe. The second line gives an explicit expression for each VFF term. The third line is the force constant parameters. Parameters are in the unit of $\frac{eV}{\text{\AA}^2}$ for the bond stretching interactions, and in the unit of eV for the angle bending interaction. The fourth line gives the initial bond length (in unit of \AA) for the bond stretching interaction and the initial angle (in unit of degrees) for the angle bending interaction.

VFF type	bond stretching		angle bending	
expression	$\frac{1}{2}K_{\text{Ga-Te}}(\Delta r)^2$	$\frac{1}{2}K_{\text{Ga-Ga}}(\Delta r)^2$	$\frac{1}{2}K_{\text{GaTeTe}}(\Delta\theta)^2$	$\frac{1}{2}K_{\text{GaGaTe}}(\Delta\theta)^2$
parameter	7.382	4.366	2.841	1.519
r_0 or θ_0	2.700	2.460	99.781	117.978

TABLE DCXXIII: Two-body SW potential parameters for GaTe used by GULP,⁸ as expressed in Eq. (3).

	A (eV)	ρ (\AA)	B (\AA^4)	r_{\min} (\AA)	r_{\max} (\AA)
Ga ₁ -Te ₁	10.179	1.849	26.572	0.0	3.817
Ga ₁ -Ga ₂	6.750	2.239	18.311	0.0	3.634

TABLE DCXXIV: Three-body SW potential parameters for GaTe used by GULP,⁸ as expressed in Eq. (4).

	K (eV)	θ_0 (degree)	ρ_1 (\AA)	ρ_2 (\AA)	$r_{\min12}$ (\AA)	$r_{\max12}$ (\AA)	$r_{\min13}$ (\AA)	$r_{\max13}$ (\AA)	$r_{\min23}$ (\AA)	$r_{\max23}$ (\AA)
Ga ₁ -Te ₁ -Te ₁	40.060	99.781	1.849	1.849	0.0	3.817	0.0	3.817	0.0	5.642
Ga ₁ -Te ₁ -Ga ₂	34.354	117.978	2.239	1.849	0.0	3.634	0.0	3.817	0.0	5.238

TABLE DCXXV: SW potential parameters for GaTe used by LAMMPS,⁹ as expressed in Eqs. (9) and (10).

	ϵ (eV)	σ (\AA)	a	λ	γ	$\cos\theta_0$	A_L	B_L	p	q	tol
Ga ₁ -Te ₁ -Te ₁	1.000	1.849	2.065	40.060	1.000	-0.170	10.179	2.274	4	0	0.0
Ga ₁ -Ga ₂ -Ga ₂	1.000	2.239	1.623	0.000	1.000	0.000	6.750	0.728	4	0	0.0
Ga ₁ -Ga ₂ -Te ₁	1.000	0.000	0.000	34.354	1.000	-0.469	0.000	0.000	4	0	0.0

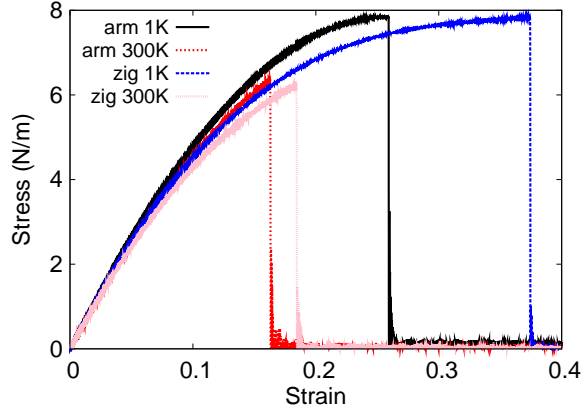


FIG. 320: (Color online) Stress-strain relations for the GaTe of size $100 \times 100 \text{ \AA}$. The GaTe is uniaxially stretched along the armchair or zigzag directions at temperatures 1 K and 300 K.

parameters, eg. the lattice constant 4.13 \AA , the bond length $d_{\text{Ga-Te}} = 2.70 \text{ \AA}$, and the bond length $d_{\text{Ga-Ga}} = 2.46 \text{ \AA}$.

Table DCXXII shows the VFF model for the single-layer GaTe. The force constant parameters are determined by fitting to the six low-frequency branches in the phonon dispersion along the ΓM as shown in Fig. 319 (a). The *ab initio* calculations for the phonon dispersion are from Ref. 115. Fig. 319 (b) shows that the VFF model and the SW potential give exactly the same phonon dispersion, as the SW potential is derived from the VFF model.

The parameters for the two-body SW potential used by GULP are shown in Tab. DCXXIII. The parameters for the three-body SW potential used by GULP are shown in Tab. DCXXIV. Parameters for the SW potential used by LAMMPS are listed in Tab. DCXXV.

We use LAMMPS to perform MD simulations for the mechanical behavior of the single-layer GaTe under uniaxial tension at 1.0 K and 300.0 K. Fig. 320 shows the stress-strain curve for the tension of a single-layer GaTe of dimension $100 \times 100 \text{ \AA}$. Periodic boundary conditions are applied in both armchair and zigzag directions. The single-layer GaTe is stretched uniaxially along the armchair or zigzag direction. The stress is calculated without involving the actual thickness of the quasi-two-dimensional structure of the single-layer GaTe. The Young's modulus can be obtained by a linear fitting of the stress-strain relation in the small strain range of $[0, 0.01]$. The Young's modulus is 55.2 N/m and 55.3 N/m along the armchair and zigzag directions, respectively. The Poisson's ratio from the VFF model and the SW

TABLE DCXXVI: The VFF model for InTe. The second line gives an explicit expression for each VFF term. The third line is the force constant parameters. Parameters are in the unit of $\frac{eV}{\text{\AA}^2}$ for the bond stretching interactions, and in the unit of eV for the angle bending interaction. The fourth line gives the initial bond length (in unit of \AA) for the bond stretching interaction and the initial angle (in unit of degrees) for the angle bending interaction.

VFF type	bond stretching		angle bending	
expression	$\frac{1}{2}K_{\text{In-Te}}(\Delta r)^2$	$\frac{1}{2}K_{\text{In-In}}(\Delta r)^2$	$\frac{1}{2}K_{\text{InTeTe}}(\Delta\theta)^2$	$\frac{1}{2}K_{\text{InInTe}}(\Delta\theta)^2$
parameter	5.592	3.928	2.419	1.227
r_0 or θ_0	2.890	2.810	99.148	118.477

TABLE DCXXVII: Two-body SW potential parameters for InTe used by GULP,⁸ as expressed in Eq. (3).

	A (eV)	ρ (\AA)	B (\AA^4)	r_{min} (\AA)	r_{max} (\AA)
In ₁ -Te ₁	8.707	1.950	34.879	0.0	4.077
In ₁ -In ₂	6.312	2.068	31.174	0.0	4.015

potential is $\nu_{xy} = \nu_{yx} = 0.23$.

There is no available value for nonlinear quantities in the single-layer GaTe. We have thus used the nonlinear parameter $B = 0.5d^4$ in Eq. (5), which is close to the value of B in most materials. The value of the third order nonlinear elasticity D can be extracted by fitting the stress-strain relation to the function $\sigma = E\epsilon + \frac{1}{2}D\epsilon^2$ with E as the Young's modulus. The values of D from the present SW potential are -183.2 N/m and -195.6 N/m along the armchair and zigzag directions, respectively. The ultimate stress is about 7.8 Nm^{-1} at the ultimate strain of 0.26 in the armchair direction at the low temperature of 1 K. The ultimate stress is about 7.8 Nm^{-1} at the ultimate strain of 0.37 in the zigzag direction at the low temperature of 1 K.

CLVII. INTE

Present studies on the InTe are based on first-principles calculations, and no empirical potential has been proposed for the InTe. We will thus parametrize a set of SW potential

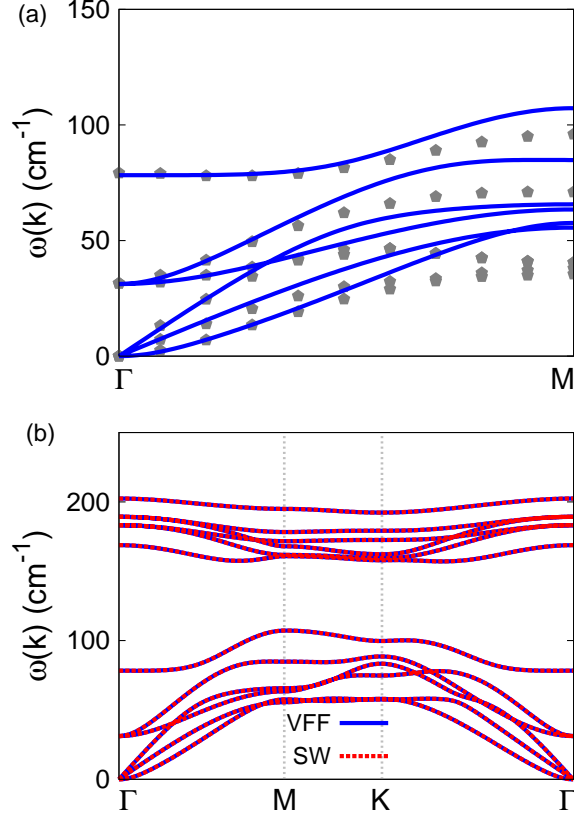


FIG. 321: (Color online) Phonon dispersion for the single-layer InTe. (a) The VFF model is fitted to the six low-frequency branches along the Γ M direction. The *ab initio* results (gray pentagons) are from Ref. 115. (b) The VFF model (blue lines) and the SW potential (red lines) give the same phonon dispersion for the InTe along Γ MK Γ .

TABLE DCXXVIII: Three-body SW potential parameters for InTe used by GULP,⁸ as expressed in Eq. (4).

	K (eV)	θ_0 (degree)	ρ_1 (Å)	ρ_2 (Å)	$r_{\min 12}$ (Å)	$r_{\max 12}$ (Å)	$r_{\min 13}$ (Å)	$r_{\max 13}$ (Å)	$r_{\min 23}$ (Å)	$r_{\max 23}$ (Å)
In ₁ -Te ₁ -Te ₁	33.178	99.148	1.950	1.950	0.0	4.077	0.0	4.077	0.0	6.011
In ₁ -Te ₁ -In ₂	22.833	118.477	2.068	1.950	0.0	4.015	0.0	4.077	0.0	5.741

for the single-layer InTe in this section.

The structure of the single-layer InTe is shown in Fig. 290 with M=In and X=Te. The structural parameters are from the *ab initio* calculations.¹¹⁵ The InTe has a bi-buckled configuration as shown in Fig. 290 (b), where the buckle is along the zigzag direction. Two

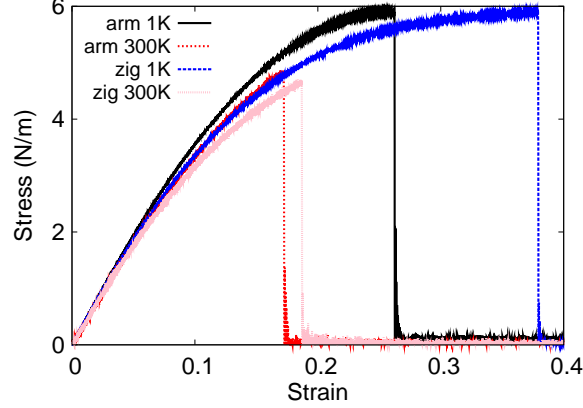


FIG. 322: (Color online) Stress-strain relations for the InTe of size $100 \times 100 \text{ \AA}$. The InTe is uniaxially stretched along the armchair or zigzag directions at temperatures 1 K and 300 K.

TABLE DCXXIX: SW potential parameters for InTe used by LAMMPS,⁹ as expressed in Eqs. (9) and (10).

	ϵ (eV)	σ (\AA)	a	λ	γ	$\cos \theta_0$	A_L	B_L	p	q	tol
In ₁ -Te ₁ -Te ₁	1.000	1.950	2.090	33.178	1.000	-0.159	8.707	2.410	4	0	0.0
In ₁ -In ₂ -In ₂	1.000	2.068	1.942	0.000	1.000	0.000	6.312	1.704	4	0	0.0
In ₁ -In ₂ -Te ₁	1.000	0.000	0.000	22.833	1.000	-0.477	0.000	0.000	4	0	0.0

buckling layers are symmetrically integrated through the interior In-In bonds, forming a bi-buckled configuration. This structure can be determined by three independent geometrical parameters, eg. the lattice constant 4.40 \AA , the bond length $d_{\text{In-Te}} = 2.89 \text{ \AA}$, and the bond length $d_{\text{In-In}} = 2.81 \text{ \AA}$.

Table DCXXVI shows the VFF model for the single-layer InTe. The force constant parameters are determined by fitting to the six low-frequency branches in the phonon dispersion along the ΓM as shown in Fig. 321 (a). The *ab initio* calculations for the phonon dispersion are from Ref. 115. Fig. 321 (b) shows that the VFF model and the SW potential give exactly the same phonon dispersion, as the SW potential is derived from the VFF model.

The parameters for the two-body SW potential used by GULP are shown in Tab. DCXXVII. The parameters for the three-body SW potential used by GULP are shown in Tab. DCXXVIII. Parameters for the SW potential used by LAMMPS are listed in Tab. DCXXIX.

We use LAMMPS to perform MD simulations for the mechanical behavior of the single-layer InTe under uniaxial tension at 1.0 K and 300.0 K. Fig. 322 shows the stress-strain curve for the tension of a single-layer InTe of dimension $100 \times 100 \text{ \AA}$. Periodic boundary conditions are applied in both armchair and zigzag directions. The single-layer InTe is stretched uniaxially along the armchair or zigzag direction. The stress is calculated without involving the actual thickness of the quasi-two-dimensional structure of the single-layer InTe. The Young's modulus can be obtained by a linear fitting of the stress-strain relation in the small strain range of $[0, 0.01]$. The Young's modulus is 40.6 N/m and 40.9 N/m along the armchair and zigzag directions, respectively. The Poisson's ratio from the VFF model and the SW potential is $\nu_{xy} = \nu_{yx} = 0.23$.

There is no available value for nonlinear quantities in the single-layer InTe. We have thus used the nonlinear parameter $B = 0.5d^4$ in Eq. (5), which is close to the value of B in most materials. The value of the third order nonlinear elasticity D can be extracted by fitting the stress-strain relation to the function $\sigma = E\epsilon + \frac{1}{2}D\epsilon^2$ with E as the Young's modulus. The values of D from the present SW potential are -130.4 N/m and -142.2 N/m along the armchair and zigzag directions, respectively. The ultimate stress is about 5.9 Nm^{-1} at the ultimate strain of 0.26 in the armchair direction at the low temperature of 1 K. The ultimate stress is about 5.9 Nm^{-1} at the ultimate strain of 0.38 in the zigzag direction at the low temperature of 1 K.

CLVIII. BOROPHENE

Most existing theoretical studies on the monolayer of boron atoms (borophene) are based on the first-principles calculations. The ReaxFF force field model was developed for the borophene recently.¹¹⁷ The present authors have provided the VFF model and the SW potential to describe the atomic interaction within the borophene,¹⁴ which includes the second-nearest-neighboring interactions. In the present work, we present a more efficient SW potential with only the first-nearest-neighboring interactions.

The structure of the borophene is shown in Fig. 323, with structural parameters from the *ab initio* calculations.¹¹⁶ Borophene has a puckered configuration as shown in Fig. 323 (b), where the pucker is perpendicular to the x-direction. The height of the pucker is $h = 0.911 \text{ \AA}$, which is the distance between the top chain and the bottom chain along the out-of-plane

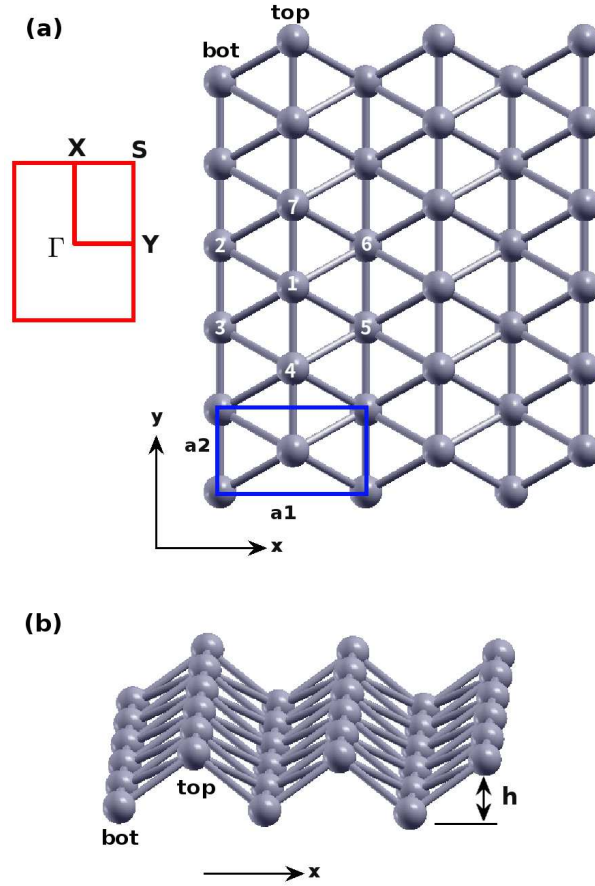


FIG. 323: (Color online) Structure for borophene. (a) Top view. Atoms are categorized into top chains and bottom chains. The top chain includes atoms like 1, 4, and 7. The bottom chain includes atoms like 2, 3, 5, and 6. The unit cell is shown by blue rectangle. The first Brillouin zone is shown by red rectangle on the left. (b) Perspective view illustrates the puckered configuration, with h as the distance between the top and bottom chains along the out-of-plane z -direction. The pucker is perpendicular to the x -axis and is parallel with the y -axis.

z -direction. The two lattice bases are $a_1 = 2.866 \text{ \AA}$ and $a_2 = 1.614 \text{ \AA}$ for the inplane rectangular unit cell. There are two inequivalent boron atoms in the unit cell. Boron atoms are categorized into the top chain and the bottom chain. The top chain includes atoms like 1, 4, and 7. The bottom chain includes atoms like 2, 3, 5, and 6.

Table [DCXXX](#) shows four VFF terms for the borophene, two of which are the bond stretching interaction shown by Eq. (1) while the other two terms are the angle bending interaction shown by Eq. (2). These force constant parameters are determined by fitting to

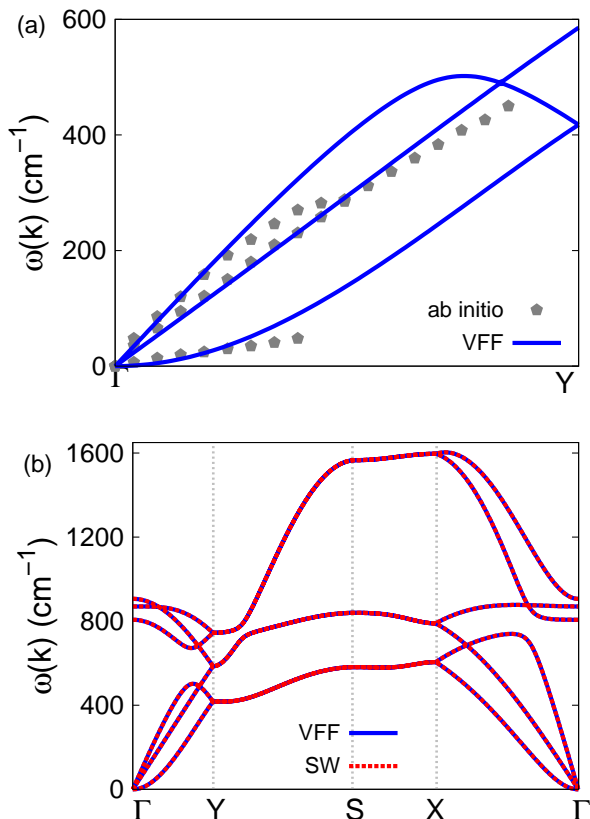


FIG. 324: (Color online) Phonon dispersion for the borophene. (a) The VFF model is fitted to the three acoustic branches in the long wave limit along the ΓY direction. The *ab initio* results (gray pentagons) are from Ref. 116. (b) The VFF model (blue lines) and the SW potential (red lines) give the same phonon dispersion for the borophene along $\Gamma Y S X \Gamma$.

the three acoustic branches in the phonon dispersion along the ΓX as shown in Fig. 324 (a). The *ab initio* calculations for the phonon dispersion are from Ref. 116. Similar phonon dispersion can also be found in other *ab initio* calculations.¹¹⁸ Fig. 324 (b) shows that the VFF model and the SW potential give exactly the same phonon dispersion, as the SW potential is derived from the VFF model.

The parameters for the two-body SW potential used by GULP are shown in Tab. DCXXXI. The parameters for the three-body SW potential used by GULP are shown in Tab. DCXXXII. Parameters for the SW potential used by LAMMPS are listed in Tab. DCXXXIII. We note that twelve atom types have been introduced for the simulation of borophene using LAMMPS, because the angles around atom 1 in Fig. 323 (a) are not

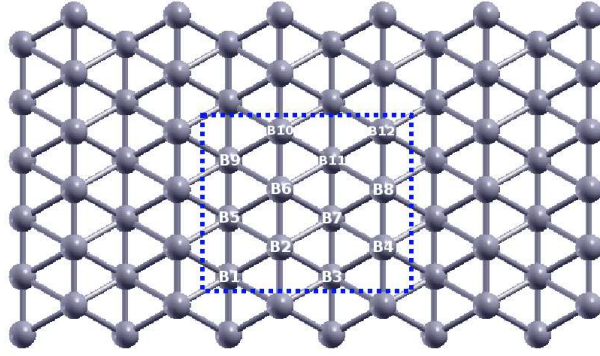


FIG. 325: (Color online) Twelve atom types are introduced for the boron atoms in the borophene. Atoms B_1 , B_3 , B_5 , B_7 , B_9 , and B_{11} are from the bottom group. Atoms B_2 , B_4 , B_6 , B_8 , B_{10} , and B_{12} are from the top group.

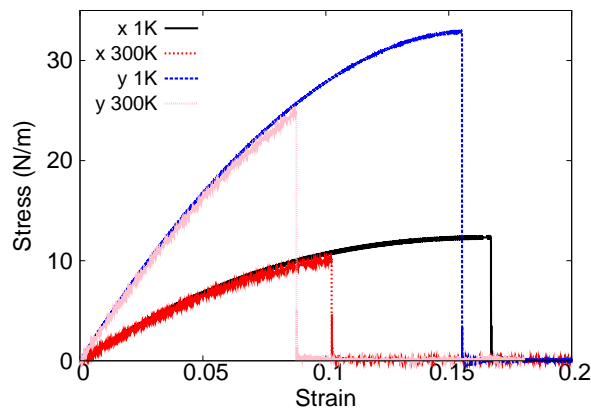


FIG. 326: (Color online) Stress-strain relations for the borophene of size $100 \times 100 \text{ \AA}$. The borophene is uniaxially stretched along the x or y directions at temperatures 1 K and 300 K.

distinguishable in LAMMPS. We thus need to differentiate these angles by assigning these six neighboring atoms (2, 3, 4, 5, 6, 7) with different atom types. Fig. 325 shows that twelve atom types are necessary for the purpose of differentiating all six neighbors around one B atom.

Fig. 326 shows the stress strain relations for the borophene of size $100 \times 100 \text{ \AA}$. The structure is uniaxially stretched in the x or y directions at 1 K and 300 K. The Young's modulus is 162.7 Nm^{-1} and 385.0 Nm^{-1} in the x and y directions respectively at 1 K, which are obtained by linear fitting of the stress strain relations in $[0, 0.01]$. These values are in

TABLE DCXXX: The VFF model for borophene. The second line gives an explicit expression for each VFF term, where atom indexes are from Fig. 323 (a). The third line is the force constant parameters. Parameters are in the unit of $\frac{\text{eV}}{\text{\AA}^2}$ for the bond stretching interactions, and in the unit of eV for the angle bending interaction. The fourth line gives the initial bond length (in unit of \AA) for the bond stretching interaction and the initial angle (in unit of degrees) for the angle bending interaction. The angle θ_{ijk} has atom i as the apex.

VFF type	bond stretching		angle bending	
expression	$\frac{1}{2}K_{14}(\Delta r_{14})^2$	$\frac{1}{2}K_{12}(\Delta r_{12})^2$	$\frac{1}{2}K_{134}(\Delta\theta_{134})^2$	$\frac{1}{2}K_{135}(\Delta\theta_{135})^2$
parameter	20.673	6.025	3.523	4.651
r_0 or θ_0	1.614	1.880	64.581	99.318

TABLE DCXXXI: Two-body SW potential parameters for borophene used by GULP,⁸ as expressed in Eq. (3). The quantity (r_{ij}) in the first line lists one representative term for the two-body SW potential between atoms i and j. Atom indexes are from Fig. 323 (a).

	A (eV)	ρ (\AA)	B (\AA^4)	r_{\min} (\AA)	r_{\max} (\AA)
r_{14}	8.974	0.971	3.393	0.0	2.240
r_{12}	2.098	0.618	6.246	0.0	2.419

good agreement with the *ab initio* results at 0 K temperature, eg. 170 Nm^{-1} and 398 Nm^{-1} in Ref. 119, or 166 Nm^{-1} and 389 Nm^{-1} in Ref. 116, or 163 Nm^{-1} and 399 Nm^{-1} in Ref. 120. Previous *ab initio* calculations obtained negative Poisson's ratio for the uniaxial stretching of the borophene in the x and y directions, e.g. -0.02 and -0.04 in Refs 119 and 116. The Poisson's ratio from the present SW potential are -0.03 and -0.07 along the x and y directions

TABLE DCXXXII: Three-body SW potential parameters for borophene used by GULP,⁸ as expressed in Eq. (4). The first line (θ_{ijk}) presents one representative term for the three-body SW potential. The angle θ_{ijk} has the atom i as the apex. Atom indexes are from Fig. 323 (a).

	K (eV)	θ_0 (degree)	ρ_1 (\AA)	ρ_2 (\AA)	$r_{\min12}$ (\AA)	$r_{\max12}$ (\AA)	$r_{\min13}$ (\AA)	$r_{\max13}$ (\AA)	$r_{\min23}$ (\AA)	$r_{\max23}$ (\AA)
θ_{134}	32.074	64.581	0.971	0.618	0.0	2.240	0.0	2.419	0.0	2.419
θ_{135}	23.668	99.318	0.618	0.618	0.0	2.419	0.0	2.410	2.240	3.047

TABLE DCXXXIII: SW potential parameters for borophene used by LAMMPS,⁹ as expressed in Eqs. (9) and (10). Atom types in the first column are displayed in Fig. 325.

	ϵ (eV)	σ (Å)	a	λ	γ	$\cos\theta_0$	A_L	B_L	p	q	tol
B ₁ -B ₅ -B ₅	1.000	0.971	2.307	0.000	1.000	0.000	8.974	3.817	4	0	0.0
B ₁ -B ₂ -B ₂	1.000	0.618	3.914	0.000	1.000	0.000	2.098	42.820	4	0	0.0
B ₁ -B ₂ -B ₅	1.000	0.000	0.000	32.074	1.000	0.429	0.000	0.000	4	0	0.0
B ₁ -B ₂ -B ₄	1.000	0.000	0.000	23.668	1.000	-0.162	0.000	0.000	4	0	0.0

respectively, which are quite comparable with the *ab initio* results.

The third-order nonlinear constant (D) can be obtained by fitting the stress strain relation to the function $\sigma = E\epsilon + \frac{1}{2}D\epsilon^2$, with E as the Young's modulus. The obtained values of D are -1100.1 Nm^{-1} and -2173.6 Nm^{-1} in the x and y directions, respectively. The ultimate stress is about 12.3 Nm^{-1} at the critical strain of 0.17 in the x-direction at the low temperature of 1 K, which agree quite well with the *ab initio* results at 0 K.^{116,118,120} The ultimate stress is about 32.9 Nm^{-1} at the critical strain of 0.16 in the y-direction at the low temperature of 1 K, which are quite comparable with *ab initio* results at 0 K.^{116,118,120}

CLIX. CONCLUSION REMARKS

As a final remark, we note some major advantages and deficiencies for the SW potential parameters provided in the present work. On the one hand, the key feature of the SW potential is its high efficiency, which is maintained by using minimum potential parameters in the present work, so the interaction range is limited to the first-nearest-neighboring atoms. As a result, the present SW potential parameters are of high computational efficiency. On the other hand, since the interaction is limited to short-range, the optical branches in the phonon spectrum are typically overestimated by the present SW potential. It is because we have ignored the long-range interactions, which contribute mostly to the acoustic phonon branches while have neglectable contribution to the optical phonon branches. The short-range interaction has thus been strengthened to give an accurate description for the acoustic phonon branches and the elastic properties, which leads to the overestimation of the optical phonon branches as a trade off. Hence, there will be systematic overestimation for simulating

optical processes using the present SW parameters.

We also note that the mathematical form of the SW potential is not suitable for the atomic-thick planar structures, such as graphene and b-BN, because the SW potential are not able to resist the bending motion of these real planar crystals.^{121,122}

In conclusion, we have provided the SW potential parameters for 156 layered crystals. The supplemental resources for all simulations in the present work are available online in Ref. 1, including a fortran code to generate crystals' structures, files for molecular dynamics simulations using LAMMPS, files for phonon calculation with the SW potential using GULP, and files for phonon calculations with the valence force field model using GULP.

Acknowledgements The work is supported by the Recruitment Program of Global Youth Experts of China, the National Natural Science Foundation of China (NSFC) under Grant No. 11504225 and the start-up funding from Shanghai University.

* Corresponding author: jiangjinwu@shu.edu.cn; jwjiang5918@hotmail.com

¹ <http://jiangjinwu.org/sw> .

² A. K. Geim and I. V. Grigorieva, *Nature* **499**, 419 (2013).

³ P. Y. Yu, *Fundamentals of Semiconductors* (Springer, New York, 2010).

⁴ F. H. Stillinger and T. A. Weber, *Physical Review B* **31**, 5262 (1985).

⁵ J. Tersoff, *Physical Review Letters* **56**, 632 (1986).

⁶ D. W. Brenner, O. A. Shenderova, J. A. Harrison, S. J. Stuart, B. Ni, and S. B. Sinnott, *Journal of Physics: Condensed Matter* **14**, 783 (2002).

⁷ J.-W. Jiang, *Nanotechnology* **26**, 315706 (2015).

⁸ J. D. Gale, *J. Chem. Soc., Faraday Trans.* **93**, 629 (1997).

⁹ lammps, <http://www.cs.sandia.gov/~sjplimp/lammps.html> (2012).

¹⁰ A. Stukowski, *Modelling and Simulation in Materials Science and Engineering* **18**, 015012 (2010).

¹¹ A. Kokalj, *Computational Materials Science* **28**, 155 (2003).

¹² C. Ataca, H. Sahin, and S. Ciraci, *Journal of Physical Chemistry C* **116**, 8983 (2012).

¹³ J.-W. Jiang, H. S. Park, and T. Rabczuk, *Journal of Applied Physics* **114**, 064307 (2013).

¹⁴ Y.-P. Zhou and J.-W. Jiang, *Scientific Reports* **7**, 45516 (2017).

- ¹⁵ J. L. Feldman, *Physical Review B* **25**, 7132 (1982).
- ¹⁶ E. B. Isaacs and C. A. Marianetti, *Physical Review B* **94**, 035120 (2016).
- ¹⁷ H. L. Zhuang, M. D. Johannes, M. N. Blonsky, and R. G. Hennig, *Applied Physics Letters* **104**, 022116 (2014).
- ¹⁸ D. Cakir, F. M. Peeters, and C. Sevik, *Applied Physics Letters* **104**, 203110 (2014).
- ¹⁹ M. M. Alyoruk, Y. Aierken, D. Cakir, F. M. Peeters, and C. Sevik, *Journal of Physical Chemistry C* **119**, 23231 (2015).
- ²⁰ J.-W. Jiang, B.-S. Wang, J.-S. Wang, and H. S. Park, *Journal of Physics: Condensed Matter* **27**, 083001 (2015).
- ²¹ W. G. FlcMullan, thesis (1983).
- ²² N. Wakabayashi, H. G. Smith, and R. M. Nicklow, *Physical Review B* **12**, 659 (1975).
- ²³ T. Liang, S. R. Phillpot, and S. B. Sinnott, *Physical Review B* **79**, 245110 (2009).
- ²⁴ V. Varshney, S. S. Patnaik, C. Muratore, A. K. Roy, A. A. Voevodin, and B. L. Farmer, *Computational Materials Science* **48**, 101 (2010).
- ²⁵ A. Kandemir, H. Yapicioglu, A. Kinaci, T. Cagin, and C. Sevik, *Nanotechnology* **27**, 055703 (2016).
- ²⁶ A. Molina-Sánchez and L. Wirtz, *Physical Review B* **84**, 155413 (2011).
- ²⁷ R. C. Cooper, C. Lee, C. A. Marianetti, X. Wei, J. Hone, and J. W. Kysar, *Physical Review B* **87**, 035423 (2013).
- ²⁸ R. C. Cooper, C. Lee, C. A. Marianetti, X. Wei, J. Hone, and J. W. Kysar, *Physical Review B* **87**, 079901 (2013).
- ²⁹ S. Bertolazzi, J. Brivio, and A. Kis, *ACS Nano* **5**, 9703 (2011).
- ³⁰ S. Horzum, H. Sahin, S. Cahangirov, P. Cudazzo, A. Rubio, T. Serin, and F. M. Peeters, *Physical Review B* **87**, 125415 (2013).
- ³¹ W. Huang, H. Da, and G. Liang, *Journal of Applied Physics* **113**, 104304 (2013).
- ³² C. Sevik, *Physical Review B* **89**, 035422 (2014).
- ³³ S. Kumar and U. Schwingenschlogl, *Chem. Mater.* **27**, 1278 (2015).
- ³⁴ Z. Huang, W. Zhang, and W. Zhang, *Materials* **9**, 716 (2016).
- ³⁵ J. Li, N. V. Medhekar, and V. B. Shenoy, *Journal of Physical Chemistry C* **117**, 15842 (2013).
- ³⁶ H. Guo, T. Yang, M. Yamamoto, L. Zhou, R. Ishikawa, K. Ueno, K. Tsukagoshi, Z. Zhang, M. S. Dresselhaus, and R. Saito, *Physical Review B* **91**, 205415 (2015).

- ³⁷ M. Kan, H. G. Nam, Y. H. Lee, and Q. Sun, *Phys. Chem. Chem. Phys.* **17**, 14866 (2015).
- ³⁸ X. Gu and R. Yang, *Applied Physics Letters* **105**, 131903 (2014).
- ³⁹ W. Huang, X. Luo, C. K. Gan, S. Y. Quek, and G. Liang, *Phys. Chem. Chem. Phys.* **16**, 10866 (2014).
- ⁴⁰ P. Norouzzadeh and D. J. Singh, *Nanotechnology* **28**, 075708 (2017).
- ⁴¹ W.-X. Zhou and K.-Q. Chen, *Scientific Reports* **5**, 15070 (2015).
- ⁴² E. Torun, H. Sahin, S. Cahangirov, A. Rubio, , and F. M. Peeters, *Journal of Applied Physics* **119**, 074307 (2016).
- ⁴³ A. Mar, S. Jobic, and J. A. Ibers, *Journal of the American Chemical Society* **114**, 8963 (1992).
- ⁴⁴ W. G. Dawson and D. W. Bullett, *Journal of Physics C: Solid State Physics* **20**, 6159 (1987).
- ⁴⁵ B. E. Brown, *Acta Crystallographica* **20**, 268 (1996).
- ⁴⁶ M. K. Jana, A. Singh, D. J. Late, C. Rajamathi, K. Biswas, C. Felser, U. V. Waghmare, and C. N. R. Rao, *Journal of Physics: Condensed Matter* **27**, 285401 (2015).
- ⁴⁷ Y. C. Jiang, J. Gao, and L. Wang, *Scientific Reports* **6**, 19624 (2016).
- ⁴⁸ L. Yu, Q. Yan, and A. Ruzsinszky, Preprint at <http://arxiv.org/abs/1701.06529> (2017).
- ⁴⁹ Y. Li, J. Kang, and J. Li, *RSC Adv.* **4**, 7396 (2014).
- ⁵⁰ G. Ding, G. Y. Gao, Z. Huang, W. Zhang, and K. Yao, *Nanotechnology* **27**, 375703 (2016).
- ⁵¹ W. Zhang, Z. Huang, W. Zhang, and Y. Li, *Nano Research* **7**, 1731 (2014).
- ⁵² J.-W. Jiang, T. Chang, X. Guo, and H. S. Park, *Nano Letters* **16**, 5286 (2016).
- ⁵³ J. Kang, H. Sahin, and F. M. Peeters, *Phys. Chem. Chem. Phys.* **17**, 27742 (2015).
- ⁵⁴ J. Chen, *Solid State Communications* **237-238**, 14 (2016).
- ⁵⁵ Z. Zhu and D. Tomanek, *Physical Review Letters* **112**, 176802 (2014).
- ⁵⁶ C. Kaneta, H. Katayama-Yoshida, and A. Morita, *Solid State Communications* **44**, 613 (1982).
- ⁵⁷ Y. Du, C. Ouyang, S. Shi, and M. Lei, *Journal of Applied Physics* **107**, 093718 (2010).
- ⁵⁸ G. Qin, Z. Qin, S.-Y. Yue, H.-J. Cui, Q.-R. Zheng, Q.-B. Yan, and G. Su, *Scientific Reports* **4**, 6946 (2014).
- ⁵⁹ M. Elahi, K. Khaliji, S. M. Tabatabaei, M. Pourfath, and R. Asgari, *Physical Review B* **91**, 115412 (2014).
- ⁶⁰ Z.-Y. Ong, Y. Cai, G. Zhang, and Y.-W. Zhang, *Journal of Physical Chemistry C* **118**, 25272 (2014).
- ⁶¹ Y. Aierken, D. Cakir, C. Sevik, and F. M. Peeters, *Physical Review B* **92**, 081408 (2015).

- ⁶² J.-W. Jiang, *Nanotechnology* **26**, 055701 (2015).
- ⁶³ A. Jain and A. J. H. McGaughey, *Scientific Reports* **5**, 8501 (2015).
- ⁶⁴ S. Zhang, M. Xie, F. Li, Z. Yan, Y. Li, E. Kan, W. Liu, Z. Chen, and H. Zeng, *Angew. Chem. Int. Ed.* **55**, 1666 (2016).
- ⁶⁵ J. Qiao, X. Kong, Z.-X. Hu, F. Yang, and W. Ji, *Nature Communications* **5**, 4475 (2014).
- ⁶⁶ Q. Wei and X. Peng, *Applied Physics Letters* **104**, 251915 (2014).
- ⁶⁷ J.-W. Jiang and H. S. Park, *Nature Communications* **5**, 4727 (2014).
- ⁶⁸ D. Midtvedt and A. Croy, *Nanotechnology* **27**, 238001 (2016).
- ⁶⁹ J.-W. Jiang, Preprint at <http://arxiv.org/abs/1605.02566v1> (2016).
- ⁷⁰ Y. Xu, B. Peng, H. Zhang, H. Shao, R. Zhang, H. Lu, D. W. Zhang, and H. Zhu, Preprint at <http://arxiv.org/abs/1604.03422v1> (2016).
- ⁷¹ Z. Zhang, J. Xie, D. Yang, Y. Wang, M. Si, and D. Xue, *Applied Physics Express* **8**, 055201 (2015).
- ⁷² C. Kamal and M. Ezawa, *Physical Review B* **91**, 085423 (2015).
- ⁷³ M. Zeraati, S. M. V. Allaei, I. A. Sarsari, M. Pourfath, and D. Donadio, *Physical Review B* **93**, 085424 (2015).
- ⁷⁴ M. Yang and W.-M. Liu, Preprint at <http://arxiv.org/abs/1501.04350v1> (2016).
- ⁷⁵ G. Wang, R. Pandey, and S. P. Karna, *ACS Appl. Mater. Interfaces* **7**, 11490 (2015).
- ⁷⁶ G. Zheng, Y. Jia, S. Gao, and S.-H. Ke, *Physical Review B* **94**, 155448 (2016).
- ⁷⁷ E. Akturk, O. U. Akturk, and S. Ciraci, *Physical Review B* **94**, 014115 (2016).
- ⁷⁸ C. Kamal, A. Chakrabarti, and M. Ezawa, *Physical Review B* **93**, 125428 (2016).
- ⁷⁹ J. M. Soler, E. Artacho, J. D. Gale, A. Garcia, J. Junquera, P. Ordejon, and D. Sanchez-Portal, *Journal of Physics: Condensed Matter* **14**, 2745 (2002).
- ⁸⁰ J. P. Perdew, K. Burke, and M. Ernzerhof, *Physical Review Letters* **77**, 3865 (1996).
- ⁸¹ G. Qin, Z. Qin, W.-Z. Fang, L.-C. Zhang, S.-Y. Yue, Q.-B. Yan, M. Hu, and G. Su, *Nanoscale* **8**, 11306 (2016).
- ⁸² L.-C. Zhang, G. Qin, W.-Z. Fang, H.-J. Cui, Q.-R. Zheng, Q.-B. Yan, and G. Su, Preprint at <http://arxiv.org/abs/1505.04590> (2016).
- ⁸³ Y. Chen, Q. Sun, and P. Jena, *J. Mater. Chem. C* **4**, 6353 (2016).
- ⁸⁴ X.-J. Ge, K.-L. Yao, and J.-T. Lu, *Physical Review B* **94**, 165433 (2016).
- ⁸⁵ A. Ince and S. Erkoç, *Computational Materials Science* **50**, 865 (2011).

- ⁸⁶ M. I. Baskes, *Physical Review B* **46**, 2727 (1992).
- ⁸⁷ Q.-X. Pei, Y.-W. Zhang, Z.-D. Sha, and V. B. Shenoy, *Journal of Applied Physics* **114**, 033526 (2013).
- ⁸⁸ J. F. Justo, M. Z. Bazant, E. Kaxiras, V. V. Bulatov, and S. Yip, *Physical Review B* **58**, 2539 (1998).
- ⁸⁹ M. R. Chavez-Castillo, M. A. Rodriguez-Meza, and L. Meza-Montes, *RSC Adv.* **5**, 96052 (2015).
- ⁹⁰ X. Zhang, H. Xie, M. Hu, H. Bao, S. Yu, G. Qin, and G. Su, *Physical Review B* **89**, 054310 (2014).
- ⁹¹ X. Li, J. T. Mullen, Z. Jin, K. M. Borysenko, M. B. Nardelli, and K. W. Kim, *Physical Review B* **87**, 115418 (2013).
- ⁹² E. Scalise, M. Houssa, G. Pourtois, B. van den Broek, V. Afanasev, and A. Stesmans, *Nano Research* **6**, 19 (2013).
- ⁹³ N. J. Roome and J. D. Carey, *ACS Appl. Mater. Interfaces* **6**, 7743 (2014).
- ⁹⁴ C. Yang, Z. Yu, P. Lu, Y. Liu, H. Ye, and T. Gao, *Computational Materials Science* **95**, 420 (2014).
- ⁹⁵ B. Wang, J. Wu, X. Gu, H. Yin, Y. Wei, R. Yang, and M. Dresselhaus, *Applied Physics Letters* **104**, 081902 (2014).
- ⁹⁶ H. Xie, M. Hu, and H. Bao, *Applied Physics Letters* **104**, 131906 (2014).
- ⁹⁷ X. Gu and R. Yang, *Journal of Applied Physics* **117**, 025102 (2015).
- ⁹⁸ L.-F. Huang, P.-L. Gong, and Z. Zeng, *Physical Review B* **91**, 205433 (2015).
- ⁹⁹ Z. Wang, T. Feng, and X. Ruan, *Journal of Applied Physics* **117**, 084317 (2015).
- ¹⁰⁰ H. Xie, T. Ouyang, E. Germaneau, G. Qin, M. Hu, and H. Bao, *Physical Review B* **93**, 075404 (2016).
- ¹⁰¹ Y. D. Kuang, L. Lindsay, S. Q. Shi, and G. P. Zheng, *Nanoscale* **8**, 3760 (2016).
- ¹⁰² B. Peng, H. Zhang, H. Shao, Y. Xu, and H. Zhu, Preprint at <http://arxiv.org/abs/1602.02266v1> (2016).
- ¹⁰³ Q. Peng, X. Wen, and S. De, *RSC Advances* **3**, 13772 (2013).
- ¹⁰⁴ M. A. Balatero, G. J. Paylaga, N. T. Paylaga, and R. V. Bantaculo, *Applied Mechanics and Materials* **772**, 67 (2015).
- ¹⁰⁵ S. J. Zaveh, M. Roknabadi, and M. M. T. Morshedloo, *Superlattices and Microstructures* **91**,

- 383 (2016).
- ¹⁰⁶ S. Mojumder, A. A. Amin, and M. M. Islam, *Journal of Applied Physics* **118**, 124305 (2015).
- ¹⁰⁷ M. Modarresi, A. Kakoei, Y. Mogulkoc, and M. Roknabadi, *Computational Materials Science* **101**, 164 (2015).
- ¹⁰⁸ M. J. Cherukara, B. Narayanan, A. Kinaci, K. Sasikumar, S. K. Gray, M. K. Chan, and S. K. R. S. Sankaranarayanan, *J. Phys. Chem. Lett.* **7**, 3752 (2016).
- ¹⁰⁹ B. van den Broek, M. Houssa, E. Scalise, G. Pourtois, V. V. Afanasev, and A. Stesmans, *2D Mater.* **1**, 021004 (2014).
- ¹¹⁰ B. Peng, H. Zhang, H. Shao, Y. Xu, X. Zhang, and H. Zhu, *Scientific Reports* **6**, 20225 (2016).
- ¹¹¹ H. Zhou, Y. Cai, G. Zhang, and Y.-W. Zhang, *Physical Review B* **94**, 045423 (2016).
- ¹¹² D. Singh, S. K. Gupta, I. Lukacevic, and Y. Sonvane, *RSC Adv.* **6**, 8006 (2016).
- ¹¹³ L. Cheng, H. Liu, X. Tan, J. Zhang, J. Wei, H. L. J. Shi, and X. Tang, *Journal of Physical Chemistry C* **118**, 904 (2013).
- ¹¹⁴ H. Sahin, S. Cahangirov, M. Topsakal, E. Bekaroglu, E. Akturk, R. T. Senger, and S. Ciraci, *Physical Review B* **80**, 155453 (2009).
- ¹¹⁵ S. Demirci, N. Avazh, E. Durgun, and S. Cahangirov, *Physical Review B* **95**, 115409 (2017).
- ¹¹⁶ H. Wang, Q. Li, Y. Gao, F. Miao, X.-F. Zhou, and X. G. Wan, *New Journal of Physics* **18**, 73016 (2016).
- ¹¹⁷ M. Q. Le, B. Mortazavi, and T. Rabczuk, *Nanotechnology* **27**, 445709 (2016).
- ¹¹⁸ Z. Pang, X. Qian, R. Yang, and Y. Wei, Preprint at <http://arxiv.org/abs/1602.05370> (2016).
- ¹¹⁹ A. J. Mannix, X.-F. Zhou, B. Kiraly, J. D. Wood, D. Alducin, B. D. Myers, X. Liu, B. L. Fisher, U. Santiago, J. R. Guest, M. J. Yacaman, A. Ponce, A. R. Oganov, M. C. Hersam, and N. P. Guisinger, *Science* **350**, 1513 (2015).
- ¹²⁰ Z. Zhang, Y. Yang, E. S. Penev, and B. I. Yakobson, *Advanced Functional Materials* **27**, 1605059 (2017).
- ¹²¹ M. Arroyo and T. Belytschko, *Physical Review B* **69**, 115415 (2004).
- ¹²² J.-W. Jiang, Z. Qi, H. S. Park, and T. Rabczuk, *Nanotechnology* **24**, 435705 (2013).